

8-2014

Development of a New Independent Monte Carlo Dose Calculation Quality Assurance Audit Tool for Clinical Trials

Austin M. Faught

Follow this and additional works at: http://digitalcommons.library.tmc.edu/utgsbs_dissertations

 Part of the [Medical Biophysics Commons](#), and the [Other Physics Commons](#)

Recommended Citation

Faught, Austin M., "Development of a New Independent Monte Carlo Dose Calculation Quality Assurance Audit Tool for Clinical Trials" (2014). *UT GSBS Dissertations and Theses (Open Access)*. Paper 486.

This Dissertation (PhD) is brought to you for free and open access by the Graduate School of Biomedical Sciences at DigitalCommons@The Texas Medical Center. It has been accepted for inclusion in UT GSBS Dissertations and Theses (Open Access) by an authorized administrator of DigitalCommons@The Texas Medical Center. For more information, please contact laurel.sanders@library.tmc.edu.

DEVELOPMENT OF A NEW INDEPENDENT MONTE CARLO DOSE CALCULATION
QUALITY ASSURANCE AUDIT TOOL FOR CLINICAL TRIALS

By

Austin Michael Faught

Approved:

David Followill, Ph.D.

Advisory Professor

Geoffrey Ibbott, Ph.D.

Stephen Kry, Ph.D.

Scott Davidson, Ph.D.

Carol Etzel, Ph.D.

Approved:

Dean, The University of Texas

Health Science Center at Houston

Graduate School of Biomedical Sciences

DEVELOPMENT OF A NEW INDEPENDENT MONTE CARLO DOSE CALCULATION
QUALITY ASSURANCE AUDIT TOOL FOR CLINICAL TRIALS

A
Dissertation

Presented to the Faculty of
The University of Texas Health Science Center at Houston
Graduate School of Biomedical Sciences

and
The University of Texas
MD Anderson Cancer Center

In Partial Fulfillment
of the Requirements
for the Degree of

Doctor of Philosophy

By

Austin Michael Faught

Houston, Texas

August, 2014

Acknowledgements

There are many people who have contributed their time, effort, and support in order for this project to be completed. For that, I am grateful to you all. Special acknowledgement is deserved by a few individuals for their extraordinary contributions. First, I am thankful for the support of my parents, Mike and Lori, who have encouraged me in all my endeavors. Two great educators played a significant role in my path towards Medical Physics. Rich Koehler, my high school science teacher, first ignited the flame of curiosity within me, and Dr. John Idoine, a physics professor at Kenyon College, introduced me to Medical Physics and mentored me throughout my undergraduate work. Dr. Rich Popple and Dr. Jonas Fontenot generously contributed their time to help with phantom measurements at their respective institutions. My advisory committee has graciously provided me with their time and guidance during this project. Dr. David Followill's role as a mentor early in my Medical Physics career has been invaluable. Finally, my soon to be wife, Jacqueline Tonigan has been a never ending source of encouragement.

Development of a New Independent Monte Carlo Dose Calculation Quality Assurance Audit Tool for Clinical Trials

Austin Michael Faught

Advisory Professor: David S. Followill, Ph.D.

Introduction: Commercially available treatment planning systems (TPS) may use a number of different radiation dose calculation algorithms during the planning process. The Radiological Physics Center (RPC), tasked with ensuring clinically comparable and consistent dose delivery amongst institutions participating in NCI funded multi-institutional clinical trials, has traditionally relied upon measurements to achieve this objective. As a supplement to the tools used by the RPC, an independent dose calculation tool is needed to determine patient dose distributions in three dimensions so as to act as a quality assurance tool for the dose calculations.

Methods: Multiple source models representing the output of Elekta 6MV and 10MV and Varian TrueBeam Flattening Filter Free (FFF) 6MV and FFF 10MV therapeutic x-ray beams were developed. The Monte Carlo technique, using the Dose Planning Method (DPM) algorithm, was used in radiation dose calculations. During validation calculations were compared to open field measurements in a water phantom. Benchmarking was a measurement based comparison of mock treatment plans in anthropomorphic phantoms. Treatment plans included intensity modulated radiation therapy and stereotactic body radiation therapy techniques. Past phantom treatment plans submitted through a remote auditing program were recalculated using the tool and compared to submitted measurement data as a test of the models' robustness.

Results: The average percentage of data passing a $\pm 2\%/2\text{mm}$ gamma criterion during validation testing was 99.5%, 99.6%, 98.1%, and 98.1% for Elekta 6MV, 10MV, Varian

TrueBeam FFF 6MV, and FFF 10MV beams, respectively. The percentage of data passing the benchmarking evaluation criterion of $\pm 3\%/2\text{mm}$ was 87.4%, 89.9%, 90.1%, and 90.8% for Elekta 6MV, Elekta 10MV, Varian TrueBeam FFF 6MV, and Varian TrueBeam FFF 10MV beams, respectively.

Conclusions: Elekta 6MV and 10MV and Varian TrueBeam FFF 6MV and FFF 10MV multiple source models based on dose calculations using the DPM Monte Carlo code were successfully developed, validated, and benchmarked against measurements. A recalculation of TPS dose from archived phantom credentialing audits was performed as a proof of concept for the models' utility as a quality assurance tool for use in clinical trial audits.

Contents

Chapter 1: Introduction	1
1.1 Statement of Problem.....	1
1.2 Benefits to Science.....	6
1.3 Hypothesis and Specific Aims	7
Chapter 2: Materials and Methods: Development, Validation, and Benchmarking.....	9
2.1 Introduction	9
2.2 Source Model.....	11
2.2.1 Hardware.....	11
2.2.2 Software.....	11
2.2.3 Source Model Commissioning.....	11
2.2.4 Machine Output Correction.....	14
2.2.5 Fluence Map	14
2.2.6 Primary Source Size.....	15
2.2.7 Electron Contamination Contribution Versus Field Size.....	15
2.3 Validation Testing.....	15
2.4 Anthropomorphic Phantoms.....	17
2.5 Benchmark Testing	20
2.5.1 Point Dose Comparisons.....	21
2.5.2 Dose Profile Comparisons.....	21
2.5.3 Gamma Map Comparisons.....	21
2.5.4 Treatment Plans.....	23
Chapter 3: Results and Discussion: Elekta 6MV and 10MV.....	30
3.1 Source Model.....	30
3.1.1 Source Model Commissioning Parameters.....	30
3.1.2 Fluence Map, Primary Source Size, and Machine Output Correction	35
3.2 Validation Testing.....	37

3.2.1 Uncertainty	37
3.2.2 Depth Dose Data	37
3.2.3 Dose Profiles	41
3.3 Benchmark Testing	46
3.3.1 Uncertainty	46
3.3.2 Deliver of IMRT H&N Phantom Plan: Point Dose Comparison.....	47
3.3.3 Delivery of IMRT H&N Phantom Plan: Dose Profile and Gamma Map Comparison.....	51
3.3.4 Delivery of SBRT Thorax Phantom Plan: Point Dose Comparison.....	60
3.3.5 Delivery of SBRT Thorax Phantom Plan: Dose Profile and Gamma Map Comparison ...	62
3.3.6 Delivery of IMRT Thorax Phantom Plan: Point Dose Comparison	71
3.3.7 Delivery of IMRT Thorax Phantom Plan: Dose Profile and Gamma Map Comparison ...	74
3.3.8 Benchmark Summary	82
3.4 Conclusion	84
Chapter 4: Results and Discussion: Varian TrueBeam 6 MV and 10MV Flattening Filter Free	
Beams	86
4.1 Source Model	86
4.1.1 Source Model Commissioning Parameters.....	86
4.1.2 Fluence Map, Primary Source Size, and Machine Output Correction	91
4.2 Validation Testing.....	91
4.2.1 Uncertainty	91
4.2.2 Depth Dose Data.....	92
4.2.3 Dose Profiles	97
4.3 Benchmark Testing	103
4.3.1 Uncertainty	103
4.3.2 Delivery of the IMRT Head and Neck Phantom Plan: Point Dose Comparison	103
4.3.3 Delivery of the IMRT Head and Neck Phantom Plan: Point Dose Comparison	107
4.3.4 Delivery of the SBRT Thorax Phantom Plan: Point Dose Comparison.....	114

4.3.5 Delivery of the SBRT Thorax Phantom Plan: Dose Profile and Gamma Map Comparison	117
4.3.6 Delivery of the IMRT Thorax Phantom Plan: Point Dose Comparison	126
4.3.7 Delivery of the IMRT Thorax Phantom Plan: Dose Profile and Gamma Map Comparison	129
4.3.8 Benchmark Summary	138
4.4 Conclusion	139
Chapter 5: Robustness Study at Outside Institutions: Elekta and Varian TrueBeam FFF 6MV and 10MV	141
5.1 Introduction	141
5.2 Materials and Methods	141
5.3 Results	144
5.3.1 Point Dose Comparison.....	144
5.3.2 Gamma Map Comparison	146
5.4 Conclusion	149
Chapter 6: Summary	151
6.1 Summary for Elekta Models	151
6.2 Summary for Varian TrueBeam FFF Models	151
6.3 Summary for Robustness Study	152
6.4 Evaluation of the Hypothesis	153
6.5 General Conclusions	154
6.6 Future Work	154
Chapter 7: Appendix	156
7.1 Elekta 6 MV: Percent Depth Dose and Dose Profiles	156
7.2 Elekta 6 MV: Gamma Maps.....	166
7.2.1 Elekta 6 MV: Delivery of IMRT Head and Neck Plan	166
7.2.2 Elekta 6 MV: Delivery of SBRT Lung Plan	169

7.2.3 Elekta 6 MV: Delivery of IMRT Lung Plan.....	173
7.3 Elekta 10 MV: Percent Depth Dose and Dose Profiles	177
7.4 Elekta 10 MV: Gamma Maps.....	187
7.4.1 Elekta 10 MV: Delivery of IMRT Head and Neck Plan	187
7.4.2 Elekta 10 MV: Delivery of SBRT Lung Plan	190
7.4.3 Elekta 10 MV: Delivery of IMRT Lung Plan.....	194
7.5 Varian TrueBeam 6 MV: Percent Depth Dose and Dose Profiles	198
7.6 Varian TrueBeam 6 MV: Gamma Maps.....	210
7.6.1 Varian TrueBeam 6 MV: Delivery of IMRT Head and Neck Plan	210
7.6.2 Varian TrueBeam 6 MV: Delivery of SBRT Lung Plan	213
7.6.3 Varian TrueBeam 6 MV: Delivery of IMRT Lung Plan	217
7.7 Varian TrueBeam 10 MV: Percent Depth Dose and Dose Profiles	221
7.8 Varian TrueBeam 10 MV: Gamma Maps.....	234
7.8.1 Varian TrueBeam 10 MV: Delivery of IMRT Head and Neck Plan.....	234
7.8.2 Varian TrueBeam 10 MV: Delivery of SBRT Lung Plan	237
7.8.3 Varian TrueBeam 10 MV: Delivery of IMRT Lung Plan	241
7.9 Outside Institution Robustness Study: Gamma Maps.....	245
7.9.1 Head and Neck Phantom Audits.....	245
7.9.2 Lung Phantom Audits	254
Chapter 8: References	273
Chapter 9: Vita	281

List of Illustrations

- Figure 2.1:** The anthropomorphic, hollow, plastic shell to the RPC's head and neck phantom with the polystyrene insert removed and opened. The polystyrene insert in the RPC's head and neck phantom is opened up to reveal a transverse, cross sectional view. The insert contains a primary PTV, secondary PTV, and critical structure made of solid water that may be distinguished from the insert in a CT scan for treatment planning purposes. Also pictured are the holes to house the thermoluminescent dosimeters (TLD) for absolute dosimetry. The orthogonal slits intersecting in the primary PTV are for sagittal and coronal films while an axial film may be placed between the two halves to the insert shown in this cross sectional image. 18
- Figure 2.2:** The outer shell of the RPC's thorax phantom with the lung insert partially removed. Within the insert are slits for the placement of radiochromic film and holes for TLD. Rods containing TLD capsules are also inserted into the shell for point dose measurements corresponding to the location of the spinal cord and heart, the representative critical structures for this treatment. Also pictured (right) is the disassembled lung insert with locations for radiochromic film and TLD and the removed TLD rods (bottom left)..... 19
- Figure 2.3:** Exclusion mask used in the evaluation of the sagittal film from the IMRT head and neck phantom. The exclusion areas are indicated by red lines and correspond to discontinuities between the superior and inferior film pieces, a cutout for the placement of the OAR TLD, and the pin pricks used to localize the film within the phantom insert. 22
- Figure 2.4:** Region of interest evaluated using gamma analysis for the axial plane of the IMRT head and neck phantom (left) and lung phantom (right) is shown with the dose cloud from a treatment plan overlaid on the CT scan. For delineation of specific structures in the CT scan in each phantom see Figures 2.5 and 2.6. 23
- Figure 2.5:** Axial (top), sagittal (bottom left), and coronal (bottom right) views of the CT scan of the head and neck phantom. Contours are the primary PTV (red), secondary PTV (green), and critical structure, the cord, (blue). The dark circles within the contours are the regions where the

TLD are placed within the phantom and the location for point dose comparisons between measurement and calculation..... 25

Figure 2.6: Axial (top), sagittal (bottom left), and coronal (bottom right) views of the CT scan of the thorax phantom. Contours are the PTV (green), heart (red), and the cord (blue). The dark circles within the contours are the regions where the TLD are placed within the phantom and the location for point dose comparisons between measurement and calculation. 27

Figure 3.1: Comparison of commissioned Elekta 6MV source model spectrum with the results from BEAM (Sheikh-Bagheri and Rogers) and Davidson et. al. 32

Figure 3.2: Comparison of commissioned Elekta 10MV source model spectrum with the results from Davidson et. al. 33

Figure 3.3: Output at a depth of 1.6cm for the measured data (blue circles), calculated data without the hyperbolic correction (red star), and the calculated data with the hyperbolic correction (green x) for the Elekta 6MV source model. 36

Figure 3.4: Output at a depth of 2.0cm for the measured data (blue circles), calculated data without the hyperbolic correction (red star), and the calculated data with the hyperbolic correction (green triangle) for the Elekta 10MV source model. 36

Figure 3.5: Calculated (blue 'x') and measured (red line) depth dose curves for an Elekta 6MV beam for a 3 x 3 cm² field size. Gamma agreement (red circles) for each point is also displayed along with any points (red star) at which a failure to meet the $\pm 2\%/2\text{mm}$ criterion. ... 38

Figure 3.6: Calculated (blue 'x') and measured (red line) depth dose curves for an Elekta 6MV beam for a 10 x 10 cm² field size. Gamma agreement (red circles) for each point is also displayed. There were no failures for this field size and as a result no failure points marked... 39

Figure 3.7: Calculated (blue 'x') and measured (red line) depth dose curves for an Elekta 6MV beam for a 30 x 30 cm² field size. Gamma agreement (red circles) for each point is also displayed along with any points (red star) at which a failure to meet the $\pm 2\%/2\text{mm}$ criterion. ... 39

Figure 3.8: Calculated (blue 'x') and measured (red line) depth dose curves for an Elekta 10MV beam for a 3 x 3 cm² field size. Gamma agreement (red circles) for each point is also displayed along with any points (red star) at which a failure to meet the ±2%/2mm criterion. ... 40

Figure 3.9: Calculated (blue 'x') and measured (red line) depth dose curves for an Elekta 10MV beam for a 10 x 10 cm² field size. Gamma agreement (red circles) for each point is also displayed along with any points (red star) at which a failure to meet the ±2%/2mm criterion. ... 40

Figure 3.10: Calculated (blue 'x') and measured (red line) depth dose curves for an Elekta 10MV beam for a 30 x 30 cm² field size. Gamma agreement (red circles) for each point is also displayed along with any points (red star) at which a failure to meet the ±2%/2mm criterion. ... 41

Figure 3.11: Calculated (red diamond) and measured (blue line) dose profiles for an Elekta 6MV beam at a field size of 3 x 3 cm²..... 42

Figure 3.12: Calculated (red diamond) and measured (blue line) dose profiles for an Elekta 6MV beam at a field size of 10 x 10 cm²..... 43

Figure 3.13: Calculated (red diamond) and measured (blue line) dose profiles for an Elekta 6MV beam at a field size of 30 x 30 cm²..... 43

Figure 3.14: Calculated (red diamond) and measured (blue line) dose profiles for an Elekta 10MV beam at a field size of 3 x 3 cm²..... 44

Figure 3.15: Calculated (red diamond) and measured (blue line) dose profiles for an Elekta 10MV beam at a field size of 10 x 10 cm²..... 44

Figure 3.16: Calculated (red diamond) and measured (blue line) dose profiles for an Elekta 10MV beam at a field size of 30 x 30 cm²..... 45

Figure 3.17: A comparison of the lateral (left to right) profile from the axial film of an IMRT H&N delivery for the 6MV model (delivery #1). 52

Figure 3.18: A comparison of the AP (anterior to posterior) profile from the axial film of an IMRT H&N delivery for the 6MV model (delivery #1). 52

Figure 3.19: A comparison of the SI (superior to inferior) profile from the axial film of an IMRT H&N delivery for the 6MV model (delivery #1). 53

Figure 3.20: A comparison of the lateral (left to right) profile from the axial film of an IMRT H&N delivery for the 10MV model (delivery #1). 53

Figure 3.21: A comparison of the AP (anterior to posterior) profile from the axial film of an IMRT H&N delivery for the 10MV model (delivery #1). 54

Figure 3.22: A comparison of the SI (superior to inferior) profile from the axial film of an IMRT H&N delivery for the 10MV model (delivery #1). 54

Figure 3.23: IMRT head and neck delivery comparison for the axial plane of delivery #1 for the Elekta 6MV model. Agreement was evaluated using a $\pm 3\%/2\text{mm}$ gamma criterion and 91.4% of pixels passed. 56

Figure 3.24: IMRT head and neck delivery comparison for the sagittal plane of delivery #1 for the Elekta 6MV model. Agreement was evaluated using a $\pm 3\%/2\text{mm}$ gamma criterion and 88.9% of pixels passed. 56

Figure 3.25: IMRT head and neck delivery comparison for the axial plane of delivery #3 for the Elekta 10MV model. Agreement was evaluated using a $\pm 3\%/2\text{mm}$ gamma criterion and 95.9% of pixels passed. 57

Figure 3.26: IMRT head and neck delivery comparison for the sagittal plane of delivery #3 for the Elekta 10MV model. Agreement was evaluated using a $\pm 3\%/2\text{mm}$ gamma criterion and 87.3% of pixels passed. 57

Figure 3.27: Dose profile comparison for IMRT head and neck delivery for 10MV Elekta model. The top profile is along the anteroposterior direction of the superior film piece, and the bottom is along the anteroposterior direction of the inferior film piece. 59

Figure 3.28: A comparison of the lateral (left to right) profile from the axial film of an SBRT lung delivery for the 6MV model (delivery #1). 63

Figure 3.29: A comparison of the AP (anterior to posterior) profile from the axial film of an SBRT lung delivery for the 6MV model (delivery #1). 63

Figure 3.30: A comparison of the SI (superior to inferior) profile from the sagittal film of an SBRT lung delivery for the 6MV model (delivery #1). 64

Figure 3.31: A comparison of the lateral (left to right) profile from the axial film of an SBRT lung delivery for the 10MV model (delivery #1).	64
Figure 3.32: A comparison of the AP (anterior to posterior) profile from the axial film of an SBRT lung delivery for the 10MV model (delivery #1).	65
Figure 3.33: A comparison of the SI (superior to inferior) profile from the sagittal film of an SBRT lung delivery for the 10MV model (delivery #1).	65
Figure 3.34: Lung SBRT delivery comparison for the axial plane of delivery #1 for the Elekta 6MV model. Agreement was evaluated using a $\pm 3\%/2\text{mm}$ gamma criterion and 85.3% of pixels passed.	66
Figure 3.35: Lung SBRT delivery comparison for the sagittal plane of delivery #1 for the Elekta 6MV model. Agreement was evaluated using a $\pm 3\%/2\text{mm}$ gamma criterion and 87.7% of pixels passed.	67
Figure 3.36: Lung SBRT delivery comparison for the coronal plane of delivery #1 for the Elekta 6MV model. Agreement was evaluated using a $\pm 3\%/2\text{mm}$ gamma criterion and 93.9% of pixels passed.	67
Figure 3.37: Lung SBRT delivery comparison for the axial plane of delivery #1 for the Elekta 10MV model. Agreement was evaluated using a $\pm 3\%/2\text{mm}$ gamma criterion and 96.5% of pixels passed.	68
Figure 3.38: Lung SBRT delivery comparison for the sagittal plane of delivery #1 for the Elekta 10MV model. Agreement was evaluated using a $\pm 3\%/2\text{mm}$ gamma criterion and 89.1% of pixels passed.	69
Figure 3.39: Lung SBRT delivery comparison for the coronal plane of delivery #1 for the Elekta 10MV model. Agreement was evaluated using a $\pm 3\%/2\text{mm}$ gamma criterion and 92.6% of pixels passed.	69
Figure 3.40: A comparison of the lateral (left to right) profile from the axial film of an IMRT lung delivery for the 6MV model.	74

Figure 3.41: A comparison of the AP (anterior to posterior) profile from the axial film of an IMRT lung delivery for the 6MV model.	75
Figure 3.42: A comparison of the SI (superior to inferior) profile from the coronal film of an IMRT lung delivery for the 6MV model.	75
Figure 3.43: A comparison of the lateral (left to right) profile from the axial film of an IMRT lung delivery for the 10MV model.	76
Figure 3.44: A comparison of the AP (anterior to posterior) profile from the axial film of an IMRT lung delivery for the 10MV model.	76
Figure 3.45: A comparison of the SI (superior to inferior) profile from the coronal film of an IMRT lung delivery for the 10MV model.	77
Figure 3.46: Lung IMRT delivery comparison for the axial plane of delivery #3 for the Elekta 6MV model. Agreement was evaluated using a $\pm 3\%/2\text{mm}$ gamma criterion and 87.5% of pixels passed.	78
Figure 3.47: Lung IMRT delivery comparison for the sagittal plane of delivery #3 for the Elekta 6MV model. Agreement was evaluated using a $\pm 3\%/2\text{mm}$ gamma criterion and 86.4% of pixels passed.	78
Figure 3.48: Lung IMRT delivery comparison for the coronal plane of delivery #3 for the Elekta 6MV model. Agreement was evaluated using a $\pm 3\%/2\text{mm}$ gamma criterion and 94.0% of pixels passed.	79
Figure 3.49: Lung IMRT delivery comparison for the axial plane of delivery #1 for the Elekta 10MV model. Agreement was evaluated using a $\pm 3\%/2\text{mm}$ gamma criterion and 94.7% of pixels passed.	80
Figure 3.50: Lung IMRT delivery comparison for the sagittal plane of delivery #1 for the Elekta 10MV model. Agreement was evaluated using a $\pm 3\%/2\text{mm}$ gamma criterion and 90.6% of pixels passed.	81

Figure 3.51: Lung IMRT delivery comparison for the coronal plane of delivery #1 for the Elekta 10MV model. Agreement was evaluated using a $\pm 3\%/2\text{mm}$ gamma criterion and 89.3% of pixels passed. 81

Figure 4.1: Comparison of commissioned TrueBeam FFF 6MV source model spectrum (red square) with the previously developed Varian 6MV source model (blue diamond)[35]..... 88

Figure 4.2: Comparison of commissioned TrueBeam FFF 10MV source model spectrum (red square) with the previously developed Varian 10MV source model (blue diamond)[35]..... 89

Figure 4.3: Calculated (blue 'x') and measured (red line) depth dose curves for a TrueBeam FFF 6MV beam for a $3 \times 3 \text{ cm}^2$ field size. Gamma agreement (red circles) for each point is also displayed along with any points (red star) at which a failure to meet the $\pm 2\%/2\text{mm}$ criterion. ... 94

Figure 4.4: Calculated (blue 'x') and measured (red line) depth dose curves for a TrueBeam FFF 6MV beam for a $10 \times 10 \text{ cm}^2$ field size. Gamma agreement (red circles) for each point is also displayed along with any points (red star) at which a failure to meet the $\pm 2\%/2\text{mm}$ criterion. 94

Figure 4.5: Calculated (blue 'x') and measured (red line) depth dose curves for a TrueBeam FFF 6MV beam for a $40 \times 40 \text{ cm}^2$ field size. Gamma agreement (red circles) for each point is also displayed along with any points (red star) at which a failure to meet the $\pm 2\%/2\text{mm}$ criterion. 95

Figure 4.6: Calculated (blue 'x') and measured (red line) depth dose curves for a TrueBeam FFF 10MV beam for a $3 \times 3 \text{ cm}^2$ field size. Gamma agreement (red circles) for each point is also displayed along with any points (red star) at which a failure to meet the $\pm 2\%/2\text{mm}$ criterion. 95

Figure 4.7: Calculated (blue 'x') and measured (red line) depth dose curves for a TrueBeam FFF 10MV beam for a $10 \times 10 \text{ cm}^2$ field size. Gamma agreement (red circles) for each point is also displayed along with any points (red star) at which a failure to meet the $\pm 2\%/2\text{mm}$ criterion. 96

Figure 4.8: Calculated (blue 'x') and measured (red line) depth dose curves for a TrueBeam FFF 10MV beam for a 40 x 40 cm ² field size. Gamma agreement (red circles) for each point is also displayed along with any points (red star) at which a failure to meet the ±2%/2mm criterion.	96
Figure 4.9: Calculated (red circle) and measured (blue line) dose profiles for a TrueBeam FFF 6MV beam at a field size of 3 x 3 cm ²	99
Figure 4.10: Calculated (red circle) and measured (blue line) dose profiles for a TrueBeam FFF 6MV beam at a field size of 10 x 10 cm ²	99
Figure 4.11: Calculated (red circle) and measured (blue line) dose profiles for a TrueBeam FFF 6MV beam at a field size of 40 x 40 cm ²	100
Figure 4.12: Calculated (red circle) and measured (blue line) dose profiles for a TrueBeam FFF 10MV beam at a field size of 3 x 3 cm ²	100
Figure 4.13: Calculated (red circle) and measured (blue line) dose profiles for a TrueBeam FFF 10MV beam at a field size of 10 x 10 cm ²	101
Figure 4.14: Calculated (red circle) and measured (blue line) dose profiles for a TrueBeam FFF 10MV beam at a field size of 40 x 40 cm ²	101
Figure 4.15: A comparison of the lateral (left to right) profile from the axial film of an IMRT H&N delivery for the FFF 6MV model (delivery #1).	108
Figure 4.16: A comparison of the AP (anterior to posterior) profile from the axial film of an IMRT H&N delivery for the FFF 6MV model (delivery #1).	108
Figure 4.17: A comparison of the SI (superior to inferior) profile from the axial film of an IMRT H&N delivery for the FFF 6MV model (delivery #1).	109
Figure 4.18: A comparison of the lateral (left to right) profile from the axial film of an IMRT H&N delivery for the FFF 10MV model (delivery #1).	109
Figure 4.19: A comparison of the AP (anterior to posterior) profile from the axial film of an IMRT H&N delivery for the FFF 10MV model (delivery #1).	110

Figure 4.20: A comparison of the SI (superior to inferior) profile from the axial film of an IMRT H&N delivery for the FFF 10MV model (delivery #1)..... 110

Figure 4.21: IMRT head and neck delivery comparison for the axial plane of delivery #1 for the TrueBeam FFF 6MV model. Agreement was evaluated using a $\pm 3\%/2\text{mm}$ gamma criterion and 93.6% of pixels passed. 112

Figure 4.22: IMRT head and neck delivery comparison for the sagittal plane of delivery #1 for the TrueBeam FFF 6MV model. Agreement was evaluated using a $\pm 3\%/2\text{mm}$ gamma criterion and 94.3% of pixels passed..... 112

Figure 4.23: IMRT head and neck delivery comparison for the axial plane of delivery #1 for the TrueBeam FFF 10MV model. Agreement was evaluated using a $\pm 3\%/2\text{mm}$ gamma criterion and 87.9% of pixels passed..... 113

Figure 4.24: IMRT head and neck delivery comparison for the sagittal plane of delivery #1 for the TrueBeam FFF 10MV model. Agreement was evaluated using a $\pm 3\%/2\text{mm}$ gamma criterion and 90.5% of pixels passed..... 113

Figure 4.25: A comparison of the lateral (left to right) profile from the axial film of an SBRT lung delivery for the FFF 6MV model (delivery #1)..... 117

Figure 4.26: A comparison of the AP (anterior to posterior) profile from the axial film of an SBRT lung delivery for the FFF 6MV model (delivery #1)..... 118

Figure 4.27: A comparison of the SI (superior to inferior) profile from the sagittal film of an SBRT lung delivery for the FFF 6MV model (delivery #1)..... 118

Figure 4.28: A comparison of the lateral (left to right) profile from the axial film of an SBRT lung delivery for the FFF 10MV model (delivery #1)..... 119

Figure 4.29: A comparison of the AP (anterior to posterior) profile from the axial film of an SBRT lung delivery for the FFF 10MV model (delivery #1)..... 119

Figure 4.30: A comparison of the SI (superior to inferior) profile from the sagittal film of an SBRT lung delivery for the FFF 10MV model (delivery #1)..... 120

Figure 4.31: Lung SBRT delivery comparison for the axial plane of delivery #1 for the TrueBeam FFF 6MV model. Agreement was evaluated using a $\pm 3\%/2\text{mm}$ gamma criterion and 91.5% of pixels passed.	121
Figure 4.32: Lung SBRT delivery comparison for the sagittal plane of delivery #1 for the TrueBeam FFF 6MV model. Agreement was evaluated using a $\pm 3\%/2\text{mm}$ gamma criterion and 85.5% of pixels passed.	122
Figure 4.33: Lung SBRT delivery comparison for the coronal plane of delivery #1 for the TrueBeam FFF 6MV model. Agreement was evaluated using a $\pm 3\%/2\text{mm}$ gamma criterion and 98.7% of pixels passed.	122
Figure 4.34: Lung SBRT delivery comparison for the axial plane of delivery #1 for the TrueBeam FFF 10MV model. Agreement was evaluated using a $\pm 3\%/2\text{mm}$ gamma criterion and 91.4% of pixels passed.....	123
Figure 4.35: Lung SBRT delivery comparison for the sagittal plane of delivery #1 for the TrueBeam FFF 10MV model. Agreement was evaluated using a $\pm 3\%/2\text{mm}$ gamma criterion and 88.9% of pixels passed.....	124
Figure 4.36: Lung SBRT delivery comparison for the coronal plane of delivery #1 for the TrueBeam FFF 10MV model. Agreement was evaluated using a $\pm 3\%/2\text{mm}$ gamma criterion and 91.9% of pixels passed.....	124
Figure 4.37: A comparison of the lateral (left to right) profile from the axial film of an IMRT lung delivery for the FFF 6MV model (delivery #1).	129
Figure 4.38: A comparison of the AP (anterior to posterior) profile from the axial film of an IMRT lung delivery for the FFF 6MV model (delivery #1).....	130
Figure 4.39: A comparison of the SI (superior to inferior) profile from the sagittal film of an IMRT lung delivery for the FFF 6MV model (delivery #1).....	130
Figure 4.40: A comparison of the lateral (left to right) profile from the axial film of an IMRT lung delivery for the FFF 10MV model (delivery #1).	131

Figure 4.41: A comparison of the AP (anterior to posterior) profile from the axial film of an IMRT lung delivery for the FFF 10MV model (delivery #1).....	131
Figure 4.42: A comparison of the SI (superior to inferior) profile from the sagittal film of an IMRT lung delivery for the FFF 10MV model (delivery #1).....	132
Figure 4.43: Lung IMRT delivery comparison for the axial plane of delivery #1 for the TrueBeam FFF 6MV model. Agreement was evaluated using a $\pm 3\%/2\text{mm}$ gamma criterion and 91.0% of pixels passed.	133
Figure 4.44: Lung IMRT delivery comparison for the sagittal plane of delivery #1 for the TrueBeam FFF 6MV model. Agreement was evaluated using a $\pm 3\%/2\text{mm}$ gamma criterion and 91.8% of pixels passed.	134
Figure 4.45: Lung IMRT delivery comparison for the coronal plane of delivery #1 for the TrueBeam FFF 6MV model. Agreement was evaluated using a $\pm 3\%/2\text{mm}$ gamma criterion and 93.9% of pixels passed.	134
Figure 4.46: Lung IMRT delivery comparison for the axial plane of delivery #3 for the TrueBeam FFF 10MV model. Agreement was evaluated using a $\pm 3\%/2\text{mm}$ gamma criterion and 92.3% of pixels passed.....	135
Figure 4.47: Lung IMRT delivery comparison for the sagittal plane of delivery #3 for the TrueBeam FFF 10MV model. Agreement was evaluated using a $\pm 3\%/2\text{mm}$ gamma criterion and 90.8% of pixels passed.....	136
Figure 4.48: Lung IMRT delivery comparison for the coronal plane of delivery #3 for the TrueBeam FFF 10MV model. Agreement was evaluated using a $\pm 3\%/2\text{mm}$ gamma criterion and 96.6% of pixels passed.....	136
Figure 7.1: Calculated (blue 'x') and measured (red line) percent depth dose curves for an Elekta 6MV beam at a field size of $3 \times 3 \text{ cm}^2$. Gamma agreement (red circles) for each point is also displayed along with any points (red star) at which a failure to meet the $\pm 2\%/2\text{mm}$ criterion. At this field size 99.43% of all data passed the gamma criterion.	156

Figure 7.2: Calculated (blue 'x') and measured (red line) percent depth dose curves for an Elekta 6MV beam at a field size of 5 x 5 cm². Gamma agreement (red circles) for each point is also displayed along with any points (red star) at which a failure to meet the ±2%/2mm criterion. At this field size 99.43% of all data passed the gamma criterion. 157

Figure 7.3: Calculated (blue 'x') and measured (red line) percent depth dose curves for an Elekta 6MV beam at a field size of 10 x 10 cm². Gamma agreement (red circles) for each point is also displayed along with any points (red star) at which a failure to meet the ±2%/2mm criterion. At this field size 100% of all data passed the gamma criterion. 157

Figure 7.4: Calculated (blue 'x') and measured (red line) percent depth dose curves for an Elekta 6MV beam at a field size of 15 x 15 cm². Gamma agreement (red circles) for each point is also displayed along with any points (red star) at which a failure to meet the ±2%/2mm criterion. At this field size 100% of all data passed the gamma criterion. 158

Figure 7.5: Calculated (blue 'x') and measured (red line) percent depth dose curves for an Elekta 6MV beam at a field size of 20 x 20 cm². Gamma agreement (red circles) for each point is also displayed along with any points (red star) at which a failure to meet the ±2%/2mm criterion. At this field size 99.43% of all data passed the gamma criterion. 158

Figure 7.6: Calculated (blue 'x') and measured (red line) percent depth dose curves for an Elekta 6MV beam at a field size of 30 x 30 cm². Gamma agreement (red circles) for each point is also displayed along with any points (red star) at which a failure to meet the ±2%/2mm criterion. At this field size 99.43% of all data passed the gamma criterion. 159

Figure 7.7: Calculated (red diamond) and measured (blue line) dose profiles for an Elekta 6MV beam at a field size of 3 x 3 cm² 160

Figure 7.8: Calculated (red diamond) and measured (blue line) dose profiles for an Elekta 6MV beam at a field size of 5 x 5 cm² 161

Figure 7.9: Calculated (red diamond) and measured (blue line) dose profiles for an Elekta 6MV beam at a field size of 10 x 10 cm² 162

Figure 7.10: Calculated (red diamond) and measured (blue line) dose profiles for an Elekta 6MV beam at a field size of 15 x 15 cm ²	163
Figure 7.11: Calculated (red diamond) and measured (blue line) dose profiles for an Elekta 6MV beam at a field size of 20 x 20 cm ²	164
Figure 7.12: Calculated (red diamond) and measured (blue line) dose profiles for an Elekta 6MV beam at a field size of 30 x 30 cm ²	165
Figure 7.13: IMRT head and neck delivery comparison for the axial plane of delivery #2 for the Elekta 6MV model. Agreement was evaluated using a $\pm 3\%/2\text{mm}$ gamma criterion and 87.6% of pixels passed.	166
Figure 7.14: IMRT head and neck delivery comparison for the sagittal plane of delivery #2 for the Elekta 6MV model. Agreement was evaluated using a $\pm 3\%/2\text{mm}$ gamma criterion and 86.7% of pixels passed.	167
Figure 7.15: IMRT head and neck delivery comparison for the axial plane of delivery #3 for the Elekta 6MV model. Agreement was evaluated using a $\pm 3\%/2\text{mm}$ gamma criterion and 82.5% of pixels passed.	167
Figure 7.16: IMRT head and neck delivery comparison for the sagittal plane of delivery #3 for the Elekta 6MV model. Agreement was evaluated using a $\pm 3\%/2\text{mm}$ gamma criterion and 86.1% of pixels passed.	168
Figure 7.17: Lung SBRT delivery comparison for the axial plane of delivery #2 for the Elekta 6MV model. Agreement was evaluated using a $\pm 3\%/2\text{mm}$ gamma criterion and 86.2% of pixels passed.	169
Figure 7.18: Lung SBRT delivery comparison for the sagittal plane of delivery #2 for the Elekta 6MV model. Agreement was evaluated using a $\pm 3\%/2\text{mm}$ gamma criterion and 85.3% of pixels passed.	170
Figure 7.19: Lung SBRT delivery comparison for the coronal plane of delivery #2 for the Elekta 6MV model. Agreement was evaluated using a $\pm 3\%/2\text{mm}$ gamma criterion and 85.9% of pixels passed.	170

Figure 7.20: Lung SBRT delivery comparison for the axial plane of delivery #3 for the Elekta 6MV model. Agreement was evaluated using a $\pm 3\%/2\text{mm}$ gamma criterion and 89.0% of pixels passed. 171

Figure 7.21: Lung SBRT delivery comparison for the sagittal plane of delivery #3 for the Elekta 6MV model. Agreement was evaluated using a $\pm 3\%/2\text{mm}$ gamma criterion and 84.2% of pixels passed. 171

Figure 7.22: Lung SBRT delivery comparison for the coronal plane of delivery #3 for the Elekta 6MV model. Agreement was evaluated using a $\pm 3\%/2\text{mm}$ gamma criterion and 88.1% of pixels passed. 172

Figure 7.23: Lung IMRT delivery comparison for the axial plane of delivery #1 for the Elekta 6MV model. Agreement was evaluated using a $\pm 3\%/2\text{mm}$ gamma criterion and 82.6% of pixels passed. 173

Figure 7.24: Lung IMRT delivery comparison for the sagittal plane of delivery #1 for the Elekta 6MV model. Agreement was evaluated using a $\pm 3\%/2\text{mm}$ gamma criterion and 92.5% of pixels passed. 174

Figure 7.25: Lung IMRT delivery comparison for the coronal plane of delivery #1 for the Elekta 6MV model. Agreement was evaluated using a $\pm 3\%/2\text{mm}$ gamma criterion and 89.8% of pixels passed. 174

Figure 7.26: Lung IMRT delivery comparison for the axial plane of delivery #2 for the Elekta 6MV model. Agreement was evaluated using a $\pm 3\%/2\text{mm}$ gamma criterion and 85.4% of pixels passed. 175

Figure 7.27: Lung IMRT delivery comparison for the sagittal plane of delivery #2 for the Elekta 6MV model. Agreement was evaluated using a $\pm 3\%/2\text{mm}$ gamma criterion and 83.5% of pixels passed. 175

Figure 7.28: Lung IMRT delivery comparison for the coronal plane of delivery #2 for the Elekta 6MV model. Agreement was evaluated using a $\pm 3\%/2\text{mm}$ gamma criterion and 89.8% of pixels passed. 176

Figure 7.29: Calculated (blue 'x') and measured (red line) percent depth dose curves for an Elekta 10MV beam at a field size of 3 x 3 cm². Gamma agreement (red circles) for each point is also displayed along with any points (red star) at which a failure to meet the ±2%/2mm criterion. At this field size 99.43% of all data passed the gamma criterion. 177

Figure 7.30: Calculated (blue 'x') and measured (red line) percent depth dose curves for an Elekta 10MV beam at a field size of 5 x 5 cm². Gamma agreement (red circles) for each point is also displayed along with any points (red star) at which a failure to meet the ±2%/2mm criterion. At this field size 99.43% of all data passed the gamma criterion. 178

Figure 7.31: Calculated (blue 'x') and measured (red line) percent depth dose curves for an Elekta 10MV beam at a field size of 10 x 10 cm². Gamma agreement (red circles) for each point is also displayed along with any points (red star) at which a failure to meet the ±2%/2mm criterion. At this field size 99.43% of all data passed the gamma criterion. 178

Figure 7.32: Calculated (blue 'x') and measured (red line) percent depth dose curves for an Elekta 10MV beam at a field size of 15 x 15 cm². Gamma agreement (red circles) for each point is also displayed along with any points (red star) at which a failure to meet the ±2%/2mm criterion. At this field size 100% of all data passed the gamma criterion. 179

Figure 7.33: Calculated (blue 'x') and measured (red line) percent depth dose curves for an Elekta 10MV beam at a field size of 20 x 20 cm². Gamma agreement (red circles) for each point is also displayed along with any points (red star) at which a failure to meet the ±2%/2mm criterion. At this field size 100% of all data passed the gamma criterion. 179

Figure 7.34: Calculated (blue 'x') and measured (red line) percent depth dose curves for an Elekta 10MV beam at a field size of 30 x 30 cm². Gamma agreement (red circles) for each point is also displayed along with any points (red star) at which a failure to meet the ±2%/2mm criterion. At this field size 100% of all data passed the gamma criterion. 180

Figure 7.35: Calculated (red diamond) and measured (blue line) dose profiles for an Elekta 10MV beam at a field size of 3 x 3 cm². 181

Figure 7.36: Calculated (red diamond) and measured (blue line) dose profiles for an Elekta 10MV beam at a field size of 5 x 5 cm ²	182
Figure 7.37: Calculated (red diamond) and measured (blue line) dose profiles for an Elekta 10MV beam at a field size of 10 x 10 cm ²	183
Figure 7.38: Calculated (red diamond) and measured (blue line) dose profiles for an Elekta 10MV beam at a field size of 15 x 15 cm ²	184
Figure 7.39: Calculated (red diamond) and measured (blue line) dose profiles for an Elekta 10MV beam at a field size of 20 x 20 cm ²	185
Figure 7.40: Calculated (red diamond) and measured (blue line) dose profiles for an Elekta 10MV beam at a field size of 30 x 30 cm ²	186
Figure 7.41: IMRT head and neck delivery comparison for the axial plane of delivery #2 for the Elekta 10MV model. Agreement was evaluated using a $\pm 3\%/2\text{mm}$ gamma criterion and 91.6% of pixels passed.	187
Figure 7.42: IMRT head and neck delivery comparison for the sagittal plane of delivery #2 for the Elekta 10MV model. Agreement was evaluated using a $\pm 3\%/2\text{mm}$ gamma criterion and 86.4% of pixels passed.	188
Figure 7.43: IMRT head and neck delivery comparison for the axial plane of delivery #3 for the Elekta 10MV model. Agreement was evaluated using a $\pm 3\%/2\text{mm}$ gamma criterion and 95.9% of pixels passed.	188
Figure 7.44: IMRT head and neck delivery comparison for the sagittal plane of delivery #3 for the Elekta 10MV model. Agreement was evaluated using a $\pm 3\%/2\text{mm}$ gamma criterion and 87.3% of pixels passed.	189
Figure 7.45: Lung SBRT delivery comparison for the axial plane of delivery #2 for the Elekta 10MV model. Agreement was evaluated using a $\pm 3\%/2\text{mm}$ gamma criterion and 86.2% of pixels passed.	190

Figure 7.46: Lung SBRT delivery comparison for the sagittal plane of delivery #2 for the Elekta 10MV model. Agreement was evaluated using a $\pm 3\%/2\text{mm}$ gamma criterion and 90.8% of pixels passed.	191
Figure 7.47: Lung SBRT delivery comparison for the coronal plane of delivery #2 for the Elekta 10MV model. Agreement was evaluated using a $\pm 3\%/2\text{mm}$ gamma criterion and 85.3% of pixels passed.	191
Figure 7.48: Lung SBRT delivery comparison for the axial plane of delivery #3 for the Elekta 10MV model. Agreement was evaluated using a $\pm 3\%/2\text{mm}$ gamma criterion and 88.1% of pixels passed.	192
Figure 7.49: Lung SBRT delivery comparison for the sagittal plane of delivery #3 for the Elekta 10MV model. Agreement was evaluated using a $\pm 3\%/2\text{mm}$ gamma criterion and 85.2% of pixels passed.	192
Figure 7.50: Lung SBRT delivery comparison for the coronal plane of delivery #3 for the Elekta 10MV model. Agreement was evaluated using a $\pm 3\%/2\text{mm}$ gamma criterion and 90.5% of pixels passed.	193
Figure 7.51: Lung IMRT delivery comparison for the axial plane of delivery #2 for the Elekta 10MV model. Agreement was evaluated using a $\pm 3\%/2\text{mm}$ gamma criterion and 85.8% of pixels passed.	194
Figure 7.52: Lung IMRT delivery comparison for the sagittal plane of delivery #2 for the Elekta 10MV model. Agreement was evaluated using a $\pm 3\%/2\text{mm}$ gamma criterion and 87.3% of pixels passed.	195
Figure 7.53: Lung IMRT delivery comparison for the coronal plane of delivery #2 for the Elekta 10MV model. Agreement was evaluated using a $\pm 3\%/2\text{mm}$ gamma criterion and 89.3% of pixels passed.	195
Figure 7.54: Lung IMRT delivery comparison for the axial plane of delivery #3 for the Elekta 10MV model. Agreement was evaluated using a $\pm 3\%/2\text{mm}$ gamma criterion and 92.5% of pixels passed.	196

Figure 7.55: Lung IMRT delivery comparison for the sagittal plane of delivery #3 for the Elekta 10MV model. Agreement was evaluated using a $\pm 3\%/2\text{mm}$ gamma criterion and 94.0% of pixels passed. 196

Figure 7.56: Lung IMRT delivery comparison for the coronal plane of delivery #3 for the Elekta 10MV model. Agreement was evaluated using a $\pm 3\%/2\text{mm}$ gamma criterion and 88.5% of pixels passed. 197

Figure 7.57: Calculated (blue 'x') and measured (red line) percent depth dose curves for a TrueBeam FFF 6MV beam at a field size of $3 \times 3 \text{ cm}^2$. Gamma agreement (red circles) for each point is also displayed along with any points (red star) at which a failure to meet the $\pm 2\%/2\text{mm}$ criterion. At this field size 100.0% of all data passed the gamma criterion. 198

Figure 7.58: Calculated (blue 'x') and measured (red line) percent depth dose curves for a TrueBeam FFF 6MV beam at a field size of $4 \times 4 \text{ cm}^2$. Gamma agreement (red circles) for each point is also displayed along with any points (red star) at which a failure to meet the $\pm 2\%/2\text{mm}$ criterion. At this field size 100.0% of all data passed the gamma criterion. 198

Figure 7.59: Calculated (blue 'x') and measured (red line) percent depth dose curves for a TrueBeam FFF 6MV beam at a field size of $6 \times 6 \text{ cm}^2$. Gamma agreement (red circles) for each point is also displayed along with any points (red star) at which a failure to meet the $\pm 2\%/2\text{mm}$ criterion. At this field size 99.33% of all data passed the gamma criterion. 199

Figure 7.60: Calculated (blue 'x') and measured (red line) percent depth dose curves for a TrueBeam FFF 6MV beam at a field size of $8 \times 8 \text{ cm}^2$. Gamma agreement (red circles) for each point is also displayed along with any points (red star) at which a failure to meet the $\pm 2\%/2\text{mm}$ criterion. At this field size 100.0% of all data passed the gamma criterion. 199

Figure 7.61: Calculated (blue 'x') and measured (red line) percent depth dose curves for a TrueBeam FFF 6MV beam at a field size of $10 \times 10 \text{ cm}^2$. Gamma agreement (red circles) for each point is also displayed along with any points (red star) at which a failure to meet the $\pm 2\%/2\text{mm}$ criterion. At this field size 100.0% of all data passed the gamma criterion. 200

Figure 7.62: Calculated (blue 'x') and measured (red line) percent depth dose curves for a TrueBeam FFF 6MV beam at a field size of 20 x 20 cm². Gamma agreement (red circles) for each point is also displayed along with any points (red star) at which a failure to meet the ±2%/2mm criterion. At this field size 100.0% of all data passed the gamma criterion. 200

Figure 7.63: Calculated (blue 'x') and measured (red line) percent depth dose curves for a TrueBeam FFF 6MV beam at a field size of 30 x 30 cm². Gamma agreement (red circles) for each point is also displayed along with any points (red star) at which a failure to meet the ±2%/2mm criterion. At this field size 100.0% of all data passed the gamma criterion. 201

Figure 7.64: Calculated (blue 'x') and measured (red line) percent depth dose curves for a TrueBeam FFF 6MV beam at a field size of 40 x 40 cm². Gamma agreement (red circles) for each point is also displayed along with any points (red star) at which a failure to meet the ±2%/2mm criterion. At this field size 100.0% of all data passed the gamma criterion. 201

Figure 7.65: Calculated (red circle) and measured (blue line) dose profiles for a TrueBeam 6MV beam at a field size of 3 x 3 cm²..... 202

Figure 7.66: Calculated (red circle) and measured (blue line) dose profiles for a TrueBeam 6MV beam at a field size of 4 x 4 cm²..... 203

Figure 7.67: Calculated (red circle) and measured (blue line) dose profiles for a TrueBeam 6MV beam at a field size of 6 x 6 cm²..... 204

Figure 7.68: Calculated (red circle) and measured (blue line) dose profiles for a TrueBeam 6MV beam at a field size of 8 x 8 cm²..... 205

Figure 7.69: Calculated (red circle) and measured (blue line) dose profiles for a TrueBeam 6MV beam at a field size of 10 x 10 cm²..... 206

Figure 7.70: Calculated (red circle) and measured (blue line) dose profiles for a TrueBeam 6MV beam at a field size of 20 x 20 cm²..... 207

Figure 7.71: Calculated (red circle) and measured (blue line) dose profiles for a TrueBeam 6MV beam at a field size of 30 x 30 cm²..... 208

Figure 7.72: Calculated (red circle) and measured (blue line) dose profiles for a TrueBeam 6MV beam at a field size of 40 x 40 cm²..... 209

Figure 7.73: IMRT head and neck delivery comparison for the axial plane of delivery #2 for the TrueBeam FFF 6MV model. Agreement was evaluated using a $\pm 3\%/2\text{mm}$ gamma criterion and 89.4% of pixels passed. 210

Figure 7.74: IMRT head and neck delivery comparison for the sagittal plane of delivery #2 for the TrueBeam FFF 6MV model. Agreement was evaluated using a $\pm 3\%/2\text{mm}$ gamma criterion and 86.6% of pixels passed..... 211

Figure 7.75: IMRT head and neck delivery comparison for the axial plane of delivery #3 for the TrueBeam FFF 6MV model. Agreement was evaluated using a $\pm 3\%/2\text{mm}$ gamma criterion and 80.3% of pixels passed. 211

Figure 7.76: IMRT head and neck delivery comparison for the sagittal plane of delivery #3 for the TrueBeam FFF 6MV model. Agreement was evaluated using a $\pm 3\%/2\text{mm}$ gamma criterion and 95.9% of pixels passed..... 212

Figure 7.77: Lung SBRT delivery comparison for the axial plane of delivery #2 for the TrueBeam FFF 6MV model. Agreement was evaluated using a $\pm 3\%/2\text{mm}$ gamma criterion and 84.5% of pixels passed. 213

Figure 7.78: Lung SBRT delivery comparison for the sagittal plane of delivery #2 for the TrueBeam FFF 6MV model. Agreement was evaluated using a $\pm 3\%/2\text{mm}$ gamma criterion and 90.3% of pixels passed. 214

Figure 7.79: Lung SBRT delivery comparison for the coronal plane of delivery #2 for the TrueBeam FFF 6MV model. Agreement was evaluated using a $\pm 3\%/2\text{mm}$ gamma criterion and 98.4% of pixels passed. 214

Figure 7.80: Lung SBRT delivery comparison for the axial plane of delivery #3 for the TrueBeam FFF 6MV model. Agreement was evaluated using a $\pm 3\%/2\text{mm}$ gamma criterion and 87.5% of pixels passed. 215

Figure 7.81: Lung SBRT delivery comparison for the sagittal plane of delivery #3 for the TrueBeam FFF 6MV model. Agreement was evaluated using a $\pm 3\%/2\text{mm}$ gamma criterion and 95.2% of pixels passed.	215
Figure 7.82: Lung SBRT delivery comparison for the coronal plane of delivery #3 for the TrueBeam FFF 6MV model. Agreement was evaluated using a $\pm 3\%/2\text{mm}$ gamma criterion and 85.5% of pixels passed.	216
Figure 7.83: Lung IMRT delivery comparison for the axial plane of delivery #2 for the TrueBeam FFF 6MV model. Agreement was evaluated using a $\pm 3\%/2\text{mm}$ gamma criterion and 91.4% of pixels passed.	217
Figure 7.84: Lung IMRT delivery comparison for the sagittal plane of delivery #2 for the TrueBeam FFF 6MV model. Agreement was evaluated using a $\pm 3\%/2\text{mm}$ gamma criterion and 87.4% of pixels passed.	218
Figure 7.85: Lung IMRT delivery comparison for the coronal plane of delivery #2 for the TrueBeam FFF 6MV model. Agreement was evaluated using a $\pm 3\%/2\text{mm}$ gamma criterion and 88.4% of pixels passed.	218
Figure 7.86: Lung IMRT delivery comparison for the axial plane of delivery #3 for the TrueBeam FFF 6MV model. Agreement was evaluated using a $\pm 3\%/2\text{mm}$ gamma criterion and 93.5% of pixels passed.	219
Figure 7.87: Lung IMRT delivery comparison for the sagittal plane of delivery #3 for the TrueBeam FFF 6MV model. Agreement was evaluated using a $\pm 3\%/2\text{mm}$ gamma criterion and 94.3% of pixels passed.	219
Figure 7.88: Lung IMRT delivery comparison for the coronal plane of delivery #3 for the TrueBeam FFF 6MV model. Agreement was evaluated using a $\pm 3\%/2\text{mm}$ gamma criterion and 92.4% of pixels passed.	220
Figure 7.89: Calculated (blue 'x') and measured (red line) percent depth dose curves for a TrueBeam FFF 10MV beam at a field size of $3 \times 3 \text{ cm}^2$. Gamma agreement (red circles) for	

each point is also displayed along with any points (red star) at which a failure to meet the $\pm 2\%/2\text{mm}$ criterion. At this field size 99.3% of all data passed the gamma criterion. 221

Figure 7.90: Calculated (blue 'x') and measured (red line) percent depth dose curves for a TrueBeam FFF 10MV beam at a field size of $4 \times 4 \text{ cm}^2$. Gamma agreement (red circles) for each point is also displayed along with any points (red star) at which a failure to meet the $\pm 2\%/2\text{mm}$ criterion. At this field size 99.3% of all data passed the gamma criterion. 222

Figure 7.91: Calculated (blue 'x') and measured (red line) percent depth dose curves for a TrueBeam FFF 10MV beam at a field size of $6 \times 6 \text{ cm}^2$. Gamma agreement (red circles) for each point is also displayed along with any points (red star) at which a failure to meet the $\pm 2\%/2\text{mm}$ criterion. At this field size 99.3% of all data passed the gamma criterion. 222

Figure 7.92: Calculated (blue 'x') and measured (red line) percent depth dose curves for a TrueBeam FFF 10MV beam at a field size of $8 \times 8 \text{ cm}^2$. Gamma agreement (red circles) for each point is also displayed along with any points (red star) at which a failure to meet the $\pm 2\%/2\text{mm}$ criterion. At this field size 100.0% of all data passed the gamma criterion. 223

Figure 7.93: Calculated (blue 'x') and measured (red line) percent depth dose curves for a TrueBeam FFF 10MV beam at a field size of $10 \times 10 \text{ cm}^2$. Gamma agreement (red circles) for each point is also displayed along with any points (red star) at which a failure to meet the $\pm 2\%/2\text{mm}$ criterion. At this field size 100.0% of all data passed the gamma criterion. 223

Figure 7.94: Calculated (blue 'x') and measured (red line) percent depth dose curves for a TrueBeam FFF 10MV beam at a field size of $20 \times 20 \text{ cm}^2$. Gamma agreement (red circles) for each point is also displayed along with any points (red star) at which a failure to meet the $\pm 2\%/2\text{mm}$ criterion. At this field size 100.0% of all data passed the gamma criterion. 224

Figure 7.95: Calculated (blue 'x') and measured (red line) percent depth dose curves for a TrueBeam FFF 10MV beam at a field size of $30 \times 30 \text{ cm}^2$. Gamma agreement (red circles) for each point is also displayed along with any points (red star) at which a failure to meet the $\pm 2\%/2\text{mm}$ criterion. At this field size 97.4% of all data passed the gamma criterion. 224

Figure 7.96: Calculated (blue 'x') and measured (red line) percent depth dose curves for a TrueBeam FFF 10MV beam at a field size of 40 x 40 cm ² . Gamma agreement (red circles) for each point is also displayed along with any points (red star) at which a failure to meet the ±2%/2mm criterion. At this field size 96.7% of all data passed the gamma criterion.	225
Figure 7.97: Calculated (red circle) and measured (blue line) dose profiles for a TrueBeam FFF 10MV beam at a field size of 3 x 3 cm ²	226
Figure 7.98: Calculated (red circle) and measured (blue line) dose profiles for a TrueBeam FFF 10MV beam at a field size of 4 x 4 cm ²	227
Figure 7.99: Calculated (red circle) and measured (blue line) dose profiles for a TrueBeam FFF 10MV beam at a field size of 6 x 6 cm ²	228
Figure 7.100: Calculated (red circle) and measured (blue line) dose profiles for a TrueBeam FFF 10MV beam at a field size of 8 x 8 cm ²	229
Figure 7.101: Calculated (red circle) and measured (blue line) dose profiles for a TrueBeam FFF 10MV beam at a field size of 10 x 10 cm ²	230
Figure 7.102: Calculated (red circle) and measured (blue line) dose profiles for a TrueBeam FFF 10MV beam at a field size of 20 x 20 cm ²	231
Figure 7.103: Calculated (red circle) and measured (blue line) dose profiles for a TrueBeam FFF 10MV beam at a field size of 30 x 30 cm ²	232
Figure 7.104: Calculated (red circle) and measured (blue line) dose profiles for a TrueBeam FFF 10MV beam at a field size of 40 x 40 cm ²	233
Figure 7.105: IMRT head and neck delivery comparison for the axial plane of delivery #2 for the TrueBeam FFF 10MV model. Agreement was evaluated using a ±3%/2mm gamma criterion and 93.1% of pixels passed.....	234
Figure 7.106: IMRT head and neck delivery comparison for the sagittal plane of delivery #2 for the TrueBeam FFF 10MV model. Agreement was evaluated using a ±3%/2mm gamma criterion and 85.9% of pixels passed.....	235

Figure 7.107: IMRT head and neck delivery comparison for the axial plane of delivery #3 for the TrueBeam FFF 10MV model. Agreement was evaluated using a $\pm 3\%/2\text{mm}$ gamma criterion and 75.5% of pixels passed..... 235

Figure 7.108: IMRT head and neck delivery comparison for the sagittal plane of delivery #3 for the TrueBeam FFF 10MV model. Agreement was evaluated using a $\pm 3\%/2\text{mm}$ gamma criterion and 90.1% of pixels passed..... 236

Figure 7.109: Lung SBRT delivery comparison for the axial plane of delivery #2 for the TrueBeam FFF 10MV model. Agreement was evaluated using a $\pm 3\%/2\text{mm}$ gamma criterion and 87.4% of pixels passed..... 237

Figure 7.110: Lung SBRT delivery comparison for the sagittal plane of delivery #2 for the TrueBeam FFF 10MV model. Agreement was evaluated using a $\pm 3\%/2\text{mm}$ gamma criterion and 88.1% of pixels passed..... 238

Figure 7.111: Lung SBRT delivery comparison for the coronal plane of delivery #2 for the TrueBeam FFF 10MV model. Agreement was evaluated using a $\pm 3\%/2\text{mm}$ gamma criterion and 92.7% of pixels passed..... 238

Figure 7.112: Lung SBRT delivery comparison for the axial plane of delivery #3 for the TrueBeam FFF 10MV model. Agreement was evaluated using a $\pm 3\%/2\text{mm}$ gamma criterion and 95.8% of pixels passed..... 239

Figure 7.113: Lung SBRT delivery comparison for the sagittal plane of delivery #3 for the TrueBeam FFF 10MV model. Agreement was evaluated using a $\pm 3\%/2\text{mm}$ gamma criterion and 91.4% of pixels passed..... 239

Figure 7.114: Lung SBRT delivery comparison for the coronal plane of delivery #3 for the TrueBeam FFF 10MV model. Agreement was evaluated using a $\pm 3\%/2\text{mm}$ gamma criterion and 98.1% of pixels passed..... 240

Figure 7.115: Lung IMRT delivery comparison for the axial plane of delivery #1 for the TrueBeam FFF 10MV model. Agreement was evaluated using a $\pm 3\%/2\text{mm}$ gamma criterion and 95.6% of pixels passed..... 241

Figure 7.116: Lung IMRT delivery comparison for the sagittal plane of delivery #1 for the TrueBeam FFF 10MV model. Agreement was evaluated using a $\pm 3\%/2\text{mm}$ gamma criterion and 84.2% of pixels passed.....	242
Figure 7.117: Lung IMRT delivery comparison for the coronal plane of delivery #1 for the TrueBeam FFF 10MV model. Agreement was evaluated using a $\pm 3\%/2\text{mm}$ gamma criterion and 92.1% of pixels passed.....	242
Figure 7.118: Lung IMRT delivery comparison for the axial plane of delivery #2 for the TrueBeam FFF 10MV model. Agreement was evaluated using a $\pm 3\%/2\text{mm}$ gamma criterion and 97.4% of pixels passed.....	243
Figure 7.119: Lung IMRT delivery comparison for the sagittal plane of delivery #2 for the TrueBeam FFF 10MV model. Agreement was evaluated using a $\pm 3\%/2\text{mm}$ gamma criterion and 93.6% of pixels passed.....	243
Figure 7.120: Lung IMRT delivery comparison for the coronal plane of delivery #2 for the TrueBeam FFF 10MV model. Agreement was evaluated using a $\pm 3\%/2\text{mm}$ gamma criterion and 96.4% of pixels passed.....	244
Figure 7.121: IMRT head and neck delivery comparison for the axial plane of Head and Neck Plan #1 with respect to DPM recalculated dose. Agreement was evaluated using a $\pm 3\%/2\text{mm}$ gamma criterion and 59.1% of pixels passed.	245
Figure 7.122: IMRT head and neck delivery comparison for the sagittal plane of Head and Neck Plan #1 with respect to DPM recalculated dose. Agreement was evaluated using a $\pm 3\%/2\text{mm}$ gamma criterion and 69.4% of pixels passed.	246
Figure 7.123: IMRT head and neck delivery comparison for the axial plane of Head and Neck Plan #1 with respect to DPM recalculated dose. Agreement was evaluated using a $\pm 5\%/3\text{mm}$ gamma criterion and 82.1% of pixels passed.	246
Figure 7.124: IMRT head and neck delivery comparison for the sagittal plane of Head and Neck Plan #1 with respect to DPM recalculated dose. Agreement was evaluated using a $\pm 5\%/3\text{mm}$ gamma criterion and 88.2% of pixels passed.	247

Figure 7.125: IMRT head and neck delivery comparison for the axial plane of Head and Neck Plan #1 with respect to TPS calculated dose. Agreement was evaluated using a $\pm 3\%/2\text{mm}$ gamma criterion and 67.6% of pixels passed. 247

Figure 7.126: IMRT head and neck delivery comparison for the sagittal plane of Head and Neck Plan #1 with respect to TPS calculated dose. Agreement was evaluated using a $\pm 3\%/2\text{mm}$ gamma criterion and 75.3% of pixels passed. 248

Figure 7.127: IMRT head and neck delivery comparison for the axial plane of Head and Neck Plan #1 with respect to TPS calculated dose. Agreement was evaluated using a $\pm 5\%/3\text{mm}$ gamma criterion and 88.6% of pixels passed. 248

Figure 7.128: IMRT head and neck delivery comparison for the sagittal plane of Head and Neck Plan #1 with respect to TPS calculated dose. Agreement was evaluated using a $\pm 5\%/3\text{mm}$ gamma criterion and 98.9% of pixels passed. 249

Figure 7.129: IMRT head and neck delivery comparison for the axial plane of Head and Neck Plan #2 with respect to DPM recalculated dose. Agreement was evaluated using a $\pm 3\%/2\text{mm}$ gamma criterion and 88.4% of pixels passed. 249

Figure 7.130: IMRT head and neck delivery comparison for the sagittal plane of Head and Neck Plan #2 with respect to DPM recalculated dose. Agreement was evaluated using a $\pm 3\%/2\text{mm}$ gamma criterion and 52.5% of pixels passed. 250

Figure 7.131: IMRT head and neck delivery comparison for the axial plane of Head and Neck Plan #2 with respect to DPM recalculated dose. Agreement was evaluated using a $\pm 5\%/3\text{mm}$ gamma criterion and 98.3% of pixels passed. 250

Figure 7.132: IMRT head and neck delivery comparison for the sagittal plane of Head and Neck Plan #2 with respect to DPM recalculated dose. Agreement was evaluated using a $\pm 5\%/3\text{mm}$ gamma criterion and 76.8% of pixels passed. 251

Figure 7.133: IMRT head and neck delivery comparison for the axial plane of Head and Neck Plan #2 with respect to TPS calculated dose. Agreement was evaluated using a $\pm 3\%/2\text{mm}$ gamma criterion and 85.9% of pixels passed. 251

Figure 7.134: IMRT head and neck delivery comparison for the axial plane of Head and Neck Plan #2 with respect to TPS calculated dose. Agreement was evaluated using a $\pm 3\%/2\text{mm}$ gamma criterion and 69.8% of pixels passed.	252
Figure 7.135: IMRT head and neck delivery comparison for the sagittal plane of Head and Neck Plan #2 with respect to TPS calculated dose. Agreement was evaluated using a $\pm 5\%/3\text{mm}$ gamma criterion and 98.4% of pixels passed.	252
Figure 7.136: IMRT head and neck delivery comparison for the sagittal plane of Head and Neck Plan #2 with respect to TPS calculated dose. Agreement was evaluated using a $\pm 5\%/3\text{mm}$ gamma criterion and 86.3% of pixels passed.	253
Figure 7.137: Lung phantom delivery comparison for the axial plane of Lung Plan #1 with respect to DPM recalculated dose. Agreement was evaluated using a $\pm 3\%/2\text{mm}$ gamma criterion and 99.7% of pixels passed.	254
Figure 7.138: Lung phantom delivery comparison for the coronal plane of Lung Plan #1 with respect to DPM recalculated dose. Agreement was evaluated using a $\pm 3\%/2\text{mm}$ gamma criterion and 99.0% of pixels passed.	255
Figure 7.139: Lung phantom delivery comparison for the sagittal plane of Lung Plan #1 with respect to DPM recalculated dose. Agreement was evaluated using a $\pm 3\%/2\text{mm}$ gamma criterion and 94.9% of pixels passed.	255
Figure 7.140: Lung phantom delivery comparison for the axial plane of Lung Plan #1 with respect to DPM recalculated dose. Agreement was evaluated using a $\pm 5\%/3\text{mm}$ gamma criterion and 99.9% of pixels passed.	256
Figure 7.141: Lung phantom delivery comparison for the coronal plane of Lung Plan #1 with respect to DPM recalculated dose. Agreement was evaluated using a $\pm 5\%/3\text{mm}$ gamma criterion and 99.0% of pixels passed.	256
Figure 7.142: Lung phantom delivery comparison for the sagittal plane of Lung Plan #1 with respect to DPM recalculated dose. Agreement was evaluated using a $\pm 5\%/3\text{mm}$ gamma criterion and 99.6% of pixels passed.	257

Figure 7.143: Lung phantom delivery comparison for the axial plane of Lung Plan #1 with respect to TPS calculated dose. Agreement was evaluated using a $\pm 3\%/2\text{mm}$ gamma criterion and 97.4% of pixels passed..... 257

Figure 7.144: Lung phantom delivery comparison for the coronal plane of Lung Plan #1 with respect to TPS calculated dose. Agreement was evaluated using a $\pm 3\%/2\text{mm}$ gamma criterion and 95.5% of pixels passed..... 258

Figure 7.145: Lung phantom delivery comparison for the sagittal plane of Lung Plan #1 with respect to TPS calculated dose. Agreement was evaluated using a $\pm 3\%/2\text{mm}$ gamma criterion and 86.8% of pixels passed..... 258

Figure 7.146: Lung phantom delivery comparison for the axial plane of Lung Plan #1 with respect to TPS calculated dose. Agreement was evaluated using a $\pm 5\%/3\text{mm}$ gamma criterion and 99.9% of pixels passed..... 259

Figure 7.147: Lung phantom delivery comparison for the coronal plane of Lung Plan #1 with respect to TPS calculated dose. Agreement was evaluated using a $\pm 5\%/3\text{mm}$ gamma criterion and 99.9% of pixels passed..... 259

Figure 7.148: Lung phantom delivery comparison for the sagittal plane of Lung Plan #1 with respect to TPS calculated dose. Agreement was evaluated using a $\pm 5\%/3\text{mm}$ gamma criterion and 99.4% of pixels passed..... 260

Figure 7.149: Lung phantom delivery comparison for the axial plane of Lung Plan #2 with respect to DPM recalculated dose. Agreement was evaluated using a $\pm 3\%/2\text{mm}$ gamma criterion and 88.4% of pixels passed. 260

Figure 7.150: Lung phantom delivery comparison for the coronal plane of Lung Plan #2 with respect to DPM recalculated dose. Agreement was evaluated using a $\pm 3\%/2\text{mm}$ gamma criterion and 79.1% of pixels passed. 261

Figure 7.151: Lung phantom delivery comparison for the sagittal plane of Lung Plan #2 with respect to DPM recalculated dose. Agreement was evaluated using a $\pm 3\%/2\text{mm}$ gamma criterion and 82.6% of pixels passed. 261

Figure 7.152: Lung phantom delivery comparison for the axial plane of Lung Plan #2 with respect to DPM recalculated dose. Agreement was evaluated using a $\pm 5\%/3\text{mm}$ gamma criterion and 99.0% of pixels passed. 262

Figure 7.153: Lung phantom delivery comparison for the coronal plane of Lung Plan #2 with respect to DPM recalculated dose. Agreement was evaluated using a $\pm 5\%/3\text{mm}$ gamma criterion and 96.9% of pixels passed. 262

Figure 7.154: Lung phantom delivery comparison for the sagittal plane of Lung Plan #2 with respect to DPM recalculated dose. Agreement was evaluated using a $\pm 5\%/3\text{mm}$ gamma criterion and 99.5% of pixels passed. 263

Figure 7.155: Lung phantom delivery comparison for the axial plane of Lung Plan #2 with respect to TPS calculated dose. Agreement was evaluated using a $\pm 3\%/2\text{mm}$ gamma criterion and 96.0% of pixels passed..... 263

Figure 7.156: Lung phantom delivery comparison for the coronal plane of Lung Plan #2 with respect to TPS calculated dose. Agreement was evaluated using a $\pm 3\%/2\text{mm}$ gamma criterion and 93.3% of pixels passed..... 264

Figure 7.157: Lung phantom delivery comparison for the sagittal plane of Lung Plan #2 with respect to TPS calculated dose. Agreement was evaluated using a $\pm 3\%/2\text{mm}$ gamma criterion and 66.8% of pixels passed..... 264

Figure 7.158: Lung phantom delivery comparison for the axial plane of Lung Plan #2 with respect to TPS calculated dose. Agreement was evaluated using a $\pm 5\%/3\text{mm}$ gamma criterion and 99.9% of pixels passed..... 265

Figure 7.159: Lung phantom delivery comparison for the coronal plane of Lung Plan #2 with respect to TPS calculated dose. Agreement was evaluated using a $\pm 5\%/3\text{mm}$ gamma criterion and 99.8% of pixels passed..... 265

Figure 7.160: Lung phantom delivery comparison for the sagittal plane of Lung Plan #2 with respect to TPS calculated dose. Agreement was evaluated using a $\pm 5\%/3\text{mm}$ gamma criterion and 93.2% of pixels passed..... 266

Figure 7.161: Lung phantom delivery comparison for the axial plane of Lung Plan #3 with respect to DPM recalculated dose. Agreement was evaluated using a $\pm 3\%/2\text{mm}$ gamma criterion and 92.1% of pixels passed.	266
Figure 7.162: Lung phantom delivery comparison for the coronal plane of Lung Plan #3 with respect to DPM recalculated dose. Agreement was evaluated using a $\pm 3\%/2\text{mm}$ gamma criterion and 92.6% of pixels passed.	267
Figure 7.163: Lung phantom delivery comparison for the sagittal plane of Lung Plan #3 with respect to DPM recalculated dose. Agreement was evaluated using a $\pm 3\%/2\text{mm}$ gamma criterion and 97.1% of pixels passed.	267
Figure 7.164: Lung phantom delivery comparison for the axial plane of Lung Plan #3 with respect to DPM recalculated dose. Agreement was evaluated using a $\pm 5\%/3\text{mm}$ gamma criterion and 99.1% of pixels passed.	268
Figure 7.165: Lung phantom delivery comparison for the coronal plane of Lung Plan #3 with respect to DPM recalculated dose. Agreement was evaluated using a $\pm 5\%/3\text{mm}$ gamma criterion and 99.6% of pixels passed.	268
Figure 7.166: Lung phantom delivery comparison for the sagittal plane of Lung Plan #3 with respect to DPM recalculated dose. Agreement was evaluated using a $\pm 5\%/3\text{mm}$ gamma criterion and 99.8% of pixels passed.	269
Figure 7.167: Lung phantom delivery comparison for the axial plane of Lung Plan #3 with respect to TPS calculated dose. Agreement was evaluated using a $\pm 3\%/2\text{mm}$ gamma criterion and 64.1% of pixels passed.	269
Figure 7.168: Lung phantom delivery comparison for the coronal plane of Lung Plan #3 with respect to TPS calculated dose. Agreement was evaluated using a $\pm 3\%/2\text{mm}$ gamma criterion and 53.6% of pixels passed.	270
Figure 7.169: Lung phantom delivery comparison for the sagittal plane of Lung Plan #3 with respect to TPS calculated dose. Agreement was evaluated using a $\pm 3\%/2\text{mm}$ gamma criterion and 64.1% of pixels passed.	270

Figure 7.170: Lung phantom delivery comparison for the axial plane of Lung Plan #3 with respect to TPS calculated dose. Agreement was evaluated using a $\pm 5\%/3\text{mm}$ gamma criterion and 85.7% of pixels passed..... 271

Figure 7.171: Lung phantom delivery comparison for the coronal plane of Lung Plan #3 with respect to TPS calculated dose. Agreement was evaluated using a $\pm 5\%/3\text{mm}$ gamma criterion and 82.5% of pixels passed..... 271

Figure 7.172: Lung phantom delivery comparison for the sagittal plane of Lung Plan #3 with respect to TPS calculated dose. Agreement was evaluated using a $\pm 5\%/3\text{mm}$ gamma criterion and 82.4% of pixels passed..... 272

Table 3.1: Optimized parameters for the source models as determined during the initial commissioning of the models. The first three parameters describe the shape and location of the spectra. The fourth through sixth parameters relate the relative contribution and energy scale of the three sources, and the final parameter is the standard deviation of the Gaussian kernel convolved with the calculated dose profiles to mimic the volume averaging effect of an ion chamber at the penumbra of dose profiles. 31

Table 3.2: Optimized coefficients to a piece-wise linear function used to describe the increase in off-axis fluence of Elekta 6MV and 10MV models. Fluence weighting values are reported with respect to the dose measured at the central axis (CAX) for the 40 x 40 cm² field size dose profile at a depth of d_{max} 34

Table 3.3: Gamma comparison agreement for Elekta 6MV and 10MV models using a $\pm 2\%/2\text{mm}$ criterion for measured and calculated depth dose data..... 38

Table 3.4: Gamma comparison agreement for Elekta 6MV and 10MV models using a $\pm 2\%/2\text{mm}$ criterion for measured and calculated dose profile data. Dose profiles were measured and calculated in-plane and cross-plane at depths of d_{max} (1.6cm for 6MV and 2.0cm for 10MV), 5cm, 10cm, 20cm, and 25cm (10MV only). 46

Table 3.5: Point dose comparisons for the Elekta 6MV IMRT head and neck phantom measurements. The measured dose is the averaged dose from the three deliveries of each plan. Comparison to calculated doses by DPM (left) and Pinnacle (right) are expressed as a ratio of calculated to measured doses. Point dose locations are indicated by Pri = Primary PTV, Sec = Secondary PTV, OAR = Organ at Risk, S = Superior, I = Inferior, A = Anterior, P = Posterior..... 48

Table 3.6: Point dose comparisons for the Elekta 10MV IMRT head and neck phantom measurements. The measured dose is the averaged dose from the three deliveries of each plan. Comparison to calculated doses by DPM (left) and Pinnacle (right) are expressed as a ratio of calculated to measured doses. Point dose locations are indicated by Pri = Primary PTV,

Sec = Secondary PTV, OAR = Organ at Risk, S = Superior, I = Inferior, A = Anterior, P = Posterior..... 50

Table 3.7: Percentage of pixels passing a $\pm 3\%/2\text{mm}$ gamma criterion for IMRT head and neck plans for both Elekta 6MV and 10MV models. Agreement was evaluated in both the axial and sagittal planes for three deliveries of each plan. 55

Table 3.8: Point dose comparisons for the Elekta 6MV SBRT lung phantom measurements. The measured dose is the averaged dose from the three deliveries of each plan. Comparison to calculated doses by DPM (left) and Pinnacle (right) are expressed as a ratio of calculated to measured doses. Point dose locations are indicated by PTV = Planning Target Volume, OAR = Organ at Risk, S = Superior, I = Inferior..... 60

Table 3.9: Point dose comparisons for the Elekta 10MV SBRT lung phantom measurements. The measured dose is the averaged dose from the three deliveries of each plan. Comparison to calculated doses by DPM (left) and Pinnacle (right) are expressed as a ratio of calculated to measured doses. Point dose locations are indicated by PTV = Planning Target Volume, OAR = Organ at Risk, S = Superior, I = Inferior..... 61

Table 3.10: Percentage of pixels passing a $\pm 3\%/2\text{mm}$ gamma criterion for SBRT lung plans for both Elekta 6MV and 10MV models. Agreement was evaluated in the axial, sagittal, and coronal planes for three deliveries of each plan..... 70

Table 3.11: Point dose comparisons for the Elekta 6MV IMRT lung phantom measurements. The measured dose is the averaged dose from the three deliveries of each plan. Comparison to calculated doses by DPM (left) and Pinnacle (right) are expressed as a ratio of calculated to measured doses. Point dose locations are indicated by PTV = Planning Target Volume, OAR = Organ at Risk, S = Superior, I = Inferior..... 72

Table 3.12: Point dose comparisons for the Elekta 10MV IMRT lung phantom measurements. The measured dose is the averaged dose from the three deliveries of each plan. Comparison to calculated doses by DPM (left) and Pinnacle (right) are expressed as a ratio of calculated to

measured doses. Point dose locations are indicated by PTV = Planning Target Volume, OAR = Organ at Risk, S = Superior, I = Inferior..... 73

Table 3.13: Percentage of pixels passing a $\pm 3\%/2\text{mm}$ gamma criterion for IMRT lung plans for both Elekta 6MV and 10MV models. Agreement was evaluated in the axial, sagittal, and coronal planes for three deliveries of each plan..... 80

Table 3.14: The average and range of the percent of pixels passing a $\pm 3\%/2\text{mm}$ gamma criterion for Elekta 6MV and 10MV source models as assessed through three repeated deliveries for three different treatment plans to anthropomorphic phantoms. 82

Table 4.1: Optimized parameters for the source models as determined during the initial commissioning of the models. The first three parameters describe the shape and location of the spectra. The fourth through sixth parameters relate the relative contribution and energy scale of the three sources, and the final parameter is the standard deviation of the Gaussian kernel convolved with the calculated dose profiles to mimic the volume averaging effect of an ion chamber at the penumbra of dose profiles. 87

Table 4.2: Optimized coefficients to a piece-wise linear function used to describe the increase in off-axis fluence of TrueBeam FFF 6MV and 10MV models. Fluence weighting values are reported with respect to the dose measured at the central axis (CAX) for the $40 \times 40 \text{ cm}^2$ field size dose profile at a depth of d_{max} 90

Table 4.3: Gamma comparison agreement for TrueBeam FFF 6MV and 10MV models using a $\pm 2\%/2\text{mm}$ criterion for measured and calculated depth dose data..... 93

Table 4.4: Gamma comparison agreement for TrueBeam FFF 6MV and FFF 10MV models using a $\pm 2\%/2\text{mm}$ criterion for measured and calculated dose profile data. Dose profiles were measured and calculated in-plane at depths of d_{max} (1.6cm for 6MV and 2.4cm for 10MV), 5cm, 10cm, 20cm, and 30cm. 98

Table 4.5: Point dose comparisons for the FFF 6MV IMRT head and neck phantom measurements. The measured dose is the averaged dose from the three deliveries of each plan. Comparison to calculated doses by DPM (left) and Eclipse (right) are expressed as a ratio

of calculated to measured doses. Point dose locations are indicated by Pri = Primary PTV, Sec = Secondary PTV, OAR = Organ at Risk, S = Superior, I = Inferior, A = Anterior, P = Posterior.
 104

Table 4.6: Point dose comparisons for the FFF 10MV IMRT head and neck phantom measurements. The measured dose is the averaged dose from the three deliveries of each plan. Comparison to calculated doses by DPM (left) and Eclipse (right) are expressed as a ratio of calculated to measured doses. Point dose locations are indicated by Pri = Primary PTV, Sec = Secondary PTV, OAR = Organ at Risk, S = Superior, I = Inferior, A = Anterior, P = Posterior.
 106

Table 4.7: Percentage of pixels passing a $\pm 3\%/2\text{mm}$ gamma criterion for IMRT head and neck plans for both TrueBeam FFF 6MV and 10MV models. Agreement was evaluated in both the axial and sagittal planes for three deliveries of each plan. 111

Table 4.8: Point dose comparisons for the FFF 6MV SBRT lung phantom measurements. The measured dose is the averaged dose from the three deliveries of each plan. Comparison to calculated doses by DPM (left) and Eclipse (right) are expressed as a ratio of calculated to measured doses. Point dose locations are indicated by PTV = Planning Target Volume, OAR = Organ at Risk, S = Superior, I = Inferior..... 115

Table 4.9: Point dose comparisons for the FFF 10MV SBRT lung phantom measurements. The measured dose is the averaged dose from the three deliveries of each plan. Comparison to calculated doses by DPM (left) and Eclipse (right) are expressed as a ratio of calculated to measured doses. Point dose locations are indicated by PTV = Planning Target Volume, OAR = Organ at Risk, S = Superior, I = Inferior..... 116

Table 4.10: Percentage of pixels passing a $\pm 3\%/2\text{mm}$ gamma criterion for SBRT lung plans for both TrueBeam FFF 6MV and FFF 10MV models. Agreement was evaluated in the axial, sagittal, and coronal planes for three deliveries of each plan..... 125

Table 4.11: Point dose comparisons for the FFF 6MV IMRT lung phantom measurements. The measured dose is the averaged dose from the three deliveries of each plan. Comparison to

calculated doses by DPM (left) and Eclipse (right) are expressed as a ratio of calculated to measured doses. Point dose locations are indicated by PTV = Planning Target Volume, OAR = Organ at Risk, S = Superior, I = Inferior..... 127

Table 4.12: Point dose comparisons for the FFF 10MV IMRT lung phantom measurements.

The measured dose is the averaged dose from the three deliveries of each plan. Comparison to calculated doses by DPM (left) and Eclipse (right) are expressed as a ratio of calculated to measured doses. Point dose locations are indicated by PTV = Planning Target Volume, OAR = Organ at Risk, S = Superior, I = Inferior..... 128

Table 4.13: Percentage of pixels passing a $\pm 3\%/2\text{mm}$ gamma criterion for IMRT lung plans for both TrueBeam FFF 6MV and 10MV models. Agreement was evaluated in the axial, sagittal, and coronal planes for three deliveries of each plan..... 137

Table 4.14: The average and range of the percent of pixels passing a $\pm 3\%/2\text{mm}$ gamma criterion for TrueBeam FFF 6MV and FFF 10MV source models as assessed through three repeated deliveries for three different treatment plans to anthropomorphic phantoms. 138

Table 5.1: Summary of head and neck phantom audits chosen for a measurement based comparison to Monte Carlo recalculation of plan dose. Both plans were step and shoot IMRT, or static MLC (SMLC), deliveries. 144

Table 5.2: Summary of lung phantom audits chosen for a measurement based comparison to Monte Carlo recalculation of plan dose. Delivery techniques were either 3D or static MLC (SMLC)..... 144

Table 5.3: Point dose comparisons for the multiple source model recalculation of the head and neck phantom audits. Comparison to calculated doses by DPM and the institution reported doses calculated by the TPS are expressed as a ratio of calculated to measured doses. Point dose locations were restricted to within the PTV. S = Superior, I = Inferior, A = Anterior, P = Posterior..... 145

Table 5.4: Point dose comparisons for the multiple source model recalculation of the lung phantom audits. Comparison to calculated doses by DPM and the institution reported doses

calculated by the TPS are expressed as a ratio of calculated to measured doses. Point dose locations were restricted to within the PTV. S = Superior, I = Inferior.	146
Table 5.5: Percentages of pixels passing a $\pm 3\%/2\text{mm}$ gamma criterion for previous head and neck audits are reported. Agreement was evaluated in the axial and sagittal planes.....	147
Table 5.6: Percentages of pixels passing a $\pm 5\%/3\text{mm}$ gamma criterion for previous head and neck audits are reported. Agreement was evaluated in the axial and sagittal planes.....	147
Table 5.7: Percentages of pixels passing a $\pm 3\%/2\text{mm}$ gamma criterion for previous lung audits are reported. Agreement was evaluated in the axial, coronal and sagittal planes.	147
Table 5.8: Percentages of pixels passing a $\pm 5\%/3\text{mm}$ gamma criterion for previous lung audits are reported. Agreement was evaluated in the axial, coronal and sagittal planes.	148
Table 7.1: Dose profile agreement between the Elekta 6MV multiple source model and measurement using a $\pm 2\%/2\text{mm}$ global gamma criterion at all depths of comparison for a $3 \times 3 \text{ cm}^2$ field size.	160
Table 7.2: Dose profile agreement between the Elekta 6MV multiple source model and measurement using a $\pm 2\%/2\text{mm}$ global gamma criterion at all depths of comparison for a $5 \times 5 \text{ cm}^2$ field size.	161
Table 7.3: Dose profile agreement between the Elekta 6MV multiple source model and measurement using a $\pm 2\%/2\text{mm}$ global gamma criterion at all depths of comparison for a $10 \times 10 \text{ cm}^2$ field size.	162
Table 7.4: Dose profile agreement between the Elekta 6MV multiple source model and measurement using a $\pm 2\%/2\text{mm}$ global gamma criterion at all depths of comparison for a $15 \times 15 \text{ cm}^2$ field size.	163
Table 7.5: Dose profile agreement between the Elekta 6MV multiple source model and measurement using a $\pm 2\%/2\text{mm}$ global gamma criterion at all depths of comparison for a $20 \times 20 \text{ cm}^2$ field size.	164

Table 7.6: Dose profile agreement between the Elekta 6MV multiple source model and measurement using a $\pm 2\%/2\text{mm}$ global gamma criterion at all depths of comparison for a 30 x 30 cm ² field size.	165
Table 7.7: Dose profile agreement between the Elekta 10MV multiple source model and measurement using a $\pm 2\%/2\text{mm}$ global gamma criterion at all depths of comparison for a 3 x 3 cm ² field size.	181
Table 7.8: Dose profile agreement between the Elekta 10MV multiple source model and measurement using a $\pm 2\%/2\text{mm}$ global gamma criterion at all depths of comparison for a 5 x 5 cm ² field size.	182
Table 7.9: Dose profile agreement between the Elekta 10MV multiple source model and measurement using a $\pm 2\%/2\text{mm}$ global gamma criterion at all depths of comparison for a 10 x 10 cm ² field size.	183
Table 7.10: Dose profile agreement between the Elekta 10MV multiple source model and measurement using a $\pm 2\%/2\text{mm}$ global gamma criterion at all depths of comparison for a 15 x 15 cm ² field size.	184
Table 7.11: Dose profile agreement between the Elekta 10MV multiple source model and measurement using a $\pm 2\%/2\text{mm}$ global gamma criterion at all depths of comparison for a 20 x 20 cm ² field size.	185
Table 7.12: Dose profile agreement between the Elekta 10MV multiple source model and measurement using a $\pm 2\%/2\text{mm}$ global gamma criterion at all depths of comparison for a 30 x 30 cm ² field size.	186
Table 7.13: Dose profile agreement between the TrueBeam FFF 6MV multiple source model and measurement using a $\pm 2\%/2\text{mm}$ global gamma criterion at all depths of comparison for a 3 x 3 cm ² field size.	202
Table 7.14: Dose profile agreement between the TrueBeam FFF 6MV multiple source model and measurement using a $\pm 2\%/2\text{mm}$ global gamma criterion at all depths of comparison for a 4 x 4 cm ² field size.	203

Table 7.15: Dose profile agreement between the TrueBeam FFF 6MV multiple source model and measurement using a $\pm 2\%/2\text{mm}$ global gamma criterion at all depths of comparison for a $6 \times 6 \text{ cm}^2$ field size.	204
Table 7.16: Dose profile agreement between the TrueBeam FFF 6MV multiple source model and measurement using a $\pm 2\%/2\text{mm}$ global gamma criterion at all depths of comparison for a $8 \times 8 \text{ cm}^2$ field size.	205
Table 7.17: Dose profile agreement between the TrueBeam FFF 6MV multiple source model and measurement using a $\pm 2\%/2\text{mm}$ global gamma criterion at all depths of comparison for a $10 \times 10 \text{ cm}^2$ field size.....	206
Table 7.18: Dose profile agreement between the TrueBeam FFF 6MV multiple source model and measurement using a $\pm 2\%/2\text{mm}$ global gamma criterion at all depths of comparison for a $20 \times 20 \text{ cm}^2$ field size.....	207
Table 7.19: Dose profile agreement between the TrueBeam FFF 6MV multiple source model and measurement using a $\pm 2\%/2\text{mm}$ global gamma criterion at all depths of comparison for a $30 \times 30 \text{ cm}^2$ field size.....	208
Table 7.20: Dose profile agreement between the TrueBeam FFF 6MV multiple source model and measurement using a $\pm 2\%/2\text{mm}$ global gamma criterion at all depths of comparison for a $40 \times 40 \text{ cm}^2$ field size.....	209
Table 7.21: Dose profile agreement between the TrueBeam FFF 10MV multiple source model and measurement using a $\pm 2\%/2\text{mm}$ global gamma criterion at all depths of comparison for a $3 \times 3 \text{ cm}^2$ field size.	226
Table 7.22: Dose profile agreement between the TrueBeam FFF 10MV multiple source model and measurement using a $\pm 2\%/2\text{mm}$ global gamma criterion at all depths of comparison for a $4 \times 4 \text{ cm}^2$ field size.	227
Table 7.23: Dose profile agreement between the TrueBeam FFF 10MV multiple source model and measurement using a $\pm 2\%/2\text{mm}$ global gamma criterion at all depths of comparison for a $6 \times 6 \text{ cm}^2$ field size.	228

Table 7.24: Dose profile agreement between the TrueBeam FFF 10MV multiple source model and measurement using a $\pm 2\%/2\text{mm}$ global gamma criterion at all depths of comparison for a $8 \times 8 \text{ cm}^2$ field size. 229

Table 7.25: Dose profile agreement between the TrueBeam FFF 10MV multiple source model and measurement using a $\pm 2\%/2\text{mm}$ global gamma criterion at all depths of comparison for a $10 \times 10 \text{ cm}^2$ field size..... 230

Table 7.26: Dose profile agreement between the TrueBeam FFF 10MV multiple source model and measurement using a $\pm 2\%/2\text{mm}$ global gamma criterion at all depths of comparison for a $20 \times 20 \text{ cm}^2$ field size..... 231

Table 7.27: Dose profile agreement between the TrueBeam FFF 10MV multiple source model and measurement using a $\pm 2\%/2\text{mm}$ global gamma criterion at all depths of comparison for a $30 \times 30 \text{ cm}^2$ field size..... 232

Table 7.28: Dose profile agreement between the TrueBeam FFF 10MV multiple source model and measurement using a $\pm 2\%/2\text{mm}$ global gamma criterion at all depths of comparison for a $40 \times 40 \text{ cm}^2$ field size..... 233

Chapter 1: Introduction

1.1 Statement of Problem

The Radiological Physics Center (RPC) is one of three National Cancer Institute (NCI) funded, quality assurance (QA) offices that provides QA auditing services to institutions participating in NCI cooperative clinical trials. The RPC has developed several programs as a means to efficiently provide dosimetric and QA services to the clinical trial community and to ensure NCI that the institutions participating in clinical trials deliver comparable and consistent radiation doses. The RPC's QA programs are comprised of on-site evaluations and remote auditing tools. The on-site evaluations consist of interviews of personnel that perform physical measurements on the therapy machines, a review of quality control procedures, measurement of basic beam dosimetry data, and a review of patient dose calculations. The remote auditing tools are used to review patient dose calculations, measure reference beam output with optically stimulated luminescence dosimeters (OSLD), and evaluate advanced treatment procedures with anthropomorphic QA phantoms. The anthropomorphic QA phantoms are designed to test the entire treatment process beginning with imaging of the patient and continuing through treatment planning, set-up, and delivery of the prescription dose. This is done by comparing measurements from the phantom's thermoluminescent dosimeters (TLD) and radiochromic film to predicted values obtained from the institutions' calculations performed by the treatment planning system[1].

Measurement based comparisons historically have provided acceptable assurance evaluating an institution's ability to accurately deliver dose for conventional treatment procedures. With recent advances in radiotherapy that allow for highly conformal dose distributions and steep dose gradients through the use of multi-leaf collimators (MLC), dynamic wedges, and advanced delivery techniques including three dimensional stereotactic

radiosurgery and intensity modulated radiation therapy (IMRT), there is a growing concern that the limits of measurement uncertainty are being approached[2]. As reported by the New York Times, increased complexity in treatment modality creates the potential for devastating errors in the administration of therapeutic radiation [3-10]. In addition, patient dose calculations in the lung or near bony anatomy using the new treatment delivery technologies require the use of heterogeneity correction dose algorithms that the RPC is currently not able to fully verify with its current QA tools. The RPC has published results detailing the associated uncertainty with TLD[11] and radiochromic film[12] as well as the results from the remote anthropomorphic phantom audit program that present the ability of institutions to conform to prescribed treatment plans[13-17]. These publications show a varying degree of compliance among the treatment plans with variability among different plans generated from the same treatment planning system (TPS). There is reason to believe that these plan variations could be from the beam commissioning process, delivery of the treatment, and the accuracy of the dose calculation algorithms used by the TPS[12, 18, 19]. The observed differences between institutions have caused concern that variations and inaccuracies in the delivery of radiation therapy between institutions could negatively impact patient safety and compromise the conclusions drawn from NCI supported multi-institutional clinical trials. Currently the RPC has no means by which to check the dose calculations made by the TPS for IMRT and heterogeneity corrected treatments to catch any errors resulting from the dose calculation algorithms. In order to evaluate the actual dosimetry and judge the accuracy of the TPS predicted dose distributions, a trusted independent dose calculation tool is needed. This would also allow for retrospective analysis of past clinical trials in which all dosimetry data could be normalized based on an independent dose calculation standard.

For this reason, the RPC began the development of a multiple source model that is executed using the Monte Carlo (MC) technique for dose calculations[20, 21]. The MC technique is a means to numerically solve the transport equation by means of simulating the stochastic processes using random sampling. It has been generally accepted as the most

accurate means of radiation dose calculation[22] and is particularly useful in calculations in which interfaces between materials along the transport path exhibit large differences in density and/or atomic numbers[23]. The accuracy of the MC technique has been tested against deterministic algorithms for a variety of codes including EGS4[24, 25], ITS[26, 27], MCNP[28], and PENELOPE[29-31]. Despite its superior accuracy compared to deterministic methods, MC based methods have not been widely implemented into the radiotherapy clinic due to the computational intensity of the calculations[22, 23]. Recent improvements in MC code and improvements in technology that have resulted in increased computational speed have motivated increased consideration to treatment planning systems utilizing MC techniques[22, 32].

The improved accuracy of the MC technique is of particular significance in calculating dose in tumors that lie near lung/air interfaces in the body [22, 33]. In these regions, tissues and air cavities may have radiological properties that are substantially different from water. This necessitates heterogeneity corrections for standard deterministic methods of calculating dose[34]. Davidson et al. have documented how these correction factors may lead to differences between measurement and calculation in heterogeneous media when using conventional analytical dose calculation algorithms[12, 18].

The RPC's previously developed multiple source model[35], a dose calculation tool for Varian (Varian Medical Systems, Palo Alto, California) 6MV and 10MV photon beams, was executed using the Dose Planning Method (DPM) code. The open source code allows for easy modification and interfacing, making it a good choice of code to execute the MC simulations. DPM uses standard condensed history modeling for electron transport, and is what's known as a mixed scheme[23]. This means that large energy transfer collisions are treated in an analogue sense (event-by-event) and small loss collisions are approximated using the continuous slowing down approximation (CSDA) using a restricted stopping power[22, 23]. Photon transport is handled on an interaction by interaction basis and is composed of photoelectric absorption, Compton scattering, and pair production[23]. By altering the transport

mechanics such that large electron transport steps may be taken, even across heterogeneous boundaries while maintaining the necessary accuracy, the computation speed has been greatly improved, keeping differences between DPM and other MC codes below 1.25% and statistical uncertainty on the order of 0.2% of the maximum dose[23].

To aid in integrating the source model with the DPM code, a graphical user interface designed to run off the Computational Environment for Radiotherapy Research (CERR)[36] software platform was designed in the application MATLAB (MathWorks Inc., Natick, MA). CERR was developed to create a common data structure for treatment plan databases that would facilitate multi-institutional collaborations amongst the radiation therapy community.

Within radiotherapy treatment planning and dose calculation, the linear accelerator output may be modeled in three primary ways. First, a complete simulation of the linear accelerator mechanics may be done and saved to a phase space plane for further simulations in the future. While more rigorous, this method is strongly influenced by hardware specifics that may be difficult to ascertain or are proprietary in nature. It also requires the most memory usage of the three methods [37-40]. Second, an analytical description of the output, based on the full simulation, may be used in the form of a multiple source model. The multiple sources arise from the grouping of photons based on their last interaction prior to being stored in the phase space plane [37-44]. The final means, and method of choice for the RPC's model, is a measurement based multiple source model in which output is matched to standard dosimetry data. This has the advantage of being independent of the complexities within the treatment head[22]. Parameters to the analytical models describing the multiple sources are derived by minimizing the difference between simulated and measured data [45-49].

Currently, the multiple source model is comprised of three analytical components describing the output of a therapeutic megavoltage photon beam. The components correspond to the primary source in the treatment head, an extra-focal scattering source, and a source to model electron contamination in the beam. The analytical model is coupled to the DPM code where

simulation of the particle transport occurs resulting in the independent dose calculation tool[20, 21].

The primary point source represents isotropically emitted photons originating from the target inside the linac head. A second, extra-focal source is added to model scattered photons within the linac head and is placed at a location corresponding to the flattening filter within the linac. While only included in the Varian 10MV model done by Davidson et al., a third source representing electron contamination may sometimes be added to the model. Studies have suggested that this source may not be necessary for linacs of nominal energies less than or equal to 10MV.

This project will be based on the extension of the currently developed multiple source model for Varian megavoltage, therapeutic, linear accelerators to include linear accelerators manufactured by Elekta (Elekta AB, Stockholm, Sweden) and Flattening Filter Free Varian TrueBeam with nominal beam energies of 6MV and 10MV. In its current stage, the calculation tool may be used as a generic model for Varian linacs of different models. By extending the tool to Elekta and Flattening Filter Free Varian TrueBeam, the RPC will be able to use the tool for most of the remaining 25% of machines used clinically. While specific models of a manufacturer have been extensively modeled using the Monte Carlo technique[39, 50, 51], there have been a limited number of studies exploring generic models meant to cover a range of models by a manufacturer[52-54]. RPC measured dosimetry data suggests that a standard dataset can match measurements from modern linear accelerators of the same nominal energy and manufacturer[55, 56].

1.2 Benefits to Science

The RPC wishes to incorporate the generic model into a fully integrated calculation tool for use in analysis of clinical trial data. This tool would allow for the accurate modeling of nearly all megavoltage, therapeutic photon beams monitored by the RPC[55, 56] and easy importation of treatment plan data including beam and MLC configurations and CT data representing the calculation grid for dose calculations. This tool will have four primary uses within the RPC's QA program:

- 1) It will complement the anthropomorphic phantom program by allowing for an additional data source in comparison of measurement data and TPS calculated dose distributions.
- 2) It may act as means to provide direct comparison of retrospective patient treatment plans from clinical trials. This would isolate the performance of the TPS dose calculation from all other variables in the treatment process.
- 3) It will allow for the comparison of TPS dose calculation algorithm performance. RPC studies[13-17] have shown that discrepancies between TPS data and measured data from the phantom QA program can be largely dependent on beam modeling errors, planning mistakes, and errors in phantom set up. By importing a single treatment plan to the institution TPS for dose calculation, the performance of the TPS calculation may be objectively compared through the use of a standard baseline established by the calculation tool using the DPM engine.
- 4) Extension of the calculation tool to include a flexible source model for Elekta and Flattening Filter Free Varian TrueBeam machines will act as a valuable quality assurance tool that allows the RPC's quality assurance program to test areas of the radiation therapy treatment process previously not possible.

The new models will be developed and commissioned in a step by step process beginning with validation against basic dosimetry data, benchmarking against phantom based

measurements, and finally benchmarking against outside institution phantom measurements previously submitted through the RPC's credentialing program. A detailed explanation of the proposed methods and issues to be resolved are contained below.

1.3 Hypothesis and Specific Aims

Hypothesis: A dose calculation quality assurance tool using the Dose Planning Method Monte Carlo technique coupled to multiple source models of Elekta 6MV and 10MV and Varian TrueBeam FFF 6MV and FFF 10MV beams can perform dose calculations to an accuracy of $\pm 3\%$ of the maximum dose and $\pm 2\text{mm}$ distance to agreement for conformal radiation therapy and intensity modulated radiation therapy in homogeneous and heterogeneous media as determined by anthropomorphic phantom based measurements.

Specific Aim 1: Modify and extend a multiple source model dose calculation tool previously developed for Varian linear accelerator (linac) 6MV and 10MV photon beams to include Elekta 6 MV and 10MV, and Varian TrueBeam FFF 6MV and FFF 10MV photon beams using the same model optimization process. The dose calculation tool will be validated, and the accuracy will be verified against depth dose data and dose profiles for field sizes up to $40 \times 40 \text{ cm}^2$. Acceptance between the dose calculation and measured dosimetry data is $\pm 2\%/2\text{mm}$ distance to agreement (DTA) for 90% of all data.

Specific Aim 2: The dose calculation tool will be benchmarked against measurements for Elekta 6MV and 10MV and Flattening Filter Free Varian TrueBeam 6MV and 10MV photon beams using the Radiological Physics Center's (RPC) anthropomorphic phantoms. These phantom measurements will include measurements for a homogeneous intensity modulated radiation therapy (IMRT) head and neck phantom, stereotactic lung phantom, and

heterogeneous IMRT lung treatments. The accuracy of the dose calculation tool will be within $\pm 3\%/2\text{mm}$ DTA of measurements for 85% of the data tested.

Specific Aim 3: The dose calculation tool will be benchmarked against measurements submitted by outside institutions as a part of the Radiological Physics Center's remote auditing program. Plans will be selected to include previously passing deliveries that will test the robustness of the models and their ability to predict dose distributions from linear accelerators whose dosimetry data were not used during commissioning and validation of the models.

Chapter 2: Materials and Methods: Development, Validation, and Benchmarking

2.1 Introduction

Interest in the Monte Carlo (MC) technique as means for dose calculations has been motivated by its superior accuracy compared to traditional, deterministic algorithms[22]. While different codes utilizing the technique have been developed[23, 25, 28-30], all operate under a similar idea that with known interaction probability distributions of electrons and photon radiation may be transported with a high degree of statistical certainty. While deterministic algorithms used by modern day treatment planning systems have been shown to perform well in dose calculations, there have been demonstrated instances of disagreement between calculated and measured data in conditions of heterogeneous media, small field sizes, and/or steep dose gradients[12, 18]. Due to challenges associated with measuring a full three-dimensional dose distribution in realistic clinical circumstances (e.g. within an anthropomorphic phantom), the MC technique is an excellent way to evaluate the performance of commercial treatment planning dose calculation algorithms.

Traditionally MC dose calculations are performed via a full simulation of the mechanics within the linear accelerator. Depending on the dosimetric quantities of interest and the measurement conditions, results may be highly dependent on the accuracy and completeness of the model geometry. Out of field doses in particular rely upon more than the general beam line components such as target, flattening filter, jaws, and multi-leaf collimator (MLC) that can model standard in field dosimetric quantities. The execution of this type of model can be cumbersome as the level of detail needed in modeling specific components may be considered proprietary information by the manufacturer and as a result not readily available. Alternate means of modeling as detailed in the American Association of Physicists in Medicine's Task Group Report No. 105 (TG-105)[22] have been implemented. These include a multiple source model based on the full simulation of an accelerator in which particles are grouped based on their points of interaction and described analytically. A third method is a measurement based

multiple source model in which an analytical description of particles is generated based on minimizing differences between resultant calculated data and measured data.

Another obstacle to the wide spread implementation of MC dose calculations has been its computational intensity. Within a clinical environment, it is not always practical to wait for a dose calculation with sufficient statistical certainty. Advances in computer technology and the use of GPU based calculations have cut the required time down substantially and renewed interest in clinical MC calculations. Additionally alternate approaches of simplifying the MC transport have been developed to cut down on calculation time [23, 57, 58].

Originally developed and commissioned for field sizes up to $10 \times 10 \text{ cm}^2$ by Joseph Deasy and his research group out of Washington University in St. Louis[20], the RPC has documented its modifications and development of an independent, dose calculation, quality assurance tool for Varian linear accelerators of nominal photon beam energies 6MV and 10MV up to field sizes of $40 \times 40 \text{ cm}^2$ including fields modulated by MLCs[21, 35]. This tool was designed with a generic model of Varian megavoltage, therapeutic, x-ray beams such that individual beam models would not be needed for every beam monitored by the RPC. In short, the model was a measurement-driven multiple source model consisting of analytical descriptions of a primary point source, an extra-focal disk source, and an electron contamination source. The model was shown to accurately account for off-axis effects, namely increased fluence and decreased mean energy, resulting from the flattening filter.

It's estimated that the current dose calculation tool covers approximately 75% of the beams monitored by the RPC. Notable exclusions are Elekta and Siemens manufactured linear accelerators and linear accelerators operating in flattening-filter-free mode, notably the Varian TrueBeam accelerator. Chapter 3 reports on the development of Elekta 6MV and 10MV therapeutic x-ray beam models to be included in the dose calculation tool, and Chapter 4 reports on the inclusion of a Varian TrueBeam linear accelerator operating in flattening filter free mode. Validation of the models was tested by comparing ion chamber measurements in a water phantom for depth dose data and dose profiles for square field sizes. Benchmarking was

performed using the RPC's anthropomorphic phantoms that contain thermo-luminescent dosimeters (TLD) and radiochromic film. In this stage the entire model was evaluated in clinically realistic scenarios including both homogenous and heterogeneous media with highly modulated and small fields.

2.2 Source Model

2.2.1 Hardware

Dose calculations were performed on a Hewlett Packard ProLiant DL585 G5 3.2 GHz server with four AMD Opteron™ processors with four core CPU's and 32 GB of RAM (Hewlett-Packard Company, Palo Alto, CA) and a Hewlett Packard ProLiant DL380 G8 server with two Xeon® CPU E5-2602 with six core CPU's (Hewlett-Packard Company, Palo Alto, CA).

2.2.2 Software

Calculations and analysis were performed with MATLAB (MathWorks Inc., Natick, MA) and the use of the Computational Environment for Radiotherapy Research (CERR)[36]. Execution of the MC code was done using the Dose Planning Method (DPM)[23] utilizing low energy electron and photon cutoffs of 200 keV and 50 keV, respectively. To cut down on calculation time, each simulation was broken into smaller batches and individual beams such that calculations were allocated to individual processors using MATLAB's Parallel Processing Toolbox.

2.2.3 Source Model Commissioning

The commissioning of a source model was completed in two steps. The first was based on central axis depth dose data from a 10 x 10 cm² field size. Separate dose calculations were performed for mono-energetic bins of 0.25 MeV increments through the nominal energy range

of the beam for both primary and extra-focal sources. The relative weight between each of the bins was adjusted during an optimization process to match measured percent depth dose data (PDD).

Optimization involved the adjustment of seven unique parameters used to describe the shape and position of the primary and extra-focal energy spectra, relative fluence of the primary and extra-focal sources, electron contamination contribution, and a parameter used to model the volume average blurring from the use of an ion chamber in collecting measurement data. The parameters used to describe the energy spectra shape were based on the product of a Fatigue-Life function and Fermi Distribution, shown below in Equation 2.1, and referred to as a Fatigue Fermi Distribution by Davidson et. al[20, 21, 35].

$$f(E) = \left(\frac{\sqrt{\frac{E-\mu}{\beta}} + \sqrt{\frac{\beta}{E-\mu}}}{2\gamma(E-\mu)} \right) \left(\frac{e^{-\left(\frac{1}{2}\right)\left(\frac{\sqrt{\frac{E-\mu}{\beta}} - \sqrt{\frac{\beta}{E-\mu}}}{\gamma}\right)^2}}{\sqrt{2\pi}} \right) \left(\frac{1}{1+e^{\frac{E-E_F}{kT}}} \right) \quad (2.1)$$

Such that $E > \mu$; $\gamma, \beta > 0$

In the above equation, E is the photon energy, E_F the cut-off energy, and μ , β , and γ shape the photon spectrum. This function was chosen for the Elekta model to 1) be consistent with the spectra modeling used for the Varian models by Davidson et al. [20, 21, 35] and 2) its ability to fit the photon spectra from numerous linac manufacturers determined from the Monte Carlo code BEAM and studied by Sheikh-Bagheri and Rogers[59] without being overly parameterized.

The distribution matched exactly with the Varian model with the exception that the locations of the extra-focal source and electron contamination source were moved to be consistent with

the location of the flattening filter within Elekta machines. Briefly, these distributions consisted of a primary point source corresponding to photons created within the target, an exponential disk source[60] used to model photons originating from scatter events in the linac head (primary collimator, jaws, MLC, flattening filter, etc.) and a uniformly distributed, circular electron contamination source. The energy distribution for the extra-focal source is modeled by the same distribution as the primary source, Equation 2.1, but scaled down in the relative fluence and maximum energy. The electron contamination source has an energy spectrum modeled by an exponential function described by Fippel et al. [53] for Elekta and Siemens linacs. Its relative contribution was determined during the optimization process and was included in both Elekta 6MV and 10MV and TrueBeam FFF 6MV and FFF 10MV models, contrary to the Varian model in which Davidson et al.[35] chose to exclude it for the 6MV model.

The output of the MC simulation is in units of energy per source particle. To convert the resultant calculations into the more useful units of dose per monitor unit (MU), the output was scaled by a constant factor to match the dose at a depth of d_{\max} for the $10 \times 10 \text{ cm}^2$ measurements and calculations.

The second step of the commissioning process is based on measured data from a $40 \times 40 \text{ cm}^2$ field size, and is executed with the intention of modeling off-axis effects such as increased off-axis fluence and decreased mean energy off-axis, collectively contributing to the Horn Effect. Using the optimized spectra from the first step and an off-axis correction for half-value layer (HVL) formulated by Taylor et al. [61] (Elekta models) and Georg et al.[62] (TrueBeam FFF Models) and implemented without change, calculations were run for 1600 $1 \times 1 \text{ cm}^2$ beamlets, making up an open $40 \times 40 \text{ cm}^2$ field. Each beamlet's contribution to the total dose was adjusted based on a piecewise linear function such that the calculated dose profiles were matched to measured dose profiles at a depth of d_{\max} .

2.2.4 Machine Output Correction

Similar to the output correction used by Davidson et al.[35], and documented in the literature[63, 64], a second order hyperbolic equation was used to correct for machine output as a function of field size for the Elekta models. This was done by a least squares fit of the ratio of calculated and measured output factors as a function of field size. The correction factor was then applied to the entire three-dimensional (3D) dose matrix after calculation. No output correction was needed for the Varian TrueBeam FFF models.

2.2.5 Fluence Map

A projected fluence map at isocenter was formed with dimensions determined by the jaw settings. This map was divided into $1 \times 1 \text{ mm}^2$ fluence segments with the option of a finer $0.5 \times 0.5 \text{ mm}^2$ at the cost of increased computation time and memory. The fluence through each fluence segment was determined from MLC position pulled from the DICOM plan file for each plan segment, the transmission through the MLC leaves, transmission through the rounded leaf ends, and the leakage between adjacent leaves. Each group of fluence segments exposed to the primary source during the plan segment were assigned a fluence based on the number of monitor units per plan segment. The transmission through the MLC assigned additional fluence to the fluence segments as a percentage of the monitor units in an amount that varied along the leaf length with the least amount being at the rounded tips of the leaves. A piecewise linear function was used to weight the fluence in this region to model the rounded tip. The fluence segments that this function was applied to corresponded to the projected width of the leaves at isocenter and an effective tip length of 5mm. This resulted in a more effective modeling of the penumbra caused by the shape of the leaves. Interleaf leakage was modeled by assigning additional fluence, expressed as a percentage of the monitor units, to the fluence segments. This was done along the fluence segments alongside the leaves in 1mm wide region with length corresponding to the leaf positions. A final, composite fluence map was calculated by summing the $1 \times 1 \text{ mm}^2$ fluence segments from all beam segments determined in the treatment

plan. The DPM calculation was then run by segmenting the fluence map into beamlets of similar monitor units.

2.2.6 Primary Source Size

The primary source corresponding to photons created within the target of the linear accelerator head was treated as a point. In reality, it is known that this is finite in size and ranges, dependent on linear accelerator manufacturer, from 0.5mm to 3.4mm in full width at half the maximum[65]. The finite size of the source results in an exaggerated penumbra, dependent on source size, distance from the collimator jaws, and distance between the collimator jaws and point of measurement, referred to as the geometric penumbra. To mimic this effect in a point source model, an offset in the MLC leaf positions was implemented in the amount of 0.4mm. This remains unchanged from the previously developed Varian model[20, 21, 35].

2.2.7 Electron Contamination Contribution Versus Field Size

Similar to the overall output correction discussed in 2.2.1.4, a field size dependent output correction was used for the electron contamination contribution in the Elekta models. This too was a second order hyperbolic equation. This correction was necessary to model the increased head scatter contribution with relation to the field size which affects the build-up region of the depth dose curves and the depth of maximum dose. No field size dependent correction factor was used for the Varian TrueBeam FFF models.

2.3 Validation Testing

Validation of the Elekta source models was done through a comparison of calculated dosimetry values to basic, measured beam data. Specifically that data consisted of depth dose

curves and dose profiles at depths of 1.6cm (d_{max}), 5.0cm, 10.0cm, and 20.0cm for the 6MV model and 2.0cm (d_{max}), 5.0cm, 10.0cm, 20.0cm, and 25.0cm for the 10MV model. These comparisons were done for field sizes of 3 x 3 cm², 5 x 5 cm², 10 x 10 cm², 15 x 15 cm², 20 x 20 cm², and 30 x 30 cm². Measurements were performed in a water phantom and calculations were done in a simulated 50 x 50 x 50 cm³ water phantom.

Validation of the Varian TrueBeam FFF 6MV and FFF 10MV models was done through a comparison of calculated dosimetry values to basic, measured beam data. Data consisted of depth dose curves and dose profiles at depths of 1.5cm (d_{max}), 5.0cm, 10.0cm, 20.0cm and 30.0cm for the FFF 6MV model and 2.4cm (d_{max}), 5.0cm, 10.0cm, 20.0cm, and 30.0cm for the FFF 10MV model. These comparisons were done for field sizes of 3 x 3 cm², 4 x 4 cm², 6 x 6 cm², 8 x 8 cm², 10 x 10 cm², 20 x 20 cm², 30 x 30 cm², and 40 x 40 cm². Measurements were performed in a water phantom and calculations were done in a simulated 50 x 50 x 50 cm³ water phantom.

The calculated data was extracted from the 3D dose matrix relative to the surface of the virtual water phantom, as defined by the skin contour. The resolution of the calculated data was 0.2cm in the depth direction, defined as 'y' in the CT data set, 0.2cm in the in-plane direction, defined as 'x' in the CT data set, and 0.3cm in the cross-plane direction, defined as 'z' in the CT data set.

The measured data was the same data used for the commissioning of the clinical treatment planning system and were performed using a Wellhöfer CC13 ionization chamber (internal volume of 0.13cc) manufactured by CNMC (Best Medical, Nashville TN) for the Elekta measurements and a PTW 31010 ionization chamber (internal volume of .125cc) (PTW, Freiburg, Germany) for the Varian TrueBeam FFF measurements. To account for volume averaging effects of the ionization chamber that exaggerate the penumbra, a Gaussian convolution was applied to all dose profiles for comparison of measured and calculated data. The standard deviation of the kernel applied in the convolution was one of the seven parameters defined during model optimization.

Agreement between measured and calculated data was evaluated using gamma analysis with a criterion of $\pm 2\%$ of the maximum dose and $\pm 2\text{mm}$ distance to agreement. For dose profile comparison, the analysis was performed out to an off-axis distance corresponding to 5% of the maximum central axis dose.

2.4 Anthropomorphic Phantoms

The RPC's anthropomorphic head and neck phantom, shown in Figure 2.1, consists of a hollow, plastic head that may be filled with water to mimic radiological properties similar to tissue. Contained within the hollow shell is a removable insert constructed of polystyrene with solid water structures representing two separate targets and a single organ at risk (OAR). Also contained in the insert is space for the placement of radiochromic film (Gafchromic EBT2, Ashland Inc., Covington, KY) in the axial and sagittal directions and thermoluminescent dosimeter (TLD) capsules (TLD-100 capsules, Radiation Detection Company, Gilroy, CA). The orientation of the insert within the shell, and the targets and OAR within the insert, are such that the phantom presents a clinically realistic challenge. For detailed specifications about the phantom design, the reader is referred to an article published by Molineu et al.[66].



Figure 2.1: The anthropomorphic, hollow, plastic shell to the RPC's head and neck phantom with the polystyrene insert removed and opened. The polystyrene insert in the RPC's head and neck phantom is opened up to reveal a transverse, cross sectional view. The insert contains a primary PTV, secondary PTV, and critical structure made of solid water that may be distinguished from the insert in a CT scan for treatment planning purposes. Also pictured are the holes to house the thermoluminescent dosimeters (TLD) for absolute dosimetry. The orthogonal slits intersecting in the primary PTV are for sagittal and coronal films while an axial film may be placed between the two halves of the insert shown in this cross sectional image.

The planning criteria established by the RPC and RTOG protocol H-002 for credentialed institutions will be used in the benchmarking study. It is as follows:

- 1) 6.6 Gy delivered to 95% of the primary PTV
- 2) 5.4 Gy delivered to 95% of the secondary PTV
- 3) Less than 1% of the PTVs may receive less than 93% of the prescription dose
- 4) OAR is to receive a dose less than 4.5 Gy

5) Normal tissue dose must be held under 110% of the prescription dose

The heterogeneous, anthropomorphic thorax phantom designed by the RPC, shown in Figure 2.2, consists of a hollow PVC shell filled by water that contains structures of varying materials representative of human anatomy including a heart (nylon), spine (PBT-polyester), lungs (compressed cork), and a lung tumor (polystyrene). To simulate the slope of a human chest, the anterior surface of the outer shell is slightly angled. At a position consistent with the left lung, the phantom contains a removable imaging/dosimetry insert. Within the dosimetry insert is space for TLD capsules and radiochromic film in the axial, sagittal, and coronal planes. A detailed description of the phantom specifications can be found in the literature[67].

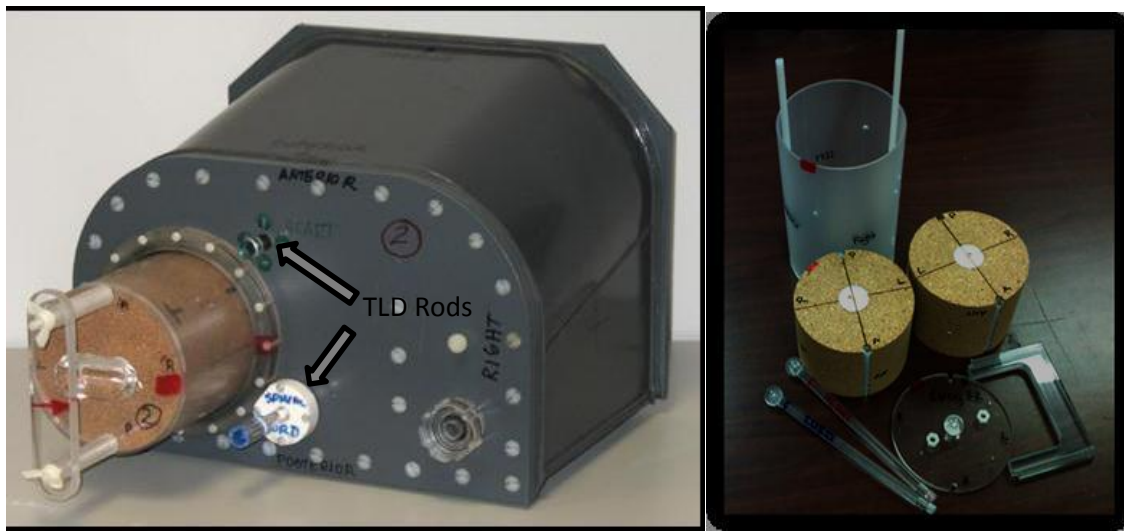


Figure 2.2: The outer shell of the RPC's thorax phantom with the lung insert partially removed. Within the insert are slits for the placement of radiochromic film and holes for TLD. Rods containing TLD capsules are also inserted into the shell for point dose measurements corresponding to the location of the spinal cord and heart, the representative critical structures for this treatment. Also pictured (right) is the disassembled lung insert with locations for radiochromic film and TLD and the removed TLD rods (bottom left).

Planning criteria decided upon by the RPC and RTOG protocol 0236 to be used in the benchmarking study are as follows:

- 1) 66 Gy to 95% of the PTV (clinically delivered in 33 fractions)
- 2) Less than 45 Gy to the spinal cord
- 3) Less than 20 Gy to 40% of the lung
- 4) Less than 40 Gy to the entire heart
- 5) Less than 50 Gy to 50% of the heart

The dosimeters contained within the phantom are all specified at doses less than the clinical constraints given above. Therefore all plans will be scaled down by a constant factor of 11 and delivered in a single fraction[35, 67].

2.5 Benchmark Testing

The benchmarking of the validated source model was designed to be done in a step by step process with increasingly difficult treatment planning and computational challenges including heterogeneous media, small field sizes, and highly modulated treatment plans. The RPC's anthropomorphic head and neck phantom was used in creating, delivering, and comparing to calculation a highly modulated, nine co-planar beam, IMRT plan to the homogenous phantom. Next benchmarking was done on the RPC's heterogeneous lung phantom with first a nine co-planar beam stereotactic body radiotherapy (SBRT) plan followed by a six co-planar, IMRT plan for 6MV and 10MV models, respectively. All treatment plans were designed to meet the credentialing criteria established by the RTOG and delivered three times to evaluate the repeatability.

The accuracy of the calculations was then assessed by comparing point doses from TLD measurements, and dose profiles and 2D gamma comparisons from film measurements.

2.5.1 Point Dose Comparisons

Point dose comparisons were made between calculated doses and measured TLD doses of the target and critical structures. The measured doses were determined from the small volume of TLD powder contained in the TLD capsule, and the calculated values were determined from a corresponding contour of the TLD in the CT scan.

2.5.2 Dose Profile Comparisons

Dose profiles along the three primary axes and passing through the target volume were used as a qualitative evaluation of agreement between the source model and measurements performed in the phantoms. Anterior posterior (AP) and left-right (LR) profiles were extracted from the axial films and profiles along the superior/inferior (SI) direction were taken from the sagittal films. Due to the sagittal films being bisected by the axial film plane, a discontinuity in the center of the measured dose profile exists where the two sagittal films meet. Measured dose in this region should be ignored as a result. While quantitative information exists in the profile comparisons, the analysis was restricted to qualitative evaluation of the models' ability to predict complex dose distributions. The quantitative assessment of distance to agreement was evaluated in the gamma analysis detailed in section 2.5.3.

2.5.3 Gamma Map Comparisons

Two dimensional dose distributions were evaluated using the gamma index technique[68] as a means of evaluating the project hypothesis. Agreement between calculated and measured dose was evaluated in the film planes intersecting the phantom target to a criterion of $\pm 3\%$ of the target TLD dose and $\pm 2\text{mm}$ distance to agreement.

Exclusion of selected regions of the film were performed in areas in which discontinuities or alterations of the film were made to allow for proper assembly of the dosimetry tools. These included cut out regions of film along the central AP axis and central lateral axis of the sagittal and coronal films in the thorax phantom that allow for arrangement of the film along a shared axis, a small cutout on the right, postero-lateral corner of the axial film for the head and neck phantom to allow for proper placement of the film, and a cutout in the sagittal film plane to allow for placement of the critical structure TLD. An example from the sagittal film plane of head and neck phantom is included in Figure 2.3.

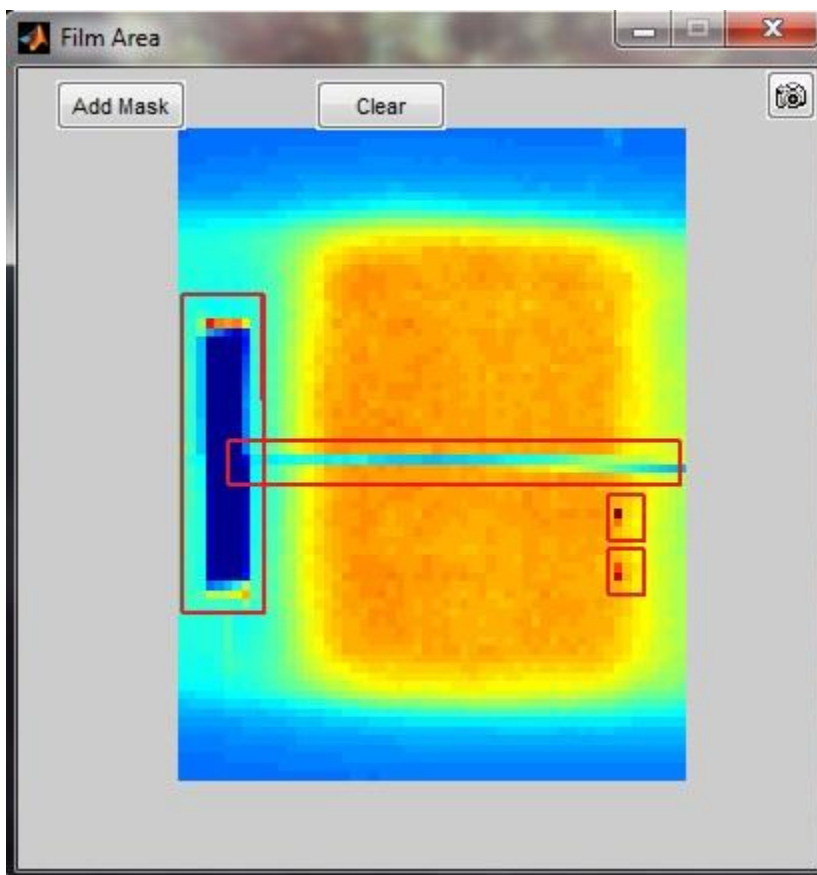


Figure 2.3: Exclusion mask used in the evaluation of the sagittal film from the IMRT head and neck phantom. The exclusion areas are indicated by red lines and correspond to discontinuities between the superior and inferior film pieces, a cutout for the placement of the OAR TLD, and the pin pricks used to localize the film within the phantom insert.

As a representative example of the area of the film that was evaluated, Figure 2.4 shows the evaluated region as dose cloud overlaid on the CT scan for the axial plane of the head and neck and lung phantoms, respectively.

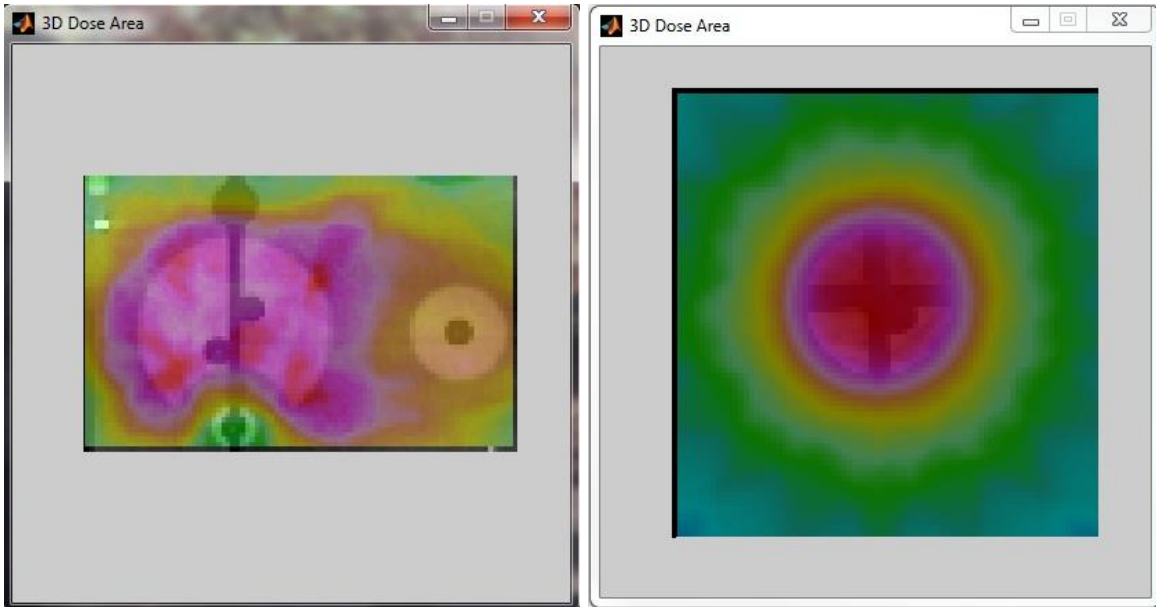


Figure 2.4: Region of interest evaluated using gamma analysis for the axial plane of the IMRT head and neck phantom (left) and lung phantom (right) is shown with the dose cloud from a treatment plan overlaid on the CT scan. For delineation of specific structures in the CT scan in each phantom see Figures 2.5 and 2.6.

2.5.4 Treatment Plans

2.5.4.1 Elekta Benchmarking

Treatment plans for the benchmarking of the Elekta 6MV and 10MV models were developed using the Pinnacle treatment planning system version 9.6 (Philips Medical Systems, Andover, MA). Evaluation of the dose constraints during planning were performed using Pinnacle's collapsed cone convolution algorithm.

The primary goal in developing the treatment plans was to increasingly challenge the dose calculation tool in clinically relevant ways. Because of this, there were some exceptions made to the planning criteria established by the RTOG and RPC in order to increase the complexity of the plan. For example, the planning criteria for the lung phantom can be met quite easily without the use of highly modulated fields. This however would not provide a satisfactory test of modulated fields in a heterogeneous medium for the calculation tool. As a result, modulation was forced in the plan at the expense of increasing the whole lung dose to a level that would otherwise be unacceptable in an institutional audit.

For the head and neck phantom, 95% of the primary PTV, constrained to the identified GTV in the CT scan as shown in Figure 2.5 with the OAR contours, was to receive at least 6.6Gy. The percentage that actually achieved this constraint was 87.4% and 90.4% for the 6MV and 10MV plans, respectively. However the volumes receiving 6.5Gy were 98.5% and 95.9% for the respective plans. The secondary PTV was to receive 5.4Gy to 95% of the volume when in actuality the plans achieved 85.7% and 98.2%, respectively. For the 6MV plan 99.9% of the secondary PTV received a dose of 5.3Gy, 10cGy less than the actual requirement. The OAR dose was to be kept below 4.5Gy for 100% of the volume. In the actual treatment plans 0.1% and 0.6% received a dose of 4.5Gy. The maximum dose to normal tissue was 7.22Gy and 7.45Gy, respectively. The total number of segments in the plan was 107 for both 6MV and 10MV plans. While the planning criteria were not strictly met, it was decided that the levels achieved provided a clinically realistic enough of a plan to still test the calculation tool's ability to model modulated fields in the homogenous phantom.

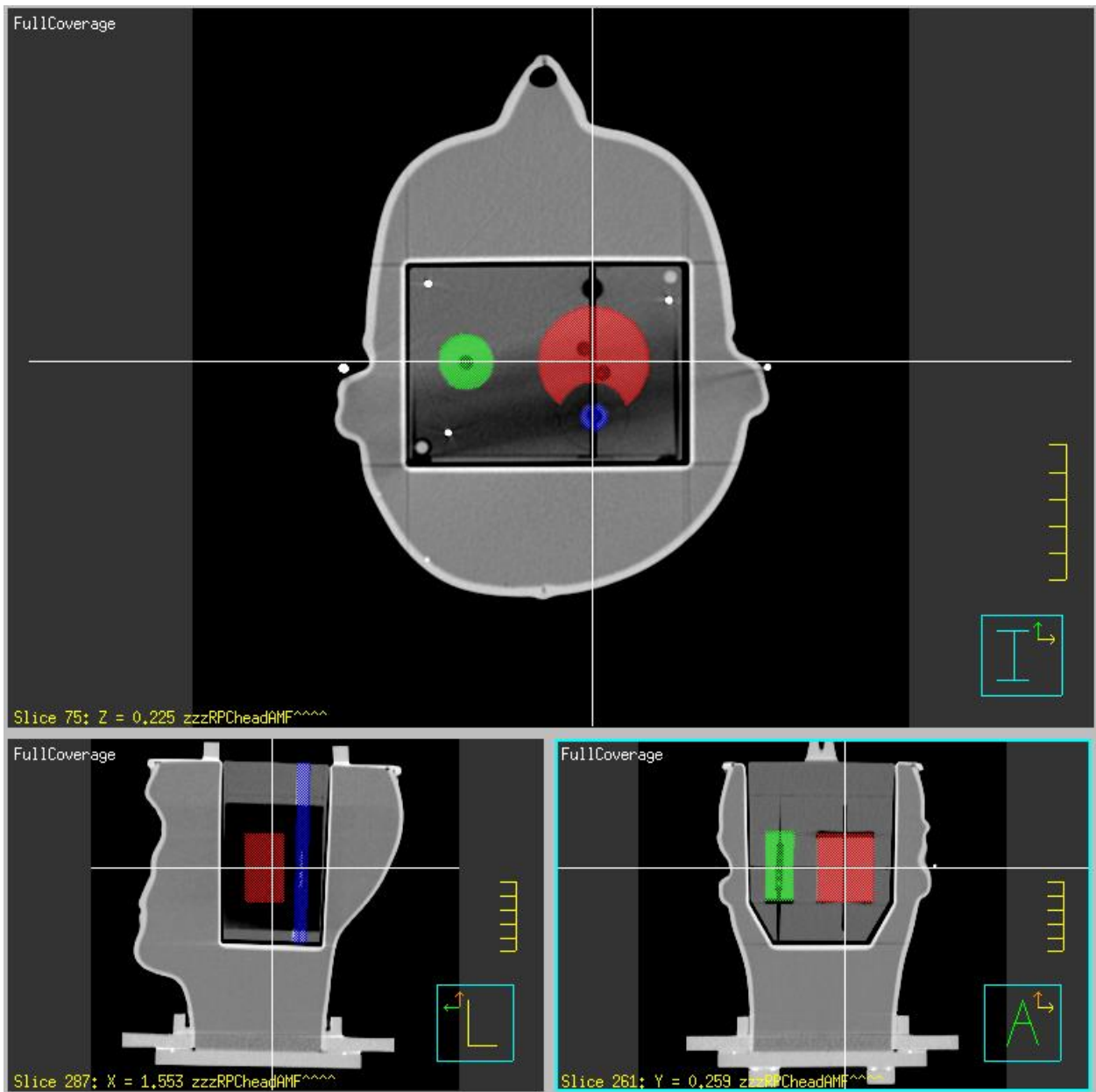


Figure 2.5: Axial (top), sagittal (bottom left), and coronal (bottom right) views of the CT scan of the head and neck phantom. Contours are the primary PTV (red), secondary PTV (green), and critical structure, the cord, (blue). The dark circles within the contours are the regions where the TLD are placed within the phantom and the location for point dose comparisons between measurement and calculation.

The planning criteria for the SBRT plans on the thorax phantom were met fully. Briefly, 97.8% and 99.4% of the PTV, defined as an expansion of 0.5cm of the GTV in the axial plane and 1.0cm expansion in the longitudinal plane and shown with the OAR in Figure 2.6, received the prescription dose for the 6MV and 10MV plans, respectively, and the maximum cord dose was kept to 2.0Gy and 2.2Gy, well below the 5.0Gy limit, for the respective plans. The dose to the heart was below 1.4Gy and 1.6Gy for the two plans. Whole lung dose was kept below 2.0Gy for 11.7% and 13.1% of the volume for each of the plans.

For the IMRT plans on the lung phantom 97.0% and 96.1% of the PTV, defined in the same way as the SBRT plan above, met prescription for the 6MV and 10MV plans, respectively. Maximum dose to the cord was held at 1.8Gy for both plans, and the maximum heart dose was 3.2Gy for 6MV and 10MV plans. The volume of the whole lung exceeding 2.0Gy was 47.8% and 47.4%, respectively, thus exceeding the desired maximum volume of 37%. Again, this was determined necessary in order to force the level of modulation desired for evaluation the model. The total number of segments in each plan were 45 and 44 for 6MV and 10MV plans, respectively.

Monte Carlo calculation resolution was matched to the CT voxel size. For the head and neck treatment plans this was $0.518 \times 0.518 \times 1.25 \text{ mm}^3$, and for the lung treatment plans it was $1.27 \times 1.27 \times 1.25 \text{ mm}^3$.

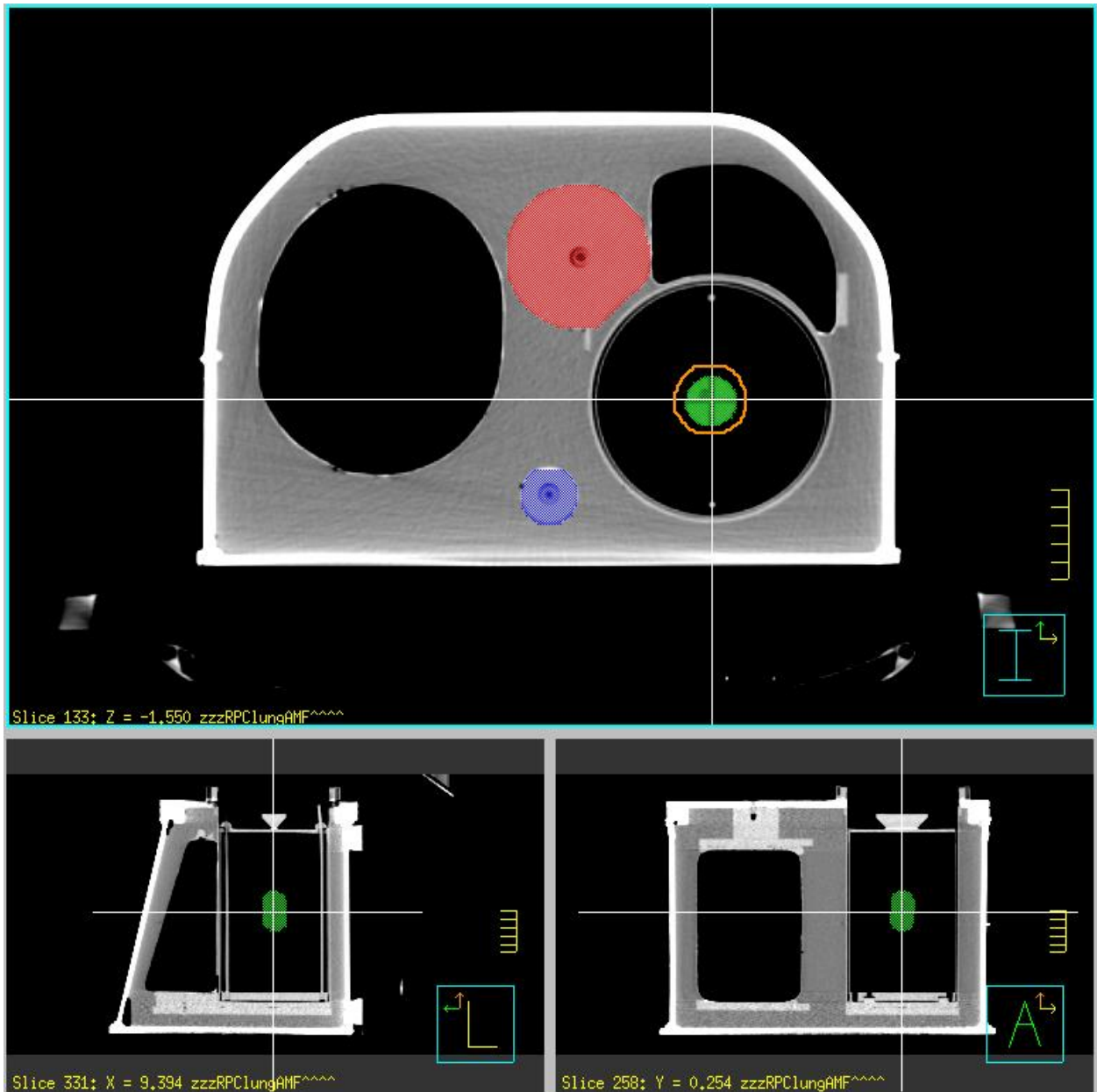


Figure 2.6: Axial (top), sagittal (bottom left), and coronal (bottom right) views of the CT scan of the thorax phantom. Contours are the PTV (green), heart (red), and the cord (blue). The dark circles within the contours are the regions where the TLD are placed within the phantom and the location for point dose comparisons between measurement and calculation.

2.5.4.2 Varian TrueBeam FFF Benchmarking

Treatment plans for the benchmarking of the Varian TrueBeam FFF 6 and FFF 10MV models were developed using the Eclipse treatment planning system version 11.0 (Varian Medical Systems, Palo Alto, CA). Evaluation of the dose constraints during planning were performed using Eclipse's analytical anisotropic algorithm (AAA).

For the head and neck phantom, 95% of the primary PTV, constrained to the identified GTV in the CT scan as shown in Figure 2.3 with the OAR contours, was to receive at least 6.6Gy. The percentage that actually achieved this constraint was 95.5% and 94.6% for the 6MV and 10MV plans, respectively. However the volume receiving 6.5Gy was 99.8% for the 10MV plan. The secondary PTV was to receive 5.4Gy to 95% of the volume when in actuality the plans achieved 98.2% and 94.1%, respectively. For the 10MV plan 99.3% of the secondary PTV received a dose of 5.3Gy, 10cGy less than the actual requirement. The OAR dose was to be kept below 4.5Gy for 100% of the volume. This was achieved in both plans and maximum doses were 4.1Gy and 3.9Gy, respectively. The maximum dose to normal tissue was 6.97Gy and 6.93Gy respectively. The total number of segments in each plan was 134 and 136 for 6MV and 10MV plans, respectively. While the planning criteria were not strictly met, it was decided that the levels achieved provided a clinically realistic enough of a plan to still test the calculation tool's ability to model modulated fields in the homogenous phantom.

The achieved planning criteria for the SBRT plans on the thorax phantom were as prescribed with the exception of a small reduction in coverage of the PTV. Briefly, 93.8% and 93.4% of the PTV, defined as an expansion of 0.5cm of the GTV in the axial plane and 1.0cm expansion in the longitudinal plane and shown with the OAR in Figure 2.4, received the prescription dose for the 6MV and 10MV plans, respectively, and the maximum cord dose was kept to 2.0Gy and 1.8Gy, well below the 5.0Gy limit, for the respective plans. The dose to the heart was below 2.4Gy and 2.2Gy for the two plans. Whole lung dose was kept below 2.0Gy for 7.3% and 7.8% of the volume for each of the plans. Despite the small coverage discrepancy

between achieved and prescribed criteria, the plan was still judged to be an adequate test of the models' performance in heterogeneous media without field modulation.

For the IMRT plans on the lung phantom 93.0% and 93.1% of the PTV, defined in the same way as the SBRT plan above. Maximum dose to the cord was held at 0.69Gy for both plans and the maximum heart dose was 1.2Gy for both plans. The volume of the whole lung exceeding 2.0Gy was 11.4% and 12.0%, respectively. The drop in coverage to the PTV for both plans was judged to be a result of placing the beams at purposefully challenging angles to increase modulation of the plan. For the purpose of testing the models' performance, this was determined to be an acceptable sacrifice. The total number of segments in the plans were 63 and 64 for 6MV and 10MV plans, respectively.

Calculation resolution was matched to the CT voxel size. For the head and neck treatment plans this was 0.68 x 0.68 x 3.00 mm³, and for the lung treatment plans it was 0.977 x 0.977 x 3.00 mm³.

Chapter 3: Results and Discussion: Elekta 6MV and 10MV

3.1 Source Model

3.1.1 Source Model Commissioning Parameters

The seven optimized parameters, determined in commissioning, that describe the photon energy spectra, fluence contributions, and volume averaging of the ion chamber leading to an exaggerated penumbra for dose profiles are reported in Table 3.1 for the Elekta 6MV and 10MV models. The first three parameters, γ , μ , and β describe the spectrum shape, peak energy location, and relative scale respectively.

Parameter	Value Elekta 6MV	Value Elekta 10MV
Fatigue-Life distribution shape parameter, γ	1.79	1.15
Fatigue-Life distribution location parameter, μ	-0.0163	-0.0165
Fatigue-Life distribution scale parameter, β	3.69	3.95
Primary spectrum to extra-focal spectrum reduction factor	1.71	3.10
Extra-focal fluence relative to the primary fluence	0.1101	0.1901
Electron Contamination contribution (relative to the primary photon contribution)	0.002	0.005
Standard deviation of Gaussian used to convolve the MC dose profile to match the measured dose profile during validation (in mm)	1.8	1.8

Table 3.1: Optimized parameters for the source models as determined during the initial commissioning of the models. The first three parameters describe the shape and location of the spectra. The fourth through sixth parameters relate the relative contribution and energy scale of the three sources, and the final parameter is the standard deviation of the Gaussian kernel convolved with the calculated dose profiles to mimic the volume averaging effect of an ion chamber at the penumbra of dose profiles.

A comparison of the 6MV spectrum from the optimization process and those from the widely accepted BEAM code[59] for simulating radiation transport in linear accelerators is shown in Figure 3.1. In Figure 2.6 a comparison of the Elekta 10MV spectrum to the Varian 10MV spectrum from Davidson et. al[35] is shown. While not an exact match for either the 6MV or

10MV models, the results from validation indicate that it is an adequate description of the photon beam. The extra-focal source was scaled in energy by a factor of 1.71 and 3.10 for 6MV and 10MV models, respectively. Their fluences, relative to the primary point source in a 10 x 10 cm² open field, were found to be 11.01% and 19.01% for 6MV and 10MV models, respectively. The electron contamination sources, while small at 0.2% and 0.5% respectively, were still included in the source model, unlike the Varian 6MV model[20, 21, 35]. For the comparison of the dose profiles, a Gaussian kernel of standard deviation 1.8mm was convolved with the calculated data to model the volume averaging effect of an ion chamber measurement.

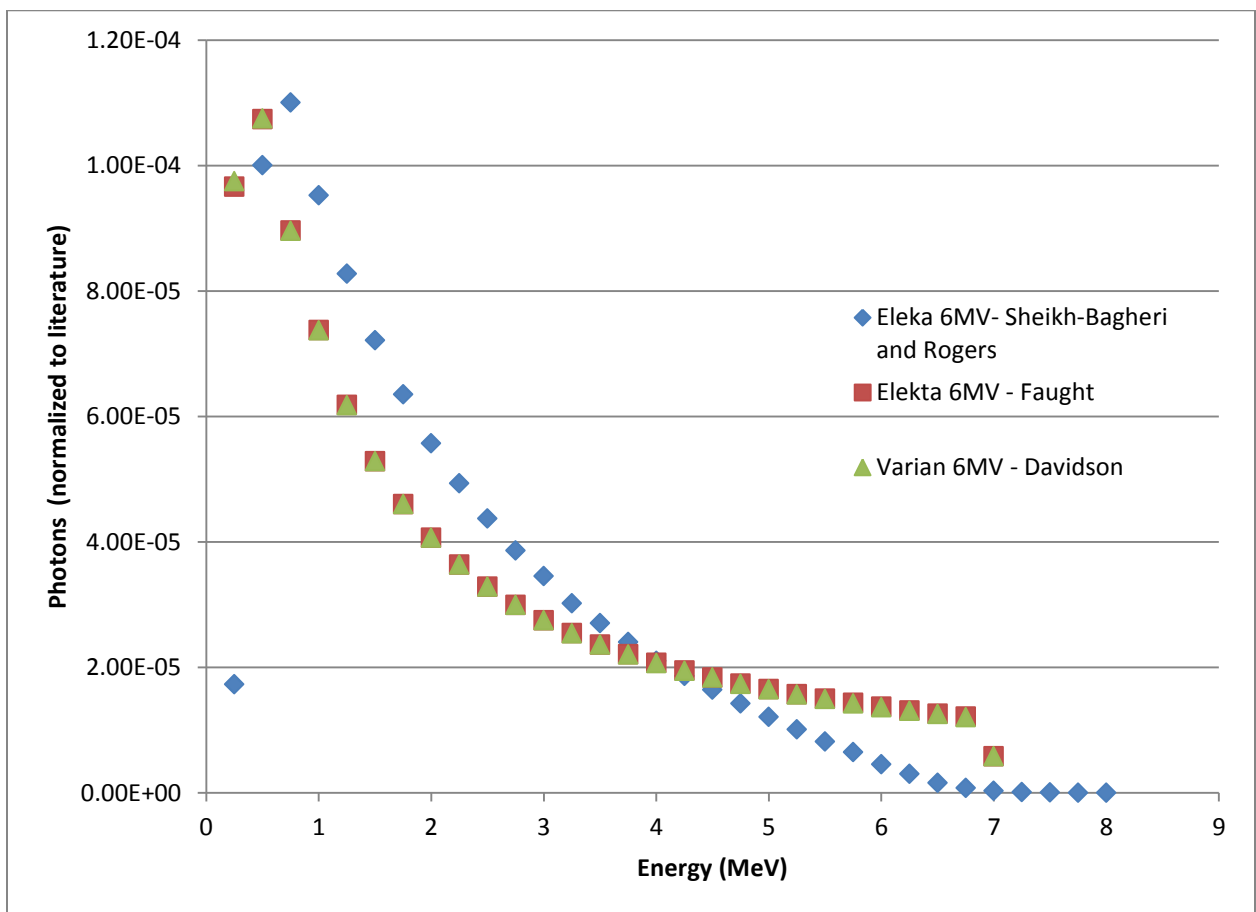


Figure 3.1: Comparison of commissioned Elekta 6MV source model spectrum with the results from BEAM (Sheikh-Bagheri and Rogers) and Davidson et. al.

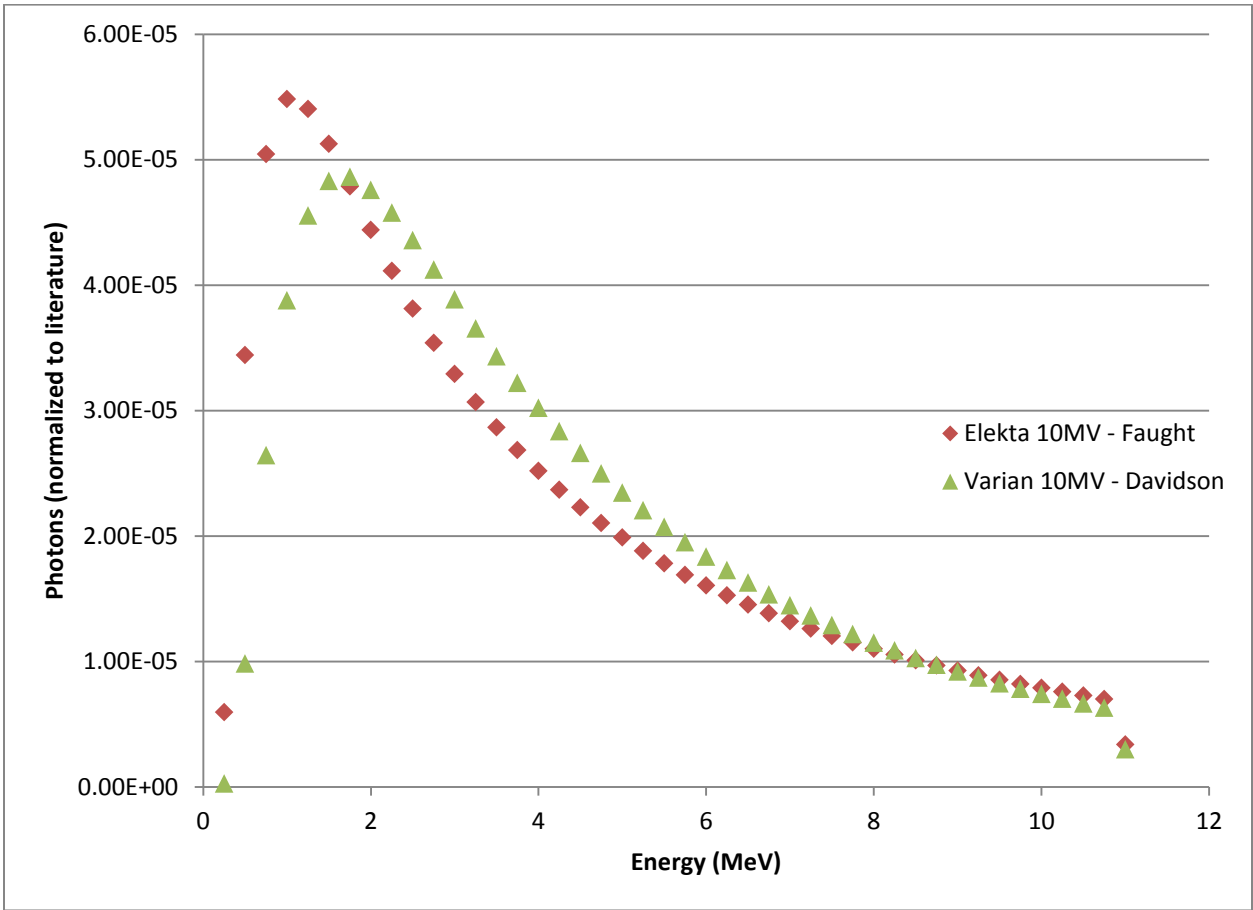


Figure 3.2: Comparison of commissioned Elekta 10MV source model spectrum with the results from Davidson et. al.

The results to the second step of the commissioning process in which the off-axis fluence was modeled by a piecewise linear function of the cosine of the off-axis angle are shown in Table 3.2. The off-axis energy correction was implemented from Taylor et al. [61] without change.

Cosine (Off-axis Angle)	Fluence Weight (Relative to CAX)	Fluence Weight (Relative to CAX)
	Elekta 6MV Model	Elekta 10 MV Model
1.00000	1.0000	1.0000
0.99970	1.0390	1.0310
0.99789	1.0488	1.0620
0.99728	1.0880	1.0980
0.99518	1.1251	1.1300
0.99250	1.1687	1.1700
0.98926	1.2143	1.2000
0.98546	1.2245	1.2200
0.98113	1.2619	1.2300
0.97630	1.2933	1.2800
0.97098	1.3193	1.3000
0.96277	1.3528	1.3200

Table 3.2: Optimized coefficients to a piece-wise linear function used to describe the increase in off-axis fluence of Elekta 6MV and 10MV models. Fluence weighting values are reported with respect to the dose measured at the central axis (CAX) for the 40 x 40 cm² field size dose profile at a depth of d_{max} .

After completing the second step of the commissioning process, the scaling factor used to convert the Monte Carlo output from energy per particle to cGy per MU was determined from the dose at d_{max} along the central axis for a 10 x 10 cm² field size. These values were 25.17 and 15.92 for the 6MV and 10MV models, respectively. This factor will be applied to all subsequent dose calculations for the corresponding linac/energy models.

3.1.2 Fluence Map, Primary Source Size, and Machine Output Correction

Fluence map generation is a process that is unique to the treatment plan, patient, phantom, or open field delivery, and beam energy. The MLC positions for each segment weight the fluence by assuming 1% transmission through the leaves and an additional 1% as interleaf leakage. The transmission and the leakage percentages were the same for 6MV and 10MV models.

Because the source model includes a point source representing photons created within the target and not a finite source size, an offset of the MLC, x_{pen} , of 0.4mm was necessary. This was the same offset used in the Varian model[20, 21, 35] and because the literature has suggested its size is nearly fixed for different nominal energies from the same manufacturer[69], it was left constant for both 6MV and 10MV models.

An empirically determined field size dependent output correction was implemented in addition to the normal output factor due to the models inability to fully model field size dependent scatter conditions. Each model, Elekta 6MV (equation 3.1) and 10MV (equation 3.2), had its own correction implemented.

Elekta 6MV Output Correction

$$y = 1.15 - \frac{2.35}{6.12+x} \quad (3.1)$$

Elekta 10MV Output Correction

$$y = 1.13 - \frac{2.07}{6.23+x} \quad (3.2)$$

In the above equations, y is the output correction and x is the field size. Graphs of the measured and uncorrected and corrected data are shown below in Figure 3.3 and Figure 3.4.

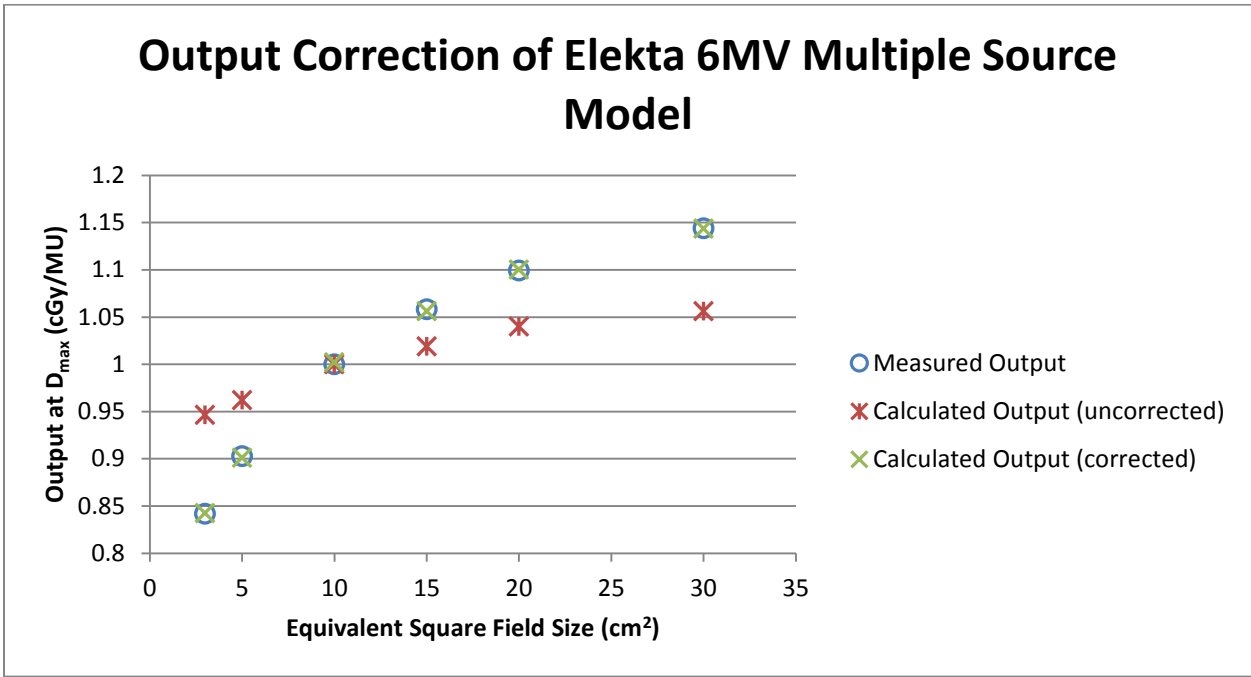


Figure 3.3: Output at a depth of 1.6cm for the measured data (blue circles), calculated data without the hyperbolic correction (red star), and the calculated data with the hyperbolic correction (green x) for the Elekta 6MV source model.

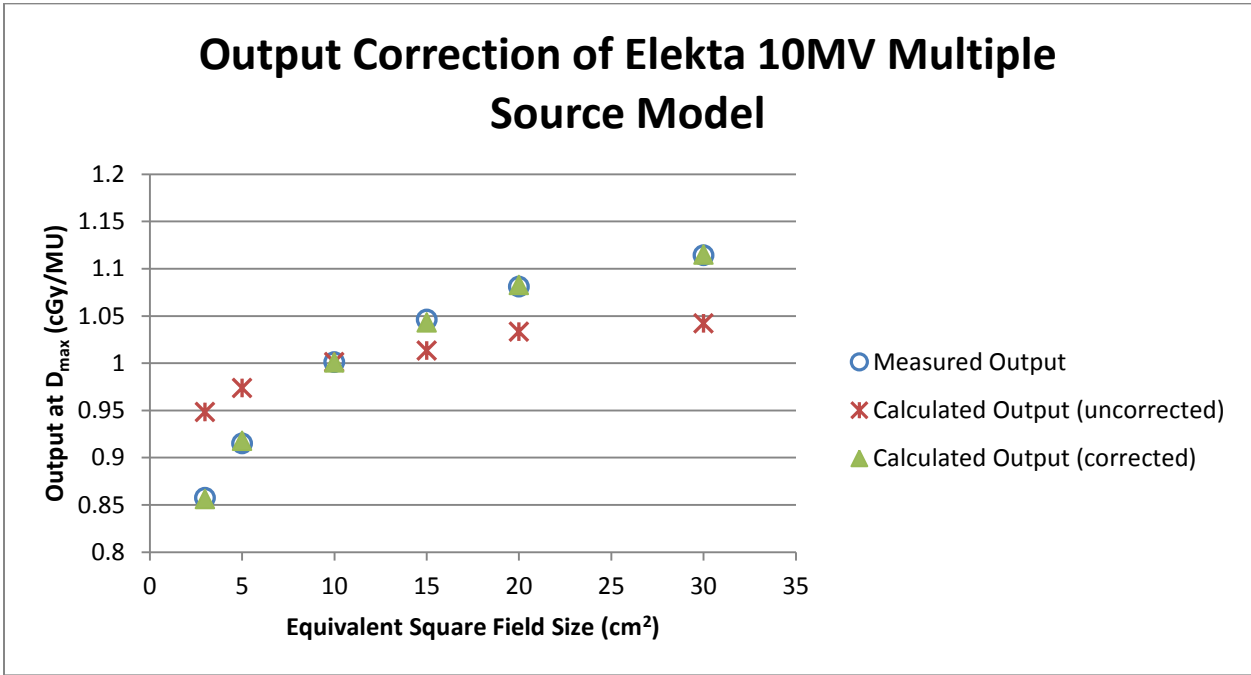


Figure 3.4: Output at a depth of 2.0cm for the measured data (blue circles), calculated data without the hyperbolic correction (red star), and the calculated data with the hyperbolic correction (green triangle) for the Elekta 10MV source model.

3.2 Validation Testing

3.2.1 Uncertainty

The uncertainty in the ion chamber measurements was estimated at 1.6% (one standard deviation) to match that reported in the literature[70]. The standard error of the mean in the dose calculations was calculated to be no more than 2.5% using the batch method described in AAPM Task Group Report No. 105[22].

3.2.2 Depth Dose Data

The comparison between measured and calculated depth dose data for the Elekta 6MV and 10MV models was performed for field sizes ranging from 3 x 3 cm² to 30 x 30 cm². Gamma analysis agreement using a $\pm 2\%/2\text{mm}$ criterion is summarized in Table 2.3. The percentage of data passing the criterion for every field size at every depth is reported in the Appendix (Chapter 6). For a graphical comparison between depth dose data of all field sizes please see the Appendix (Chapter 6). As representative summary the smallest (3 x 3 cm²), nominal (10 x 10 cm²), and largest (30 x 30 cm²) field sizes are shown for the Elekta 6MV model in Figures 3.5, 3.6, and 3.7, respectively. The same field sizes are shown for the Elekta 10MV model in Figure 3.8, 3.9, and 3.10, respectively.

Validation Results –Depth Dose Data

Field Size (cm ²)	% Pixels Passing	
	Elekta 6MV Model	Elekta 10MV Model
3 x 3	99.4	99.4
5 x 5	99.4	99.4
10 x 10	100.0	99.4
15 x 15	100.0	100.0
20 x 20	99.4	100.0
30 x 30	99.4	100.0

Table 3.3: Gamma comparison agreement for Elekta 6MV and 10MV models using a $\pm 2\%/2\text{mm}$ criterion for measured and calculated depth dose data

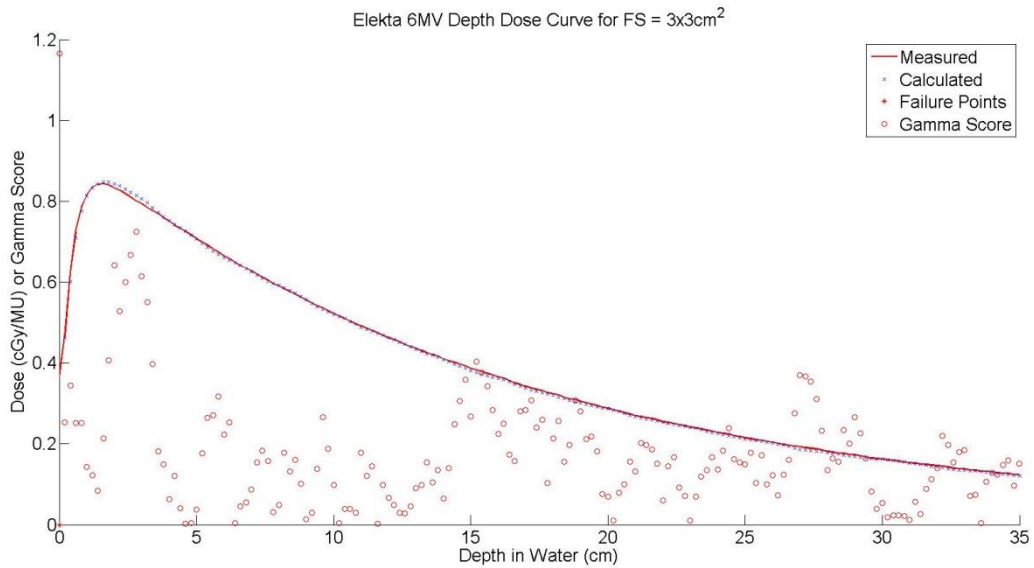


Figure 3.5: Calculated (blue 'x') and measured (red line) depth dose curves for an Elekta 6MV beam for a 3 x 3 cm² field size. Gamma agreement (red circles) for each point is also displayed along with any points (red star) at which a failure to meet the $\pm 2\%/2\text{mm}$ criterion.

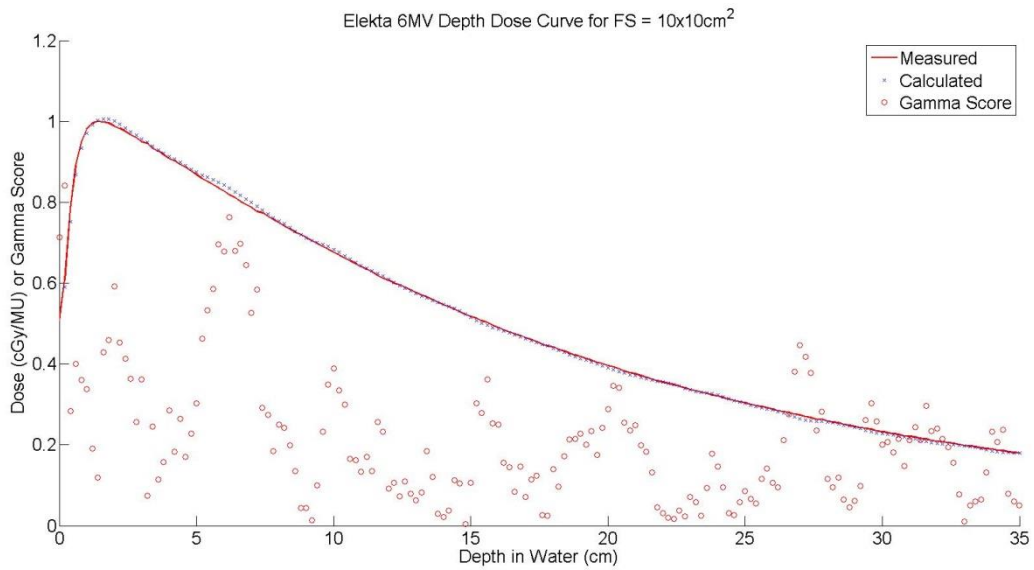


Figure 3.6: Calculated (blue 'x') and measured (red line) depth dose curves for an Elekta 6MV beam for a 10 x 10 cm² field size. Gamma agreement (red circles) for each point is also displayed. There were no failures for this field size and as a result no failure points marked.

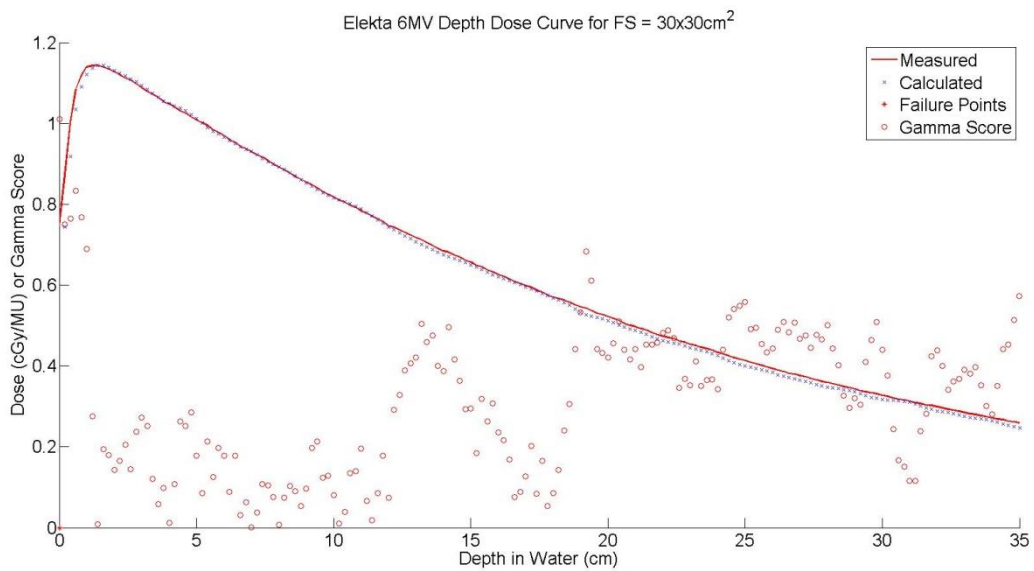


Figure 3.7: Calculated (blue 'x') and measured (red line) depth dose curves for an Elekta 6MV beam for a 30 x 30 cm² field size. Gamma agreement (red circles) for each point is also displayed along with any points (red star) at which a failure to meet the $\pm 2\%/2\text{mm}$ criterion.

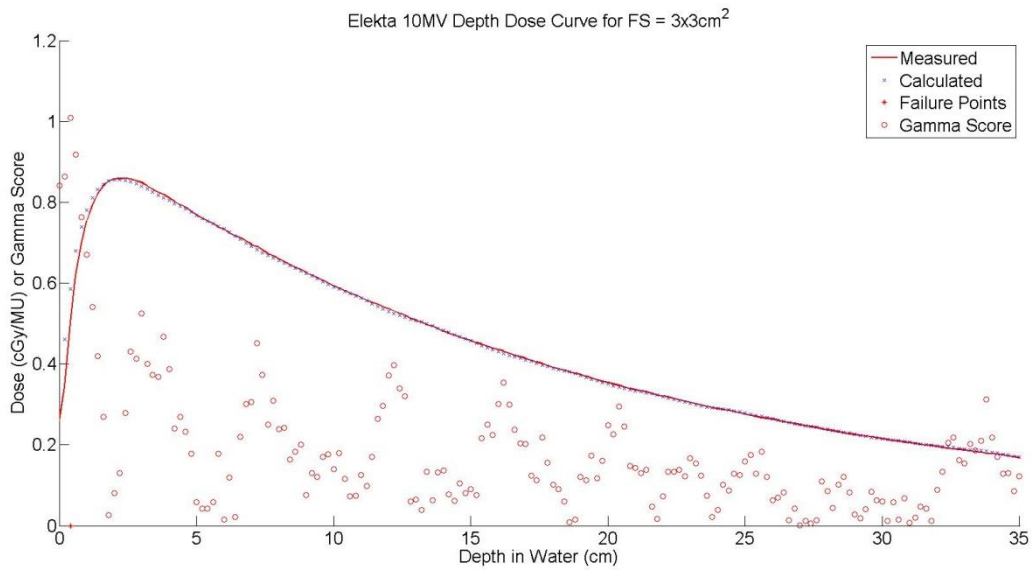


Figure 3.8: Calculated (blue 'x') and measured (red line) depth dose curves for an Elekta 10MV beam for a 3 x 3 cm² field size. Gamma agreement (red circles) for each point is also displayed along with any points (red star) at which a failure to meet the $\pm 2\%/2\text{mm}$ criterion.

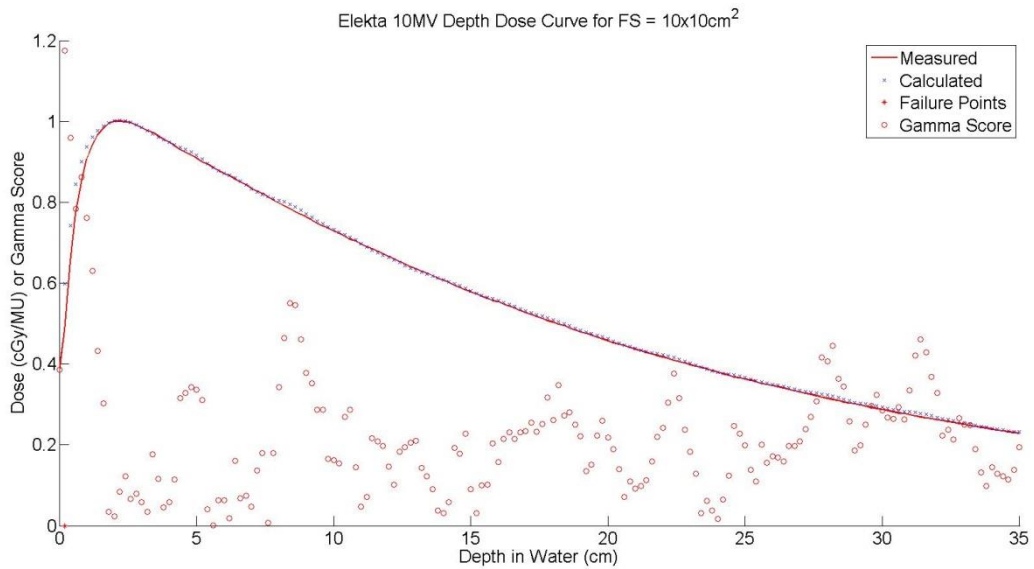


Figure 3.9: Calculated (blue 'x') and measured (red line) depth dose curves for an Elekta 10MV beam for a 10 x 10 cm² field size. Gamma agreement (red circles) for each point is also displayed along with any points (red star) at which a failure to meet the $\pm 2\%/2\text{mm}$ criterion.

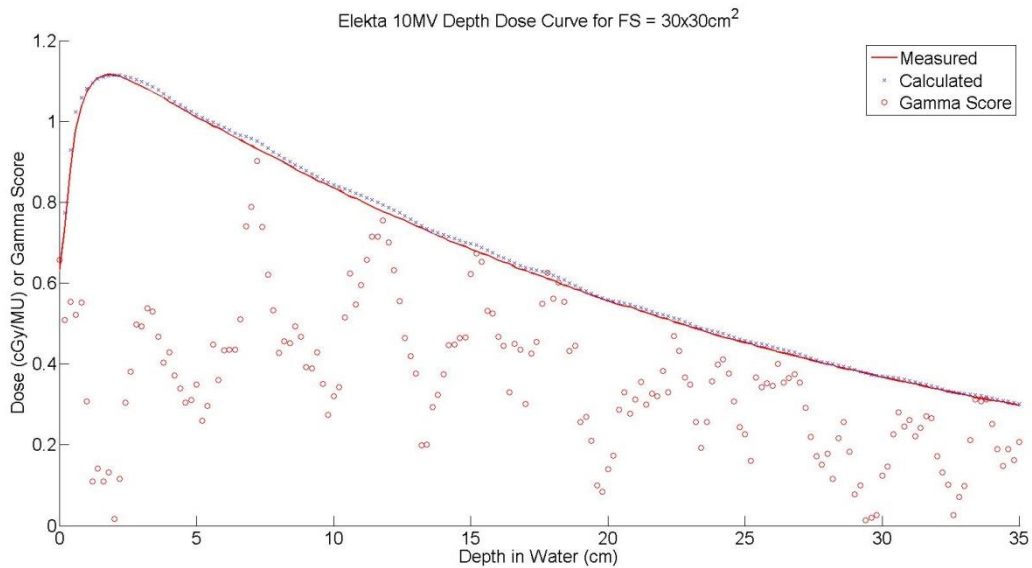


Figure 3.10: Calculated (blue 'x') and measured (red line) depth dose curves for an Elekta 10MV beam for a 30 x 30 cm² field size. Gamma agreement (red circles) for each point is also displayed along with any points (red star) at which a failure to meet the $\pm 2\%/2\text{mm}$ criterion.

3.2.3 Dose Profiles

A comparison of calculated dose profiles to measurements was performed for both Elekta 6MV and 10MV models at depths of d_{max} , 5cm, 10cm, and 20cm for field sizes ranging from 3 x 3 cm² to 30 x 30 cm². An additional comparison at depths of 25cm was performed for the Elekta 10MV model. Gamma analysis with $\pm 2\%/2\text{mm}$ criteria was used as the means of comparison and is summarized in Table 3.4. The percentages of pixels passing for each profile compared are reported in the Appendix (Chapter 6) along with graphs of each comparison. As a representative summary the smallest (3 x 3 cm²), nominal (10 x 10 cm²), and largest (30 x 30 cm²) field sizes are shown for the Elekta 6MV model in Figures 3.11, 3.12, and 3.13, respectively. The same field sizes are shown for the Elekta 10MV model in Figure 3.14, 3.15, and 3.16, respectively.

As can be seen in Figures 3.11 through 3.16, comparisons were performed on both in-plane and cross-plane profiles. The Monte Carlo model however assumes an equal distance from the target for the x-jaws and y-jaws resulting in identical calculated dose profiles for in-plane and cross-plane. As a result, the overlapping calculated data appears as a single profile in the comparisons. The Appendix reports the agreement along both directions, and based on the observed agreement of these results it was decided the assumption of the model was reasonable.

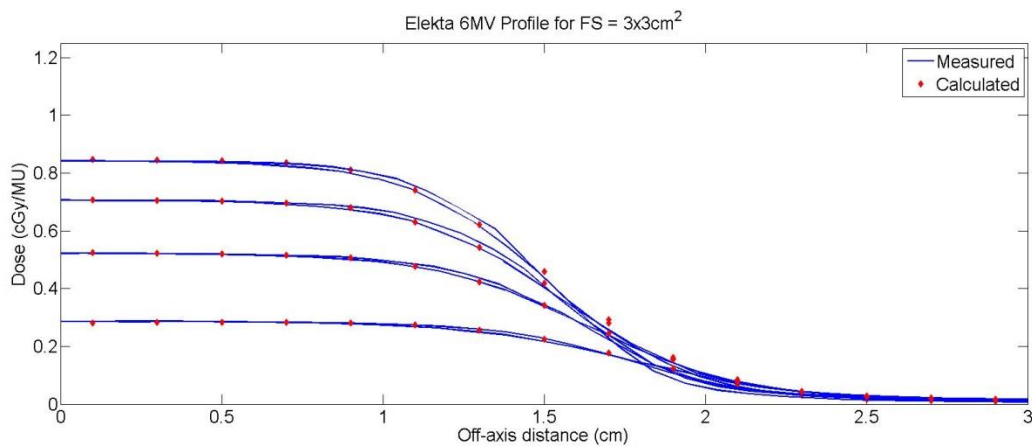


Figure 3.11: Calculated (red diamond) and measured (blue line) dose profiles for an Elekta 6MV beam at a field size of 3 x 3 cm².

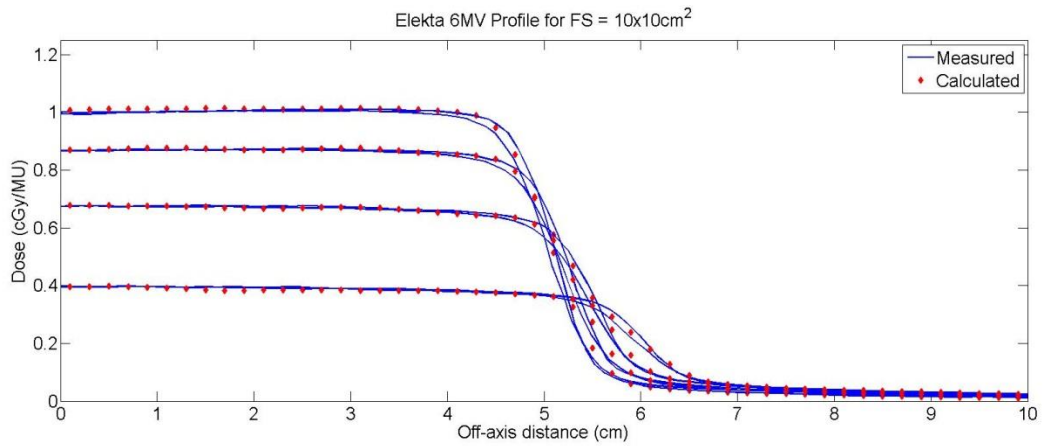


Figure 3.12: Calculated (red diamond) and measured (blue line) dose profiles for an Elekta 6MV beam at a field size of 10 x 10 cm².

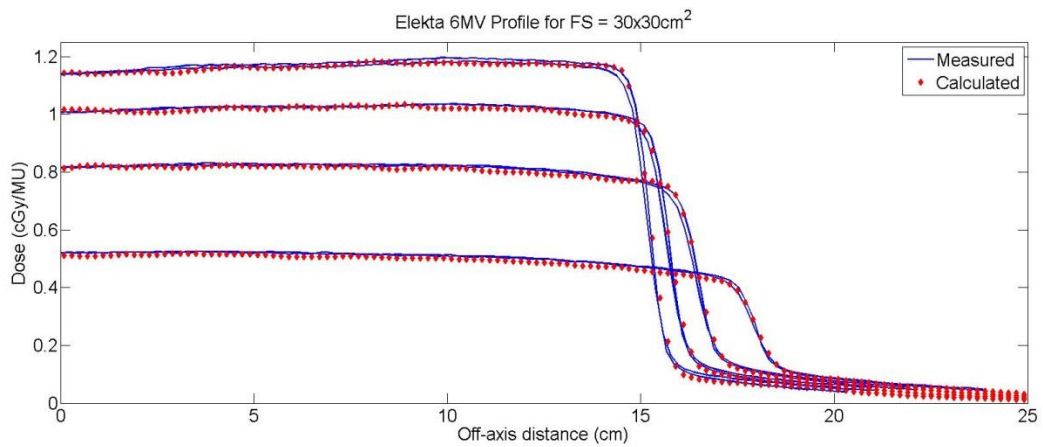


Figure 3.13: Calculated (red diamond) and measured (blue line) dose profiles for an Elekta 6MV beam at a field size of 30 x 30 cm².

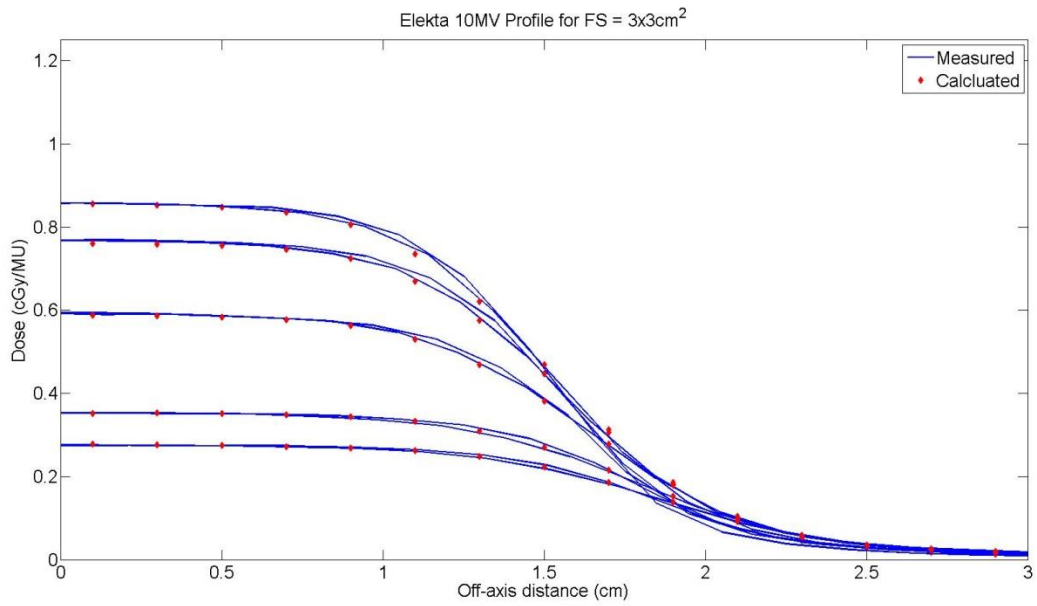


Figure 3.14: Calculated (red diamond) and measured (blue line) dose profiles for an Elekta 10MV beam at a field size of $3 \times 3 \text{ cm}^2$.

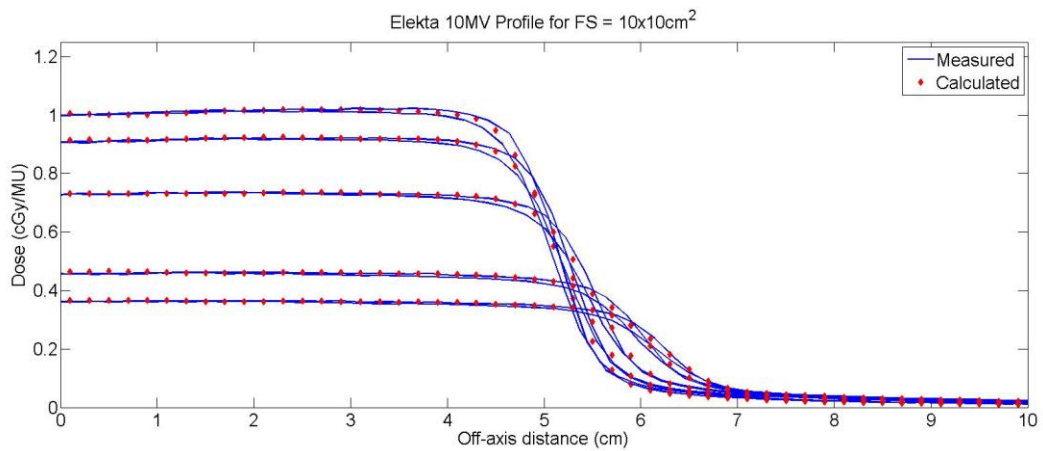


Figure 3.15: Calculated (red diamond) and measured (blue line) dose profiles for an Elekta 10MV beam at a field size of $10 \times 10 \text{ cm}^2$.

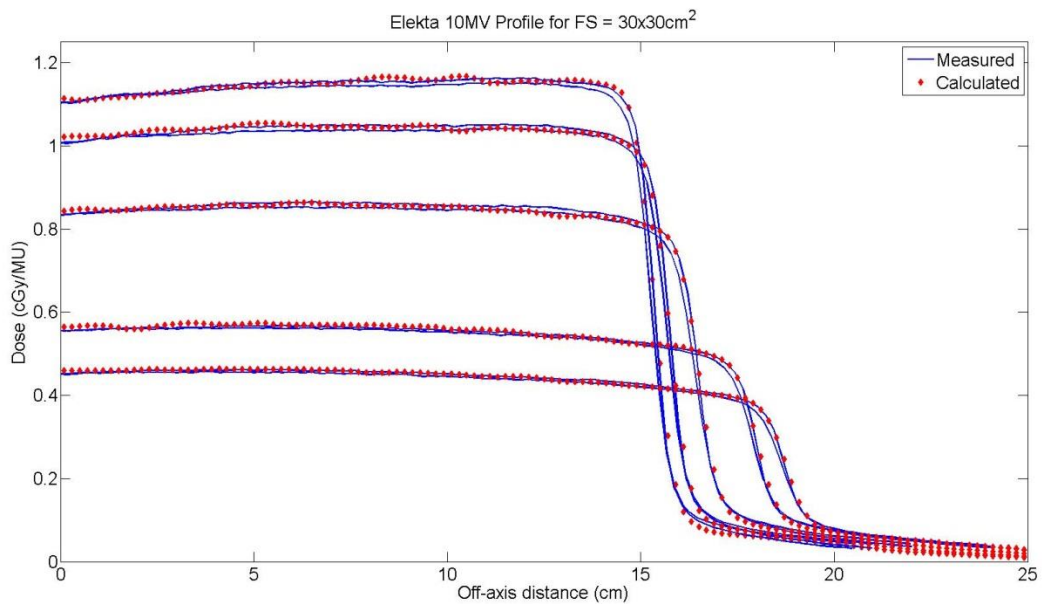


Figure 3.16: Calculated (red diamond) and measured (blue line) dose profiles for an Elekta 10MV beam at a field size of 30 x 30 cm².

Agreement between calculated and measured profile data was assessed using the gamma technique with an evaluation criterion of $\pm 2\%/2\text{mm}$. Profiles at all field sizes and depths showed excellent agreement with the minimum percentage of pixels passing each individual profile being 94.8% and 91.0% for 6MV and 10MV models, respectively. The average percentage of pixels passing the gamma analysis was 99.4% and 99.6% for 6MV and 10MV models respectively. Table 3.4 displays the average agreement by field size for both 6MV and 10MV models.

Validation Results – Dose Profile Data

Field Size (cm ²)	% Pixels Passing	
	Elekta 6MV Model	Elekta 10MV Model
3 x 3	99.0	99.6
5 x 5	99.5	100.0
10 x 10	99.5	100.0
15 x 15	99.4	99.5
20 x 20	99.8	99.9
30 x 30	99.4	99.9

Table 3.4: Gamma comparison agreement for Elekta 6MV and 10MV models using a $\pm 2\%/2\text{mm}$ criterion for measured and calculated dose profile data. Dose profiles were measured and calculated in-plane and cross-plane at depths of d_{max} (1.6cm for 6MV and 2.0cm for 10MV), 5cm, 10cm, 20cm, and 25cm (10MV only).

3.3 Benchmark Testing

3.3.1 Uncertainty

The measurement uncertainty in the dose distributions in the radiochromic film, normalized to the adjacent TLD doses, was estimated in previous studies to be between 2.6% and 3.5% at one standard deviation[12, 35]. By normalizing the film to the TLD dose, the uncertainty related to differences between the film calibration process and the actual film used in benchmarking was minimized. The literature details the estimated uncertainty of the TLD dose[11], the film uniformity, film-to-film variation, and the fit of the sensitometric curve[71].

The estimated single voxel standard error of the mean in the phantom plan simulations was 1.1% using 12 million particles per square centimeter.

3.3.2 Deliver of IMRT H&N Phantom Plan: Point Dose Comparison

Results comparing TLD measurements to predicted doses by the multiple source model are shown in Table 3.5 for the Elekta 6MV model and Table 3.6 for the Elekta 10MV model. TLD capsules were contained within the center of the primary PTV (four capsules), center of the secondary PTV (two capsules) and the center of a mock organ at risk (two capsules). Included in the table are average dose measurements, percent standard deviation from the three deliveries of each plan, a comparison of the DPM predicted dose with measurement expressed as a ratio of calculated dose to measured dose, and, for reference, a comparison of Pinnacle calculated dose with measurement expressed as a ratio of calculated to measured dose.

TLD								
Point Dose Location	Measurement		DPM Calculation			Pinnacle Calculation		
	Avg. (cGy)	% Std. Dev.	Avg. (cGy)	% Std. Dev.	Ratio Calc/Meas	Avg. (cGy)	% Std. Dev.	Ratio Calc/Meas
Pri – SP	644.7	0.7	672.5	1.9	1.043	667.8	0.7	1.036
Pri – SA	654.9	0.1	655.1	1.9	1.000	666.6	0.7	1.018
Pri – IP	634.9	0.7	649.4	2.1	1.023	664.7	0.6	1.047
Pri – IA	646.3	0.7	638.6	2.0	0.988	664.9	0.7	1.029
Pri Avg.					1.014			1.032
Sec – S	527.3	0.4	529.6	1.4	1.004	542.1	0.5	1.028
Sec – I	523.6	0.1	521.6	2.0	0.996	542.1	0.2	1.035
Sec Avg.					1.000			1.032
OAR – S	277.1	0.2	288.2	11.7	1.040	316.7	1.3	1.143
OAR – I	294.6	0.4	304.5	10.0	1.033	339.0	1.4	1.151
OAR Avg.					1.037			1.147

Table 3.5: Point dose comparisons for the Elekta 6MV IMRT head and neck phantom measurements. The measured dose is the averaged dose from the three deliveries of each plan. Comparison to calculated doses by DPM (left) and Pinnacle (right) are expressed as a ratio of calculated to measured doses. Point dose locations are indicated by Pri = Primary PTV, Sec = Secondary PTV, OAR = Organ at Risk, S = Superior, I = Inferior, A = Anterior, P = Posterior.

For the Elekta 6MV model the average agreement between the DPM multiple source model calculation and measurement in the primary PTV was 1.014. The range of calculated to measured dose ratios was from 0.988 to 1.043. The secondary PTV showed an average agreement of 1.000 with a range from 0.996 to 1.004. The averaged ratio for the OAR TLD was 1.037 with a range of 1.033 to 1.040. The poorer agreement with the OAR measured dose could largely be attributed to the high dose gradient in the region due to the OAR's close proximity to the primary PTV.

Point Dose Location	TLD Measurement		DPM Calculation			Pinnacle Calculation		
	Avg. (cGy)	% Std. Dev.	Avg. (cGy)	% Std. Dev.	Ratio Calc/Meas	Avg. (cGy)	% Std. Dev.	Ratio Calc/Meas
Pri – SP	625.1	0.4	676.8	2.0	1.083	677.0	0.8	1.083
Pri – SA	657.2	0.3	645.2	1.7	0.982	672.7	1.5	1.024
Pri – IP	639.4	0.2	658.2	1.7	1.029	676.3	0.7	1.058
Pri – IA	662.1	0.8	653.4	2.1	0.987	686.7	0.7	1.037
Pri Avg.					1.020			1.050
Sec – S	531.0	0.5	529.4	1.4	0.997	550.8	0.0	1.037
Sec – I	526.8	0.7	520.2	1.0	0.987	551.0	0.0	1.046
Sec Avg.					0.992			1.042
OAR – S	252.9	0.9	288.9	7.9	1.142	307.4	0.4	1.216
OAR – I	260.5	0.6	297.4	6.2	1.141	321.5	0.3	1.234
OAR Avg.					1.142			1.225

Table 3.6: Point dose comparisons for the Elekta 10MV IMRT head and neck phantom measurements. The measured dose is the averaged dose from the three deliveries of each plan. Comparison to calculated doses by DPM (left) and Pinnacle (right) are expressed as a ratio of calculated to measured doses. Point dose locations are indicated by Pri = Primary PTV, Sec = Secondary PTV, OAR = Organ at Risk, S = Superior, I = Inferior, A = Anterior, P = Posterior.

Results for the Elekta 10MV model show an average agreement between the DPM code and measurement in the primary PTV of 1.020. The range contributing to this average was from 0.982 to 1.083. The poor agreement seen in the superior posterior TLD is suspected to be due to its proximity to a high dose gradient. Further examination of the dose field showed that a setup error as small as 1.5mm could contribute to the 8% change in dose. Agreement in the secondary PTV was 0.992 with a range of 0.987 to 0.997. Comparisons in the OAR showed an average agreement of 1.142 with a range of 1.141 to 1.142. Similar to the 6MV model, the OAR showed an overall poorer agreement with measurement. This was again attributed to the high dose gradient in the region.

While the benchmarking of the multiple source model was based exclusively on measurement, comparisons to doses calculated by Pinnacle are included as means of comparison against an actively used and state of the art treatment planning system dose calculation algorithm. A comparison between average agreement of DPM to measured doses and Pinnacle to measured doses shows superior performance for the Monte Carlo based calculation technique.

3.3.3 Delivery of IMRT H&N Phantom Plan: Dose Profile and Gamma Map Comparison

Dose profile comparison between the multiple source model and measurement are shown for all three major planes in Figures 3.17, 3.18, 3.19 for the 6MV model and Figures 3.20, 3.21, and 3.22 for the 10MV model. These comparisons are meant to be a qualitative assessment of the models ability to predict complex dose distributions across the volume of the PTV. All profiles showed good agreement between calculation and measurement.

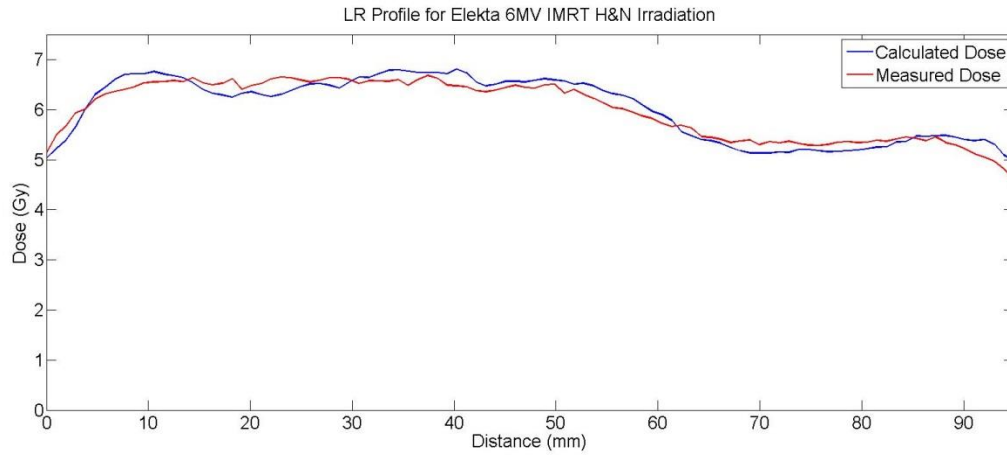


Figure 3.17: A comparison of the lateral (left to right) profile from the axial film of an IMRT H&N delivery for the 6MV model (delivery #1).

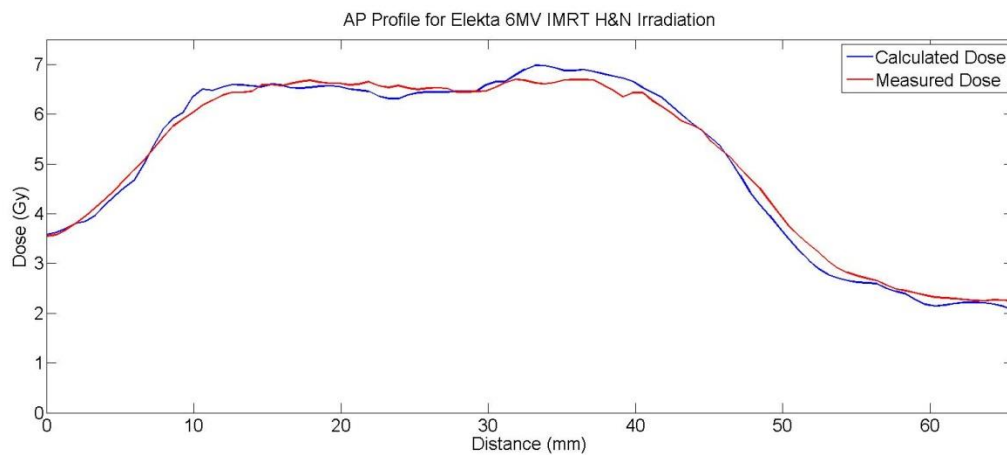


Figure 3.18: A comparison of the AP (anterior to posterior) profile from the axial film of an IMRT H&N delivery for the 6MV model (delivery #1).

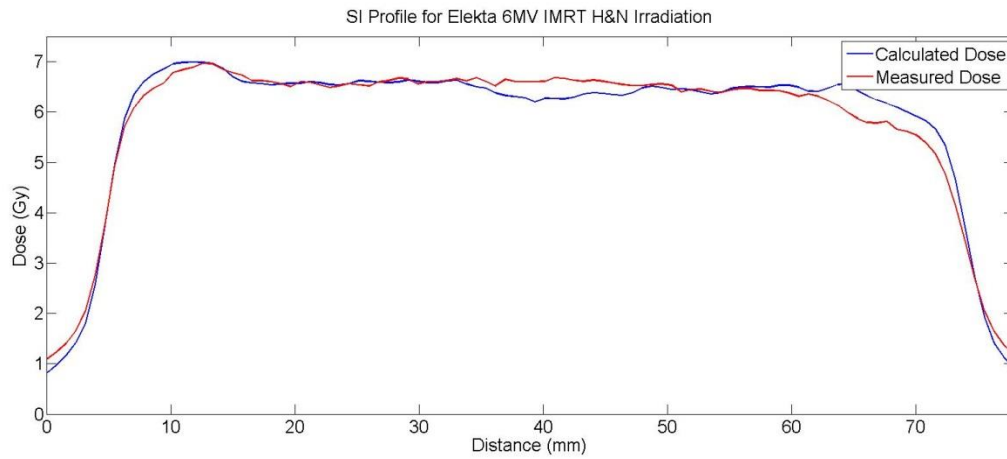


Figure 3.19: A comparison of the SI (superior to inferior) profile from the axial film of an IMRT H&N delivery for the 6MV model (delivery #1).

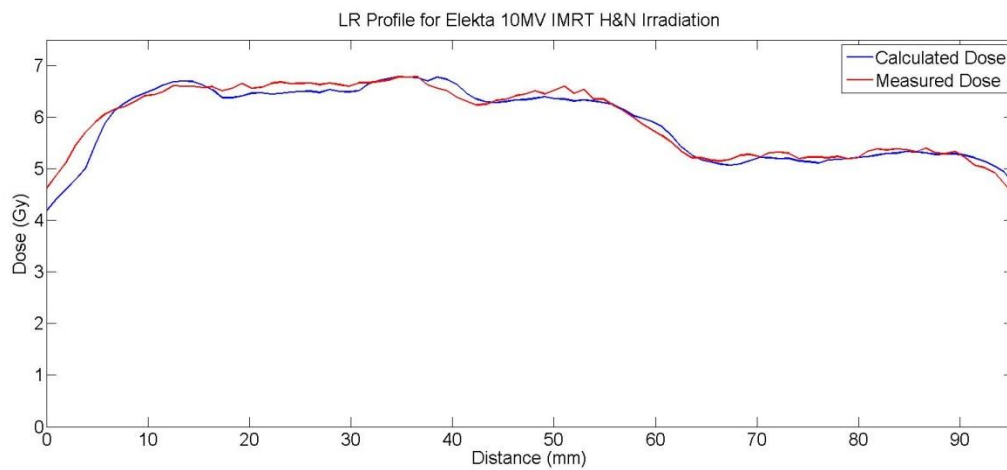


Figure 3.20: A comparison of the lateral (left to right) profile from the axial film of an IMRT H&N delivery for the 10MV model (delivery #1).

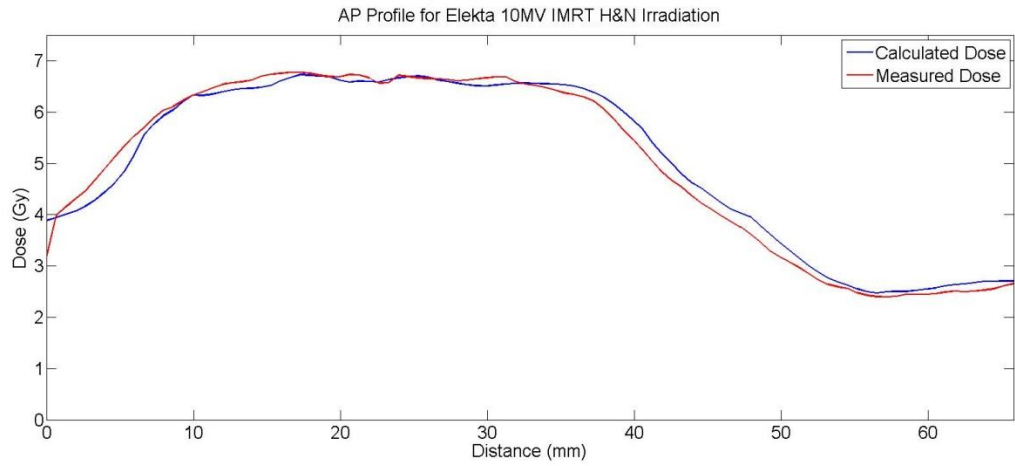


Figure 3.21: A comparison of the AP (anterior to posterior) profile from the axial film of an IMRT H&N delivery for the 10MV model (delivery #1).

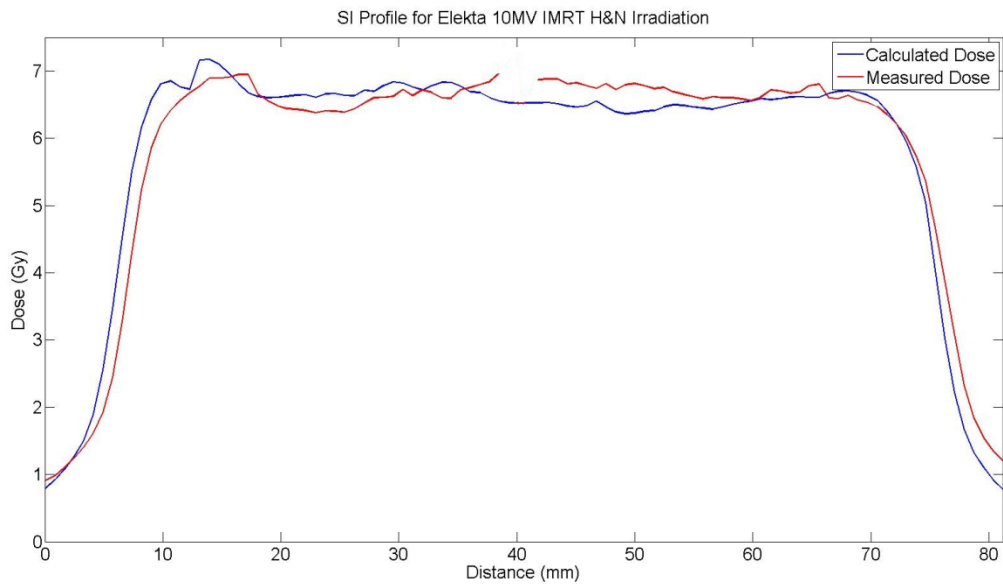


Figure 3.22: A comparison of the SI (superior to inferior) profile from the axial film of an IMRT H&N delivery for the 10MV model (delivery #1).

To evaluate the models performance at describing the penumbra, MLC leakage, rounded leaf tips, and leaf transmission in highly modulated fields, gamma analysis was performed using a $\pm 3\%/2\text{mm}$ criterion. The analysis considers dose differences as relative percentage and the distance to agreement to assess overall agreement and identify locations of difficulty to the model. The resulting gamma maps from a single irradiation in the axial and sagittal plans are shown in Figure 3.23 and Figure 3.24 for the 6MV model and Figure 3.25 and Figure 3.26 for the 10MV model. Gamma maps for all three deliveries of each nominal energy are included in the Appendix. For the IMRT head and neck plan, the average percent of pixels passing for the 6MV comparison was 87.2% with a range of 82.5% to 91.4%. The 10MV comparison averaged 90.5% of pixels passing the $\pm 3\%/2\text{mm}$ criterion with a range of 86.4% to 95.9%. Table 3.7 reports the average agreement in the sagittal and axial planes for both the 6MV and 10MV models.

	Elekta 6MV		Elekta 10MV	
	Axial	Sagittal	Axial	Sagittal
Delivery #1	91.4	88.9	91.3	87.9
Delivery #2	87.6	86.7	91.6	86.4
Delivery #3	82.5	86.1	95.9	87.3
Average	87.2	87.3	92.9	87.2

Table 3.7: Percentage of pixels passing a $\pm 3\%/2\text{mm}$ gamma criterion for IMRT head and neck plans for both Elekta 6MV and 10MV models. Agreement was evaluated in both the axial and sagittal planes for three deliveries of each plan.

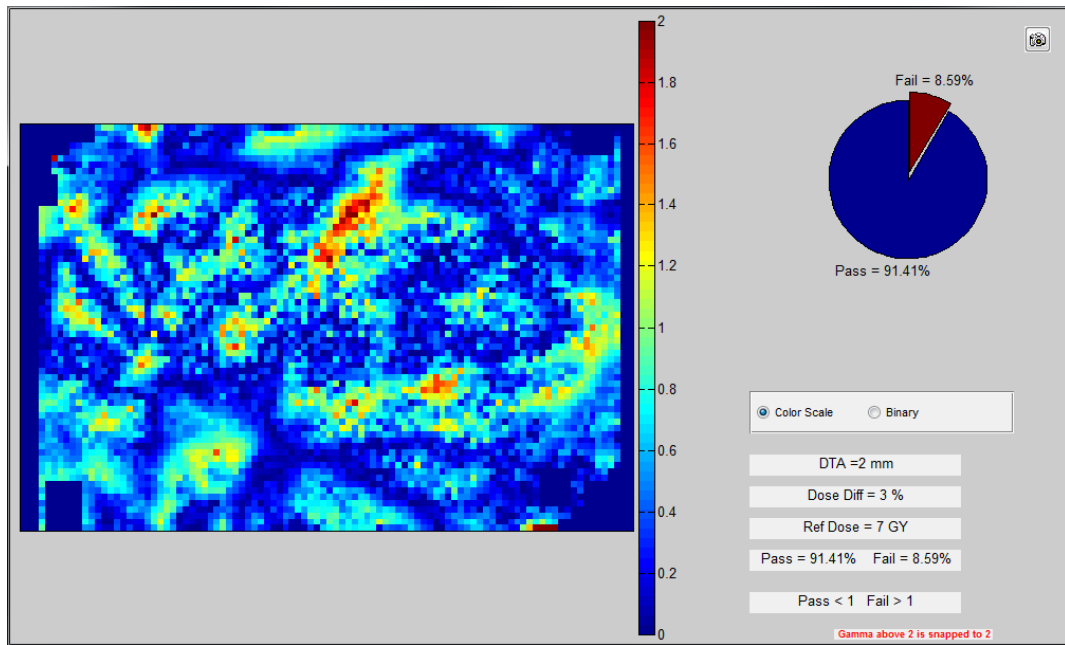


Figure 3.23: IMRT head and neck delivery comparison for the axial plane of delivery #1 for the Elekta 6MV model. Agreement was evaluated using a $\pm 3\%/2\text{mm}$ gamma criterion and 91.4% of pixels passed.

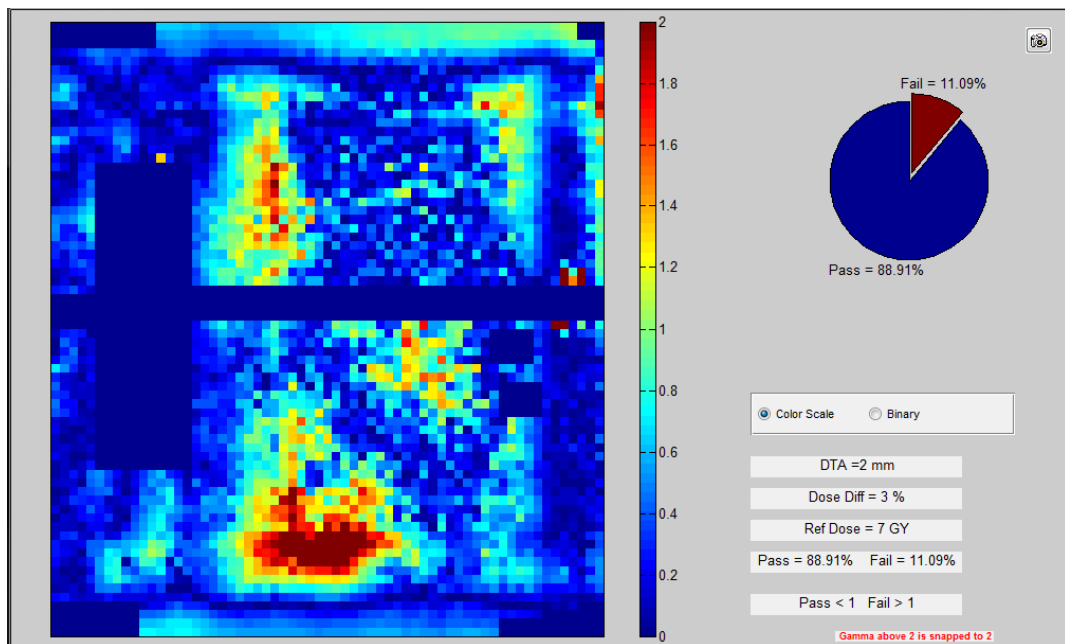


Figure 3.24: IMRT head and neck delivery comparison for the sagittal plane of delivery #1 for the Elekta 6MV model. Agreement was evaluated using a $\pm 3\%/2\text{mm}$ gamma criterion and 88.9% of pixels passed.

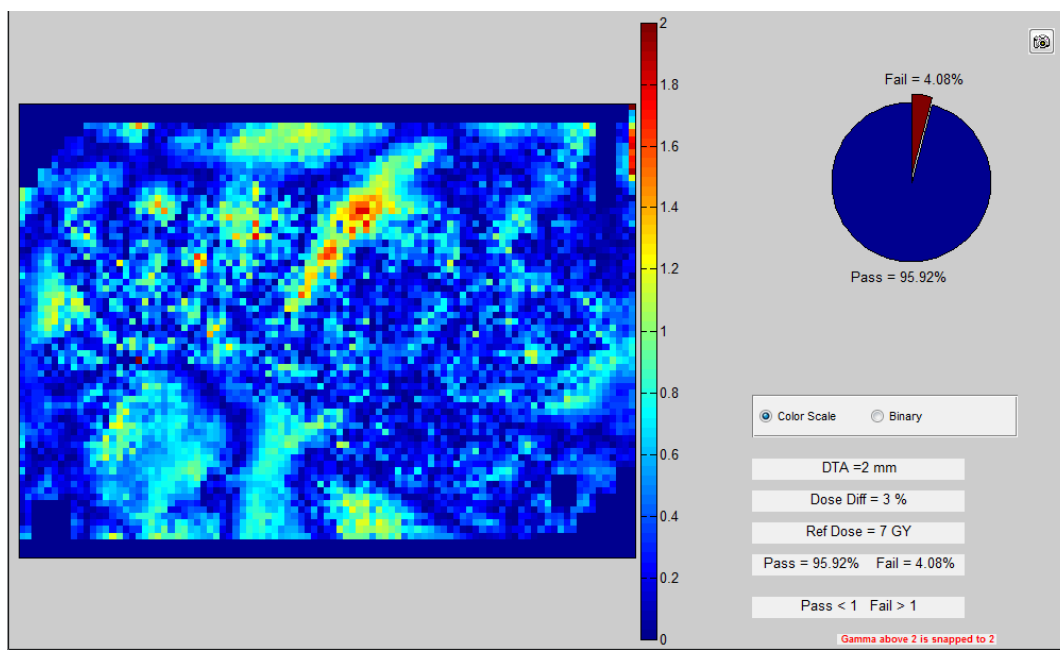


Figure 3.25: IMRT head and neck delivery comparison for the axial plane of delivery #3 for the Elekta 10MV model. Agreement was evaluated using a $\pm 3\%/2\text{mm}$ gamma criterion and 95.9% of pixels passed.

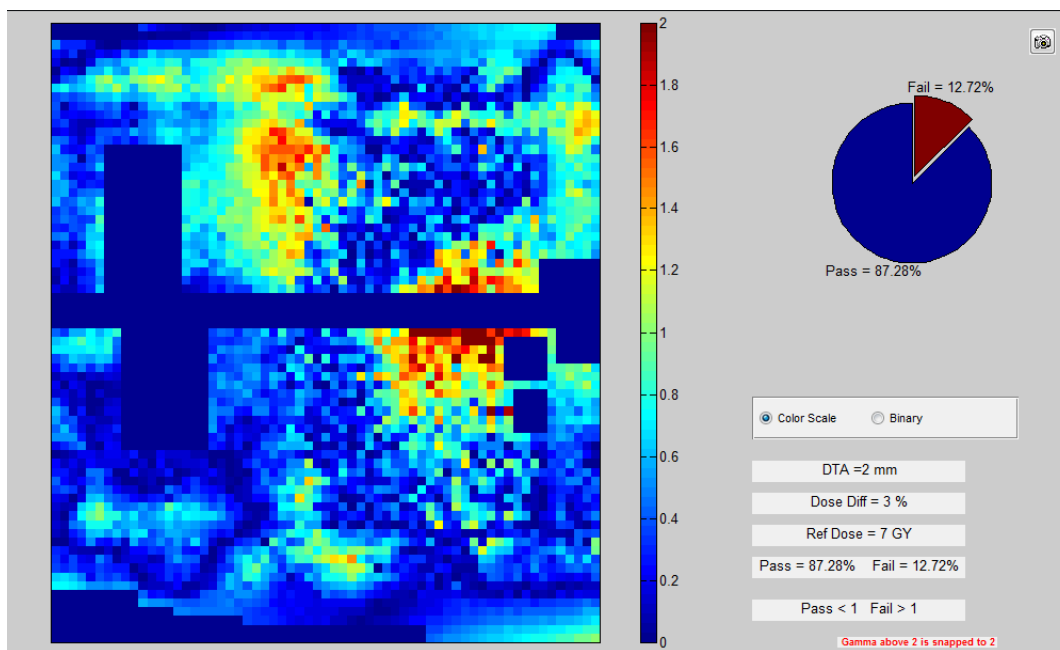
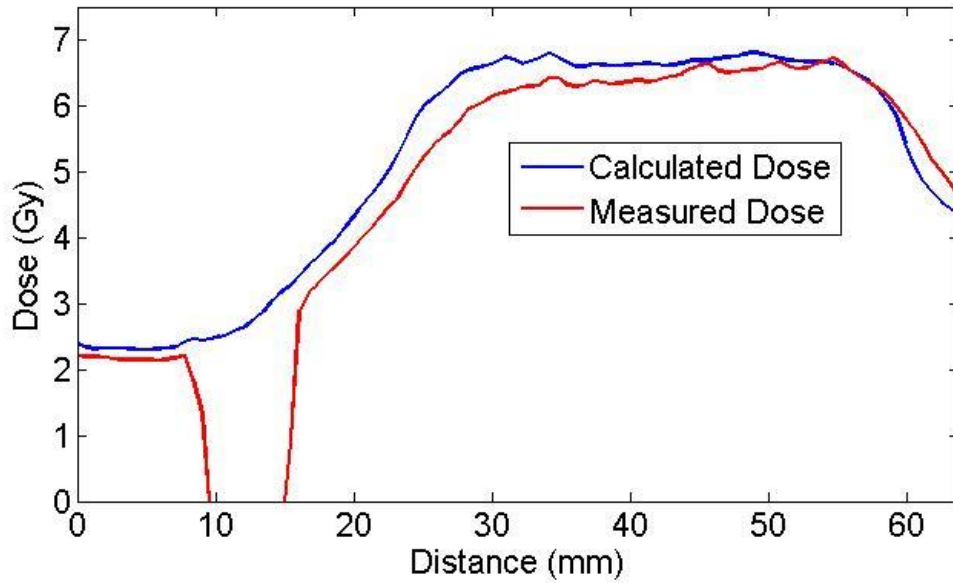


Figure 3.26: IMRT head and neck delivery comparison for the sagittal plane of delivery #3 for the Elekta 10MV model. Agreement was evaluated using a $\pm 3\%/2\text{mm}$ gamma criterion and 87.3% of pixels passed.

Qualitative evaluation of the axial gamma maps revealed no consistent failure regions in the dose distribution for either the 6MV or 10MV comparisons. Failure regions of the sagittal gamma maps were consistently along the posterior edge of the PTV in the superior film piece for both 6MV and 10MV comparisons. This is largely attributed to the sensitivity of the comparison to the registration of film to the phantom. Because the sagittal comparisons consist of two pieces of film that need to be aligned during scanning, the registration uncertainty is higher than for the axial plane which consists of single piece of film. Dose profiles shown in Figure 3.27 suggest that there could be an approximately 1mm offset in the alignment of the superior piece of film with respect to the inferior piece of film. Even with the increased registration uncertainty, passing rates were above the pre-established threshold of 85%.

AP Profile for Elekta 10MV IMRT H&N Irradiation (Superior Film Piece)



AP Profile for Elekta 10MV IMRT H&N Irradiation (Inferior Film Piece)

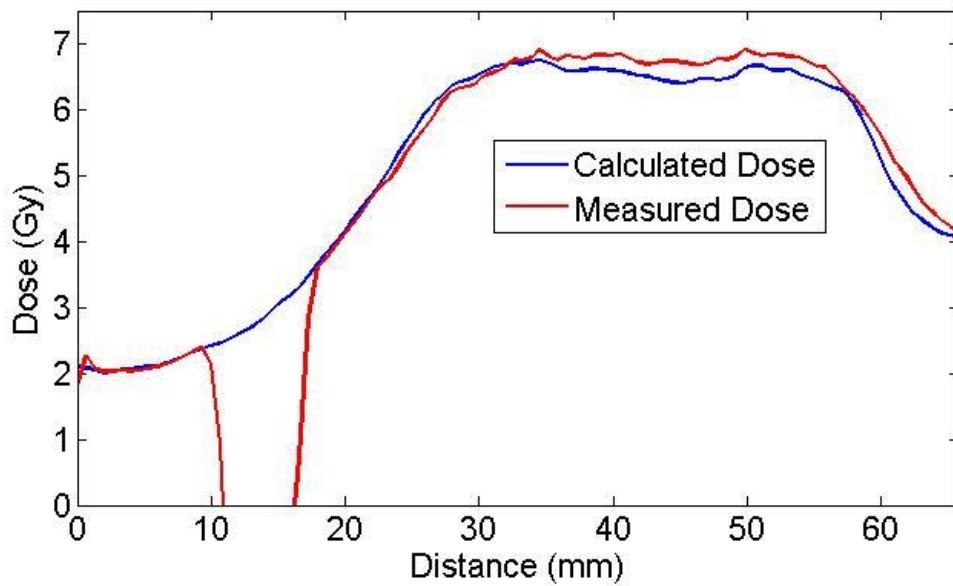


Figure 3.27: Dose profile comparison for IMRT head and neck delivery for 10MV Elekta model. The top profile is along the anteroposterior direction of the superior film piece, and the bottom is along the anteroposterior direction of the inferior film piece.

3.3.4 Delivery of SBRT Thorax Phantom Plan: Point Dose Comparison

The results to point dose comparisons between the developed model and TLD measurements in the anthropomorphic thorax phantom are shown in Table 3.8 and Table 3.9. Double packed TLD were contained in the center of the target (two), in the heart (one), and in the spinal cord (one). The table includes average dose measurements, percent standard deviation from the three deliveries of each plan, a comparison of the DPM predicted dose with measurement expressed as a ratio of calculated dose to measured dose, and, for reference, a comparison of Pinnacle calculated doses with measurement expressed as a ratio of measured to calculated dose.

TLD								
	Measurement		DPM Calculation			Pinnacle Calculation		
Point Dose	Avg.	% Std.	Avg.	% Std.	Ratio	Avg.	% Std.	Ratio
Location	(cGy)	Dev.	(cGy)	Dev.	Calc/Meas	(cGy)	Dev.	Calc/Meas
PTV – S	657.6	0.4	677.2	0.7	1.030	658.0	3.0	1.001
PTV – I	659.8	0.3	679.1	0.7	1.029	661.7	2.8	1.003
PTV Avg.					1.030			1.002
OAR – Heart	99.0	0.2	107.4	2.1	1.085	99.6	5.8	1.006
OAR – Cord	122.6	0.4	130.3	1.8	1.062	136.8	2.4	1.115

Table 3.8: Point dose comparisons for the Elekta 6MV SBRT lung phantom measurements.

The measured dose is the averaged dose from the three deliveries of each plan. Comparison to calculated doses by DPM (left) and Pinnacle (right) are expressed as a ratio of calculated to measured doses. Point dose locations are indicated by PTV = Planning Target Volume, OAR = Organ at Risk, S = Superior, I = Inferior.

For the Elekta 6MV model the average agreement between the DPM multiple source model calculation and measurement in the PTV was 1.030. The range of calculated to measured dose ratios was from 1.029 to 1.030. The ratio for the heart TLD was 1.085, and the ratio for the cord TLD was 1.062.

Point Dose Location	TLD Measurement		DPM Calculation			Pinnacle Calculation		
	Avg. (cGy)	% Std. Dev.	Avg. (cGy)	% Std. Dev.	Ratio Calc/Meas	Avg. (cGy)	% Std. Dev.	Ratio Calc/Meas
PTV – S	664.5	0.2	679.1	1.0	1.022	672.8	3.1	1.012
PTV – I	675.0	0.7	681.6	0.8	1.010	674.9	3.1	1.000
PTV Avg.					1.016			1.006
OAR – Heart	99.1	0.2	105.2	4.1	1.061	100.5	7.1	1.014
OAR – Cord	122.5	0.8	130.0	0.0	1.061	136.2	2.9	1.112

Table 3.9: Point dose comparisons for the Elekta 10MV SBRT lung phantom measurements.

The measured dose is the averaged dose from the three deliveries of each plan. Comparison to calculated doses by DPM (left) and Pinnacle (right) are expressed as a ratio of calculated to measured doses. Point dose locations are indicated by PTV = Planning Target Volume, OAR = Organ at Risk, S = Superior, I = Inferior.

The average agreement between the DPM model and the PTV for the Elekta 10MV model was 1.016. The range of the values for the PTV agreement was from 1.010 to 1.022. The calculated to measured ratio for both the heart and cord TLDs was 1.061.

It is important to note that while the OAR calculated doses showed poorer agreement with measurements for 6MV and 10MV models, the uncertainty in the measured dose is unknown at such low doses. The standards used for low dose measurements are done at doses of 8Gy

and 3Gy, nearly 3 times the dose of both the heart and cord measurement for the lower of the two standard doses. At doses near 1Gy, as seen in both of the OAR TLD, the RPC does not have data documenting the accuracy of their TLD measurement process for phantom irradiations.

Even though the benchmarking of the multiple source model was based exclusively on measurement, comparisons to doses calculated by Pinnacle are included as means of comparison against an actively used and state of the art treatment planning system dose calculation algorithm. A direct comparison between the DPM calculated doses and the Pinnacle calculated doses show the DPM calculation to be comparable with measurement results in the OARs and within the PTVs.

3.3.5 Delivery of SBRT Thorax Phantom Plan: Dose Profile and Gamma Map Comparison

Dose profile comparison between the multiple source model and measurement are shown for all three major planes in Figures 3.28, 3.29, 3.30 for the 6MV model and Figures 3.31, 3.32, and 3.33 for the 10MV model. These comparisons are meant to be a qualitative assessment of the models ability to predict complex dose distributions across the volume of the PTV. All profiles showed good agreement between calculation and measurement.

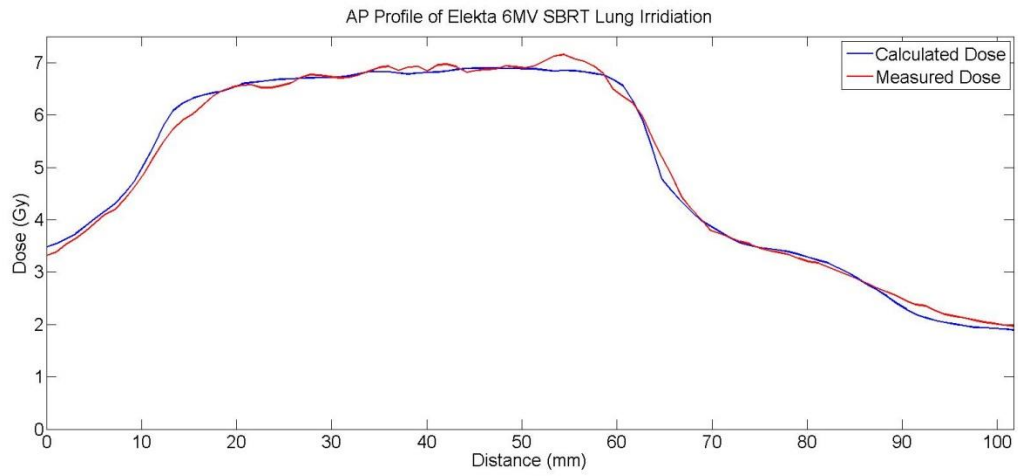


Figure 3.28: A comparison of the lateral (left to right) profile from the axial film of an SBRT lung delivery for the 6MV model (delivery #1).

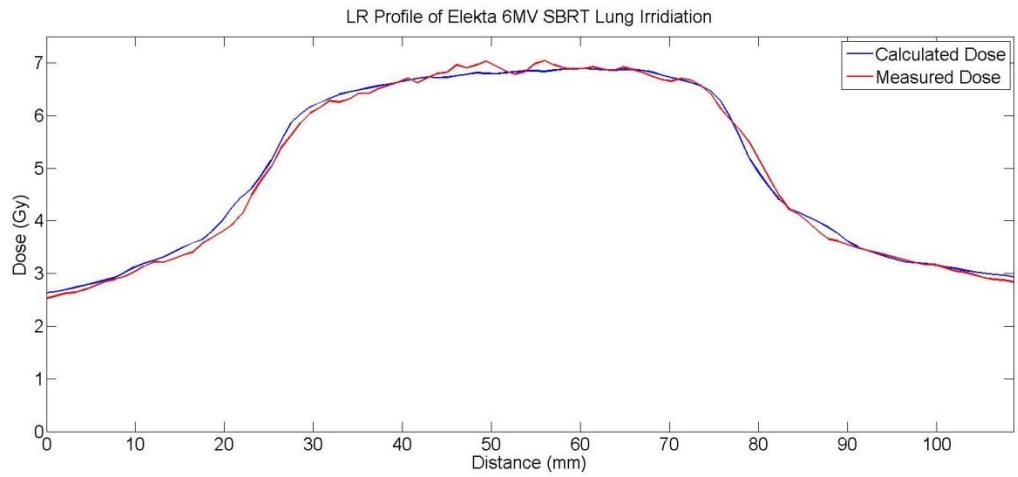


Figure 3.29: A comparison of the AP (anterior to posterior) profile from the axial film of an SBRT lung delivery for the 6MV model (delivery #1).

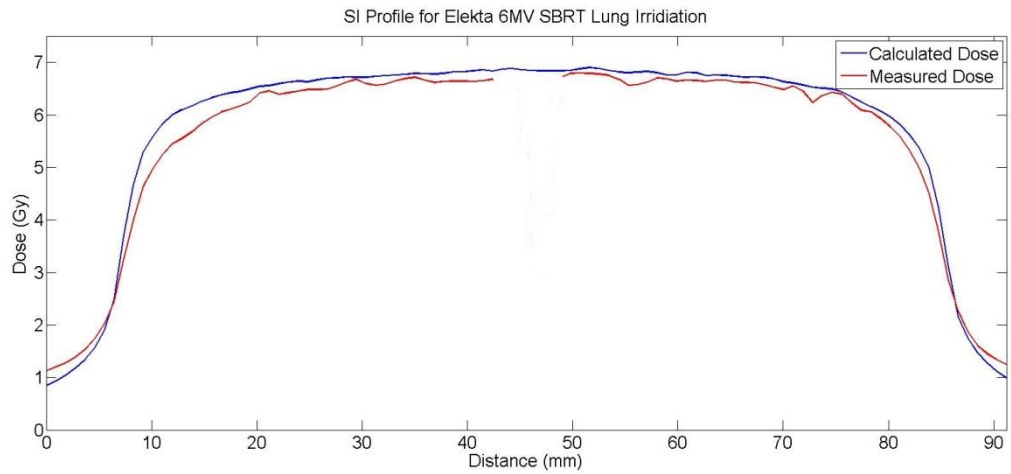


Figure 3.30: A comparison of the SI (superior to inferior) profile from the sagittal film of an SBRT lung delivery for the 6MV model (delivery #1).

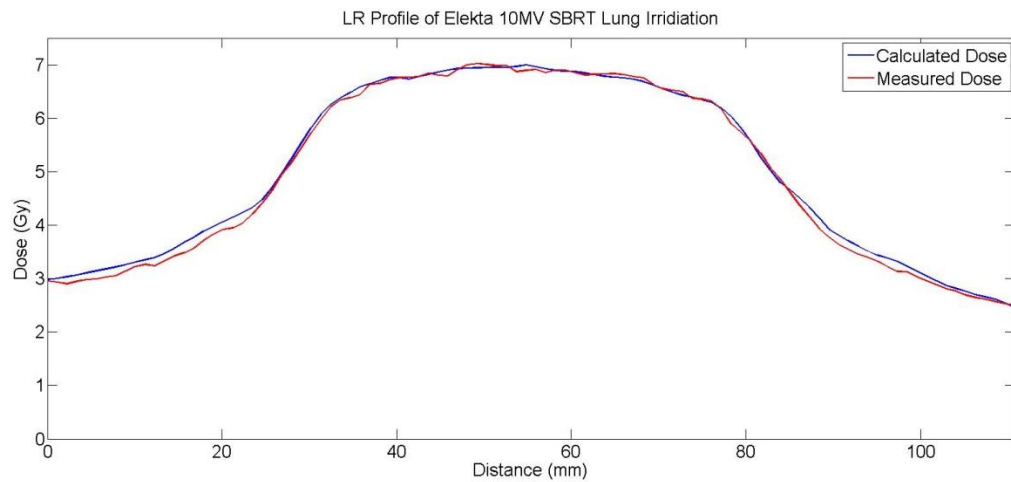


Figure 3.31: A comparison of the lateral (left to right) profile from the axial film of an SBRT lung delivery for the 10MV model (delivery #1).

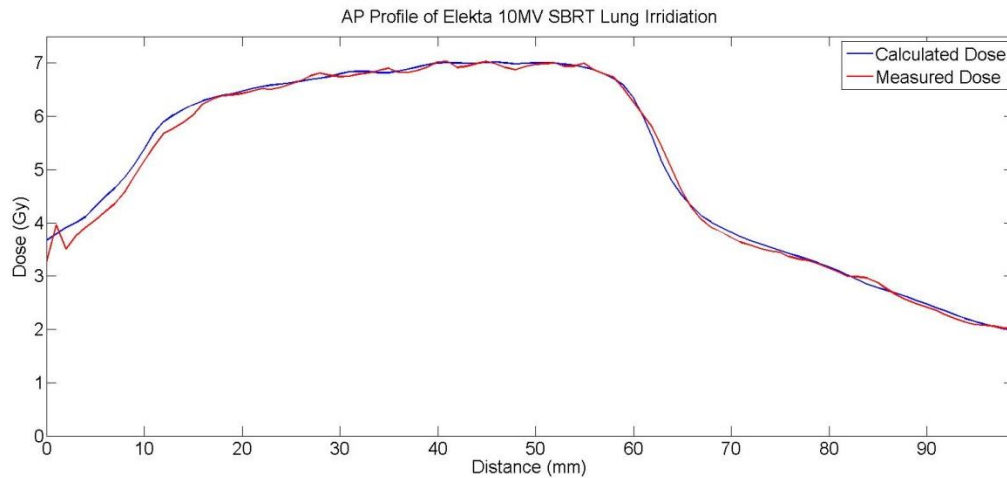


Figure 3.32: A comparison of the AP (anterior to posterior) profile from the axial film of an SBRT lung delivery for the 10MV model (delivery #1).

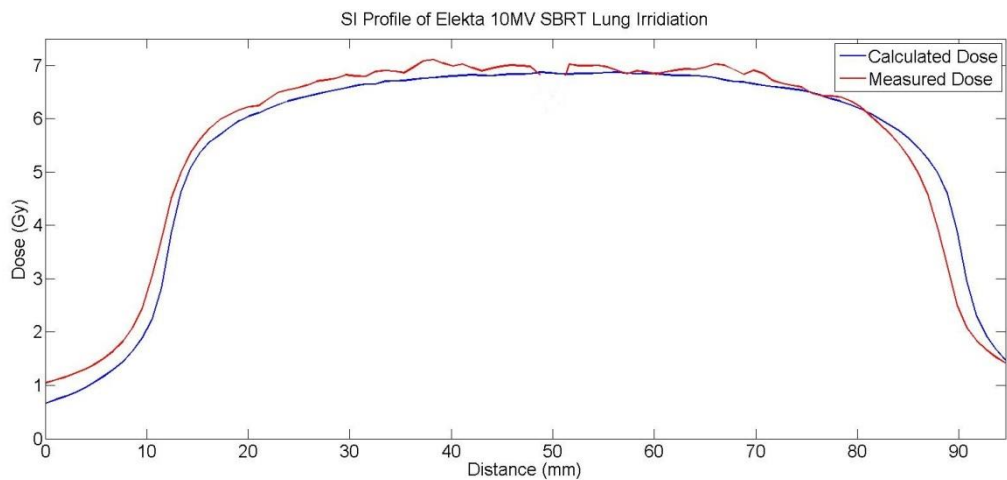


Figure 3.33: A comparison of the SI (superior to inferior) profile from the sagittal film of an SBRT lung delivery for the 10MV model (delivery #1).

The model's ability to describe the beam penumbra, MLC leakage, rounded leaf tips, and leaf transmission in unmodulated fields in a heterogeneous medium provided by the lung phantom was evaluated using the gamma technique with a $\pm 3\%/2\text{mm}$ criterion. The analysis considers the dose differences as a percentage of the maximum dose and distance to

agreement to assess overall agreement between dose distributions calculated by the multiple source model and measured by the radiochromic film in the phantom. In this way resulting gamma maps can be used to identify areas where the model may be deficient while allowing for positional measurement uncertainty to be accounted for in the distance to agreement criterion.

The gamma maps for a single irradiation and comparison to source model calculation for the 6MV model are showing in Figures 3.34, 3.35, and 3.36 for the axial, sagittal, and coronal planes respectively. Gamma maps for each delivery are included in the Appendix. The average agreement, expressed as a percentage of pixels passing the gamma criterion, were 86.8%, 86.9%, and 87.8% for axial, sagittal, and coronal planes, respectively. Agreement for the axial plane ranged from 85.3% to 89.0%. Agreement for the sagittal plane ranged from 85.9% to 87.7%, and the range of agreement for the coronal plane was 84.2% to 93.9%.

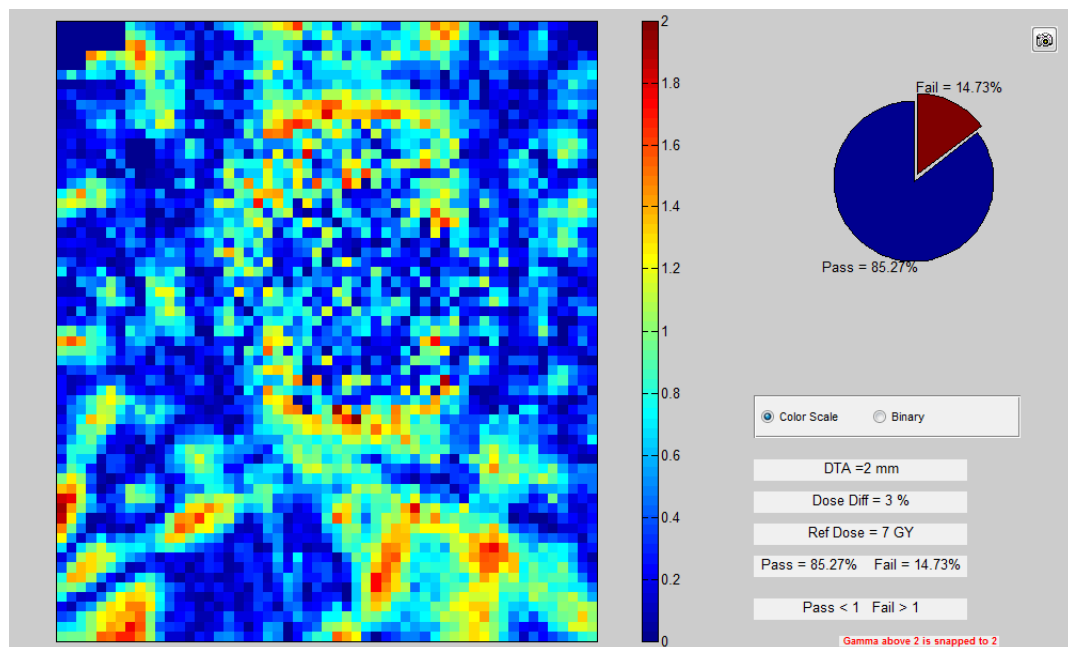


Figure 3.34: Lung SBRT delivery comparison for the axial plane of delivery #1 for the Elekta 6MV model. Agreement was evaluated using a $\pm 3\%/2\text{mm}$ gamma criterion and 85.3% of pixels passed.

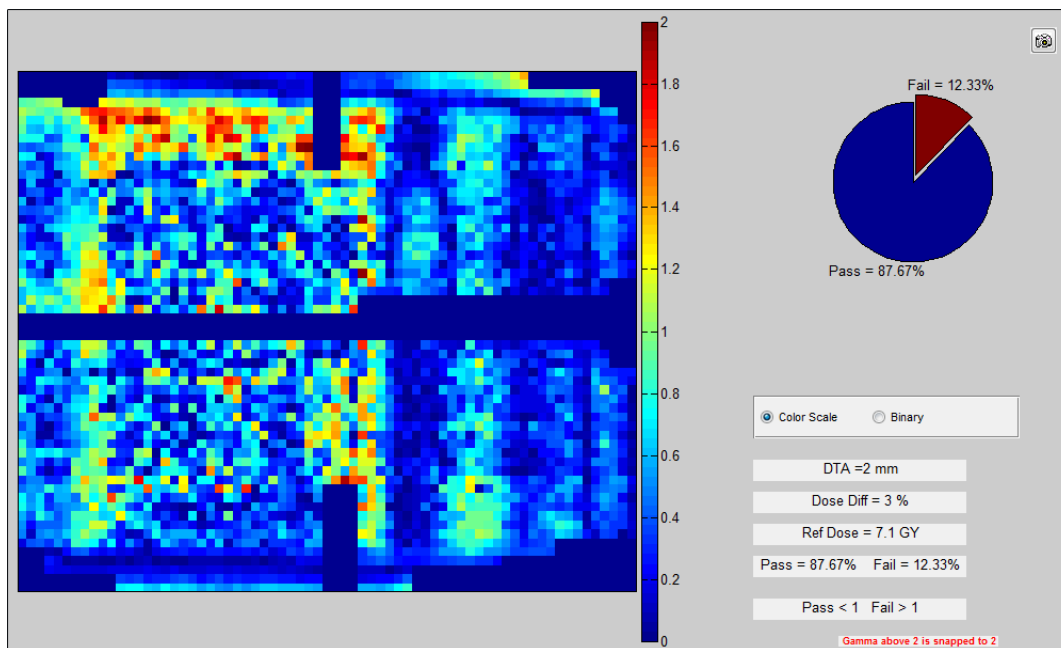


Figure 3.35: Lung SBRT delivery comparison for the sagittal plane of delivery #1 for the Elekta 6MV model. Agreement was evaluated using a $\pm 3\%/2\text{mm}$ gamma criterion and 87.7% of pixels passed.

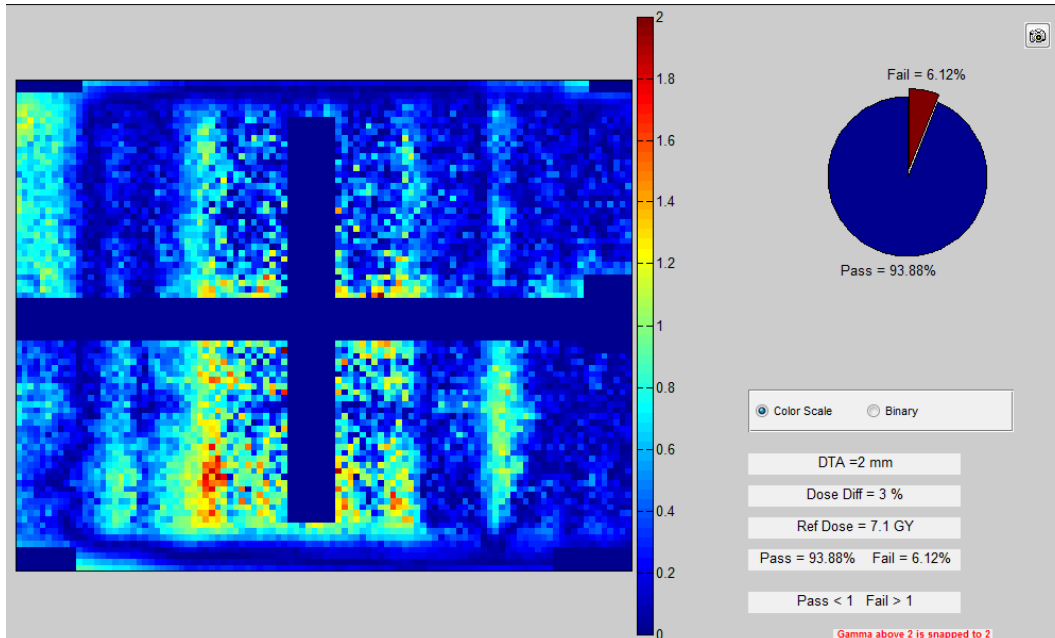


Figure 3.36: Lung SBRT delivery comparison for the coronal plane of delivery #1 for the Elekta 6MV model. Agreement was evaluated using a $\pm 3\%/2\text{mm}$ gamma criterion and 93.9% of pixels passed.

The gamma maps corresponding to the comparison of a single irradiation to the calculated dose of the 10MV source model are showing in Figures 3.37, 3.38, and 3.39 for axial, sagittal, and coronal planes, respectively. Gamma maps from all other deliveries are included in the Appendix for reference. The average agreement was 90.2%, 88.3%, and 89.5% for axial, sagittal, and coronal planes, respectively. The range of values for the axial plane was 86.2% to 96.5%, for the sagittal plane 85.2% to 90.8%, and for the coronal plane 85.3% to 92.6%.

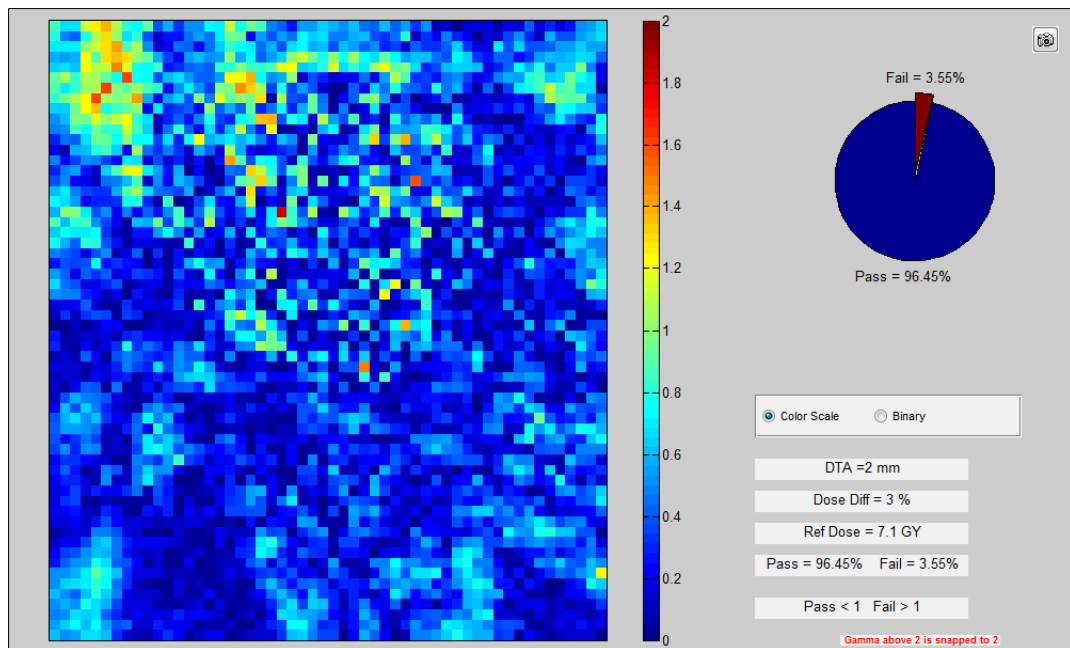


Figure 3.37: Lung SBRT delivery comparison for the axial plane of delivery #1 for the Elekta 10MV model. Agreement was evaluated using a $\pm 3\%/2\text{mm}$ gamma criterion and 96.5% of pixels passed.

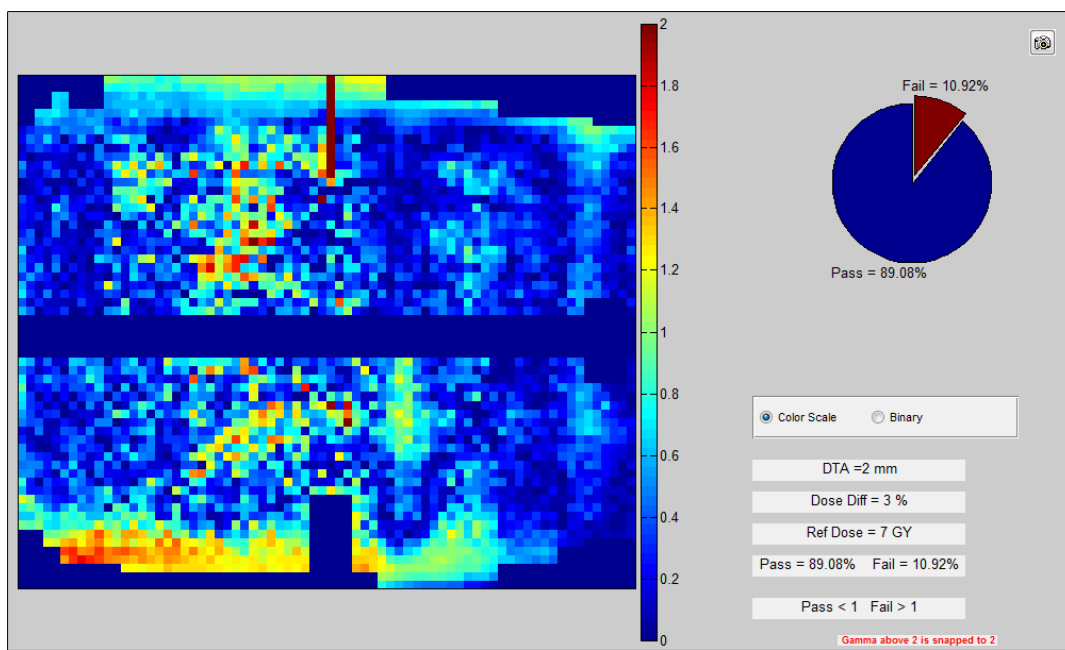


Figure 3.38: Lung SBRT delivery comparison for the sagittal plane of delivery #1 for the Elekta 10MV model. Agreement was evaluated using a $\pm 3\%/2\text{mm}$ gamma criterion and 89.1% of pixels passed.

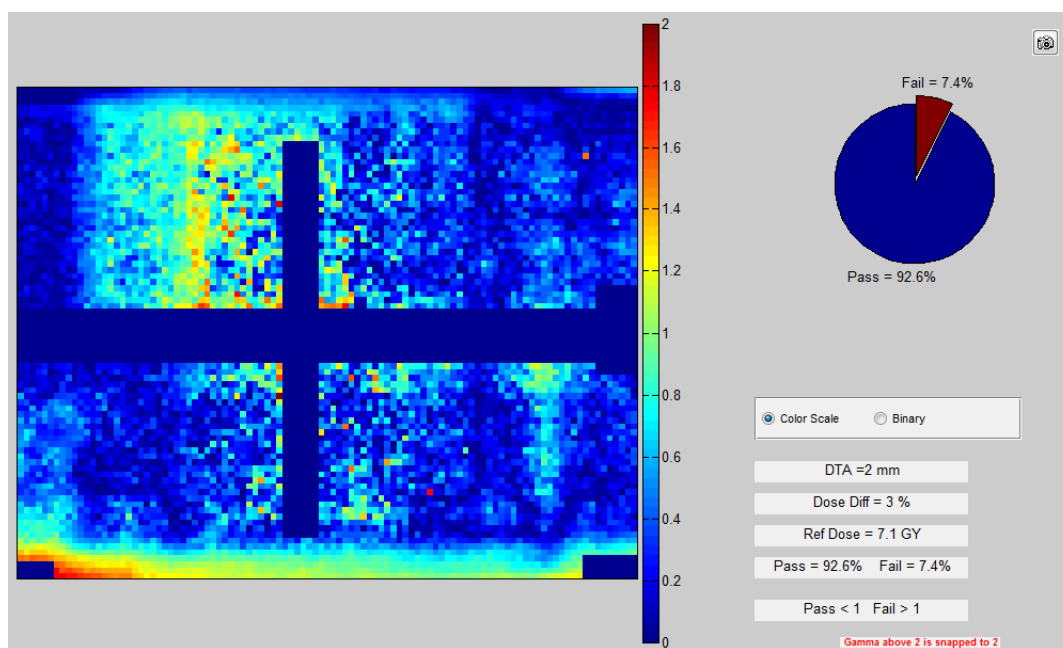


Figure 3.39: Lung SBRT delivery comparison for the coronal plane of delivery #1 for the Elekta 10MV model. Agreement was evaluated using a $\pm 3\%/2\text{mm}$ gamma criterion and 92.6% of pixels passed.

The passing rate of comparisons for each plane for all three deliveries with respect to the DPM source model calculation is shown for both 6MV and 10MV models in Table 3.10.

	Elekta 6MV			Elekta 10MV		
	Axial	Sagittal	Coronal	Axial	Sagittal	Coronal
Delivery #1	85.3	87.7	93.9	96.5	89.1	92.6
Delivery #2	86.2	85.9	85.3	86.2	90.8	85.3
Delivery #3	89.0	87.0	84.2	88.1	85.2	90.5
Average	86.8	86.9	87.8	90.2	88.3	89.5

Table 3.10: Percentage of pixels passing a $\pm 3\%/2\text{mm}$ gamma criterion for SBRT lung plans for both Elekta 6MV and 10MV models. Agreement was evaluated in the axial, sagittal, and coronal planes for three deliveries of each plan.

A qualitative evaluation of the gamma maps showed no consistent failure regions in the comparison in the axial plane. The agreement in the sagittal and coronal planes appeared to be challenged most at the edges of the PTV. This is largely attributed to the sensitivity of the comparison to the registration of film to the phantom. Because both film plane comparisons consist of two pieces of film that need to be aligned during scanning, the registration uncertainty is higher than for the axial plane which consists of single piece of film. Furthermore the high dose gradients at the edges of the PTV make the analysis more sensitive to a small translational shift either in the film registration or phantom setup. Even with the increased registration uncertainty, passing rates were above the pre-established threshold of 85%.

3.3.6 Delivery of IMRT Thorax Phantom Plan: Point Dose Comparison

The results of the point dose comparisons between the developed model and TLD measurements in the anthropomorphic thorax phantom are shown in Table 3.11 and Table 3.12. Double packed TLD were contained in the center of the target (two), in the heart (one), and in the spinal cord (one). The table includes dose measurements, a comparison of the DPM predicted dose with measurement expressed as a ratio of calculated dose to measured dose, and, for reference, a comparison of Pinnacle calculated doses with measurement expressed as a ratio of measured to calculated dose.

TLD								
Point Dose Location	Measurement		DPM Calculation			Pinnacle Calculation		
	Avg. (cGy)	% Std. Dev.	Avg. (cGy)	% Std. Dev.	Ratio Calc/Meas	Avg. (cGy)	% Std. Dev.	Ratio Calc/Meas
PTV – S	611.9	0.4	614.0	0.7	1.003	611.9	0.5	1.000
PTV – I	607.9	0.4	610.5	0.3	1.004	608.2	0.5	1.000
PTV Avg.					1.004			1.000
OAR – Heart	98.1	0.8	90.0	0.0	0.917	94.9	3.7	0.967
OAR – Cord	221.7	0.4	227.0	1.8	1.024	212.8	6.9	0.960

Table 3.11: Point dose comparisons for the Elekta 6MV IMRT lung phantom measurements.

The measured dose is the averaged dose from the three deliveries of each plan. Comparison to calculated doses by DPM (left) and Pinnacle (right) are expressed as a ratio of calculated to measured doses. Point dose locations are indicated by PTV = Planning Target Volume, OAR = Organ at Risk, S = Superior, I = Inferior.

For the Elekta 6MV model the average agreement between the DPM multiple source model calculation and measurement in the PTV was 1.004. The range of calculated to measured dose ratios within the PTV was 1.003 to 1.004. The ratio for the heart TLD was 0.917, and the ratio for the cord TLD was 1.024.

Point Dose Location	TLD Measurement		DPM Calculation			Pinnacle Calculation		
	Avg. (cGy)	% Std. Dev.	Avg. (cGy)	% Std. Dev.	Ratio Calc/Meas	Avg. (cGy)	% Std. Dev.	Ratio Calc/Meas
PTV – S	594.6	0.4	608.4	1.6	1.023	622.8	0.6	1.047
PTV – I	591.4	0.1	602.2	0.8	1.018	613.8	0.6	1.038
PTV Avg.					1.021			1.043
OAR – Heart	95.8	0.3	90.0	0.0	0.940	97.5	3.0	1.018
OAR – Cord	242.5	0.5	234.8	6.4	0.968	234.6	7.6	0.967

Table 3.12: Point dose comparisons for the Elekta 10MV IMRT lung phantom measurements.

The measured dose is the averaged dose from the three deliveries of each plan. Comparison to calculated doses by DPM (left) and Pinnacle (right) are expressed as a ratio of calculated to measured doses. Point dose locations are indicated by PTV = Planning Target Volume, OAR = Organ at Risk, S = Superior, I = Inferior.

The average agreement between the DPM model and the PTV for the Elekta 10MV model was 1.021. The range of the values for the PTV agreement was from 1.018 to 1.023. The calculated to measured ratio for the heart and cord TLDs were 0.940 and 0.968, respectively.

It is important to note that while the OAR calculated doses showed poorer agreement with measurements for 6MV and 10MV models, the uncertainty in the measured dose is unknown at such low doses. The standards used for low dose measurements are done at doses of 8Gy and 3Gy, nearly 3 times the dose of both the heart and cord measurement for the lower of the two standard doses. At doses near 1Gy, as seen in both of the OAR TLD, the RPC does not have data documenting the accuracy of their TLD measurement process for phantom irradiations.

Even though the benchmarking of the multiple source model was based exclusively on measurement, comparisons to doses calculated by Pinnacle are included as means of comparison against an actively used and state of the art treatment planning system dose calculation algorithm. A direct comparison between the DPM calculated dose performance to the Pinnacle calculated dose performance shows superior results in the PTV TLD capsules and comparable performance within the OARs.

3.3.7 Delivery of IMRT Thorax Phantom Plan: Dose Profile and Gamma Map Comparison

Dose profile comparison between the multiple source model and measurement are shown for all three major planes in Figures 3.40, 3.41, 3.42 for the 6MV model and Figures 3.43, 3.44, and 3.45 for the 10MV model. These comparisons are meant to be a qualitative assessment of the models ability to predict complex dose distributions across the volume of the PTV. All profiles showed good agreement between calculation and measurement.

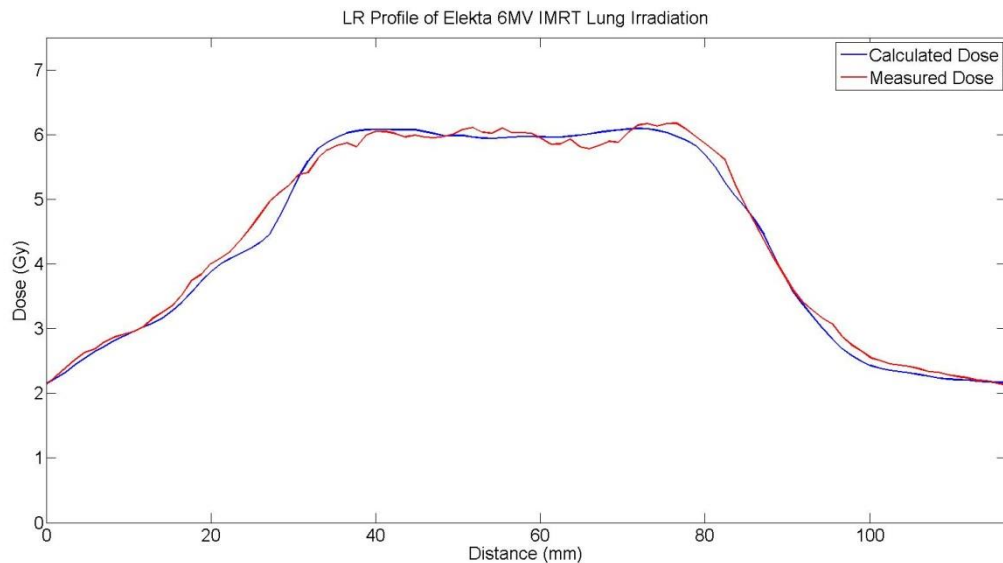


Figure 3.40: A comparison of the lateral (left to right) profile from the axial film of an IMRT lung delivery for the 6MV model.

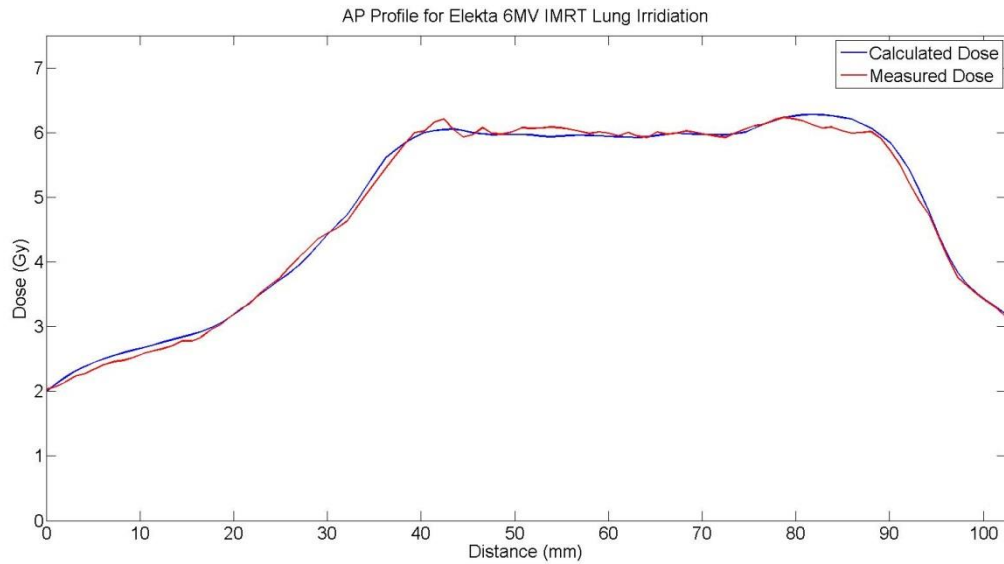


Figure 3.41: A comparison of the AP (anterior to posterior) profile from the axial film of an IMRT lung delivery for the 6MV model.

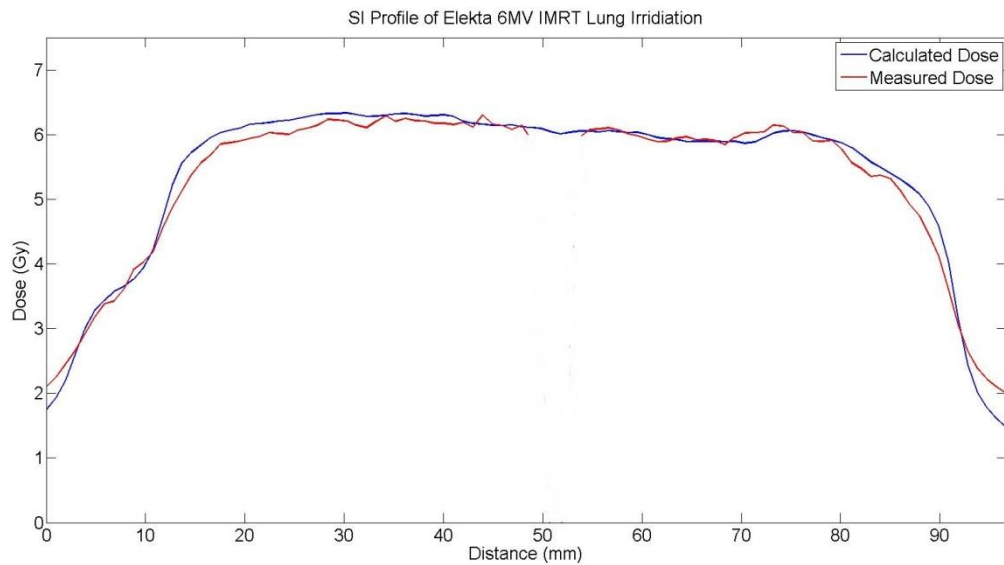


Figure 3.42: A comparison of the SI (superior to inferior) profile from the coronal film of an IMRT lung delivery for the 6MV model.

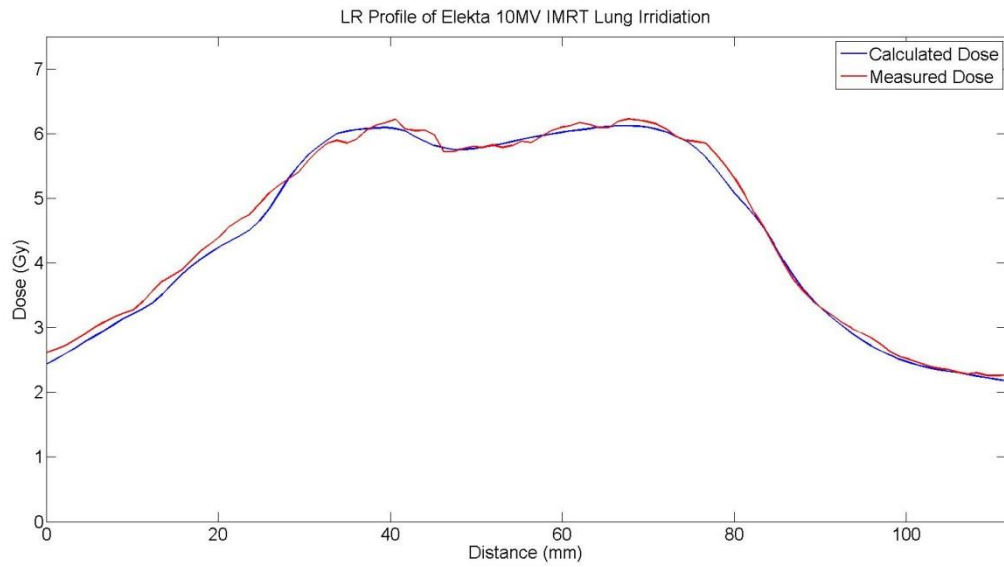


Figure 3.43: A comparison of the lateral (left to right) profile from the axial film of an IMRT lung delivery for the 10MV model.

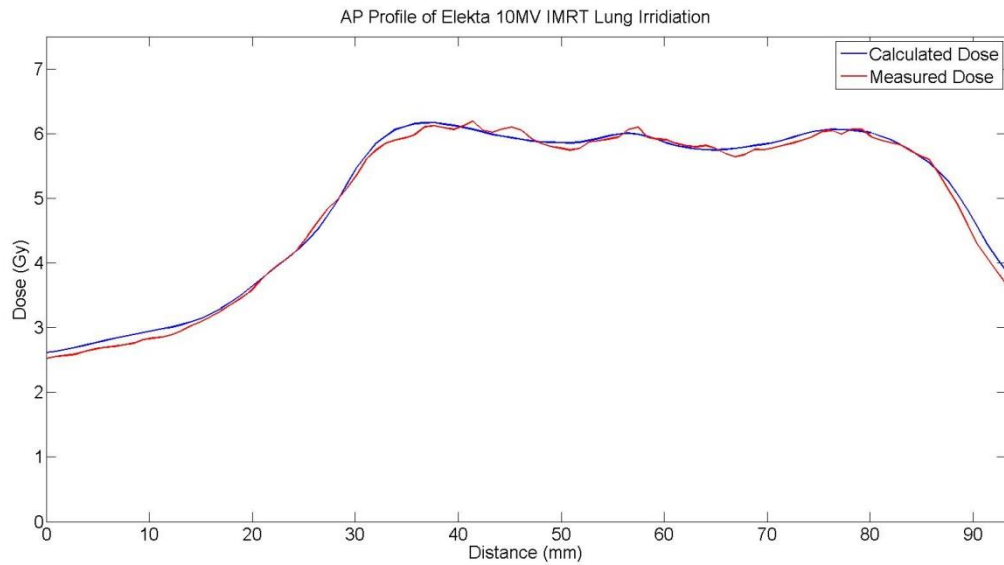


Figure 3.44: A comparison of the AP (anterior to posterior) profile from the axial film of an IMRT lung delivery for the 10MV model.

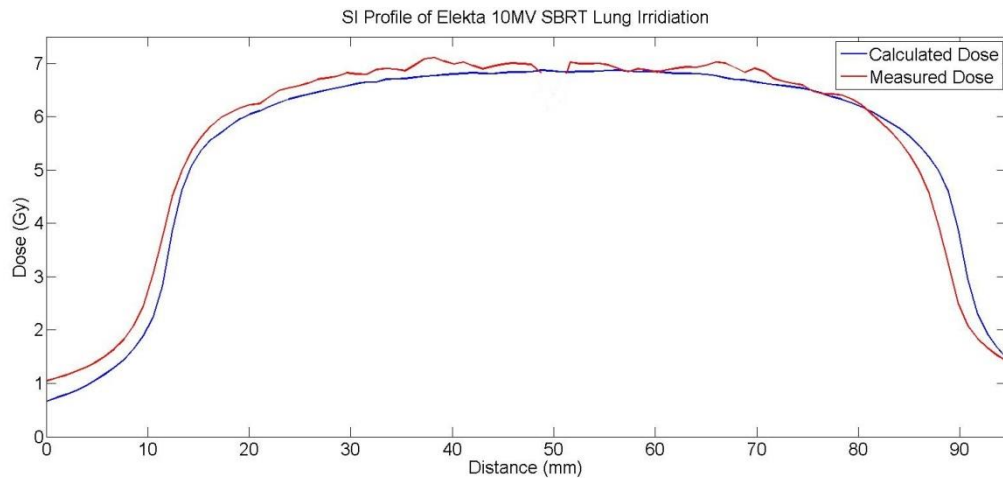


Figure 3.45: A comparison of the SI (superior to inferior) profile from the coronal film of an IMRT lung delivery for the 10MV model.

The model's ability to describe the beam penumbra, MLC leakage, rounded leaf tips, and leaf transmission in unmodulated fields in a heterogeneous medium provided by the lung phantom was evaluated using the gamma technique with a $\pm 3\%/2\text{mm}$ criterion. The analysis considers the dose differences as a percentage of the maximum dose and distance to agreement to assess overall agreement between dose distributions calculated by the multiple source model and measured by the radiochromic film in the phantom. In this way resulting gamma maps can be used to identify areas where the model may be deficient while allowing for positional measurement uncertainty to be accounted for in the distance to agreement criterion.

The gamma maps and comparison to source model calculation for the 6MV model are shown in Figures 3.46, 3.47, and 3.48 for the axial, sagittal, and coronal planes respectively. The agreement, expressed as a percentage of pixels passing the gamma criterion, were 85.2%, 90.0%, and 88.6% for axial, sagittal, and coronal planes, respectively. The individual passing rates for each film plane in each deliver are presented in Table 3.12.

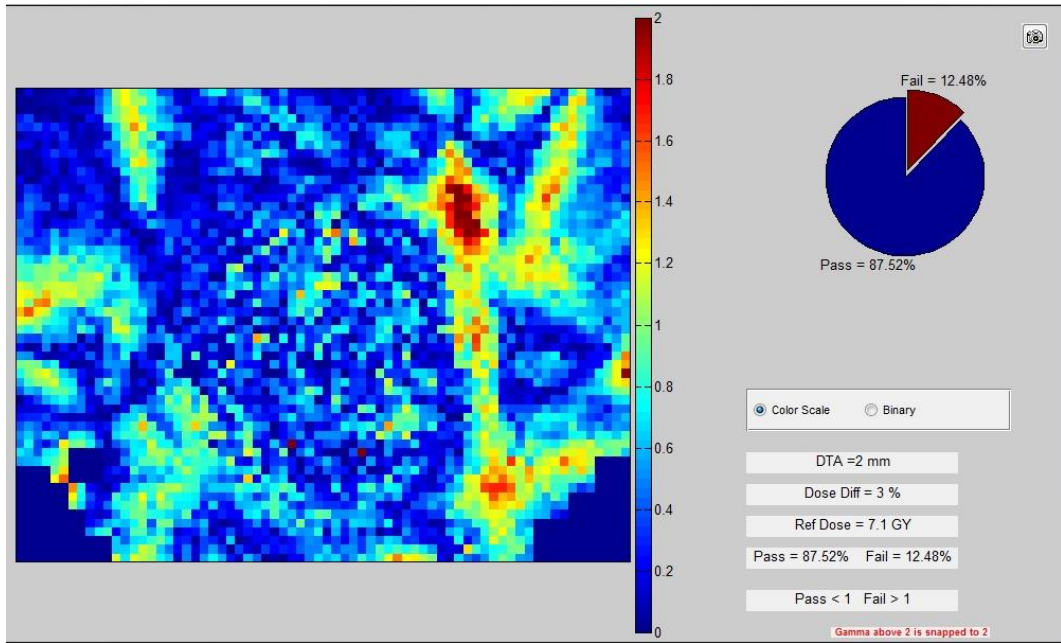


Figure 3.46: Lung IMRT delivery comparison for the axial plane of delivery #3 for the Elekta 6MV model. Agreement was evaluated using a $\pm 3\%/2\text{mm}$ gamma criterion and 87.5% of pixels passed.

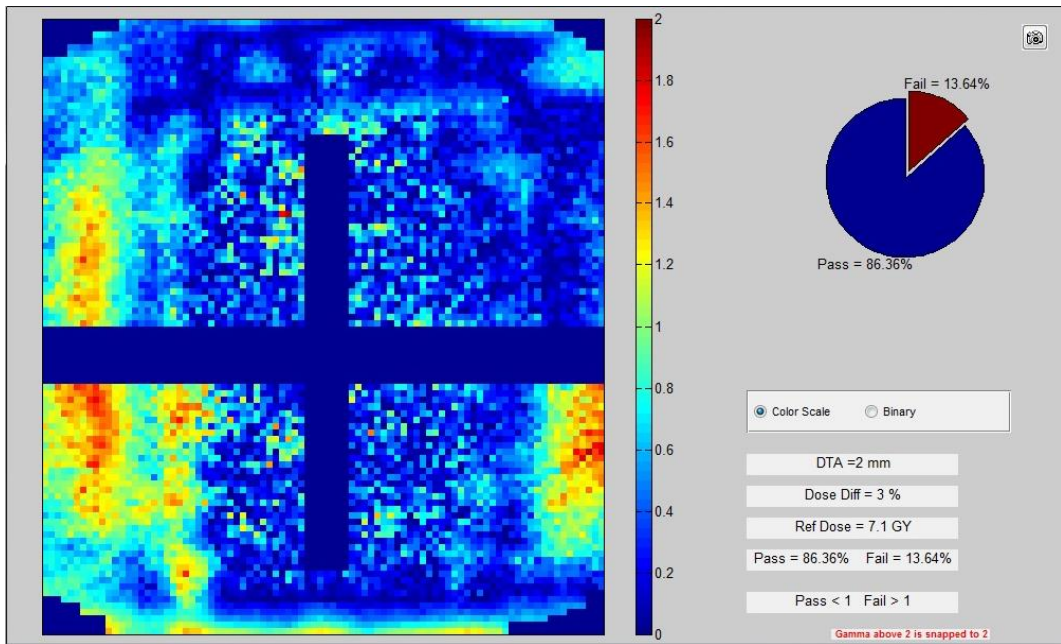


Figure 3.47: Lung IMRT delivery comparison for the sagittal plane of delivery #3 for the Elekta 6MV model. Agreement was evaluated using a $\pm 3\%/2\text{mm}$ gamma criterion and 86.4% of pixels passed.

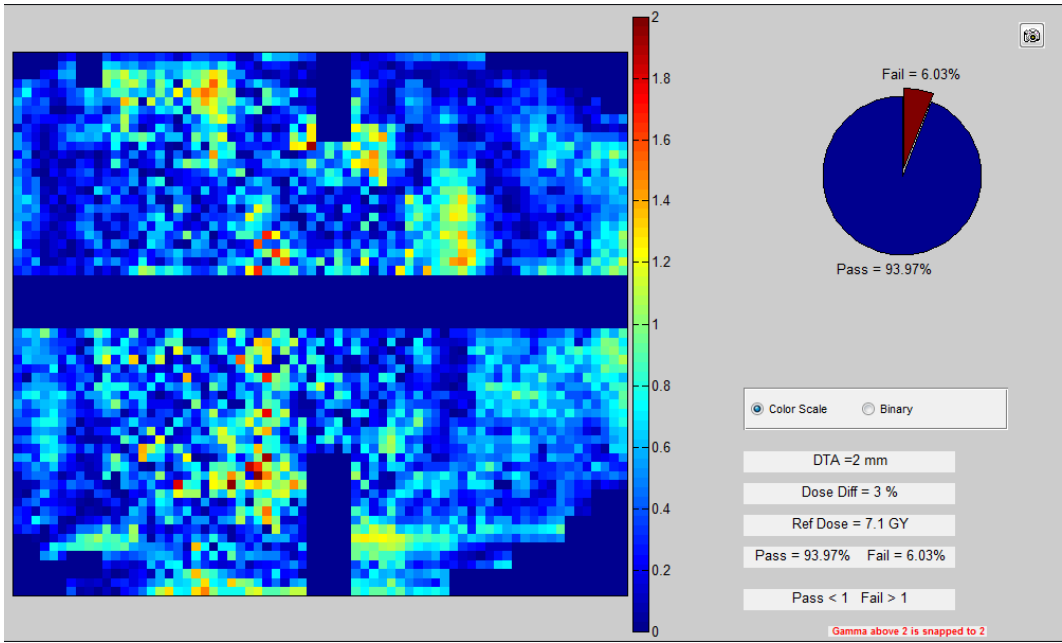


Figure 3.48: Lung IMRT delivery comparison for the coronal plane of delivery #3 for the Elekta 6MV model. Agreement was evaluated using a $\pm 3\%/2\text{mm}$ gamma criterion and 94.0% of pixels passed.

The gamma maps corresponding to the comparison of a single irradiation to the calculated dose of the 10MV source model are shown in Figures 3.49, 3.50, and 3.51 for axial, sagittal, and coronal planes, respectively. The agreement was 91.2%, 90.6%, and 88.0% for axial, sagittal, and coronal planes, respectively. Individual passing rates for each plane in each delivery are presented in Table 3.13.

	Elekta 6MV			Elekta 10MV		
	Axial	Sagittal	Coronal	Axial	Sagittal	Coronal
Delivery #1	82.6	92.5	89.8	94.7	90.6	89.29
Delivery #2	85.4	83.5	89.8	86.6	87.3	86.03
Delivery #3	87.5	94.0	86.4	92.5	94.0	88.53
Average	85.2	90.0	88.6	91.2	90.6	88.0

Table 3.13: Percentage of pixels passing a $\pm 3\%/2\text{mm}$ gamma criterion for IMRT lung plans for both Elekta 6MV and 10MV models. Agreement was evaluated in the axial, sagittal, and coronal planes for three deliveries of each plan.

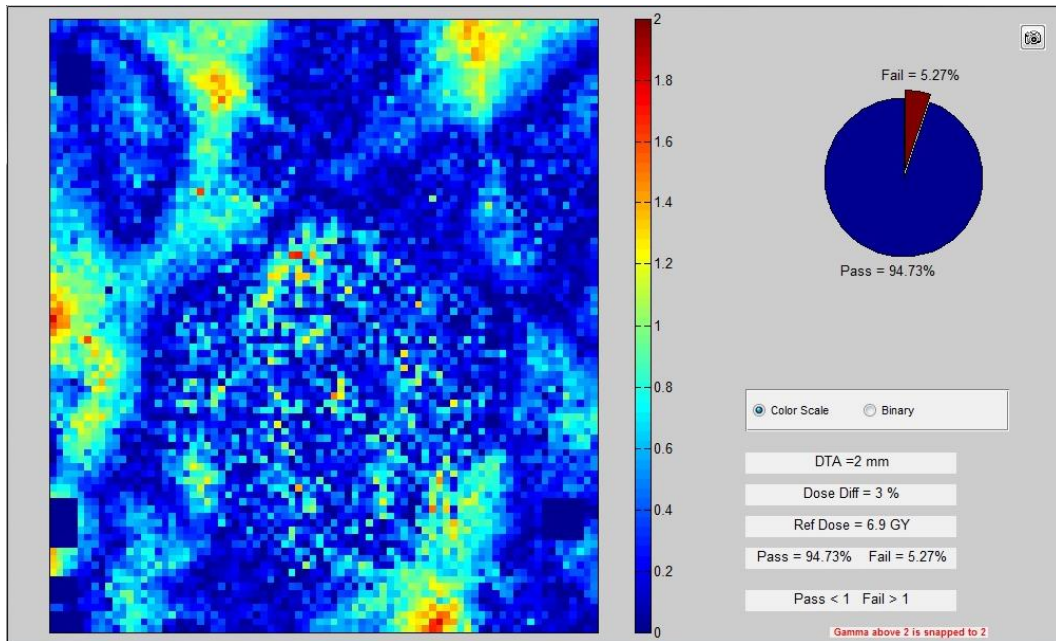


Figure 3.49: Lung IMRT delivery comparison for the axial plane of delivery #1 for the Elekta 10MV model. Agreement was evaluated using a $\pm 3\%/2\text{mm}$ gamma criterion and 94.7% of pixels passed.

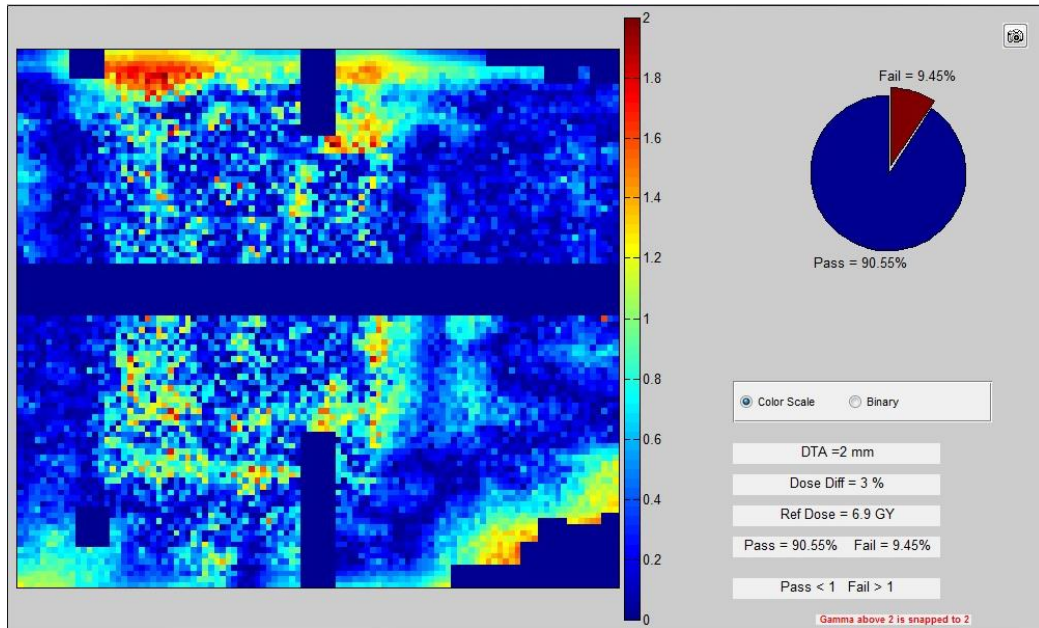


Figure 3.50: Lung IMRT delivery comparison for the sagittal plane of delivery #1 for the Elekta 10MV model. Agreement was evaluated using a $\pm 3\%/2\text{mm}$ gamma criterion and 90.6% of pixels passed.

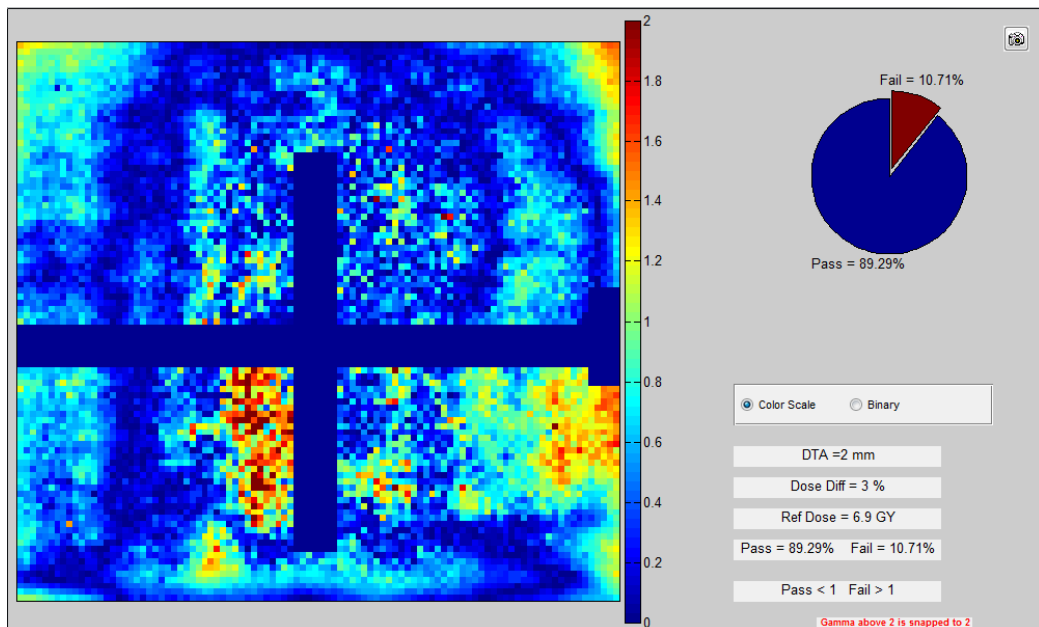


Figure 3.51: Lung IMRT delivery comparison for the coronal plane of delivery #1 for the Elekta 10MV model. Agreement was evaluated using a $\pm 3\%/2\text{mm}$ gamma criterion and 89.3% of pixels passed.

A qualitative evaluation of the gamma maps showed no consistent failure regions in the comparison in the axial plane. The agreement in the sagittal and coronal planes appeared to be challenged most at the edges of the PTV. This is largely attributed to the sensitivity of the comparison to the registration of film to the phantom. Because both film plane comparisons consist of two pieces of film that need to be aligned during scanning, the registration uncertainty is higher than for the axial plane which consists of single piece of film. Furthermore the high dose gradients at the edges of the PTV make the analysis more sensitive to a small translational shift either in the film registration or phantom setup. Even with the increased registration uncertainty, passing rates were above the pre-established threshold of 85%.

3.3.8 Benchmark Summary

The average and range of the percent of pixels passing a $\pm 3\%/2\text{mm}$ global gamma criterion for each phantom for both Elekta 6MV and 10MV source models is presented in Table 3.14.

		IMRT H&N	SBRT Lung	IMRT Lung
Elekta	Average	87.2	87.2	87.9
6MV	Range	82.5 – 91.4	84.2 – 93.9	82.6 – 94.0
Elekta	Average	90.5	89.3	89.9
10MV	Range	86.4 – 95.9	85.2 – 96.5	86.0 – 94.7

Table 3.14: The average and range of the percent of pixels passing a $\pm 3\%/2\text{mm}$ gamma criterion for Elekta 6MV and 10MV source models as assessed through three repeated deliveries for three different treatment plans to anthropomorphic phantoms.

Each multiple source model was benchmarked against three progressively challenging treatment plans delivered to anthropomorphic phantoms using SBRT and IMRT techniques in homogeneous and heterogeneous media. A 9 co-planar beam IMRT plan was designed and delivered to a head and neck phantom for both 6MV and 10MV nominal energies. Agreement was assessed using the gamma technique with a passing criterion of $\pm 3\%$ of the maximum dose and $\pm 2\text{mm}$ distance to agreement. The average percent of pixels passing the criterion was 87.2% and 90.5% for 6MV and 10MV models, respectively. The models showed a range of passing percentages in the sagittal and axial planes of 82.5% to 91.4% for the 6MV model and 86.4% to 95.9% for the 10MV model. In general disagreement was limited to the edges of the PTV in the sagittal plane where measurement uncertainty associated with film registration was most likely to have an effect on the analysis due to the steep dose gradient in the region.

An un-modulated, 9 co-planar beam SBRT plan was delivered to the RPC's anthropomorphic lung phantom. Each beam was defined by a static MLC configuration designed to conform the dose to the PTV. The average percent of pixels passing a $\pm 3\%/2\text{mm}$ global gamma criterion was 87.2% and 89.3% for 6MV and 10MV models, respectively. The range of pixels passing for the 6MV model was 84.2% to 93.9% and 85.2% to 96.5% for the 10MV model. Similar to the head and neck benchmark results, the only consistent region of disagreement was along the edges of the PTV in the sagittal and coronal planes in the regions of the steepest dose gradient.

Moderately modulated, 6 co-planar beam, 6MV and 10MV IMRT plans were delivered to the anthropomorphic lung phantom. The addition of modulation to the heterogeneous phantom increased the challenge to the dose calculation tool while maintaining a clinically relevant setup. The average percent of pixels passing a $\pm 3\%/2\text{mm}$ global gamma criterion was 87.9% and 89.9% for 6MV and 10MV models, respectively. The range of pixels passing the $\pm 3\%/2\text{mm}$ criterion was 82.6% to 94.0% for the 6MV model and 86.0% to 94.7% for the 10MV model. Even with the increased difficulty of the calculation conditions, disagreement between measurement and calculation was minimal.

3.4 Conclusion

An analytical, multiple source model for Elekta 6MV and 10MV beams using the Dose Planning Method (DPM) Monte Carlo code was developed and validated within $\pm 2\%$ of the maximum dose and $\pm 2\text{mm}$ distance to agreement against open field depth dose and dose profile measurements for field sizes ranging from $3 \times 3 \text{ cm}^2$ to $30 \times 30 \text{ cm}^2$. On average 99.5% and 99.6% of the data tested for 6MV and 10MV models, respectively, met the above criterion using gamma analysis.

The first step in the commissioning process used measured percent depth dose data from a nominal $10 \times 10 \text{ cm}^2$ field size to determine the energy spectra and relative fluences for a primary point source and an extra-focal disk source through an optimization process fitting relative contributions of 0.25 MeV energy bins to a Fatigue-Fermi Distribution. In the same optimization process the relative contribution of an electron disk source was determined. Particle distribution was implemented directly from the literature for the extra-focal[60] and electron[53] sources.

The second step of the commissioning process matched measured and calculated dose profiles for an open $40 \times 40 \text{ cm}^2$ field in order to model the increase in off-axis fluence. The decrease in mean energy off-axis was implemented without change from Taylor et al[61]. An output correction was empirically applied to match the increased scatter contribution with increasing field size. Upon completion of the commissioning process an accurate model of Elekta 6MV and 10MV therapeutic x-ray beams was developed to run basic open beam dose calculations using the DPM Monte Carlo code.

The commissioned and validated multiple source models were then benchmarked against increasingly challenging treatment plans delivered to homogenous and heterogeneous anthropomorphic phantoms. The model was shown to be accurate within $\pm 3\%$ and $\pm 2\text{mm}$ based on comparisons of calculated dose to enclosed thermoluminescent dosimeters (TLD)

and radiochromic film. Average agreement assessed using the gamma technique and a 3%/2mm global criterion was 87.4% and 89.9% for 6MV and 10MV source models, respectively.

Chapter 4: Results and Discussion: Varian TrueBeam 6 MV and 10MV Flattening Filter Free Beams

4.1 Source Model

4.1.1 Source Model Commissioning Parameters

The seven optimized parameters, determined in commissioning, that describe the photon energy spectra, fluence contributions, and volume averaging of the ion chamber leading to an exaggerated penumbra for dose profiles are reported in Table 4.1 for the Varian TrueBeam FFF 6MV and 10MV models. The first three parameters, γ , μ , and β describe the spectrum shape, peak energy location, and relative scale respectively. Figure 4.1 and Figure 4.2 show a graphical comparison between the Varian TrueBeam FFF models and the Varian models with the flattening filter in place developed by Davidson et al.[35] for nominal energies of 6MV and 10MV, respectively.

Parameter	Value	Value
	TrueBeam FFF 6MV	TrueBeam FFF 10MV
Fatigue-Life distribution shape parameter, γ	9.00	12.50
Fatigue-Life distribution location parameter, μ	0.0500	-0.0154
Fatigue-Life distribution scale parameter, β	3.50	3.88
Primary spectrum to extra-focal spectrum reduction factor	4.28	4.47
Extra-focal fluence relative to the primary fluence	0.0900	0.1003
Electron Contamination contribution (relative to the primary photon contribution)	0.0025	0.0015
Standard deviation of Gaussian used to convolve the MC dose profile to match the measured dose profile during validation (in mm)	1.2	1.2

Table 4.1: Optimized parameters for the source models as determined during the initial commissioning of the models. The first three parameters describe the shape and location of the spectra. The fourth through sixth parameters relate the relative contribution and energy scale of the three sources, and the final parameter is the standard deviation of the Gaussian kernel convolved with the calculated dose profiles to mimic the volume averaging effect of an ion chamber at the penumbra of dose profiles.

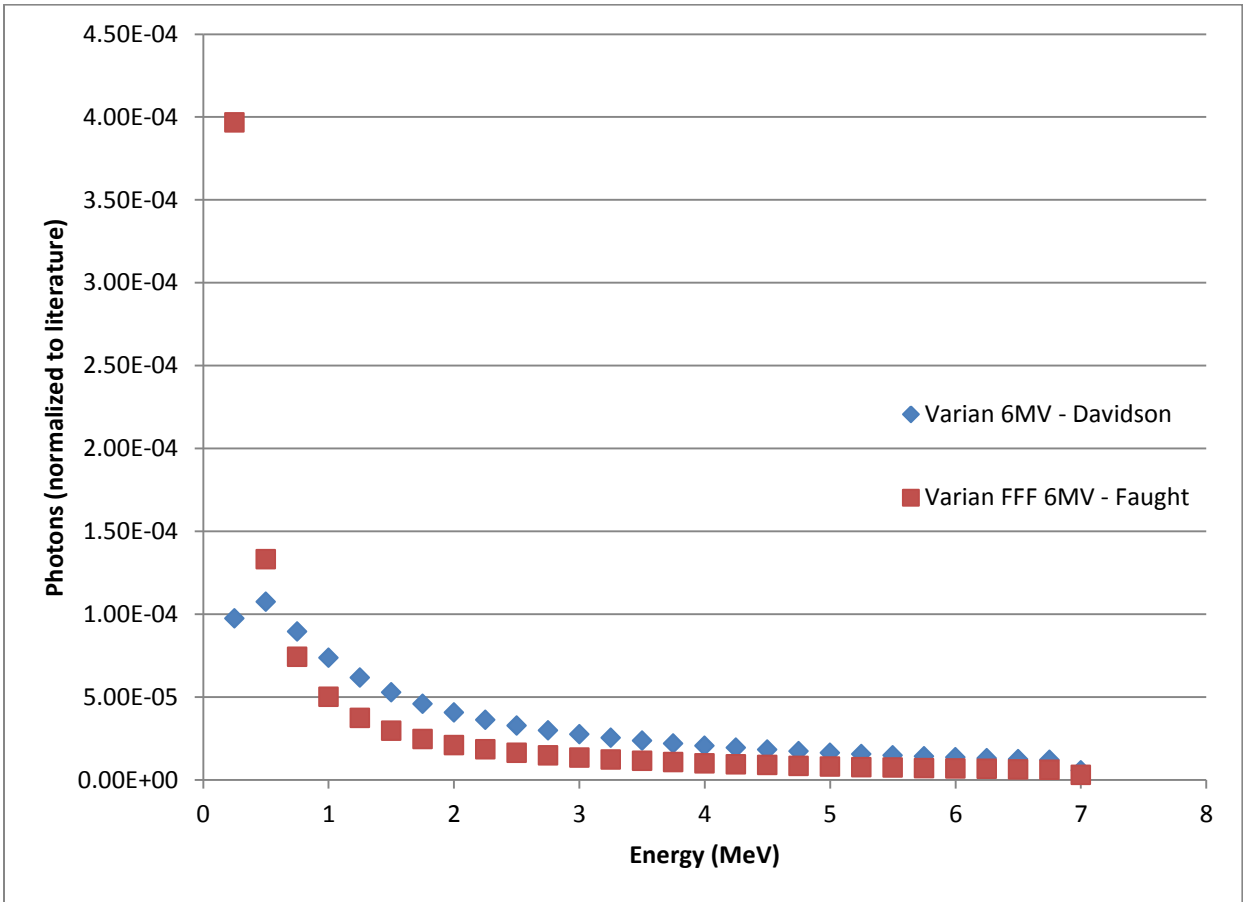


Figure 4.1: Comparison of commissioned TrueBeam FFF 6MV source model spectrum (red square) with the previously developed Varian 6MV source model (blue diamond)[35].

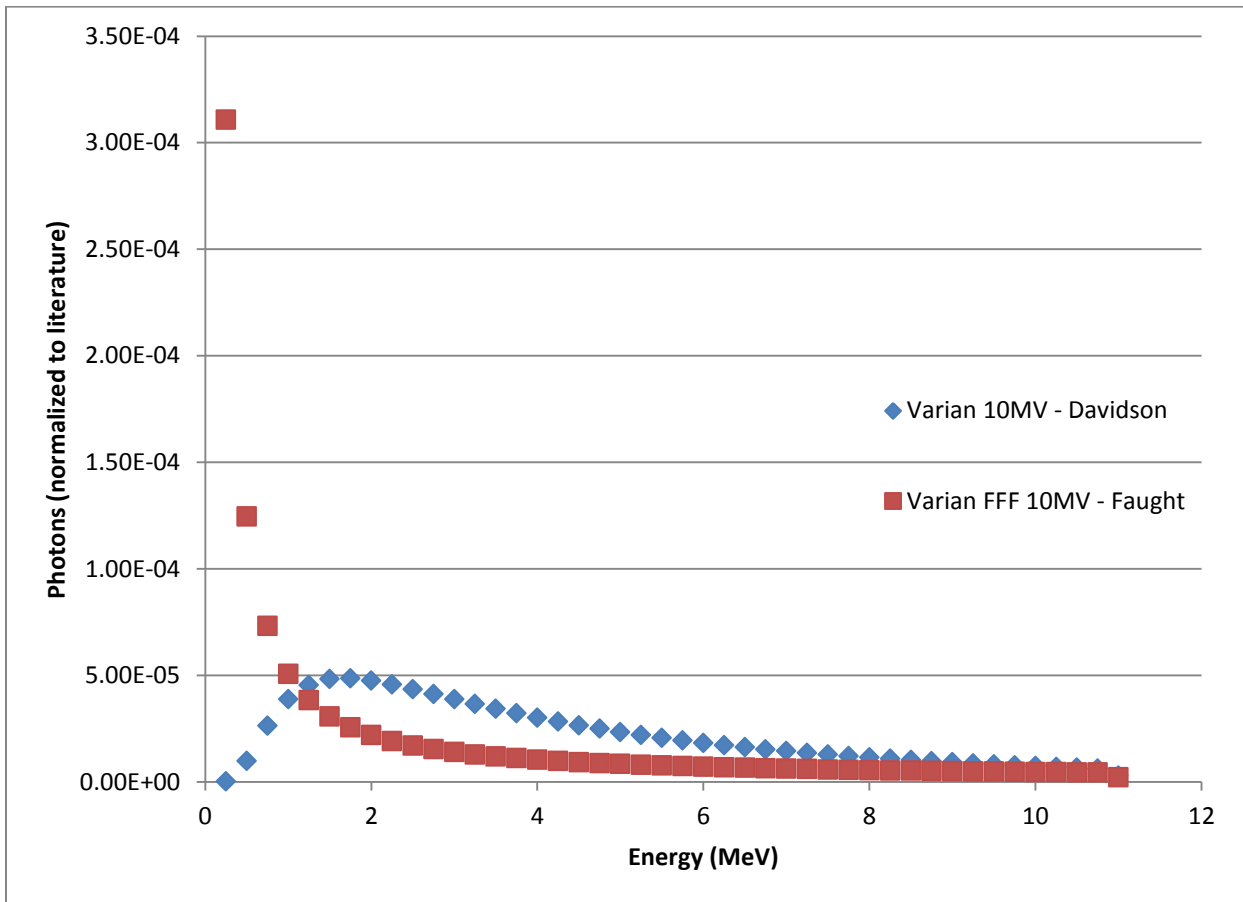


Figure 4.2: Comparison of commissioned TrueBeam FFF 10MV source model spectrum (red square) with the previously developed Varian 10MV source model (blue diamond)[35].

The extra-focal source was scaled in energy by a factor of 4.28 and 4.47 for 6MV and 10MV models, respectively. Their fluences, relative to the primary point source in a 10 x 10 cm² open field, were found to be 9.00% and 10.03% for 6MV and 10MV models, respectively. The electron contamination sources, while small at 0.25% and 0.15%, respectively, were still included in the source model, unlike the Varian 6MV model[20, 21, 35]. For the comparison of the dose profiles, a Gaussian kernel of standard deviation 1.2mm was convolved with the calculated data to model the volume averaging effect of an ion chamber measurement.

The results to the second step of the commissioning process in which the off-axis fluence was modeled by a piecewise linear function of the cosine of the off-axis angle are shown in

Table 4.2. The off-axis energy correction was implemented from Georg et al.[62] without change.

Cosine (Off-axis Angle)	Fluence Weight (Relative to CAX)	
	TrueBeam FFF 6MV Model	TrueBeam FFF 10 MV Model
1.00000	1.0000	1.0000
0.99970	0.9597	0.9010
0.99789	0.8973	0.7852
0.99728	0.8310	0.6850
0.99518	0.7563	0.5950
0.99250	0.6939	0.5260
0.98926	0.6299	0.4609
0.98546	0.5759	0.4073
0.98113	0.5191	0.3490
0.97630	0.4600	0.1591
0.97098	0.4000	0.1167
0.96277	0.3400	0.0700

Table 4.2: Optimized coefficients to a piece-wise linear function used to describe the increase in off-axis fluence of TrueBeam FFF 6MV and 10MV models. Fluence weighting values are reported with respect to the dose measured at the central axis (CAX) for the 40 x 40 cm² field size dose profile at a depth of d_{max} .

After completing the second step of the commissioning process, the scaling factor used to convert the Monte Carlo output from energy per particle to cGy per MU was determined from

the dose at d_{\max} along the central axis for a $10 \times 10 \text{ cm}^2$ field size. These values were 41.79 and 29.49 for the 6MV and 10MV models, respectively. This factor will be applied to all subsequent dose calculations for the corresponding energy models.

4.1.2 Fluence Map, Primary Source Size, and Machine Output Correction

Fluence map generation is a process that is unique to the treatment plan, patient, phantom, or open field delivery, and beam energy. The MLC positions for each segment weight the fluence by assuming 1% transmission through the leaves and an additional 1% as interleaf leakage. The transmission and the leakage percentages were the same for 6MV and 10MV models.

Because the source model includes a point source representing photons created within the target and not a finite source size, an offset of the MLC, x_{pen} , of 0.4mm was necessary. This was the same offset used in the Varian model[20, 21, 35] and because the literature has suggested its size is nearly fixed for different nominal energies from the same manufacturer[69], it was left constant for both 6MV and 10MV models.

Unlike the previously developed Varian[35] and Elekta (Chapter 3) models, an empirically determined field size dependent output correction was not needed to match the calculated to measured dosimetry data. This is likely due to the difference in scatter contributions when removing the flattening filter from the linear accelerator head.

4.2 Validation Testing

4.2.1 Uncertainty

The uncertainty in the ion chamber measurements was estimated at 1.6% (one standard deviation) to match that reported in the literature[70]. The standard error of the mean in the

dose calculations was calculated to be no more than 1.2% using the batch method described in AAPM Task Group Report No. 105[22].

4.2.2 Depth Dose Data

The comparison between measured and calculated percent depth dose data for the TrueBeam FFF 6MV and 10MV models was performed for field sizes ranging from 3 x 3 cm² to 40 x 40 cm². Gamma analysis agreement using a $\pm 2\%/2\text{mm}$ criterion is summarized in Table 4.3. The percentage of data passing the criterion for every field size at every depth is reported in the Appendix (Chapter 7). For a graphical comparison between depth dose curves of all field sizes please see the Appendix (Chapter 7). As representative summary the smallest (3 x 3 cm²), nominal (10 x 10 cm²), and largest (40 x 40 cm²) field sizes are shown for the TrueBeam FFF 6MV model in Figures 4.3, 4.4, and 4.5, respectively. The same field sizes are shown for the TrueBeam FFF 10MV model in Figure 4.6, 4.7, and 4.8, respectively.

Validation Results –Depth Dose Data

Field Size (cm ²)	% Pixels Passing	
	TrueBeam FFF 6MV Model	TrueBeam FFF 10MV Model
3 x 3	100.0	99.3
4 x 4	100.0	99.3
6 x 6	99.3	99.3
8 x 8	100.0	100.0
10 x 10	100.0	100.0
20 x 20	100.0	100.0
30 x 30	100.0	97.4
40 x 40	100.0	96.7

Table 4.3: Gamma comparison agreement for TrueBeam FFF 6MV and 10MV models using a $\pm 2\%/2\text{mm}$ criterion for measured and calculated depth dose data

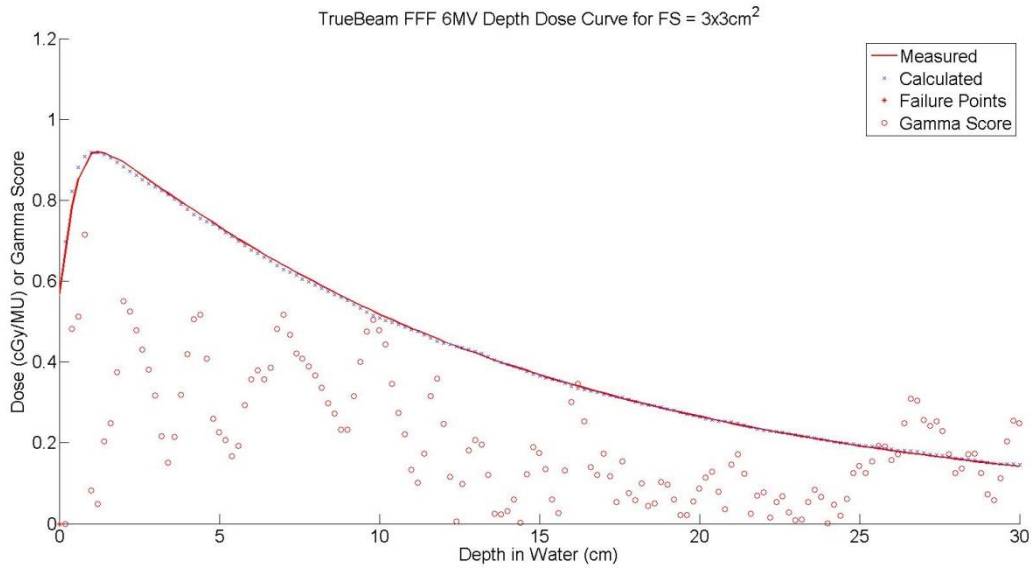


Figure 4.3: Calculated (blue 'x') and measured (red line) depth dose curves for a TrueBeam FFF 6MV beam for a 3 x 3 cm² field size. Gamma agreement (red circles) for each point is also displayed along with any points (red star) at which a failure to meet the $\pm 2\%/2\text{mm}$ criterion.

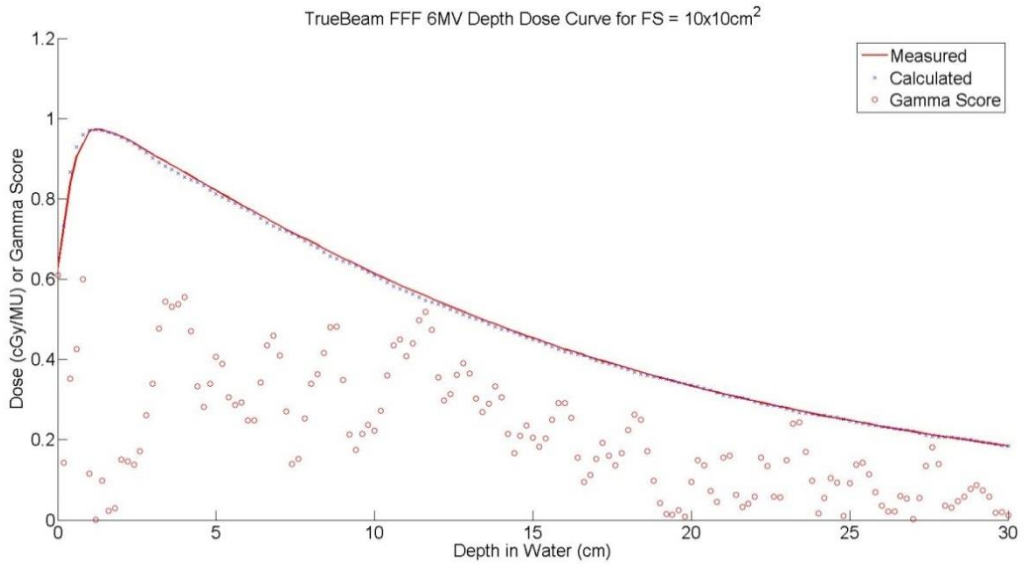


Figure 4.4: Calculated (blue 'x') and measured (red line) depth dose curves for a TrueBeam FFF 6MV beam for a 10 x 10 cm² field size. Gamma agreement (red circles) for each point is also displayed along with any points (red star) at which a failure to meet the $\pm 2\%/2\text{mm}$ criterion.

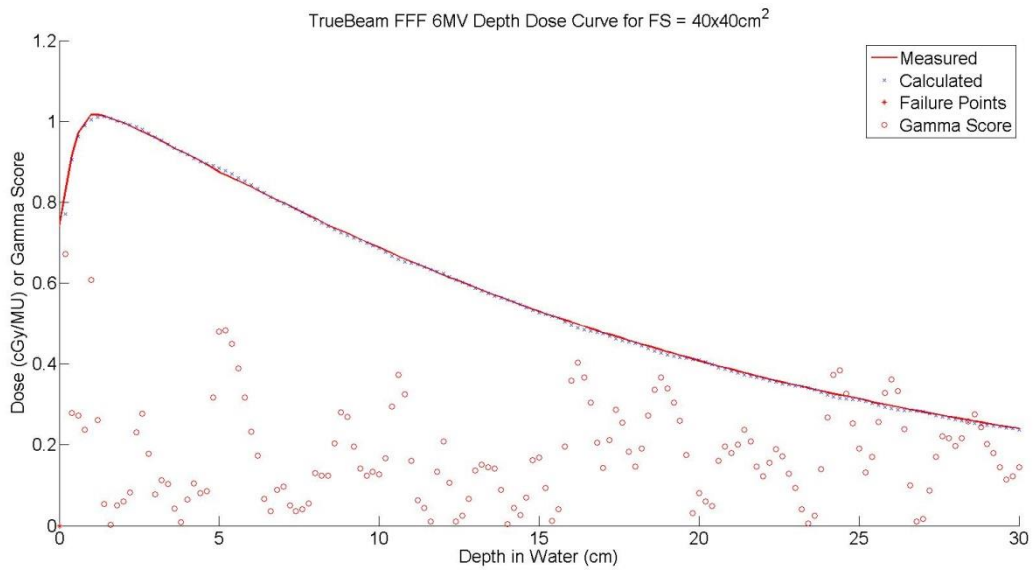


Figure 4.5: Calculated (blue 'x') and measured (red line) depth dose curves for a TrueBeam FFF 6MV beam for a 40 x 40 cm² field size. Gamma agreement (red circles) for each point is also displayed along with any points (red star) at which a failure to meet the $\pm 2\%/2\text{mm}$ criterion.

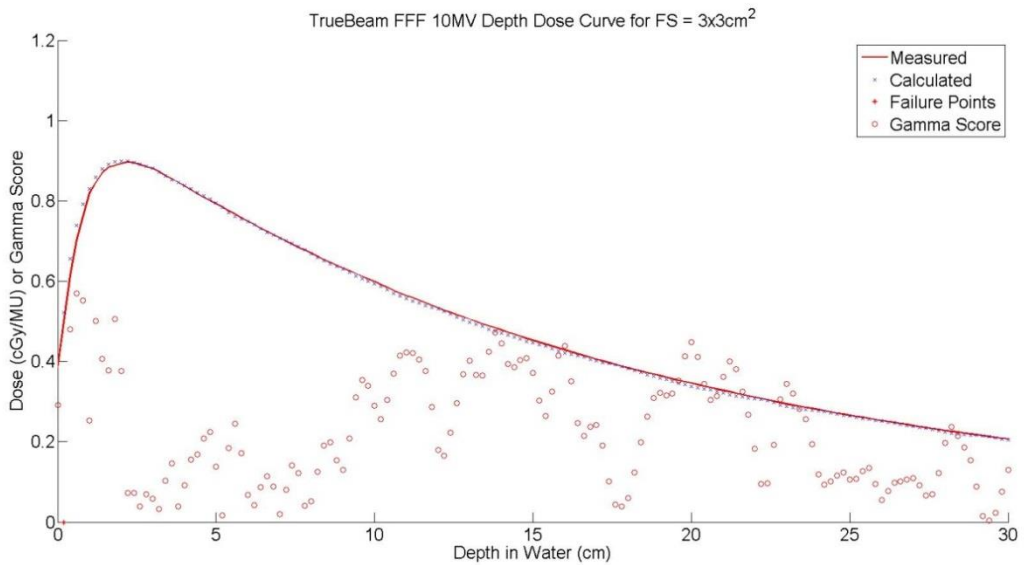


Figure 4.6: Calculated (blue 'x') and measured (red line) depth dose curves for a TrueBeam FFF 10MV beam for a 3 x 3 cm² field size. Gamma agreement (red circles) for each point is also displayed along with any points (red star) at which a failure to meet the $\pm 2\%/2\text{mm}$ criterion.

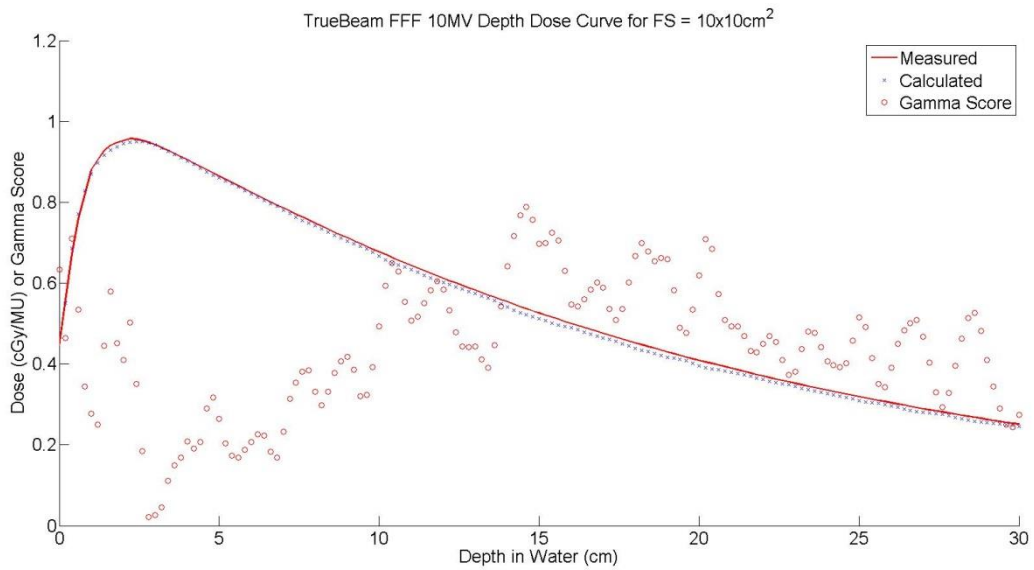


Figure 4.7: Calculated (blue 'x') and measured (red line) depth dose curves for a TrueBeam FFF 10MV beam for a 10 x 10 cm² field size. Gamma agreement (red circles) for each point is also displayed along with any points (red star) at which a failure to meet the $\pm 2\%/2\text{mm}$ criterion.

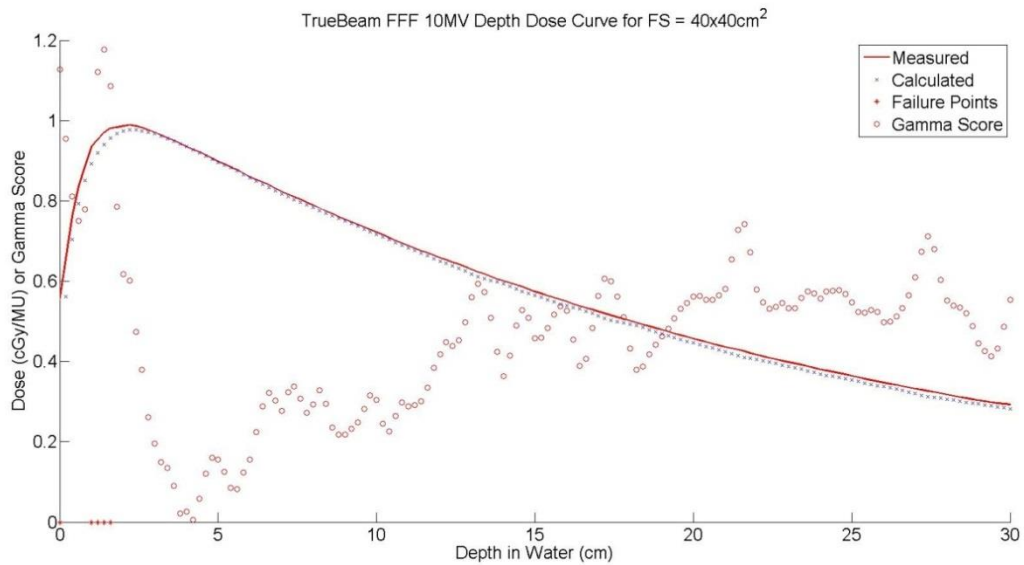


Figure 4.8: Calculated (blue 'x') and measured (red line) depth dose curves for a TrueBeam FFF 10MV beam for a 40 x 40 cm² field size. Gamma agreement (red circles) for each point is also displayed along with any points (red star) at which a failure to meet the $\pm 2\%/2\text{mm}$ criterion.

4.2.3 Dose Profiles

A comparison of calculated dose profiles to measurements was performed for both TrueBeam FFF 6MV and FFF 10MV models at depths of d_{\max} , 5cm, 10cm, 20cm, and 30cm for field sizes ranging from $3 \times 3 \text{ cm}^2$ to $40 \times 40 \text{ cm}^2$. Gamma analysis with $\pm 2\%/2\text{mm}$ criteria was used as the means of comparison and is summarized in Table 4.4. The percentages of pixels passing for each profile compared are reported in the Appendix (Chapter 6) along with graphs of each comparison. As a representative summary the smallest ($3 \times 3 \text{ cm}^2$), nominal ($10 \times 10 \text{ cm}^2$), and largest ($40 \times 40 \text{ cm}^2$) field sizes are shown for the TrueBeam FFF 6MV model in Figures 4.9, 4.10, and 4.11, respectively. The same field sizes are shown for the FFF 10MV model in Figure 4.12, 4.13, and 4.14, respectively.

Validation Results – Dose Profile Data

Field Size (cm ²)	% Pixels Passing	
	TrueBeam FFF 6MV Model	TrueBeam FFF 10MV Model
3 x 3	99.4	98.9
4 x 4	99.0	99.7
6 x 6	99.6	99.6
8 x 8	99.2	98.3
10 x 10	98.7	96.2
20 x 20	95.4	98.5
30 x 30	95.3	96.1
40 x 40	96.1	95.7

Table 4.4: Gamma comparison agreement for TrueBeam FFF 6MV and FFF 10MV models using a $\pm 2\%/2\text{mm}$ criterion for measured and calculated dose profile data. Dose profiles were measured and calculated in-plane at depths of d_{max} (1.6cm for 6MV and 2.4cm for 10MV), 5cm, 10cm, 20cm, and 30cm.

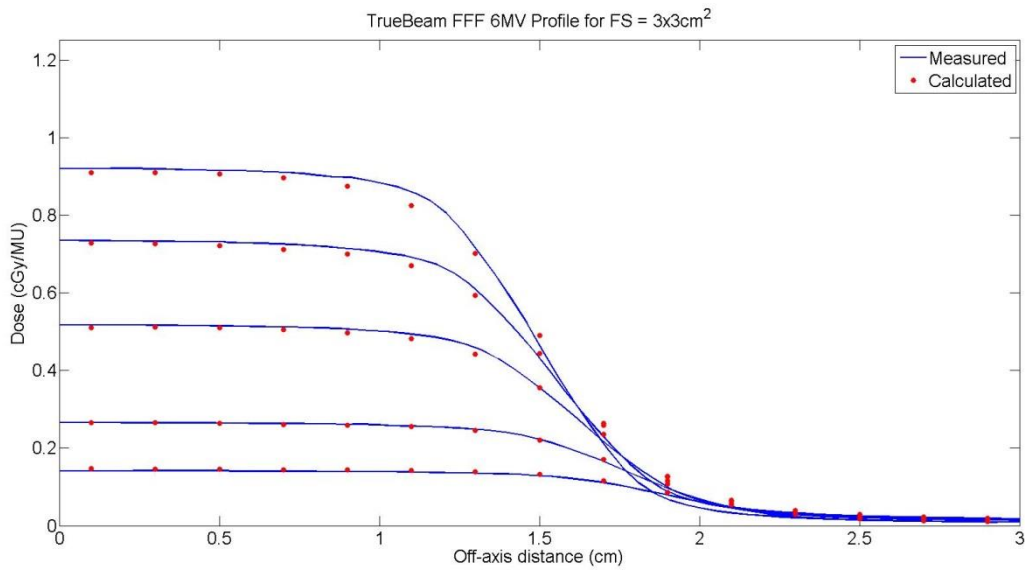


Figure 4.9: Calculated (red circle) and measured (blue line) dose profiles for a TrueBeam FFF 6MV beam at a field size of 3 x 3 cm².

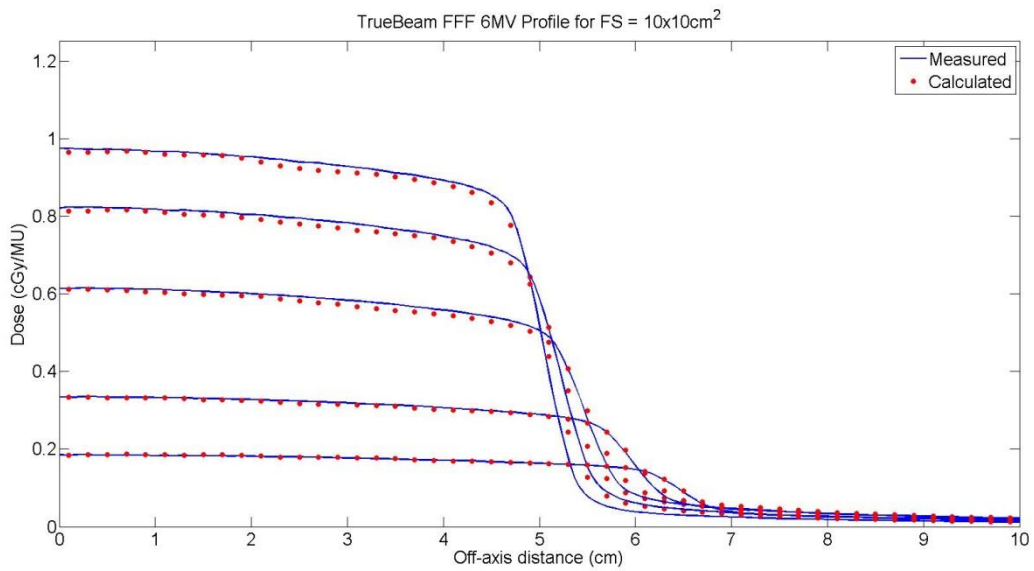


Figure 4.10: Calculated (red circle) and measured (blue line) dose profiles for a TrueBeam FFF 6MV beam at a field size of 10 x 10 cm².

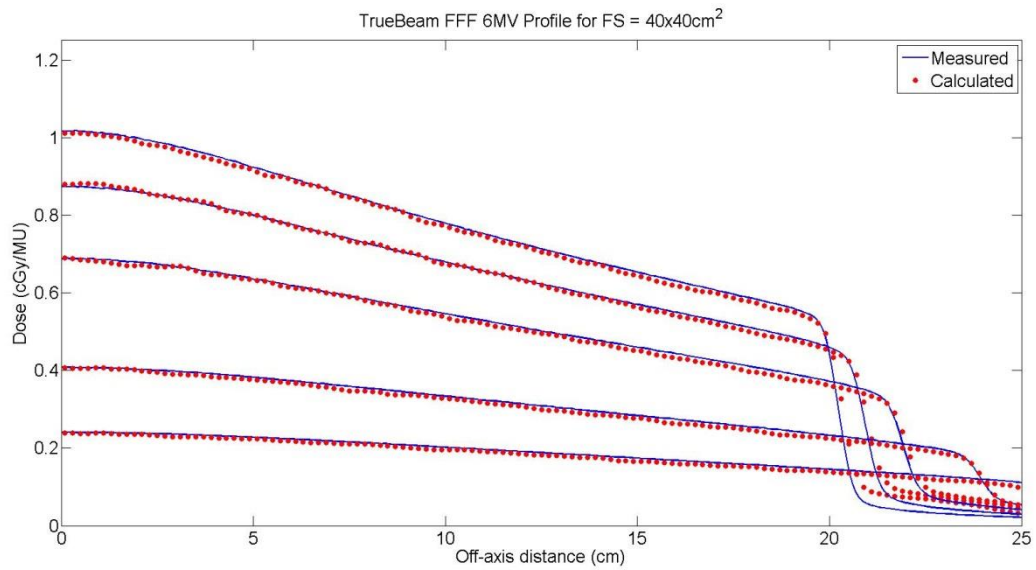


Figure 4.11: Calculated (red circle) and measured (blue line) dose profiles for a TrueBeam FFF 6MV beam at a field size of 40 x 40 cm².

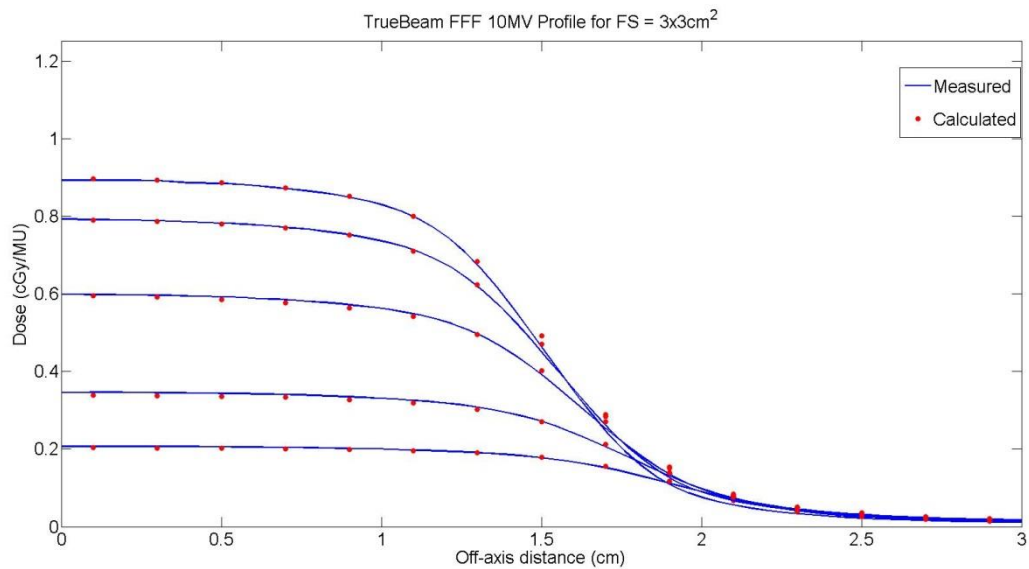


Figure 4.12: Calculated (red circle) and measured (blue line) dose profiles for a TrueBeam FFF 10MV beam at a field size of 3 x 3 cm².

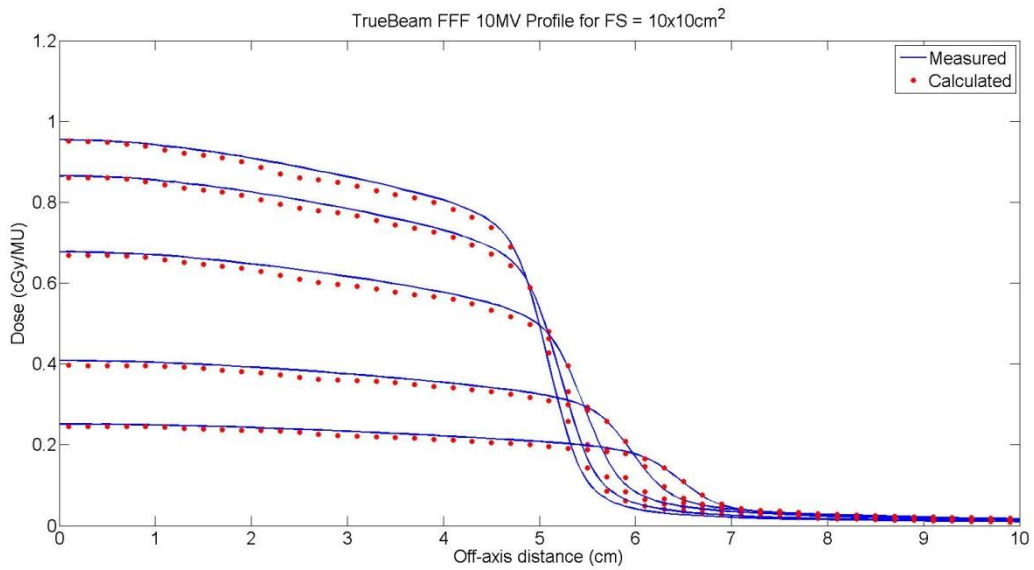


Figure 4.13: Calculated (red circle) and measured (blue line) dose profiles for a TrueBeam FFF 10MV beam at a field size of 10 x 10 cm².

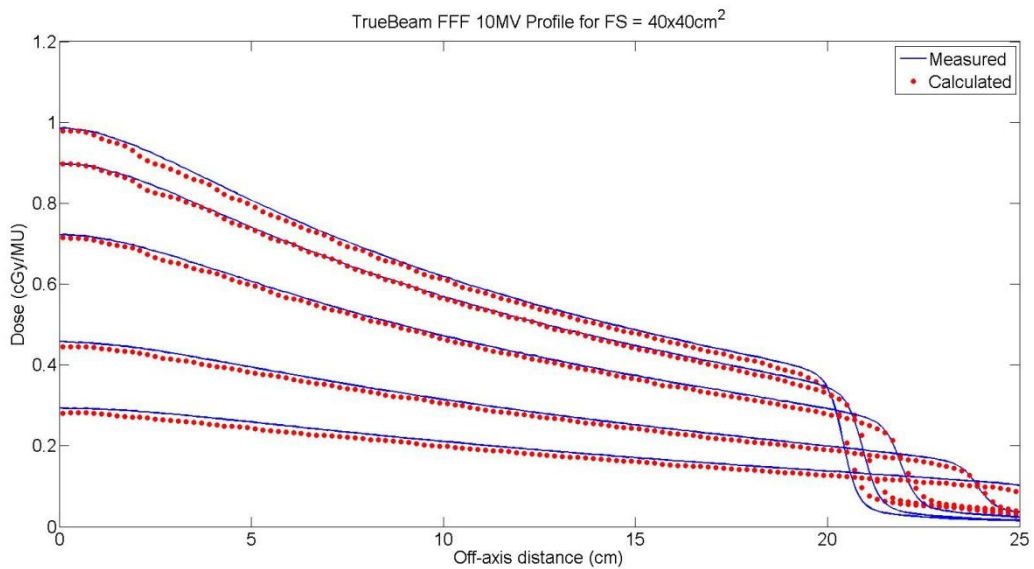


Figure 4.14: Calculated (red circle) and measured (blue line) dose profiles for a TrueBeam FFF 10MV beam at a field size of 40 x 40 cm².

Agreement between calculated and measured profile data was assessed using the gamma technique with an evaluation criterion of $\pm 2\%/2\text{mm}$. Profiles at all field sizes and depths showed good agreement with the minimum percentage of pixels passing being 88.0% and 88.6% for 6MV and 10MV models respectively. The average percentage of pixels passing the gamma analysis was 97.8% and 97.9% for 6MV and 10MV models, respectively. Table 4.4 displays the average agreement by field size for both 6MV and 10MV models.

Among the 40 profiles compared for the TrueBeam FFF 6MV model, 5 failed to achieve the pre-established minimum of 90% of pixels passing a $\pm 2\%/2\text{mm}$ gamma criterion. These failures occurred at field sizes of $20 \times 20 \text{ cm}^2$ at depths of 1.5cm (88.0%) and 5cm (89.0%), $30 \times 30 \text{ cm}^2$ at depths of 1.5cm (88.1%) and 5cm (89.0%), and $40 \times 40 \text{ cm}^2$ at a depth of 1.5cm (89.9%). Among the profiles compared for the TrueBeam FFF 10MV model, a single profile at a depth of 2.4cm for a field size of $40 \times 40 \text{ cm}^2$ failed to meet the 90% requirement (88.6%). Failure points for both models were located in the low dose region just beyond the penumbra for all failing profiles. It is suspected that the model over predicts the scatter dose at these points just outside the field edge. Because all failing profiles were within 2% of the pre-established criterion and occurred for larger field sizes only, it was determined that the disagreement would have minimal impact on the use of the calculation model for flattening filter free beams. One of the primary advantages of a flattening filter free beam is the increased dose rate achieved by removing the flattening filter and by extension reduced treatment time. For larger field sizes a higher degree of modulation is required to achieve desirable dose distributions due to the lack of flatness of the beam. This negates, and sometimes makes worse, the reduced treatment time achieved from the higher dose rate. It is therefore unlikely that a clinical plan would use field sizes at the size of the failing profiles.

4.3 Benchmark Testing

4.3.1 Uncertainty

The measurement uncertainty in the dose distributions in the radiochromic film, normalized to the adjacent TLD doses, was estimated in previous studies to be between 2.6% and 3.5% at one standard deviation[12, 35]. By normalizing the film to the TLD dose, the uncertainty related to differences between the film calibration process and the actual film used in benchmarking was minimized. The literature details the estimated uncertainty of the TLD dose[11], the film uniformity, film-to-film variation, and the fit of the sensitometric curve[71].

The estimated single voxel standard error of the mean in the phantom plan simulations was 1.0% using 12 million particles per square centimeter.

4.3.2 Delivery of the IMRT Head and Neck Phantom Plan: Point Dose Comparison

Results comparing TLD measurements to predicted doses by the multiple source model are shown in Table 4.5 for the TrueBeam FFF 6MV model and Table 4.6 for the TrueBeam FFF 10MV model. TLD capsules were contained within the center of the primary PTV (four capsules), center of the secondary PTV (two capsules) and the center of a mock organ at risk (two capsules). Included in the table are average dose measurements, percent standard deviation from the three deliveries of each plan, a comparison of the DPM predicted dose with measurement expressed as a ratio of calculated dose to measured dose, and, for reference, a comparison of Eclipse calculated dose with measurement expressed as a ratio of calculated to measured dose.

TLD								
Point Dose Location	Measurement		DPM Calculation			Eclipse Calculation		
	Avg. (cGy)	% Std. Dev.	Avg. (cGy)	% Std. Dev.	Ratio Calc/Meas	Avg. (cGy)	% Std. Dev.	Ratio Calc/Meas
Pri – SP	663.7	0.2	654.4	1.0	0.986	668.0	1.4	1.006
Pri – SA	680.8	0.2	664.8	0.7	0.976	681.9	1.7	1.002
Pri – IP	660.5	0.6	653.6	0.6	0.990	665.9	0.0	1.008
Pri – IA	672.2	0.6	660.4	0.8	0.983	674.0	1.9	1.003
Pri Avg.					0.984			1.005
Sec – S	571.8	0.4	568.9	0.4	0.995	577.8	2.3	1.010
Sec – I	567.5	0.4	552.7	0.9	0.974	569.5	2.1	1.003
Sec Avg.					0.984			1.007
OAR – S	286.8	0.3	290.9	0.8	1.014	297.2	4.8	1.036
OAR – I	295.7	0.6	299.5	1.1	1.013	302.4	0.0	1.023
OAR Avg.					1.014			1.029

Table 4.5: Point dose comparisons for the FFF 6MV IMRT head and neck phantom measurements. The measured dose is the averaged dose from the three deliveries of each plan. Comparison to calculated doses by DPM (left) and Eclipse (right) are expressed as a ratio of calculated to measured doses. Point dose locations are indicated by Pri = Primary PTV, Sec = Secondary PTV, OAR = Organ at Risk, S = Superior, I = Inferior, A = Anterior, P = Posterior.

For the TrueBeam FFF 6MV model the average agreement between the DPM multiple source model calculation and measurement in the primary PTV was 0.984. The range of calculated to measured dose ratios was 0.976 to 0.990. The secondary PTV showed an average agreement of 0.984 with a range of 0.974 to 0.995. The averaged ratio for the OAR TLD was 1.014 with a range of 1.013 to 1.014.

Point Dose Location	TLD Measurement		DPM Calculation			Eclipse Calculation		
	Avg. (cGy)	% Std. Dev.	Avg. (cGy)	% Std. Dev.	Ratio Calc/Meas	Avg. (cGy)	% Std. Dev.	Ratio Calc/Meas
Pri – SP	658.3	0.7	670.0	0.6	1.018	662.7	1.9	1.007
Pri – SA	662.5	0.4	671.5	0.7	1.014	666.0	0.0	1.005
Pri – IP	660.1	0.7	676.4	0.6	1.025	665.1	0.0	1.008
Pri – IA	658.7	0.7	672.4	0.6	1.021	665.0	0.0	1.010
Pri Avg.					1.019			1.007
Sec – S	559.7	1.3	565.6	0.4	1.010	563.3	1.1	1.006
Sec – I	556.8	0.3	568.2	0.4	1.020	562.1	2.4	1.009
Sec Avg.					1.015			1.008
OAR – S	288.2	1.0	328.2	0.7	1.139	305.2	0.0	1.059
OAR – I	289.7	1.1	325.2	0.0	1.123	302.4	2.9	1.044
OAR Avg.					1.131			1.051

Table 4.6: Point dose comparisons for the FFF 10MV IMRT head and neck phantom measurements. The measured dose is the averaged dose from the three deliveries of each plan. Comparison to calculated doses by DPM (left) and Eclipse (right) are expressed as a ratio of calculated to measured doses. Point dose locations are indicated by Pri = Primary PTV, Sec = Secondary PTV, OAR = Organ at Risk, S = Superior, I = Inferior, A = Anterior, P = Posterior.

Results for the TrueBeam FFF 10MV model show an average agreement between the DPM code and measurement in the primary PTV of 1.019. The range contributing to this average was from 1.014 to 1.025. Agreement in the secondary PTV was 1.015 with a range of 1.010 to 1.020. Comparisons in the OAR showed an average agreement of 1.131 with a range of 1.123 to 1.139. The poorer agreement with measurement displayed in the OAR was attributed to the high dose gradient in the region that was necessary to meet the plan criteria.

While the benchmarking of the multiple source model was based exclusively on measurement, comparisons to doses calculated by Eclipse are included as means of comparison against an actively used and state of the art treatment planning system dose calculation algorithm. A comparison between average agreement of DPM to measured doses and Eclipse to measured doses shows superior agreement for the Eclipse results in both FFF 6MV and FFF 10MV models. The superior performance in Eclipse calculations in the PTV was limited to being no more than 1.1% and 1.2% better for FFF 6MV and FFF 10MV models, respectively.

4.3.3 Delivery of the IMRT Head and Neck Phantom Plan: Dose Profile and Gamma Map Comparison

Dose profile comparison between the multiple source model and measurement are shown for all three major planes in Figures 4.15, 4.16, and 4.17 for the 6MV model and Figures 4.18, 4.19, and 4.20 for the 10MV model. These comparisons are meant to be a qualitative assessment of the models ability to predict complex dose distributions across the volume of the PTV. All profiles showed good agreement between calculation and measurement.

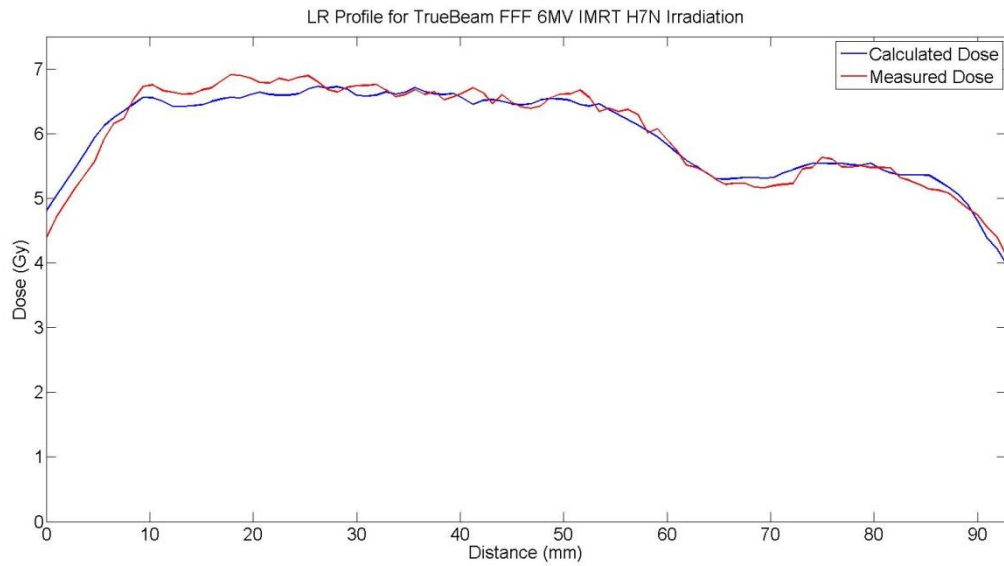


Figure 4.15: A comparison of the lateral (left to right) profile from the axial film of an IMRT H&N delivery for the FFF 6MV model (delivery #1).

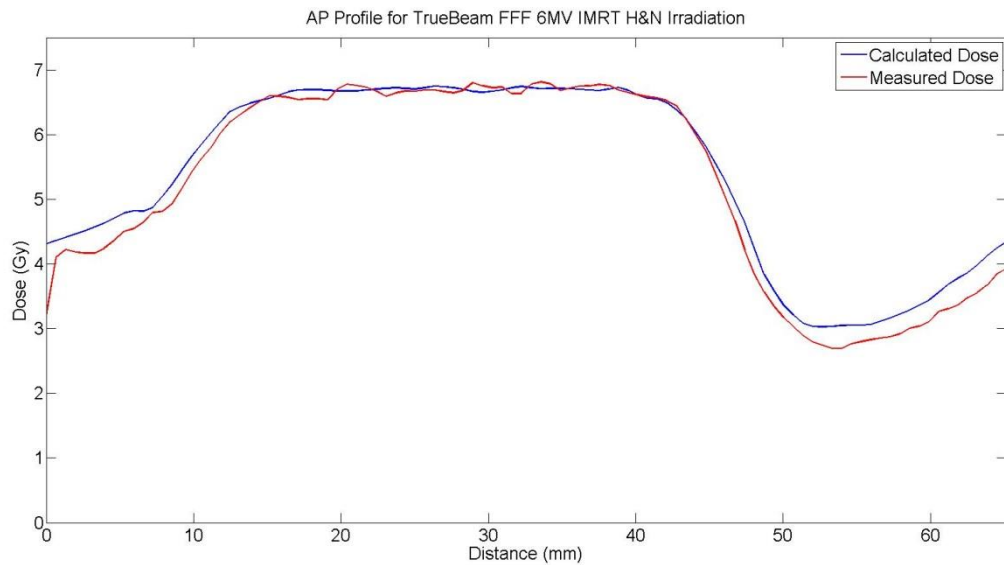


Figure 4.16: A comparison of the AP (anterior to posterior) profile from the axial film of an IMRT H&N delivery for the FFF 6MV model (delivery #1).

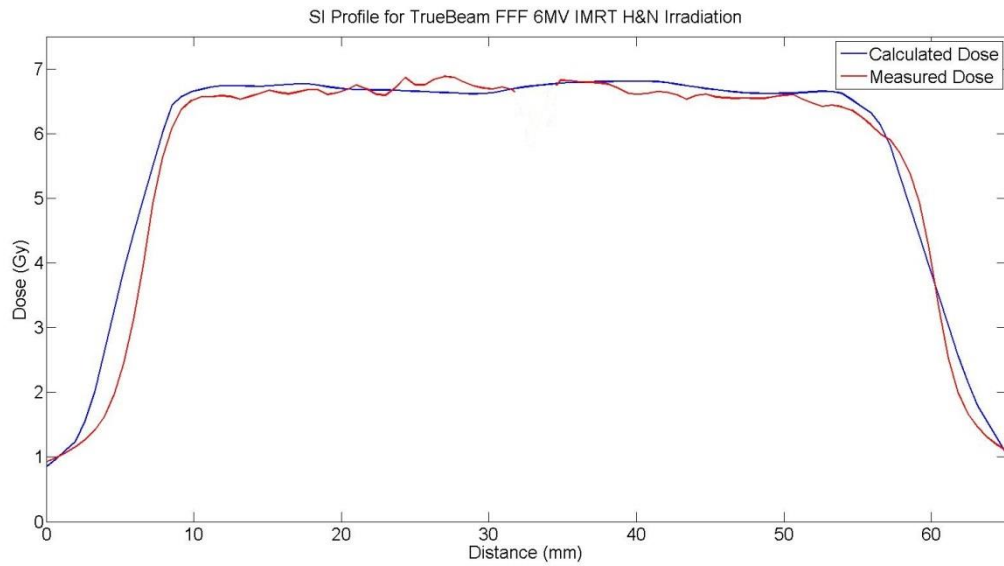


Figure 4.17: A comparison of the SI (superior to inferior) profile from the axial film of an IMRT H&N delivery for the FFF 6MV model (delivery #1).

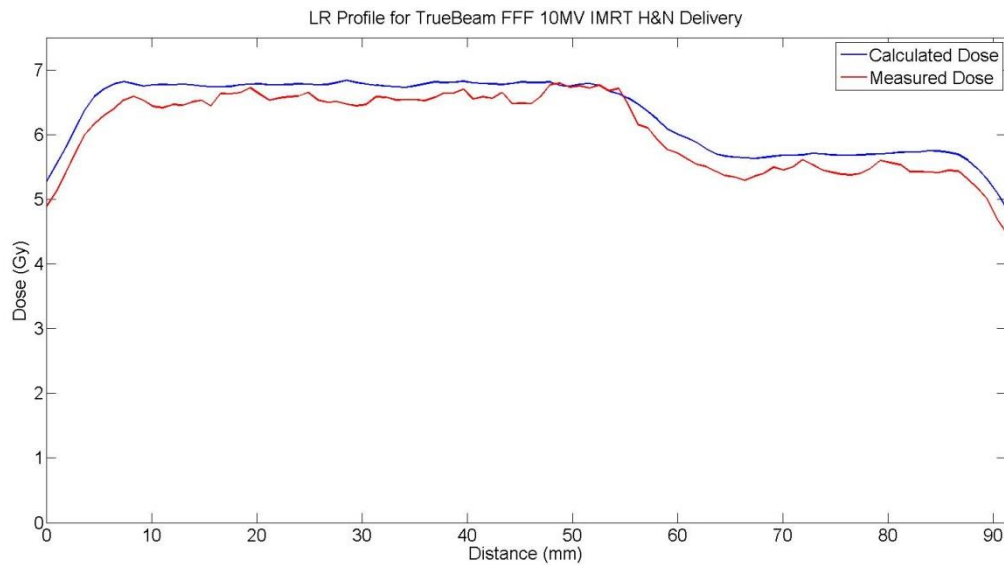


Figure 4.18: A comparison of the lateral (left to right) profile from the axial film of an IMRT H&N delivery for the FFF 10MV model (delivery #1).

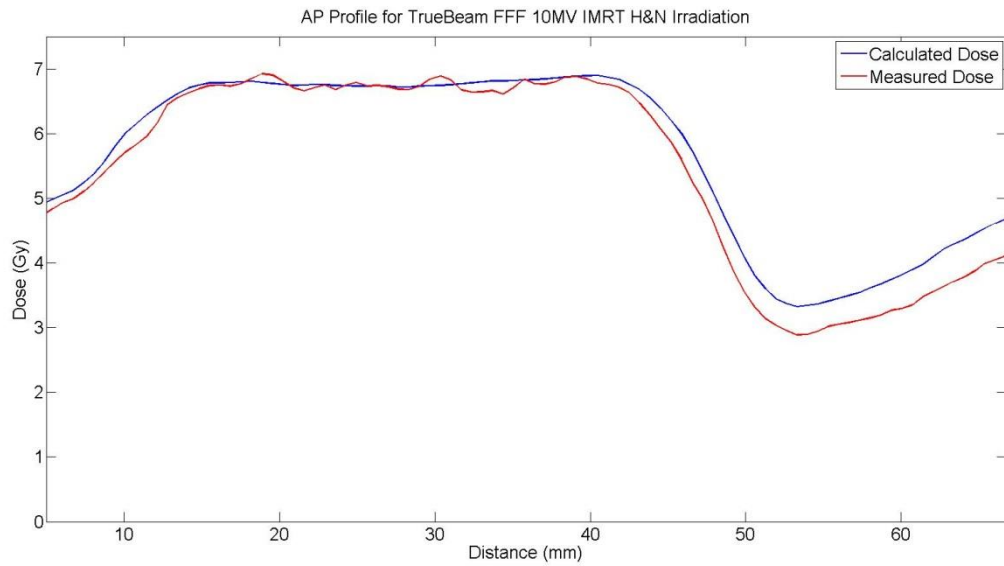


Figure 4.19: A comparison of the AP (anterior to posterior) profile from the axial film of an IMRT H&N delivery for the FFF 10MV model (delivery #1).

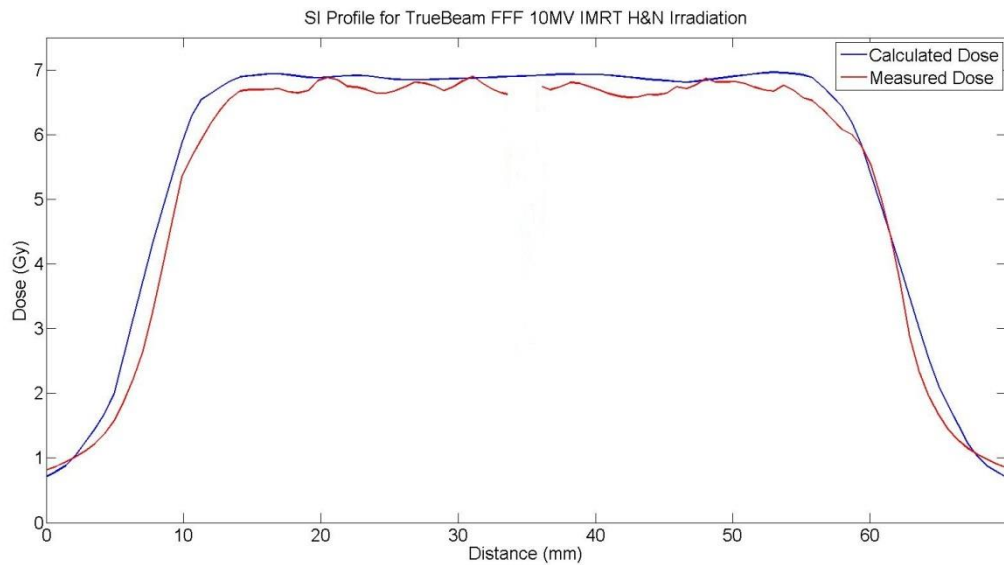


Figure 4.20: A comparison of the SI (superior to inferior) profile from the axial film of an IMRT H&N delivery for the FFF 10MV model (delivery #1).

To evaluate the models performance at describing the penumbra, MLC leakage, rounded leaf tips, and leaf transmission in highly modulated fields, gamma analysis was performed using a $\pm 3\%/2\text{mm}$ criterion. The analysis considers dose differences as relative percentage and the distance to agreement to assess overall agreement and identify locations of difficulty to the model. The resulting gamma maps from a single irradiation in the axial and sagittal plans are shown in Figure 4.21 and Figure 4.22 for the 6MV model and Figure 4.23 and Figure 4.24 for the 10MV model. Gamma maps for all three deliveries of each nominal energy are included in the Appendix. For the IMRT head and neck plan, the average percent of pixels passing for the 6MV comparison was 90.1% with a range of 80.3% to 95.9%. The 10MV comparison averaged 87.2% of pixels passing the $\pm 3\%/2\text{mm}$ criterion with a range of 75.5% to 93.1%. Table 4.7 reports the average agreement in the sagittal and axial planes for both the 6MV and 10MV models.

	TrueBeam FFF 6MV		TrueBeam FFF 10MV	
	Axial	Sagittal	Axial	Sagittal
Delivery #1	93.6	94.3	87.9	90.5
Delivery #2	89.4	86.6	93.1	85.9
Delivery #3	80.3	95.9	75.5	90.1
Average	87.8	92.3	85.5	88.8

Table 4.7: Percentage of pixels passing a $\pm 3\%/2\text{mm}$ gamma criterion for IMRT head and neck plans for both TrueBeam FFF 6MV and 10MV models. Agreement was evaluated in both the axial and sagittal planes for three deliveries of each plan.

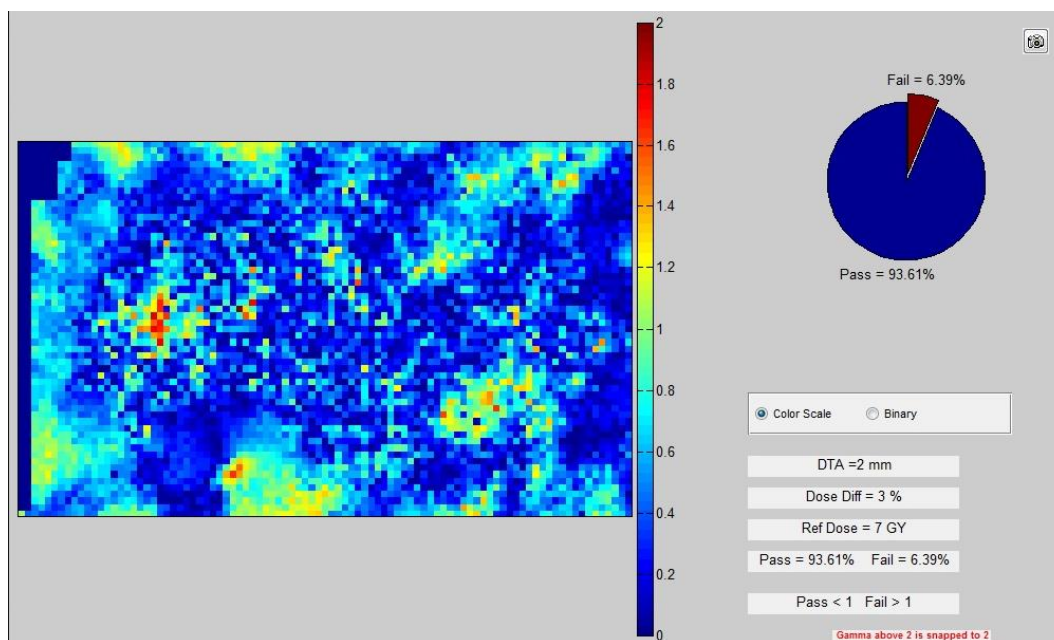


Figure 4.21: IMRT head and neck delivery comparison for the axial plane of delivery #1 for the TrueBeam FFF 6MV model. Agreement was evaluated using a $\pm 3\%/2\text{mm}$ gamma criterion and 93.6% of pixels passed.

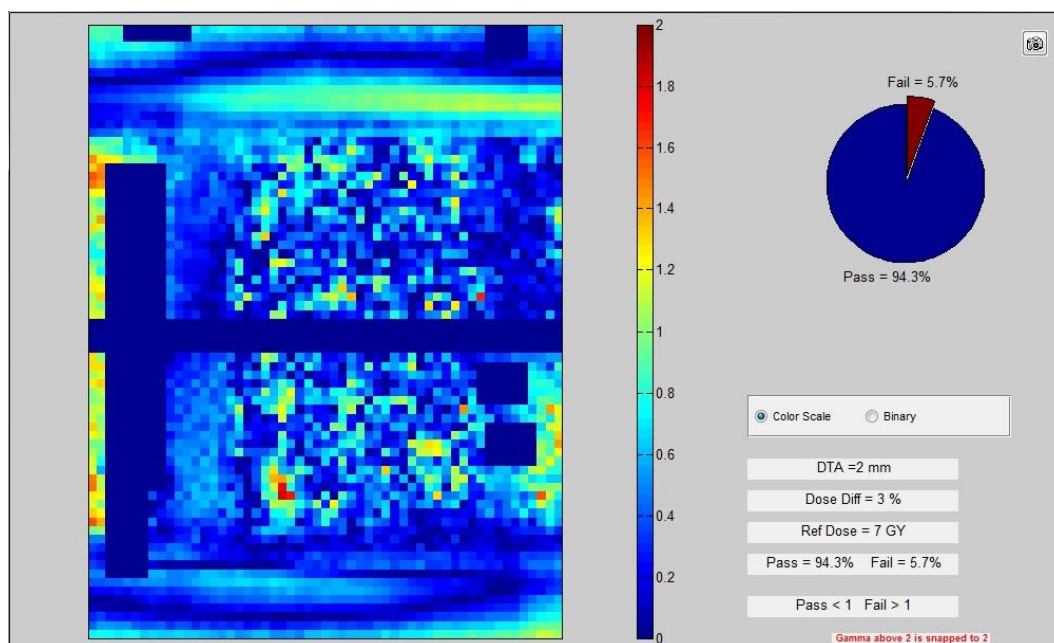


Figure 4.22: IMRT head and neck delivery comparison for the sagittal plane of delivery #1 for the TrueBeam FFF 6MV model. Agreement was evaluated using a $\pm 3\%/2\text{mm}$ gamma criterion and 94.3% of pixels passed.

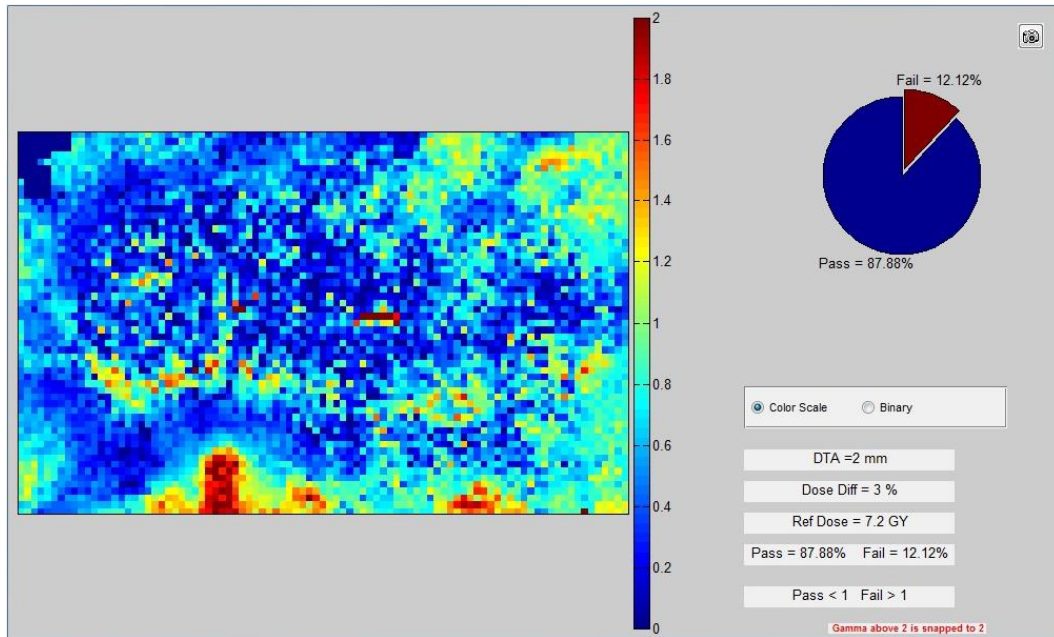


Figure 4.23: IMRT head and neck delivery comparison for the axial plane of delivery #1 for the TrueBeam FFF 10MV model. Agreement was evaluated using a $\pm 3\%/2\text{mm}$ gamma criterion and 87.9% of pixels passed.

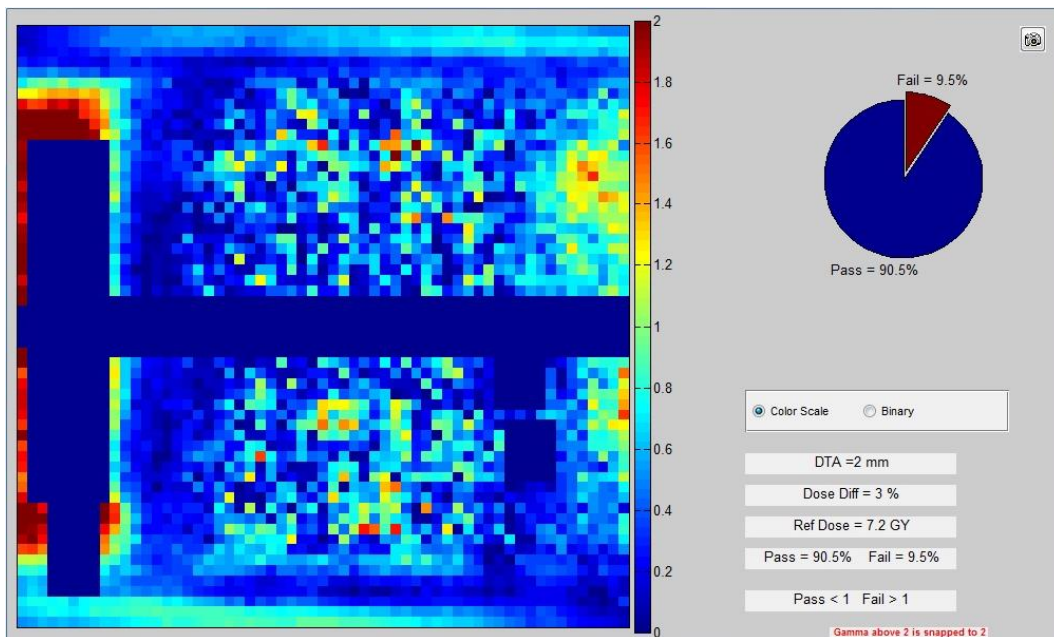


Figure 4.24: IMRT head and neck delivery comparison for the sagittal plane of delivery #1 for the TrueBeam FFF 10MV model. Agreement was evaluated using a $\pm 3\%/2\text{mm}$ gamma criterion and 90.5% of pixels passed.

Qualitative evaluation of the axial gamma maps suggested that the model was challenged most near the OAR where the dose gradient would be steepest. Failure regions of the sagittal gamma maps were consistent with the axial gamma maps in suggesting that the model was challenged most posterior to the PTV in the region near the OAR. Even with the increased challenge near the steep dose gradient, passing rates were above the pre-established threshold of 85%.

4.3.4 Delivery of the SBRT Thorax Phantom Plan: Point Dose Comparison

The results to point dose comparisons between the developed model and TLD measurements in the anthropomorphic thorax phantom are shown in Table 4.8 and Table 4.9. Double packed TLD were contained in the center of the target (two), in the heart (one), and in the spinal cord (one). The table includes average dose measurements, percent standard deviation from the three deliveries of each plan, a comparison of the DPM predicted dose with measurement expressed as a ratio of calculated dose to measured dose, and, for reference, a comparison of Eclipse calculated doses with measurement expressed as a ratio of measured to calculated dose.

TLD								
	Measurement		DPM Calculation			Eclipse Calculation		
Point Dose	Avg.	% Std.	Avg.	% Std.	Ratio	Avg.	% Std.	Ratio
Location	(cGy)	Dev.	(cGy)	Dev.	Calc/Meas	(cGy)	Dev.	Calc/Meas
PTV – S	788.2	0.4	796.7	0.5	1.011	812.9	0.0	1.031
PTV – I	783.0	0.1	786.3	0.4	1.004	803.1	0.5	1.026
PTV Avg.					1.007			1.028
OAR – Heart	170.6	0.4	177.5	1.7	1.040	168.8	0.0	0.989
OAR – Cord	155.2	0.0	177.5	2.6	1.144	179.4	2.6	1.156

Table 4.8: Point dose comparisons for the FFF 6MV SBRT lung phantom measurements. The measured dose is the averaged dose from the three deliveries of each plan. Comparison to calculated doses by DPM (left) and Eclipse (right) are expressed as a ratio of calculated to measured doses. Point dose locations are indicated by PTV = Planning Target Volume, OAR = Organ at Risk, S = Superior, I = Inferior.

For the TrueBeam FFF 6MV model the average agreement between the DPM multiple source model calculation and measurement in the PTV was 1.007. The range of calculated to measured dose ratios was 1.004 to 1.011. The ratio for the heart TLD was 1.040, and the ratio for the cord TLD was 1.144.

Point Dose Location	TLD Measurement		DPM Calculation			Eclipse Calculation		
	Avg. (cGy)	% Std. Dev.	Avg. (cGy)	% Std. Dev.	Ratio Calc/Meas	Avg. (cGy)	% Std. Dev.	Ratio Calc/Meas
PTV – S	819.6	0.6	828.3	0.6	1.011	836.6	0.6	1.021
PTV – I	813.9	0.4	810.0	2.1	0.995	821.3	0.6	1.009
PTV Avg.					1.003			1.015
OAR – Heart	155.5	0.7	152.0	2.6	0.978	155.0	0.0	0.997
OAR – Cord	150.5	0.5	170.0	0.0	1.130	169.9	0.0	1.129

Table 4.9: Point dose comparisons for the FFF 10MV SBRT lung phantom measurements. The measured dose is the averaged dose from the three deliveries of each plan. Comparison to calculated doses by DPM (left) and Eclipse (right) are expressed as a ratio of calculated to measured doses. Point dose locations are indicated by PTV = Planning Target Volume, OAR = Organ at Risk, S = Superior, I = Inferior.

The average agreement between the DPM model and the PTV for the TrueBeam FFF 10MV model was 1.003. The range of the values for the PTV agreement was 0.995 to 1.011. The calculated to measured ratios for the heart and cord TLDs were 0.978 and 1.130, respectively.

It is important to note that while the OAR calculated doses showed poorer agreement with measurements for 6MV and 10MV models, the uncertainty in the measured dose is unknown at such low doses. The standards used for low dose measurements are done at doses of 8Gy and 3Gy, nearly 3 times the dose of both the heart and cord measurement for the lower of the two standard doses. At doses near 1Gy, as seen in both of the OAR TLD, the RPC does not have data documenting the accuracy of their TLD measurement process for phantom irradiations.

Even though the benchmarking of the multiple source model was based exclusively on measurement, comparisons to doses calculated by Eclipse are included as means of comparison against an actively used and state of the art treatment planning system dose calculation algorithm. A direct comparison between the DPM calculated doses and the Eclipse calculated doses show the DPM calculation to agree better with measurement results in the PTVs and comparably within the OARs.

4.3.5 Delivery of the SBRT Thorax Phantom Plan: Dose Profile and Gamma Map

Comparison

Dose profile comparison between the multiple source model and measurement are shown for all three major planes in Figures 4.25, 4.26, 4.27 for the FFF 6MV model and Figures 4.28, 4.29, and 4.30 for the FFF 10MV model. These comparisons are meant to be a qualitative assessment of the models ability to predict complex dose distributions across the volume of the PTV. All profiles showed good agreement between calculation and measurement.

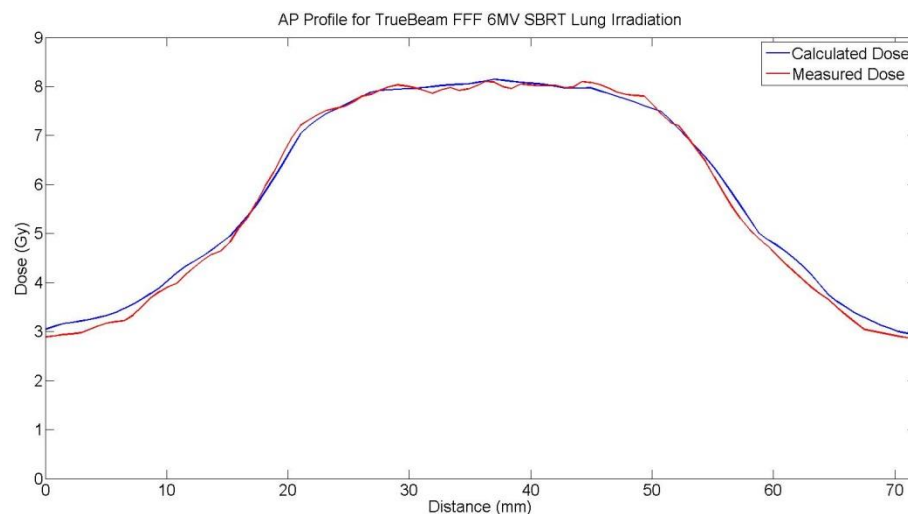


Figure 4.25: A comparison of the lateral (left to right) profile from the axial film of an SBRT lung delivery for the FFF 6MV model (delivery #1).

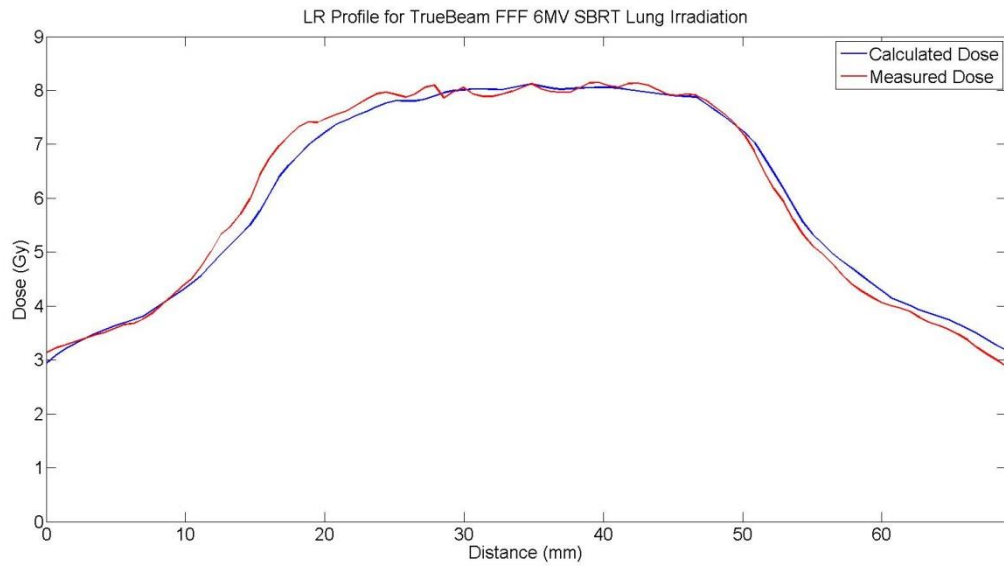


Figure 4.26: A comparison of the AP (anterior to posterior) profile from the axial film of an SBRT lung delivery for the FFF 6MV model (delivery #1).

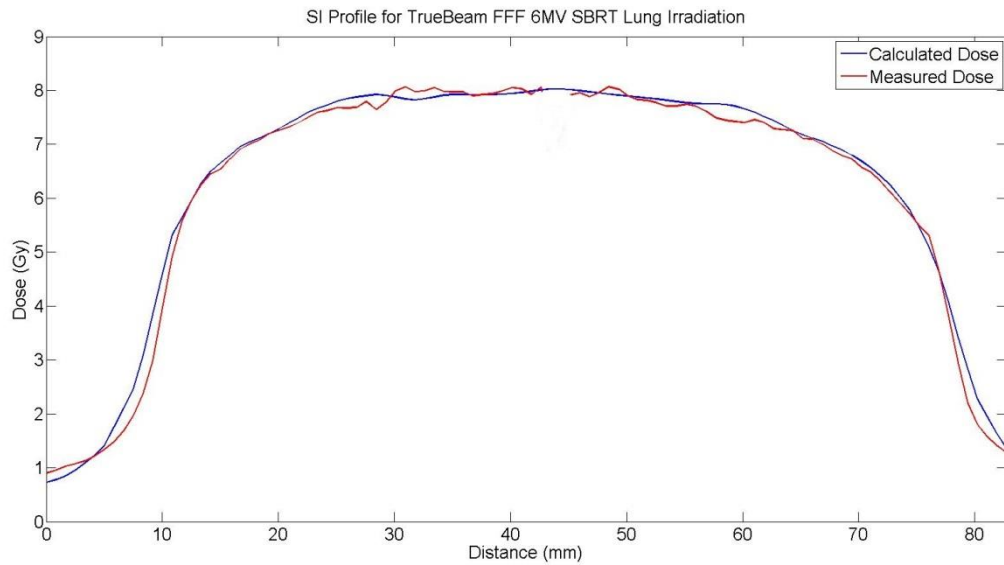


Figure 4.27: A comparison of the SI (superior to inferior) profile from the sagittal film of an SBRT lung delivery for the FFF 6MV model (delivery #1).

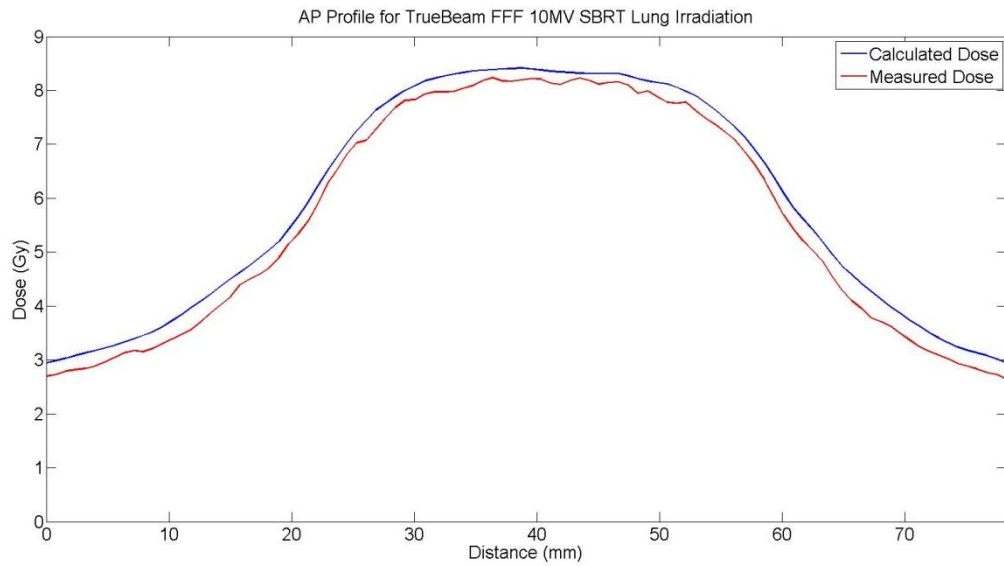


Figure 4.28: A comparison of the lateral (left to right) profile from the axial film of an SBRT lung delivery for the FFF 10MV model (delivery #1).

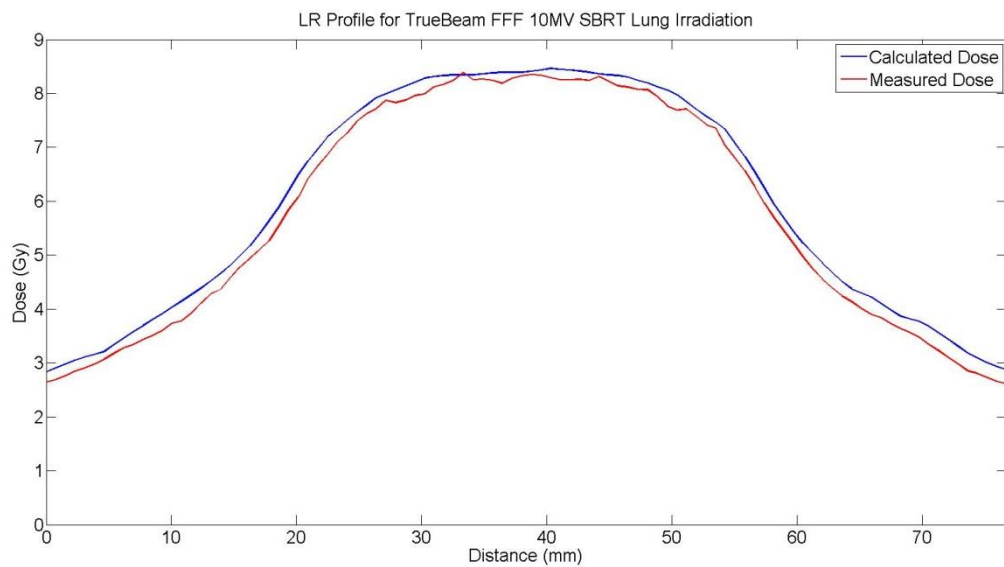


Figure 4.29: A comparison of the AP (anterior to posterior) profile from the axial film of an SBRT lung delivery for the FFF 10MV model (delivery #1).

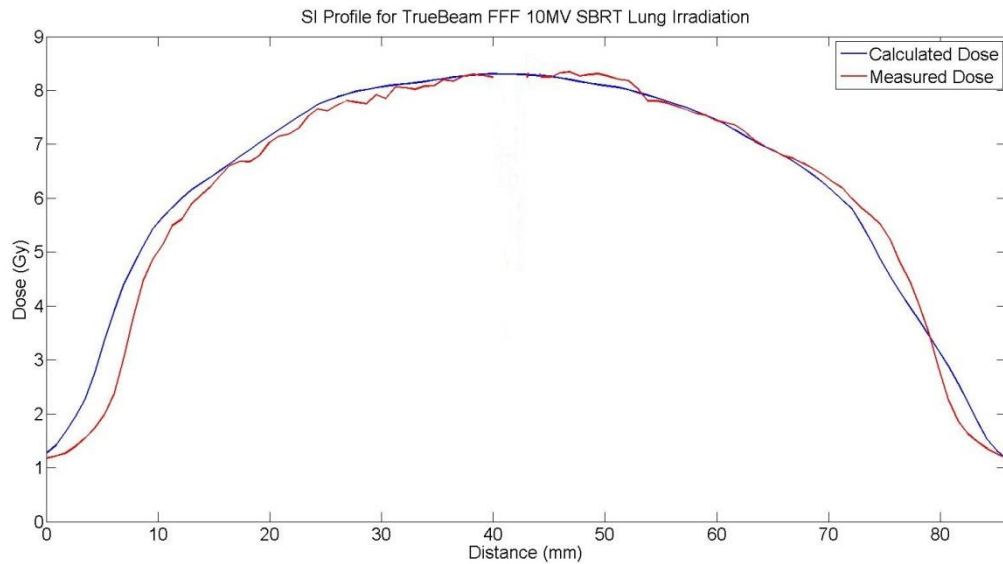


Figure 4.30: A comparison of the SI (superior to inferior) profile from the sagittal film of an SBRT lung delivery for the FFF 10MV model (delivery #1).

The model's ability to describe the beam penumbra, MLC leakage, rounded leaf tips, and leaf transmission in unmodulated fields in a heterogeneous medium provided by the lung phantom was evaluated using the gamma technique with a $\pm 3\%/2\text{mm}$ criterion. The analysis considers the dose differences as a percentage of the maximum dose and distance to agreement to assess overall agreement between dose distributions calculated by the multiple source model and measured by the radiochromic film in the phantom. In this way resulting gamma maps can be used to identify areas where the model may be deficient while allowing for positional measurement uncertainty to be accounted for in the distance to agreement criterion.

The gamma maps for a single irradiation and comparison to source model calculation for the 6MV model are shown in Figures 4.31, 4.32, and 4.33 for the axial, sagittal, and coronal planes, respectively. Gamma maps for each delivery are included in the Appendix. The average agreement, expressed as a percentage of pixels passing the gamma criterion, were 87.8%, 90.4%, and 94.2% for axial, sagittal, and coronal planes, respectively. Agreement for

the axial plane ranged from 84.5% to 91.5%. Agreement for the sagittal plane ranged from 85.5% to 95.2%, and the range of agreement for the coronal plane was 85.5% to 98.7%.

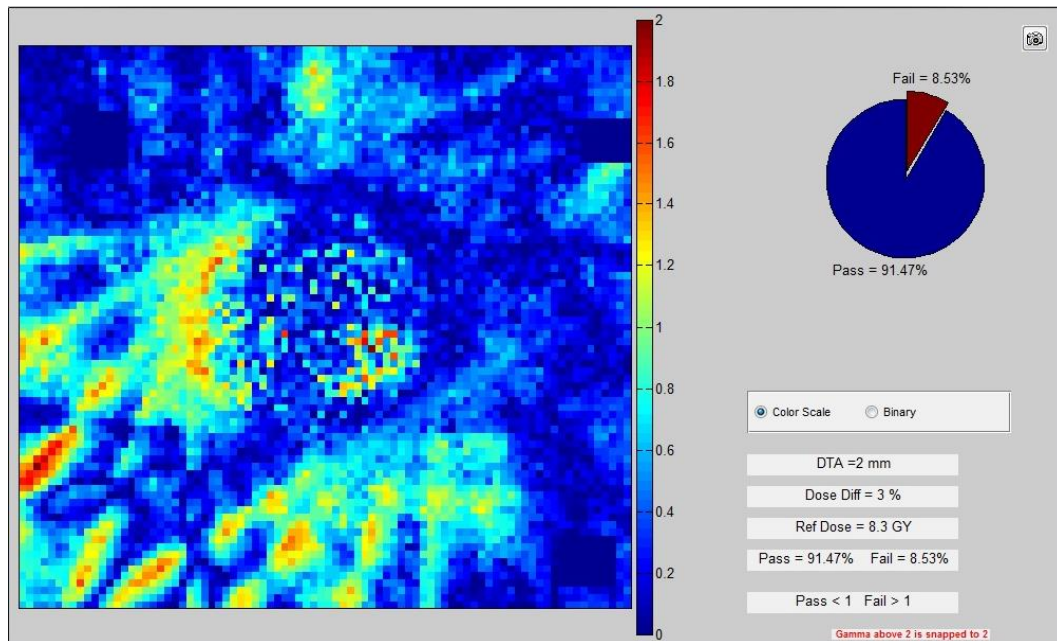


Figure 4.31: Lung SBRT delivery comparison for the axial plane of delivery #1 for the TrueBeam FFF 6MV model. Agreement was evaluated using a $\pm 3\%/2\text{mm}$ gamma criterion and 91.5% of pixels passed.

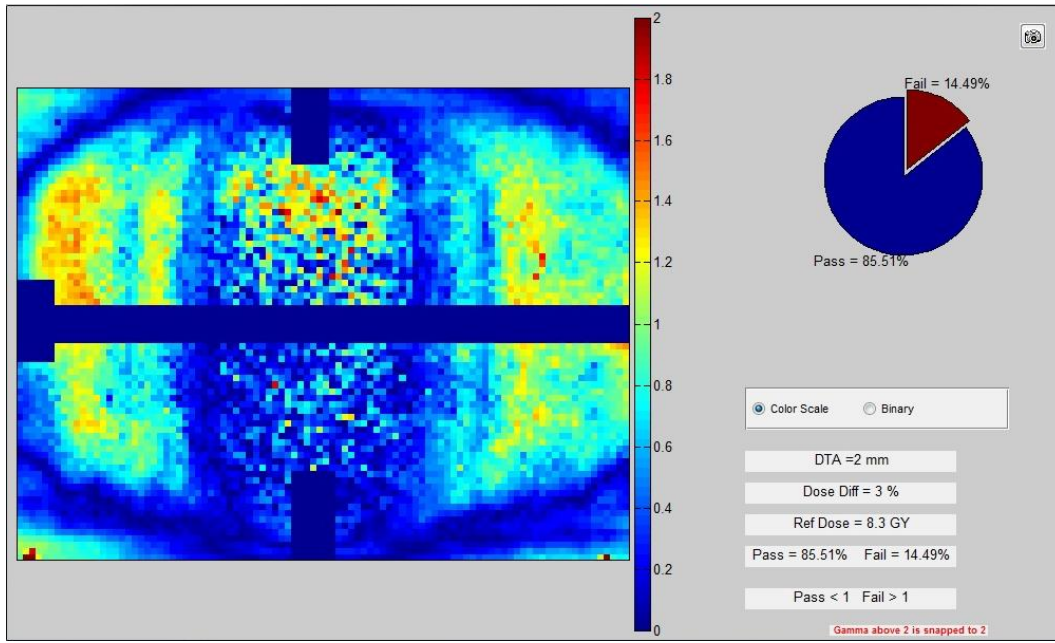


Figure 4.32: Lung SBRT delivery comparison for the sagittal plane of delivery #1 for the TrueBeam FFF 6MV model. Agreement was evaluated using a $\pm 3\%/2\text{mm}$ gamma criterion and 85.5% of pixels passed.

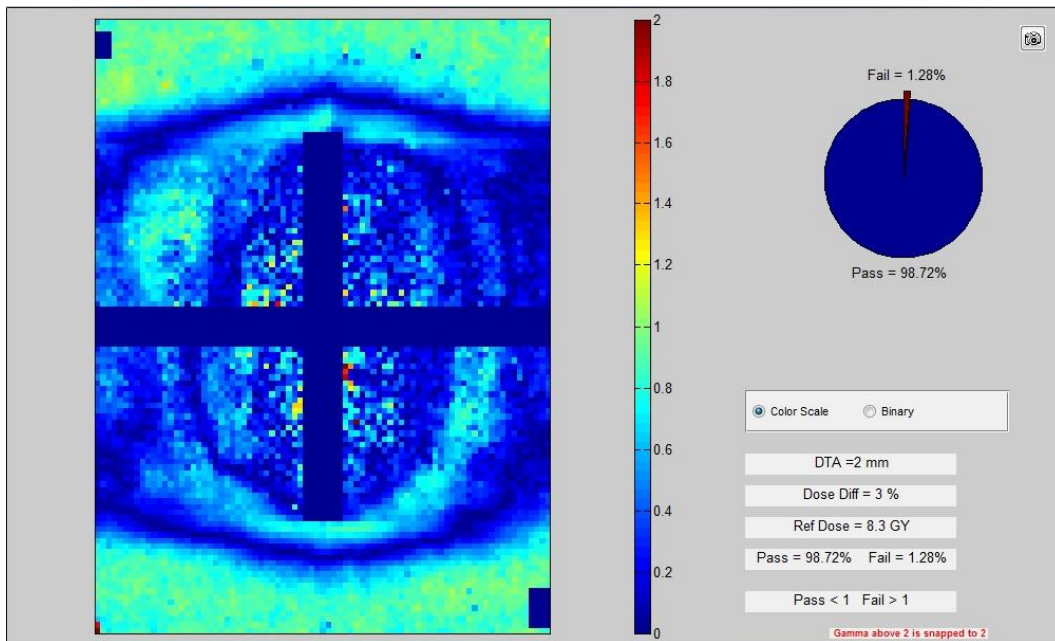


Figure 4.33: Lung SBRT delivery comparison for the coronal plane of delivery #1 for the TrueBeam FFF 6MV model. Agreement was evaluated using a $\pm 3\%/2\text{mm}$ gamma criterion and 98.7% of pixels passed.

The gamma maps corresponding to the comparison of a single irradiation to the calculated dose of the 10MV source model are showing in Figures 4.34, 4.35, and 4.36 for axial, sagittal, and coronal planes, respectively. Gamma maps from all other deliveries are included in the Appendix for reference. The average agreement was 91.5%, 89.5%, and 94.2% for axial, sagittal, and coronal planes, respectively. The range of values for the axial plane was 87.4% to 95.8%, for the sagittal plane 88.1% to 91.4%, and for the coronal plane 91.9% to 98.1%.

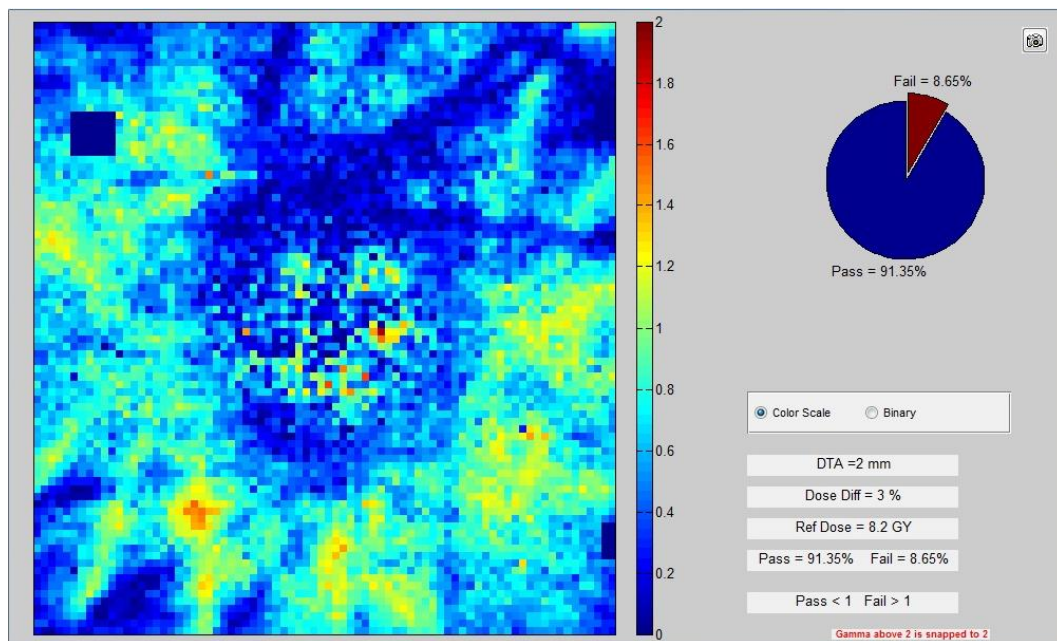


Figure 4.34: Lung SBRT delivery comparison for the axial plane of delivery #1 for the TrueBeam FFF 10MV model. Agreement was evaluated using a $\pm 3\%/2\text{mm}$ gamma criterion and 91.4% of pixels passed.

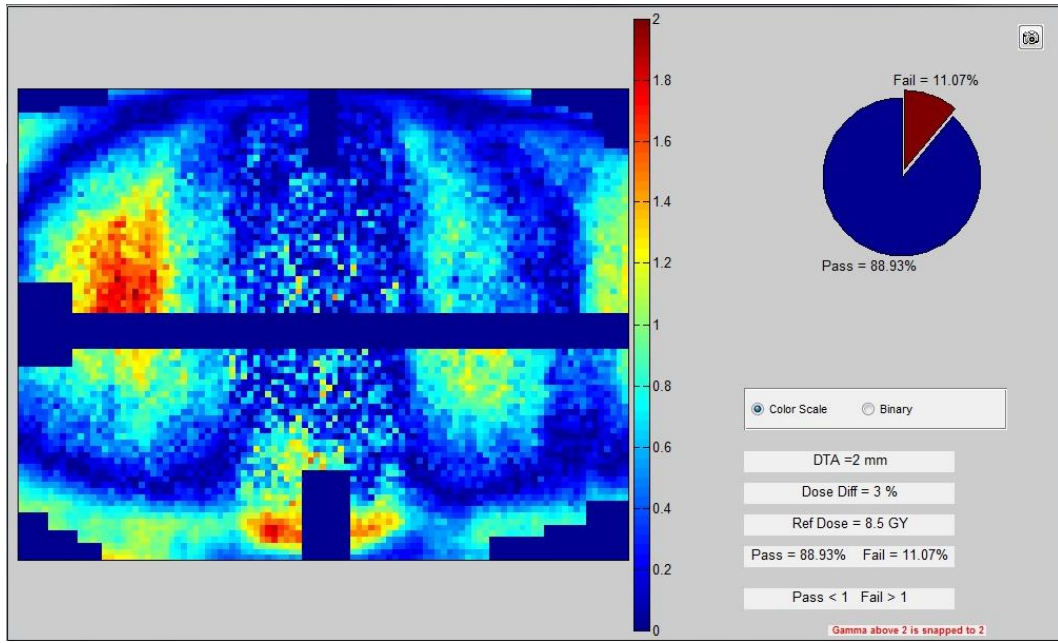


Figure 4.35: Lung SBRT delivery comparison for the sagittal plane of delivery #1 for the TrueBeam FFF 10MV model. Agreement was evaluated using a $\pm 3\%/2\text{mm}$ gamma criterion and 88.9% of pixels passed.

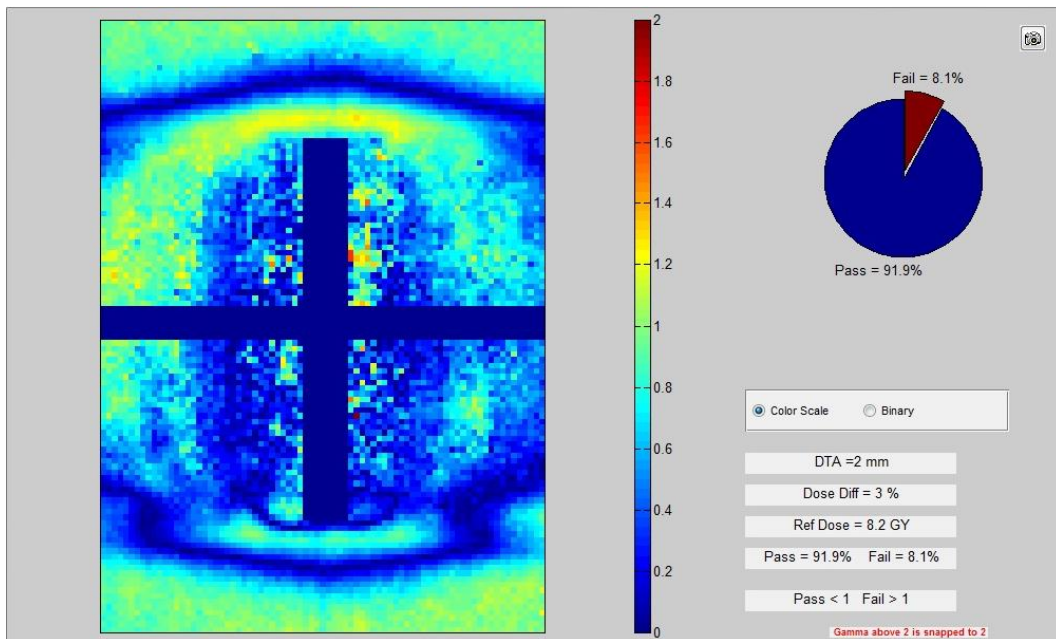


Figure 4.36: Lung SBRT delivery comparison for the coronal plane of delivery #1 for the TrueBeam FFF 10MV model. Agreement was evaluated using a $\pm 3\%/2\text{mm}$ gamma criterion and 91.9% of pixels passed.

The passing rate of comparisons for each plane for all three deliveries with respect to the DPM source model calculation is shown for both 6MV and 10MV models in Table 4.10.

	TrueBeam FFF 6MV			TrueBeam FFF 10MV		
	Axial	Sagittal	Coronal	Axial	Sagittal	Coronal
Delivery #1	91.5	85.5	98.7	91.4	88.9	91.9
Delivery #2	84.5	90.3	98.4	87.4	88.1	92.7
Delivery #3	87.5	95.2	85.5	95.8	91.4	98.1
Average	87.8	90.4	94.2	90.2	88.3	89.5

Table 4.10: Percentage of pixels passing a $\pm 3\%/2\text{mm}$ gamma criterion for SBRT lung plans for both TrueBeam FFF 6MV and FFF 10MV models. Agreement was evaluated in the axial, sagittal, and coronal planes for three deliveries of each plan.

A qualitative evaluation of the gamma maps showed no consistent failure regions in the comparison in the axial plane. The agreement in the sagittal and coronal planes appeared to be challenged most at the edges of the PTV. This is largely attributed to the sensitivity of the comparison to the registration of film to the phantom. Because both film plane comparisons consist of two pieces of film that need to be aligned during scanning, the registration uncertainty is higher than for the axial plane which consists of single piece of film. Furthermore the high dose gradients at the edges of the PTV make the analysis more sensitive to a small translational shift either in the film registration or phantom setup. Even with the increased registration uncertainty, passing rates were above the pre-established threshold of 85%.

4.3.6 Delivery of the IMRT Thorax Phantom Plan: Point Dose Comparison

The results to point dose comparisons between the developed model and TLD measurements in the anthropomorphic thorax phantom are shown in Table 4.11 and Table 4.12. Double packed TLD were contained in the center of the target (two), in the heart (one), and in the spinal cord (one). The table includes dose measurements, a comparison of the DPM predicted dose with measurement expressed as a ratio of calculated dose to measured dose, and, for reference, a comparison of Eclipse calculated doses with measurement expressed as a ratio of calculated to measured dose.

TLD								
Point Dose Location	Measurement		DPM Calculation			Eclipse Calculation		
	Avg. (cGy)	% Std. Dev.	Avg. (cGy)	% Std. Dev.	Ratio Calc/Meas	Avg. (cGy)	% Std. Dev.	Ratio Calc/Meas
PTV – S	625.4	0.5	616.7	0.8	0.986	636.0	0.7	1.017
PTV – I	625.1	1.0	630.0	1.2	1.008	644.1	0.0	1.030
PTV Avg.					0.997			1.024
OAR – Heart	62.5	1.0	58.0	8.4	0.927	60.0	8.3	0.959
OAR – Cord	47.5	0.4	50.0	0.0	1.054	57.8	0.0	1.218

Table 4.11: Point dose comparisons for the FFF 6MV IMRT lung phantom measurements. The measured dose is the averaged dose from the three deliveries of each plan. Comparison to calculated doses by DPM (left) and Eclipse (right) are expressed as a ratio of calculated to measured doses. Point dose locations are indicated by PTV = Planning Target Volume, OAR = Organ at Risk, S = Superior, I = Inferior.

For the TrueBeam FFF 6MV model the average agreement between the DPM multiple source model calculation and measurement in the PTV was 0.997. The range of calculated to measured dose ratios was 0.986 to 1.008. The ratio for the heart TLD was 0.927, and the ratio for the cord TLD was 1.054.

Point Dose Location	TLD Measurement		DPM Calculation			Eclipse Calculation		
	Avg. (cGy)	% Std. Dev.	Avg. (cGy)	% Std. Dev.	Ratio Calc/Meas	Avg. (cGy)	% Std. Dev.	Ratio Calc/Meas
PTV – S	624.2	0.5	630.0	0.0	1.009	631.0	0.0	1.011
PTV – I	643.4	0.5	630.0	0.0	0.979	626.9	0.0	0.974
PTV Avg.					0.994			0.993
OAR – Heart	62.4	1.3	68.0	0.0	1.090	61.5	8.0	0.985
OAR – Cord	52.5	0.8	50.0	0.0	0.953	51.0	0.0	0.972

Table 4.12: Point dose comparisons for the FFF 10MV IMRT lung phantom measurements.

The measured dose is the averaged dose from the three deliveries of each plan. Comparison to calculated doses by DPM (left) and Eclipse (right) are expressed as a ratio of calculated to measured doses. Point dose locations are indicated by PTV = Planning Target Volume, OAR = Organ at Risk, S = Superior, I = Inferior.

The average agreement between the DPM model and the PTV for the TrueBeam FFF 10MV model was 0.994. The range of the values for the PTV agreement was 0.979 to 1.009. The calculated to measured ratio for the heart and cord TLDs were 1.090 and 0.953, respectively.

It is important to note that while the OAR calculated doses showed poorer agreement with measurements for 6MV and 10MV models, the uncertainty in the measured dose is unknown at such low doses. The standards used for low dose measurements are done at doses of 8Gy and 3Gy, nearly 3 times the dose of both the heart and cord measurement for the lower of the two standard doses. At doses near 1Gy, as seen in both of the OAR TLD, the RPC does not have data documenting the accuracy of their TLD measurement process for phantom irradiations.

Even though the benchmarking of the multiple source model was based exclusively on measurement, comparisons to doses calculated by Eclipse are included as means of comparison against an actively used and state of the art treatment planning system dose calculation algorithm. A direct comparison between the DPM calculated dose performance to the Eclipse calculated dose performance shows comparable results in the PTV TLD capsules and inferior performance within the OARs.

4.3.7 Delivery of the IMRT Thorax Phantom Plan: Dose Profile and Gamma Map

Comparison

Dose profile comparison between the multiple source model and measurement are shown for all three major planes in Figures 4.37, 4.38, 4.39 for the 6MV model and Figures 4.40, 4.41, and 4.42 for the 10MV model. These comparisons are meant to be a qualitative assessment of the models ability to predict complex dose distributions across the volume of the PTV. All profiles showed good agreement between calculation and measurement.

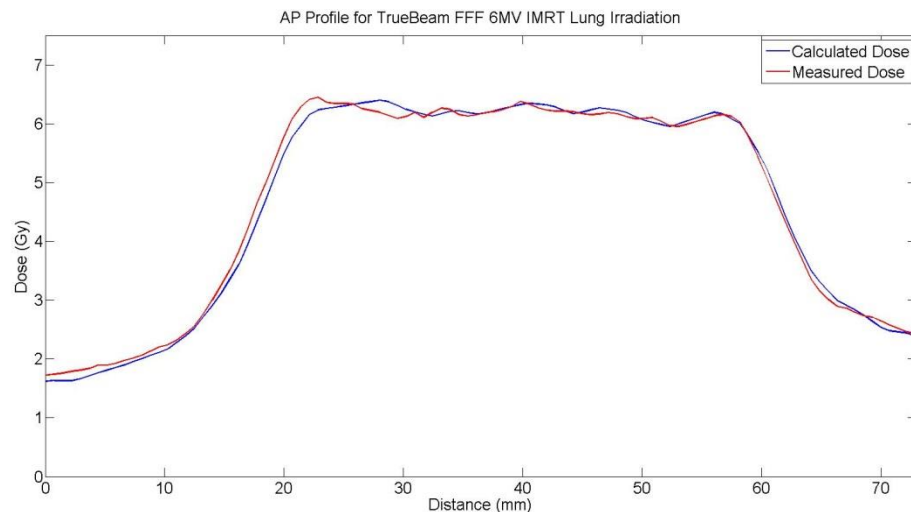


Figure 4.37: A comparison of the lateral (left to right) profile from the axial film of an IMRT lung delivery for the FFF 6MV model (delivery #1).

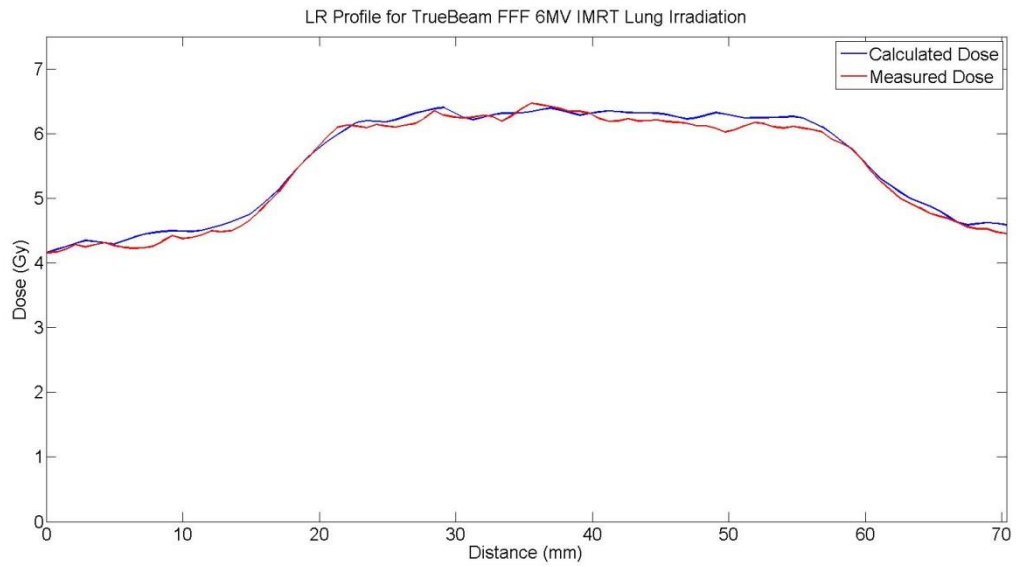


Figure 4.38: A comparison of the AP (anterior to posterior) profile from the axial film of an IMRT lung delivery for the FFF 6MV model (delivery #1).

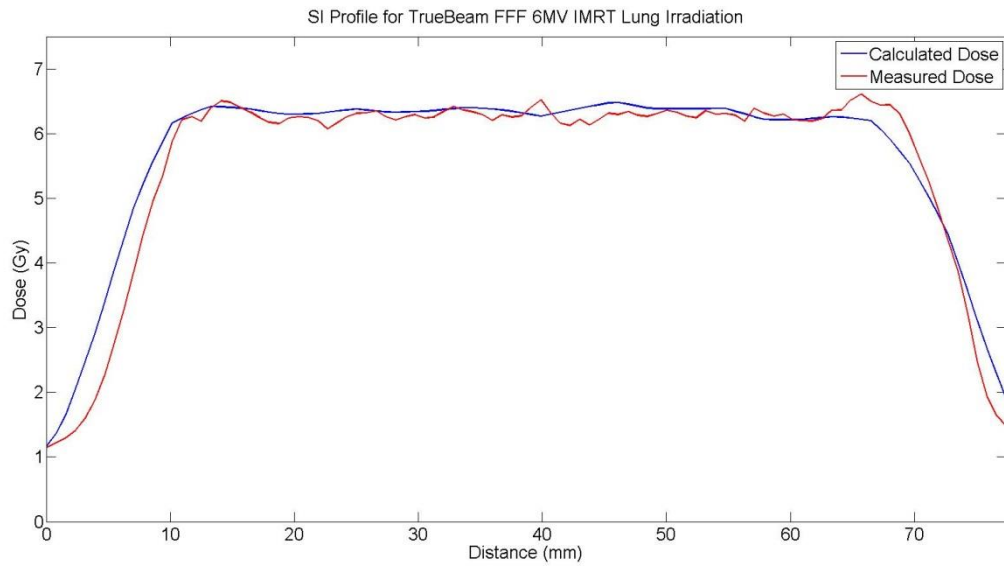


Figure 4.39: A comparison of the SI (superior to inferior) profile from the sagittal film of an IMRT lung delivery for the FFF 6MV model (delivery #1).

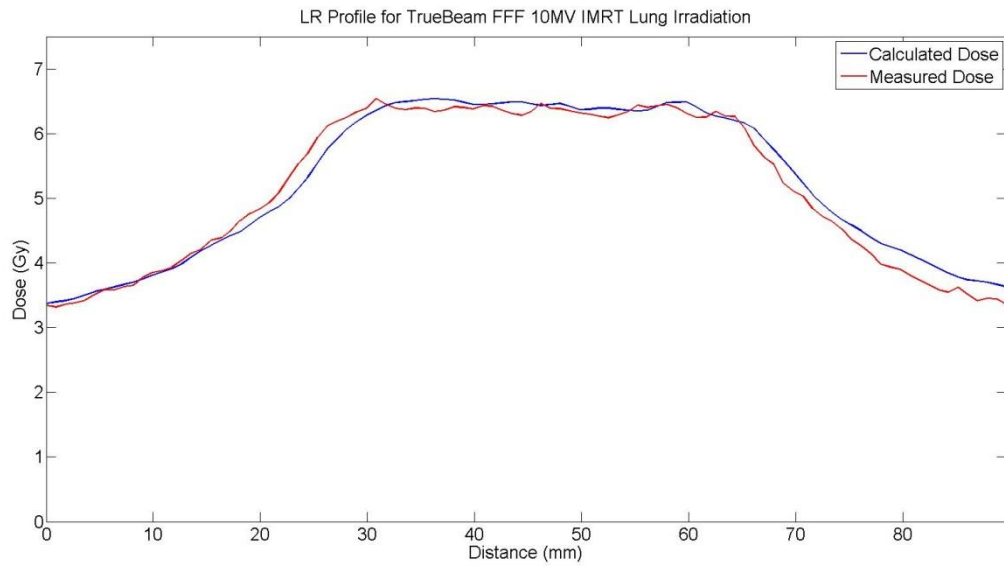


Figure 4.40: A comparison of the lateral (left to right) profile from the axial film of an IMRT lung delivery for the FFF 10MV model (delivery #1).

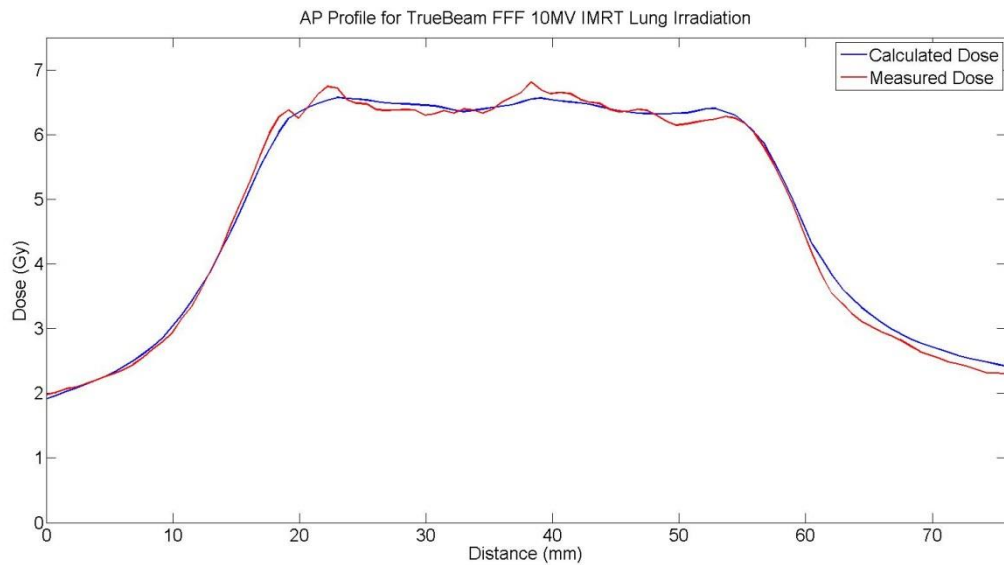


Figure 4.41: A comparison of the AP (anterior to posterior) profile from the axial film of an IMRT lung delivery for the FFF 10MV model (delivery #1).

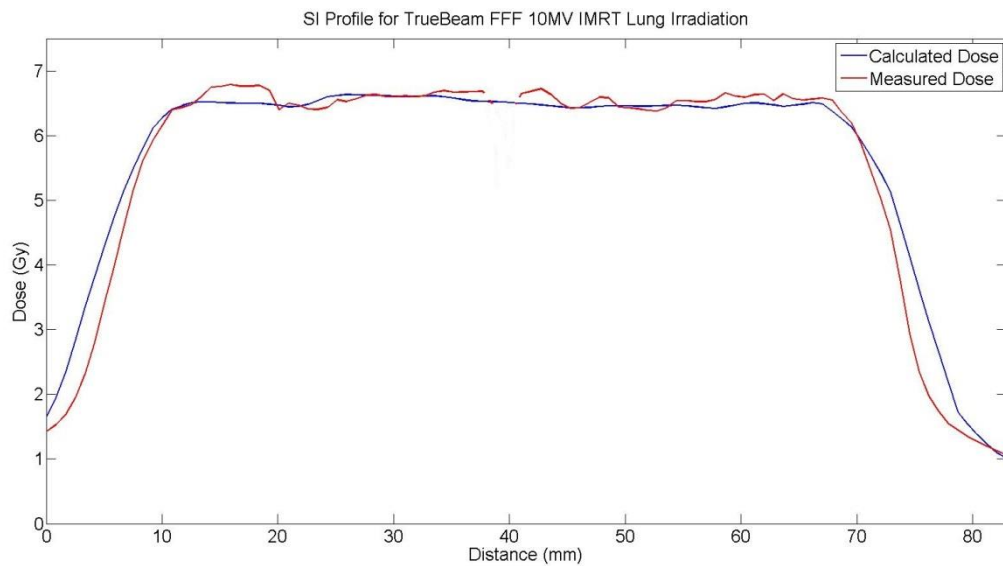


Figure 4.42: A comparison of the SI (superior to inferior) profile from the sagittal film of an IMRT lung delivery for the FFF 10MV model (delivery #1).

The model's ability to describe the beam penumbra, MLC leakage, rounded leaf tips, and leaf transmission in unmodulated fields in a heterogeneous medium provided by the lung phantom was evaluated using the gamma technique with a $\pm 3\%/2\text{mm}$ criterion. The analysis considers the dose differences as a percentage of the maximum dose and distance to agreement to assess overall agreement between dose distributions calculated by the multiple source model and measured by the radiochromic film in the phantom. In this way resulting gamma maps can be used to identify areas where the model may be deficient while allowing for positional measurement uncertainty to be accounted for in the distance to agreement criterion.

The gamma maps for a single irradiation and comparison to source model calculation for the FFF 6MV model are shown in Figures 4.43, 4.44, and 4.45 for the axial, sagittal, and coronal planes respectively. Gamma maps for each delivery are included in the Appendix. The average agreement, expressed as a percentage of pixels passing the gamma criterion, were 92.0%, 91.2%, and 91.5% for axial, sagittal, and coronal planes, respectively. Agreement for the axial

plane ranged from 91.0% to 93.5%. Agreement for the sagittal plane ranged from 87.4% to 94.3%, and the range of agreement for the coronal plane was 88.4% to 93.9%.

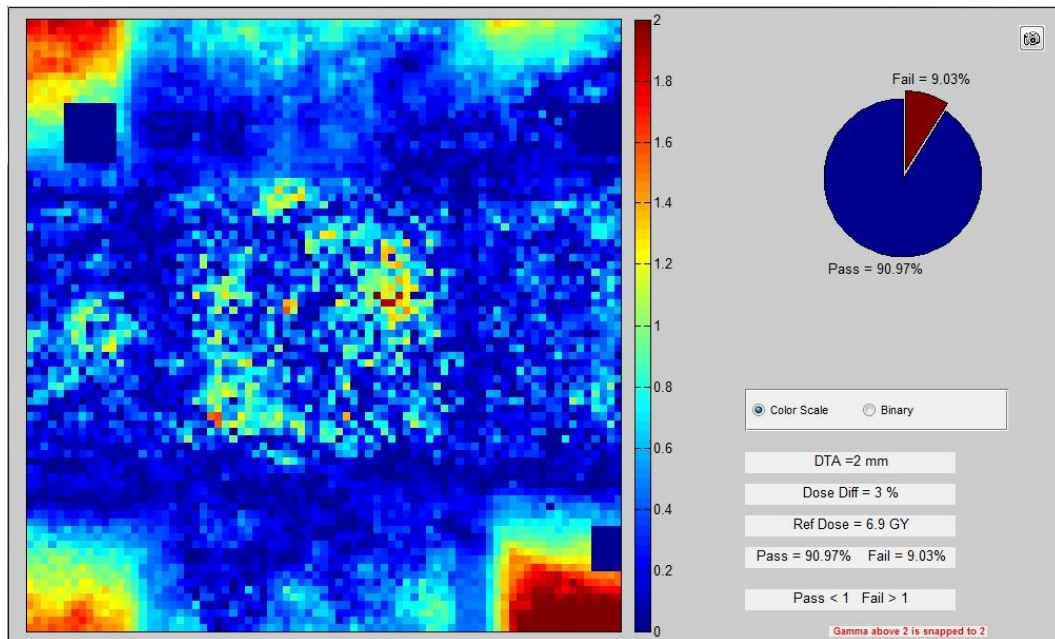


Figure 4.43: Lung IMRT delivery comparison for the axial plane of delivery #1 for the TrueBeam FFF 6MV model. Agreement was evaluated using a $\pm 3\%/2\text{mm}$ gamma criterion and 91.0% of pixels passed.

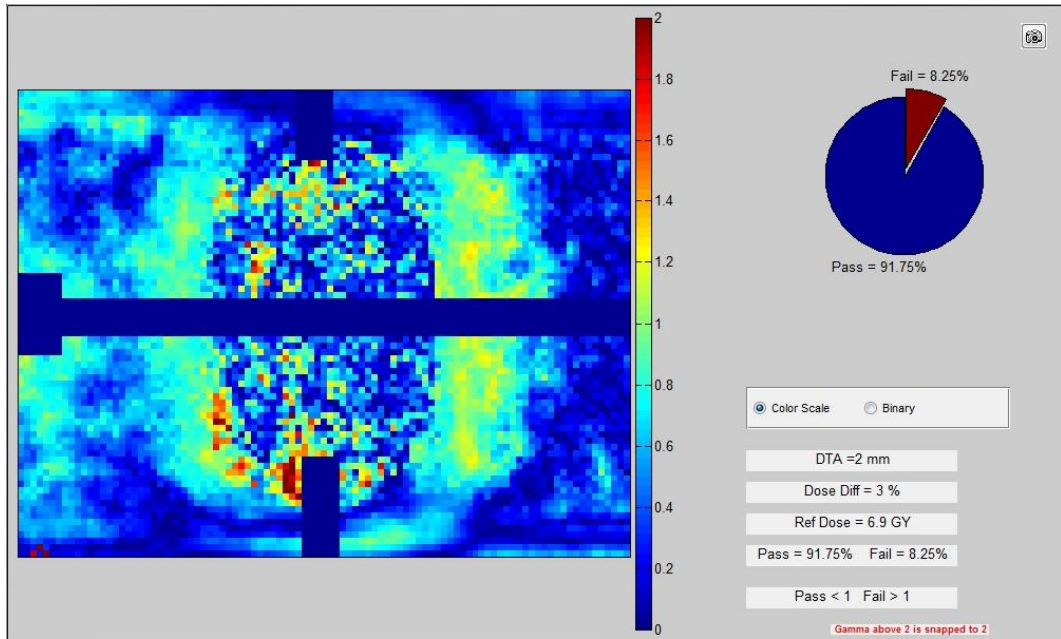


Figure 4.44: Lung IMRT delivery comparison for the sagittal plane of delivery #1 for the TrueBeam FFF 6MV model. Agreement was evaluated using a $\pm 3\%/2\text{mm}$ gamma criterion and 91.8% of pixels passed.

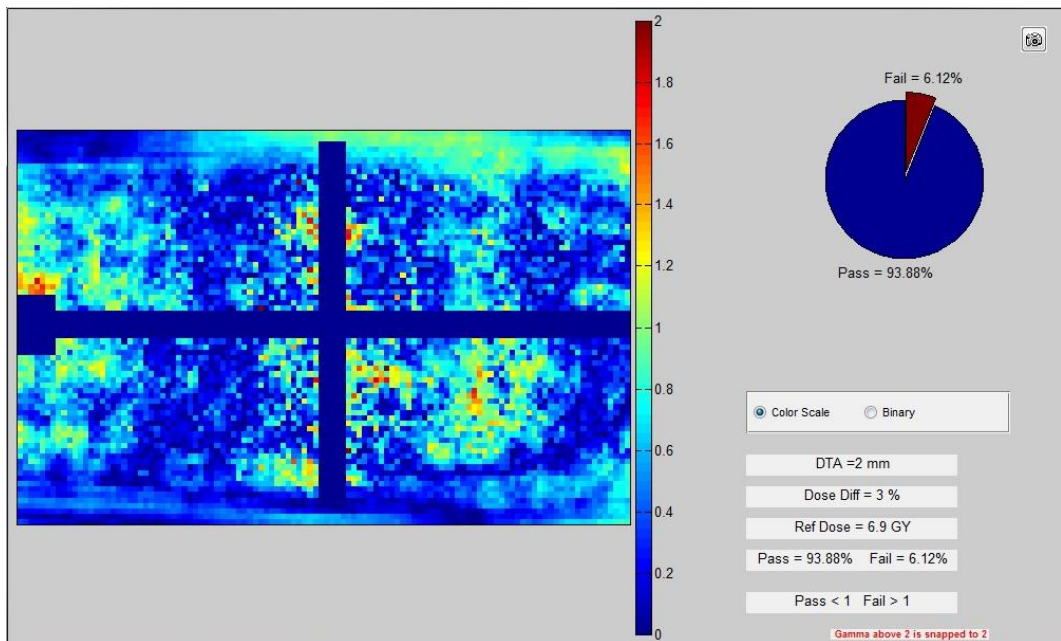


Figure 4.45: Lung IMRT delivery comparison for the coronal plane of delivery #1 for the TrueBeam FFF 6MV model. Agreement was evaluated using a $\pm 3\%/2\text{mm}$ gamma criterion and 93.9% of pixels passed.

The gamma maps corresponding to the comparison of a single irradiation to the calculated dose of the FFF 10MV source model are showing in Figures 4.46, 4.47, and 4.48 for axial, sagittal, and coronal planes, respectively. Gamma maps from all other deliveries are included in the Appendix for reference. The average agreement was 95.3%, 89.9%, and 95.0% for axial, sagittal, and coronal planes, respectively. The range of values for the axial plane was 93.0% to 97.4%, for the sagittal plane 85.2% to 93.6%, and for the coronal plane 92.1% to 96.6%.

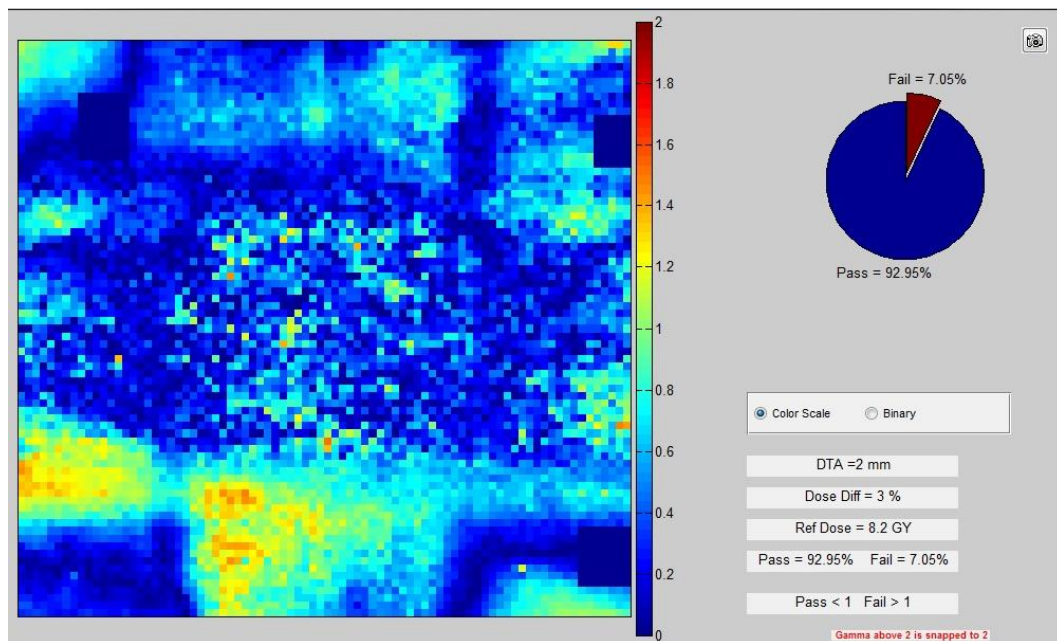


Figure 4.46: Lung IMRT delivery comparison for the axial plane of delivery #3 for the TrueBeam FFF 10MV model. Agreement was evaluated using a $\pm 3\%/2\text{mm}$ gamma criterion and 92.3% of pixels passed.

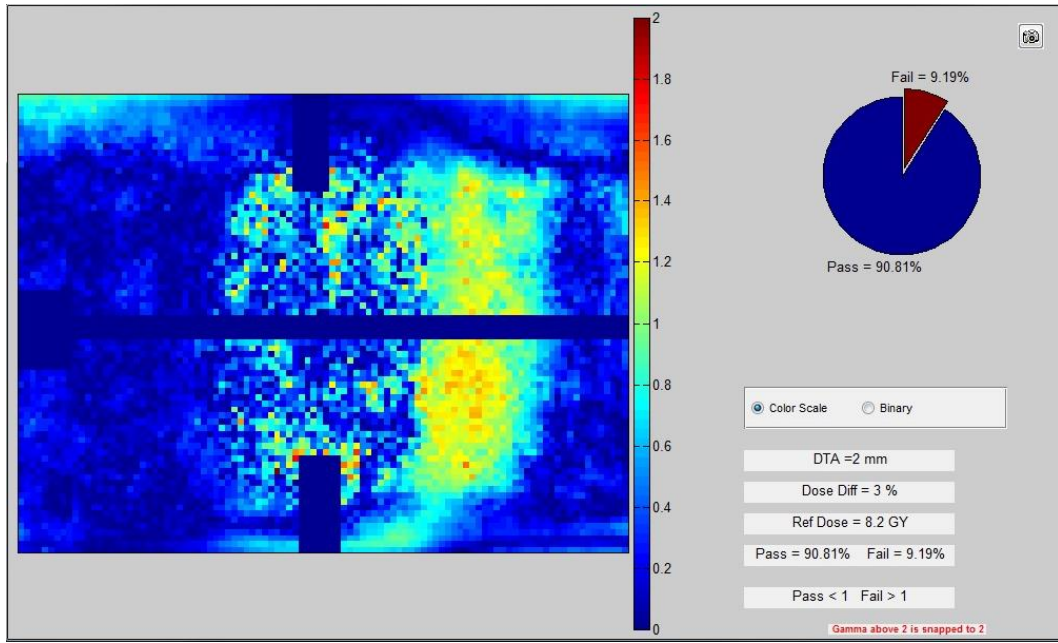


Figure 4.47: Lung IMRT delivery comparison for the sagittal plane of delivery #3 for the TrueBeam FFF 10MV model. Agreement was evaluated using a $\pm 3\%/2\text{mm}$ gamma criterion and 90.8% of pixels passed.

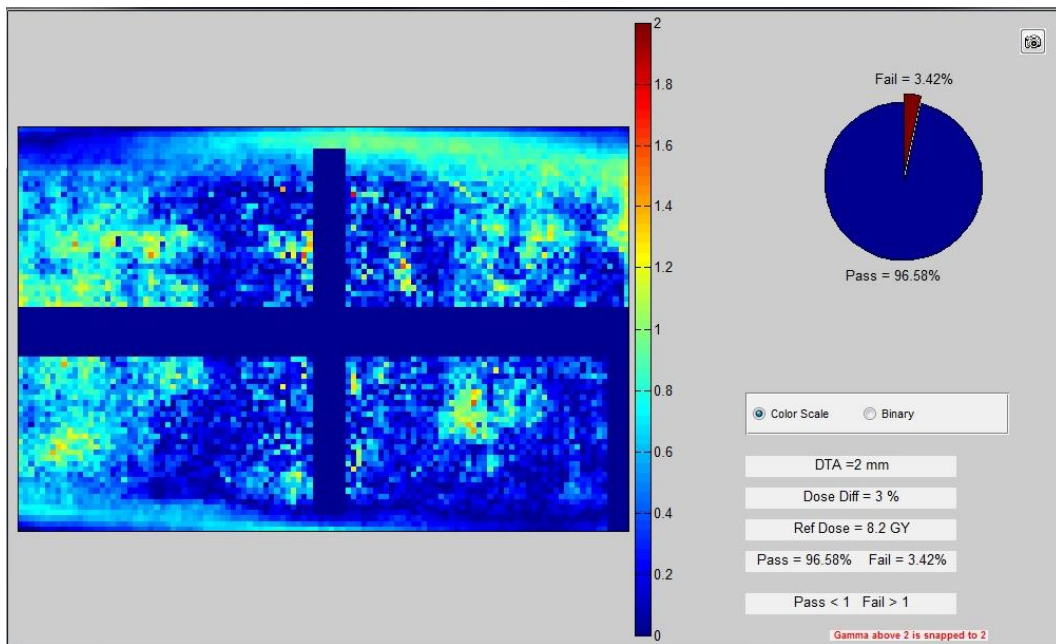


Figure 4.48: Lung IMRT delivery comparison for the coronal plane of delivery #3 for the TrueBeam FFF 10MV model. Agreement was evaluated using a $\pm 3\%/2\text{mm}$ gamma criterion and 96.6% of pixels passed.

The passing rate of comparisons for each plane for all three deliveries with respect to the DPM source model calculation is shown for both FFF 6MV and FFF 10MV models in Table 4.13.

	TrueBeam FFF 6MV			TrueBeam FFF 10MV		
	Axial	Sagittal	Coronal	Axial	Sagittal	Coronal
Delivery #1	91.0	91.8	93.9	95.6	85.2	92.1
Delivery #2	91.4	87.4	88.4	97.4	93.6	96.4
Delivery #3	93.5	94.3	92.4	93.0	90.8	96.6
Average	92.0	90.4	91.5	95.3	89.9	95.0

Table 4.13: Percentage of pixels passing a $\pm 3\%/2\text{mm}$ gamma criterion for IMRT lung plans for both TrueBeam FFF 6MV and 10MV models. Agreement was evaluated in the axial, sagittal, and coronal planes for three deliveries of each plan.

A qualitative evaluation of the gamma maps showed the model was challenged most along the edges of the beam profile outside of the PTV region. This region is more sensitive to the rotational positioning of the film during scanning because of the combination of the steeper dose gradient and the increased distance from the axis of rotation at the center of the film. The agreement in the sagittal and coronal planes appeared to be challenged most at the edges of the PTV. This is largely attributed to the sensitivity of the comparison to the registration of film to the phantom. Additionally, the film measurement for the FFF 6MV comparisons yielded doses lower than 1Gy at the corners of the axial films. At doses in this region the sensitometric curve used results in lower accuracy of the measured dose. Because both film plane comparisons consist of two pieces of film that need to be aligned during scanning, the registration uncertainty is higher than for the axial plane which consists of single piece of film.

Furthermore the high dose gradients at the edges of the PTV make the analysis more sensitive to a small translational shift either in the film registration or phantom setup. Even with the increased registration and position uncertainty, passing rates were above the pre-established threshold of 85%.

4.3.8 Benchmark Summary

The average and range of the percent of pixels passing a $\pm 3\%/2\text{mm}$ global gamma criterion for each phantom for both TrueBeam FFF 6MV and FFF 10MV source models is presented in Table 4.14.

		IMRT H&N	SBRT Lung	IMRT Lung
TrueBeam	Average	90.0	90.8	89.6
FFF 6MV	Range	80.3 – 95.9	84.5 – 98.4	85.1 – 97.5
TrueBeam	Average	87.2	91.7	93.4
FFF 10MV	Range	75.5 – 93.1	87.4 – 98.1	85.2 – 97.4

Table 4.14: The average and range of the percent of pixels passing a $\pm 3\%/2\text{mm}$ gamma criterion for TrueBeam FFF 6MV and FFF 10MV source models as assessed through three repeated deliveries for three different treatment plans to anthropomorphic phantoms.

Each multiple source model was benchmarked against three progressively challenging treatment plans delivered to anthropomorphic phantoms using SBRT and IMRT techniques in homogeneous and heterogeneous media. A 9 co-planar beam IMRT plan was designed and delivered to a head and neck phantom for both FFF 6MV and FFF 10MV nominal energies. Agreement was assessed using the gamma technique with a passing criterion of $\pm 3\%$ of the

maximum dose and ± 2 mm distance to agreement. The average percent of pixels passing the criterion was 90.0% and 87.2% for FFF 6MV and FFF 10MV models, respectively. The models showed a range of passing percentages in the sagittal and axial planes of 80.3% to 95.9% for the FFF 6MV model and 75.5% to 93.1% for the FFF 10MV model. In general disagreement was limited to regions near the organ at risk where the dose gradient was greatest.

An un-modulated, 9 co-planar beam SBRT plan was delivered to the RPC's anthropomorphic lung phantom. Each beam was defined by a static MLC configuration designed to conform the dose to the PTV. The average percent of pixels passing a $\pm 3\%/2$ mm global gamma criterion was 90.8% and 91.7% for 6MV and 10MV models, respectively. The range of pixels passing for the FFF 6MV model was 84.5% to 98.4% and 87.4% to 98.1% for the FFF 10MV model.

Moderately modulated, 6 co-planar beam, FFF 6MV and FFF 10MV IMRT plans were delivered to the anthropomorphic lung phantom. The addition of modulation to the heterogeneous phantom increased the challenge to the dose calculation tool while maintaining a clinically relevant setup. The average percent of pixels passing a $\pm 3\%/2$ mm global gamma criterion was 89.6% and 93.4% for FFF 6MV and FFF 10MV models, respectively. The range of pixels passing the criterion was 85.1% to 97.5% for the FFF 6MV model and 85.2% to 97.4% for the FFF 10MV model. Even with the increased difficulty of the calculation conditions, disagreement between measurement and calculation was minimal.

4.4 Conclusion

An analytical, multiple source model for TrueBeam FFF 6MV and FFF 10MV beams using the Dose Planning Method (DPM) Monte Carlo code was developed and validated within $\pm 2\%$ of the maximum dose and ± 2 mm distance to agreement against open field depth dose and dose profile measurements for field sizes ranging from $3 \times 3 \text{ cm}^2$ to $40 \times 40 \text{ cm}^2$. On average

98.1% of the data tested for both 6MV and 10MV models met the above criterion using gamma analysis.

The first step in the commissioning process used measured percent depth dose data from a nominal 10 x 10 cm² field size to determine the energy spectra and relative fluences for a primary point source and an extra-focal disk source through an optimization process fitting relative contributions of 0.25 MeV energy bins to a Fatigue-Fermi Distribution. In the same optimization process the relative contribution of an electron disk source was determined. Particle distribution was implemented directly from the literature for the extra-focal[60] and electron[53] sources.

The second step of the commissioning process matched measured and calculated dose profiles for an open 40 x 40 cm² field in order to model the increase in off-axis fluence. The decrease in mean energy off-axis was implemented without change from Georg et al[62]. Upon completion of the commissioning process an accurate model of TrueBeam FFF 6MV and FFF 10MV therapeutic x-ray beams was developed to run basic open beam dose calculations using the DPM Monte Carlo code.

The commissioned and validated multiple source models were then benchmarked against increasingly challenging treatment plans delivered to homogenous and heterogeneous anthropomorphic phantoms. The model was shown to be accurate within $\pm 3\%$ and $\pm 2\text{mm}$ based on comparisons of calculated dose to enclosed thermoluminescent dosimeters (TLD) and radiochromic film. Average agreement assessed using the gamma technique and a $\pm 3\%/2\text{mm}$ global criterion was 90.1% and 90.8% for FFF 6MV and FFF 10MV source models, respectively.

Chapter 5: Robustness Study at Outside Institutions: Elekta and Varian TrueBeam FFF 6MV and 10MV

5.1 Introduction

The Radiological Physics Center (RPC) has published the results for its anthropomorphic phantom audit program showing varying degrees of success amongst institutions[13, 17]. There is reason to believe that one potential source of discrepancy between these measurement to calculated dose comparisons is the accuracy of the dose calculations algorithms in heterogeneous media[12, 18]. Previously, the RPC has been unable to verify the accuracy of this step in the radiation therapy treatment process[19]. In order to ensure a higher degree of consistency among institutions participating in National Cancer Institute (NCI) funded clinical trials and improve upon patient safety, the RPC began the development of an independent dose calculation tool to be used in the auditing process[20, 21, 35].

In its current state, the dose calculation tool includes models of Varian 6MV and 10MV therapeutic linear accelerators. Chapters 3 and 4 detailed the inclusion of Elekta 6MV and 10MV models and Varian TrueBeam FFF 6MV and FFF 10MV models, respectively. The addition of these four models were intended to cover the majority of the approximately 25% of monitored beams not modeled by the dose calculation tool. In order to be truly useful as an auditing tool, the models must be able to accurately predict dose distributions for all linear accelerators of a common manufacturer and not just the linear accelerator whose dosimetry data was used during commissioning of the models. RPC collected dosimetry data suggests that this is possible as over 90% of all beams from a common manufacturer have shown agreement within $\pm 2\%$ [55].

5.2 Materials and Methods

The RPC conducts their phantom audits through a comparison of TLD measurement and film measurement to institution submitted calculated dosimetry data. The measurement data

from the phantom irradiation along with the institution submitted treatment plan data and calculated doses are archived with the auditing report sent to the institution. While it is not required for the audit, if the treatment plan data contains the plan information contained within the DICOM RT plan (RP) file, this archived plan file can be used as input to the Monte Carlo models described in Chapters 2-4. This provides all the necessary information to run a comparison between Monte Carlo calculated doses and phantom measurements similar to the model benchmarking performed in Chapter 3 Section 3 and Chapter 4 Section 3.

To evaluate the models performance against measurements on beams not used in the commissioning of the model, a comparison between Monte Carlo calculated dose and measurement dose from past phantom audits will be performed. Audits chosen for the comparison will be selected based on three criteria.

First, the phantom audit must have passed the RPC's criteria. For the IMRT head and neck phantom this requires TLD measurements to be within $\pm 7\%$ of the predicted calculated dose and gamma agreement to be $>85\%$ at a $\pm 7\%/4\text{mm}$ criterion. For the lung phantom the TLD measurements must be within $\pm 5\%$ of a measured to calculated dose ratio of 0.97 for deterministic dose calculation algorithms and $\pm 5\%$ of a ratio of 1.00 for Monte Carlo dose calculation algorithms. An analysis of past audits on the lung phantom has shown a systematic disagreement between measurement and deterministic calculations of 3-4%[72]. By requiring the measurement to be within $\pm 5\%$ of a ratio of 0.97 the systematic offset is accounted for in comparisons to doses calculated by deterministic algorithms. Additionally, the gamma analysis of the film measurement compared to dose calculation must be in agreement for $>85\%$ of data tested with a $\pm 5\%/5\text{mm}$ criterion.

The RPC's phantoms act as an end to end test of the treatment process. The AAPM Task Group Report Number 85 breaks down the acceptable uncertainties of the entire treatment process, of which the dose calculations are a small part[73]. For this reason, the past phantom audits to be compared to the tool must show agreement between measurement and calculated data superior to the minimum requirements for passing the audit. Preference will be given to

audits with TLD measurements within $\pm 3\%$ of the predicted calculated dose. For the lung phantom audits, the $\pm 3\%$ acceptance criteria will be centered on a measured to calculated dose ratio of 0.97 for doses calculated by deterministic algorithms. To minimize the impact of measurement uncertainty caused by collecting data from phantoms irradiated by outside institutions, comparisons will be restricted to the TLD contained in the PTV for both phantoms.

The final assessment for selection of the phantom audit will be based on a comparison of the dose profile agreement included in the institution's audit report. This will be a subjective evaluation of the dose distribution shape and phantom alignment. While offsets within $\pm 3\text{mm}$ in the phantom positioning can be accounted for in the registration of the calculated dose to the film measurements, accounting for larger offsets would increase the uncertainty in the comparison to unacceptable levels. While some offsets can be accounted for, a delivery error resulting in a different dose distribution cannot be accurately predicted to input into the multiple source model calculation. While this change may not affect the passing rate using a $\pm 7\%/4\text{mm}$ or $\pm 5\%/5\text{mm}$ gamma criterion in the phantom audit, it will likely cause failure at the more restrictive $\pm 3\%/2\text{mm}$ criterion that has been used on the benchmarking studies of the model.

Table 5.1 and Table 5.2 report the phantom audits chosen for the comparison of multiple source model calculations to past measurements for head and neck phantoms and lung phantoms, respectively. Because FFF is relatively new delivery technique and 10MV beams are less common than 6MV beams, there were no TrueBeam FFF 10MV phantom audits. Likewise, only the lung phantom has been used for auditing TrueBeam FFF 6MV beams. The use of Elekta 10MV beams is also uncommon among RPC audited institutions. There were no Elekta 10MV phantom audits that met the selection criteria.

Delivery	Manufacturer	Model	Energy (MV)	Technique	TPS
H&N Plan #1	Elekta	Synergy	6MV	SMLC	Pinnacle
H&N Plan #2	Elekta	Agility S	6MV	SMLC	Pinnacle

Table 5.1: Summary of head and neck phantom audits chosen for a measurement based comparison to Monte Carlo recalculation of plan dose. Both plans were step and shoot IMRT, or static MLC (SMLC), deliveries.

Delivery	Manufacturer	Model	Energy (MV)	Technique	TPS
Lung Plan #1	Varian	TrueBeam	6MV FFF	3D	Pinnacle
Lung Plan #2	Varian	TrueBeam	6MV FFF	3D	Pinnacle
Lung Plan #3	Elekta	Synergy	6MV	SMLC	Pinnacle

Table 5.2: Summary of lung phantom audits chosen for a measurement based comparison to Monte Carlo recalculation of plan dose. Delivery techniques were either 3D or static MLC (SMLC).

5.3 Results

5.3.1 Point Dose Comparison

The results to the point dose comparisons for the past audit study are reported in Table 5.3 for head and neck phantom audits. The recalculation of doses for the head and neck audits resulted in an average calculated to measured TLD dose ratio in the PTV of 1.019. The institution reported TLD doses as determined by the TPS yielded an average agreement of

1.020 in the PTV. The mean agreement of the two calculated doses was not significant according to a paired t-test ($p=0.9293$). The range of agreement in the PTV for the multiple source model recalculated doses was 1.005 to 1.030. The corresponding range for TPS agreement was 0.991 to 1.050.

Delivery	PTV TLD SA		PTV TLD IA		PTV TLD SP		PTV TLD IP		PTV TLD Avg.	
	TPS	DPM	TPS	DPM	TPS	DPM	TPS	DPM	TPS	DPM
H&N Plan #1	1.003	1.005	1.015	1.027	0.991	1.019	1.010	1.027	1.005	1.020
H&N Plan #2	1.040	1.015	1.050	1.028	1.019	1.003	1.031	1.030	1.035	1.019

Table 5.3: Point dose comparisons for the multiple source model recalculation of the head and neck phantom audits. Comparison to calculated doses by DPM and the institution reported doses calculated by the TPS are expressed as a ratio of calculated to measured doses. Point dose locations were restricted to within the PTV. S = Superior, I = Inferior, A = Anterior, P = Posterior.

The results to the point dose comparisons for the past lung phantom audit study is reported in Table 5.4. The averaged ratio of DPM recalculated dose to measurement was 0.986 compared to 1.023 for institution submitted doses calculated by the TPS. The mean agreement was determined to be significant using a paired t-test ($p=0.0004$). Using the same statistical analysis, the difference from 1.000 was not shown to be significantly better for the DPM recalculated doses with respect to the TPS calculated doses ($p=0.3276$). The range of the agreement for recalculated doses was 0.975 to 0.995. The range of the ratio of TPS calculated doses to measurement was 1.007 to 1.042.

Delivery	PTV TLD S		PTV TLD I		PTV TLD Avg.	
	TPS	DPM	TPS	DPM	TPS	DPM
Lung Plan #1	1.021	0.994	1.013	0.989	1.017	0.991
Lung Plan #2	1.007	0.975	1.015	0.978	1.011	0.977
Lung Plan #3	1.038	0.988	1.042	0.995	1.040	0.992

Table 5.4: Point dose comparisons for the multiple source model recalculation of the lung phantom audits. Comparison to calculated doses by DPM and the institution reported doses calculated by the TPS are expressed as a ratio of calculated to measured doses. Point dose locations were restricted to within the PTV. S = Superior, I = Inferior.

5.3.2 Gamma Map Comparison

To compare the multiple source models' accuracy in modeling the beam penumbra, MLC leaf tips, MLC transmission, and MLC leakage for outside institution beams, agreement between DPM recalculated doses and archived film measurements were evaluated using the gamma technique[68]. The analysis considers dose differences as relative percentage and the distance to agreement to assess overall agreement and identify locations of difficulty to the model. The analysis was performed with $\pm 3\%/2\text{mm}$ and $\pm 5\%/3\text{mm}$ criteria. All film measurements were also compared to the TPS calculated dose submitted by the audited institution using the same technique and criteria. The results of the comparisons are reported in Table 5.5 and Table 5.6 for head and neck audits using $\pm 3\%/2\text{mm}$ and $\pm 5\%/3\text{mm}$ criteria, respectively. Table 5.7 and Table 5.8 report the agreement for the lung audits using $\pm 3\%/2\text{mm}$ and $\pm 5\%/3\text{mm}$ criteria, respectively. The corresponding gamma maps for each comparison at each criterion are presented in the Appendix (Chapter 7).

Delivery	DPM		TPS	
	Axial	Sagittal	Axial	Sagittal
H&N Plan #1	59.1	69.4	67.6	75.3
H&N Plan #2	88.4	52.5	85.9	69.8

Table 5.5: Percentages of pixels passing a $\pm 3\%/2\text{mm}$ gamma criterion for previous head and neck audits are reported. Agreement was evaluated in the axial and sagittal planes.

Delivery	DPM		TPS	
	Axial	Sagittal	Axial	Sagittal
H&N Plan #1	82.1	88.2	88.6	98.9
H&N Plan #2	98.3	76.8	98.4	86.3

Table 5.6: Percentages of pixels passing a $\pm 5\%/3\text{mm}$ gamma criterion for previous head and neck audits are reported. Agreement was evaluated in the axial and sagittal planes.

Delivery	DPM			TPS		
	Axial	Coronal	Sagittal	Axial	Coronal	Sagittal
Lung Plan #1	99.7	99.0	94.9	97.4	95.5	86.8
Lung Plan #2	88.4	79.1	82.6	96.0	93.3	66.8
Lung Plan #3	92.1	92.6	97.1	64.1	53.6	64.1

Table 5.7: Percentages of pixels passing a $\pm 3\%/2\text{mm}$ gamma criterion for previous lung audits are reported. Agreement was evaluated in the axial, coronal and sagittal planes.

Delivery	DPM			TPS		
	Axial	Coronal	Sagittal	Axial	Coronal	Sagittal
Lung Plan #1	99.9	99.0	99.6	99.9	99.9	99.4
Lung Plan #2	99.0	96.9	99.5	99.9	99.8	93.2
Lung Plan #3	99.1	99.6	99.8	85.7	82.5	82.4

Table 5.8: Percentages of pixels passing a $\pm 5\%/3\text{mm}$ gamma criterion for previous lung audits are reported. Agreement was evaluated in the axial, coronal and sagittal planes.

The average agreement in the head and neck phantom audits using a $\pm 3\%/2\text{mm}$ gamma criterion was 67.3% and 74.7% for DPM recalculated doses and TPS calculated doses, respectively. At a less restrictive $\pm 5\%/3\text{mm}$ criterion the average agreement was 86.3% and 93.0% for the DPM recalculated doses and TPS calculated doses, respectively. Among the four film comparison (2 axial, 2 sagittal), TPS calculated doses showed better agreement in three comparisons at the $\pm 3\%/2\text{mm}$ criterion and all four comparisons at the $\pm 5\%/3\text{mm}$ criterion.

The average agreement in the lung phantom audits using a $\pm 3\%/2\text{mm}$ gamma criterion was 91.7% and 79.7% for DPM recalculated doses and TPS calculated doses, respectively. Using a $\pm 5\%/3\text{mm}$ criterion the average agreement was 99.2% and 93.6% for DPM recalculated doses and TPS calculated doses, respectively. Among the nine film comparisons (3 axial, 3 coronal, 3 sagittal), the DPM recalculate doses showed superior agreement in seven comparisons at the $\pm 3\%/2\text{mm}$ criterion and five comparisons at a $\pm 5\%/3\text{mm}$ criterion.

Due to the low number of phantom audits meeting the recalculation selection criteria, it is difficult to establish significance or meaning behind the discrepancy in performance for DPM recalculated doses and TPS calculated doses. The superior agreement in the lung phantom audits can likely be explained by the superior accuracy in radiation transport utilizing the Monte Carlo technique compared to deterministic algorithms. It is possible that the inferior

performance of the multiple source models in the head and neck phantom audits could be due to poorer leaf modeling by the calculation tool. The head and neck phantoms require more modulation to achieve the planning criteria compared to the lung phantoms. The increased modulation could compound the effects of small differences in modeling techniques.

5.4 Conclusion

The multiple source models developed for the RPC's dose calculation quality assurance tool have been used to recalculate doses to the RPC's anthropomorphic phantoms from previous credentialing audits. By using archived CT data sets, DICOM RT plan files, and TLD and film measurements, the models' performance could be assessed against outside institution measurements and against the performance of commercial treatment planning systems. This assessment was done for five previous credentialing audits consisting of two head and neck phantom audits and three lung phantom audits. Audits were chosen based on the availability of the necessary archived data and superior performance in the credentialing process.

Point dose comparisons using the enclosed TLD capsules in the head and neck phantoms showed an average calculated to measurement ratio of 1.019 and 1.020 for DPM recalculated doses and TPS calculated doses, respectively. Comparisons in the lung phantoms showed an average calculated to measurement ratio of 0.986 and 1.023 for DPM recalculated doses and TPS calculated doses, respectively. Differences in the head and neck phantom were not significant, and while significantly different in the lung phantoms, the performance was not significantly better for either calculation method.

To assess the ability of the two dose calculation methods' ability to predict complex dose distributions in both homogenous and heterogeneous media, a comparison of film measurement to calculated dose was performed for both phantoms using the gamma technique. At a $\pm 3\%/2\text{mm}$ criterion the average agreement for DPM recalculated dose was 67.3% and 91.7% for head and neck phantoms and lung phantoms, respectively. The TPS calculated dose showed average agreements for the same gamma criterion of 74.7% and

79.7% for head and neck phantoms and lung phantoms, respectively. Differences in performance suspected to be attributable to superior accuracy in transport in heterogeneous media for the Monte Carlo technique and more accurate leaf modeling by the TPS. More comparisons between DPM recalculated dose and TPS calculated dose are needed fully assess these differences.

Chapter 6: Summary

6.1 Summary for Elekta Models

Multiple source models for Elekta 6MV and 10MV beams were developed (Chapter 3) in a two-step commissioning process. First energy spectra were optimized by a comparison of central axis depth dose data in water for Monte Carlo calculated dose and measured dose. Next off-axis effects were accounted for in matching Monte Carlo calculated dose profiles to measured dose profiles for a 40 x 40 cm² field size. The commissioned models were then validated against open field measurements consisting of depth dose curves and dose profiles at field sizes from 3 x 3 cm² to 30 x 30 cm². Agreement was evaluated using the gamma technique and a criterion of $\pm 2\%$ of the maximum dose and ± 2 mm distance to agreement. All depth dose and dose profile comparisons exceeded 90% of data passing the criterion.

The multiple source models were then benchmarked against clinically realistic treatment deliveries using measurements from anthropomorphic phantoms. Treatments consisted of an IMRT head and neck plan, a 3D conformal SBRT lung plan, and an IMRT lung plan. Measurements from TLD and film were used to compare the models' performance to measurement. Agreement for dose distributions measured by the film was assessed using the gamma technique and a $\pm 3\%$ of the maximum dose and ± 2 mm distance to agreement criterion. All film planes for each treatment delivery averaged over 85% of data passing the established criterion.

6.2 Summary for Varian TrueBeam FFF Models

Multiple source models for Varian TrueBeam FFF 6MV and FFF 10MV beams were developed (Chapter 4) in a two-step commissioning process. First the energy spectra were determined from an optimization process based on a comparison of Monte Carlo calculated central axis depth dose data to measured central axis depth dose data. Next the off-axis effects were accounted for by matching calculated dose profiles measured dose profiles for a 40 x 40

cm² field size. The models were then validated against open field measurements in a water tank at field sizes from 3 x 3 cm² to 40 x 40 cm². Agreement between calculation and measurement was assessed using the gamma technique and a criterion of $\pm 2\%$ of the maximum dose and ± 2 mm distance to agreement. All depth dose and dose profile comparisons exceeded 88% of the data passing the criterion.

The developed source models were then benchmarked against clinically realistic treatment deliveries using anthropomorphic phantoms. The treatment plans designed to increasingly challenge the models and consisted of an IMRT head and neck delivery, a 3D conformal SBRT lung delivery, and an IMRT lung delivery. Performance of the model was assessed through a comparison of dose calculations to TLD measurement and film measurement. Dose distribution agreement was assessed in the film comparison using the gamma technique and a $\pm 3\%$ of the maximum dose and ± 2 mm distance to agreement criterion. All film planes from all deliveries averaged over 85% of data passing the criterion.

6.3 Summary for Robustness Study

To evaluate the robustness of the multiple source models developed in Chapter 3 and Chapter 4 and their feasibility for use in a dose calculation quality assurance audit tool, a retrospective analysis of recalculated dose with respect to measurement was performed on archived credentialing audits (Chapter 5). Phantom audits that were performed on therapeutic x-ray beams fitting the description of the models and with superior performance on the audit were chosen for analysis. Selected audits for comparison consisted of both lung phantom deliveries and head and neck phantom deliveries. Archived DICOM RT files were used to recalculate the phantom dose using the multiple source models and performance was evaluated by comparing to archived measurements from the audit. Performance of the multiple source model comparisons was then compared to performance of the treatment planning system calculated dose.

Point dose comparisons using the calculated dose to TLD measured dose ratio from the head and neck phantoms showed comparable performance for the DPM recalculated dose, 1.019, with respect to the TPS calculated dose, 1.020. Dose distribution comparisons of calculated dose to film measurements evaluated using the gamma technique and a $\pm 3\%$ of the maximum dose and $\pm 2\text{mm}$ distance to agreement showed superior performance from the TPS calculations, 74.7% of data passing, compared to the DPM recalculated dose, 67.3% of data passing.

Point dose comparisons using the calculated dose to TLD measured dose ratio from the lung phantoms showed statistically significant differences between DPM recalculated dose, 0.986 and TPS calculated dose, 1.023. Accuracy, however, was not significant. The dose distributions were evaluated using film measurement and the gamma technique with a $\pm 3\%$ of the maximum dose and $\pm 2\text{mm}$ distance to agreement criterion. The average percent of pixels passing was higher in the DPM recalculated dose, 91.7%, compared to the TPS calculated dose, 79.7%.

6.4 Evaluation of the Hypothesis

The hypothesis to the project was that Monte Carlo, multiple source models of Elekta 6MV, Elekta 10MV, Varian TrueBeam FFF 6MV, and Varian TrueBeam FFF 10MV beams could be developed based on measurements to an accuracy of $\pm 3\%$ of the maximum dose and $\pm 2\text{mm}$ distance to agreement in anthropomorphic phantom measurements.

The development and validation of the source models (Specific Aim #1) is documented in Chapter 3 (Elekta) and Chapter 4 (Varian TrueBeam FFF). This needed to be done at an accuracy of $\pm 2\%$ of the maximum dose and $\pm 2\text{mm}$ distance to agreement compared to open field, water tank measurements.

The hypothesis was then evaluated in benchmark testing performed against anthropomorphic phantoms. The conditions under which the hypothesis was tested are outlined

in Specific Aim #2 and Chapter 3 (Elekta) and Chapter 4 (Varian TrueBeam FFF). The treatment plans for the phantoms were designed to present increasingly challenging dose calculation conditions and consisted of an IMRT head and neck plan, a 3D conformal SBRT lung plan, and an IMRT lung plan. Reported average agreement for all four multiple source models in each plane of evaluation for all treatment plans exceeded 85%. The results of the benchmark testing proved the hypothesis true.

6.5 General Conclusions

Development of an independent, dose calculation, quality assurance tool for clinical trial audits was completed through the addition of multiple source models of Elekta 6MV and 10MV and Varian TrueBeam FFF 6MV and FFF 10MV beams to the already developed Varian 6MV and 10MV models. The new models were validated against water tank measurements for open fields with excellent agreement. The models then met the benchmarking criteria established to show a high degree of accuracy in clinically realistic treatment plans delivered to anthropomorphic phantoms. These treatment plans consisted of modulated and un-modulated plans delivered to homogeneous and heterogeneous media. As a proof of concept of the tool's utility in this role, a retrospective analysis of past phantom credentialing audits was performed with the dose calculation tool. The excellent agreement in the benchmarking studies and successful use in a retrospective study suggest that the tool is ready for implementation in the RPC's quality assurance program.

6.6 Future Work

The addition of Elekta 6MV and 10MV and Varian TrueBeam FFF 6MV and FFF 10MV beams to the previously existing Varian 6MV and 10MV models makes the independent dose calculation quality assurance tool developed useful for auditing purposes. Deficiencies in the models' benchmarking and ability to handle some treatment techniques still exist. To date,

models have only been benchmarked against step and shoot technique for IMRT deliveries. While adaptation to a sliding window technique will not fundamentally change the way the model calculates dose, the models should be benchmarked to confirm this. A more significant modification of the model will be needed to account for volumetric arc therapy (VMAT) deliveries. These have become increasingly popular treatment techniques and due to the way in which the model breaks the calculations down by beam and samples particle origin by fluence segments, VMAT deliveries cannot not be currently handled by the tool. Inclusion of this technique will require a modification to the sampling done in particle generation.

With a functioning dose calculation tool it will also be increasingly important that institutions submit DICOM RT plan files as a part of phantom audits. This is necessary if the dose calculations submitted by institutions are to be checked and will allow for larger scale data collection in comparing the performance of specific dose calculation algorithms to the dose calculation tool. Chapter 5 suffered from a lack of data points caused largely by a lack of archived audits containing DICOM RT plan information needed for the dose calculations.

Chapter 7: Appendix

7.1 Elekta 6 MV: Percent Depth Dose and Dose Profiles

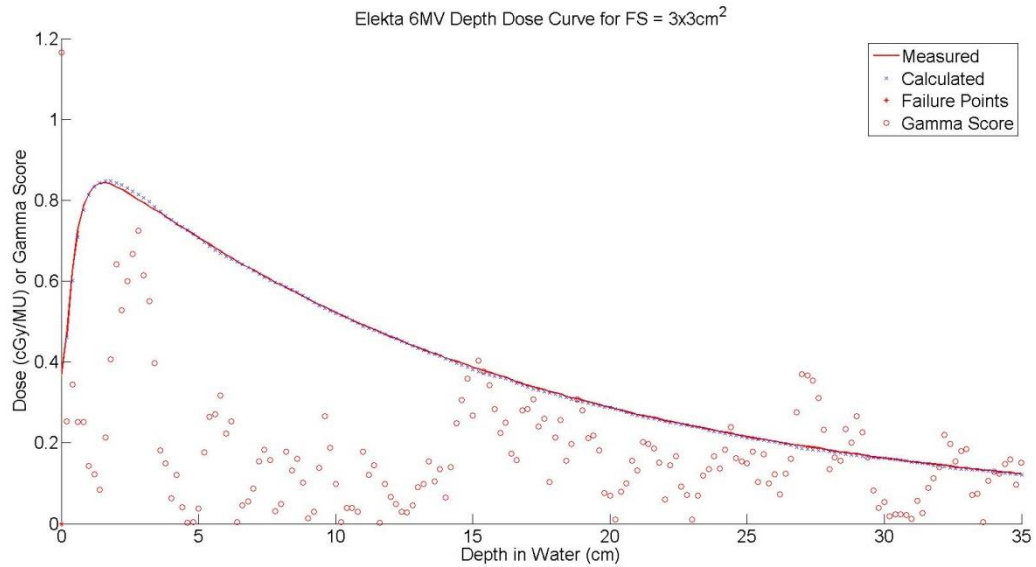


Figure 7.1: Calculated (blue 'x') and measured (red line) percent depth dose curves for an Elekta 6MV beam at a field size of 3 x 3 cm². Gamma agreement (red circles) for each point is also displayed along with any points (red star) at which a failure to meet the $\pm 2\%/2\text{mm}$ criterion. At this field size 99.43% of all data passed the gamma criterion.

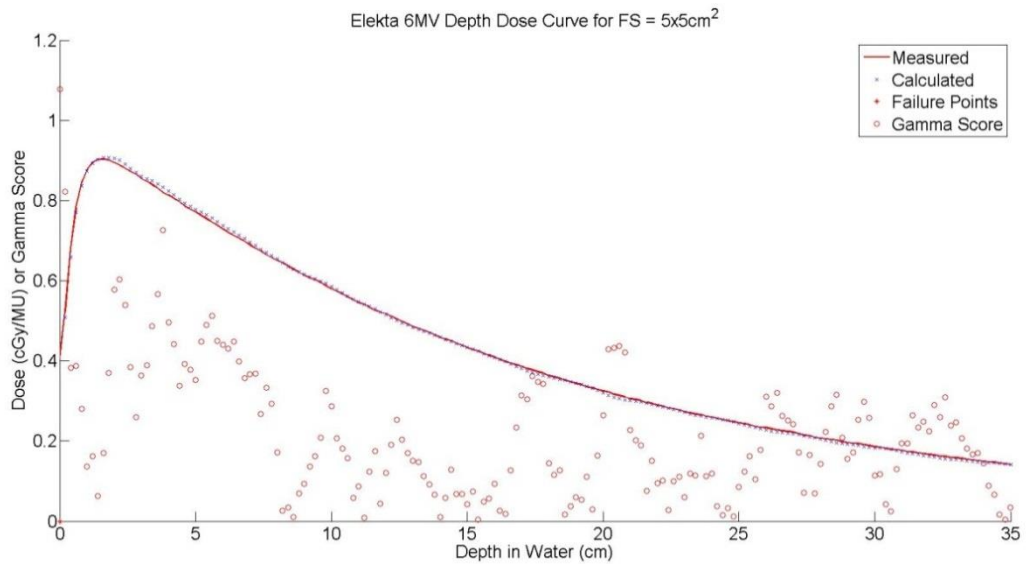


Figure 7.2: Calculated (blue 'x') and measured (red line) percent depth dose curves for an Elekta 6MV beam at a field size of 5 x 5 cm². Gamma agreement (red circles) for each point is also displayed along with any points (red star) at which a failure to meet the $\pm 2\%/2\text{mm}$ criterion. At this field size 99.43% of all data passed the gamma criterion.

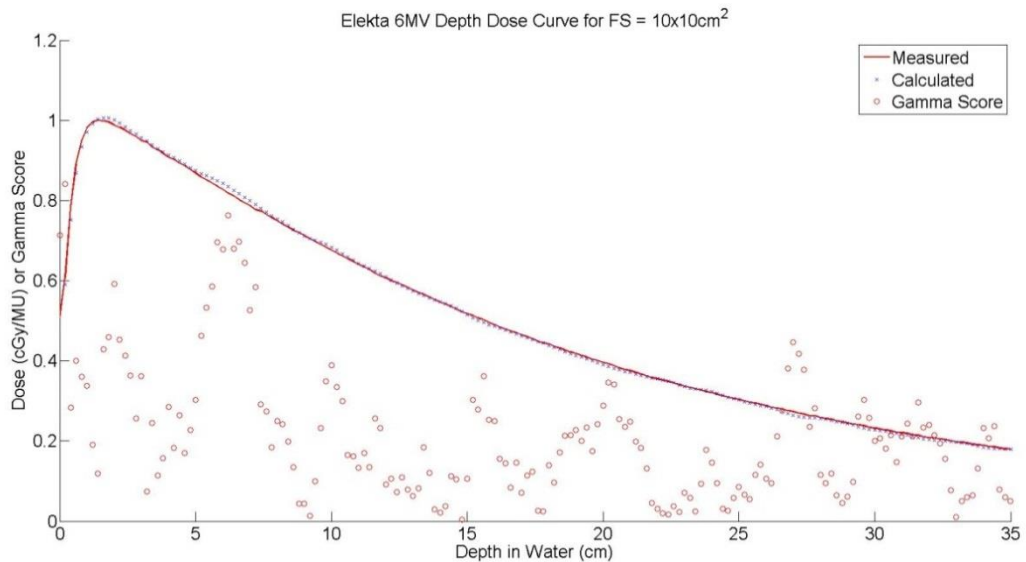


Figure 7.3: Calculated (blue 'x') and measured (red line) percent depth dose curves for an Elekta 6MV beam at a field size of 10 x 10 cm². Gamma agreement (red circles) for each point is also displayed along with any points (red star) at which a failure to meet the $\pm 2\%/2\text{mm}$ criterion. At this field size 100% of all data passed the gamma criterion.

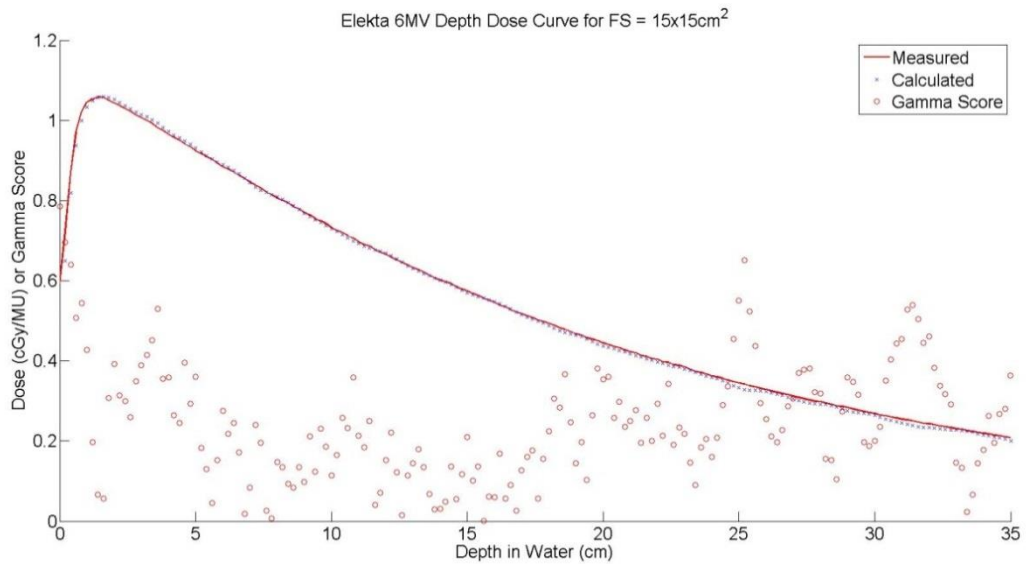


Figure 7.4: Calculated (blue 'x') and measured (red line) percent depth dose curves for an Elekta 6MV beam at a field size of 15 x 15 cm². Gamma agreement (red circles) for each point is also displayed along with any points (red star) at which a failure to meet the $\pm 2\%/2\text{mm}$ criterion. At this field size 100% of all data passed the gamma criterion.

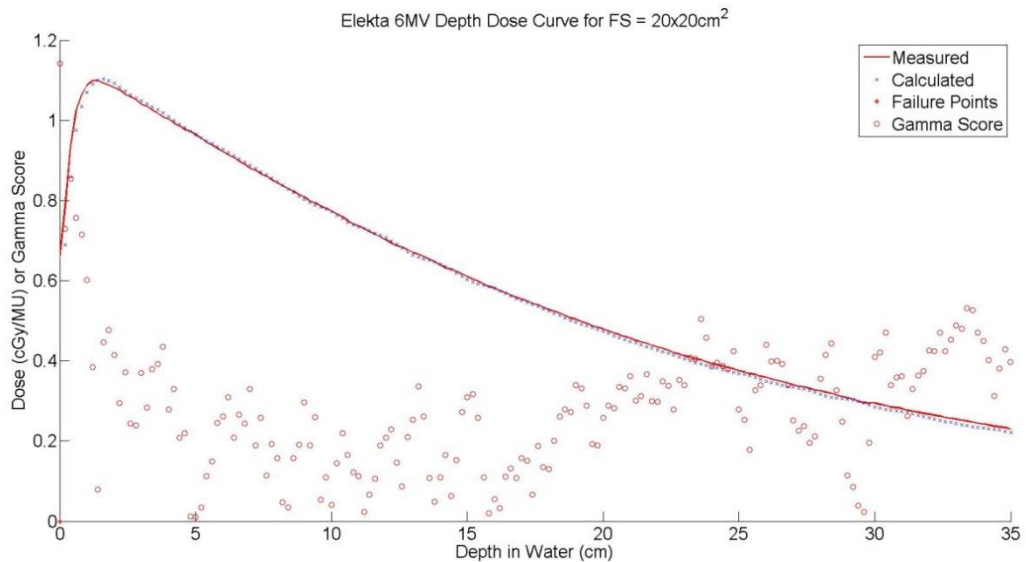


Figure 7.5: Calculated (blue 'x') and measured (red line) percent depth dose curves for an Elekta 6MV beam at a field size of 20 x 20 cm². Gamma agreement (red circles) for each point is also displayed along with any points (red star) at which a failure to meet the $\pm 2\%/2\text{mm}$ criterion. At this field size 99.43% of all data passed the gamma criterion.

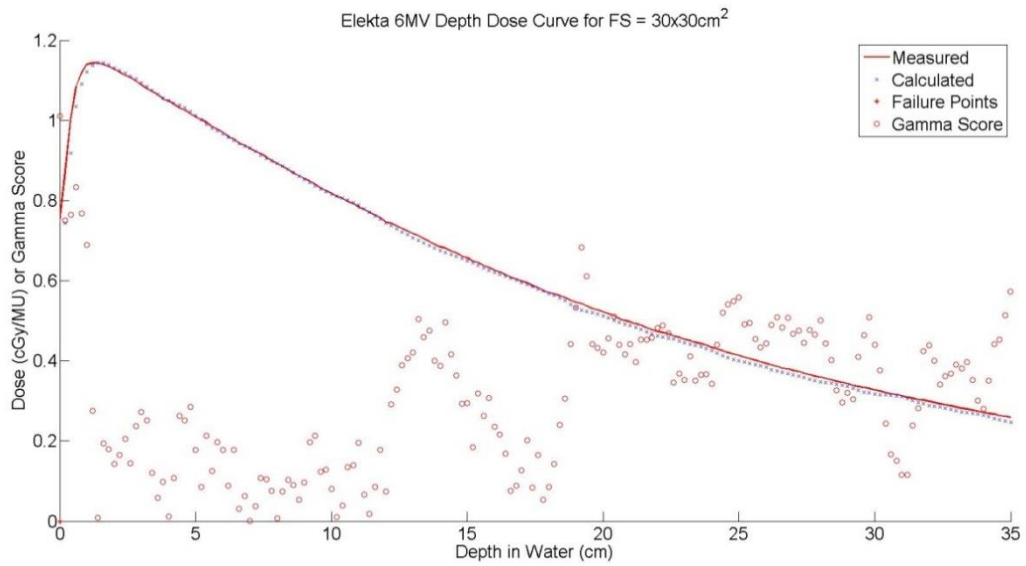


Figure 7.6: Calculated (blue 'x') and measured (red line) percent depth dose curves for an Elekta 6MV beam at a field size of 30 x 30 cm². Gamma agreement (red circles) for each point is also displayed along with any points (red star) at which a failure to meet the $\pm 2\%/2\text{mm}$ criterion. At this field size 99.43% of all data passed the gamma criterion.

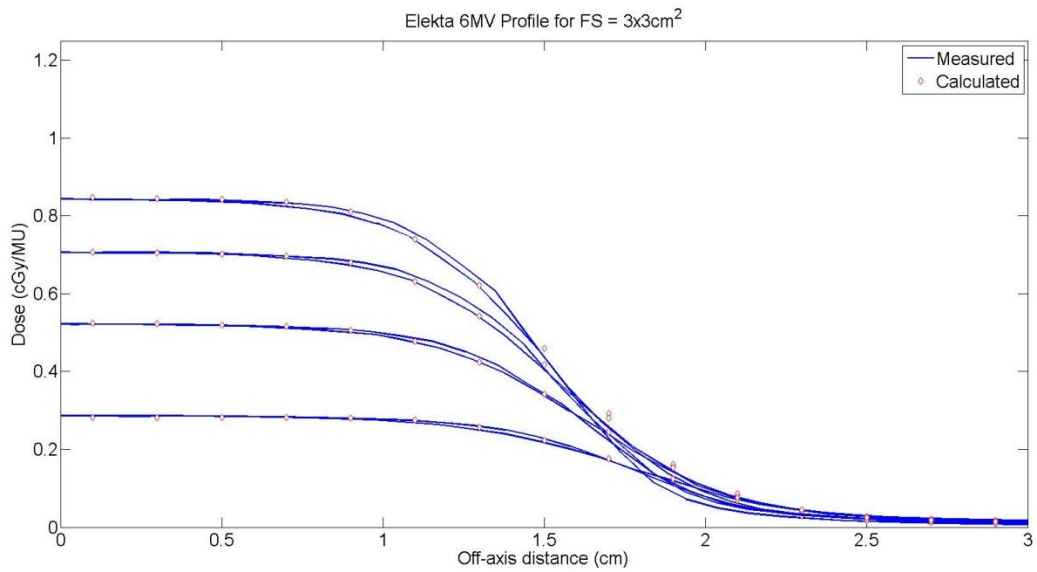


Figure 7.7: Calculated (red diamond) and measured (blue line) dose profiles for an Elekta 6MV beam at a field size of 3 x 3 cm².

Field Size (cm ²)	Direction	Depth (cm)	% Passing (2%/2mm)
3 x 3	x	1.6	95.00
	x	5	100.00
	x	10	100.00
	x	20	100.00
	y	1.6	97.14
	y	5	100.00
	y	10	100.00
	y	20	100.00

Table 7.1: Dose profile agreement between the Elekta 6MV multiple source model and measurement using a $\pm 2\%/2\text{mm}$ global gamma criterion at all depths of comparison for a 3 x 3 cm² field size.

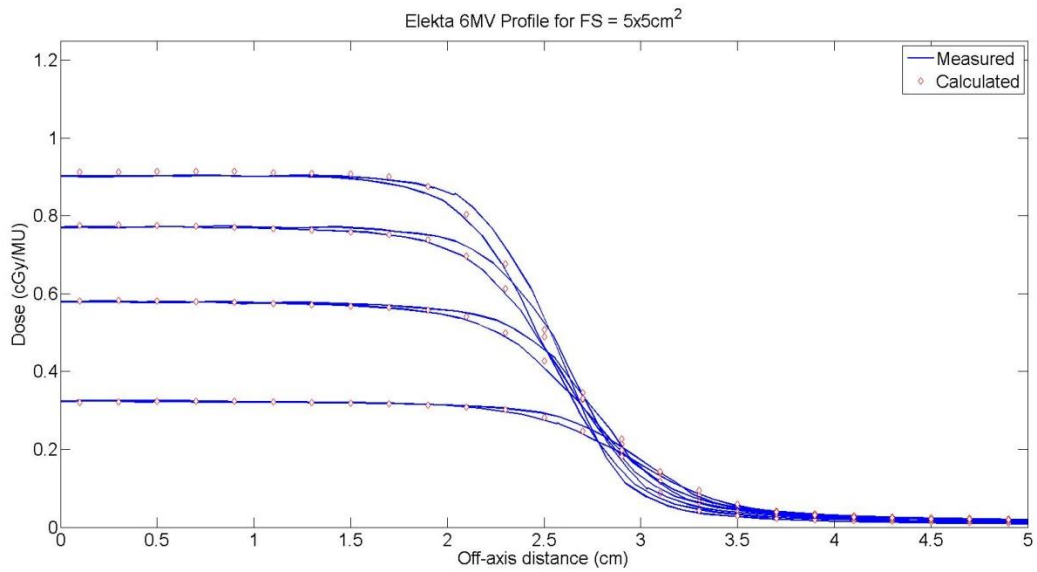


Figure 7.8: Calculated (red diamond) and measured (blue line) dose profiles for an Elekta 6MV beam at a field size of 5 x 5 cm².

Field Size (cm ²)	Direction	Depth (cm)	% Passing (2%/2mm)
5 x 5	x	1.6	98.04
	x	5	100.00
	x	10	100.00
	x	20	100.00
	y	1.6	97.92
	y	5	100.00
	y	10	100.00
	y	20	100.00

Table 7.2: Dose profile agreement between the Elekta 6MV multiple source model and measurement using a ±2%/2mm global gamma criterion at all depths of comparison for a 5 x 5 cm² field size.

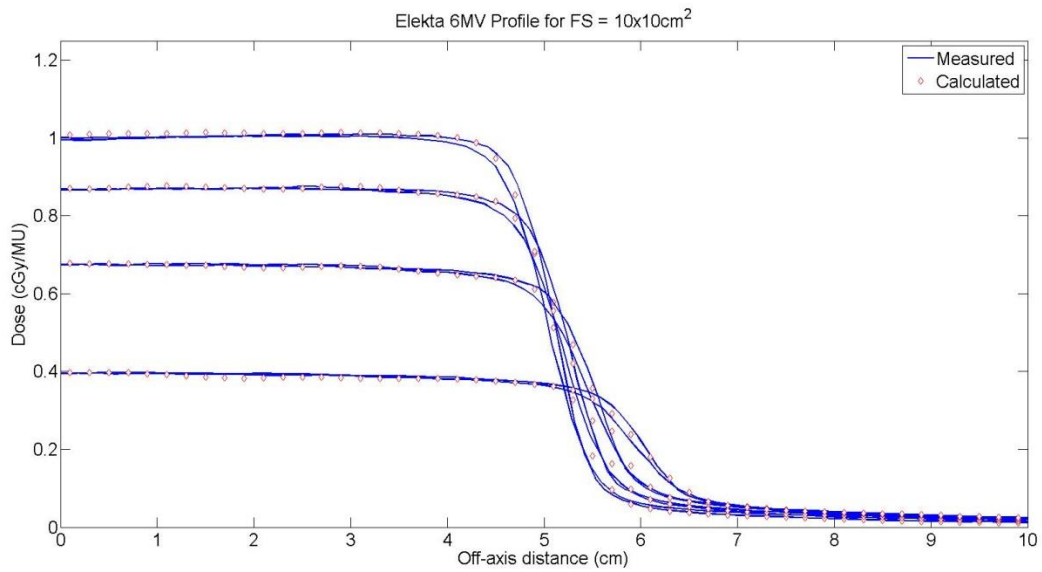


Figure 7.9: Calculated (red diamond) and measured (blue line) dose profiles for an Elekta 6MV beam at a field size of 10 x 10 cm².

Field Size (cm ²)	Direction	Depth (cm)	% Passing (2%/2mm)
10 x 10	x	1.6	96.34
	x	5	100.00
	x	10	100.00
	x	20	100.00
	y	1.6	100.00
	y	5	100.00
	y	10	100.00
	y	20	100.00

Table 7.3: Dose profile agreement between the Elekta 6MV multiple source model and measurement using a $\pm 2\%/2\text{mm}$ global gamma criterion at all depths of comparison for a 10 x 10 cm² field size.

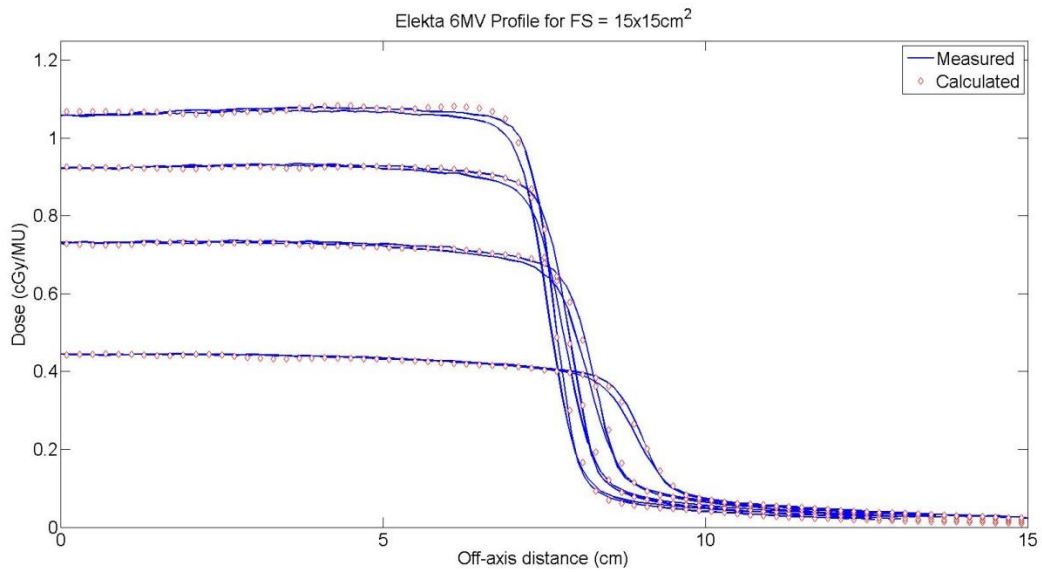


Figure 7.10: Calculated (red diamond) and measured (blue line) dose profiles for an Elekta 6MV beam at a field size of 15 x 15 cm².

Field Size (cm ²)	Direction	Depth (cm)	% Passing (2%/2mm)
15 x 15	x	1.6	94.78
	x	5	100.00
	x	10	100.00
	x	20	100.00
	y	1.6	100.00
	y	5	100.00
	y	10	100.00
	y	20	100.00

Table 7.4: Dose profile agreement between the Elekta 6MV multiple source model and measurement using a $\pm 2\%/2\text{mm}$ global gamma criterion at all depths of comparison for a 15 x 15 cm² field size.

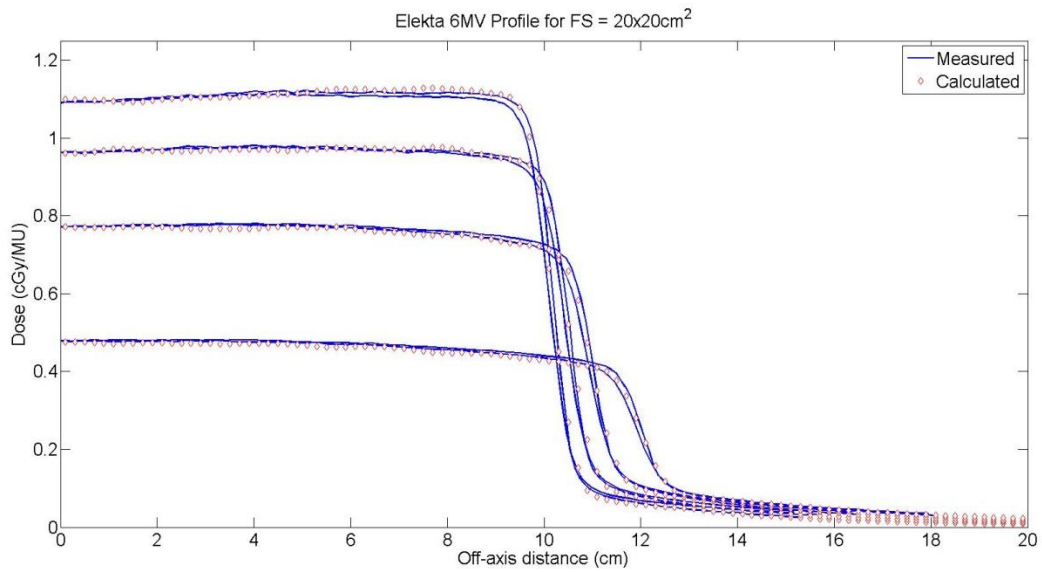


Figure 7.11: Calculated (red diamond) and measured (blue line) dose profiles for an Elekta 6MV beam at a field size of 20 x 20 cm².

Field Size (cm ²)	Direction	Depth (cm)	% Passing (2%/2mm)
20 x 20	x	1.6	98.68
	x	5	99.51
	x	10	100.00
	x	20	100.00
	y	1.6	97.98
	y	5	100.00
	y	10	99.51
	y	20	100.00

Table 7.5: Dose profile agreement between the Elekta 6MV multiple source model and measurement using a $\pm 2\%/2\text{mm}$ global gamma criterion at all depths of comparison for a 20 x 20 cm² field size.

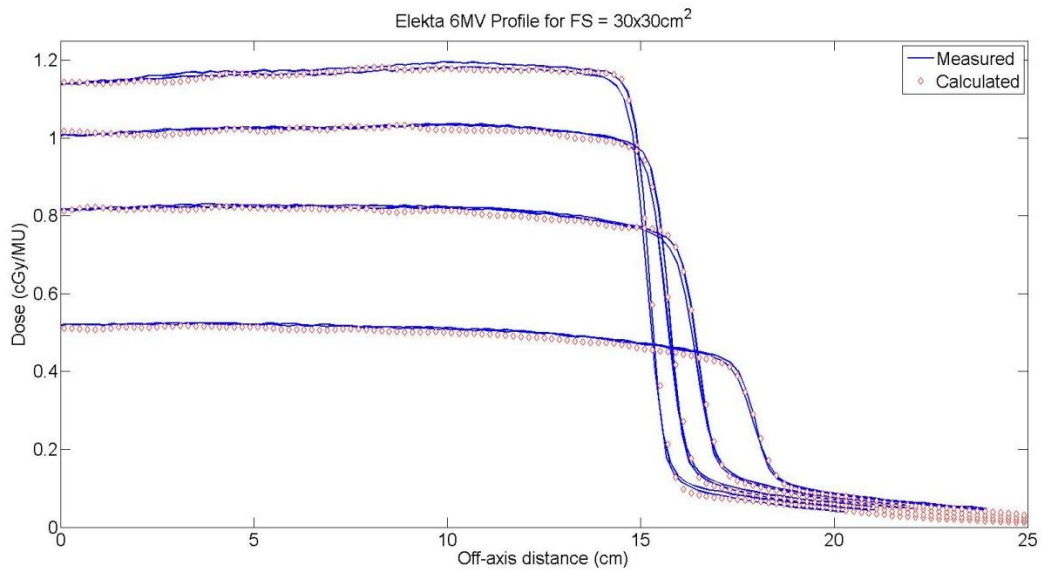


Figure 7.12: Calculated (red diamond) and measured (blue line) dose profiles for an Elekta 6MV beam at a field size of 30 x 30 cm².

Field Size (cm ²)	Direction	Depth (cm)	% Passing (2%/2mm)
30 x 30	x	1.6	98.50
	x	5	99.51
	x	10	100.00
	x	20	100.00
	y	1.6	97.98
	y	5	100.00
	y	10	99.51
	y	20	100.00

Table 7.6: Dose profile agreement between the Elekta 6MV multiple source model and measurement using a $\pm 2\%/2\text{mm}$ global gamma criterion at all depths of comparison for a 30 x 30 cm² field size.

7.2 Elekta 6 MV: Gamma Maps

7.2.1 Elekta 6 MV: Delivery of IMRT Head and Neck Plan

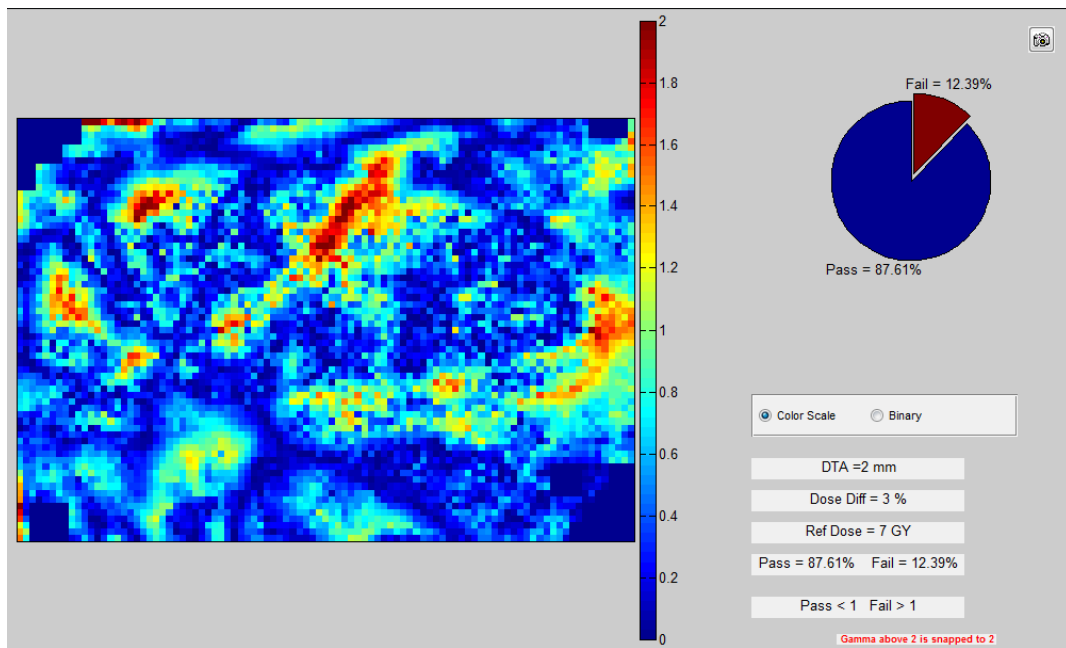


Figure 7.13: IMRT head and neck delivery comparison for the axial plane of delivery #2 for the Elekta 6MV model. Agreement was evaluated using a $\pm 3\%/2\text{mm}$ gamma criterion and 87.6% of pixels passed.

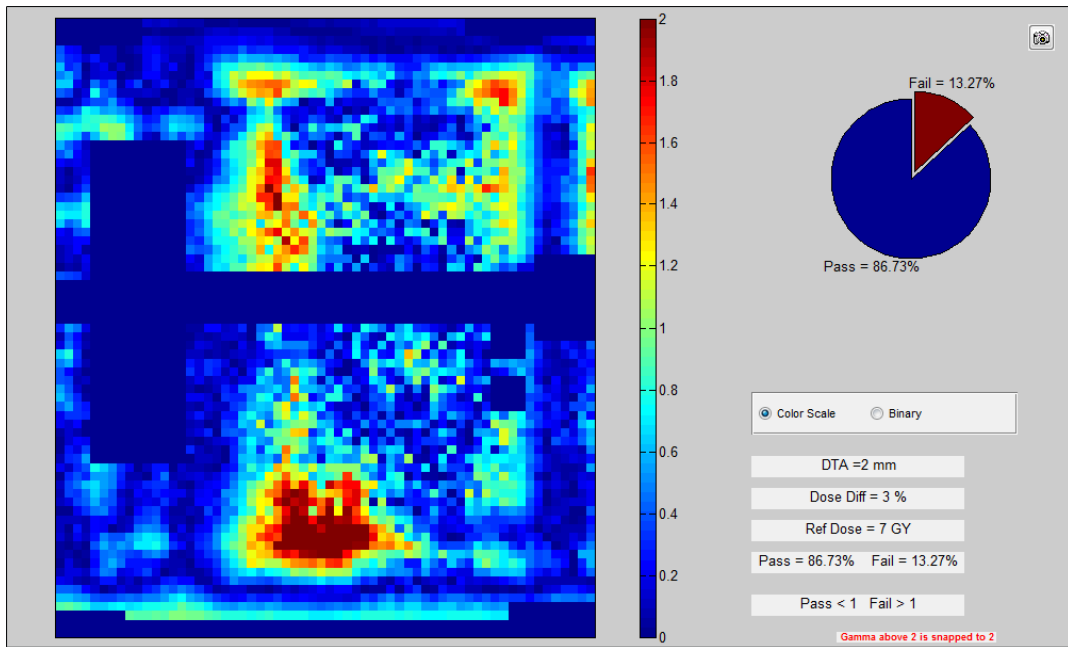


Figure 7.14: IMRT head and neck delivery comparison for the sagittal plane of delivery #2 for the Elekta 6MV model. Agreement was evaluated using a $\pm 3\%/2\text{mm}$ gamma criterion and 86.7% of pixels passed.

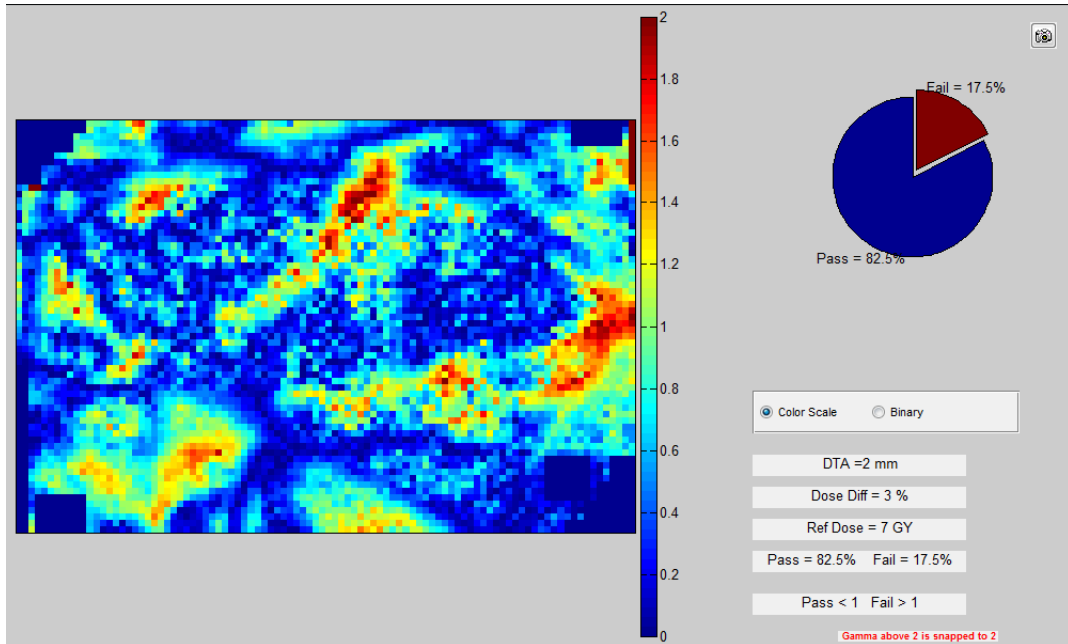


Figure 7.15: IMRT head and neck delivery comparison for the axial plane of delivery #3 for the Elekta 6MV model. Agreement was evaluated using a $\pm 3\%/2\text{mm}$ gamma criterion and 82.5% of pixels passed.

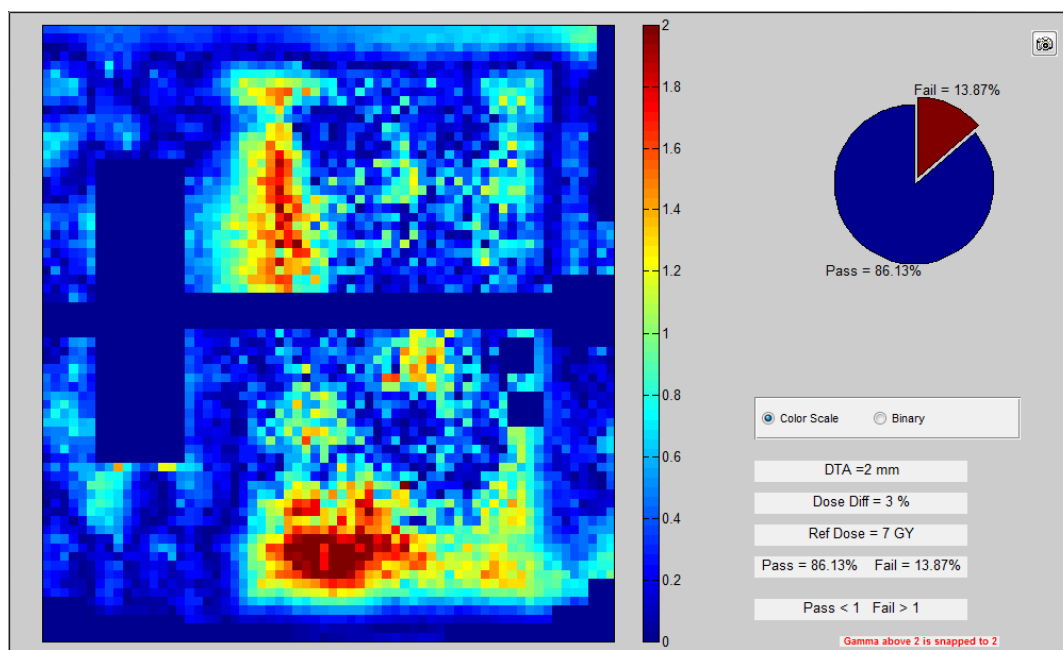


Figure 7.16: IMRT head and neck delivery comparison for the sagittal plane of delivery #3 for the Elekta 6MV model. Agreement was evaluated using a $\pm 3\%/2\text{mm}$ gamma criterion and 86.1% of pixels passed.

7.2.2 Elekta 6 MV: Delivery of SBRT Lung Plan

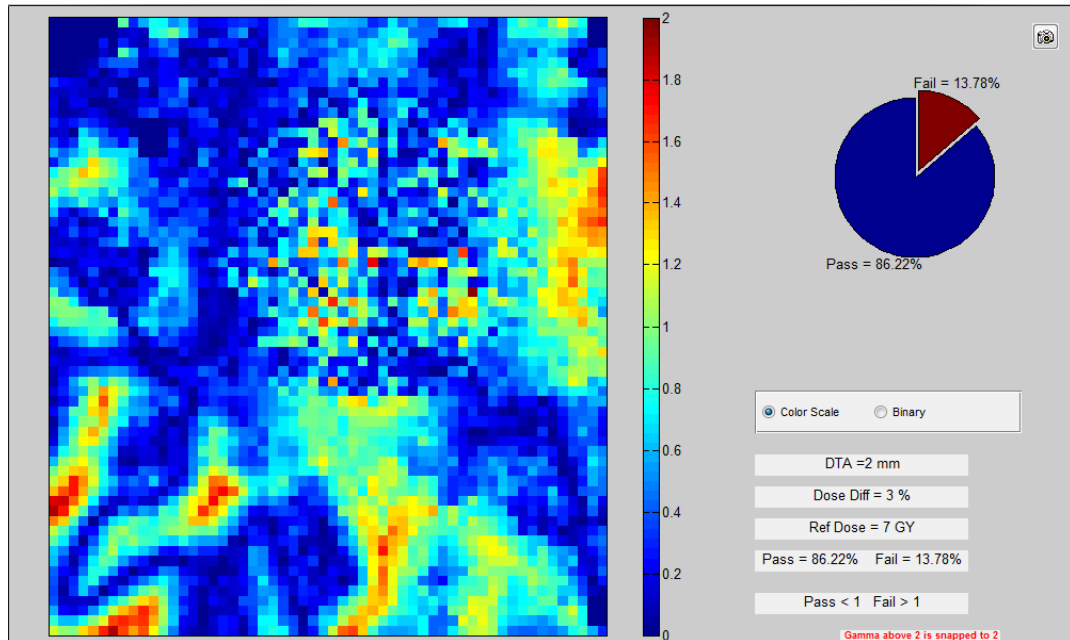


Figure 7.17: Lung SBRT delivery comparison for the axial plane of delivery #2 for the Elekta 6MV model. Agreement was evaluated using a $\pm 3\%/2\text{mm}$ gamma criterion and 86.2% of pixels passed.

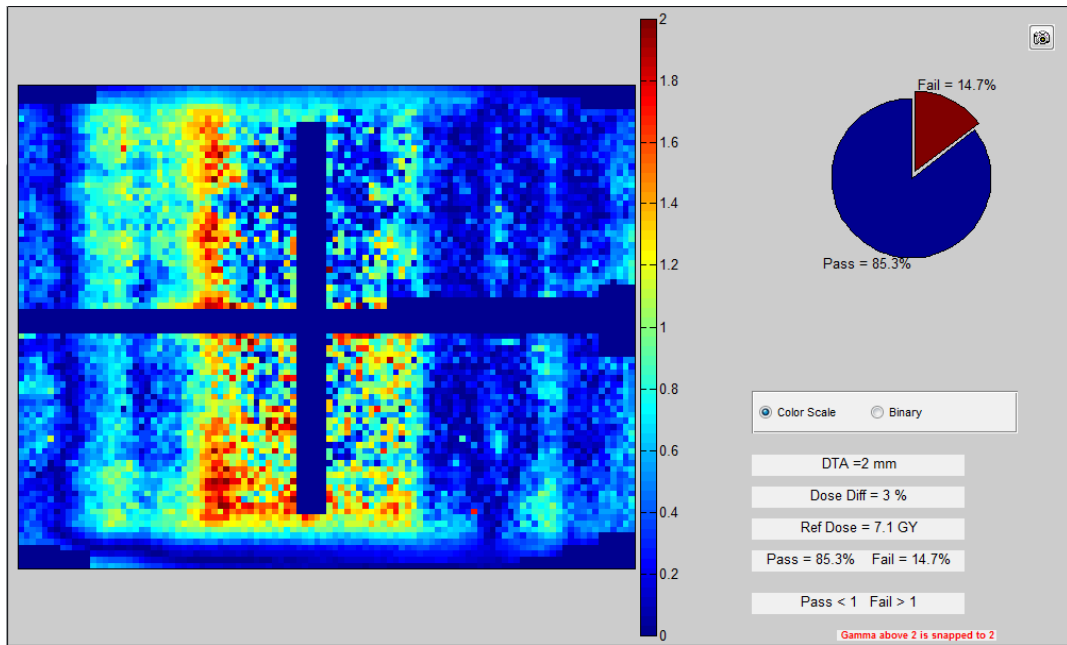


Figure 7.18: Lung SBRT delivery comparison for the sagittal plane of delivery #2 for the Elekta 6MV model. Agreement was evaluated using a $\pm 3\%/2\text{mm}$ gamma criterion and 85.3% of pixels passed.

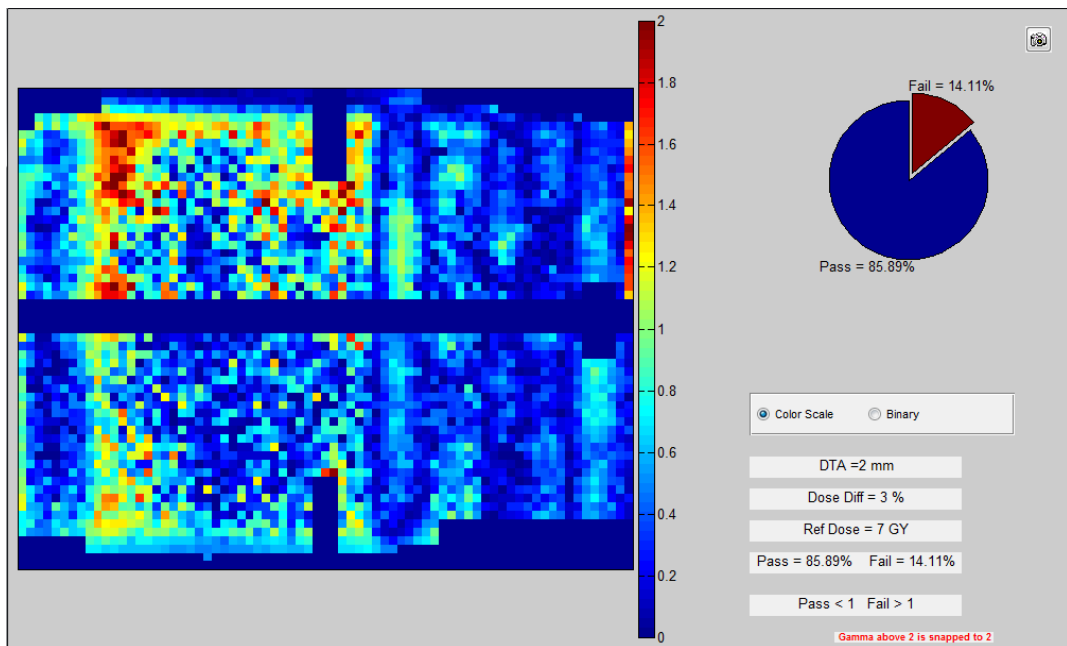


Figure 7.19: Lung SBRT delivery comparison for the coronal plane of delivery #2 for the Elekta 6MV model. Agreement was evaluated using a $\pm 3\%/2\text{mm}$ gamma criterion and 85.9% of pixels passed.

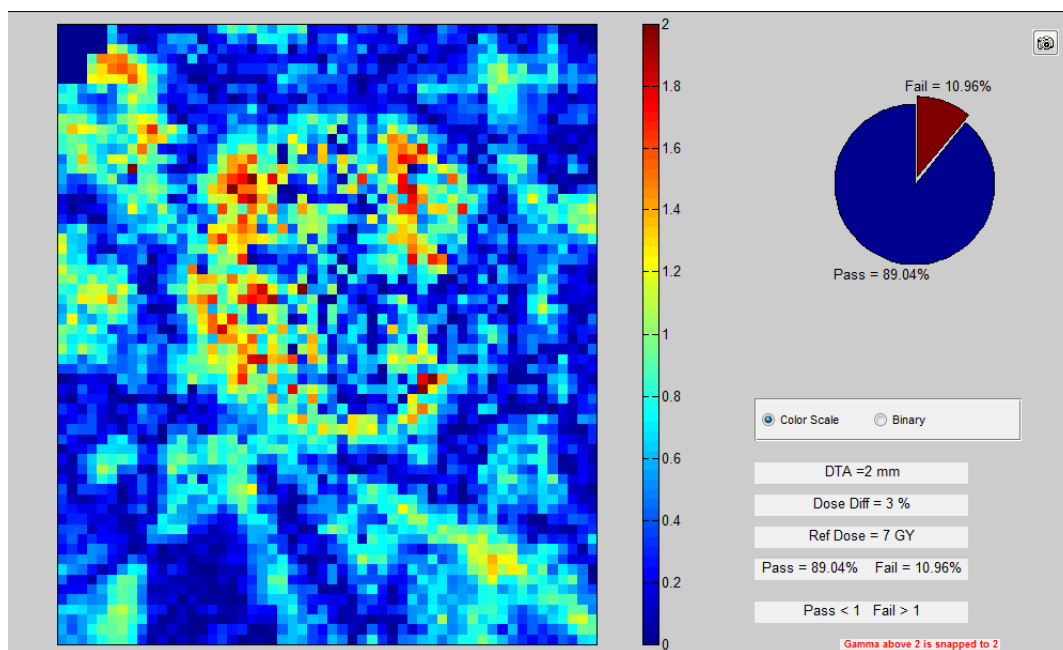


Figure 7.20: Lung SBRT delivery comparison for the axial plane of delivery #3 for the Elekta 6MV model. Agreement was evaluated using a $\pm 3\%/2\text{mm}$ gamma criterion and 89.0% of pixels passed.

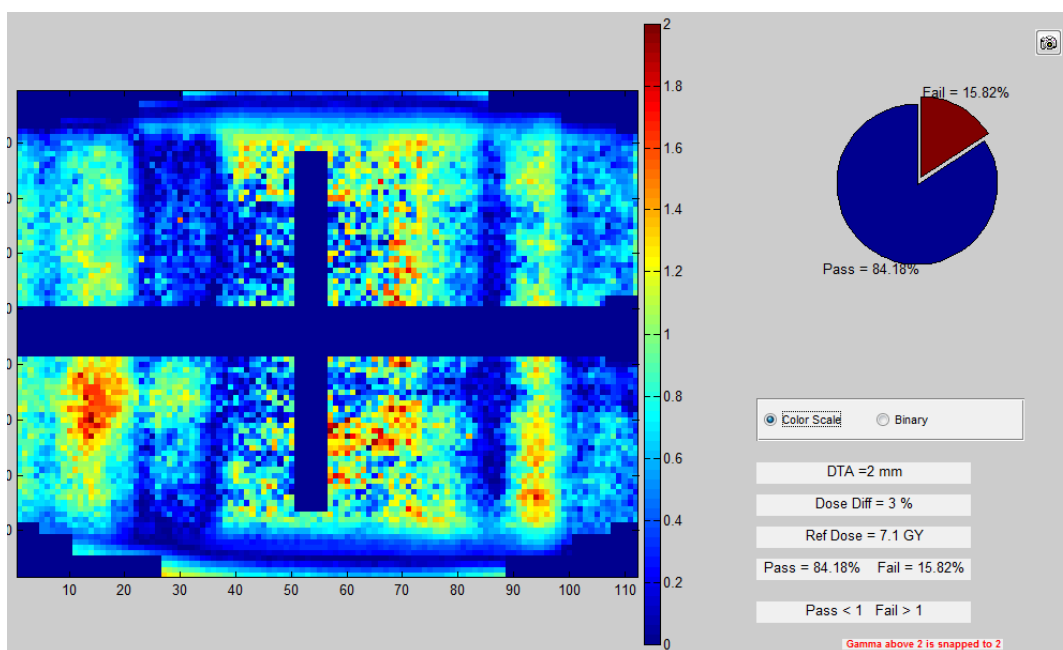


Figure 7.21: Lung SBRT delivery comparison for the sagittal plane of delivery #3 for the Elekta 6MV model. Agreement was evaluated using a $\pm 3\%/2\text{mm}$ gamma criterion and 84.2% of pixels passed.

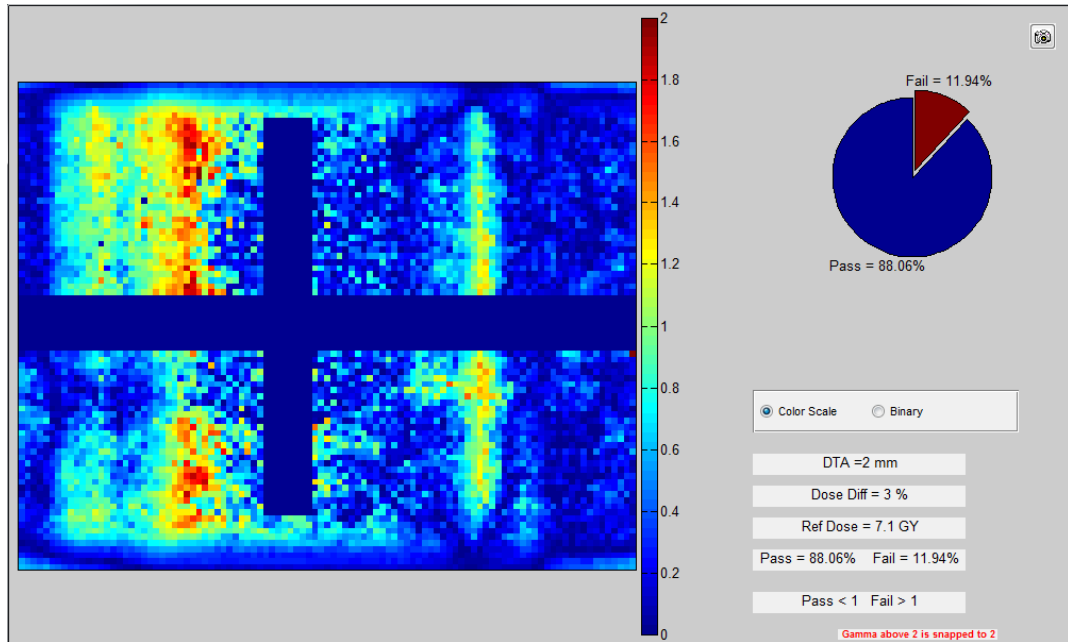


Figure 7.22: Lung SBRT delivery comparison for the coronal plane of delivery #3 for the Elekta 6MV model. Agreement was evaluated using a $\pm 3\%/2\text{mm}$ gamma criterion and 88.1% of pixels passed.

7.2.3 Elekta 6 MV: Delivery of IMRT Lung Plan

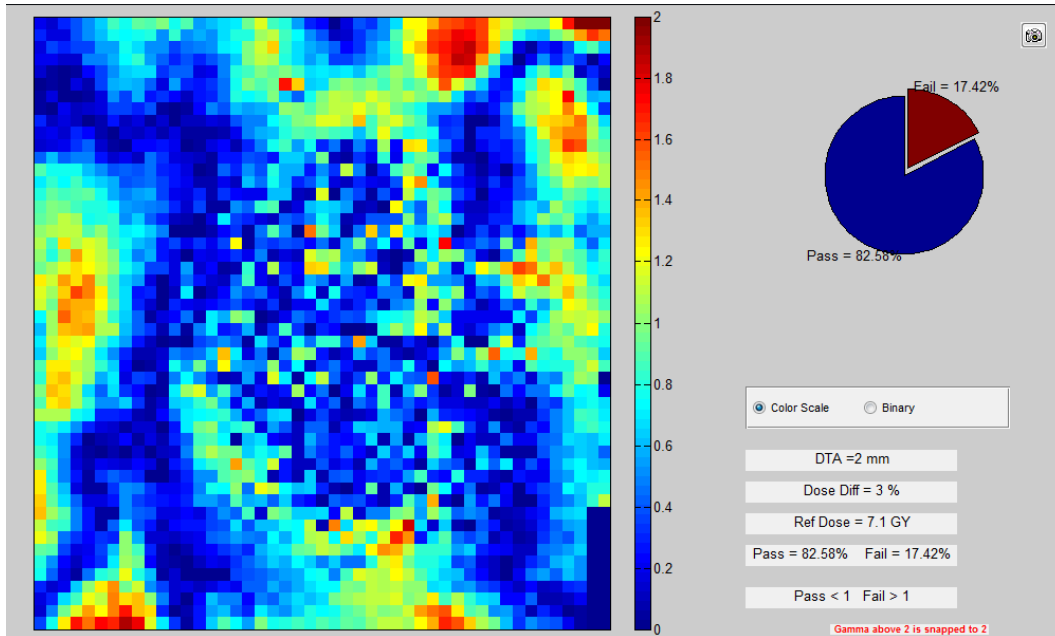


Figure 7.23: Lung IMRT delivery comparison for the axial plane of delivery #1 for the Elekta 6MV model. Agreement was evaluated using a $\pm 3\%/2\text{mm}$ gamma criterion and 82.6% of pixels passed.

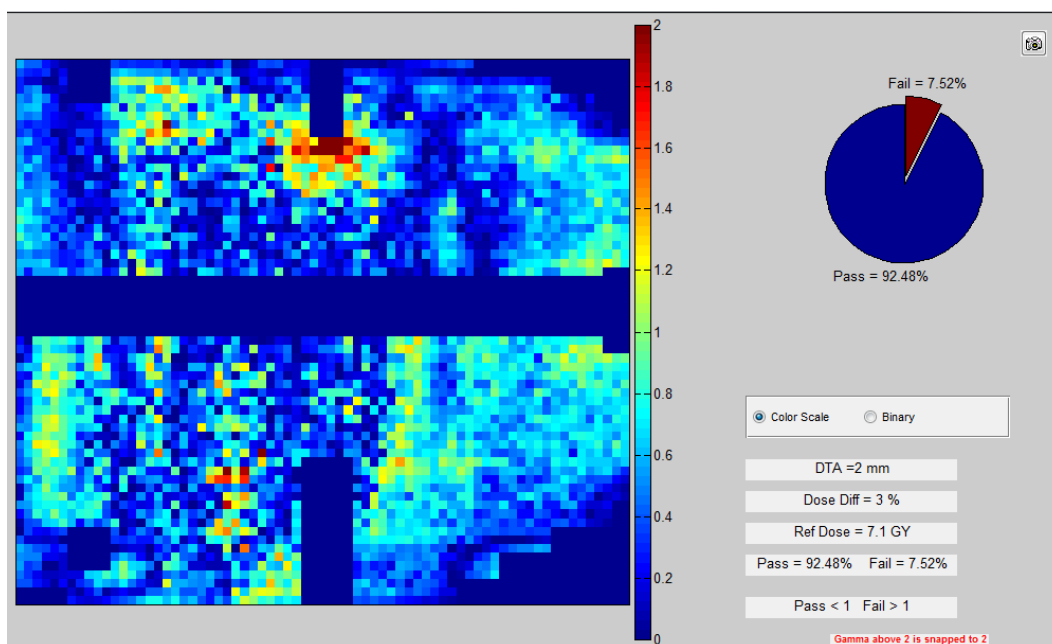


Figure 7.24: Lung IMRT delivery comparison for the sagittal plane of delivery #1 for the Elekta 6MV model. Agreement was evaluated using a $\pm 3\%/2\text{mm}$ gamma criterion and 92.5% of pixels passed.

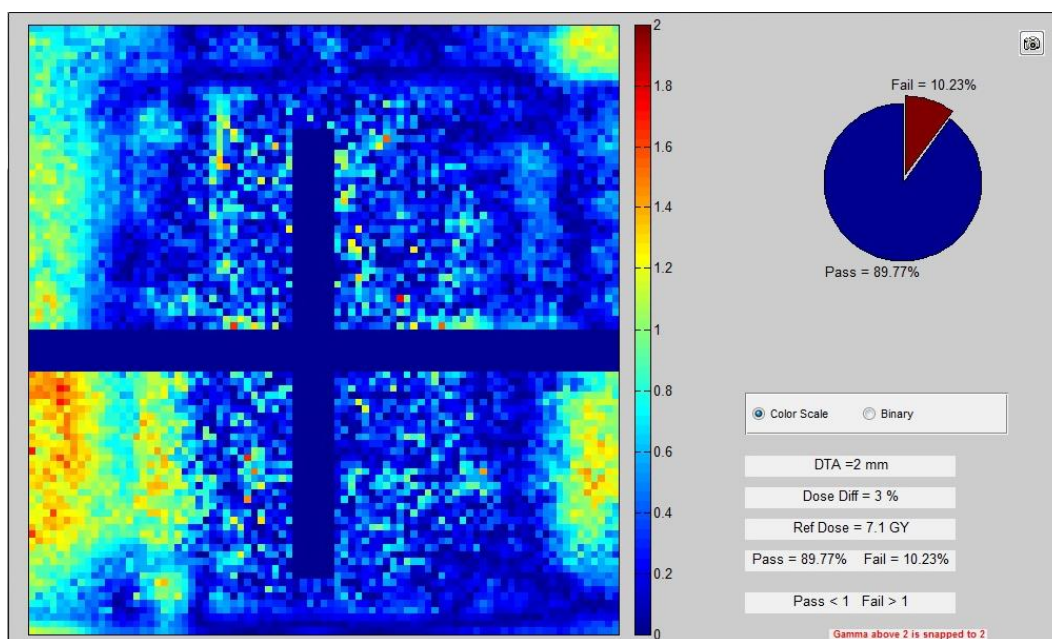


Figure 7.25: Lung IMRT delivery comparison for the coronal plane of delivery #1 for the Elekta 6MV model. Agreement was evaluated using a $\pm 3\%/2\text{mm}$ gamma criterion and 89.8% of pixels passed.

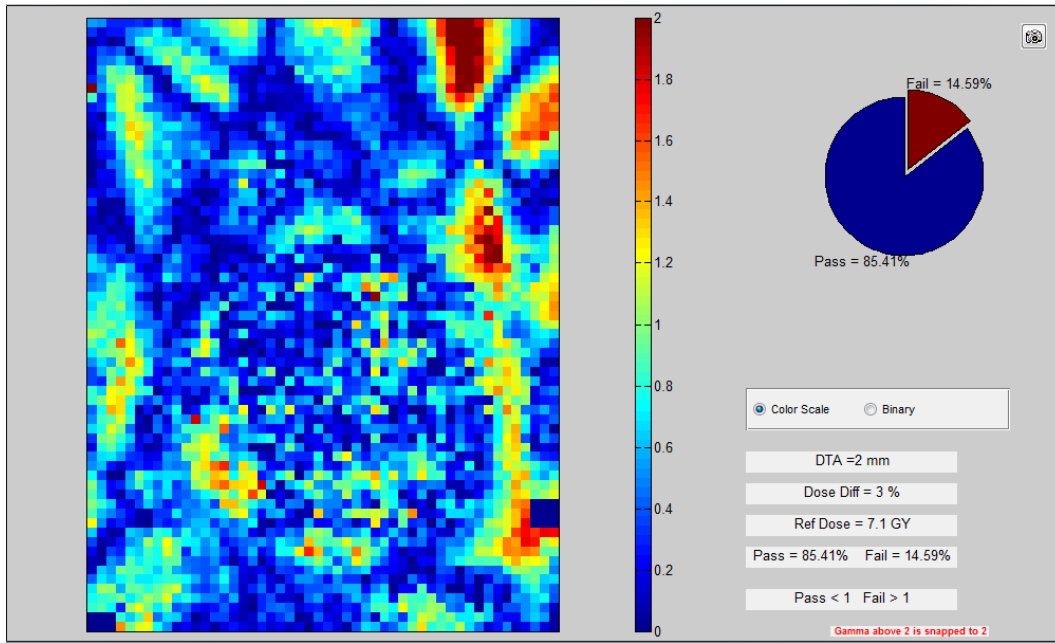


Figure 7.26: Lung IMRT delivery comparison for the axial plane of delivery #2 for the Elekta 6MV model. Agreement was evaluated using a $\pm 3\%/2\text{mm}$ gamma criterion and 85.4% of pixels passed.

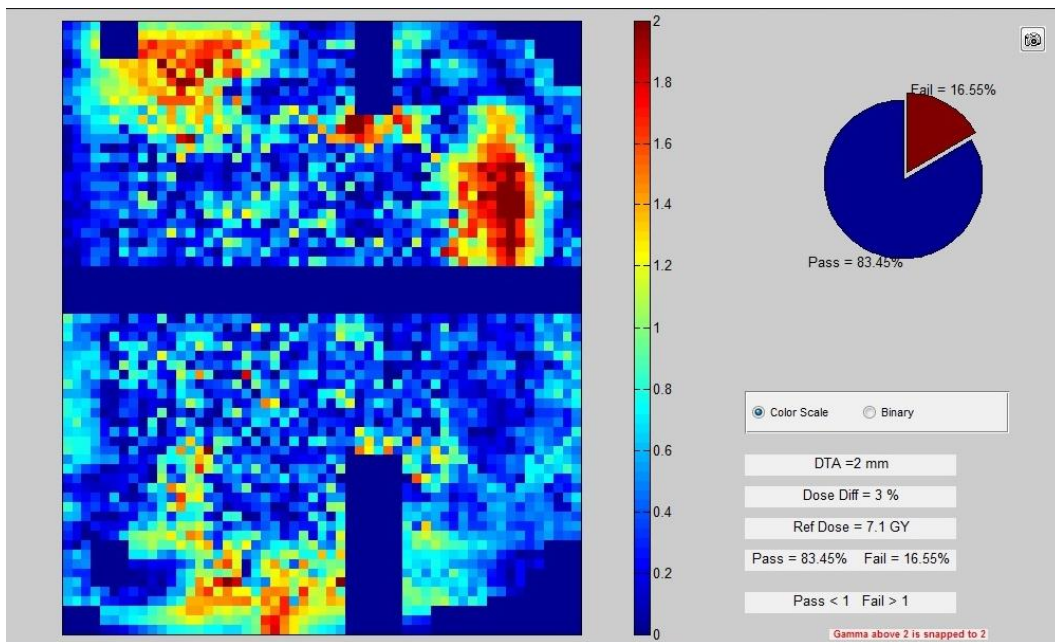


Figure 7.27: Lung IMRT delivery comparison for the sagittal plane of delivery #2 for the Elekta 6MV model. Agreement was evaluated using a $\pm 3\%/2\text{mm}$ gamma criterion and 83.5% of pixels passed.

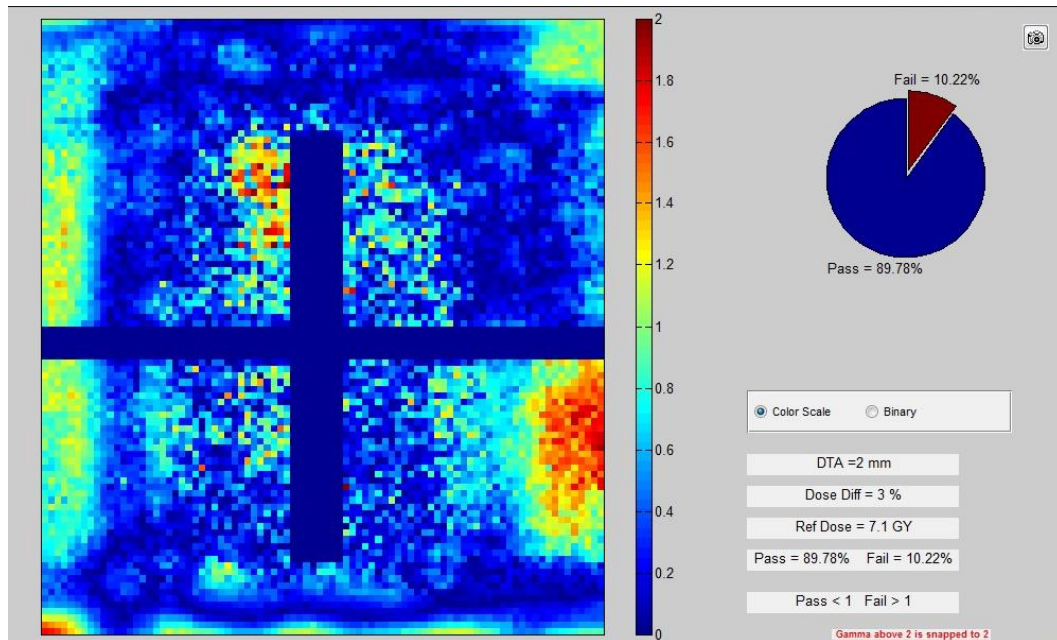


Figure 7.28: Lung IMRT delivery comparison for the coronal plane of delivery #2 for the Elekta 6MV model. Agreement was evaluated using a $\pm 3\%/2\text{mm}$ gamma criterion and 89.8% of pixels passed.

7.3 Elekta 10 MV: Percent Depth Dose and Dose Profiles

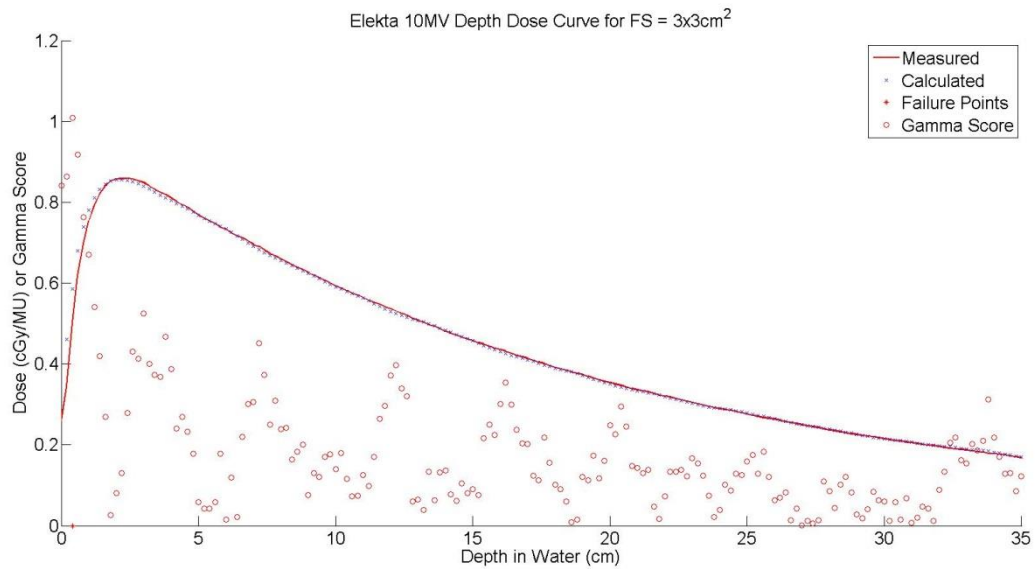


Figure 7.29: Calculated (blue 'x') and measured (red line) percent depth dose curves for an Elekta 10MV beam at a field size of 3 x 3 cm². Gamma agreement (red circles) for each point is also displayed along with any points (red star) at which a failure to meet the $\pm 2\%/2\text{mm}$ criterion. At this field size 99.43% of all data passed the gamma criterion.

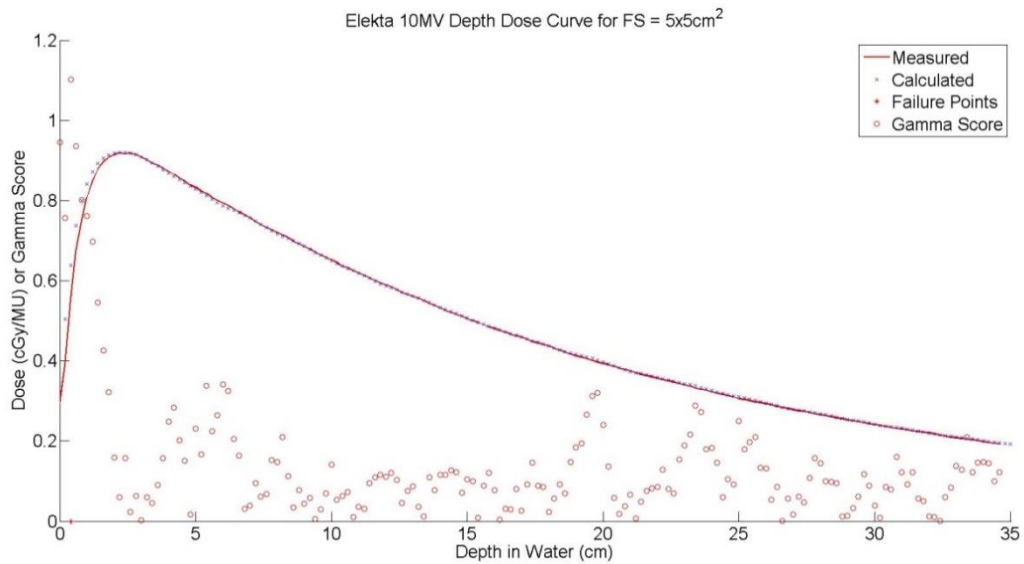


Figure 7.30: Calculated (blue 'x') and measured (red line) percent depth dose curves for an Elekta 10MV beam at a field size of 5 x 5 cm². Gamma agreement (red circles) for each point is also displayed along with any points (red star) at which a failure to meet the $\pm 2\%/2\text{mm}$ criterion. At this field size 99.43% of all data passed the gamma criterion.

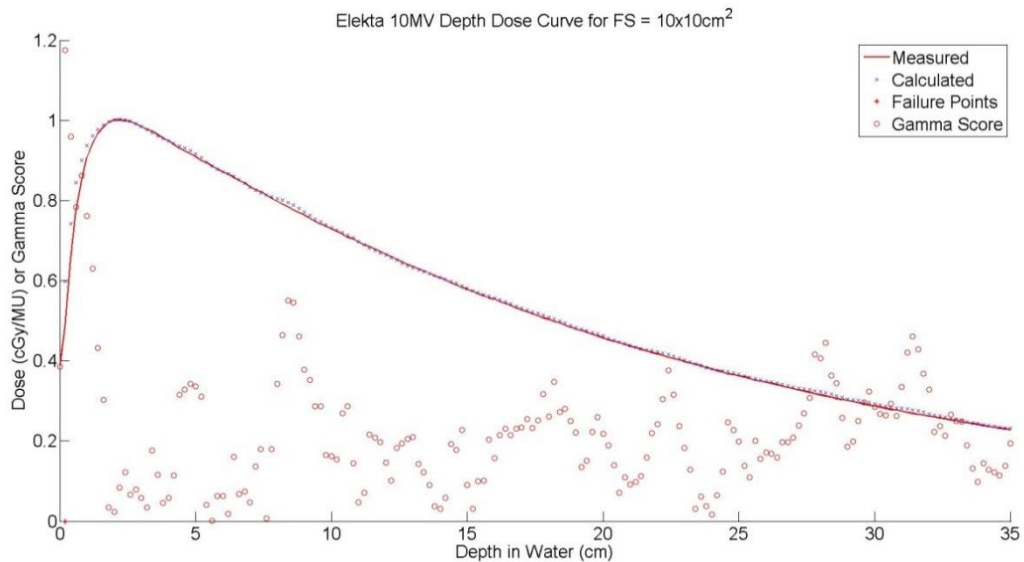


Figure 7.31: Calculated (blue 'x') and measured (red line) percent depth dose curves for an Elekta 10MV beam at a field size of 10 x 10 cm². Gamma agreement (red circles) for each point is also displayed along with any points (red star) at which a failure to meet the $\pm 2\%/2\text{mm}$ criterion. At this field size 99.43% of all data passed the gamma criterion.

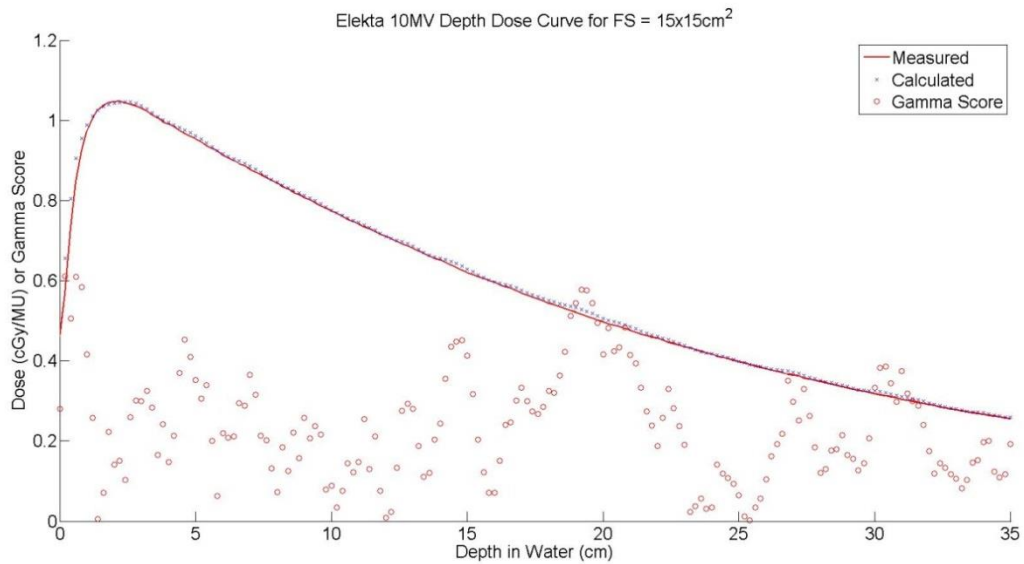


Figure 7.32: Calculated (blue 'x') and measured (red line) percent depth dose curves for an Elekta 10MV beam at a field size of 15 x 15 cm². Gamma agreement (red circles) for each point is also displayed along with any points (red star) at which a failure to meet the $\pm 2\%/2\text{mm}$ criterion. At this field size 100% of all data passed the gamma criterion.

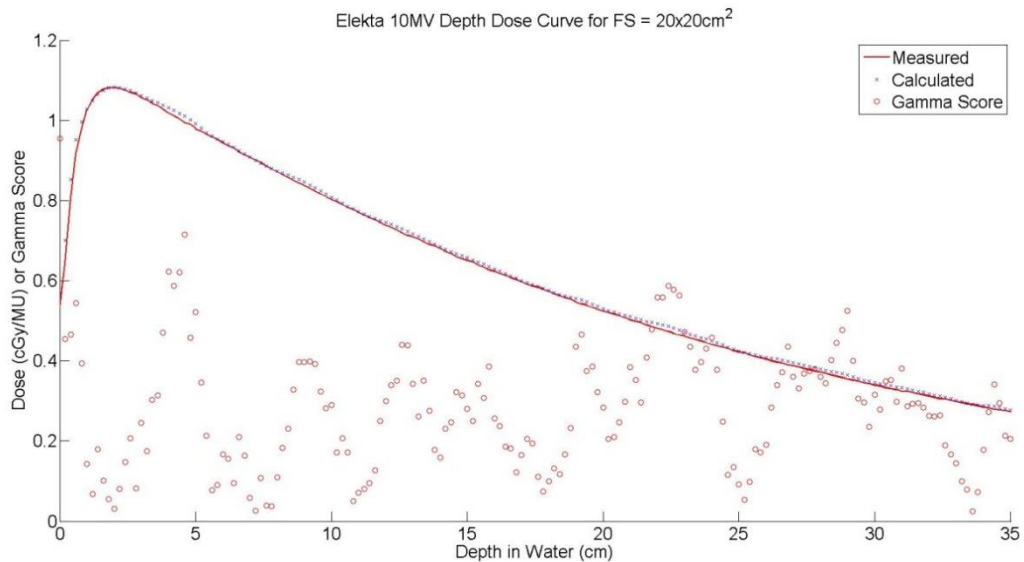


Figure 7.33: Calculated (blue 'x') and measured (red line) percent depth dose curves for an Elekta 10MV beam at a field size of 20 x 20 cm². Gamma agreement (red circles) for each point is also displayed along with any points (red star) at which a failure to meet the $\pm 2\%/2\text{mm}$ criterion. At this field size 100% of all data passed the gamma criterion.

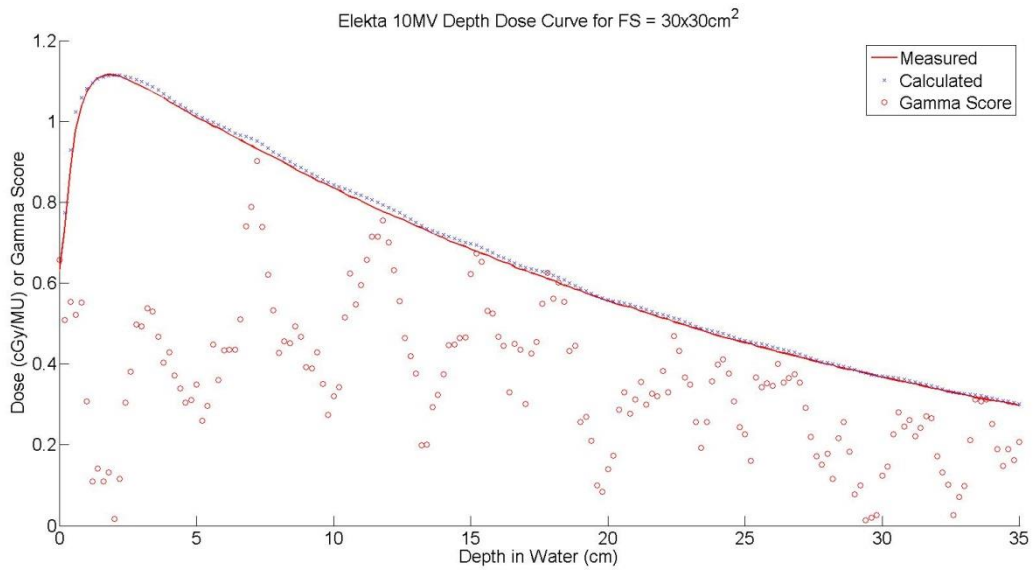


Figure 7.34: Calculated (blue 'x') and measured (red line) percent depth dose curves for an Elekta 10MV beam at a field size of 30 x 30 cm². Gamma agreement (red circles) for each point is also displayed along with any points (red star) at which a failure to meet the $\pm 2\%/2\text{mm}$ criterion. At this field size 100% of all data passed the gamma criterion.

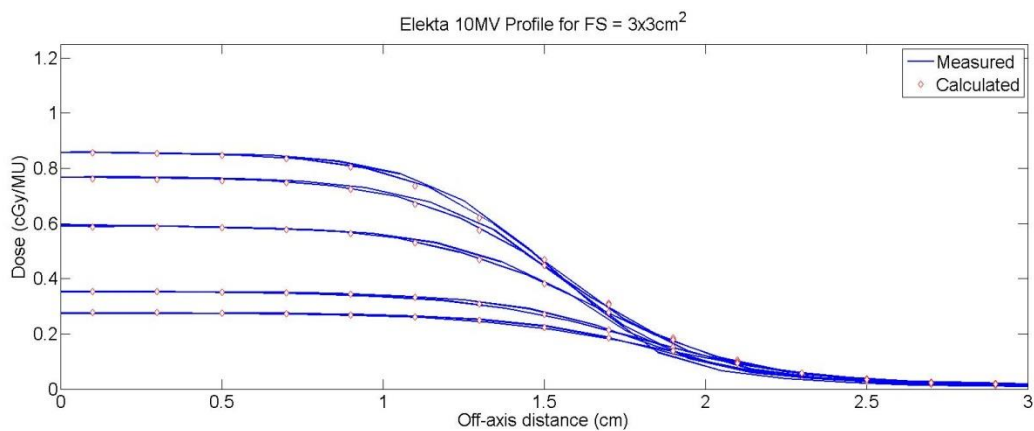


Figure 7.35: Calculated (red diamond) and measured (blue line) dose profiles for an Elekta 10MV beam at a field size of 3 x 3 cm².

Field Size (cm ²)	Direction	Depth (cm)	% Passing (2%/2mm)
3 x 3	x	1.6	95.65
	x	5	100.00
	x	10	100.00
	x	20	100.00
	x	25	100.00
	y	1.6	100.00
	y	5	100.00
	y	10	100.00
	y	20	100.00
y	25	100.00	

Table 7.7: Dose profile agreement between the Elekta 10MV multiple source model and measurement using a $\pm 2\%/2\text{mm}$ global gamma criterion at all depths of comparison for a 3 x 3 cm² field size.

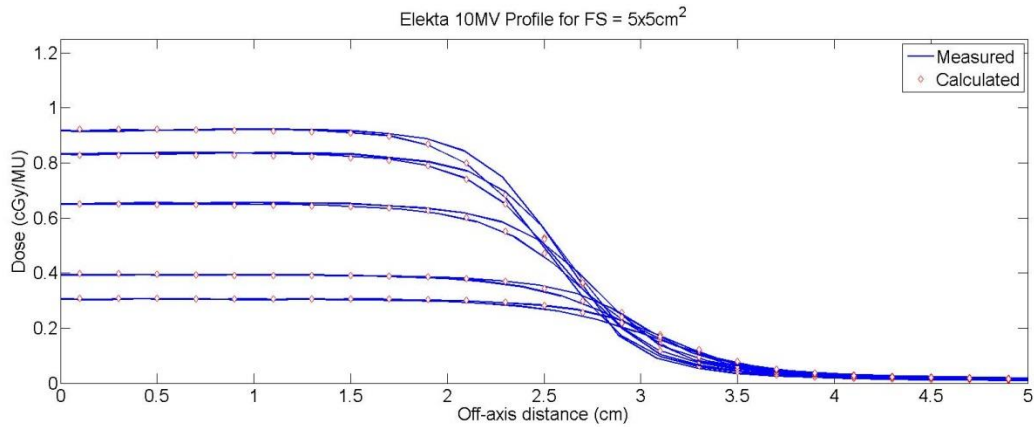


Figure 7.36: Calculated (red diamond) and measured (blue line) dose profiles for an Elekta 10MV beam at a field size of 5 x 5 cm².

Field Size (cm ²)	Direction	Depth (cm)	% Passing (2%/2mm)
5 x 5	x	1.6	100.00
	x	5	100.00
	x	10	100.00
	x	20	100.00
	x	25	100.00
	y	1.6	100.00
	y	5	100.00
	y	10	100.00
	y	20	100.00
	y	25	100.00

Table 7.8: Dose profile agreement between the Elekta 10MV multiple source model and measurement using a $\pm 2\%/2\text{mm}$ global gamma criterion at all depths of comparison for a 5 x 5 cm² field size.

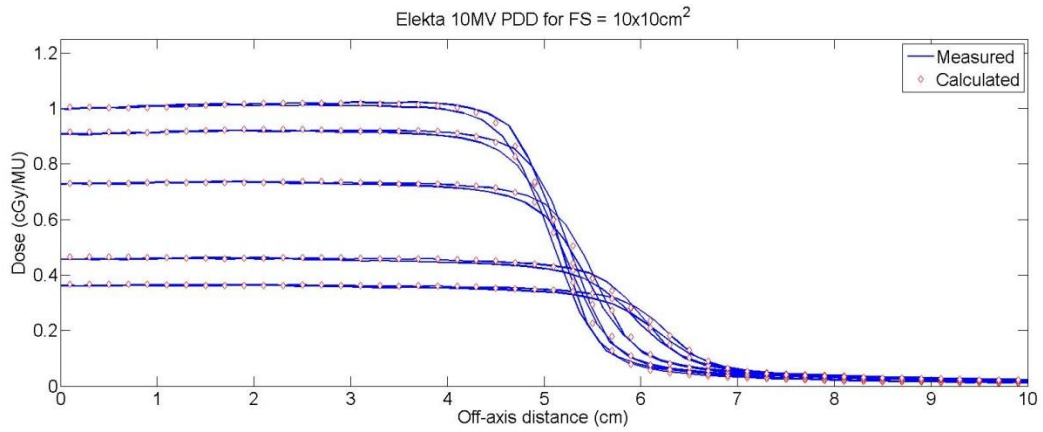


Figure 7.37: Calculated (red diamond) and measured (blue line) dose profiles for an Elekta 10MV beam at a field size of 10 x 10 cm².

Field Size (cm ²)	Direction	Depth (cm)	% Passing (2%/2mm)
10 x 10	x	1.6	100.00
	x	5	100.00
	x	10	100.00
	x	20	100.00
	x	25	100.00
	y	1.6	100.00
	y	5	100.00
	y	10	100.00
	y	20	100.00
	y	25	100.00

Table 7.9: Dose profile agreement between the Elekta 10MV multiple source model and measurement using a $\pm 2\%/2\text{mm}$ global gamma criterion at all depths of comparison for a 10 x 10 cm² field size.

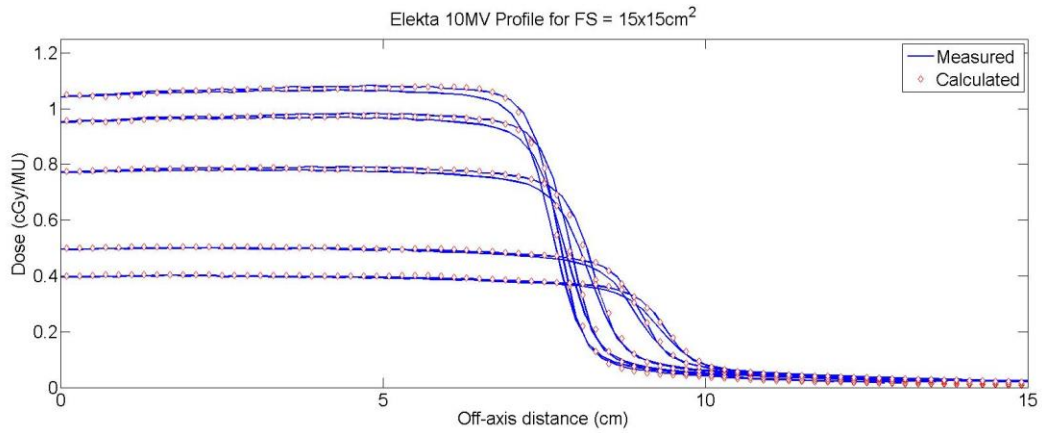


Figure 7.38: Calculated (red diamond) and measured (blue line) dose profiles for an Elekta 10MV beam at a field size of 15 x 15 cm².

Field Size (cm ²)	Direction	Depth (cm)	% Passing (2%/2mm)
15 x 15	x	1.6	94.95
	x	5	100.00
	x	10	100.00
	x	20	100.00
	x	25	100.00
	y	1.6	100.00
	y	5	100.00
	y	10	100.00
	y	20	100.00
	y	25	100.00

Table 7.10: Dose profile agreement between the Elekta 10MV multiple source model and measurement using a $\pm 2\%/2\text{mm}$ global gamma criterion at all depths of comparison for a 15 x 15 cm² field size.

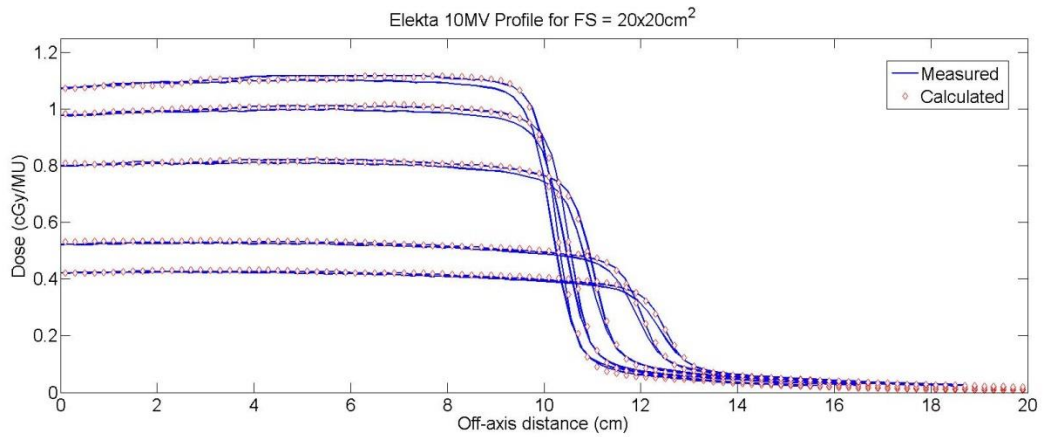


Figure 7.39: Calculated (red diamond) and measured (blue line) dose profiles for an Elekta 10MV beam at a field size of 20 x 20 cm².

Field Size (cm ²)	Direction	Depth (cm)	% Passing (2%/2mm)
20 x 20	x	1.6	90.98
	x	5	98.51
	x	10	100.00
	x	20	100.00
	x	25	100.00
	y	1.6	99.19
	y	5	100.00
	y	10	100.00
	y	20	100.00
	y	25	100.00

Table 7.11: Dose profile agreement between the Elekta 10MV multiple source model and measurement using a $\pm 2\%/2\text{mm}$ global gamma criterion at all depths of comparison for a 20 x 20 cm² field size.

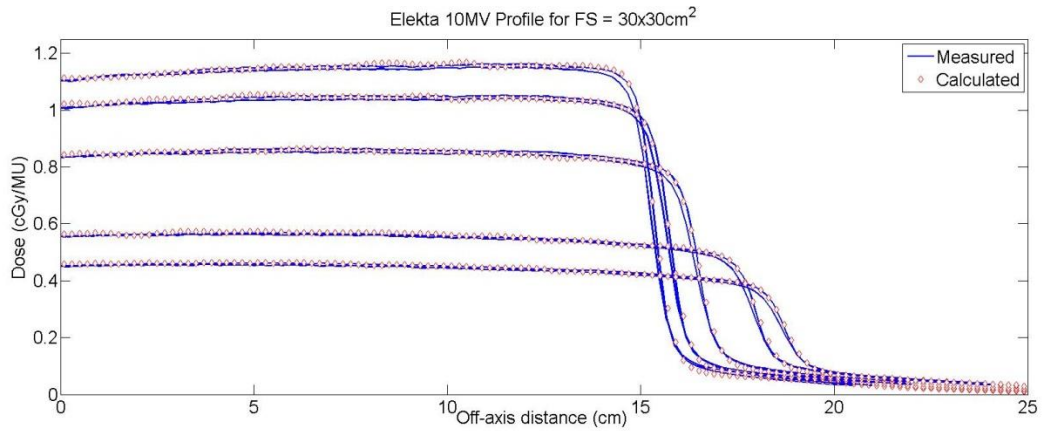


Figure 7.40: Calculated (red diamond) and measured (blue line) dose profiles for an Elekta 10MV beam at a field size of 30 x 30 cm².

Field Size (cm ²)	Direction	Depth (cm)	% Passing (2%/2mm)
30 x 30	x	1.6	98.97
	x	5	100.00
	x	10	100.00
	x	20	100.00
	x	25	100.00
	y	1.6	99.45
	y	5	100.00
	y	10	100.00
	y	20	100.00
	y	25	100.00

Table 7.12: Dose profile agreement between the Elekta 10MV multiple source model and measurement using a $\pm 2\%/2\text{mm}$ global gamma criterion at all depths of comparison for a 30 x 30 cm² field size.

7.4 Elekta 10 MV: Gamma Maps

7.4.1 Elekta 10 MV: Delivery of IMRT Head and Neck Plan

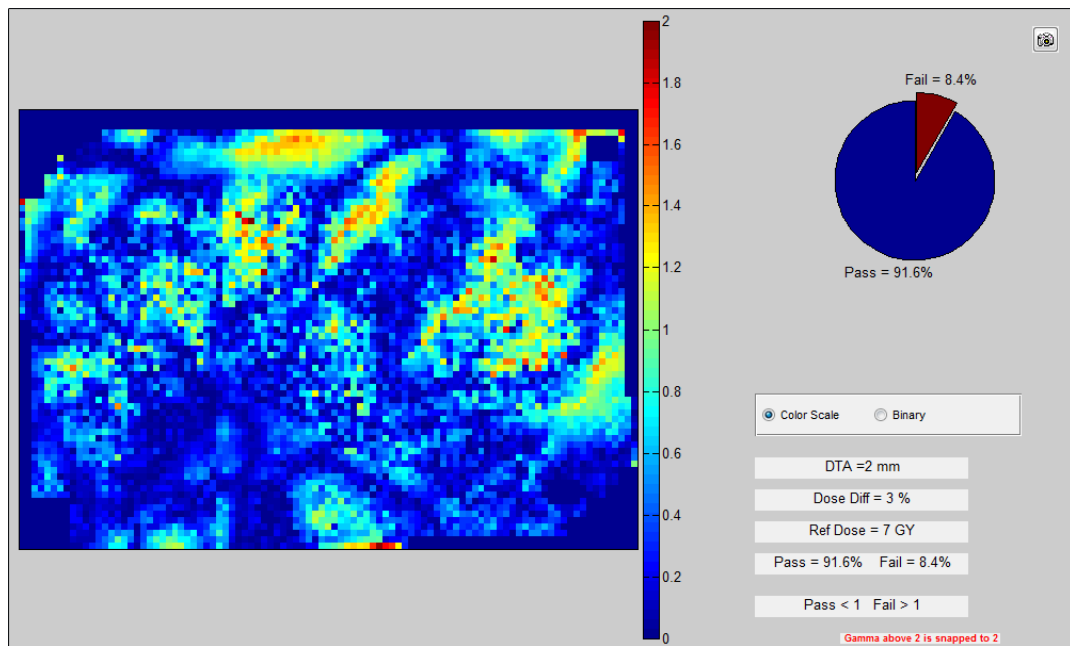


Figure 7.41: IMRT head and neck delivery comparison for the axial plane of delivery #2 for the Elekta 10MV model. Agreement was evaluated using a $\pm 3\%/2\text{mm}$ gamma criterion and 91.6% of pixels passed.

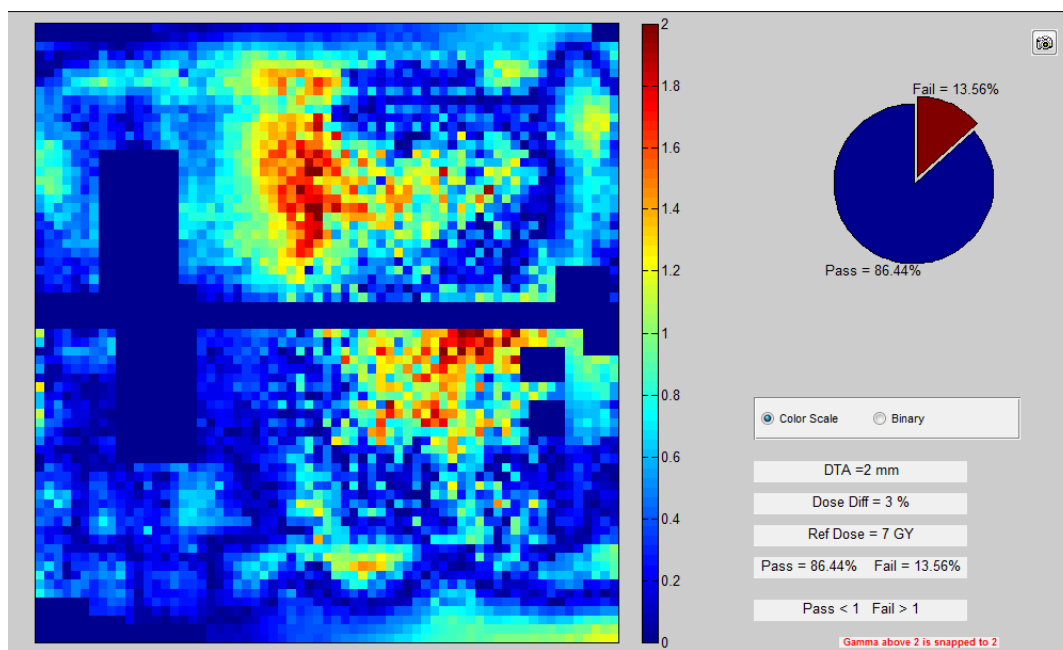


Figure 7.42: IMRT head and neck delivery comparison for the sagittal plane of delivery #2 for the Elekta 10MV model. Agreement was evaluated using a $\pm 3\%/2\text{mm}$ gamma criterion and 86.4% of pixels passed.

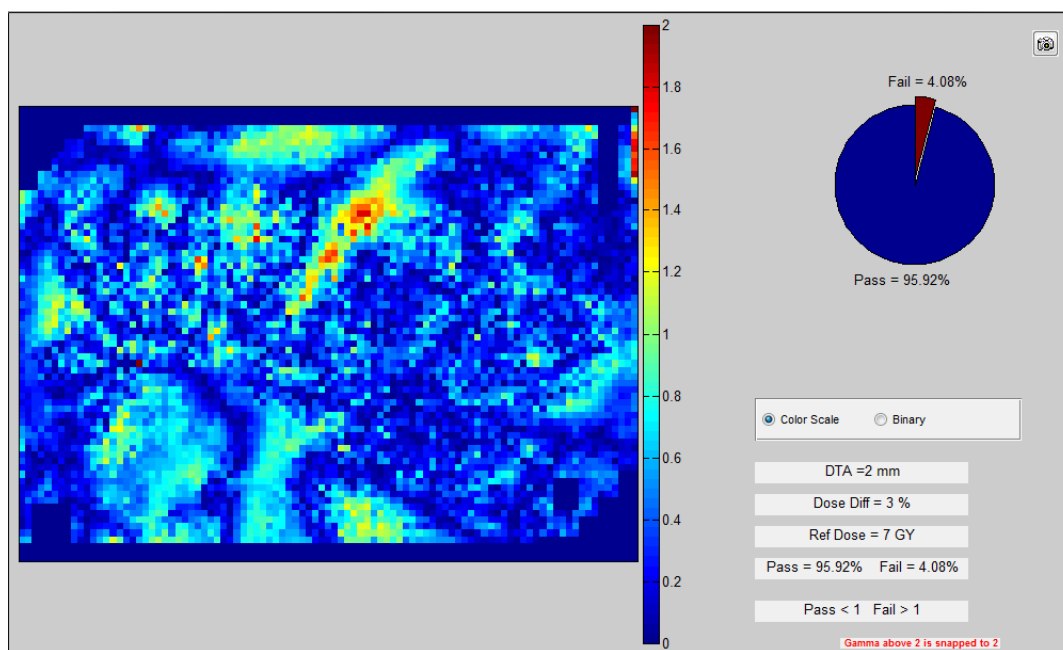


Figure 7.43: IMRT head and neck delivery comparison for the axial plane of delivery #3 for the Elekta 10MV model. Agreement was evaluated using a $\pm 3\%/2\text{mm}$ gamma criterion and 95.9% of pixels passed.

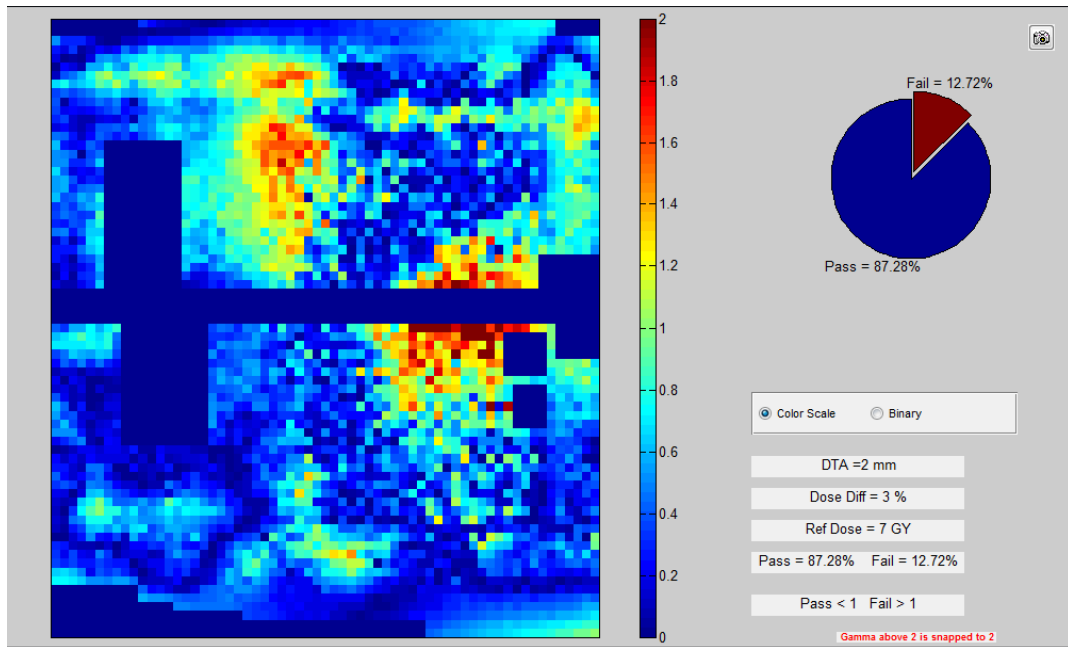


Figure 7.44: IMRT head and neck delivery comparison for the sagittal plane of delivery #3 for the Elekta 10MV model. Agreement was evaluated using a $\pm 3\%/2\text{mm}$ gamma criterion and 87.3% of pixels passed.

7.4.2 Elekta 10 MV: Delivery of SBRT Lung Plan

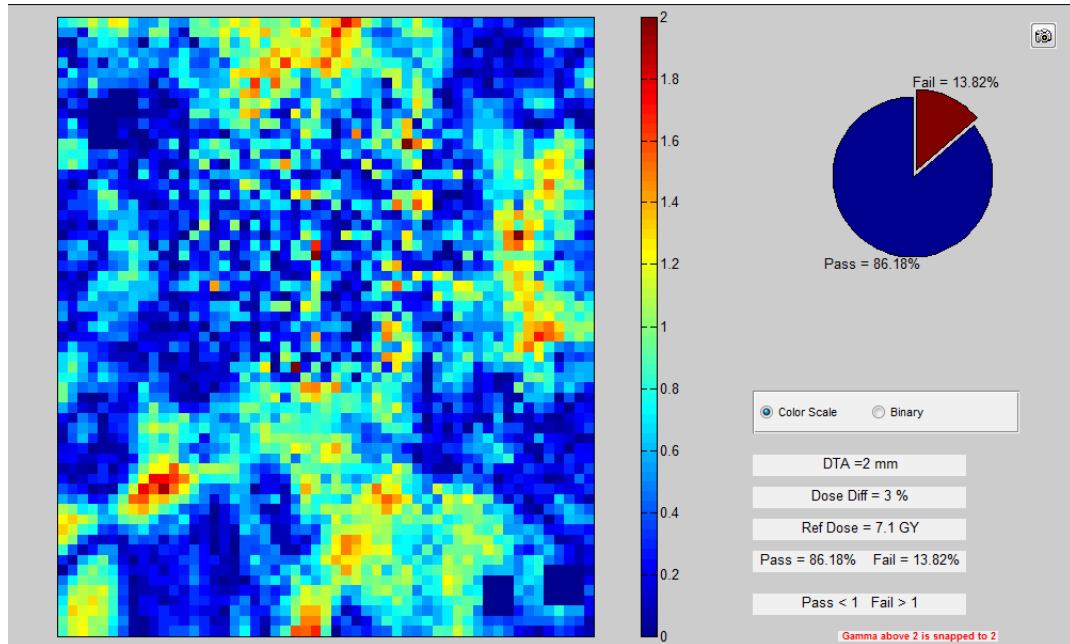


Figure 7.45: Lung SBRT delivery comparison for the axial plane of delivery #2 for the Elekta 10MV model. Agreement was evaluated using a $\pm 3\%/2\text{mm}$ gamma criterion and 86.2% of pixels passed.

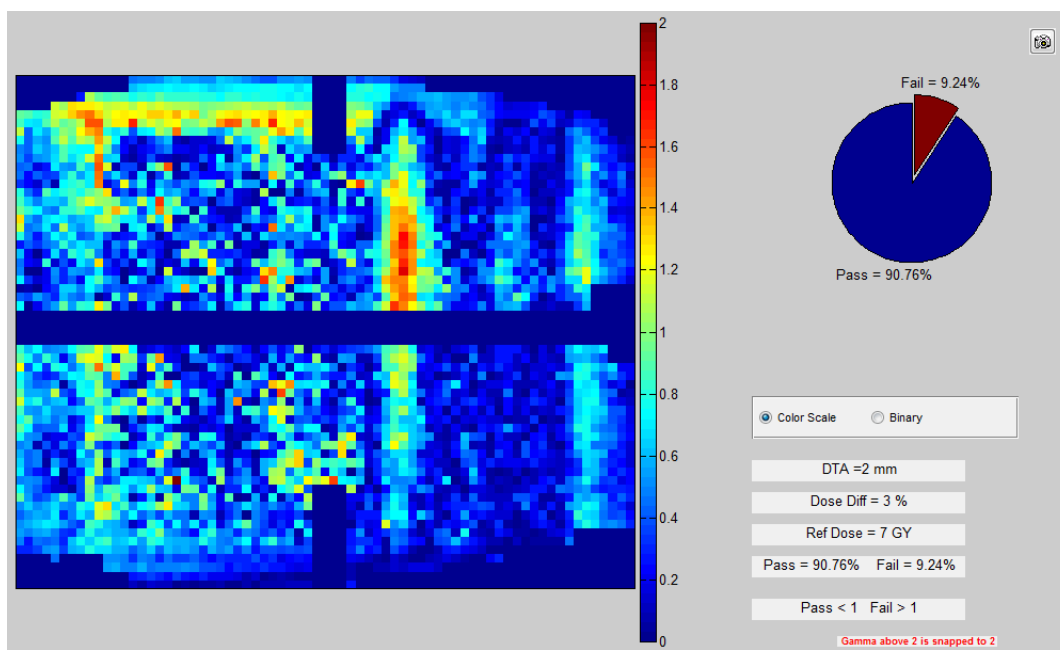


Figure 7.46: Lung SBRT delivery comparison for the sagittal plane of delivery #2 for the Elekta 10MV model. Agreement was evaluated using a $\pm 3\%/2\text{mm}$ gamma criterion and 90.8% of pixels passed.

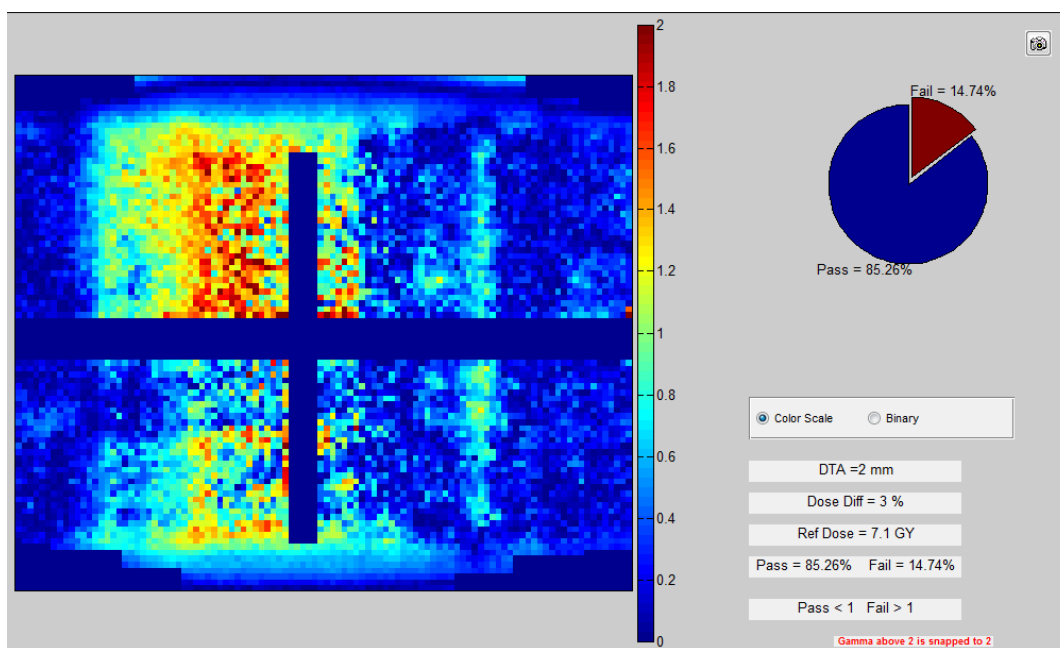


Figure 7.47: Lung SBRT delivery comparison for the coronal plane of delivery #2 for the Elekta 10MV model. Agreement was evaluated using a $\pm 3\%/2\text{mm}$ gamma criterion and 85.3% of pixels passed.

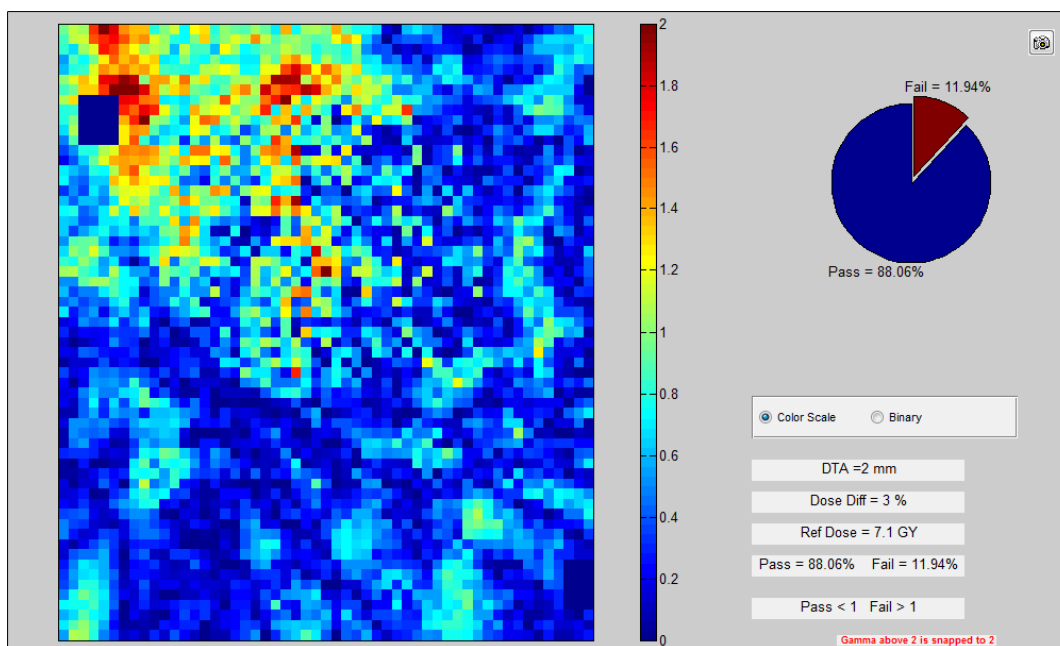


Figure 7.48: Lung SBRT delivery comparison for the axial plane of delivery #3 for the Elekta 10MV model. Agreement was evaluated using a $\pm 3\%/2\text{mm}$ gamma criterion and 88.1% of pixels passed.

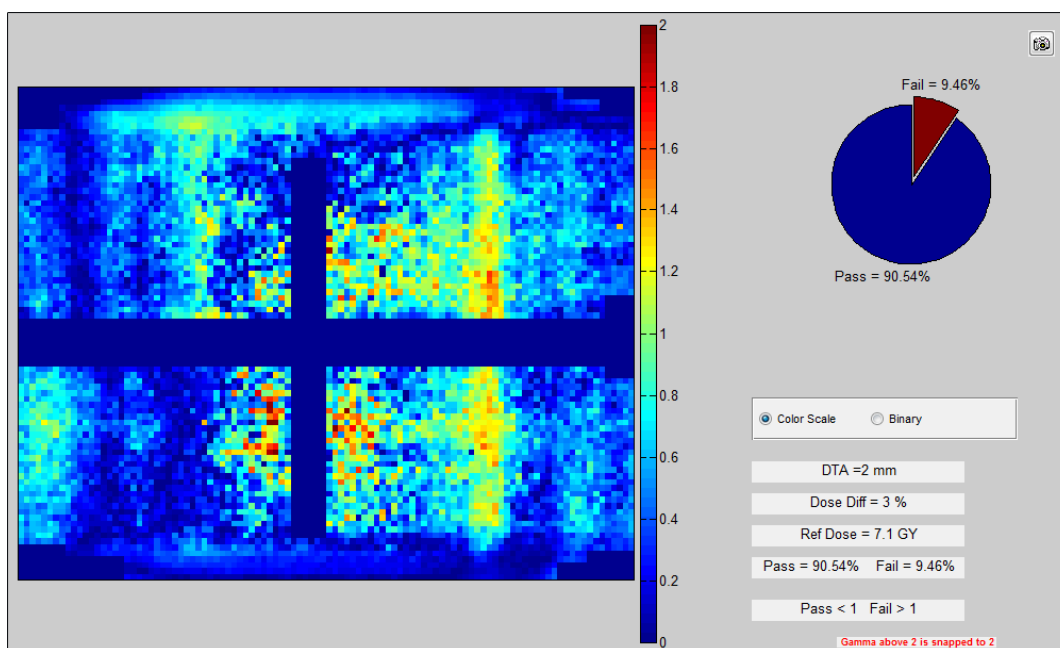


Figure 7.49: Lung SBRT delivery comparison for the sagittal plane of delivery #3 for the Elekta 10MV model. Agreement was evaluated using a $\pm 3\%/2\text{mm}$ gamma criterion and 85.2% of pixels passed.

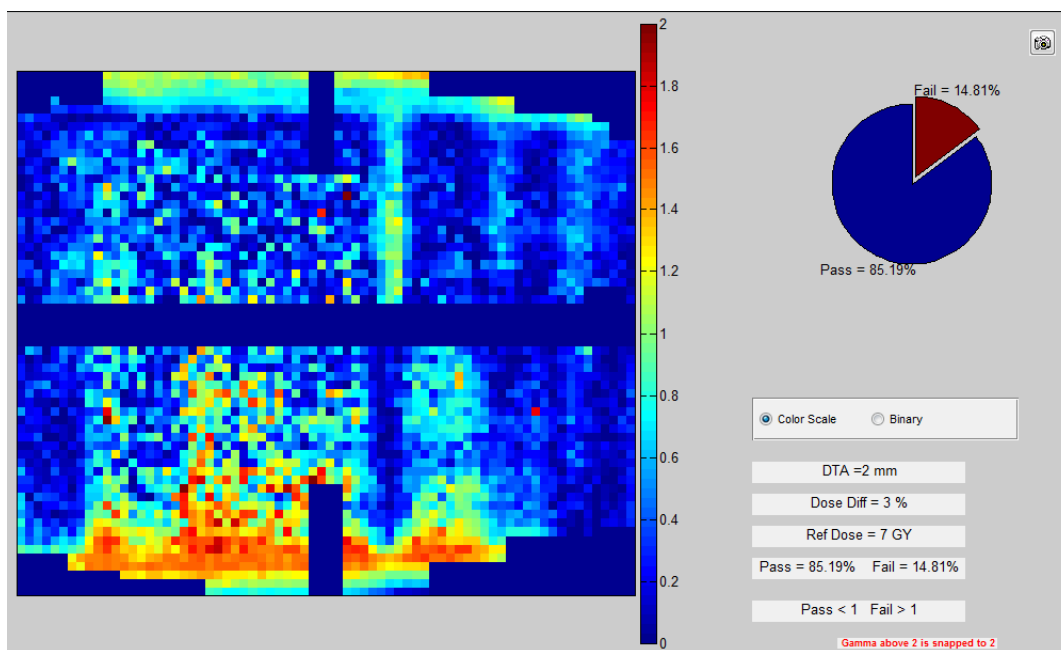


Figure 7.50: Lung SBRT delivery comparison for the coronal plane of delivery #3 for the Elekta 10MV model. Agreement was evaluated using a $\pm 3\%/2\text{mm}$ gamma criterion and 90.5% of pixels passed.

7.4.3 Elekta 10 MV: Delivery of IMRT Lung Plan

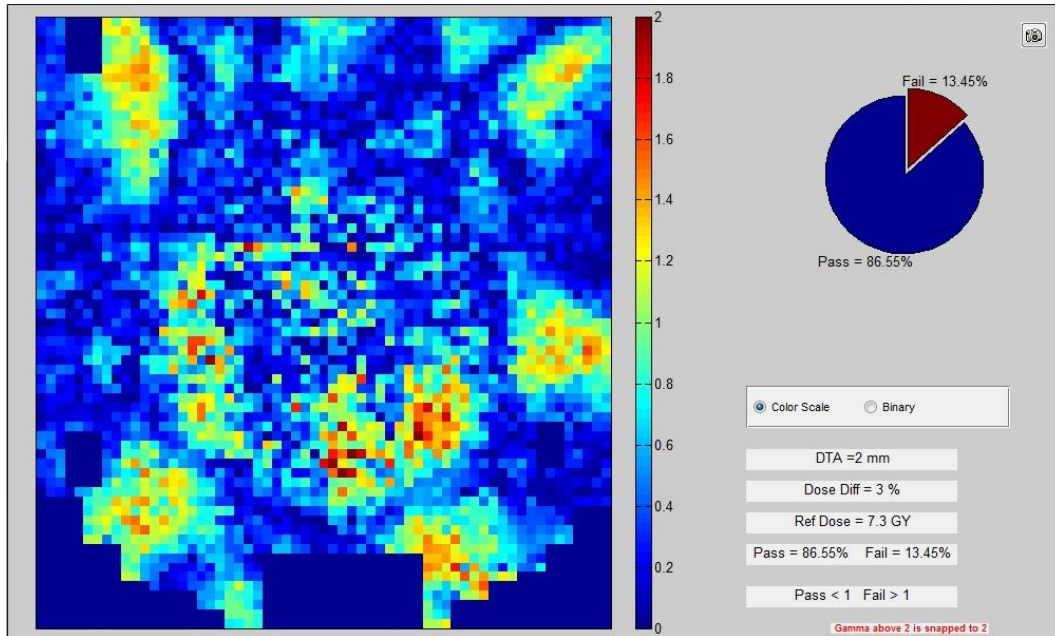


Figure 7.51: Lung IMRT delivery comparison for the axial plane of delivery #2 for the Elekta 10MV model. Agreement was evaluated using a $\pm 3\%/2\text{mm}$ gamma criterion and 85.8% of pixels passed.

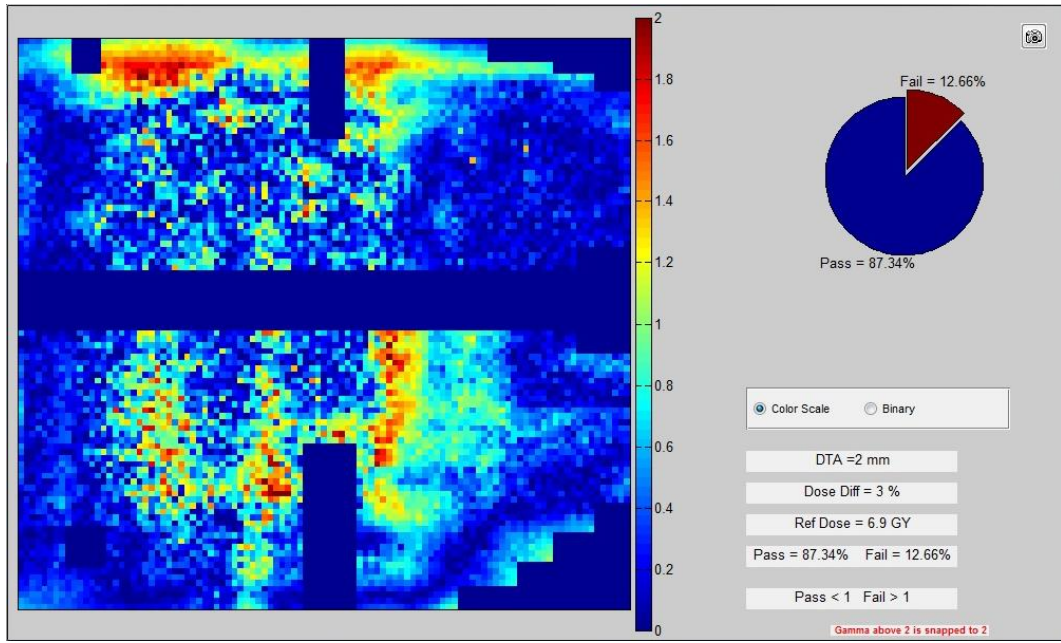


Figure 7.52: Lung IMRT delivery comparison for the sagittal plane of delivery #2 for the Elekta 10MV model. Agreement was evaluated using a $\pm 3\%/2\text{mm}$ gamma criterion and 87.3% of pixels passed.

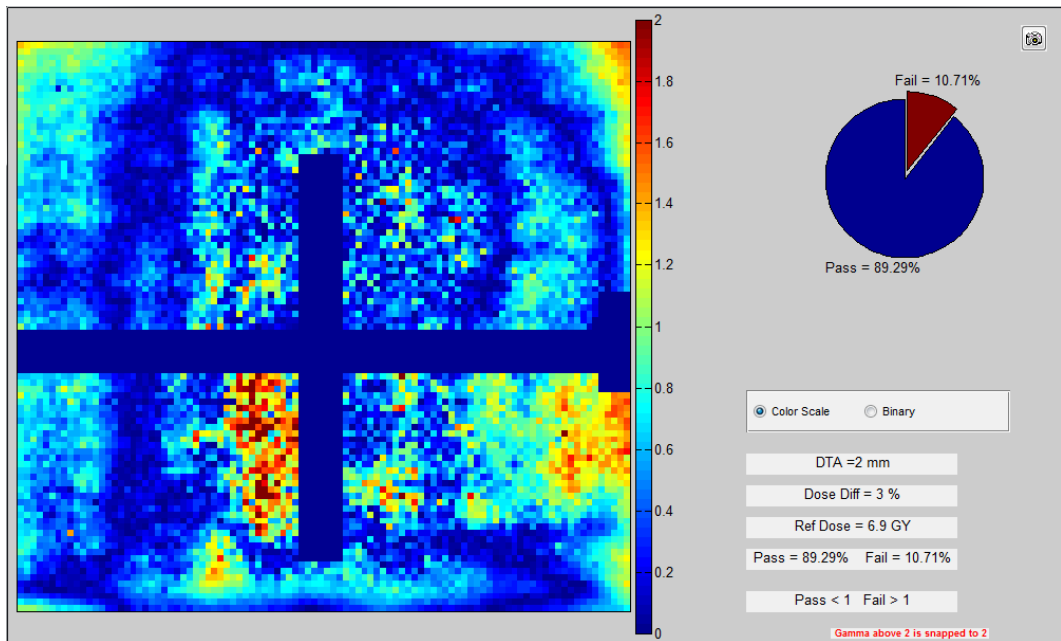


Figure 7.53: Lung IMRT delivery comparison for the coronal plane of delivery #2 for the Elekta 10MV model. Agreement was evaluated using a $\pm 3\%/2\text{mm}$ gamma criterion and 89.3% of pixels passed.

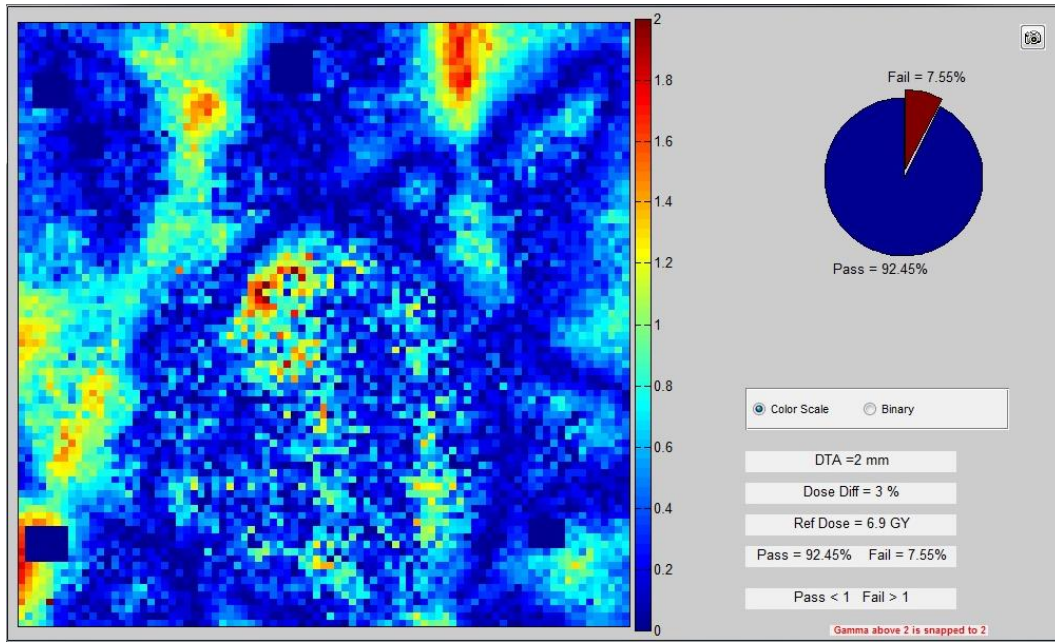


Figure 7.54: Lung IMRT delivery comparison for the axial plane of delivery #3 for the Elekta 10MV model. Agreement was evaluated using a $\pm 3\%/2\text{mm}$ gamma criterion and 92.5% of pixels passed.

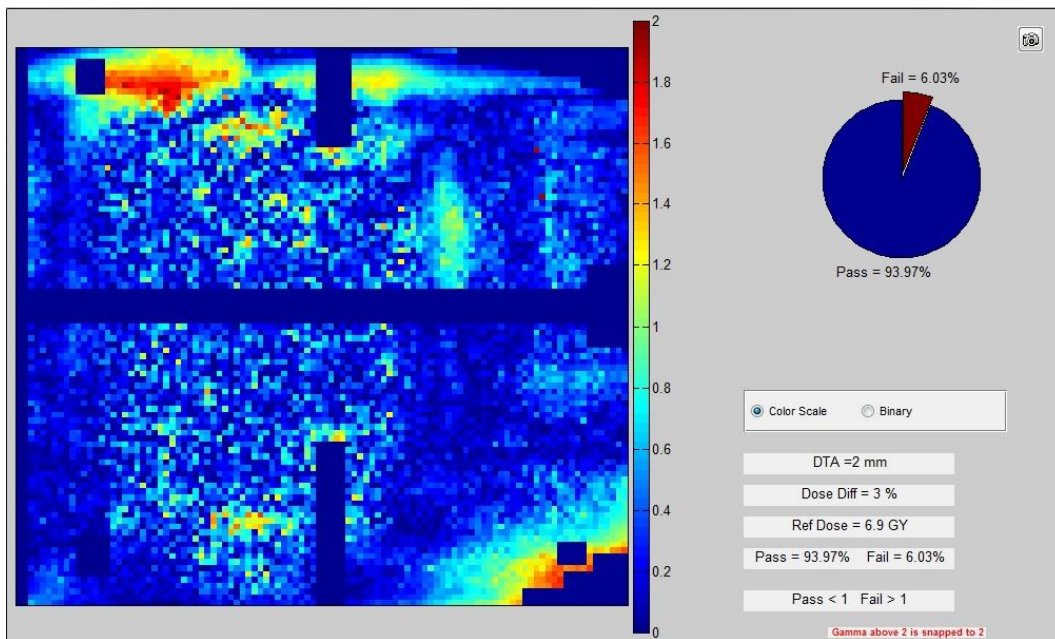


Figure 7.55: Lung IMRT delivery comparison for the sagittal plane of delivery #3 for the Elekta 10MV model. Agreement was evaluated using a $\pm 3\%/2\text{mm}$ gamma criterion and 94.0% of pixels passed.

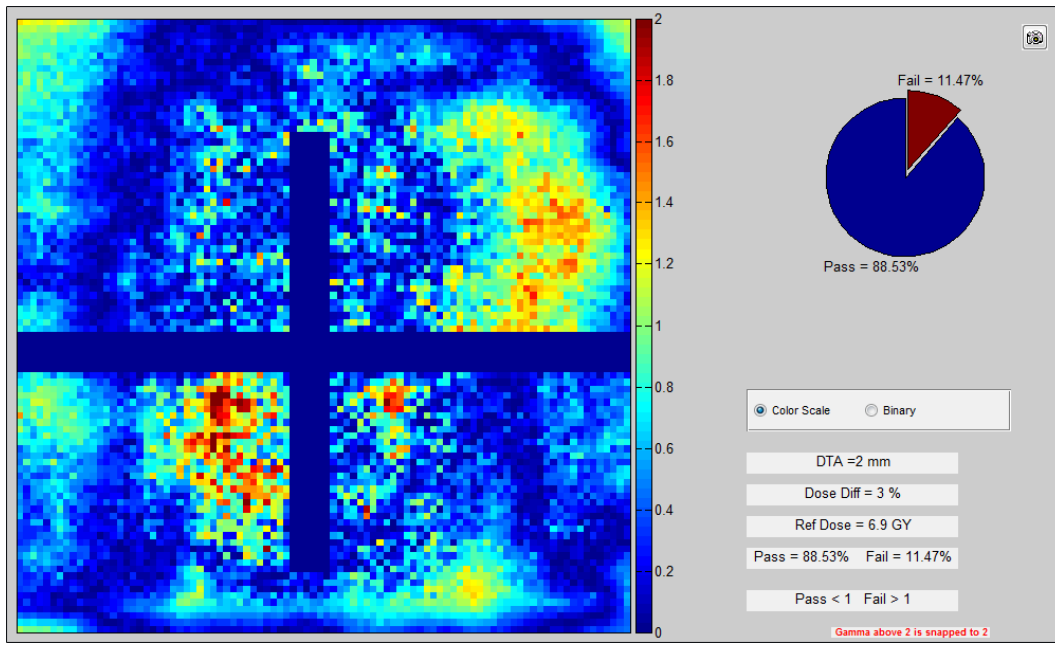


Figure 7.56: Lung IMRT delivery comparison for the coronal plane of delivery #3 for the Elekta 10MV model. Agreement was evaluated using a $\pm 3\%/2\text{mm}$ gamma criterion and 88.5% of pixels passed.

7.5 Varian TrueBeam 6 MV: Percent Depth Dose and Dose Profiles

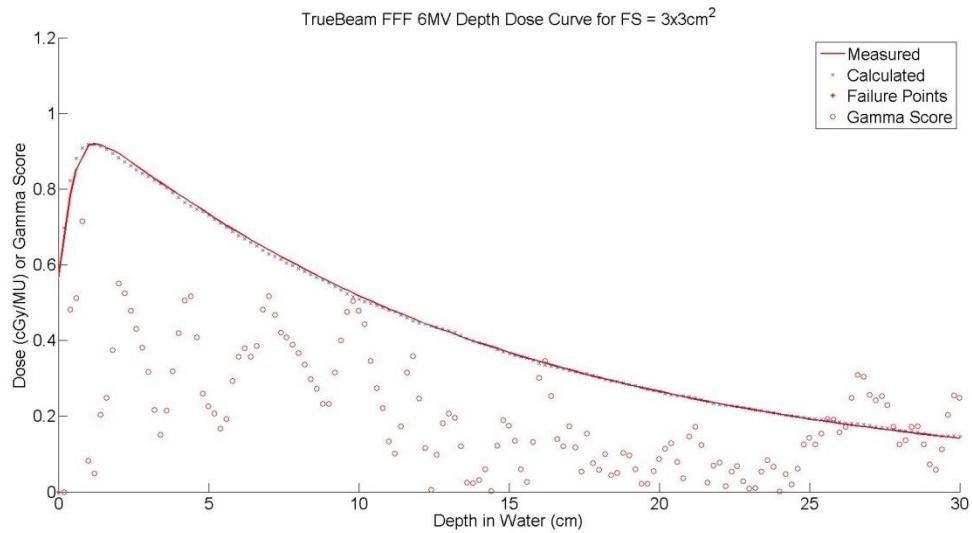


Figure 7.57: Calculated (blue 'x') and measured (red line) percent depth dose curves for a TrueBeam FFF 6MV beam at a field size of 3 x 3 cm². Gamma agreement (red circles) for each point is also displayed along with any points (red star) at which a failure to meet the $\pm 2\%/2\text{mm}$ criterion. At this field size 100.0% of all data passed the gamma criterion.

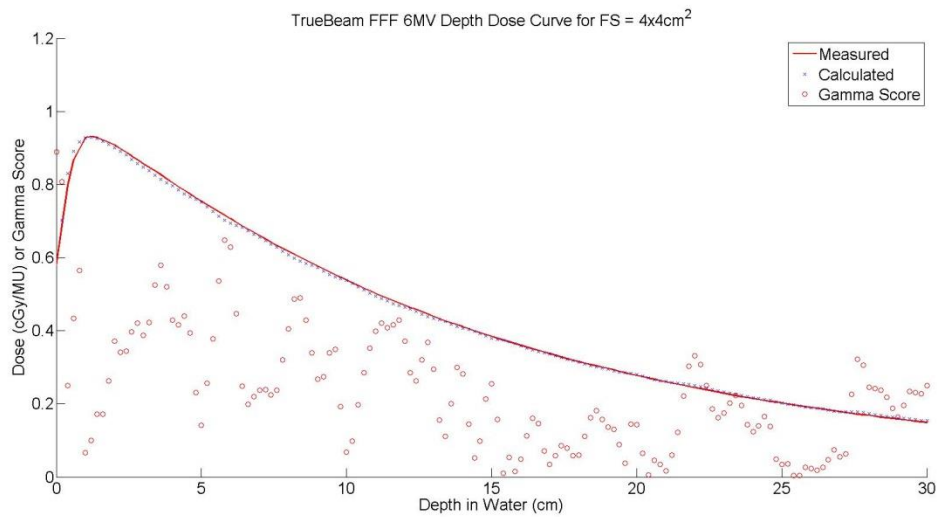


Figure 7.58: Calculated (blue 'x') and measured (red line) percent depth dose curves for a TrueBeam FFF 6MV beam at a field size of 4 x 4 cm². Gamma agreement (red circles) for each point is also displayed along with any points (red star) at which a failure to meet the $\pm 2\%/2\text{mm}$ criterion. At this field size 100.0% of all data passed the gamma criterion.

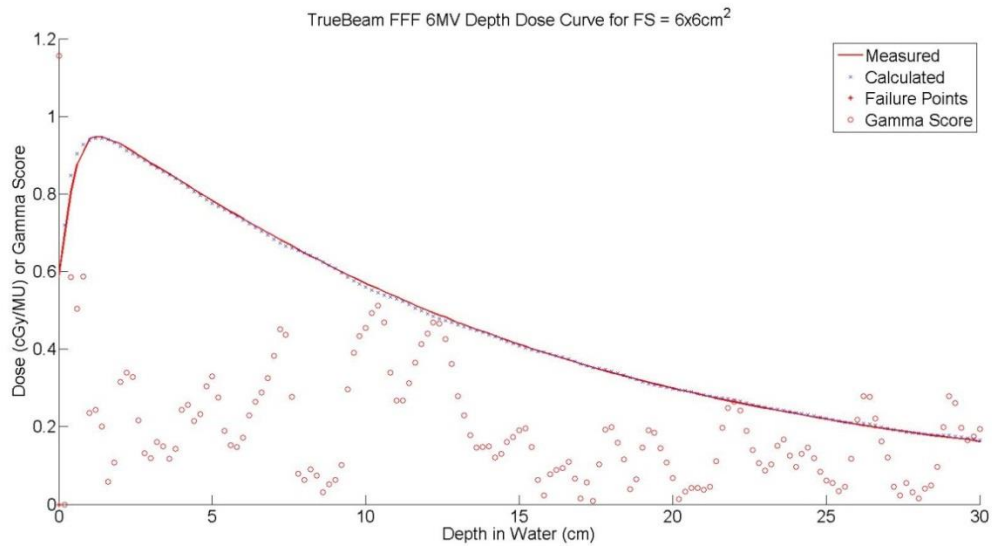


Figure 7.59: Calculated (blue 'x') and measured (red line) percent depth dose curves for a TrueBeam FFF 6MV beam at a field size of 6 x 6 cm². Gamma agreement (red circles) for each point is also displayed along with any points (red star) at which a failure to meet the $\pm 2\%/2\text{mm}$ criterion. At this field size 99.33% of all data passed the gamma criterion.

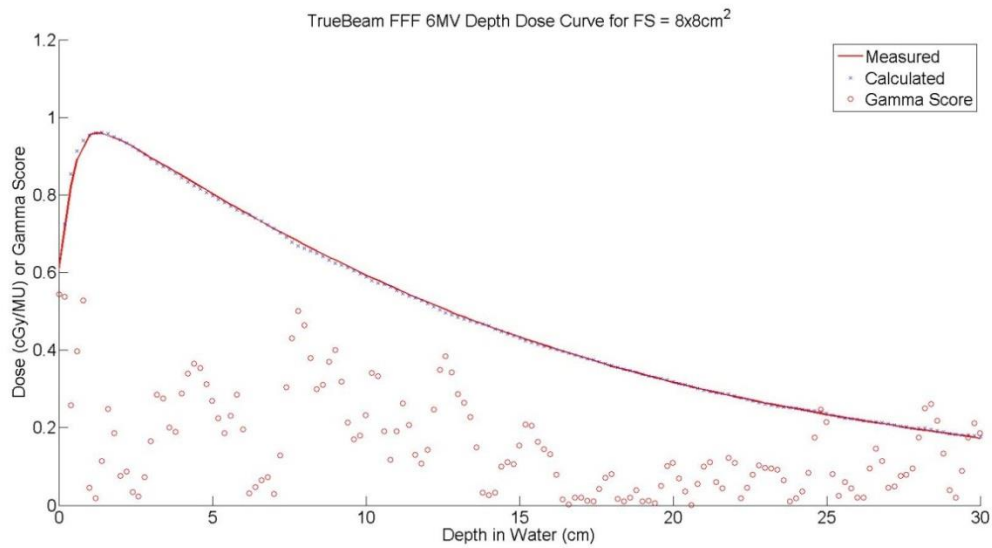


Figure 7.60: Calculated (blue 'x') and measured (red line) percent depth dose curves for a TrueBeam FFF 6MV beam at a field size of 8 x 8 cm². Gamma agreement (red circles) for each point is also displayed along with any points (red star) at which a failure to meet the $\pm 2\%/2\text{mm}$ criterion. At this field size 100.0% of all data passed the gamma criterion.

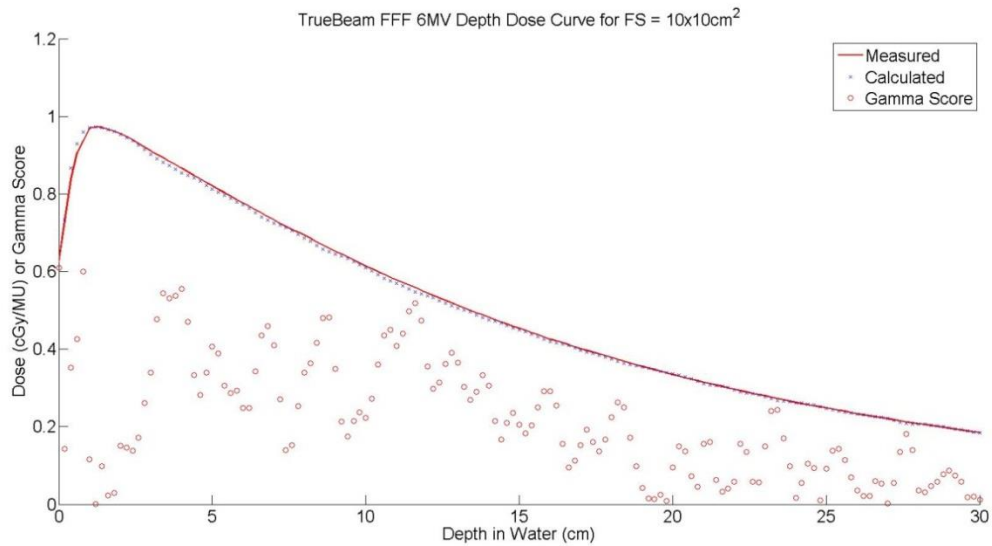


Figure 7.61: Calculated (blue 'x') and measured (red line) percent depth dose curves for a TrueBeam FFF 6MV beam at a field size of 10 x 10 cm². Gamma agreement (red circles) for each point is also displayed along with any points (red star) at which a failure to meet the $\pm 2\%/2\text{mm}$ criterion. At this field size 100.0% of all data passed the gamma criterion.

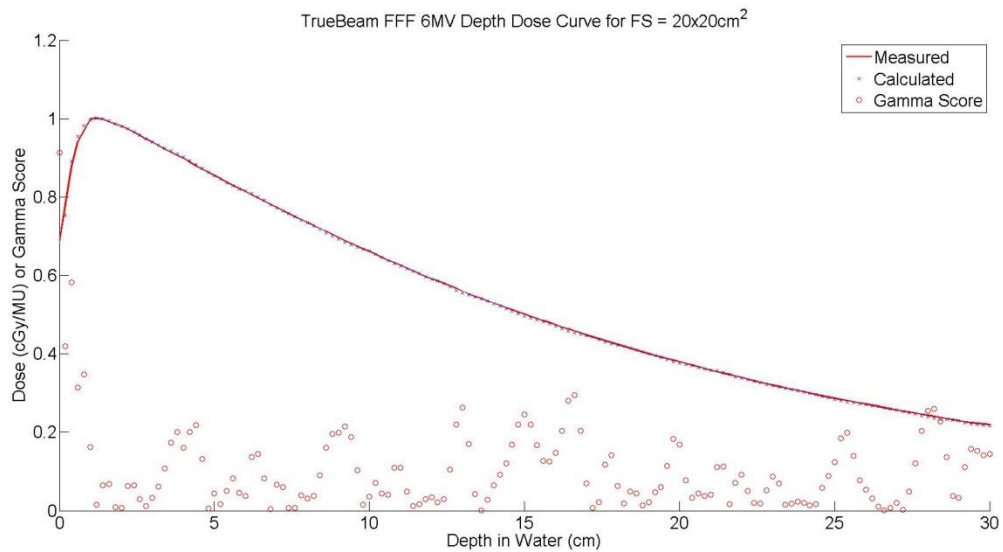


Figure 7.62: Calculated (blue 'x') and measured (red line) percent depth dose curves for a TrueBeam FFF 6MV beam at a field size of 20 x 20 cm². Gamma agreement (red circles) for each point is also displayed along with any points (red star) at which a failure to meet the $\pm 2\%/2\text{mm}$ criterion. At this field size 100.0% of all data passed the gamma criterion.

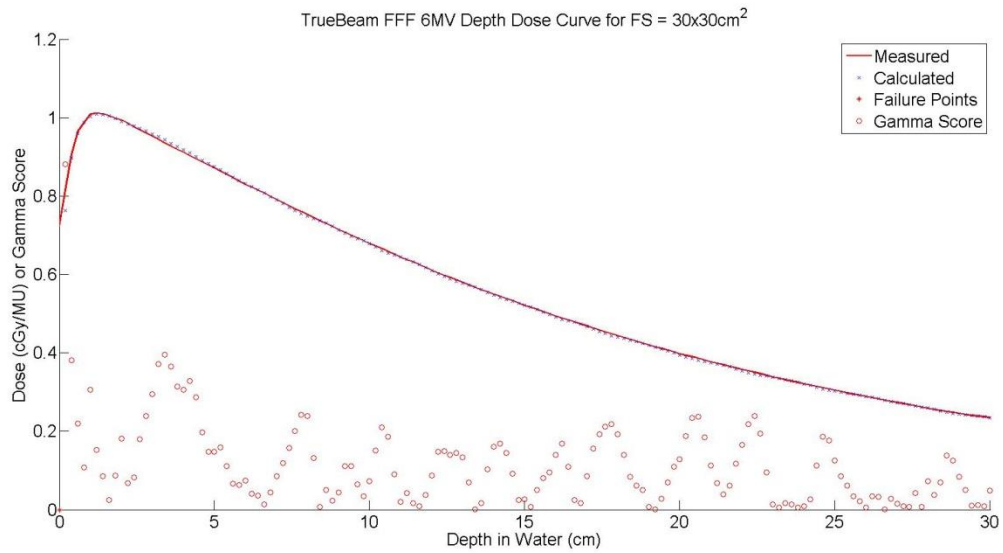


Figure 7.63: Calculated (blue 'x') and measured (red line) percent depth dose curves for a TrueBeam FFF 6MV beam at a field size of 30 x 30 cm². Gamma agreement (red circles) for each point is also displayed along with any points (red star) at which a failure to meet the $\pm 2\%/2\text{mm}$ criterion. At this field size 100.0% of all data passed the gamma criterion.

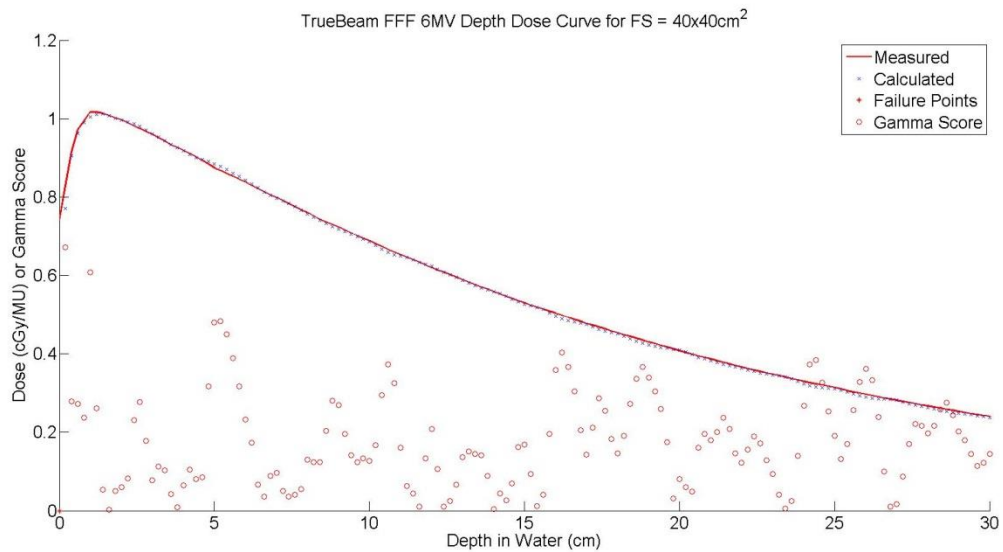


Figure 7.64: Calculated (blue 'x') and measured (red line) percent depth dose curves for a TrueBeam FFF 6MV beam at a field size of 40 x 40 cm². Gamma agreement (red circles) for each point is also displayed along with any points (red star) at which a failure to meet the $\pm 2\%/2\text{mm}$ criterion. At this field size 100.0% of all data passed the gamma criterion.

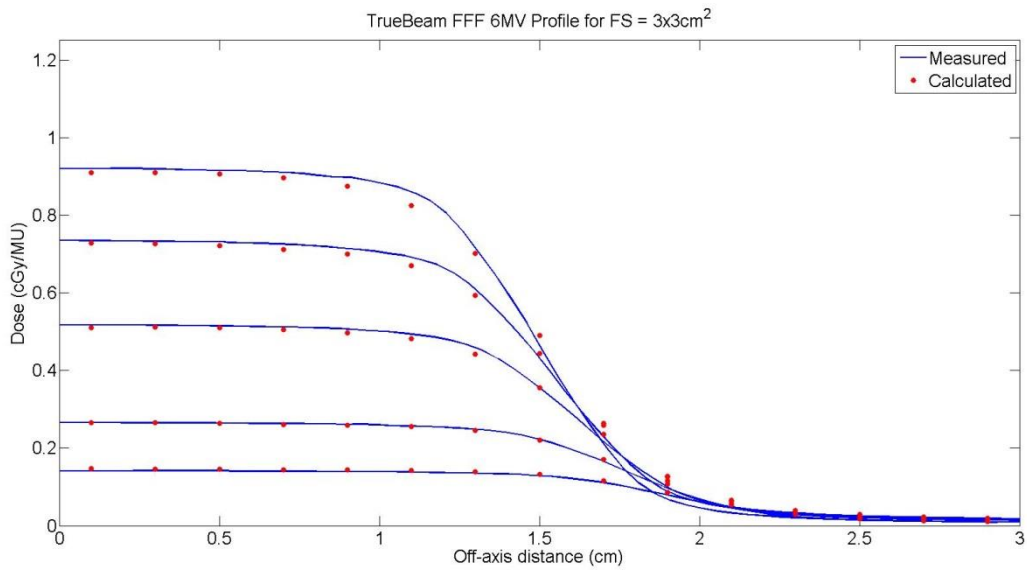


Figure 7.65: Calculated (red circle) and measured (blue line) dose profiles for a TrueBeam 6MV beam at a field size of 3 x 3 cm².

Field Size (cm ²)	Direction	Depth (cm)	% Passing (2%/2mm)
3 x 3	x	1.5	98.45
	x	5	98.45
	x	10	100.00
	x	20	100.00
	x	30	100.00

Table 7.13: Dose profile agreement between the TrueBeam FFF 6MV multiple source model and measurement using a $\pm 2\%/2\text{mm}$ global gamma criterion at all depths of comparison for a 3 x 3 cm² field size.

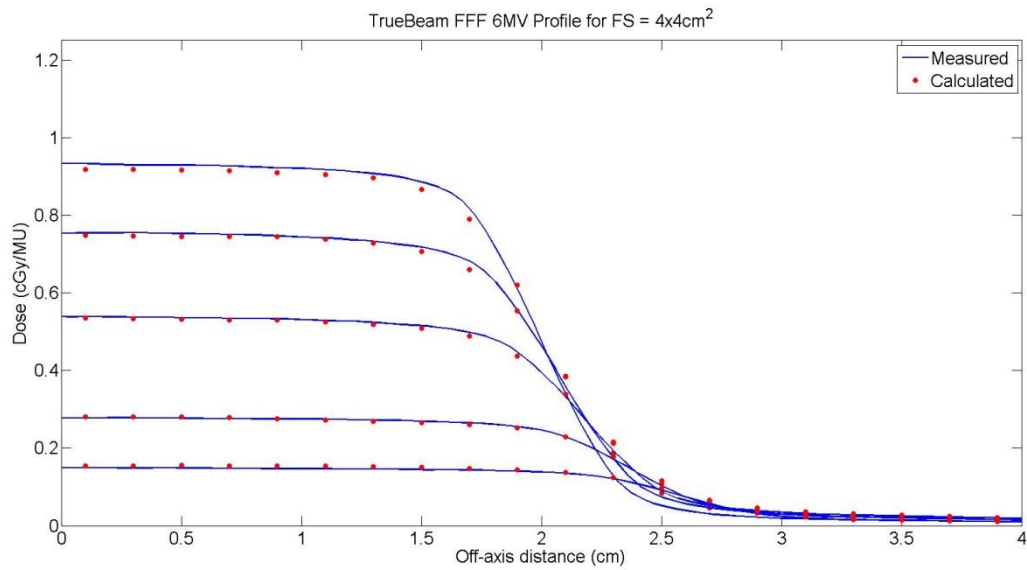


Figure 7.66: Calculated (red circle) and measured (blue line) dose profiles for a TrueBeam 6MV beam at a field size of 4 x 4 cm².

Field Size (cm ²)	Direction	Depth (cm)	% Passing (2%/2mm)
4 x 4	x	1.5	96.45
	x	5	98.58
	x	10	100.00
	x	20	100.00
	x	30	100.00

Table 7.14: Dose profile agreement between the TrueBeam FFF 6MV multiple source model and measurement using a $\pm 2\%/2\text{mm}$ global gamma criterion at all depths of comparison for a 4 x 4 cm² field size.

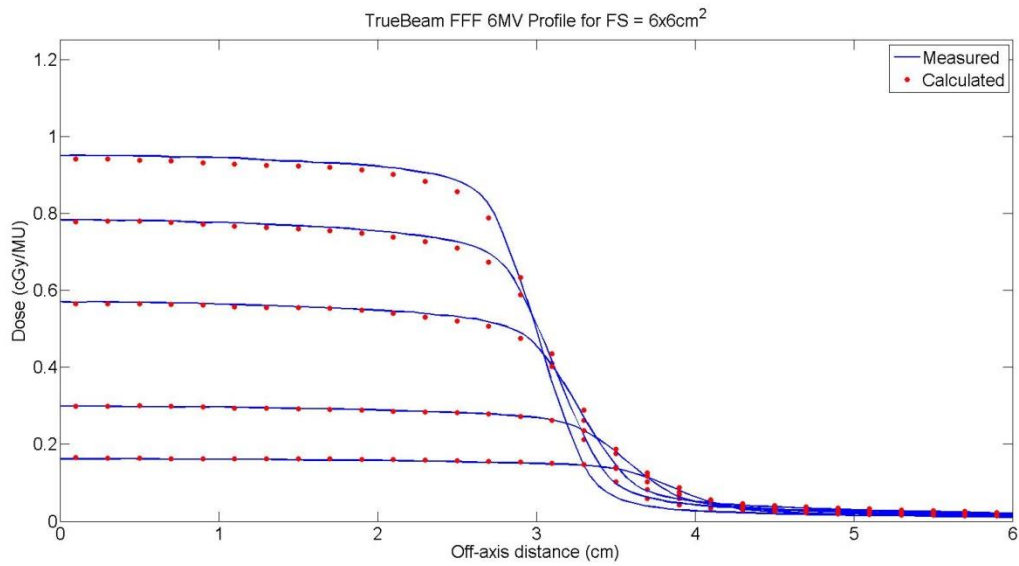


Figure 7.67: Calculated (red circle) and measured (blue line) dose profiles for a TrueBeam 6MV beam at a field size of 6 x 6 cm².

Field Size (cm ²)	Direction	Depth (cm)	% Passing (2%/2mm)
6 x 6	x	1.5	98.76
	x	5	99.34
	x	10	100.00
	x	20	100.00
	x	30	100.00

Table 7.15: Dose profile agreement between the TrueBeam FFF 6MV multiple source model and measurement using a $\pm 2\%/2\text{mm}$ global gamma criterion at all depths of comparison for a 6 x 6 cm² field size.

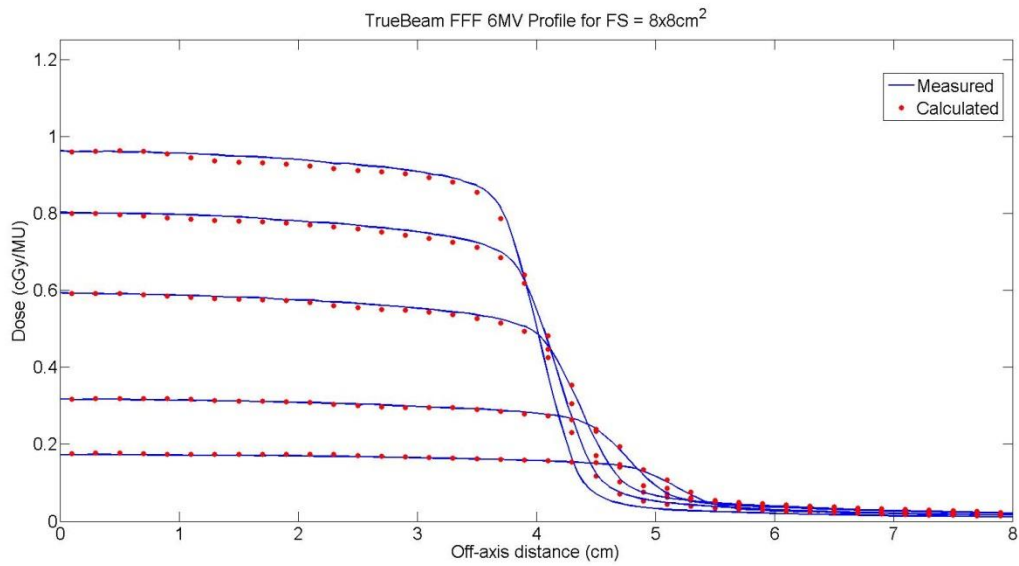


Figure 7.68: Calculated (red circle) and measured (blue line) dose profiles for a TrueBeam 6MV beam at a field size of 8 x 8 cm².

Field Size (cm ²)	Direction	Depth (cm)	% Passing (2%/2mm)
8 x 8	x	1.5	96.13
	x	5	100.00
	x	10	100.00
	x	20	100.00
	x	30	100.00

Table 7.16: Dose profile agreement between the TrueBeam FFF 6MV multiple source model and measurement using a $\pm 2\%/2\text{mm}$ global gamma criterion at all depths of comparison for a 8 x 8 cm² field size.

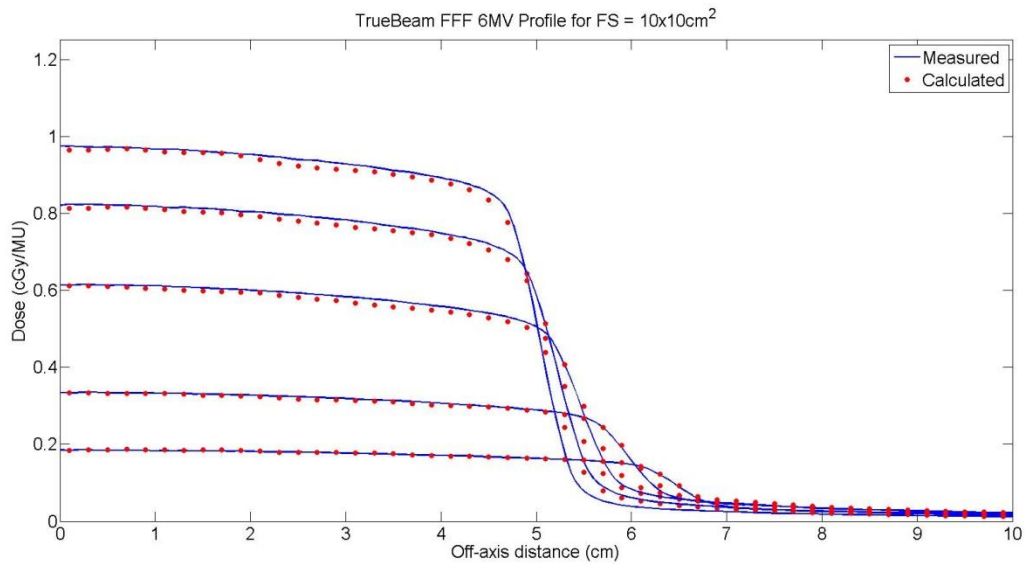


Figure 7.69: Calculated (red circle) and measured (blue line) dose profiles for a TrueBeam 6MV beam at a field size of 10 x 10 cm².

Field Size (cm ²)	Direction	Depth (cm)	% Passing (2%/2mm)
10 x 10	x	1.5	93.97
	x	5	99.50
	x	10	100.00
	x	20	100.00
	x	30	100.00

Table 7.17: Dose profile agreement between the TrueBeam FFF 6MV multiple source model and measurement using a $\pm 2\%/2\text{mm}$ global gamma criterion at all depths of comparison for a 10 x 10 cm² field size.

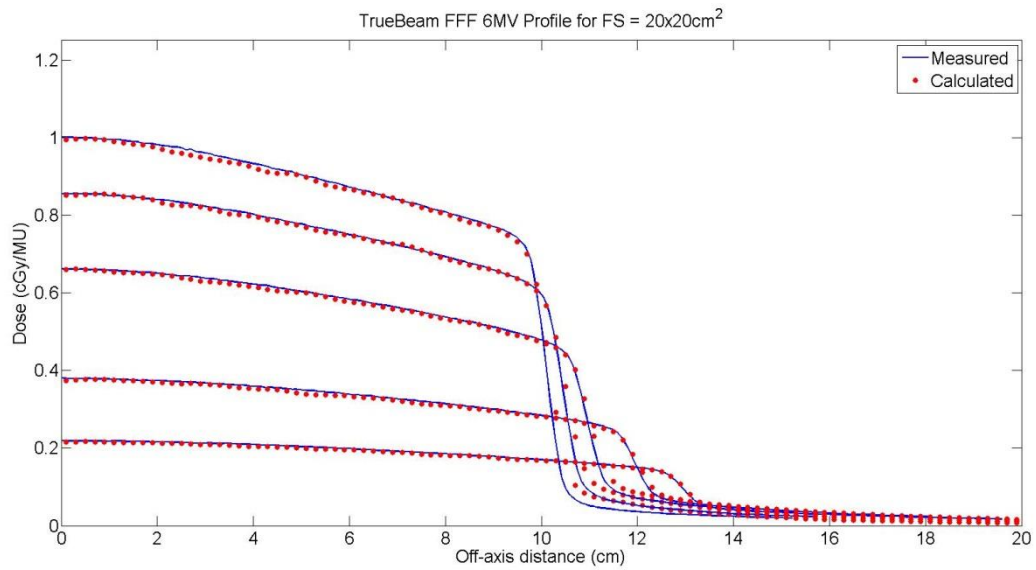


Figure 7.70: Calculated (red circle) and measured (blue line) dose profiles for a TrueBeam 6MV beam at a field size of 20 x 20 cm².

Field Size (cm ²)	Direction	Depth (cm)	% Passing (2%/2mm)
20 x 20	x	1.5	88.04
	x	5	89.04
	x	10	100.00
	x	20	100.00
	x	30	100.00

Table 7.18: Dose profile agreement between the TrueBeam FFF 6MV multiple source model and measurement using a $\pm 2\%/2\text{mm}$ global gamma criterion at all depths of comparison for a 20 x 20 cm² field size.

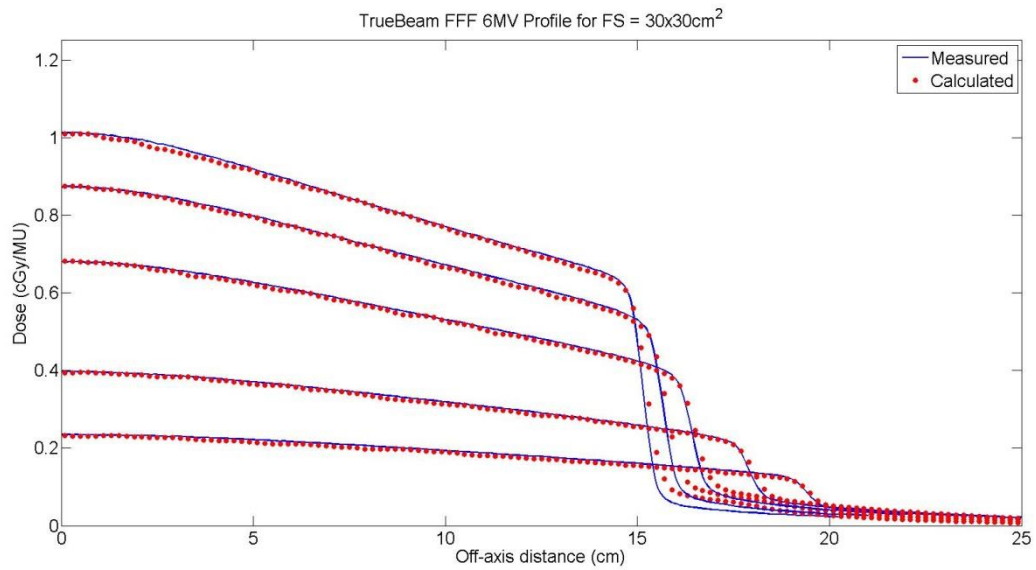


Figure 7.71: Calculated (red circle) and measured (blue line) dose profiles for a TrueBeam 6MV beam at a field size of 30 x 30 cm².

Field Size (cm ²)	Direction	Depth (cm)	% Passing (2%/2mm)
30 x 30	x	1.5	88.04
	x	5	89.04
	x	10	100.00
	x	20	100.00
	x	30	100.00

Table 7.19: Dose profile agreement between the TrueBeam FFF 6MV multiple source model and measurement using a $\pm 2\%/2\text{mm}$ global gamma criterion at all depths of comparison for a 30 x 30 cm² field size.

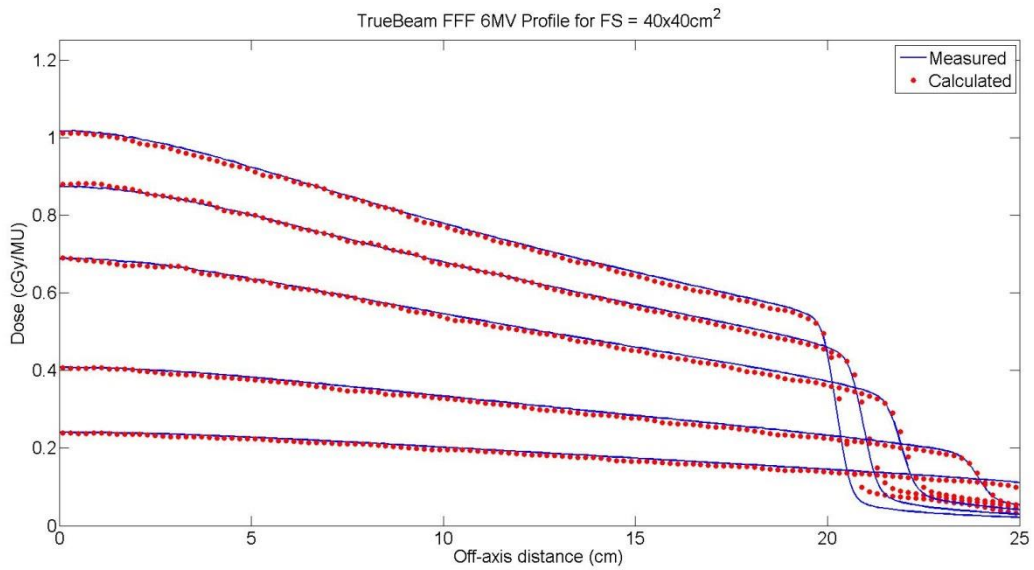


Figure 7.72: Calculated (red circle) and measured (blue line) dose profiles for a TrueBeam 6MV beam at a field size of 40 x 40 cm².

Field Size (cm ²)	Direction	Depth (cm)	% Passing (2%/2mm)
40 x 40	x	1.5	89.91
	x	5	90.50
	x	10	100.00
	x	20	100.00
	x	30	100.00

Table 7.20: Dose profile agreement between the TrueBeam FFF 6MV multiple source model and measurement using a $\pm 2\%/2\text{mm}$ global gamma criterion at all depths of comparison for a 40 x 40 cm² field size.

7.6 Varian TrueBeam 6 MV: Gamma Maps

7.6.1 Varian TrueBeam 6 MV: Delivery of IMRT Head and Neck Plan

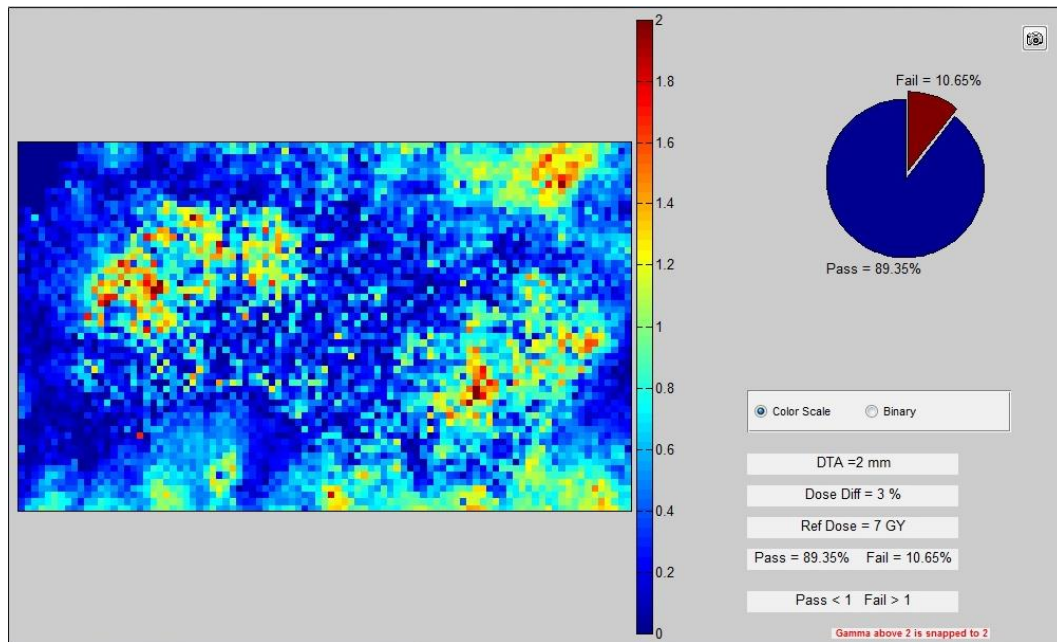


Figure 7.73: IMRT head and neck delivery comparison for the axial plane of delivery #2 for the TrueBeam FFF 6MV model. Agreement was evaluated using a $\pm 3\%/2\text{mm}$ gamma criterion and 89.4% of pixels passed.

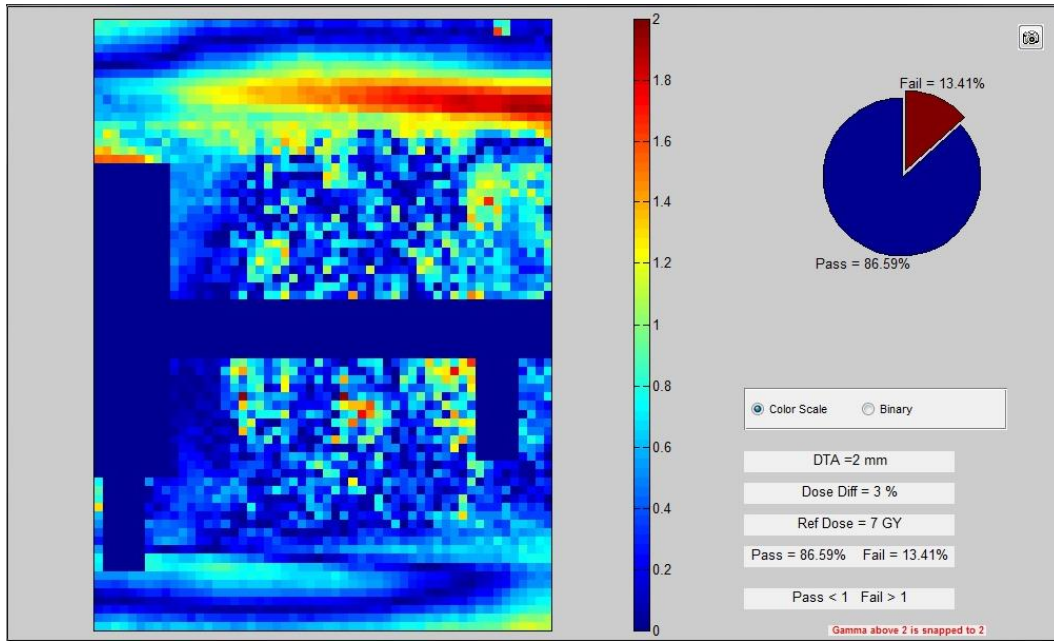


Figure 7.74: IMRT head and neck delivery comparison for the sagittal plane of delivery #2 for the TrueBeam FFF 6MV model. Agreement was evaluated using a $\pm 3\%/2\text{mm}$ gamma criterion and 86.6% of pixels passed.

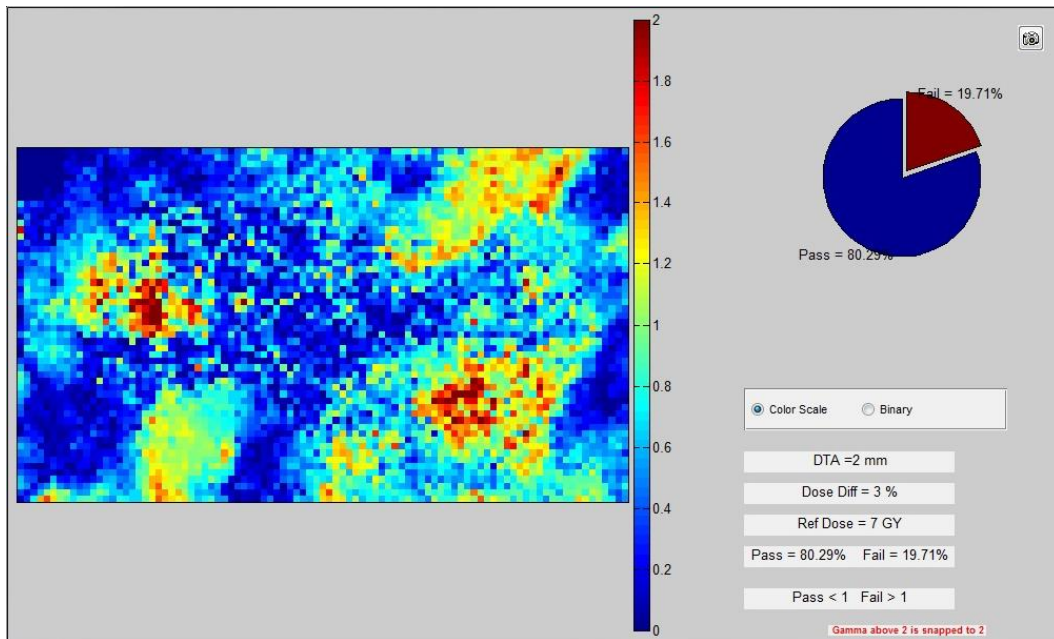


Figure 7.75: IMRT head and neck delivery comparison for the axial plane of delivery #3 for the TrueBeam FFF 6MV model. Agreement was evaluated using a $\pm 3\%/2\text{mm}$ gamma criterion and 80.3% of pixels passed.

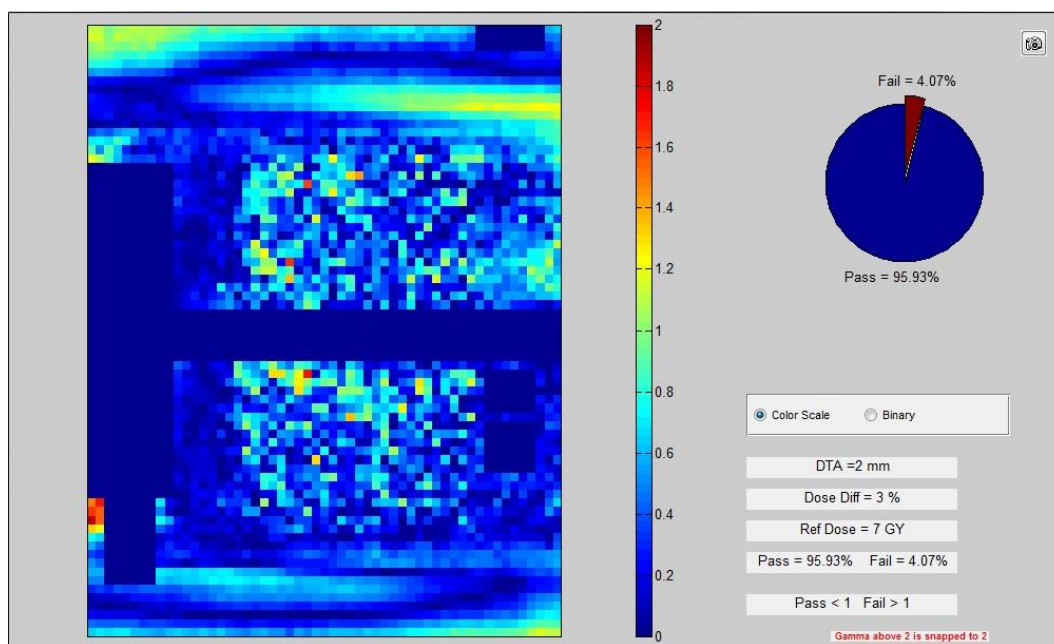


Figure 7.76: IMRT head and neck delivery comparison for the sagittal plane of delivery #3 for the TrueBeam FFF 6MV model. Agreement was evaluated using a $\pm 3\%/2\text{mm}$ gamma criterion and 95.9% of pixels passed.

7.6.2 Varian TrueBeam 6 MV: Delivery of SBRT Lung Plan

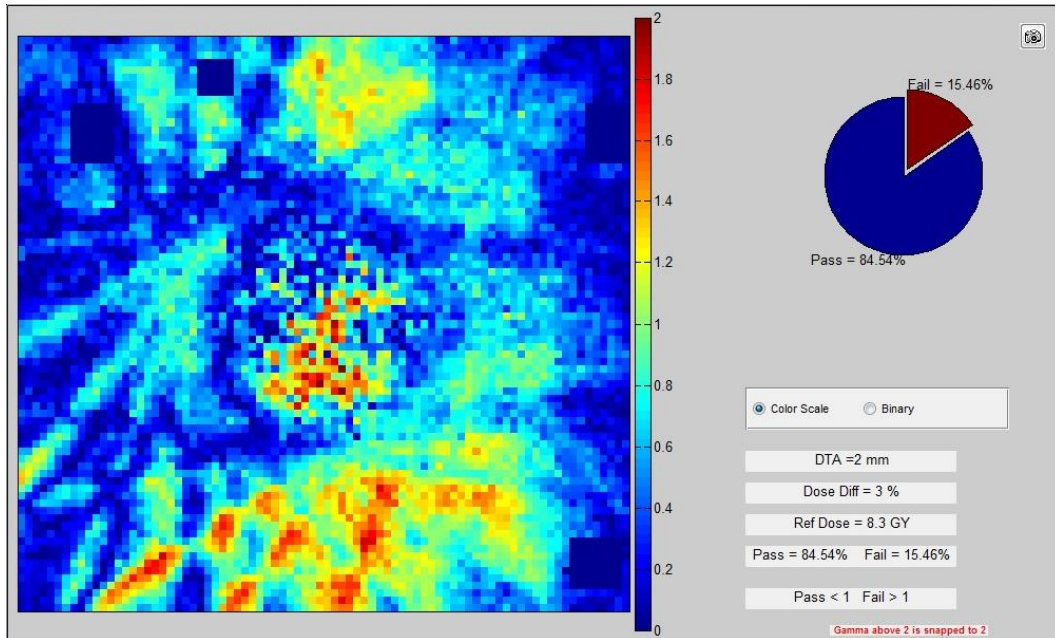


Figure 7.77: Lung SBRT delivery comparison for the axial plane of delivery #2 for the TrueBeam FFF 6MV model. Agreement was evaluated using a $\pm 3\%/2\text{mm}$ gamma criterion and 84.5% of pixels passed.

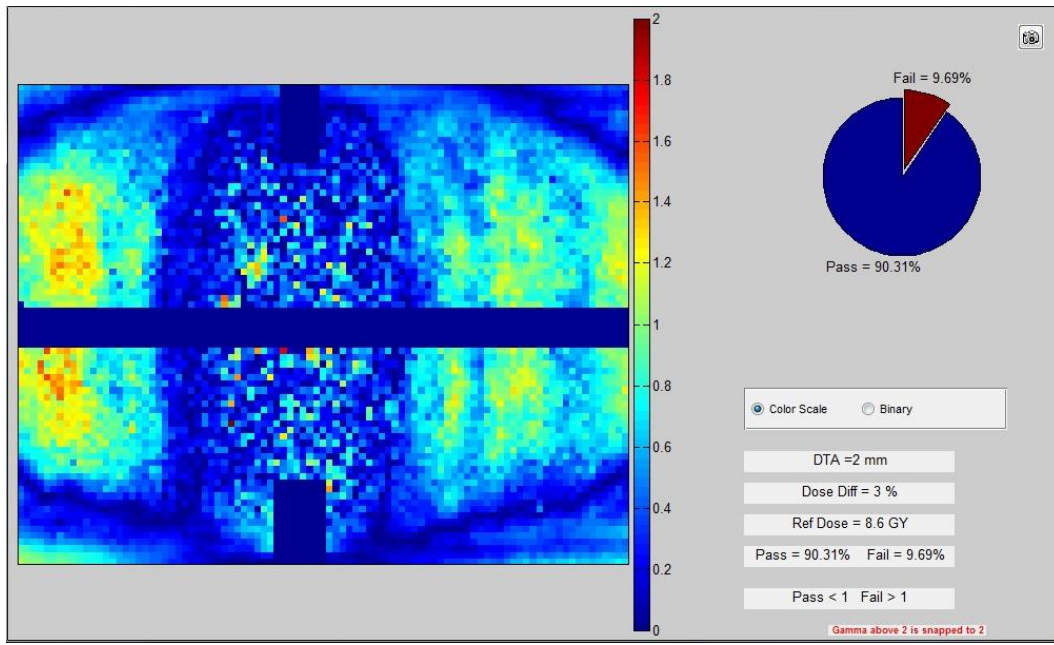


Figure 7.78: Lung SBRT delivery comparison for the sagittal plane of delivery #2 for the TrueBeam FFF 6MV model. Agreement was evaluated using a $\pm 3\%/2\text{mm}$ gamma criterion and 90.3% of pixels passed.

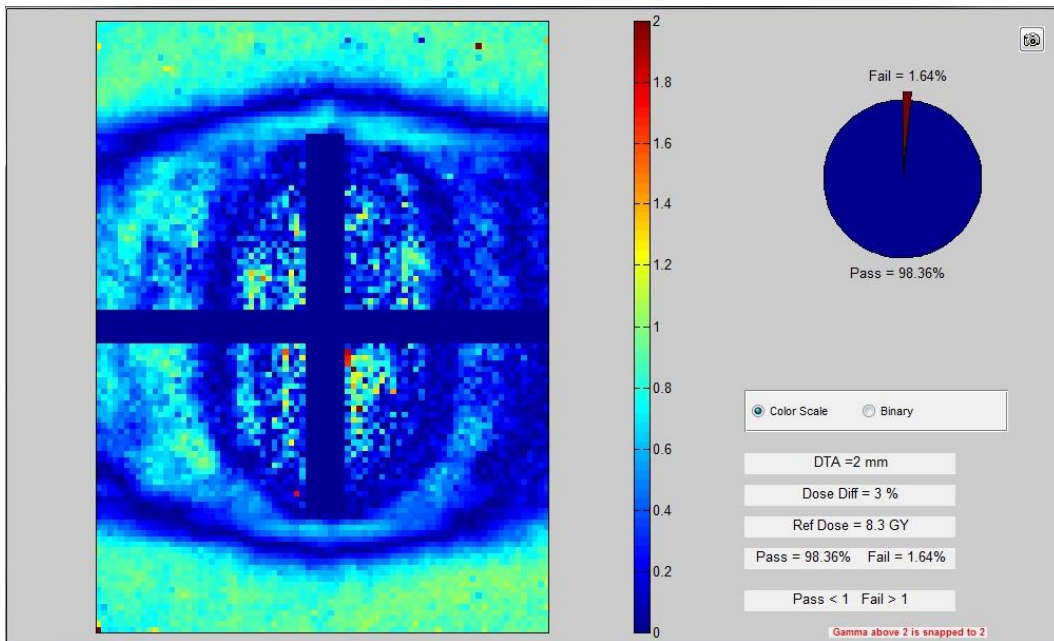


Figure 7.79: Lung SBRT delivery comparison for the coronal plane of delivery #2 for the TrueBeam FFF 6MV model. Agreement was evaluated using a $\pm 3\%/2\text{mm}$ gamma criterion and 98.4% of pixels passed.

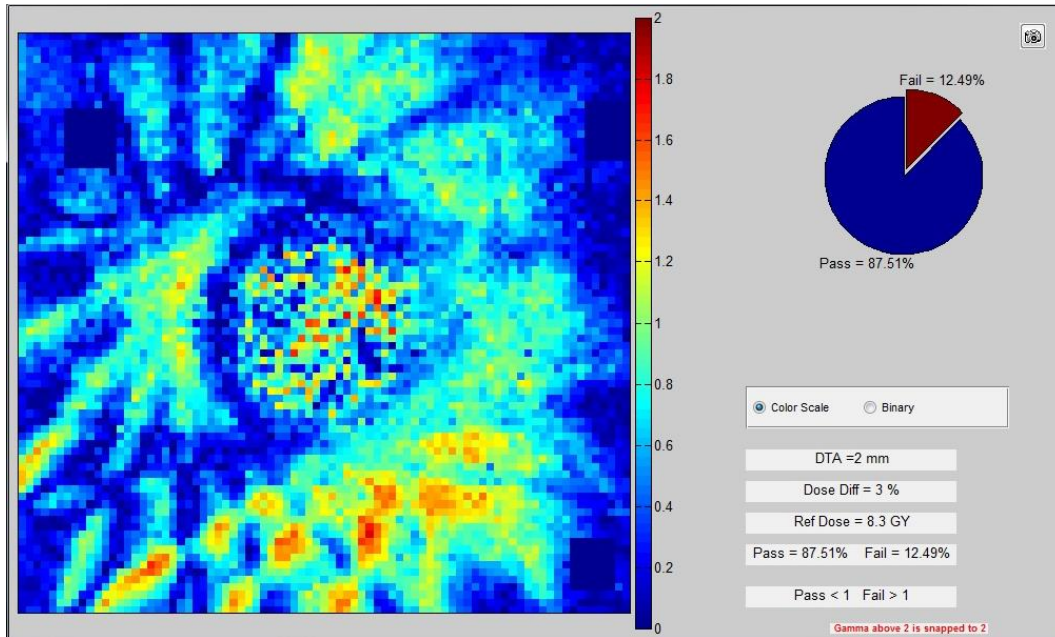


Figure 7.80: Lung SBRT delivery comparison for the axial plane of delivery #3 for the TrueBeam FFF 6MV model. Agreement was evaluated using a $\pm 3\%/2\text{mm}$ gamma criterion and 87.5% of pixels passed.

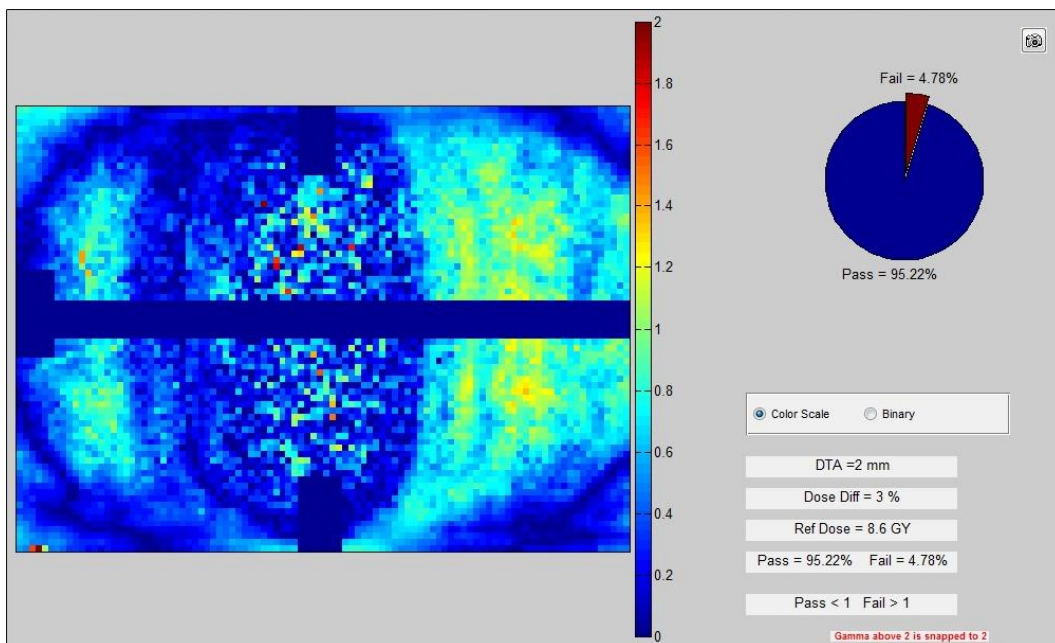


Figure 7.81: Lung SBRT delivery comparison for the sagittal plane of delivery #3 for the TrueBeam FFF 6MV model. Agreement was evaluated using a $\pm 3\%/2\text{mm}$ gamma criterion and 95.2% of pixels passed.

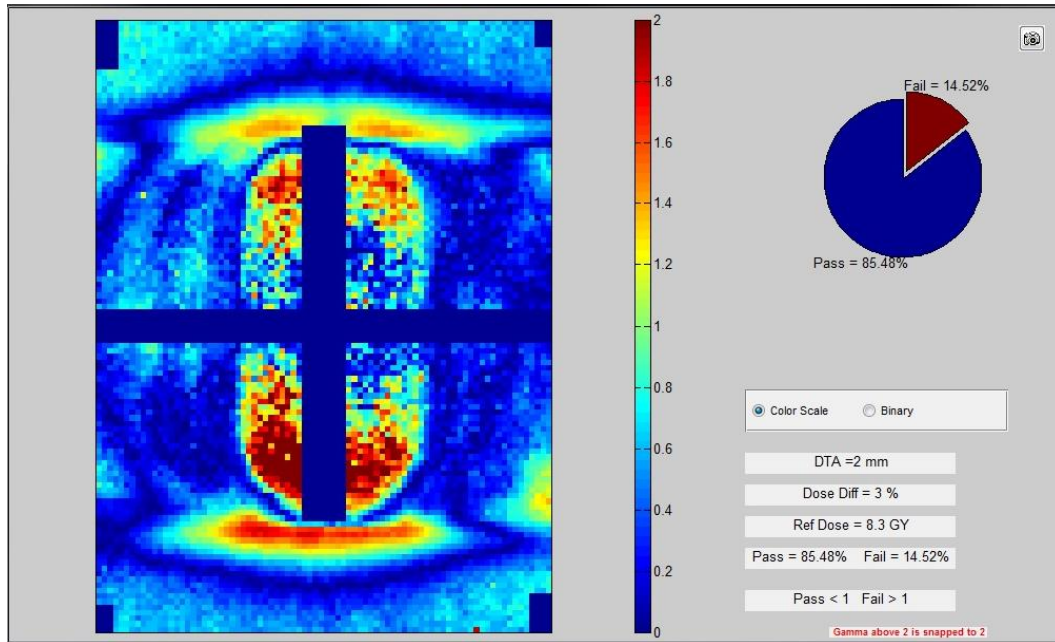


Figure 7.82: Lung SBRT delivery comparison for the coronal plane of delivery #3 for the TrueBeam FFF 6MV model. Agreement was evaluated using a $\pm 3\%/2\text{mm}$ gamma criterion and 85.5% of pixels passed.

7.6.3 Varian TrueBeam 6 MV: Delivery of IMRT Lung Plan

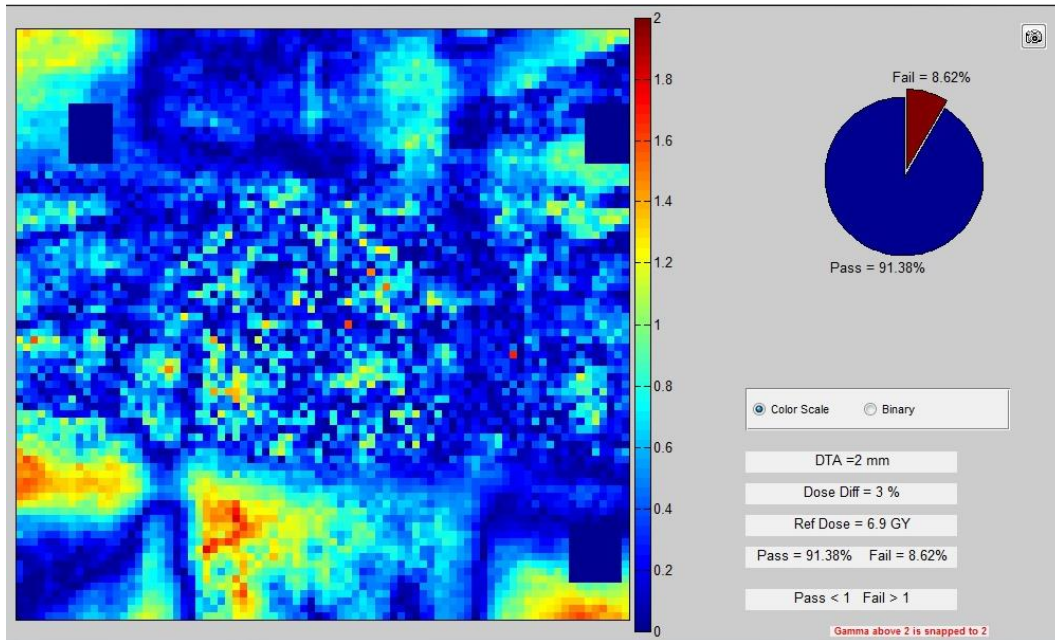


Figure 7.83: Lung IMRT delivery comparison for the axial plane of delivery #2 for the TrueBeam FFF 6MV model. Agreement was evaluated using a $\pm 3\%/2\text{mm}$ gamma criterion and 91.4% of pixels passed.

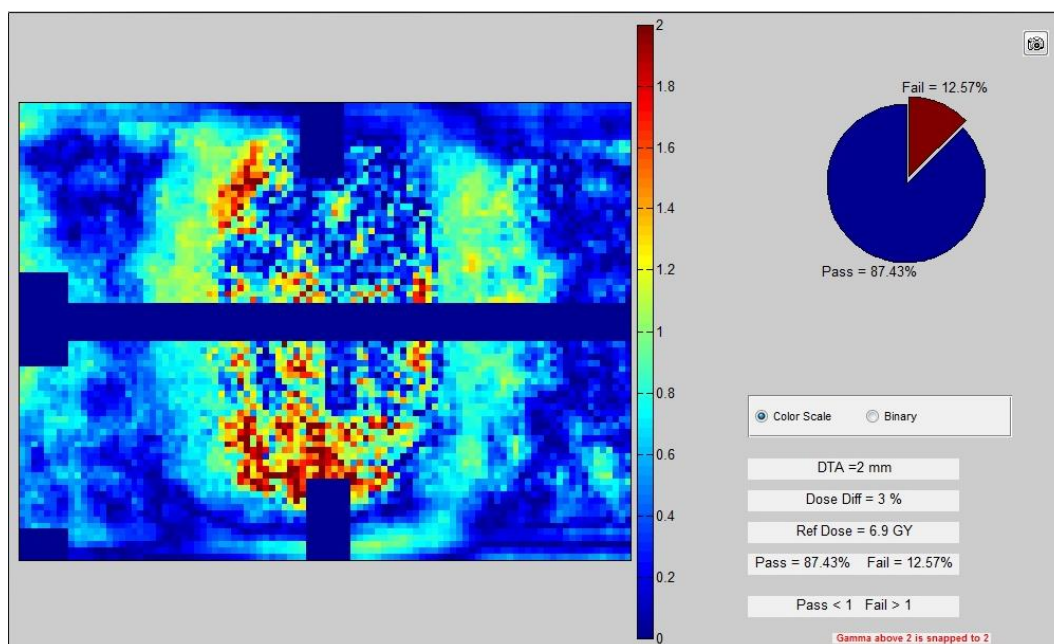


Figure 7.84: Lung IMRT delivery comparison for the sagittal plane of delivery #2 for the TrueBeam FFF 6MV model. Agreement was evaluated using a $\pm 3\%/2\text{mm}$ gamma criterion and 87.4% of pixels passed.

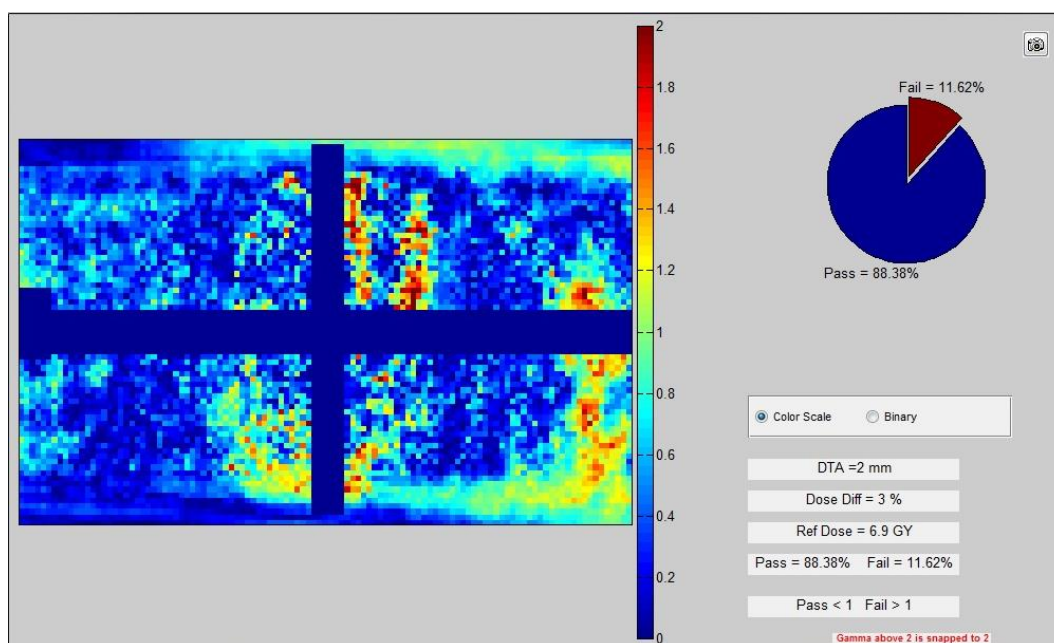


Figure 7.85: Lung IMRT delivery comparison for the coronal plane of delivery #2 for the TrueBeam FFF 6MV model. Agreement was evaluated using a $\pm 3\%/2\text{mm}$ gamma criterion and 88.4% of pixels passed.

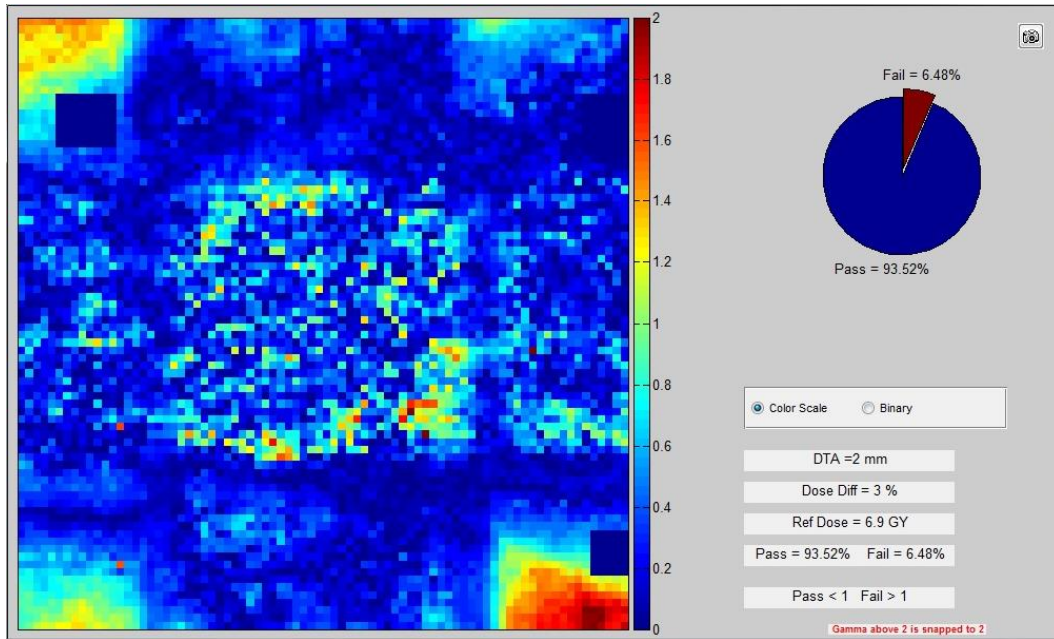


Figure 7.86: Lung IMRT delivery comparison for the axial plane of delivery #3 for the TrueBeam FFF 6MV model. Agreement was evaluated using a $\pm 3\%/2\text{mm}$ gamma criterion and 93.5% of pixels passed.

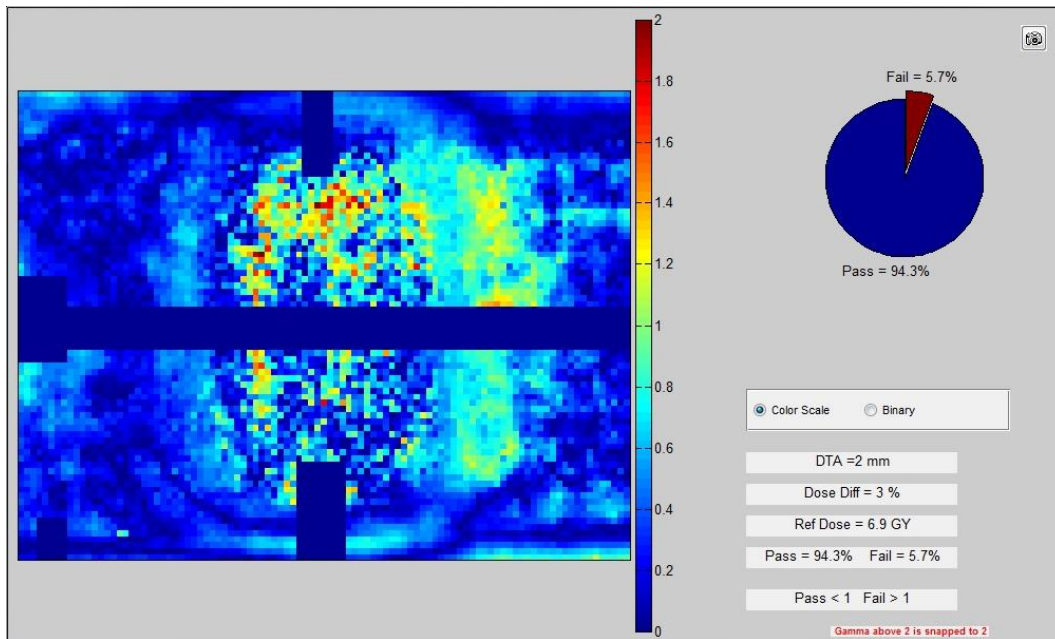


Figure 7.87: Lung IMRT delivery comparison for the sagittal plane of delivery #3 for the TrueBeam FFF 6MV model. Agreement was evaluated using a $\pm 3\%/2\text{mm}$ gamma criterion and 94.3% of pixels passed.

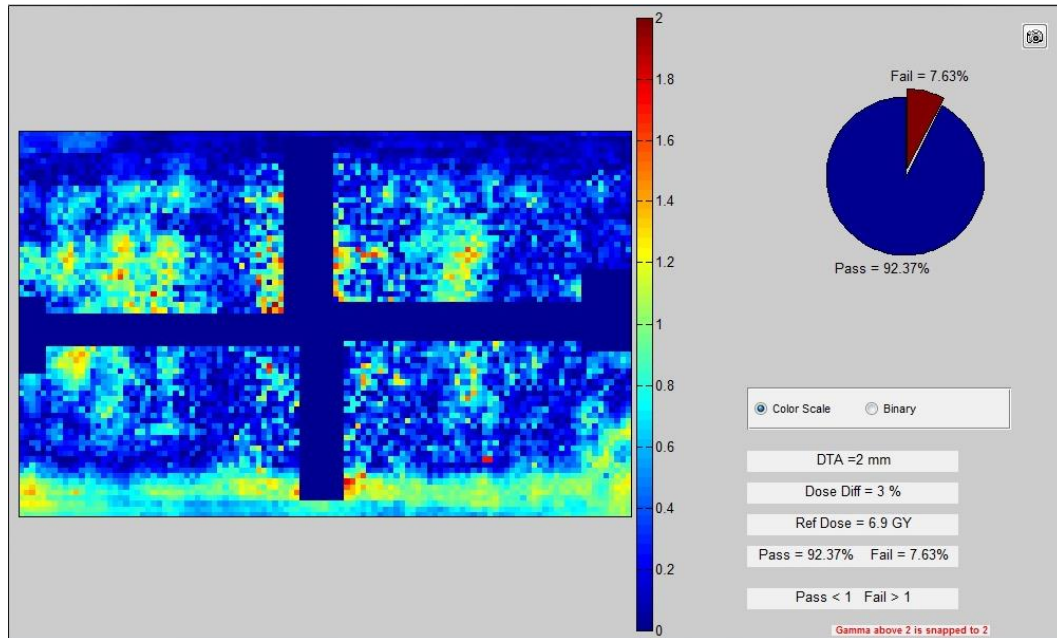


Figure 7.88: Lung IMRT delivery comparison for the coronal plane of delivery #3 for the TrueBeam FFF 6MV model. Agreement was evaluated using a $\pm 3\%/2\text{mm}$ gamma criterion and 92.4% of pixels passed.

7.7 Varian TrueBeam 10 MV: Percent Depth Dose and Dose Profiles

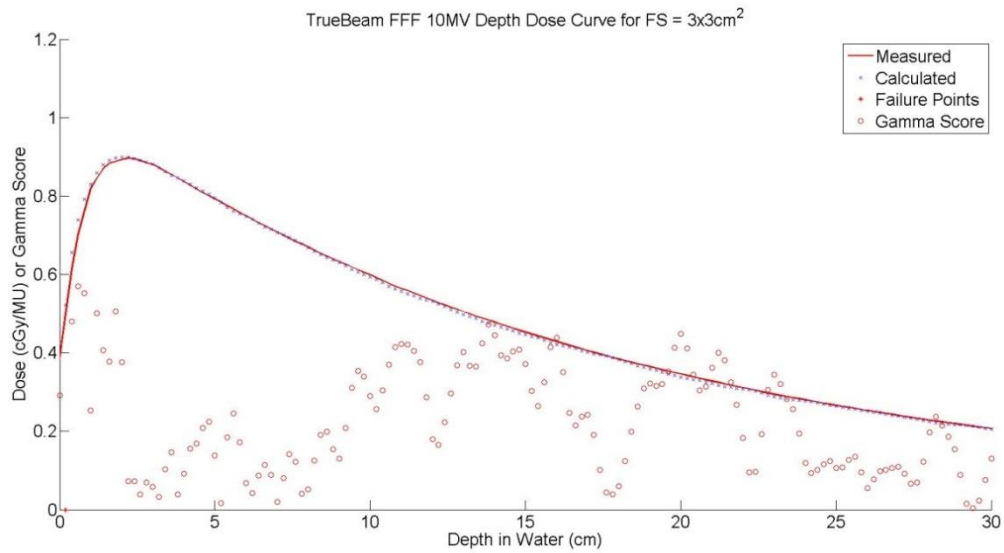


Figure 7.89: Calculated (blue 'x') and measured (red line) percent depth dose curves for a TrueBeam FFF 10MV beam at a field size of 3 x 3 cm². Gamma agreement (red circles) for each point is also displayed along with any points (red star) at which a failure to meet the $\pm 2\%/2\text{mm}$ criterion. At this field size 99.3% of all data passed the gamma criterion.

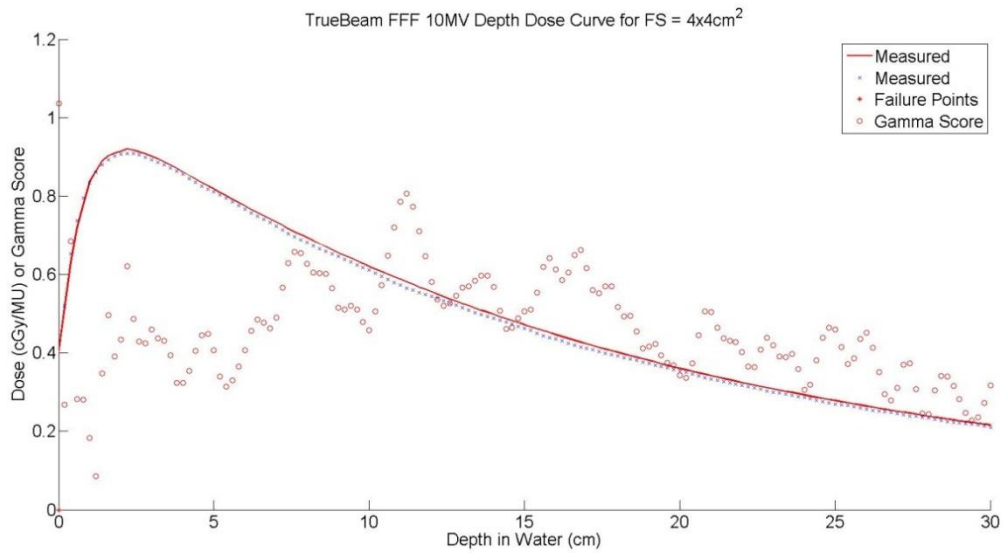


Figure 7.90: Calculated (blue 'x') and measured (red line) percent depth dose curves for a TrueBeam FFF 10MV beam at a field size of 4 x 4 cm². Gamma agreement (red circles) for each point is also displayed along with any points (red star) at which a failure to meet the $\pm 2\%/2\text{mm}$ criterion. At this field size 99.3% of all data passed the gamma criterion.

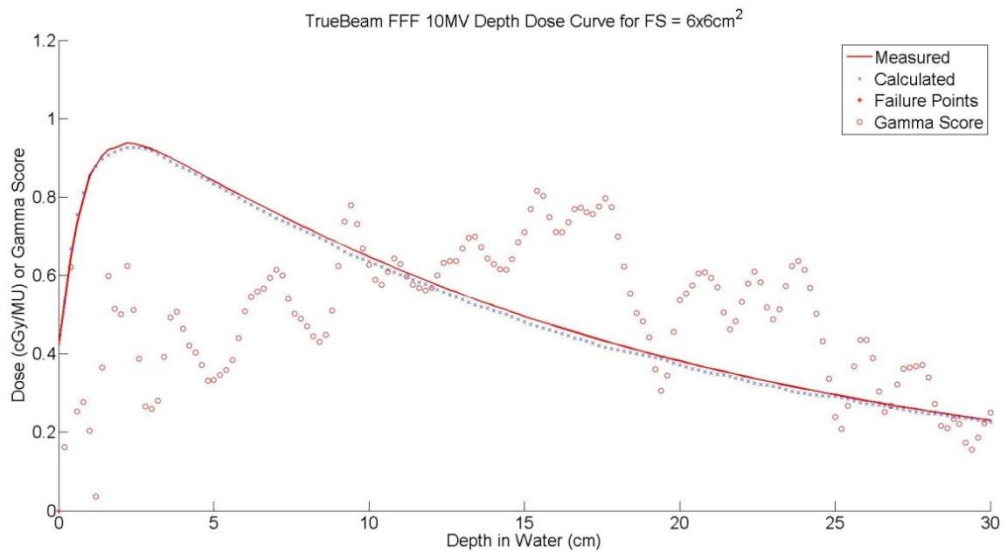


Figure 7.91: Calculated (blue 'x') and measured (red line) percent depth dose curves for a TrueBeam FFF 10MV beam at a field size of 6 x 6 cm². Gamma agreement (red circles) for each point is also displayed along with any points (red star) at which a failure to meet the $\pm 2\%/2\text{mm}$ criterion. At this field size 99.3% of all data passed the gamma criterion.

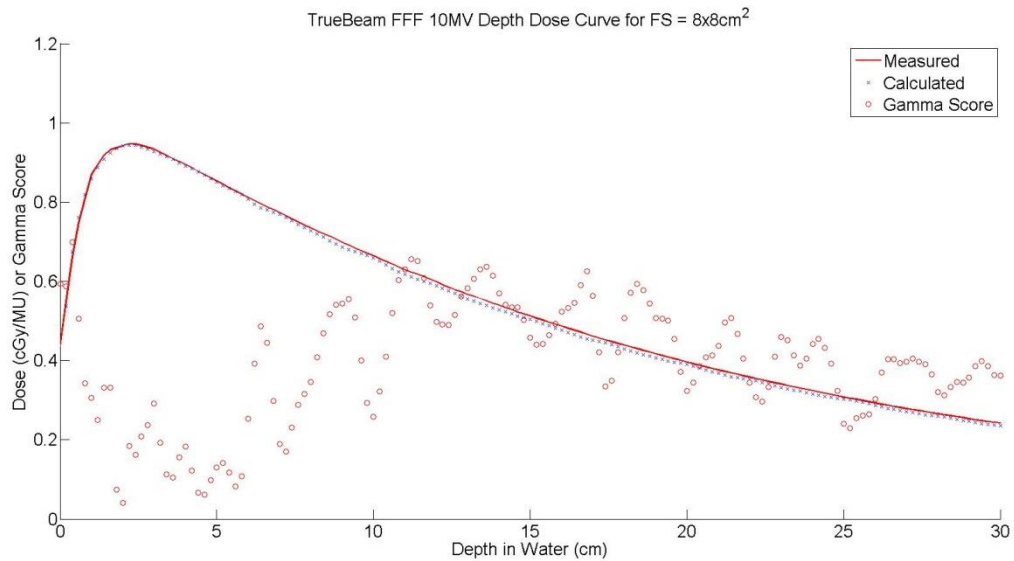


Figure 7.92: Calculated (blue 'x') and measured (red line) percent depth dose curves for a TrueBeam FFF 10MV beam at a field size of 8 x 8 cm². Gamma agreement (red circles) for each point is also displayed along with any points (red star) at which a failure to meet the $\pm 2\%/2\text{mm}$ criterion. At this field size 100.0% of all data passed the gamma criterion.

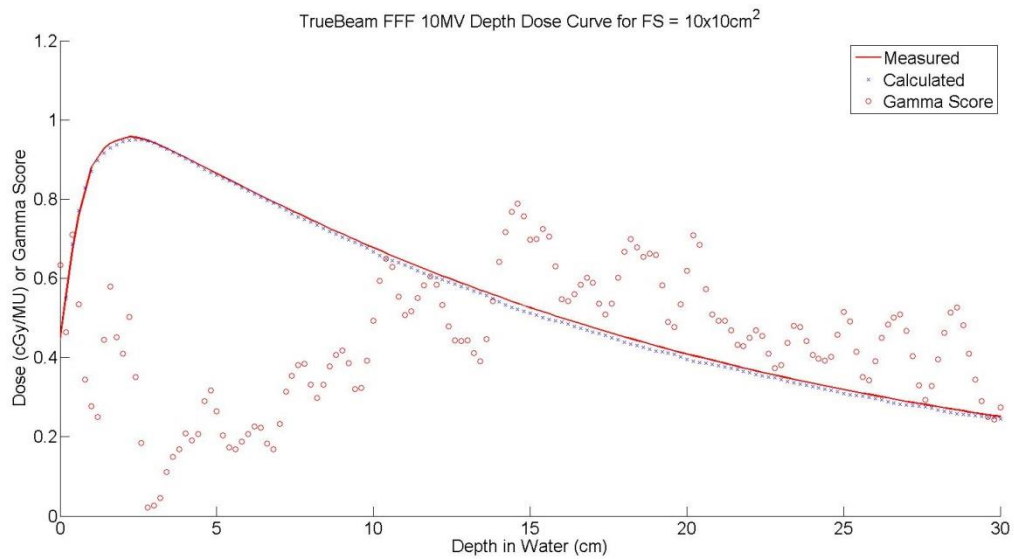


Figure 7.93: Calculated (blue 'x') and measured (red line) percent depth dose curves for a TrueBeam FFF 10MV beam at a field size of 10 x 10 cm². Gamma agreement (red circles) for each point is also displayed along with any points (red star) at which a failure to meet the $\pm 2\%/2\text{mm}$ criterion. At this field size 100.0% of all data passed the gamma criterion.

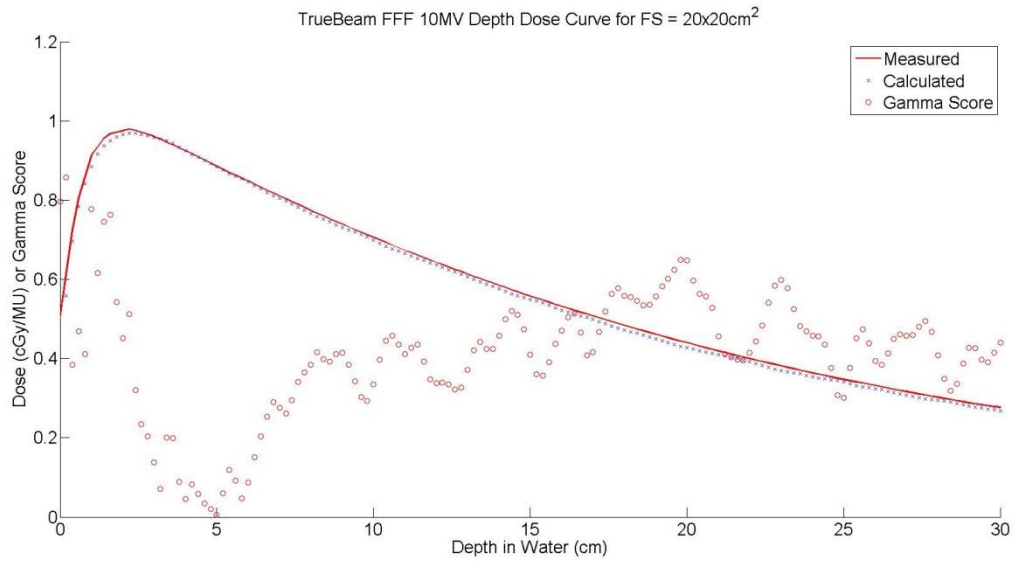


Figure 7.94: Calculated (blue 'x') and measured (red line) percent depth dose curves for a TrueBeam FFF 10MV beam at a field size of 20 x 20 cm². Gamma agreement (red circles) for each point is also displayed along with any points (red star) at which a failure to meet the $\pm 2\%/2\text{mm}$ criterion. At this field size 100.0% of all data passed the gamma criterion.

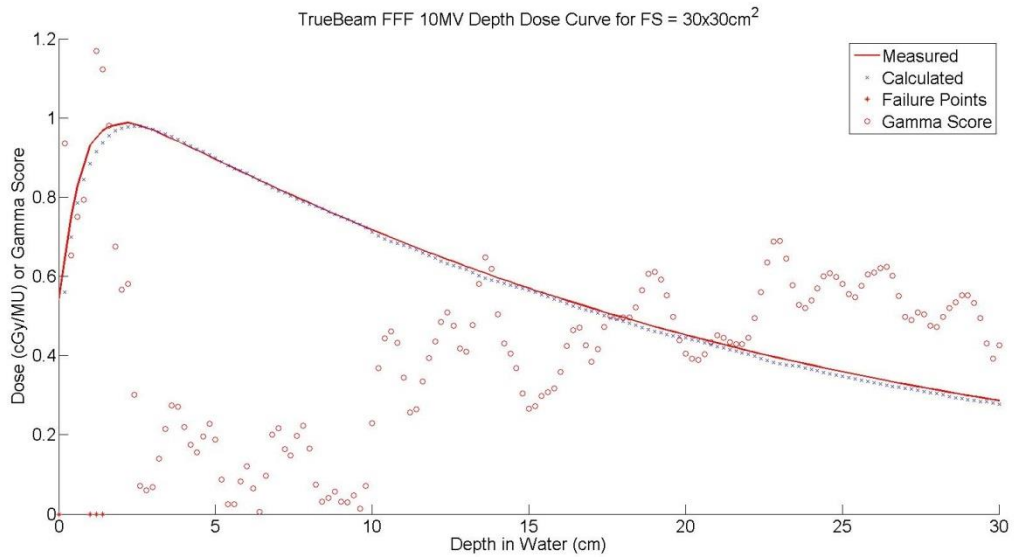


Figure 7.95: Calculated (blue 'x') and measured (red line) percent depth dose curves for a TrueBeam FFF 10MV beam at a field size of 30 x 30 cm². Gamma agreement (red circles) for each point is also displayed along with any points (red star) at which a failure to meet the $\pm 2\%/2\text{mm}$ criterion. At this field size 97.4% of all data passed the gamma criterion.

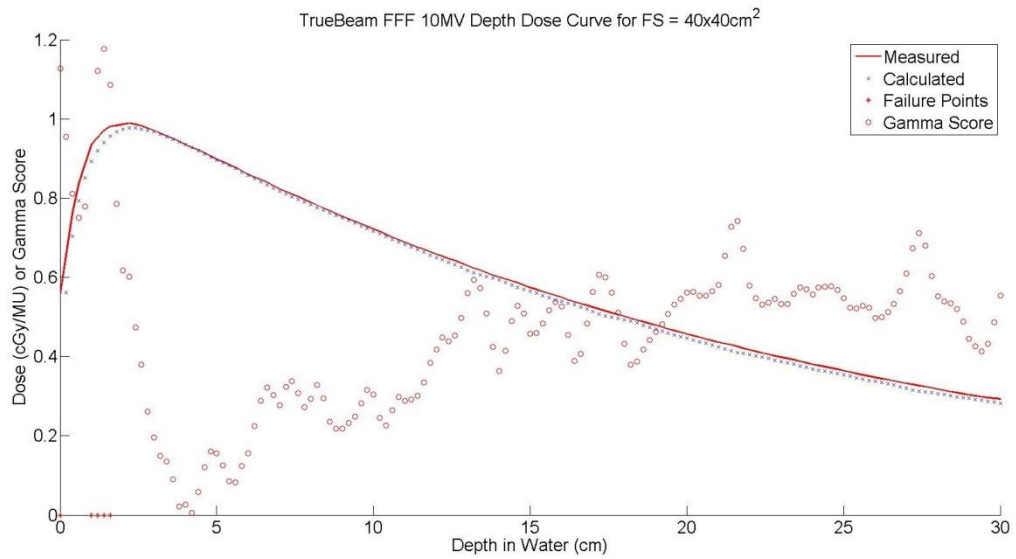


Figure 7.96: Calculated (blue 'x') and measured (red line) percent depth dose curves for a TrueBeam FFF 10MV beam at a field size of 40 x 40 cm². Gamma agreement (red circles) for each point is also displayed along with any points (red star) at which a failure to meet the $\pm 2\%/2\text{mm}$ criterion. At this field size 96.7% of all data passed the gamma criterion.

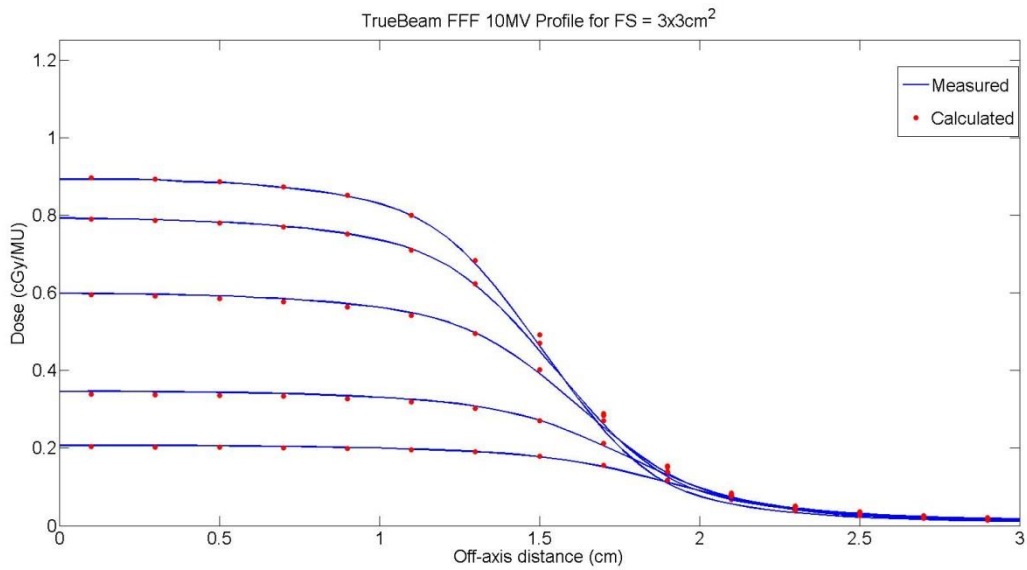


Figure 7.97: Calculated (red circle) and measured (blue line) dose profiles for a TrueBeam FFF 10MV beam at a field size of 3 x 3 cm².

Field Size (cm ²)	Direction	Depth (cm)	% Passing (2%/2mm)
3 x 3	x	2.4	94.57
	x	5	100.00
	x	10	100.00
	x	20	100.00
	x	30	100.00

Table 7.21: Dose profile agreement between the TrueBeam FFF 10MV multiple source model and measurement using a $\pm 2\%/2\text{mm}$ global gamma criterion at all depths of comparison for a 3 x 3 cm² field size.

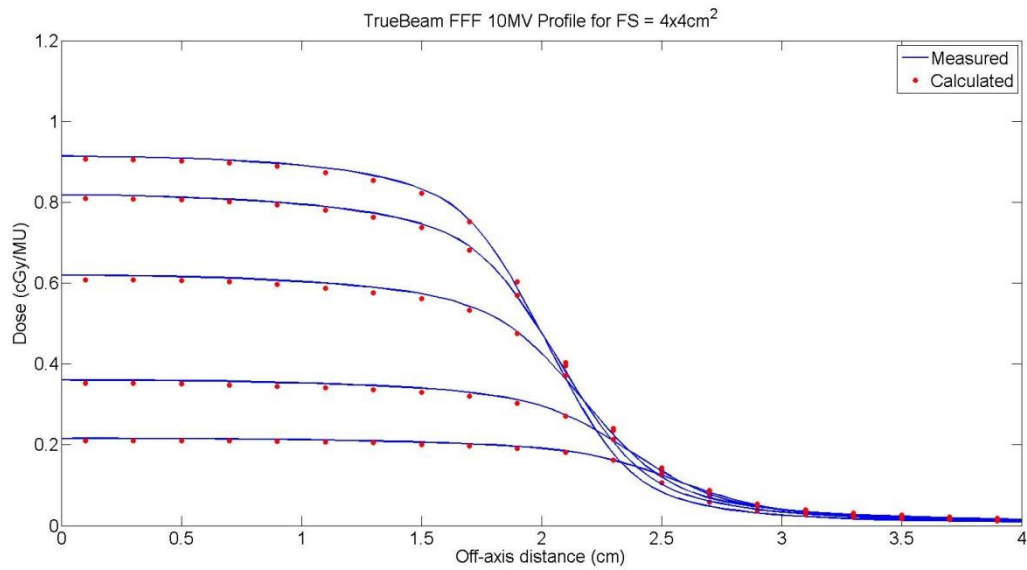


Figure 7.98: Calculated (red circle) and measured (blue line) dose profiles for a TrueBeam FFF 10MV beam at a field size of 4 x 4 cm².

Field Size (cm ²)	Direction	Depth (cm)	% Passing (2%/2mm)
4 x 4	x	2.4	100.00
	x	5	98.56
	x	10	100.00
	x	20	100.00
	x	30	100.00

Table 7.22: Dose profile agreement between the TrueBeam FFF 10MV multiple source model and measurement using a $\pm 2\%/2\text{mm}$ global gamma criterion at all depths of comparison for a 4 x 4 cm² field size.

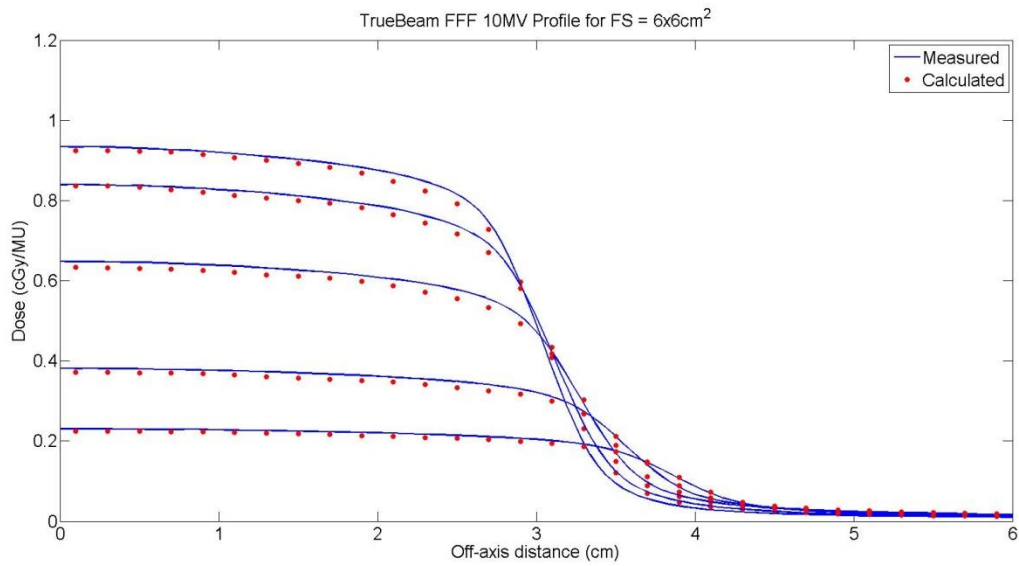


Figure 7.99: Calculated (red circle) and measured (blue line) dose profiles for a TrueBeam FFF 10MV beam at a field size of 6 x 6 cm².

Field Size (cm ²)	Direction	Depth (cm)	% Passing (2%/2mm)
6 x 6	x	2.4	98.74
	x	5	99.37
	x	10	100.00
	x	20	100.00
	x	30	100.00

Table 7.23: Dose profile agreement between the TrueBeam FFF 10MV multiple source model and measurement using a $\pm 2\%/2\text{mm}$ global gamma criterion at all depths of comparison for a 6 x 6 cm² field size.

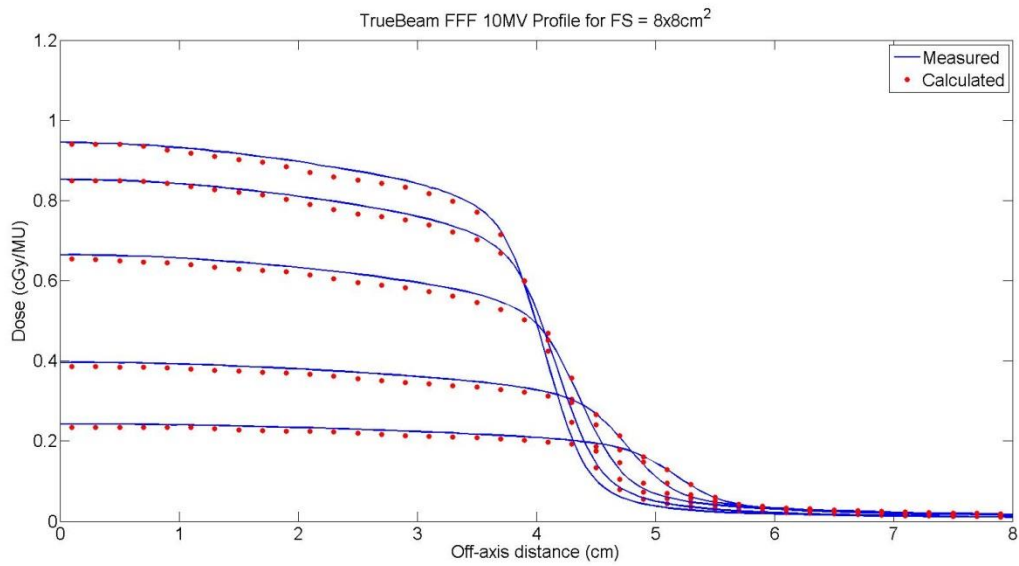


Figure 7.100: Calculated (red circle) and measured (blue line) dose profiles for a TrueBeam FFF 10MV beam at a field size of 8 x 8 cm².

Field Size (cm ²)	Direction	Depth (cm)	% Passing (2%/2mm)
8 x 8	x	2.4	96.10
	x	5	98.88
	x	10	96.65
	x	20	100.00
	x	30	100.00

Table 7.24: Dose profile agreement between the TrueBeam FFF 10MV multiple source model and measurement using a $\pm 2\%/2\text{mm}$ global gamma criterion at all depths of comparison for a 8 x 8 cm² field size.

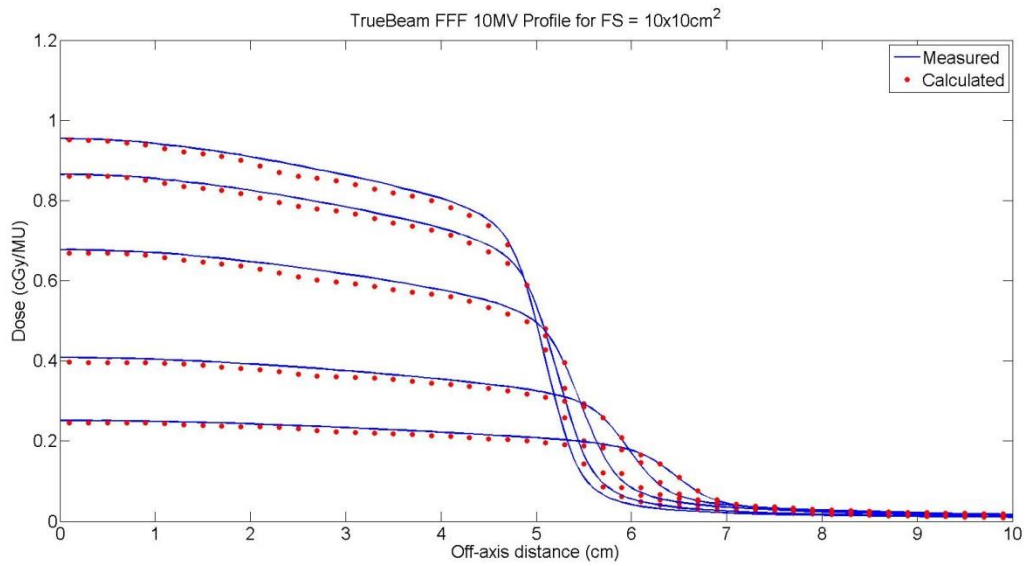


Figure 7.101: Calculated (red circle) and measured (blue line) dose profiles for a TrueBeam FFF 10MV beam at a field size of 10 x 10 cm².

Field Size (cm ²)	Direction	Depth (cm)	% Passing (2%/2mm)
10 x 10	x	2.4	93.47
	x	5	96.98
	x	10	90.45
	x	20	100.00
	x	30	100.00

Table 7.25: Dose profile agreement between the TrueBeam FFF 10MV multiple source model and measurement using a $\pm 2\%/2\text{mm}$ global gamma criterion at all depths of comparison for a 10 x 10 cm² field size.

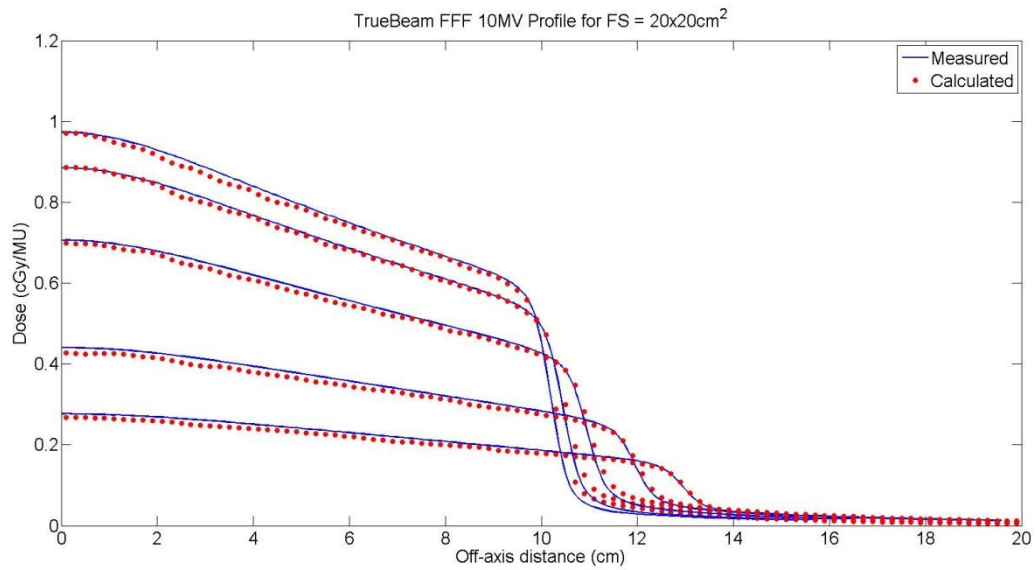


Figure 7.102: Calculated (red circle) and measured (blue line) dose profiles for a TrueBeam FFF 10MV beam at a field size of 20 x 20 cm².

Field Size (cm ²)	Direction	Depth (cm)	% Passing (2%/2mm)
20 x 20	x	2.4	99.67
	x	5	93.07
	x	10	100.00
	x	20	100.00
	x	30	100.00

Table 7.26: Dose profile agreement between the TrueBeam FFF 10MV multiple source model and measurement using a $\pm 2\%/2\text{mm}$ global gamma criterion at all depths of comparison for a 20 x 20 cm² field size.

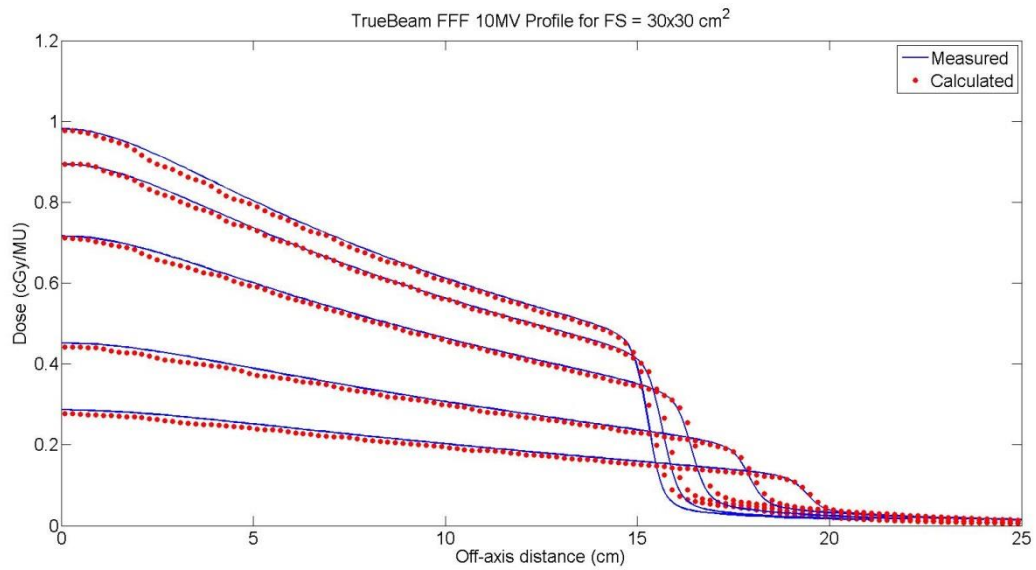


Figure 7.103: Calculated (red circle) and measured (blue line) dose profiles for a TrueBeam FFF 10MV beam at a field size of 30 x 30 cm².

Field Size (cm ²)	Direction	Depth (cm)	% Passing (2%/2mm)
30 x 30	x	2.4	90.17
	x	5	90.42
	x	10	100.00
	x	20	100.00
	x	30	100.00

Table 7.27: Dose profile agreement between the TrueBeam FFF 10MV multiple source model and measurement using a $\pm 2\%/2\text{mm}$ global gamma criterion at all depths of comparison for a 30 x 30 cm² field size.

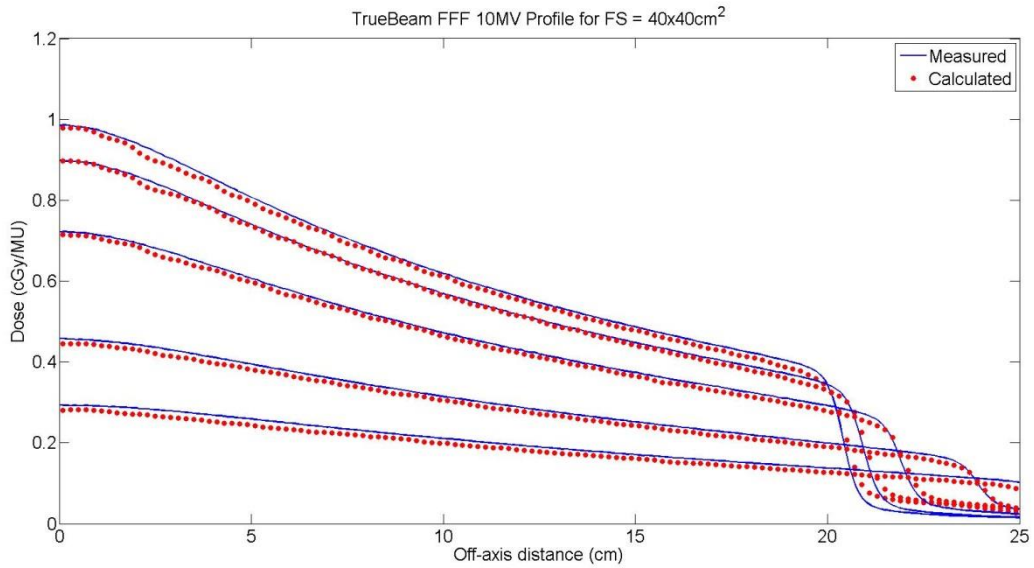


Figure 7.104: Calculated (red circle) and measured (blue line) dose profiles for a TrueBeam FFF 10MV beam at a field size of 40 x 40 cm².

Field Size (cm ²)	Direction	Depth (cm)	% Passing (2%/2mm)
40 x 40	x	2.4	88.61
	x	5	90.18
	x	10	100.00
	x	20	100.00
	x	30	99.61

Table 7.28: Dose profile agreement between the TrueBeam FFF 10MV multiple source model and measurement using a $\pm 2\%/2\text{mm}$ global gamma criterion at all depths of comparison for a 40 x 40 cm² field size.

7.8 Varian TrueBeam 10 MV: Gamma Maps

7.8.1 Varian TrueBeam 10 MV: Delivery of IMRT Head and Neck Plan

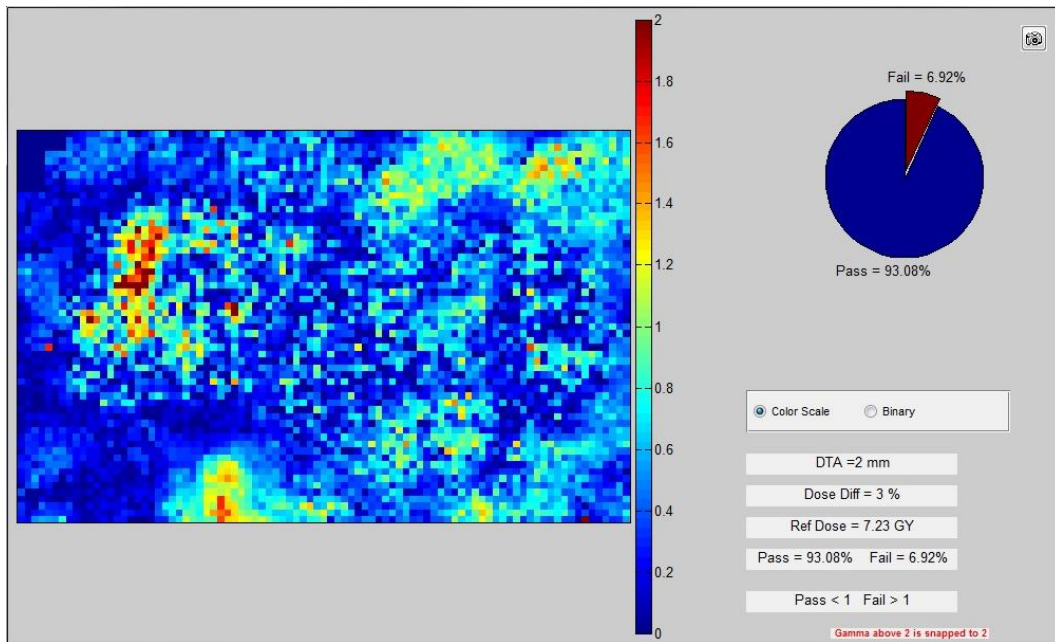


Figure 7.105: IMRT head and neck delivery comparison for the axial plane of delivery #2 for the TrueBeam FFF 10MV model. Agreement was evaluated using a $\pm 3\%/2\text{mm}$ gamma criterion and 93.1% of pixels passed.

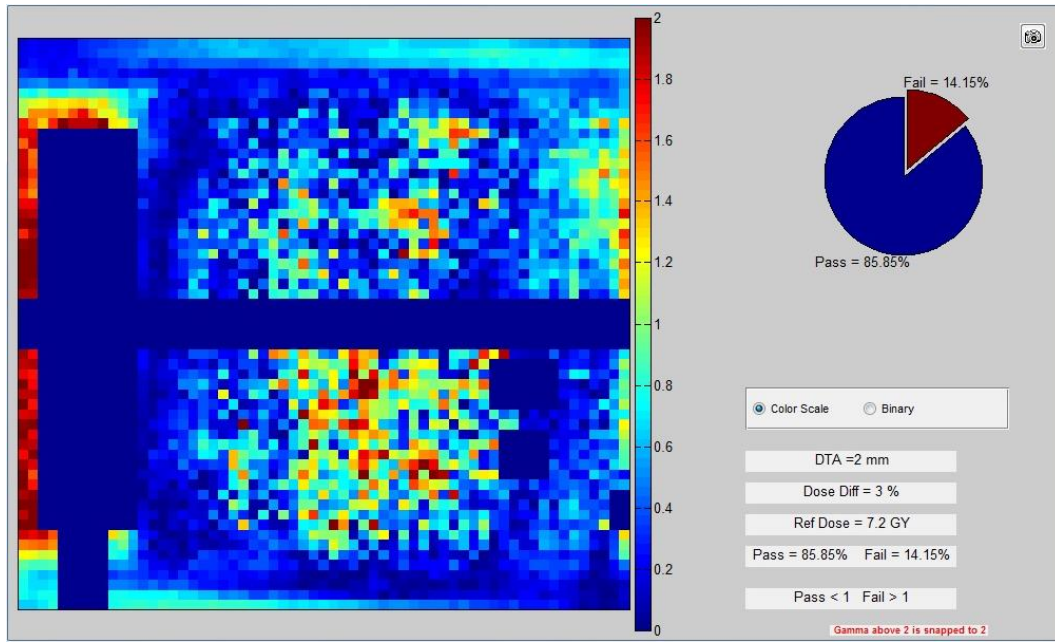


Figure 7.106: IMRT head and neck delivery comparison for the sagittal plane of delivery #2 for the TrueBeam FFF 10MV model. Agreement was evaluated using a $\pm 3\%/2\text{mm}$ gamma criterion and 85.9% of pixels passed.

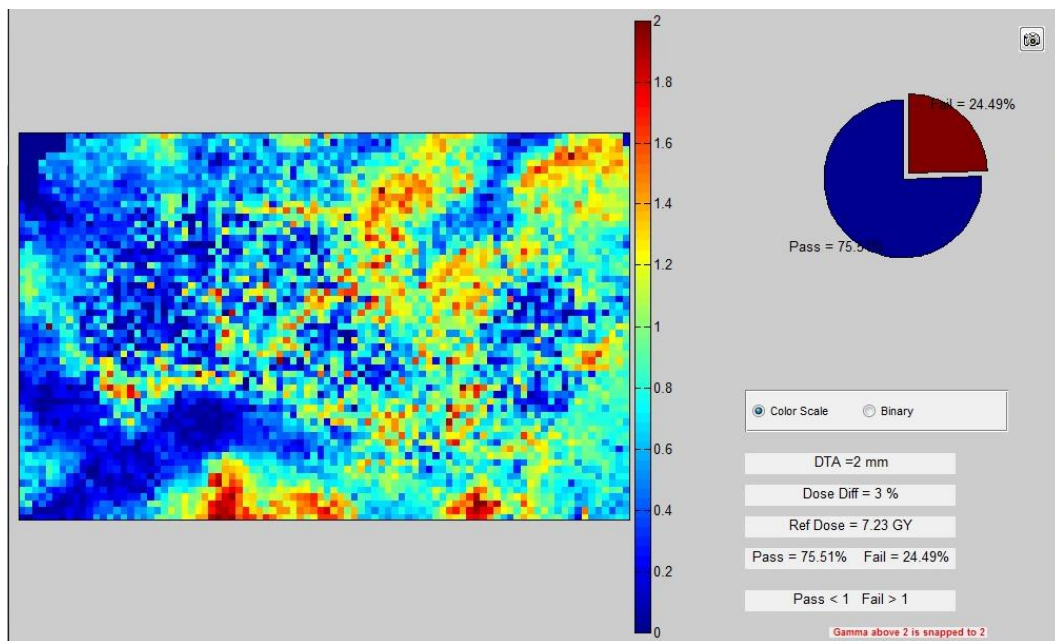


Figure 7.107: IMRT head and neck delivery comparison for the axial plane of delivery #3 for the TrueBeam FFF 10MV model. Agreement was evaluated using a $\pm 3\%/2\text{mm}$ gamma criterion and 75.5% of pixels passed.

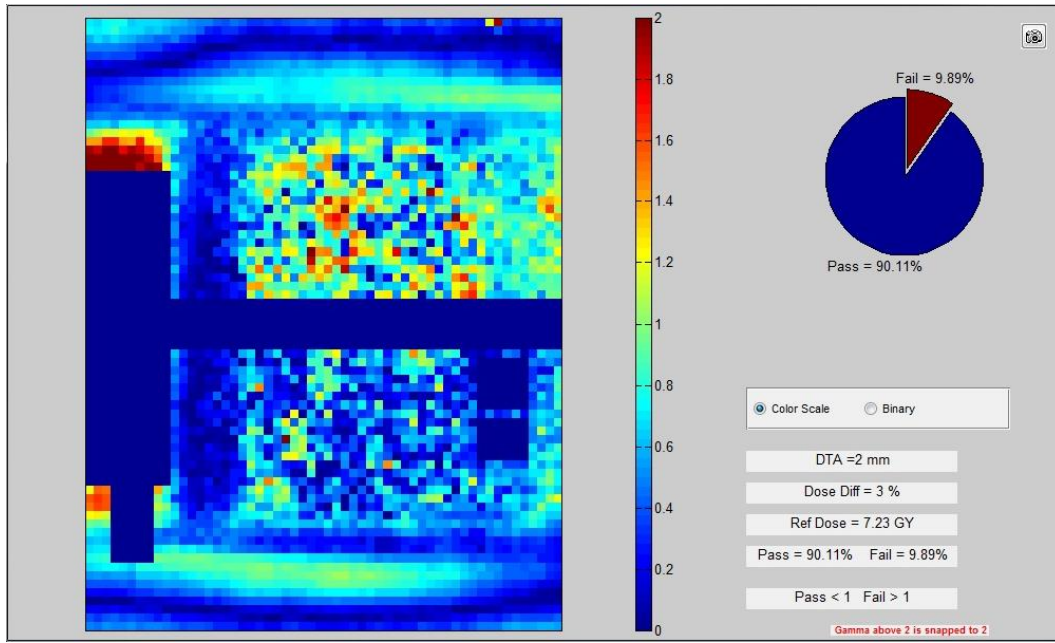


Figure 7.108: IMRT head and neck delivery comparison for the sagittal plane of delivery #3 for the TrueBeam FFF 10MV model. Agreement was evaluated using a $\pm 3\%/2\text{mm}$ gamma criterion and 90.1% of pixels passed.

7.8.2 Varian TrueBeam 10 MV: Delivery of SBRT Lung Plan

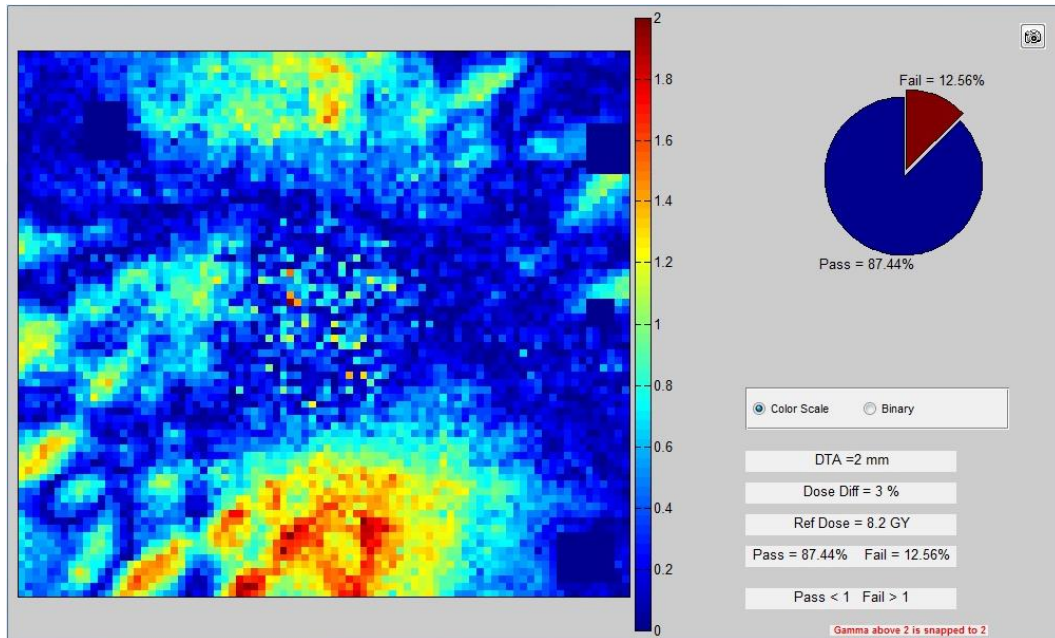


Figure 7.109: Lung SBRT delivery comparison for the axial plane of delivery #2 for the TrueBeam FFF 10MV model. Agreement was evaluated using a $\pm 3\%/2\text{mm}$ gamma criterion and 87.4% of pixels passed.

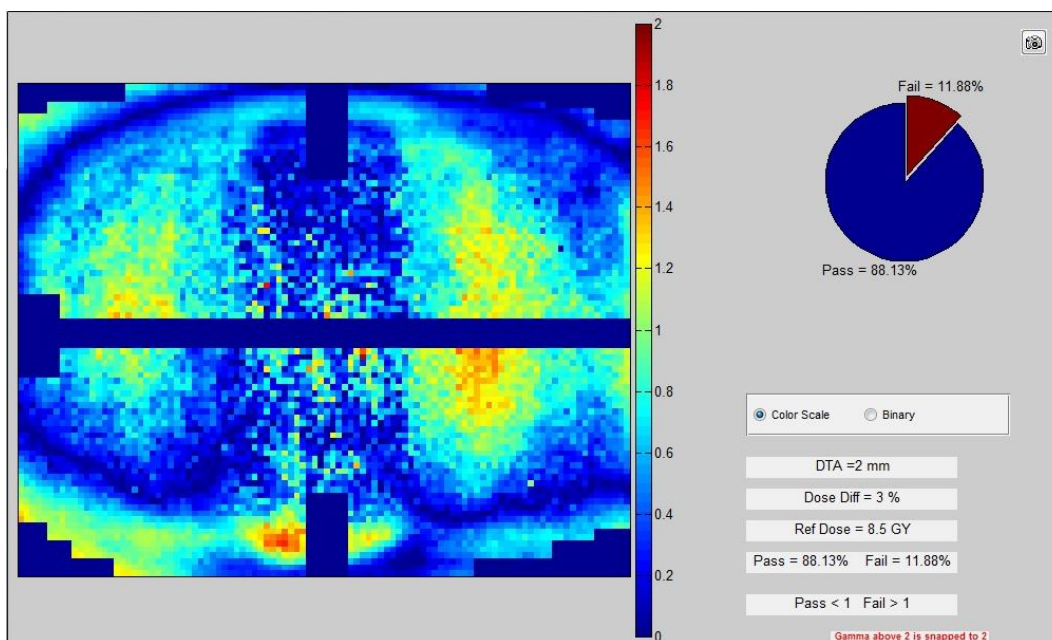


Figure 7.110: Lung SBRT delivery comparison for the sagittal plane of delivery #2 for the TrueBeam FFF 10MV model. Agreement was evaluated using a $\pm 3\%/2\text{mm}$ gamma criterion and 88.1% of pixels passed.

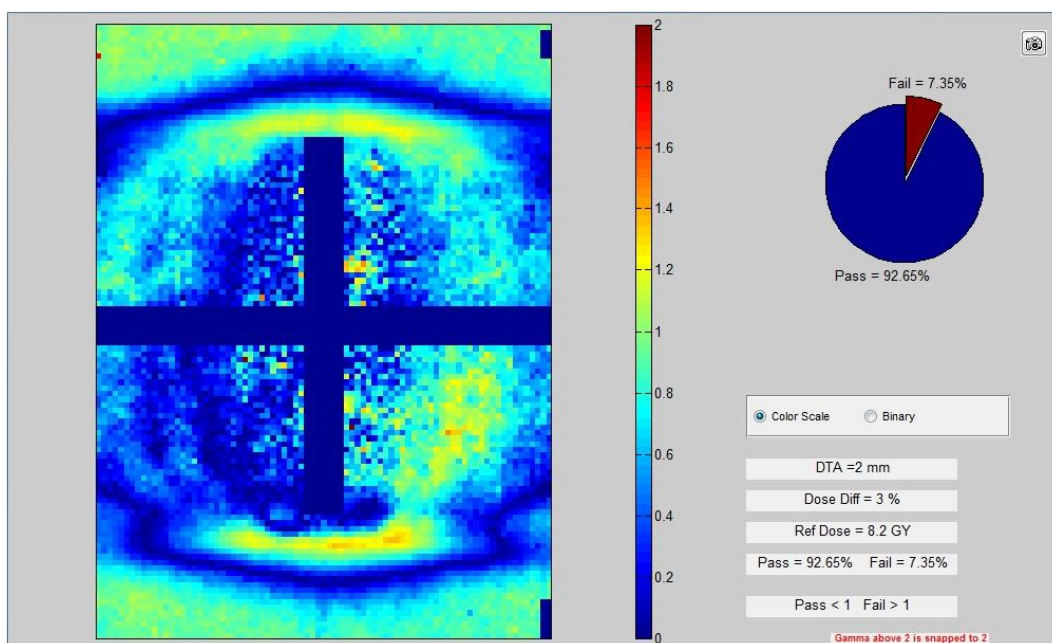


Figure 7.111: Lung SBRT delivery comparison for the coronal plane of delivery #2 for the TrueBeam FFF 10MV model. Agreement was evaluated using a $\pm 3\%/2\text{mm}$ gamma criterion and 92.7% of pixels passed.

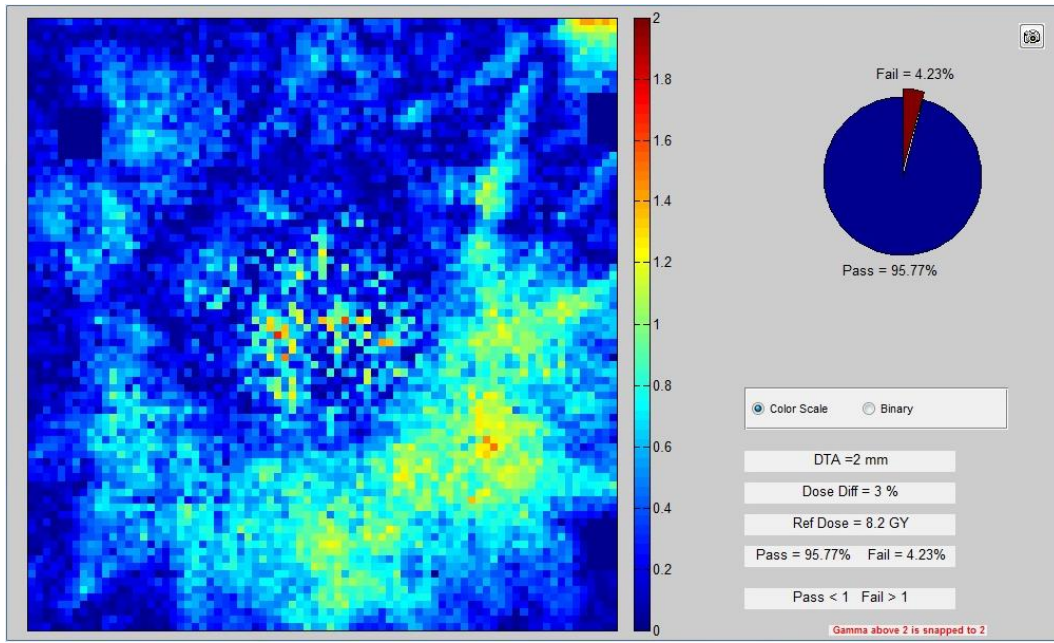


Figure 7.112: Lung SBRT delivery comparison for the axial plane of delivery #3 for the TrueBeam FFF 10MV model. Agreement was evaluated using a $\pm 3\%/2\text{mm}$ gamma criterion and 95.8% of pixels passed.

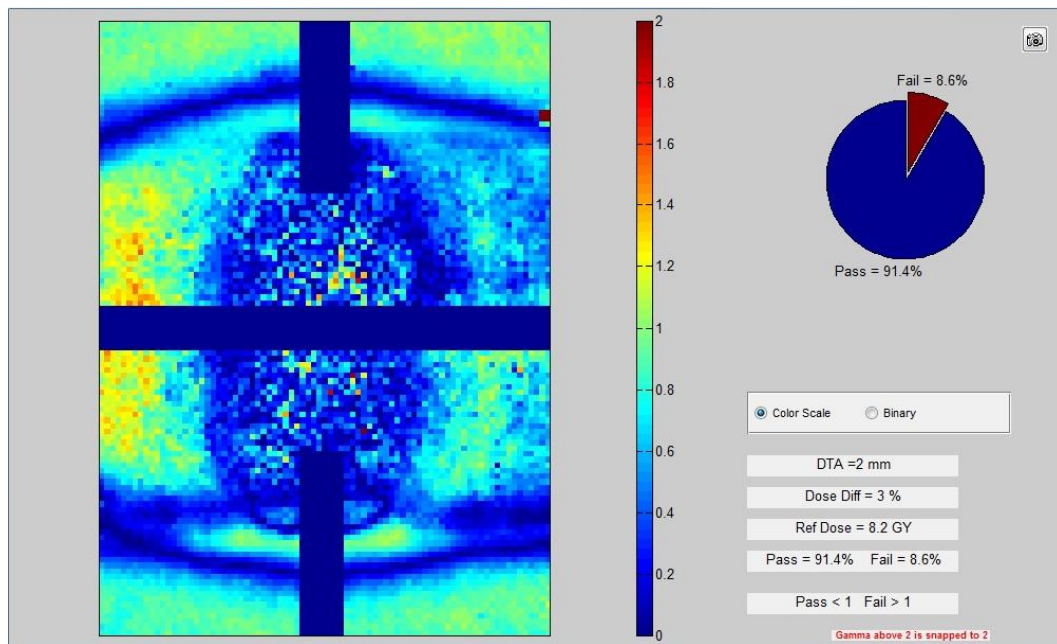


Figure 7.113: Lung SBRT delivery comparison for the sagittal plane of delivery #3 for the TrueBeam FFF 10MV model. Agreement was evaluated using a $\pm 3\%/2\text{mm}$ gamma criterion and 91.4% of pixels passed.

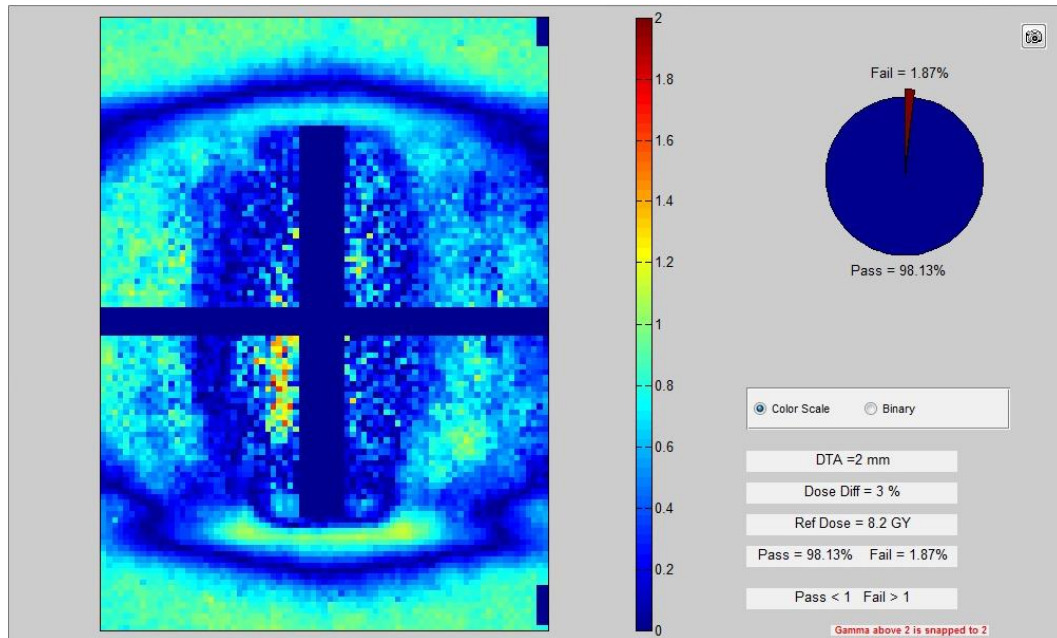


Figure 7.114: Lung SBRT delivery comparison for the coronal plane of delivery #3 for the TrueBeam FFF 10MV model. Agreement was evaluated using a $\pm 3\%/2\text{mm}$ gamma criterion and 98.1% of pixels passed.

7.8.3 Varian TrueBeam 10 MV: Delivery of IMRT Lung Plan

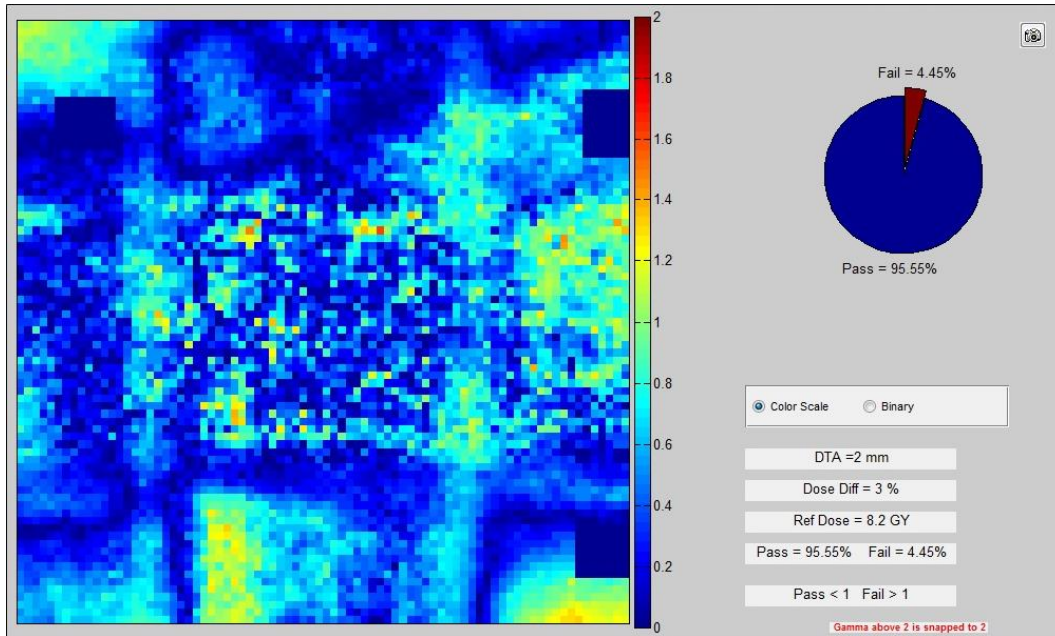


Figure 7.115: Lung IMRT delivery comparison for the axial plane of delivery #1 for the TrueBeam FFF 10MV model. Agreement was evaluated using a $\pm 3\%/2\text{mm}$ gamma criterion and 95.6% of pixels passed.

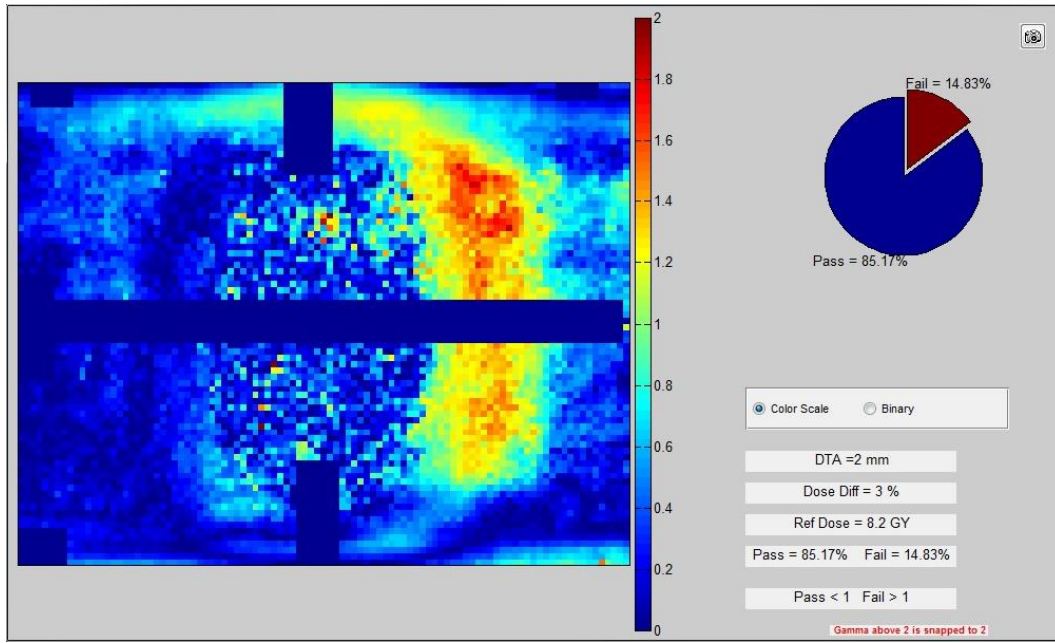


Figure 7.116: Lung IMRT delivery comparison for the sagittal plane of delivery #1 for the TrueBeam FFF 10MV model. Agreement was evaluated using a $\pm 3\%/2\text{mm}$ gamma criterion and 84.2% of pixels passed.

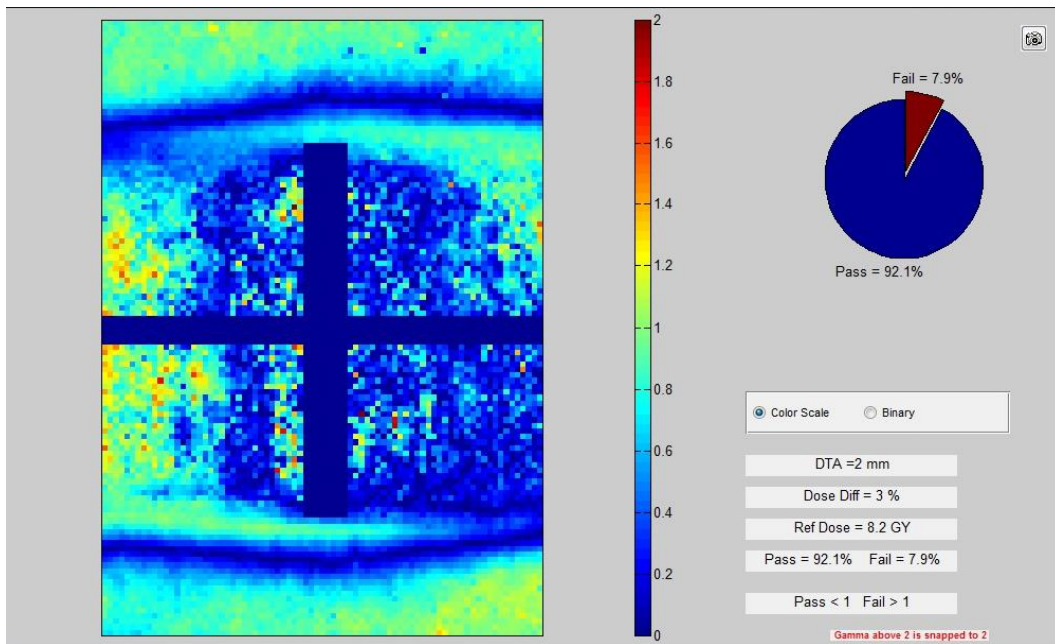


Figure 7.117: Lung IMRT delivery comparison for the coronal plane of delivery #1 for the TrueBeam FFF 10MV model. Agreement was evaluated using a $\pm 3\%/2\text{mm}$ gamma criterion and 92.1% of pixels passed.

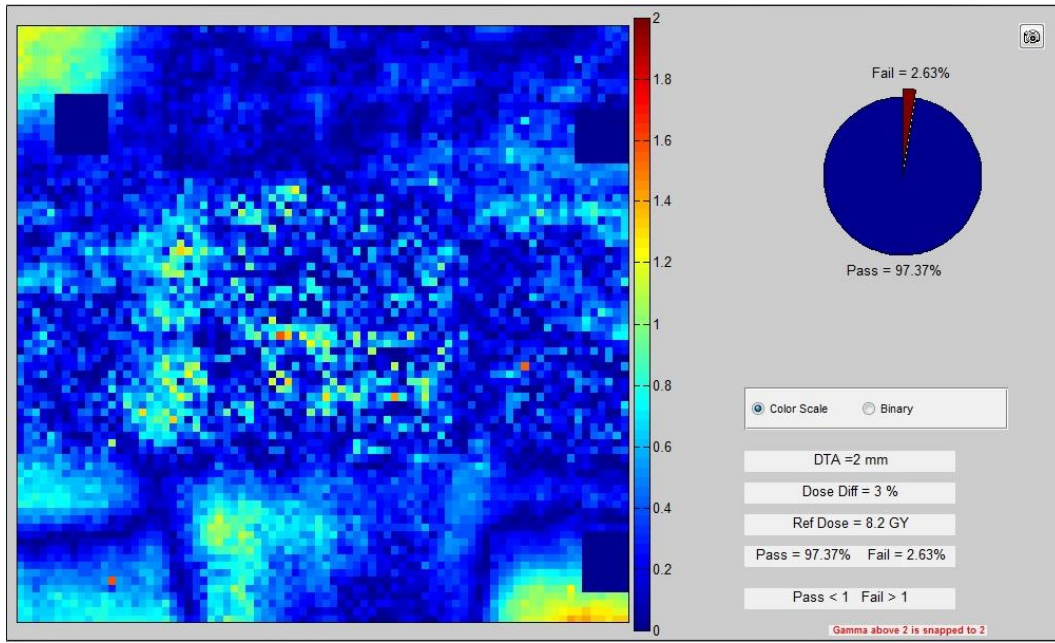


Figure 7.118: Lung IMRT delivery comparison for the axial plane of delivery #2 for the TrueBeam FFF 10MV model. Agreement was evaluated using a $\pm 3\%/2\text{mm}$ gamma criterion and 97.4% of pixels passed.

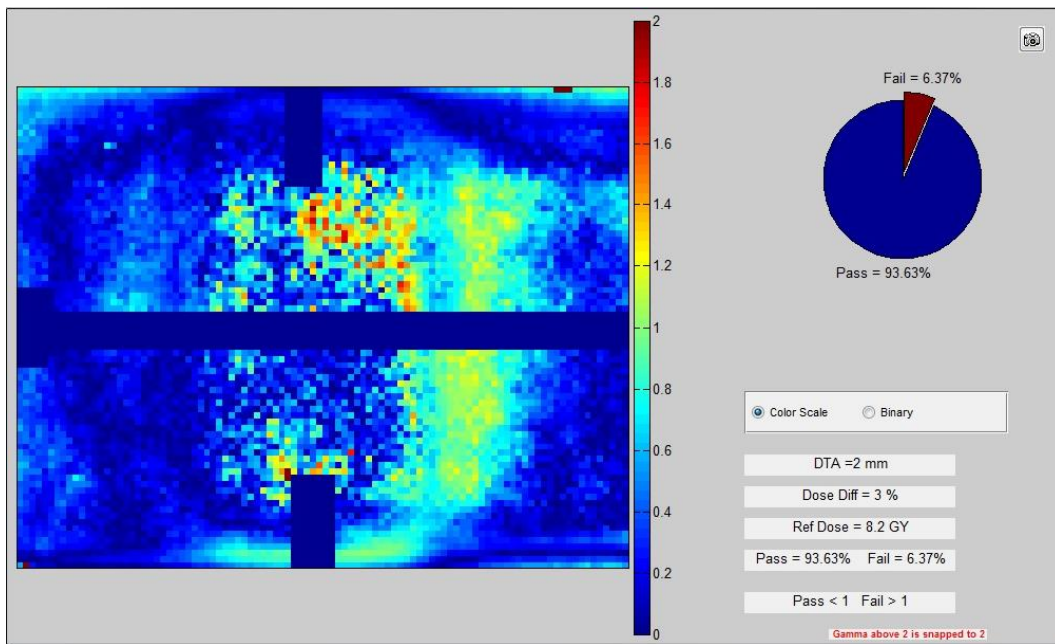


Figure 7.119: Lung IMRT delivery comparison for the sagittal plane of delivery #2 for the TrueBeam FFF 10MV model. Agreement was evaluated using a $\pm 3\%/2\text{mm}$ gamma criterion and 93.6% of pixels passed.

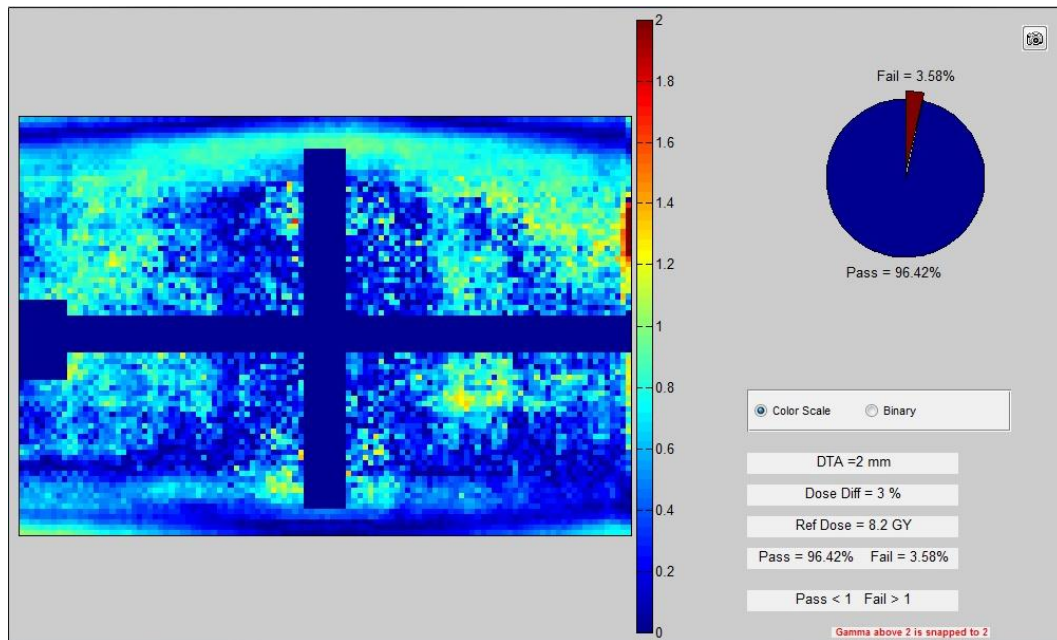


Figure 7.120: Lung IMRT delivery comparison for the coronal plane of delivery #2 for the TrueBeam FFF 10MV model. Agreement was evaluated using a $\pm 3\%/2\text{mm}$ gamma criterion and 96.4% of pixels passed.

7.9 Outside Institution Robustness Study: Gamma Maps

7.9.1 Head and Neck Phantom Audits

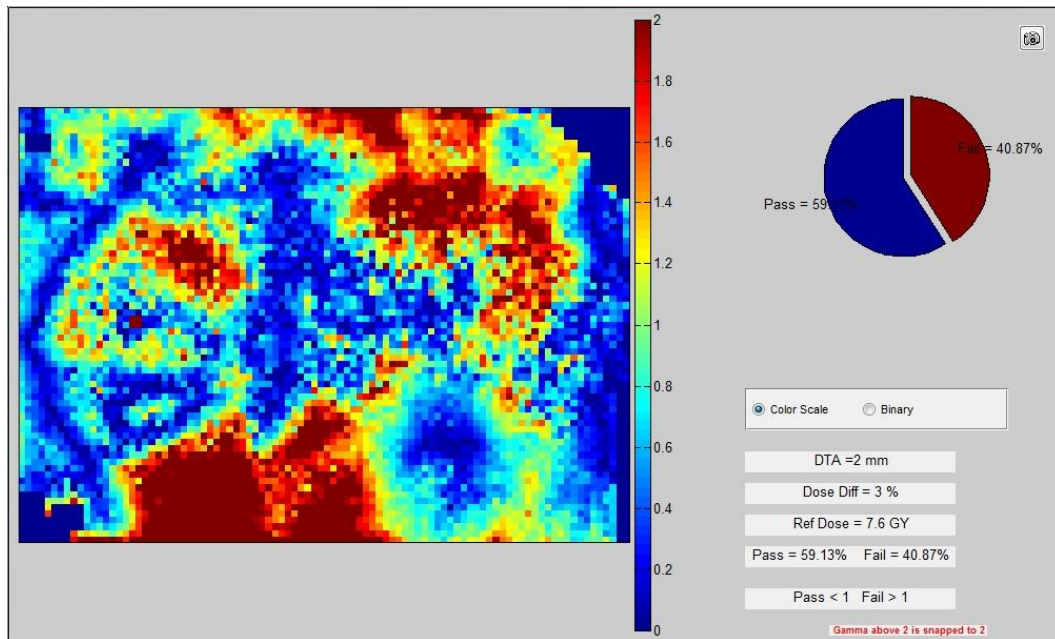


Figure 7.121: IMRT head and neck delivery comparison for the axial plane of Head and Neck Plan #1 with respect to DPM recalculated dose. Agreement was evaluated using a $\pm 3\%/2\text{mm}$ gamma criterion and 59.1% of pixels passed.

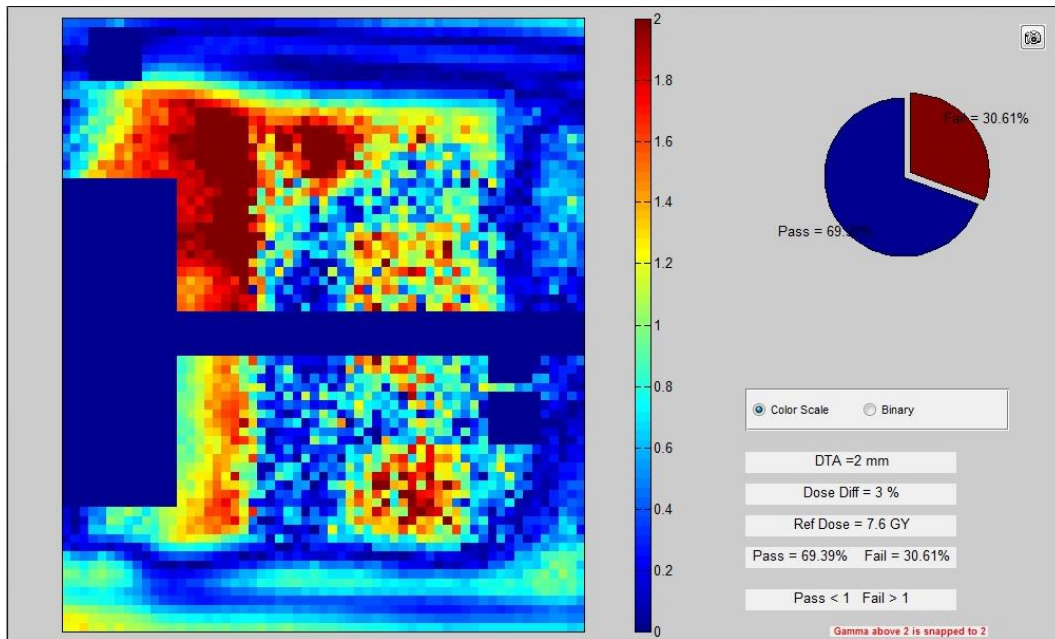


Figure 7.122: IMRT head and neck delivery comparison for the sagittal plane of Head and Neck Plan #1 with respect to DPM recalculated dose. Agreement was evaluated using a $\pm 3\%/2\text{mm}$ gamma criterion and 69.4% of pixels passed.

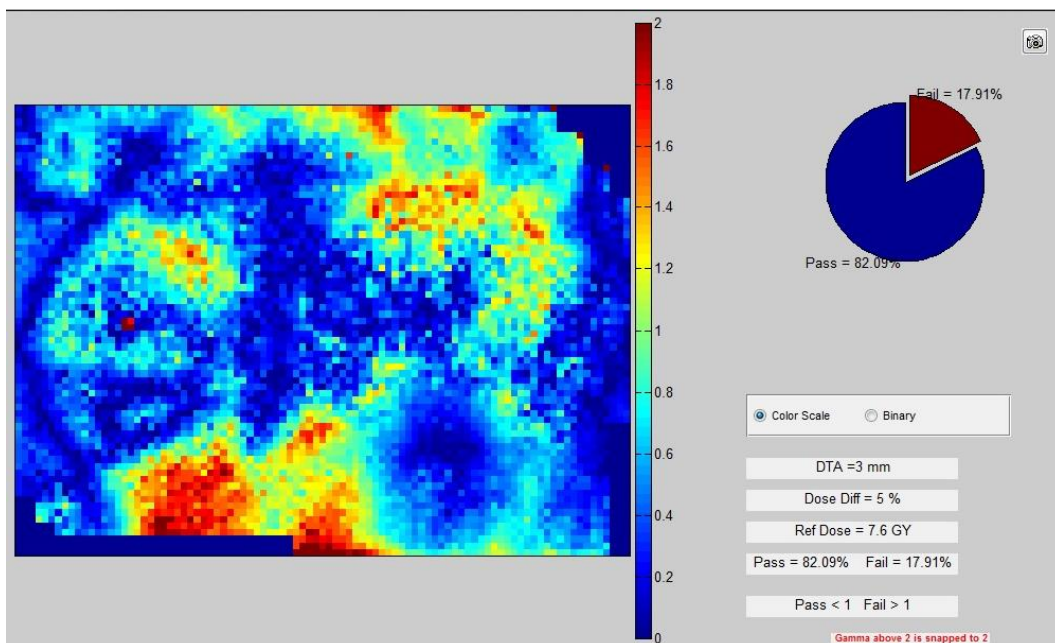


Figure 7.123: IMRT head and neck delivery comparison for the axial plane of Head and Neck Plan #1 with respect to DPM recalculated dose. Agreement was evaluated using a $\pm 5\%/3\text{mm}$ gamma criterion and 82.1% of pixels passed.

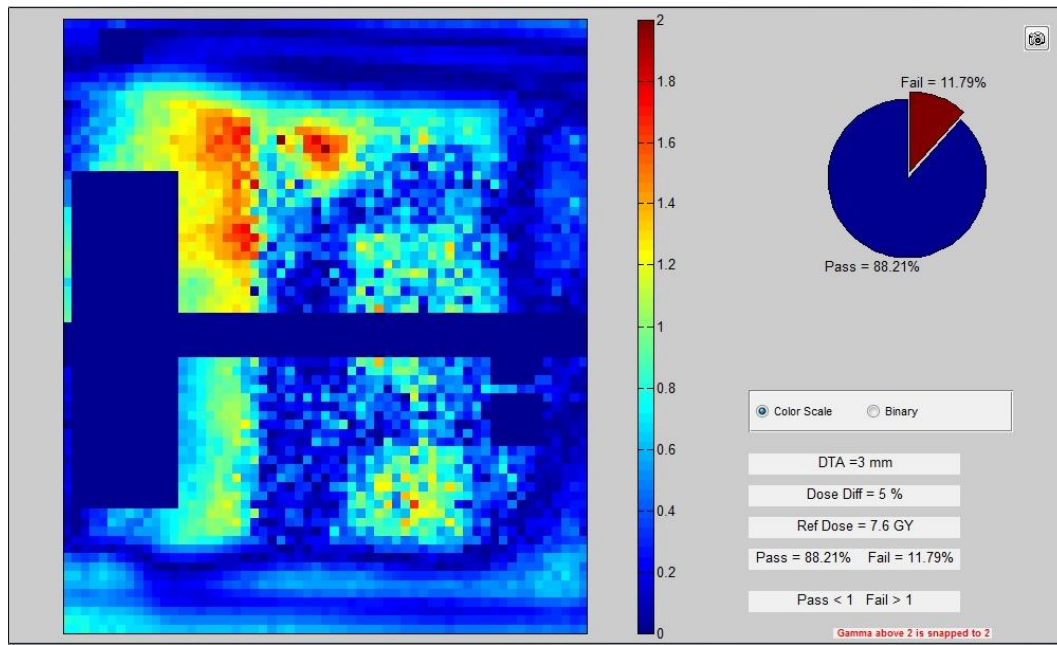


Figure 7.124: IMRT head and neck delivery comparison for the sagittal plane of Head and Neck Plan #1 with respect to DPM recalculated dose. Agreement was evaluated using a $\pm 5\%/3\text{mm}$ gamma criterion and 88.2% of pixels passed.

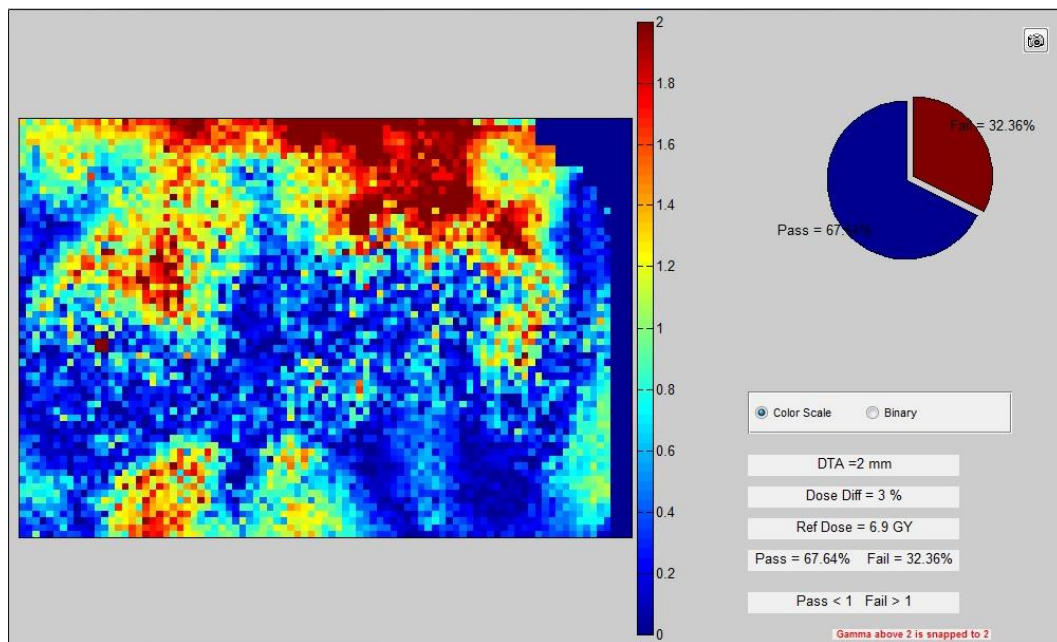


Figure 7.125: IMRT head and neck delivery comparison for the axial plane of Head and Neck Plan #1 with respect to TPS calculated dose. Agreement was evaluated using a $\pm 3\%/2\text{mm}$ gamma criterion and 67.6% of pixels passed.

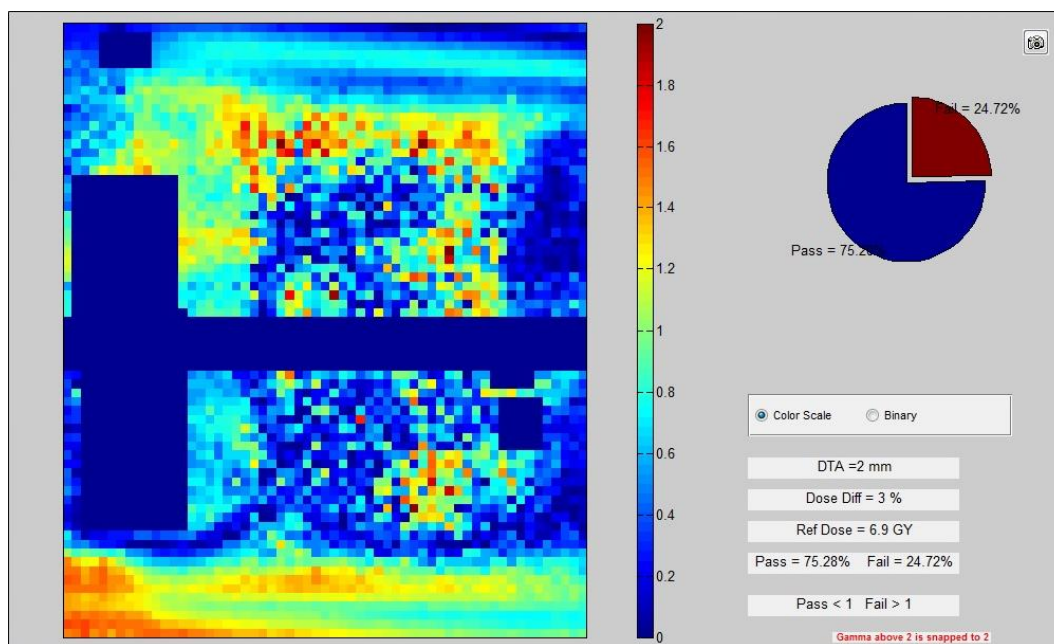


Figure 7.126: IMRT head and neck delivery comparison for the sagittal plane of Head and Neck Plan #1 with respect to TPS calculated dose. Agreement was evaluated using a $\pm 3\%/2\text{mm}$ gamma criterion and 75.3% of pixels passed.

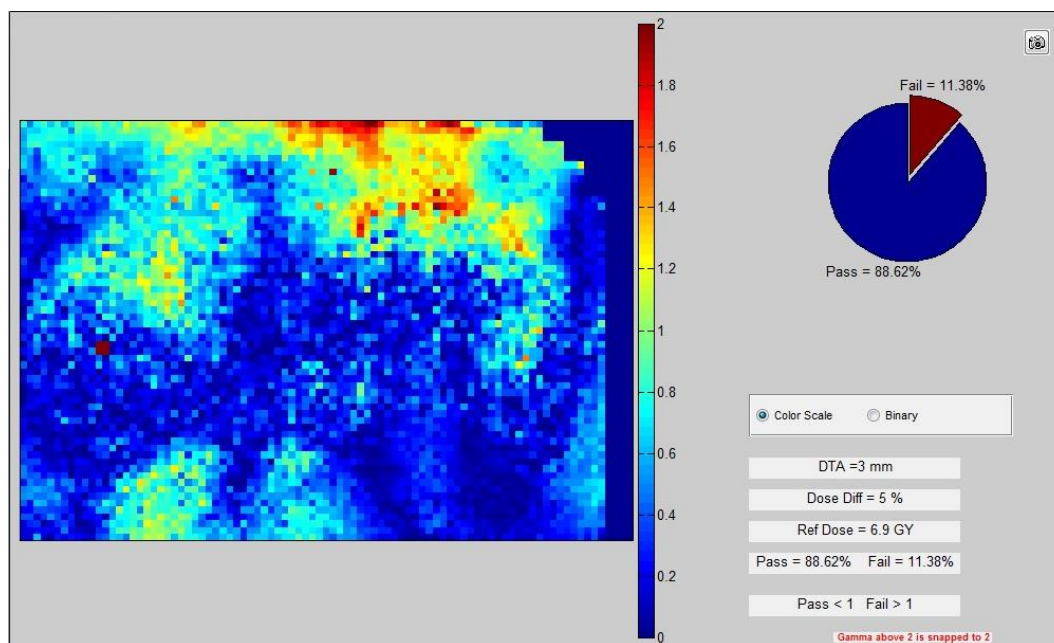


Figure 7.127: IMRT head and neck delivery comparison for the axial plane of Head and Neck Plan #1 with respect to TPS calculated dose. Agreement was evaluated using a $\pm 5\%/3\text{mm}$ gamma criterion and 88.6% of pixels passed.

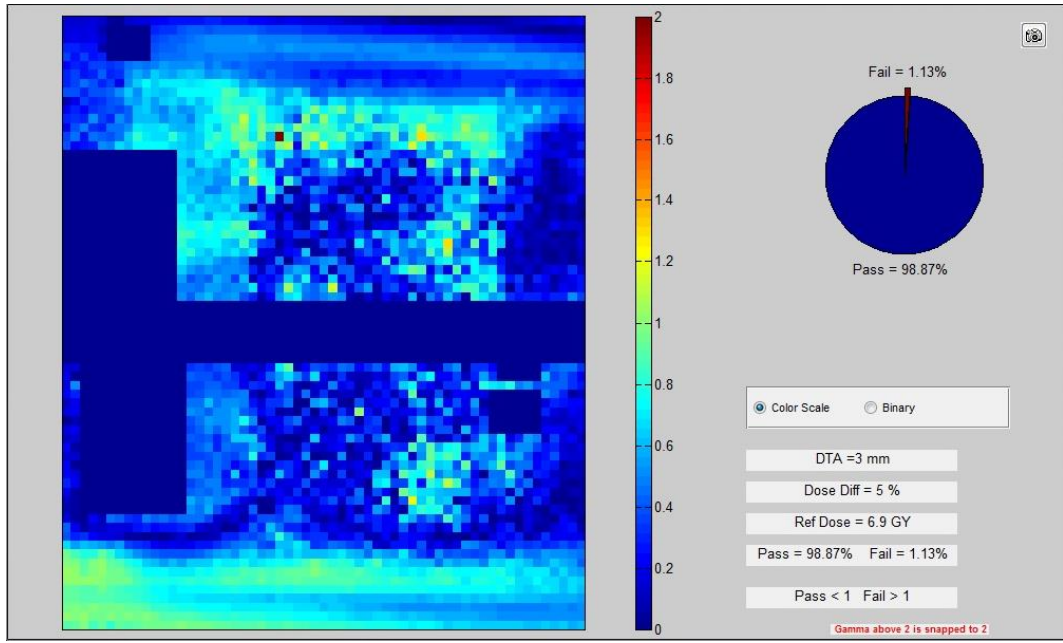


Figure 7.128: IMRT head and neck delivery comparison for the sagittal plane of Head and Neck Plan #1 with respect to TPS calculated dose. Agreement was evaluated using a $\pm 5\%/3\text{mm}$ gamma criterion and 98.9% of pixels passed.

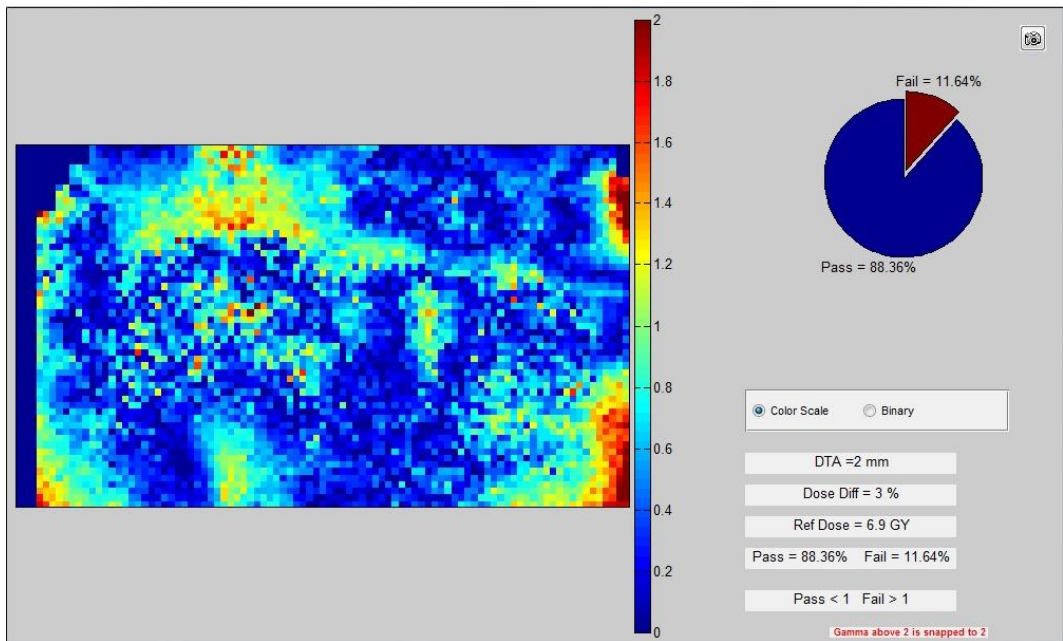


Figure 7.129: IMRT head and neck delivery comparison for the axial plane of Head and Neck Plan #2 with respect to DPM recalculated dose. Agreement was evaluated using a $\pm 3\%/2\text{mm}$ gamma criterion and 88.4% of pixels passed.

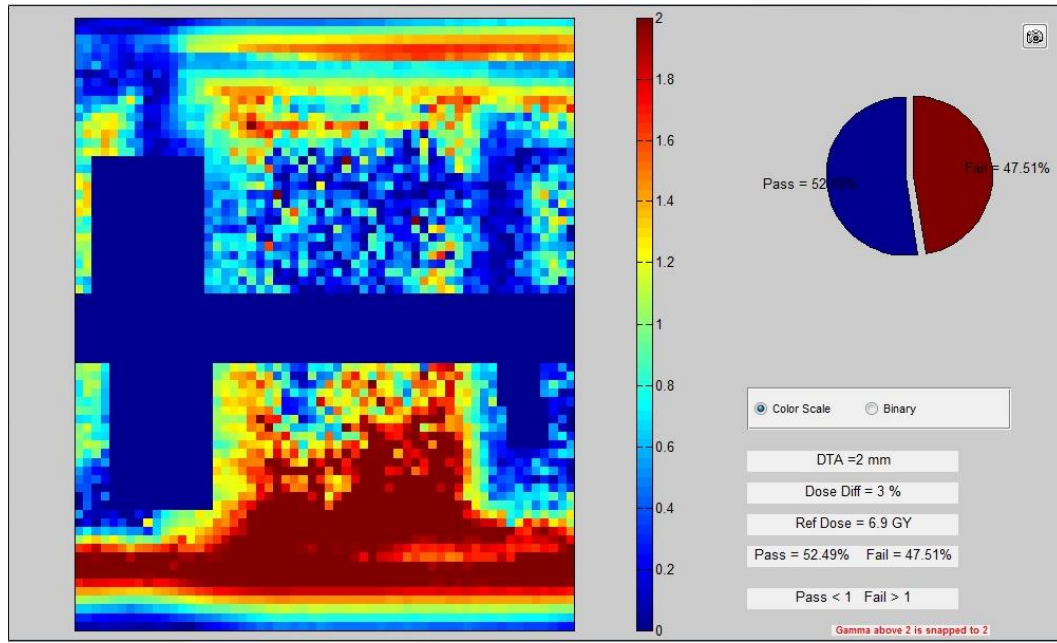


Figure 7.130: IMRT head and neck delivery comparison for the sagittal plane of Head and Neck Plan #2 with respect to DPM recalculated dose. Agreement was evaluated using a $\pm 3\%/2\text{mm}$ gamma criterion and 52.5% of pixels passed.

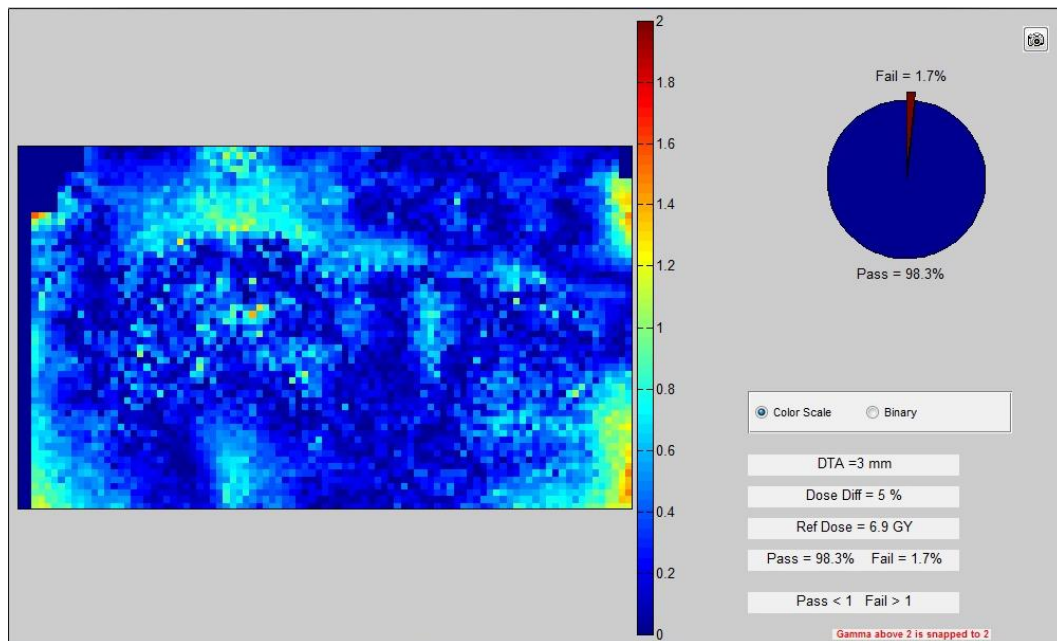


Figure 7.131: IMRT head and neck delivery comparison for the axial plane of Head and Neck Plan #2 with respect to DPM recalculated dose. Agreement was evaluated using a $\pm 5\%/3\text{mm}$ gamma criterion and 98.3% of pixels passed.

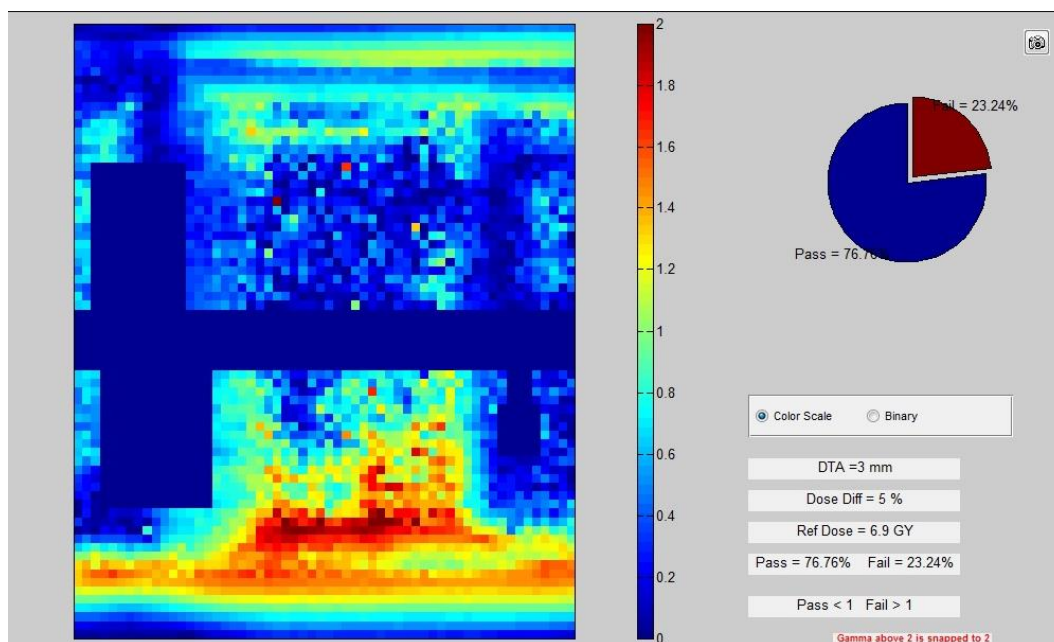


Figure 7.132: IMRT head and neck delivery comparison for the sagittal plane of Head and Neck Plan #2 with respect to DPM recalculated dose. Agreement was evaluated using a $\pm 5\%/3\text{mm}$ gamma criterion and 76.8% of pixels passed.

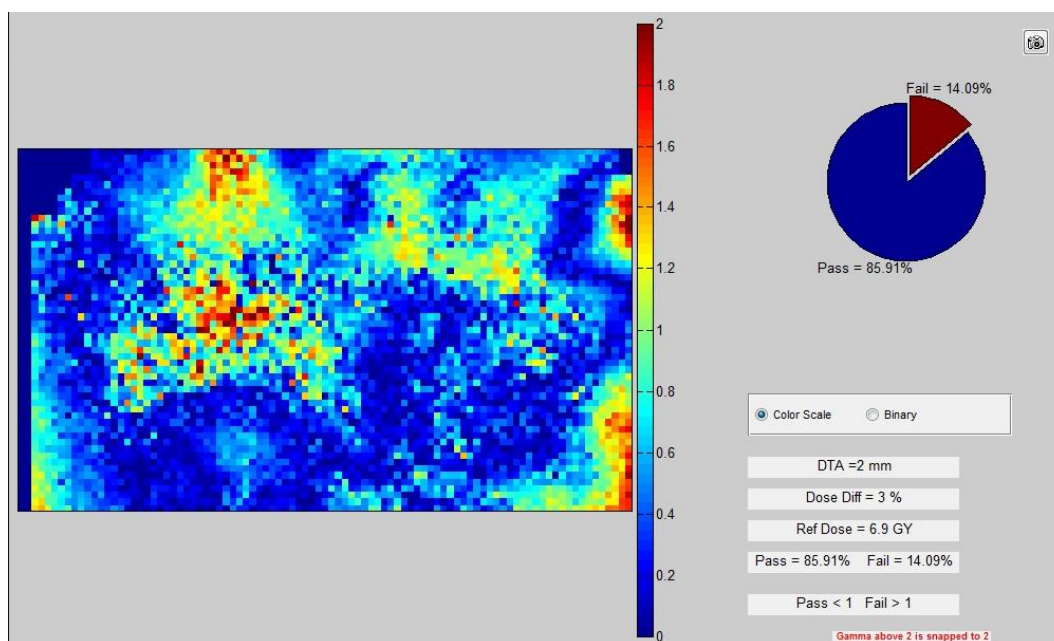


Figure 7.133: IMRT head and neck delivery comparison for the axial plane of Head and Neck Plan #2 with respect to TPS calculated dose. Agreement was evaluated using a $\pm 3\%/2\text{mm}$ gamma criterion and 85.9% of pixels passed.

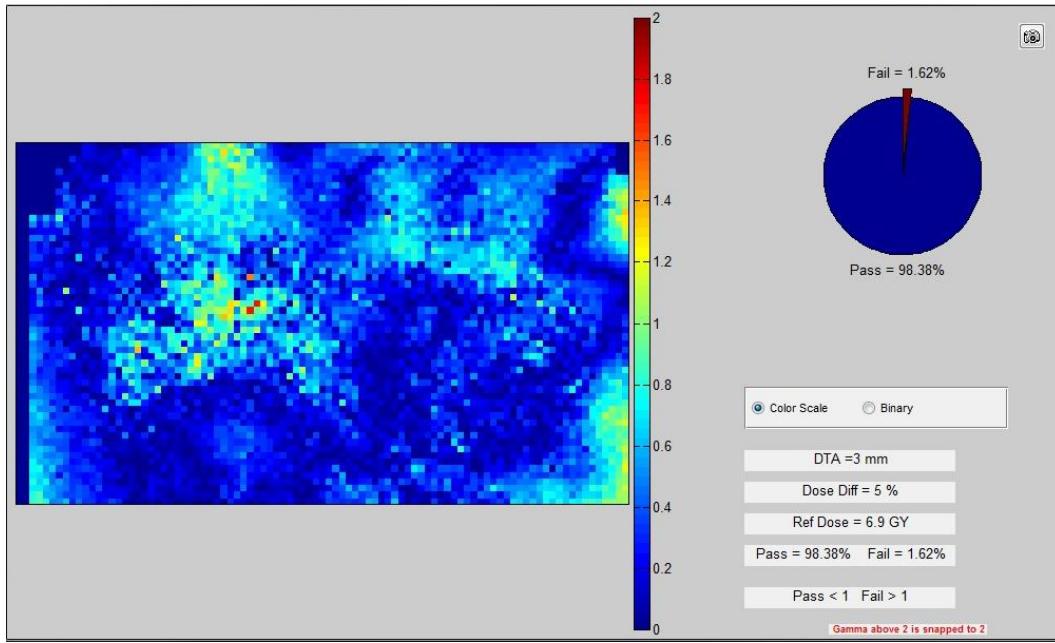


Figure 7.134: IMRT head and neck delivery comparison for the axial plane of Head and Neck Plan #2 with respect to TPS calculated dose. Agreement was evaluated using a $\pm 3\%/2\text{mm}$ gamma criterion and 69.8% of pixels passed.

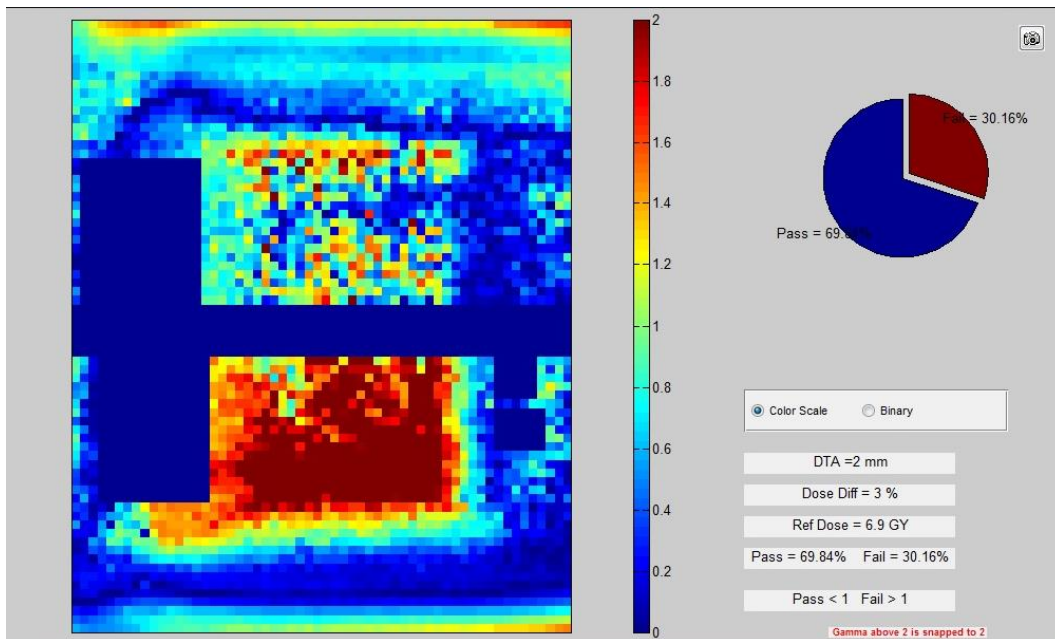


Figure 7.135: IMRT head and neck delivery comparison for the sagittal plane of Head and Neck Plan #2 with respect to TPS calculated dose. Agreement was evaluated using a $\pm 5\%/3\text{mm}$ gamma criterion and 98.4% of pixels passed.

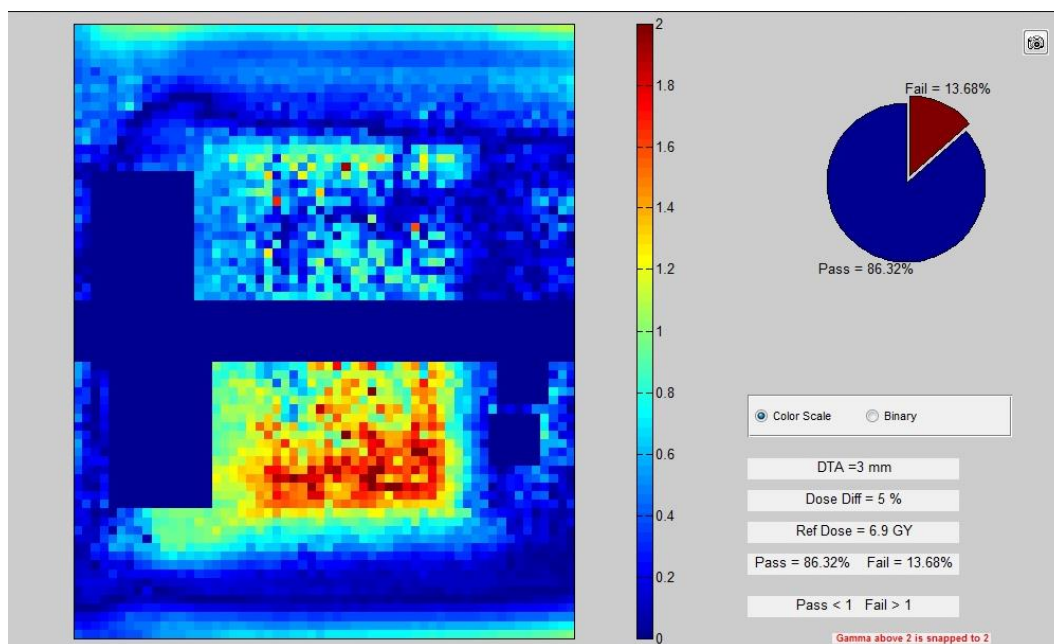


Figure 7.136: IMRT head and neck delivery comparison for the sagittal plane of Head and Neck Plan #2 with respect to TPS calculated dose. Agreement was evaluated using a $\pm 5\%/3\text{mm}$ gamma criterion and 86.3% of pixels passed.

7.9.2 Lung Phantom Audits

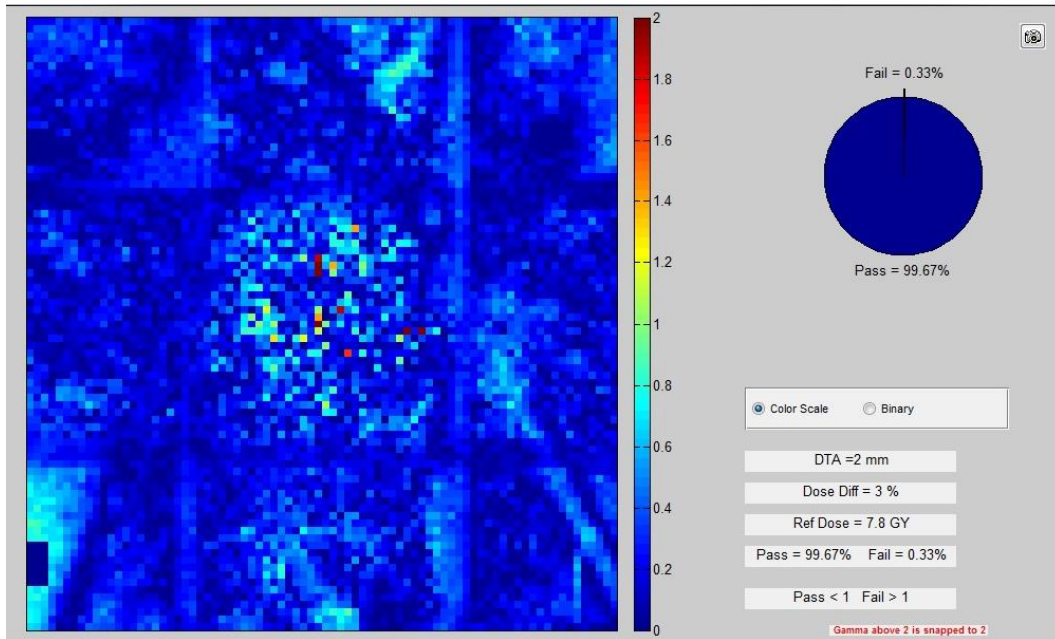


Figure 7.137: Lung phantom delivery comparison for the axial plane of Lung Plan #1 with respect to DPM recalculated dose. Agreement was evaluated using a $\pm 3\%/2\text{mm}$ gamma criterion and 99.7% of pixels passed.

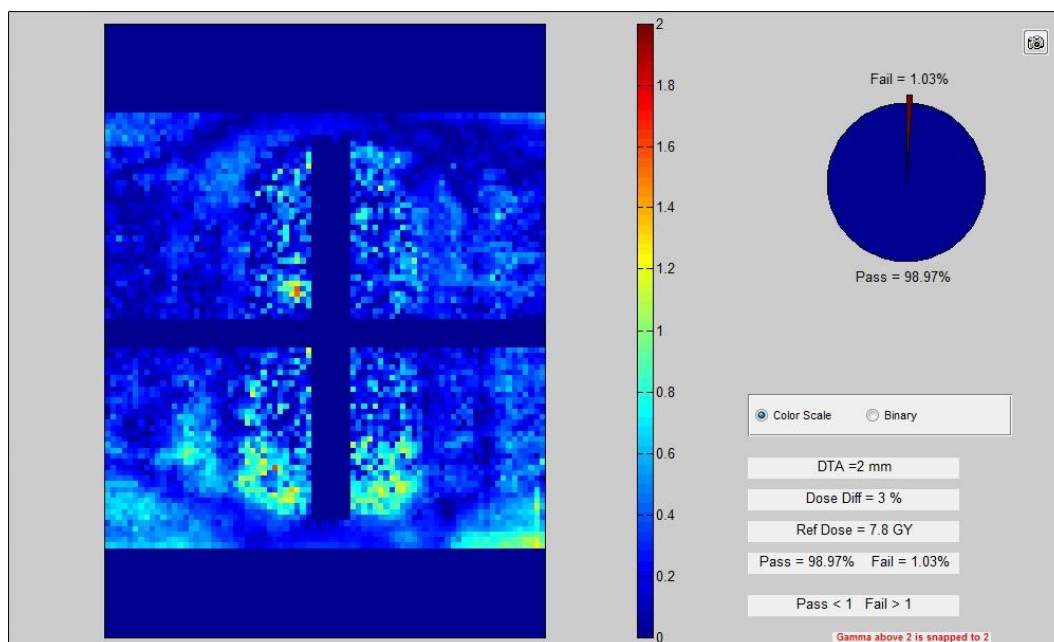


Figure 7.138: Lung phantom delivery comparison for the coronal plane of Lung Plan #1 with respect to DPM recalculated dose. Agreement was evaluated using a $\pm 3\%/2\text{mm}$ gamma criterion and 99.0% of pixels passed.

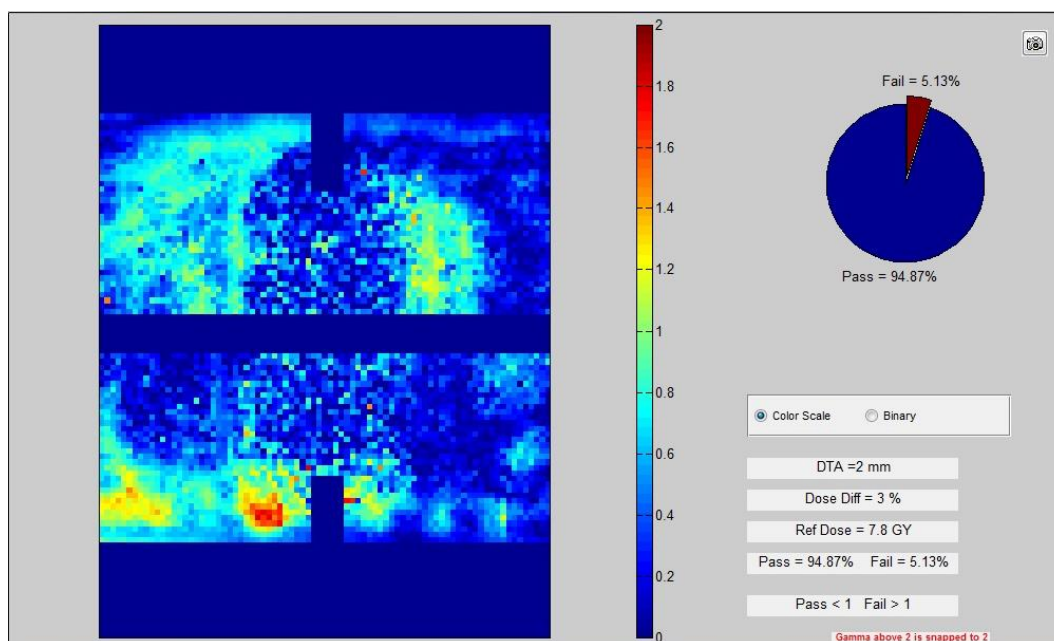


Figure 7.139: Lung phantom delivery comparison for the sagittal plane of Lung Plan #1 with respect to DPM recalculated dose. Agreement was evaluated using a $\pm 3\%/2\text{mm}$ gamma criterion and 94.9% of pixels passed.

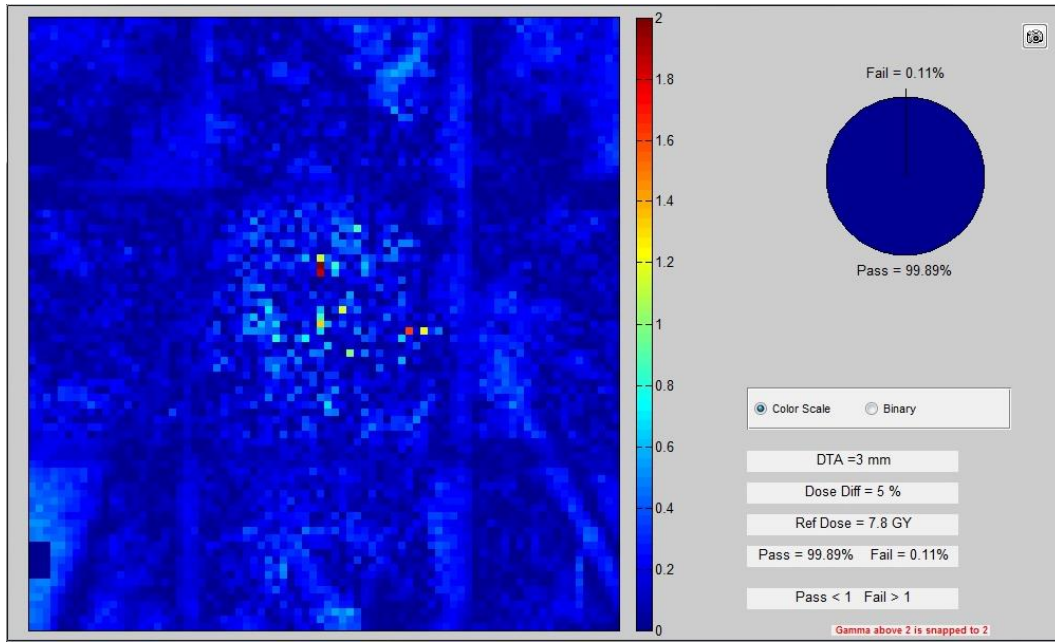


Figure 7.140: Lung phantom delivery comparison for the axial plane of Lung Plan #1 with respect to DPM recalculated dose. Agreement was evaluated using a $\pm 5\%/3\text{mm}$ gamma criterion and 99.9% of pixels passed.

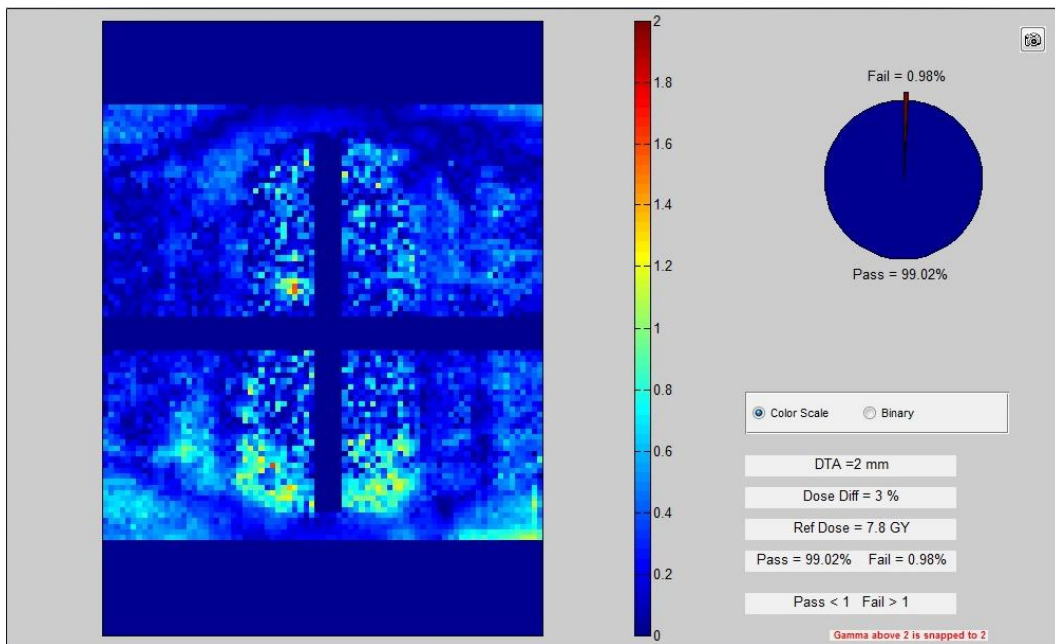


Figure 7.141: Lung phantom delivery comparison for the coronal plane of Lung Plan #1 with respect to DPM recalculated dose. Agreement was evaluated using a $\pm 5\%/3\text{mm}$ gamma criterion and 99.0% of pixels passed.

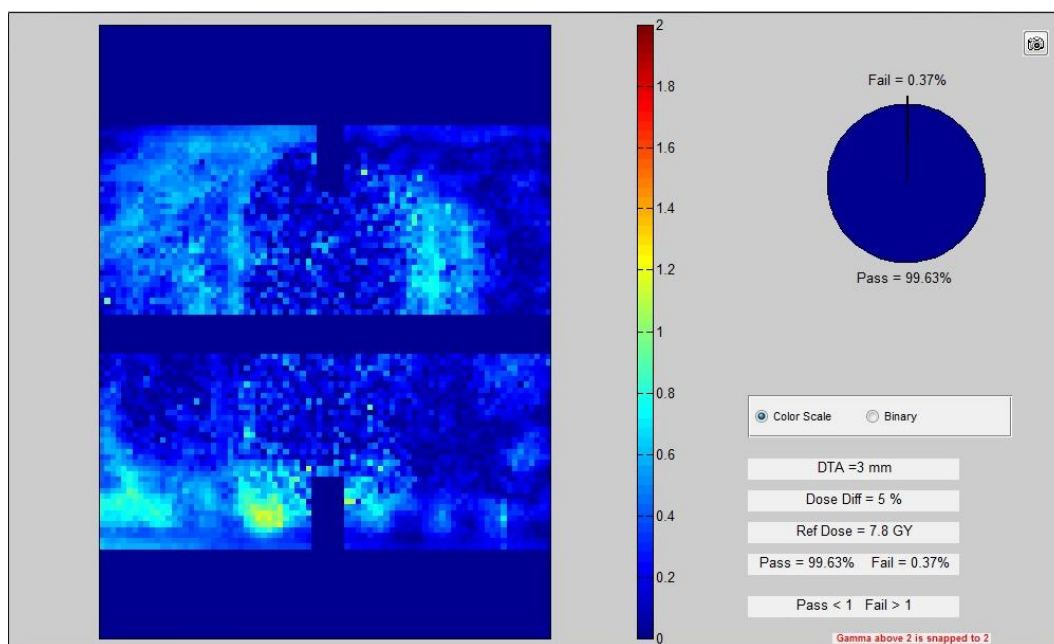


Figure 7.142: Lung phantom delivery comparison for the sagittal plane of Lung Plan #1 with respect to DPM recalculated dose. Agreement was evaluated using a $\pm 5\%/3\text{mm}$ gamma criterion and 99.6% of pixels passed.

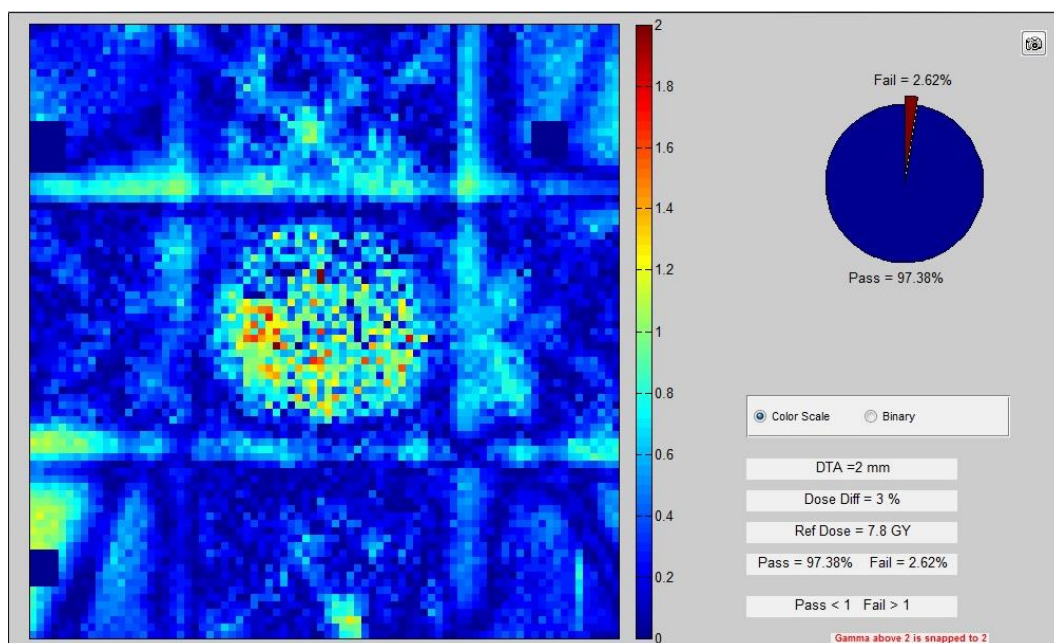


Figure 7.143: Lung phantom delivery comparison for the axial plane of Lung Plan #1 with respect to TPS calculated dose. Agreement was evaluated using a $\pm 3\%/2\text{mm}$ gamma criterion and 97.4% of pixels passed.

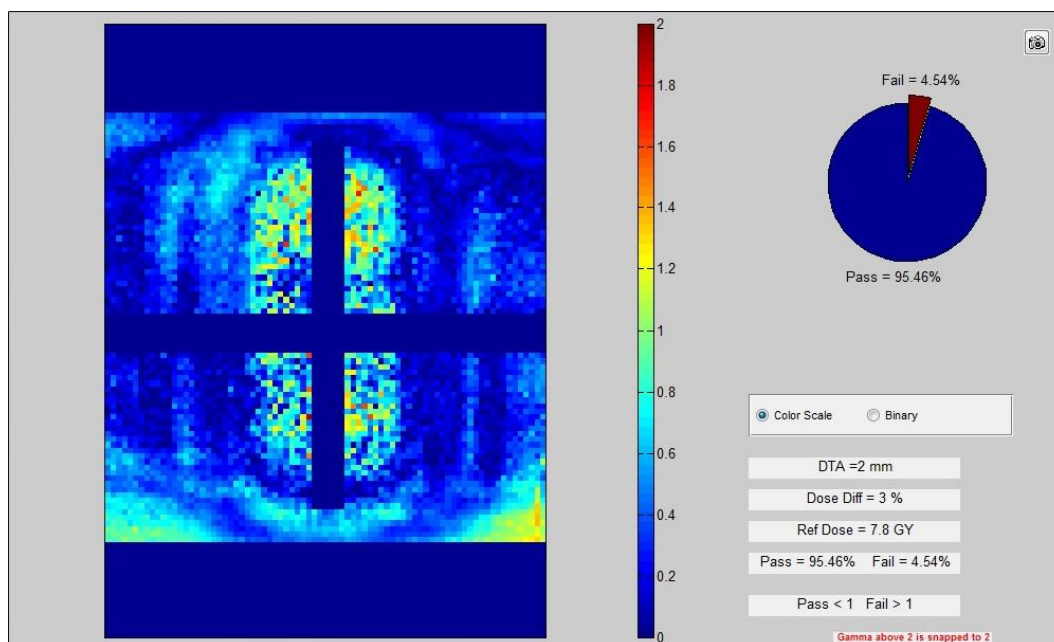


Figure 7.144: Lung phantom delivery comparison for the coronal plane of Lung Plan #1 with respect to TPS calculated dose. Agreement was evaluated using a $\pm 3\%/2\text{mm}$ gamma criterion and 95.5% of pixels passed.

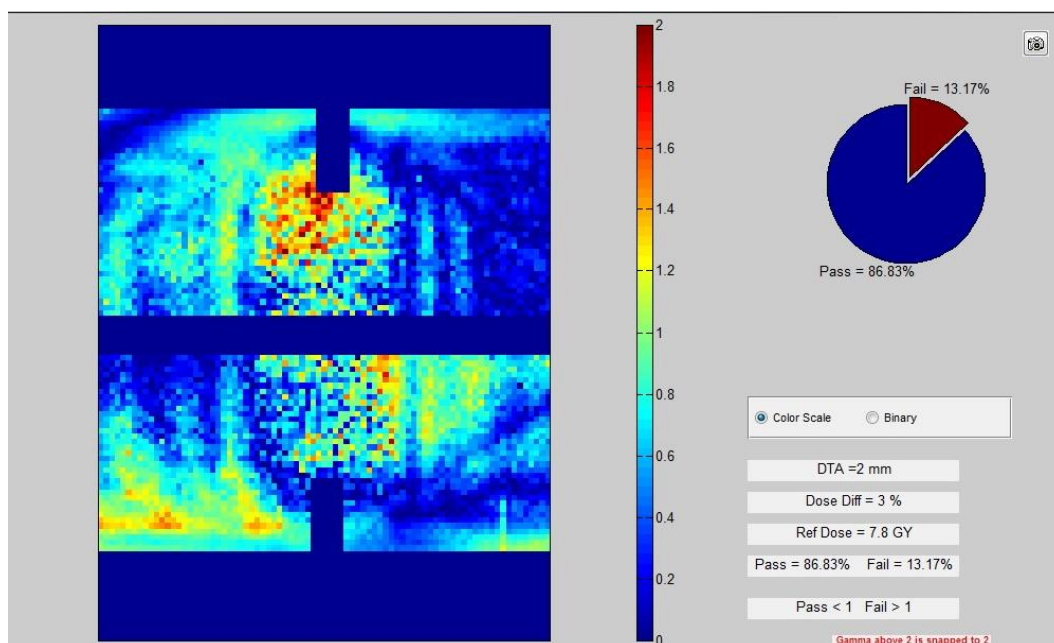


Figure 7.145: Lung phantom delivery comparison for the sagittal plane of Lung Plan #1 with respect to TPS calculated dose. Agreement was evaluated using a $\pm 3\%/2\text{mm}$ gamma criterion and 86.8% of pixels passed.

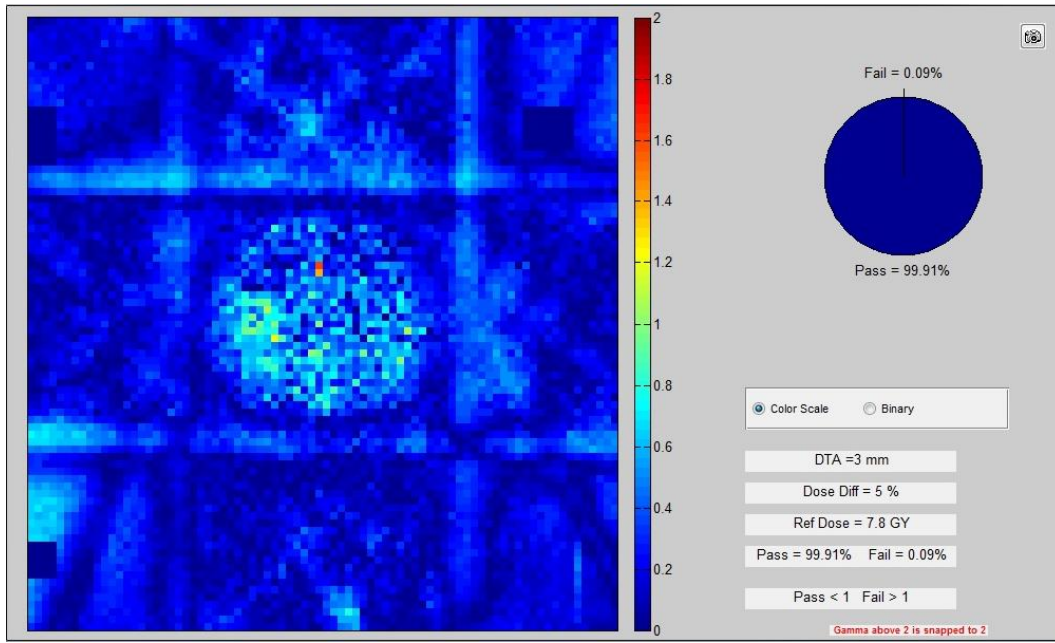


Figure 7.146: Lung phantom delivery comparison for the axial plane of Lung Plan #1 with respect to TPS calculated dose. Agreement was evaluated using a $\pm 5\%/3\text{mm}$ gamma criterion and 99.9% of pixels passed.

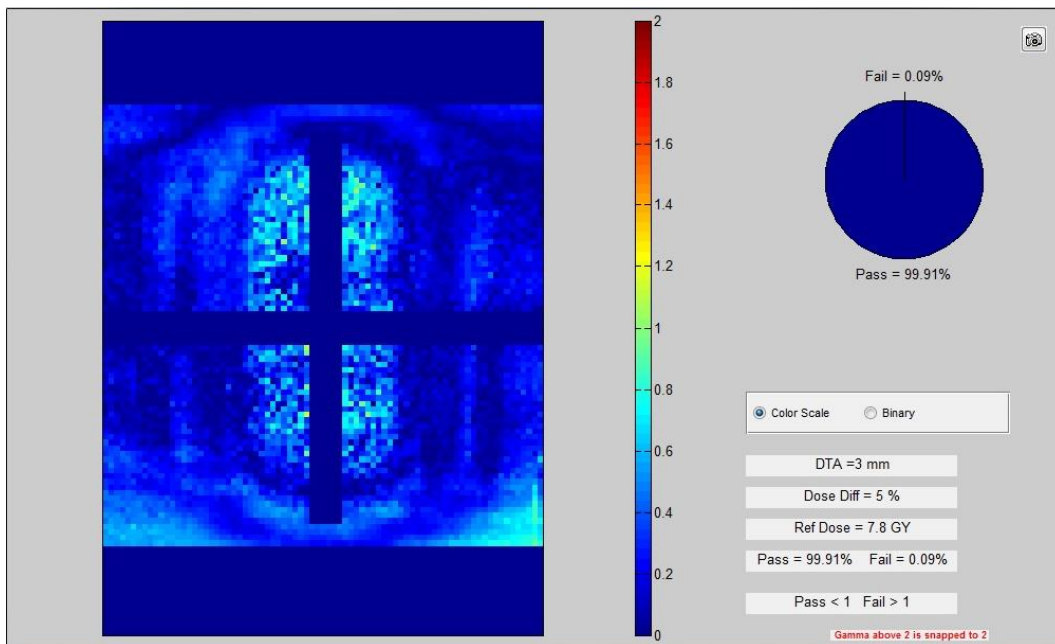


Figure 7.147: Lung phantom delivery comparison for the coronal plane of Lung Plan #1 with respect to TPS calculated dose. Agreement was evaluated using a $\pm 5\%/3\text{mm}$ gamma criterion and 99.9% of pixels passed.

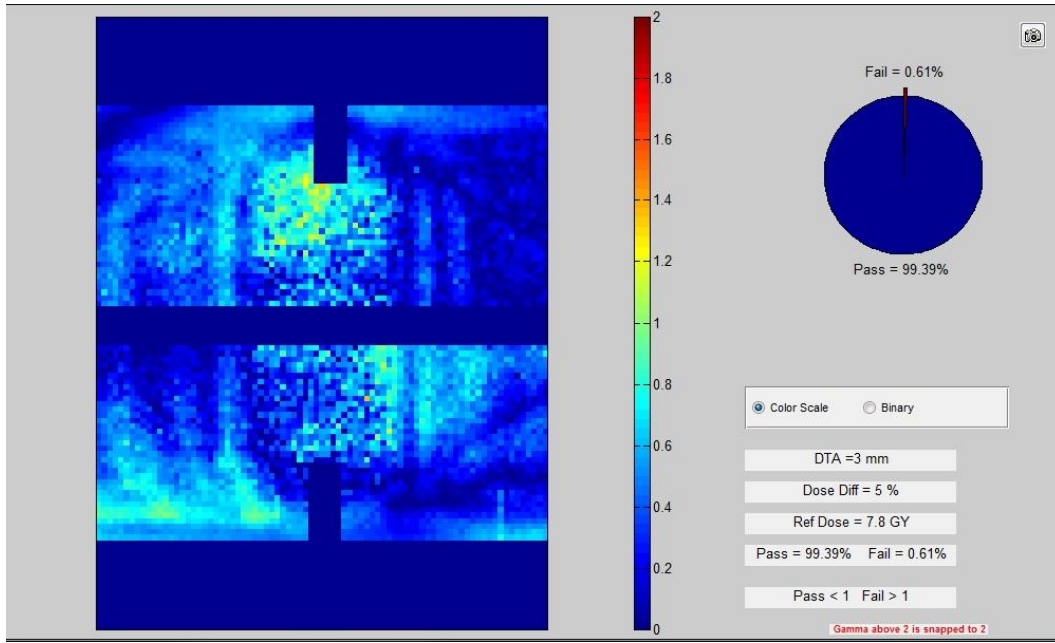


Figure 7.148: Lung phantom delivery comparison for the sagittal plane of Lung Plan #1 with respect to TPS calculated dose. Agreement was evaluated using a $\pm 5\%/3\text{mm}$ gamma criterion and 99.4% of pixels passed.

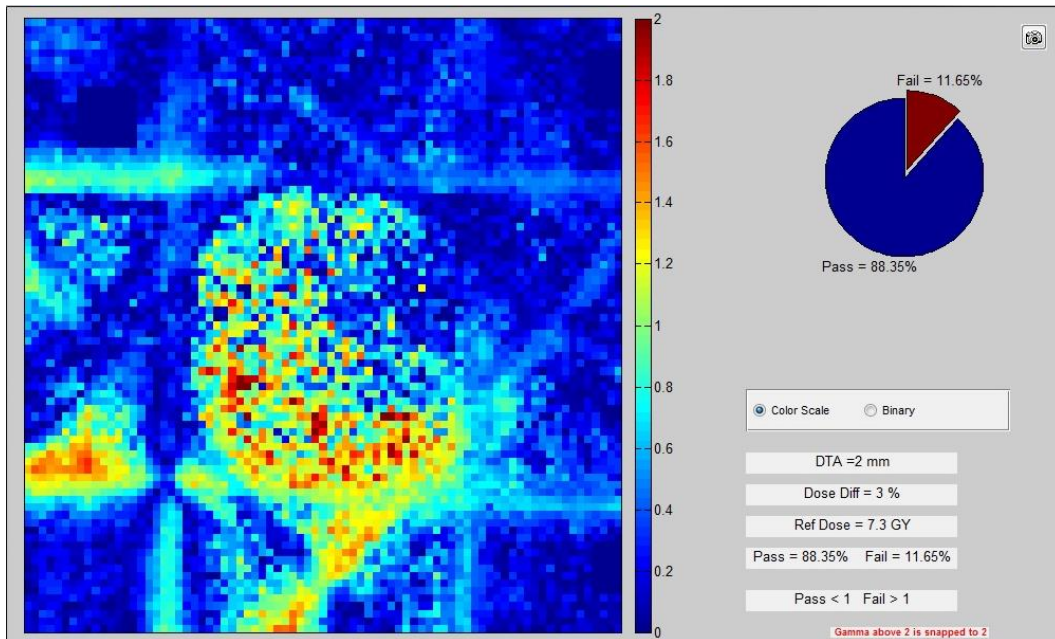


Figure 7.149: Lung phantom delivery comparison for the axial plane of Lung Plan #2 with respect to DPM recalculated dose. Agreement was evaluated using a $\pm 3\%/2\text{mm}$ gamma criterion and 88.4% of pixels passed.

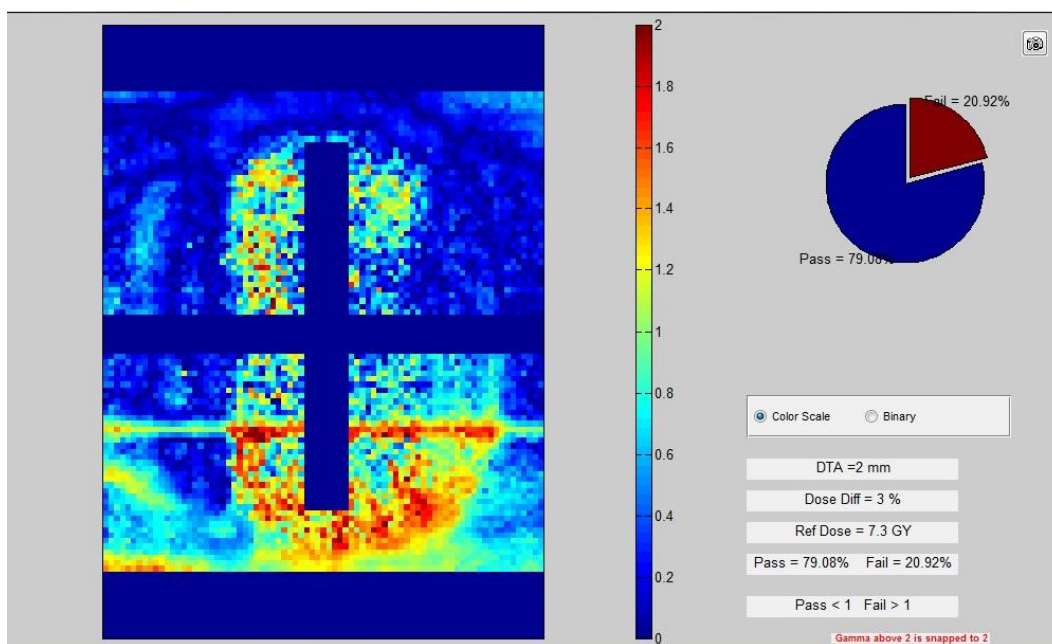


Figure 7.150: Lung phantom delivery comparison for the coronal plane of Lung Plan #2 with respect to DPM recalculated dose. Agreement was evaluated using a $\pm 3\%/2\text{mm}$ gamma criterion and 79.1% of pixels passed.

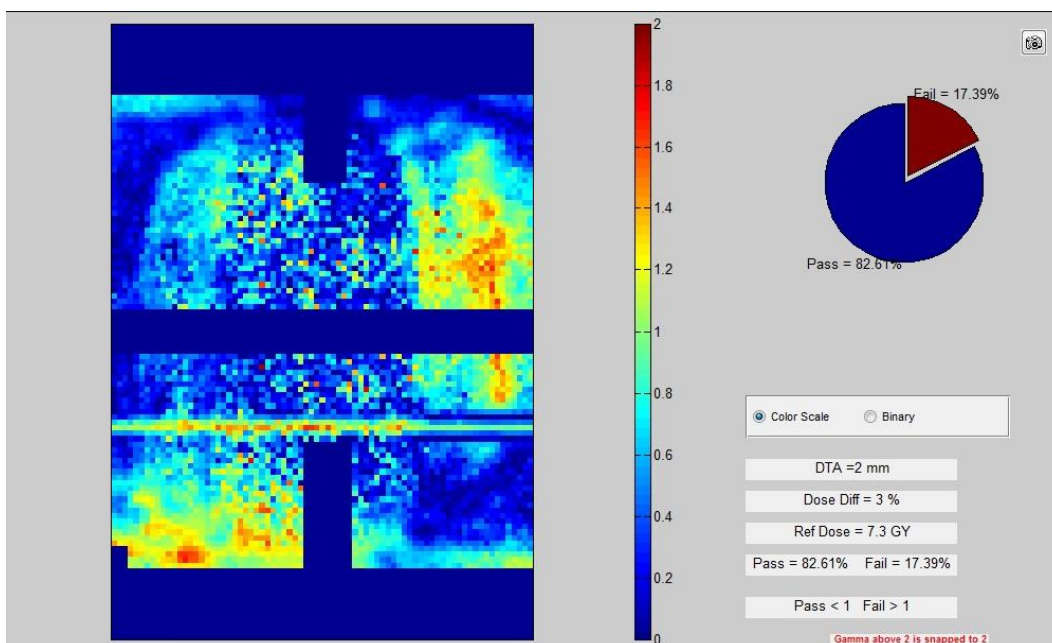


Figure 7.151: Lung phantom delivery comparison for the sagittal plane of Lung Plan #2 with respect to DPM recalculated dose. Agreement was evaluated using a $\pm 3\%/2\text{mm}$ gamma criterion and 82.6% of pixels passed.

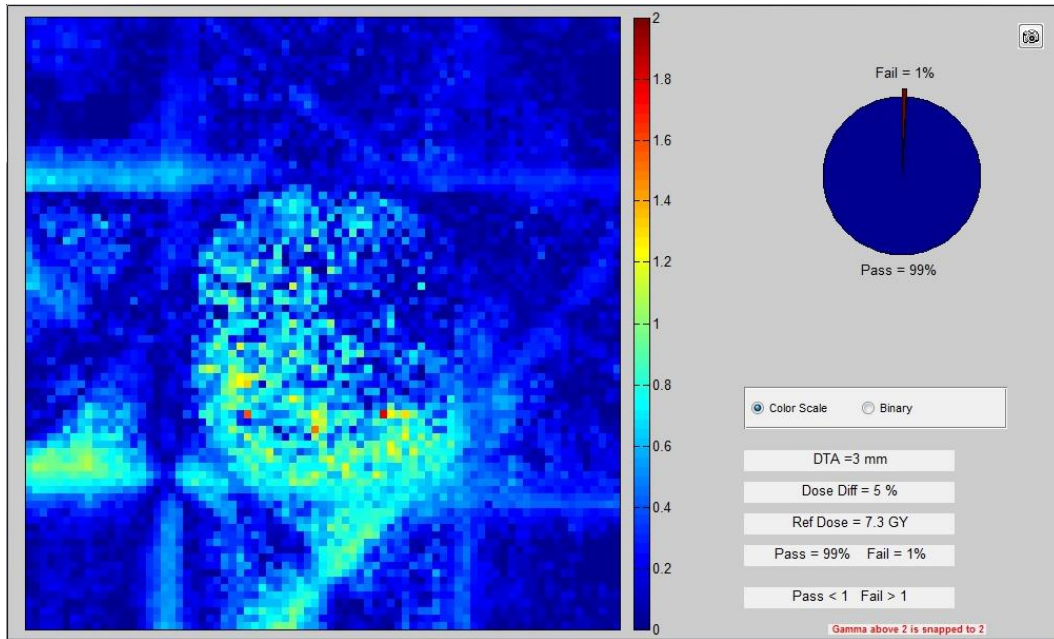


Figure 7.152: Lung phantom delivery comparison for the axial plane of Lung Plan #2 with respect to DPM recalculated dose. Agreement was evaluated using a $\pm 5\%/3\text{mm}$ gamma criterion and 99.0% of pixels passed.

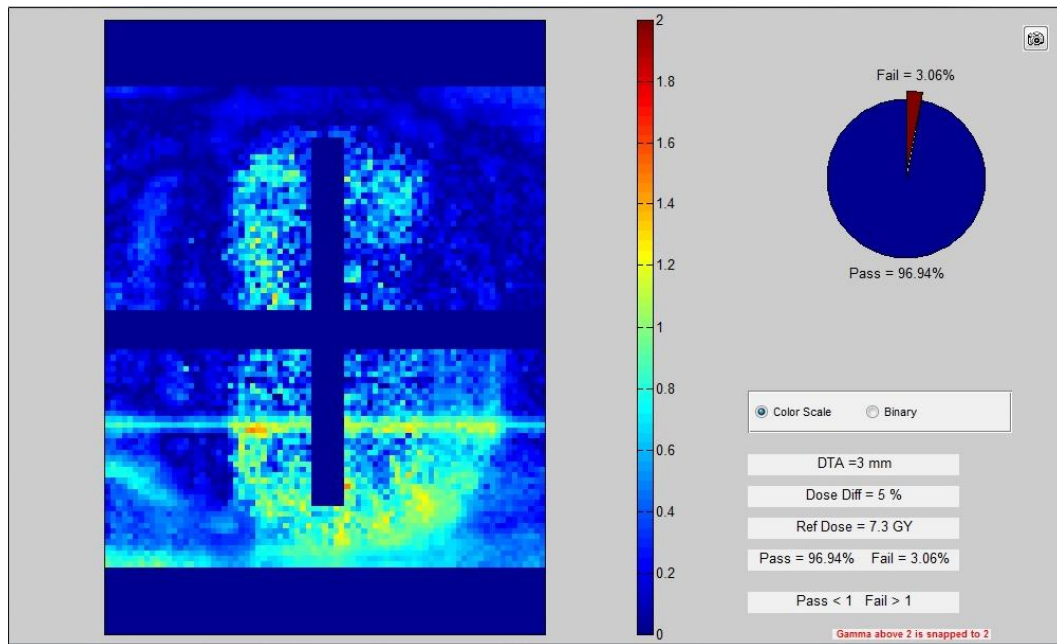


Figure 7.153: Lung phantom delivery comparison for the coronal plane of Lung Plan #2 with respect to DPM recalculated dose. Agreement was evaluated using a $\pm 5\%/3\text{mm}$ gamma criterion and 96.9% of pixels passed.

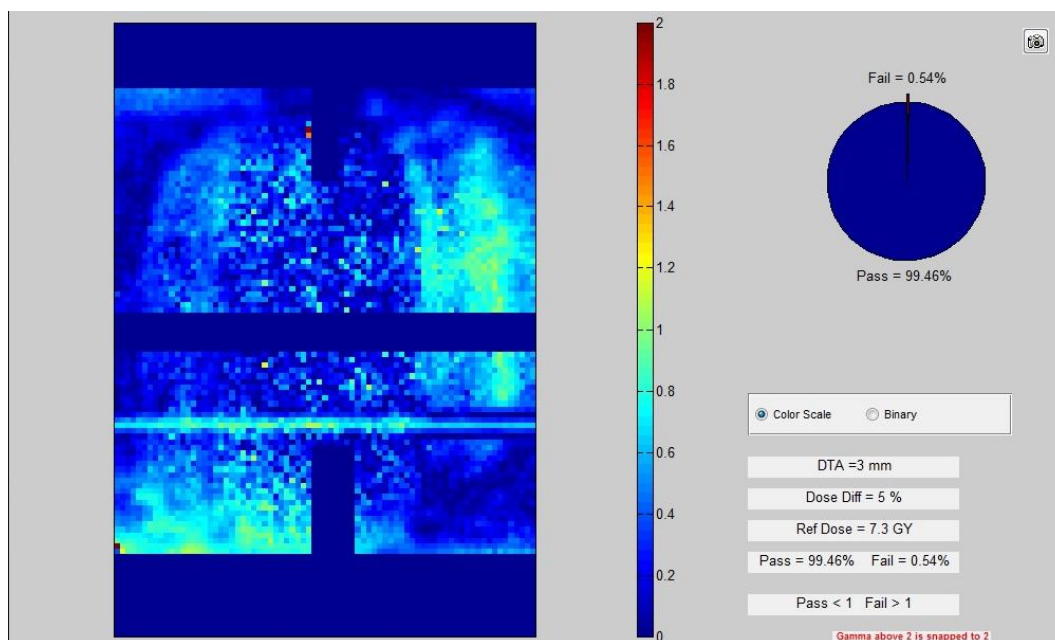


Figure 7.154: Lung phantom delivery comparison for the sagittal plane of Lung Plan #2 with respect to DPM recalculated dose. Agreement was evaluated using a $\pm 5\%/3\text{mm}$ gamma criterion and 99.5% of pixels passed.

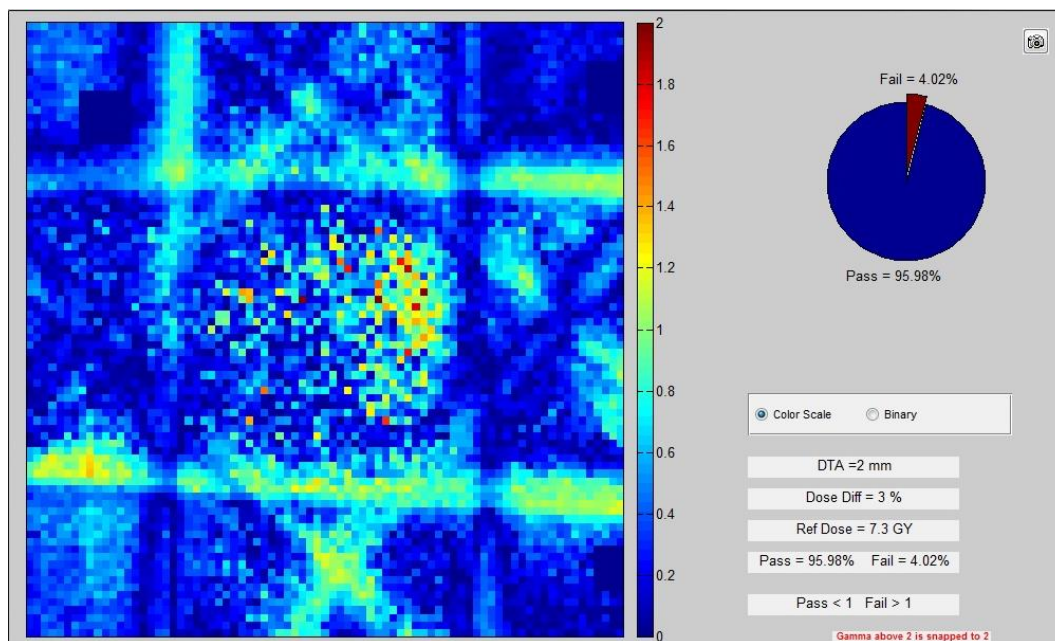


Figure 7.155: Lung phantom delivery comparison for the axial plane of Lung Plan #2 with respect to TPS calculated dose. Agreement was evaluated using a $\pm 3\%/2\text{mm}$ gamma criterion and 96.0% of pixels passed.

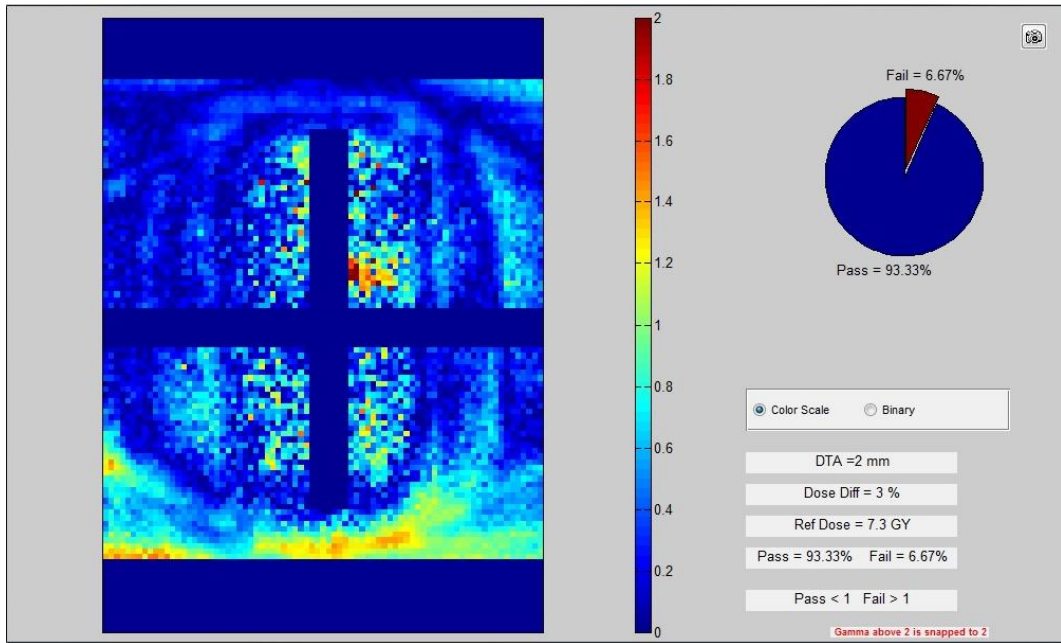


Figure 7.156: Lung phantom delivery comparison for the coronal plane of Lung Plan #2 with respect to TPS calculated dose. Agreement was evaluated using a $\pm 3\%/2\text{mm}$ gamma criterion and 93.3% of pixels passed.

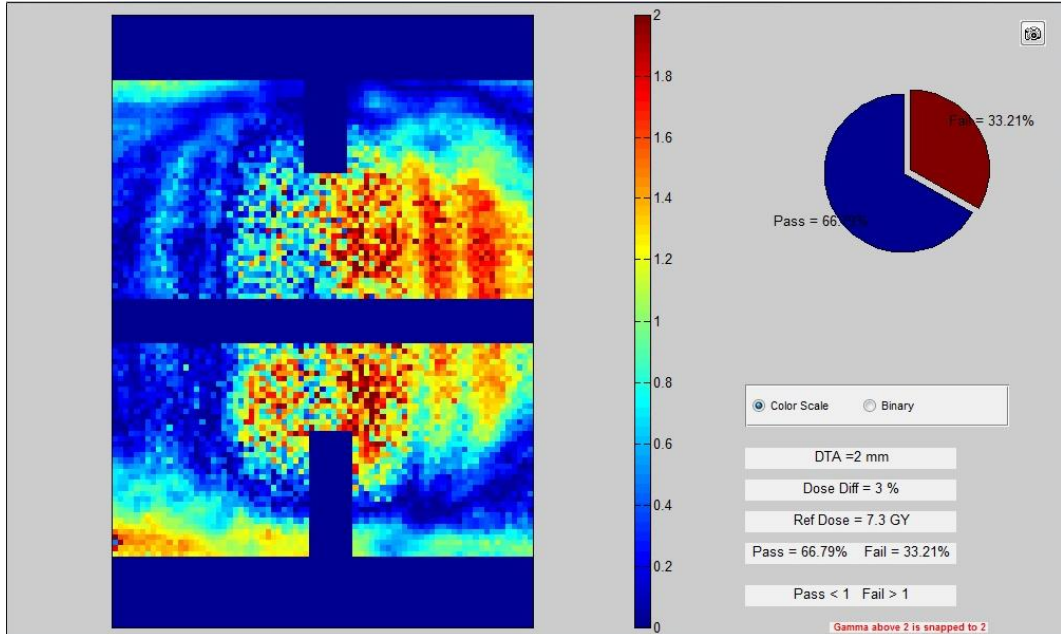


Figure 7.157: Lung phantom delivery comparison for the sagittal plane of Lung Plan #2 with respect to TPS calculated dose. Agreement was evaluated using a $\pm 3\%/2\text{mm}$ gamma criterion and 66.8% of pixels passed.

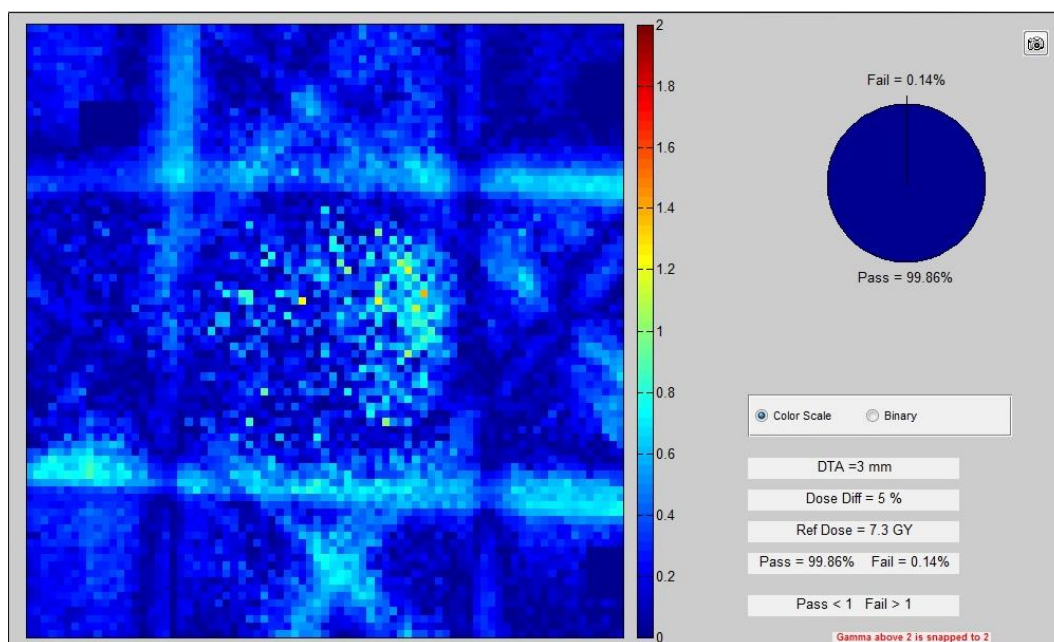


Figure 7.158: Lung phantom delivery comparison for the axial plane of Lung Plan #2 with respect to TPS calculated dose. Agreement was evaluated using a $\pm 5\%/3\text{mm}$ gamma criterion and 99.9% of pixels passed.

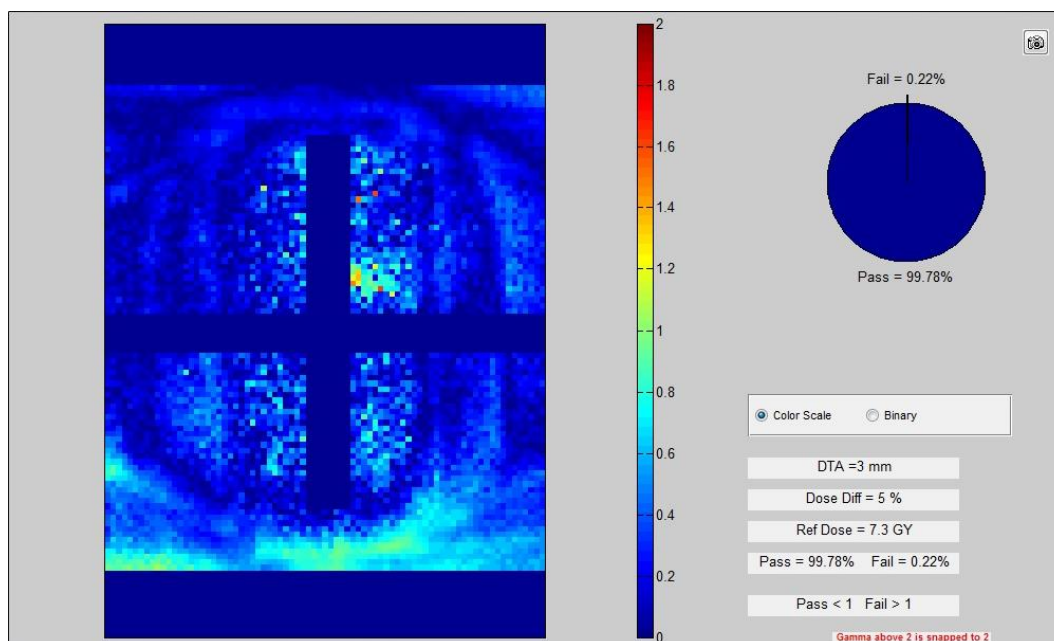


Figure 7.159: Lung phantom delivery comparison for the coronal plane of Lung Plan #2 with respect to TPS calculated dose. Agreement was evaluated using a $\pm 5\%/3\text{mm}$ gamma criterion and 99.8% of pixels passed.

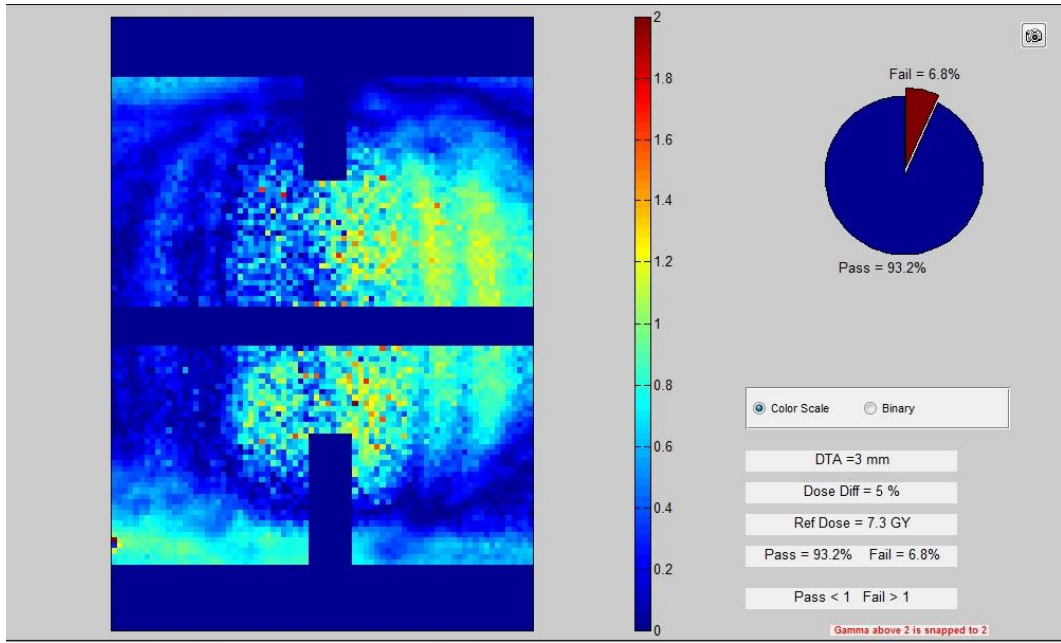


Figure 7.160: Lung phantom delivery comparison for the sagittal plane of Lung Plan #2 with respect to TPS calculated dose. Agreement was evaluated using a $\pm 5\%/3\text{mm}$ gamma criterion and 93.2% of pixels passed.

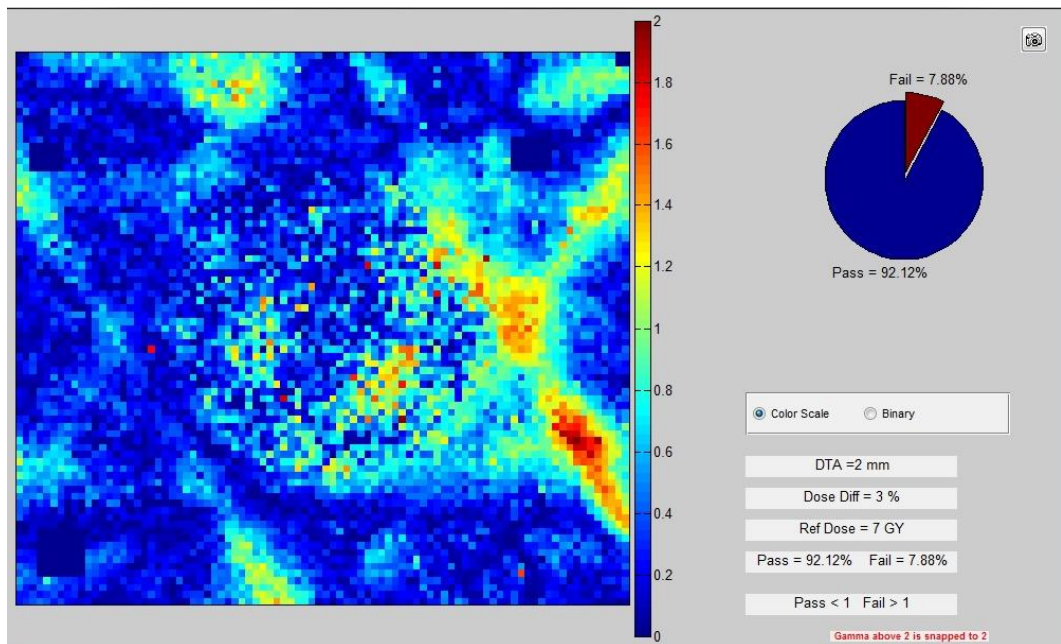


Figure 7.161: Lung phantom delivery comparison for the axial plane of Lung Plan #3 with respect to DPM recalculated dose. Agreement was evaluated using a $\pm 3\%/2\text{mm}$ gamma criterion and 92.1% of pixels passed.

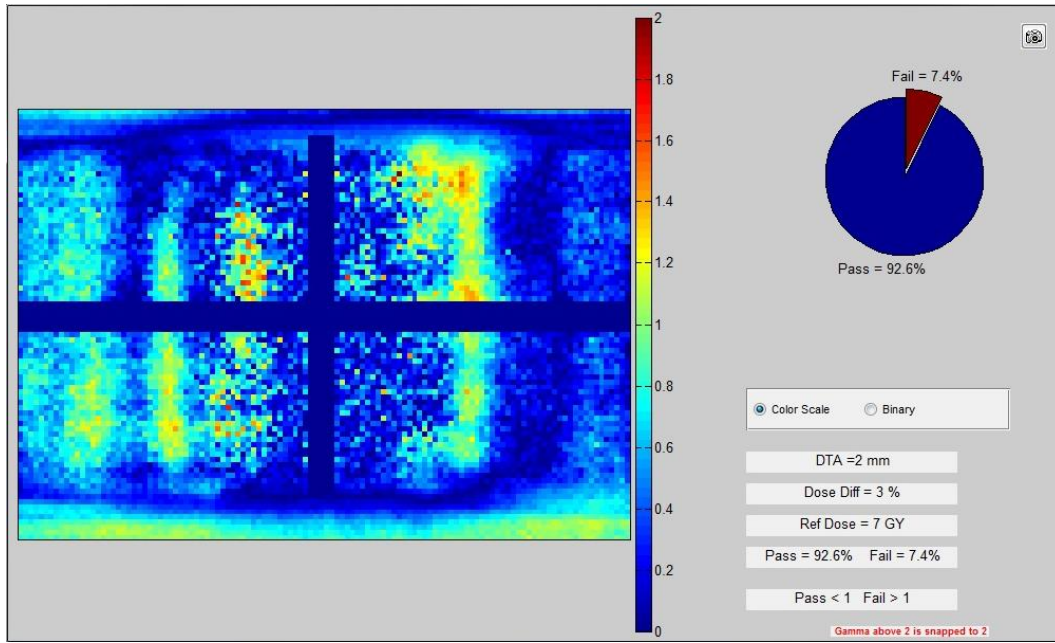


Figure 7.162: Lung phantom delivery comparison for the coronal plane of Lung Plan #3 with respect to DPM recalculated dose. Agreement was evaluated using a $\pm 3\%/2\text{mm}$ gamma criterion and 92.6% of pixels passed.

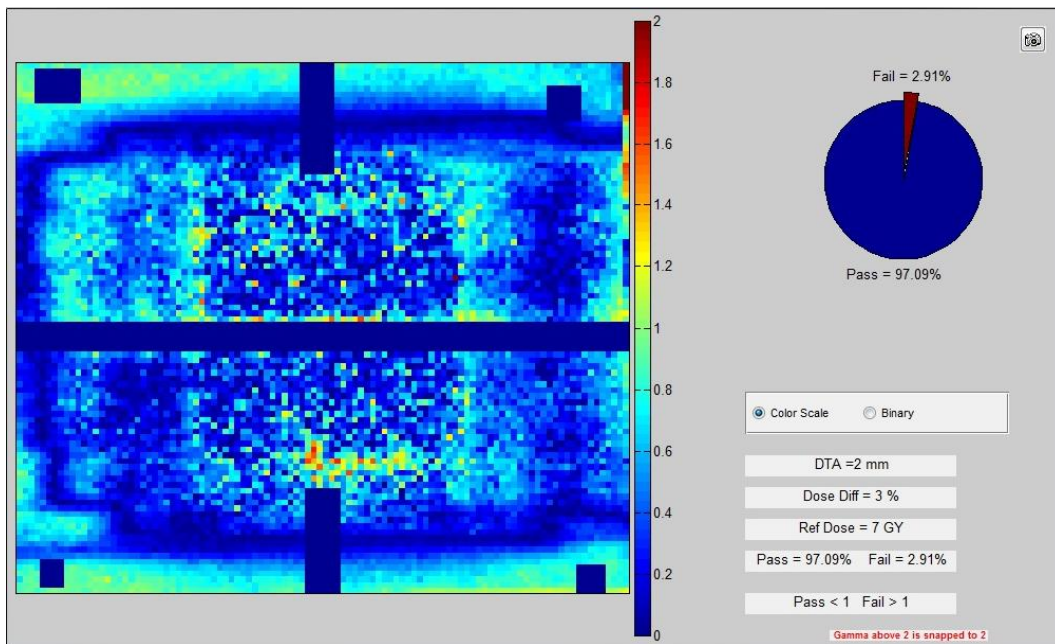


Figure 7.163: Lung phantom delivery comparison for the sagittal plane of Lung Plan #3 with respect to DPM recalculated dose. Agreement was evaluated using a $\pm 3\%/2\text{mm}$ gamma criterion and 97.1% of pixels passed.

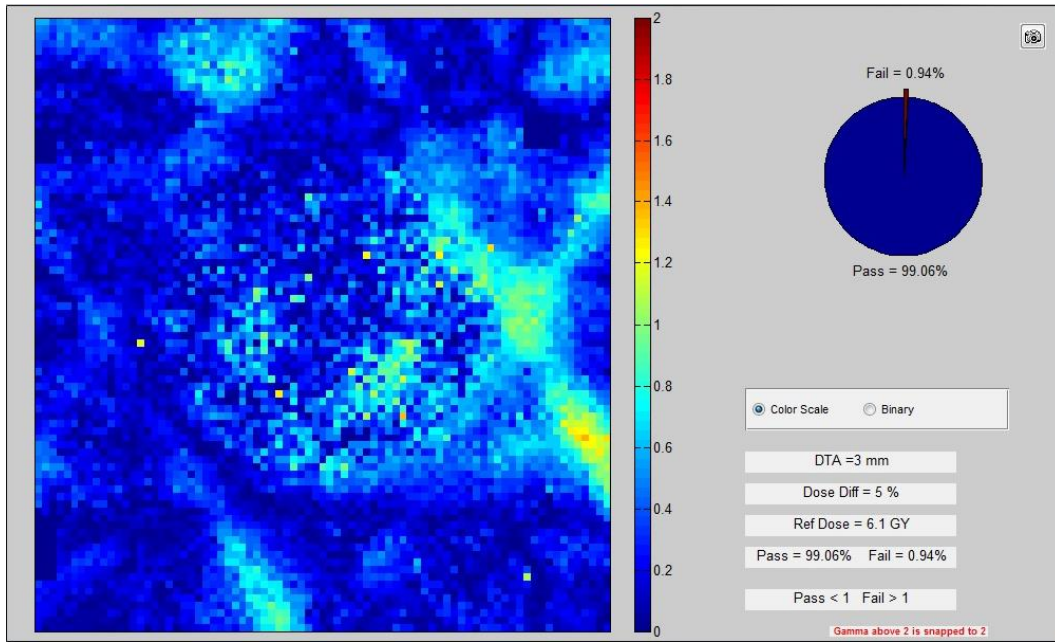


Figure 7.164: Lung phantom delivery comparison for the axial plane of Lung Plan #3 with respect to DPM recalculated dose. Agreement was evaluated using a $\pm 5\%/3\text{mm}$ gamma criterion and 99.1% of pixels passed.

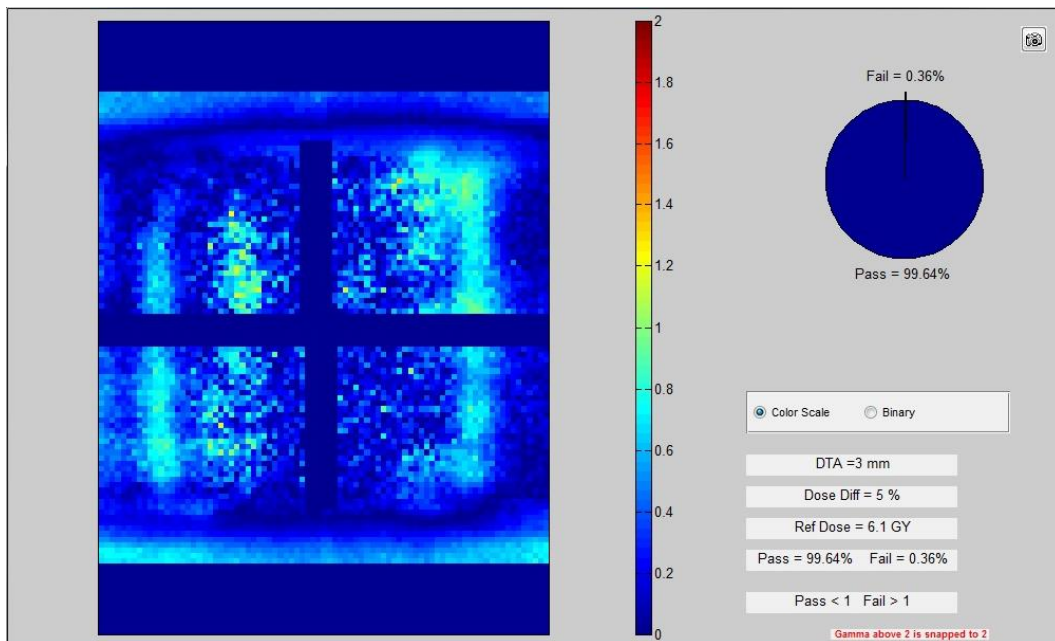


Figure 7.165: Lung phantom delivery comparison for the coronal plane of Lung Plan #3 with respect to DPM recalculated dose. Agreement was evaluated using a $\pm 5\%/3\text{mm}$ gamma criterion and 99.6% of pixels passed.

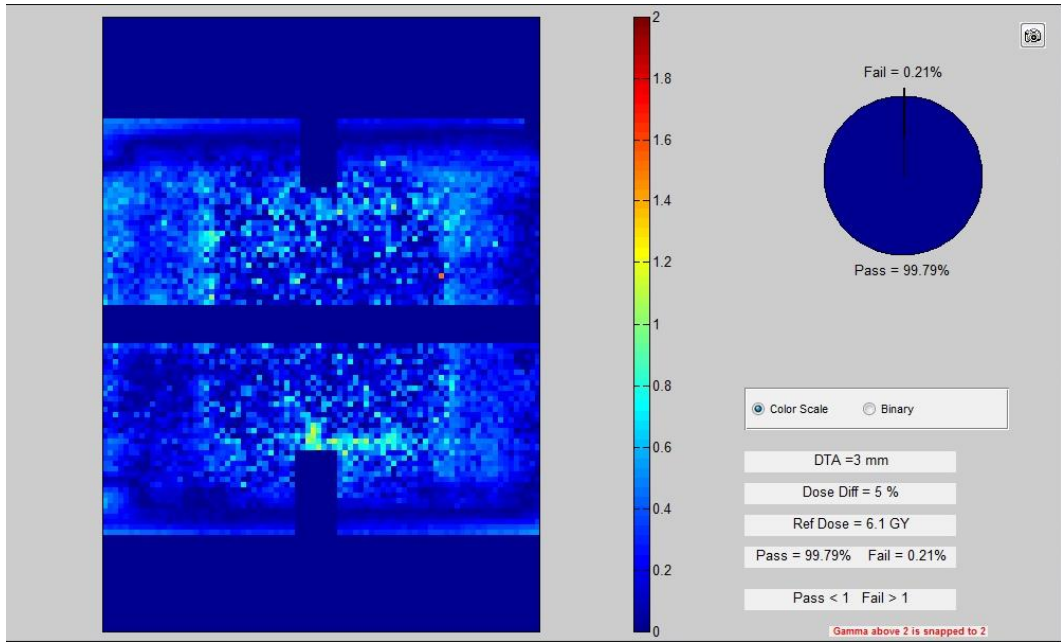


Figure 7.166: Lung phantom delivery comparison for the sagittal plane of Lung Plan #3 with respect to DPM recalculated dose. Agreement was evaluated using a $\pm 5\%/3\text{mm}$ gamma criterion and 99.8% of pixels passed.

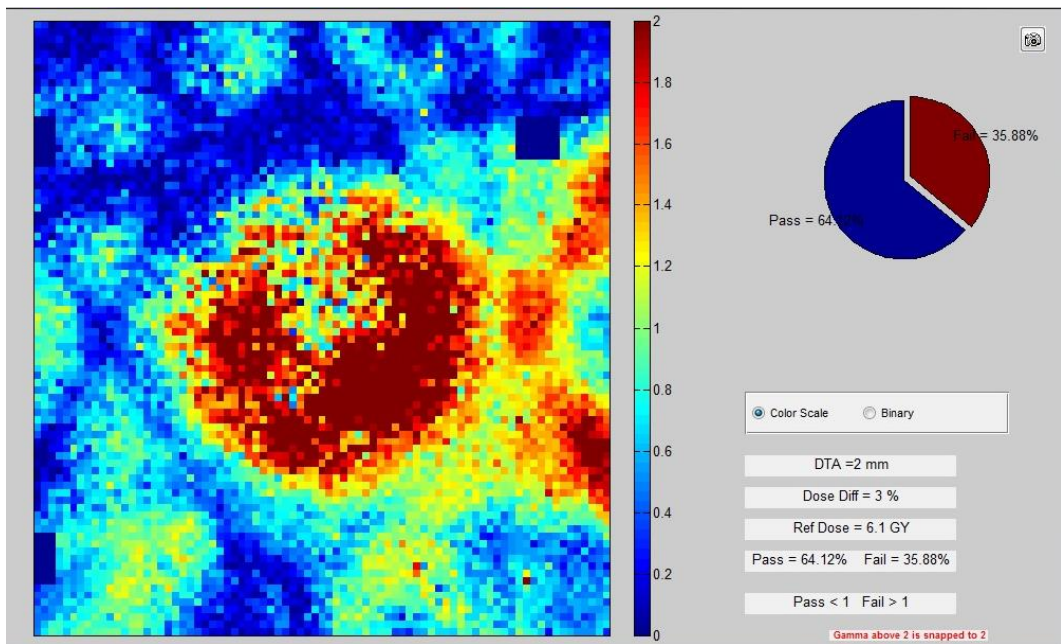


Figure 7.167: Lung phantom delivery comparison for the axial plane of Lung Plan #3 with respect to TPS calculated dose. Agreement was evaluated using a $\pm 3\%/2\text{mm}$ gamma criterion and 64.1% of pixels passed.

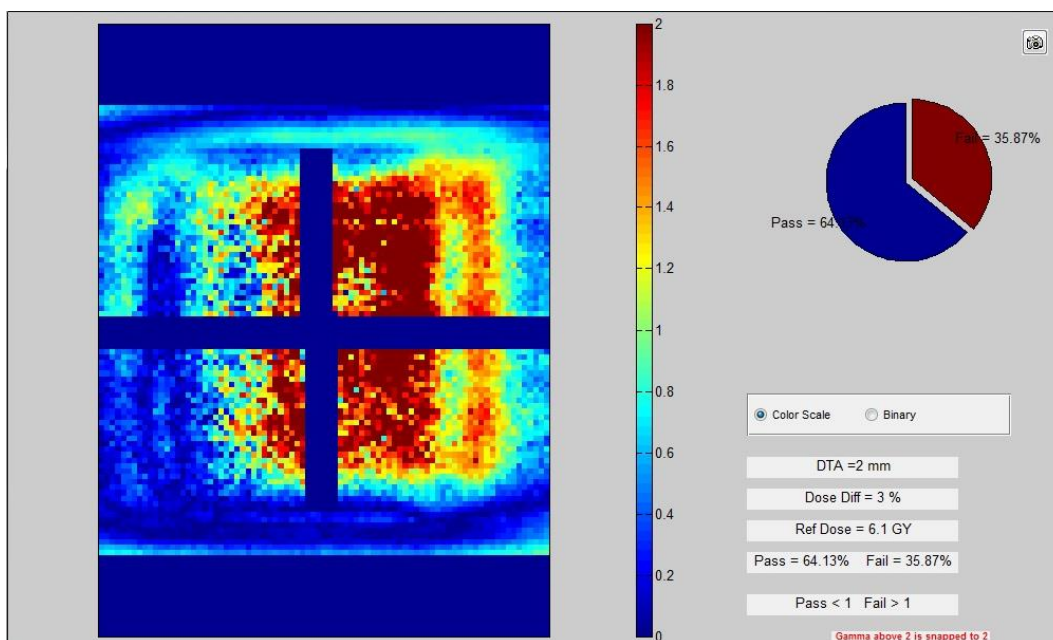


Figure 7.168: Lung phantom delivery comparison for the coronal plane of Lung Plan #3 with respect to TPS calculated dose. Agreement was evaluated using a $\pm 3\%/2\text{mm}$ gamma criterion and 53.6% of pixels passed.

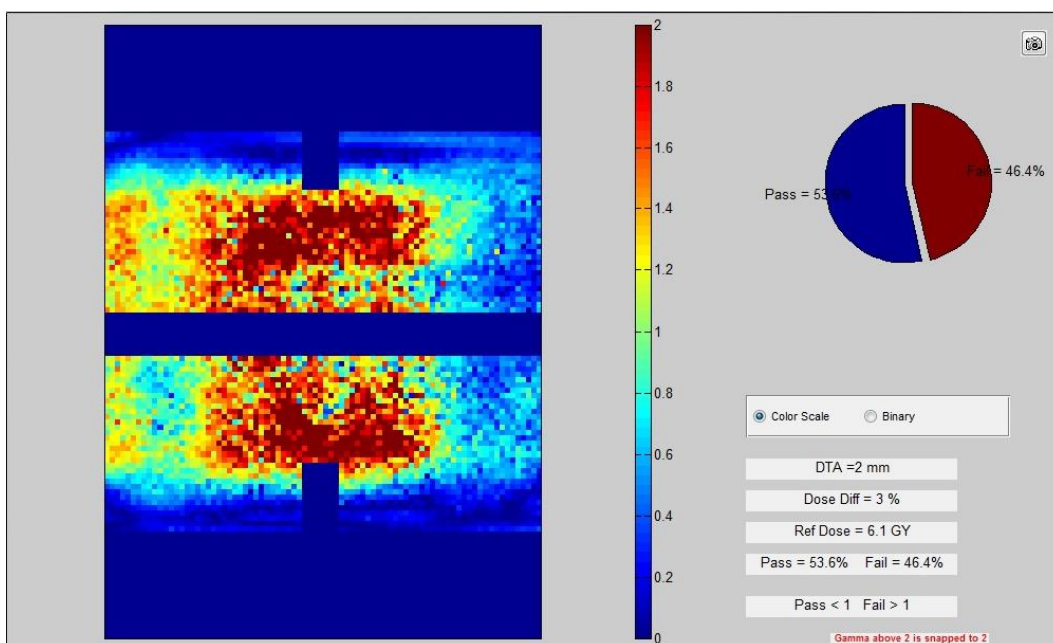


Figure 7.169: Lung phantom delivery comparison for the sagittal plane of Lung Plan #3 with respect to TPS calculated dose. Agreement was evaluated using a $\pm 3\%/2\text{mm}$ gamma criterion and 64.1% of pixels passed.

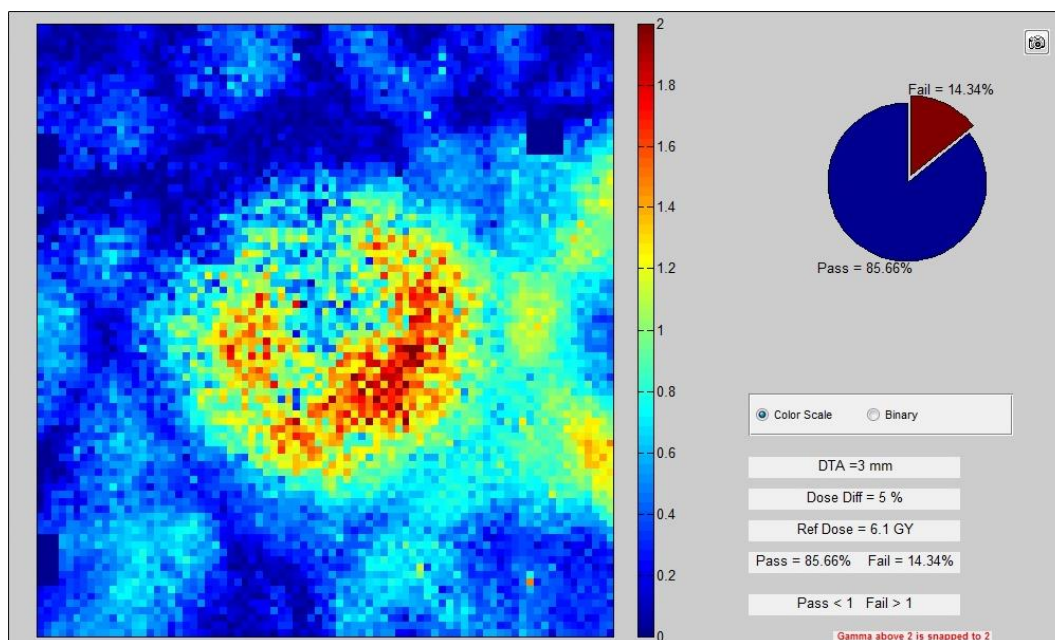


Figure 7.170: Lung phantom delivery comparison for the axial plane of Lung Plan #3 with respect to TPS calculated dose. Agreement was evaluated using a $\pm 5\%/3\text{mm}$ gamma criterion and 85.7% of pixels passed.

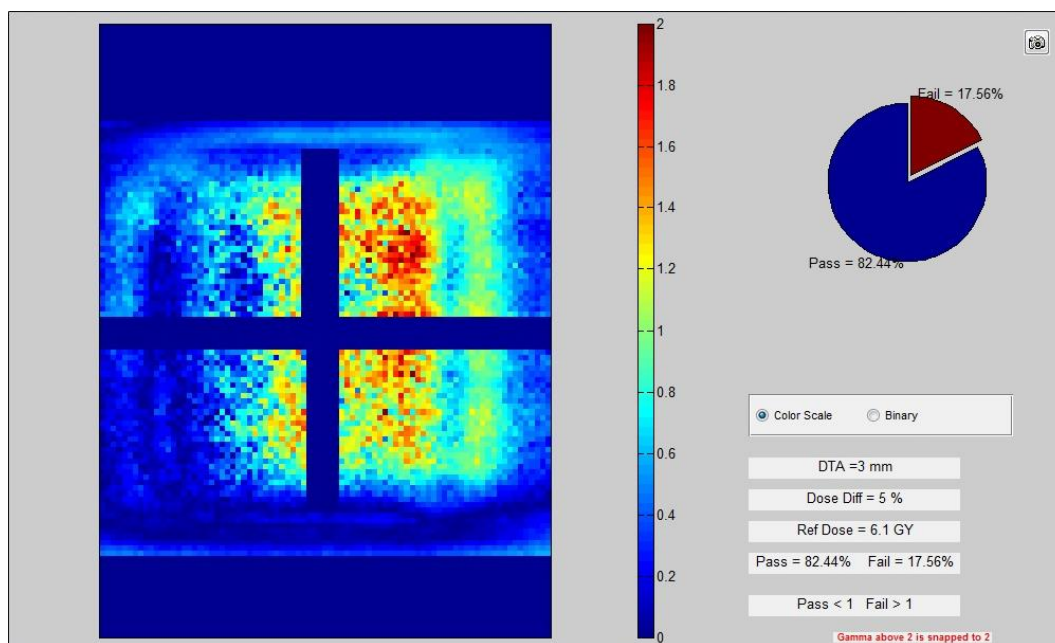


Figure 7.171: Lung phantom delivery comparison for the coronal plane of Lung Plan #3 with respect to TPS calculated dose. Agreement was evaluated using a $\pm 5\%/3\text{mm}$ gamma criterion and 82.5% of pixels passed.

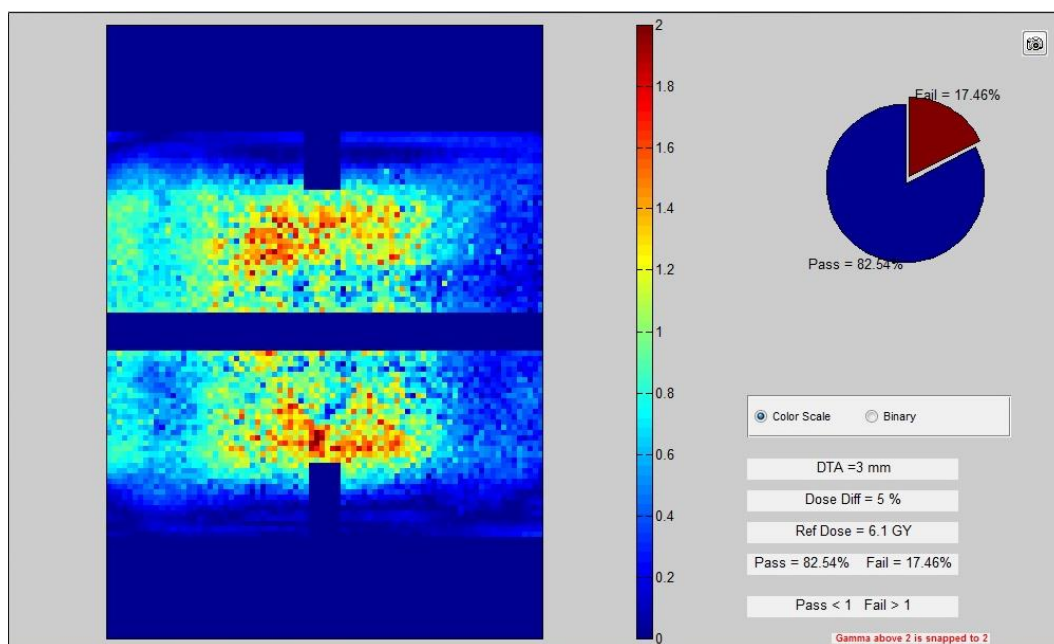


Figure 7.172: Lung phantom delivery comparison for the sagittal plane of Lung Plan #3 with respect to TPS calculated dose. Agreement was evaluated using a $\pm 5\%/3\text{mm}$ gamma criterion and 82.4% of pixels passed.

Chapter 8: References

1. Ibbott, G. *MO-A-BRC-01: Credentialing for Clinical Trials: The Role of the RPC*. in *AAPM Annual Meeting*. 2009. AAPM.
2. Ezzell, G.A., J.M. Galvin, D. Low, J.R. Palta, I. Rosen, M.B. Sharpe, P. Xia, Y. Xiao, L. Xing, and C.X. Yu, *Guidance document on delivery, treatment planning, and clinical implementation of IMRT: Report of the IMRT subcommittee of the AAPM radiation therapy committee*. *Medical Physics*, 2003. **30**(8): p. 2089-2115.
3. *Radiation Therapy's Harmful Side*, in *The New York Times*2010: New York. p. A26.
4. Bogdanich, W., *Radiation Offers New Cures, and Ways to Do Harm*, in *The New York Times*2010: New York.
5. Bogdanich, W., *As Technology Surges, radiation Safeguards Lag*, in *The New York Times*2010: New York.
6. Bogdanich, W., *Case Studies: When Medical Radiation Goes Awry*, in *The New York Times*2010: New York.
7. Bogdanich, W., *They Check the Medical Equipment, but Who is Checking Up on Them?*, in *The New York Times*2010: New York.
8. Parker-Pope, T., *Treatment Errors for Men With Prostate Cancer*, in *The New York Times*2009: New York.
9. Parker-Pope, T., *When Radiation Treatment Turns Deadly*, in *The New York Times*2010: New York.
10. Parker-Pope, T., *More Protection for Radiation Patients*, in *The New York Times*2010: New York.
11. Kirby, T.H., W.F. Hanson, and D.A. Johnston, *Uncertainty analysis of absorbed dose calculations from thermoluminescence dosimeters*. *Medical Physics*, 1992. **19**(6): p. 1427-1433.

12. Davidson, S.E., R.A. Popple, G.S. Ibbott, and D.S. Followill, *Technical Note: Heterogeneity dose calculation accuracy in IMRT: Study of five commercial treatment planning systems using an anthropomorphic thorax phantom*. Med. Phys., 2008. **35**(12): p. 5434-5439.
13. Alvarez, P., A. Molineu, N. Hernandez, D. Followill, and G. Ibbott, *SU-FF-T-403: Evaluation of doses delivered by SBRT to the lung of an anthropomorphic thorax phantom*. Medical Physics, 2005. **32**(6): p. 2043-2044.
14. Alvarez, P., A. Molineu, N. Hernandez, D. Followill, and G. Ibbott, *TU-E-224A-01: Evaluation of heterogeneity corrections algorithms through the irradiation of a lung phantom*. Medical Physics, 2006. **33**(6): p. 2214.
15. Alvarez, P., A. Molineu, N. Hernandez, D. Followill, and G. Ibbott, *MO-D-AUD-04: A comparison of heterogeneity correction algorithms within a lung PTV*. Medical Physics, 2007. **34**(6): p. 2521.
16. Followill, D., A. Molineu, P. Alvarez, and G. Ibbott, *TH-D-224C-02: The state of radiotherapy physics through the eyes of a quality auditor*. Medical Physics, 2006. **33**(6): p. 2283.
17. Molineu, A., N. Hernandez, P. Alvarez, D. Followill, and G. Ibbott, *SU-FF-T-148: IMRT head and neck phantom irradiations: Correlation of results with institution size*. Medical Physics, 2005. **32**(6): p. 1983-1984.
18. Davidson, S.E., G.S. Ibbott, K.L. Prado, L. Dong, Z. Liao, and D.S. Followill, *Accuracy of two heterogeneity dose calculation algorithms for IMRT in treatment plans designed using an anthropomorphic thorax phantom*. Med. Phys., 2007. **34**(5): p. 1850-1857.
19. Kry, S.F., P. Alvarez, A. Molineu, C. Amador, J. Galvin, and D.S. Followill, *Algorithms Used in Heterogeneous Dose Calculations Show Systematic Differences as Measured With the Radiological Physics Center's Anthropomorphic Thorax Phantom Used for RTOG Credentialing*. International Journal of Radiation Oncology*Biophysics*Physics, 2013. **85**(1): p. e95-e100.

20. Davidson, S., J. Cui, D. Followill, G. Ibbott, and J. Deasy, *A flexible Monte Carlo tool for patient or phantom specific calculations: comparison with preliminary validation measurements*. Journal of Physics: Conference Series, 2008. **102**.
21. Davidson, S., S. Kry, J. Cui, J. Deasy, G. Ibbott, M. Vicic, A. White, and D. Followill. *DPM Monte Carlo with multi-source model: validation and benchmark results*. in *Proceedings of the XVIth ICCR*. 2010. Amsterdam, North Holland, Netherlands.
22. Chetty, I.J., B. Curran, J.E. Cygler, J.J. DeMarco, G. Ezzell, B.A. Faddegon, I. Kawrakow, P.J. Keall, H. Liu, C.-M.C. Ma, D.W.O. Rogers, J. Seuntjens, D. Sheikh-Bagheri, and J.V. Siebers, *Report of the AAPM Task Group No. 105: Issues associated with clinical implementation of Monte Carlo-based photon and electron external beam treatment planning*. Medical Physics, 2007. **34**(12): p. 4818-4853.
23. Sempau, J., S.J. Wilderman, and A.F. Bielajew, *DPM, a fast, accurate Monte Carlo code optimized for photon and electron radiotherapy treatment planning dose calculations*. Phys. Med. Biol., 2000. **45**: p. 2263-2291.
24. Bielajew, A.F. *Monte Carlo modelling in external electron-beam radiotherapy - why leave it to chance?* in *Proc. of the 11th Conf. on the Use of Computers in Radiotherapy*. 1994. Madison, WI: Medical Physics Publishing.
25. Nelson, W.R., H. Hirayama, and D.W.O. Rodgers, *The EGS4 code system*, 1985, Stanford Linear Accelerator Center.
26. Halbleib, J., *Structure and operation of the ITS code system in Monte Carlo Transport of Electrons and Photons*, T. Jenkins, Editor 1989, Plenum: New York. p. 249-262.
27. Halbleib, J., R.P. Kensek, T.A. Mehlhorn, G.D. Valdez, S.M. Seltzer, and M.J. Berger, *ITS Version 3.0: the integrated TIGER series of coupled electron/photon Monte Carlo transport codes*, 1992, Sandia Report.
28. Briesmeister, J.F., *MCNP - a general Monte Carlo N-particle transport code*, 1993, Los Alamos National Laboratory: Los Alamos, NM.

29. Baro, J., J. Sempau, J.M. Fernandez-Varea, and F. Salvat, *PENELOPE: an algorithm for Monte Carlo simulation of the penetration and energy loss of electrons and positrons in matter*. Nucl. Instrum. Methods, 1995. **100**: p. 31-46.
30. Salvat, F., J.M. Fernandez-Varea, J. Baro, and J. Sempau, *PENELOPE, an algorithm and computer code for Monte Carlo simulation of electron-photon showers*, 1996, Centro de Investigaciones Energeticas, Medioambientales y Tecnologicas.
31. Sempau, J., E. Acosta, J. Baro, J.M. Fernandez-Varea, and F. Salvat, *An algorithm for Monte Carlo simulation of coupled electron-photon showers*. Nucl. Instrum. Methods, 1997. **132**: p. 377-390.
32. Fragoso, M., S. Pillai, T.D. Solberg, and I.J. Chetty, *Experimental verification and clinical implementation of a commercial Monte Carlo electron beam dose calculation algorithm*. Med. Phys., 2008. **35**: p. 1028-1038.
33. Ulmer, W., J. Pyry, and W. Kaissl, *A 3D photon superposition/convolution algorithm and its foundation on results of Monte Carlo calculations*. Physics in Medicine and Biology, 2005. **50**(8): p. 1767.
34. Papanikolaou, N., J.J. Battista, A.L. Boyer, C. Kappas, E. Klein, T.R. Mackie, M. Sharpe, and J.V. Dyk, *Report of Task Group No. 65 of the Radiation Therapy Committee of the American Association of Physicists in Medicine: Tissue inhomogeneity corrections for megavoltage photon beams*, 2004, American Association of Physicists in Medicine.
35. Davidson, S., *Benchmarking and implementation of a new independent Monte Carlo dose calculation quality assurance audit tool for clinical trials*, in *Medical Physics 2010*, The University of Texas Health Science Center at Houston - Graduate School of Biomedical Sciences: Houston, TX. p. 197.
36. Deasy, J.O., A.I. Blanco, and V.H. Clark, *CERR: A computational environment for radiotherapy research*. Med. Phys., 2003. **30**(5): p. 979-985.

37. Fix, M.K., P. Manser, E.J. Born, R. Mini, and P. Ruegsegger, *A multiple source model for 6 MV photon beam dose calculations using Monte Carlo*. *Physics in Medicine and Biology*, 2001. **46**(5): p. 1407.
38. Ma, C.M., B.A. Faddegon, D.W.O. Rogers, and T.R. Mackie, *Accurate characterization of Monte Carlo calculated electron beams for radiotherapy*. *Med. Phys.*, 1997. **24**: p. 401-416.
39. Ma, C.-M., E. Mok, A. Kapur, T. Pawlicki, D. Findley, S. Brain, K. Forster, and A.L. Boyer, *Clinical implementation of a Monte Carlo treatment planning system*. *Med. Phys.*, 1999. **26**: p. 2133-2143.
40. Wittenau, A.E.S.v., L.J. Cox, P.M. Bergstrom, W.P. Chandler, C.L.H. Siantar, and R. Mohan, *Correlated histogram representation of Monte Carlo derived medical accelerator photon-output phase space*. *Med. Phys.*, 1999. **26**: p. 1196-1211.
41. Chetty, I., J.J. DeMarco, and T.D. Solberg, *A virtual source model for Monte Carlo modeling of arbitrary intensity distributions*. *Med. Phys.*, 2000. **27**: p. 166-172.
42. Deng, J., S.B. Jiang, A. Kapur, J. Li, T. Pawlicki, and C.M. Ma, *Photon beam characterization and modelling for Monte Carlo treatment planning*. *Physics in Medicine and Biology*, 2000. **45**(2): p. 411.
43. Fix, M.K., H. Keller, P. Ruegsegger, and E.J. Born, *Simple beam models for Monte Carlo photon beam dose calculations in radiotherapy*. *Med. Phys.*, 2000. **27**: p. 2739-2747.
44. Ma, C.-M., *Characterization of computer simulated radiotherapy beams for Monte-Carlo treatment planning*. *Radiation Physics and Chemistry*, 1998. **53**(3): p. 329-344.
45. Aljarrah, K., G.C. Sharp, T. Neicu, and S.B. Jiang, *Determination of the initial beam parameters in Monte Carlo linac simulation*. Vol. 33. 2006: AAPM. 850-858.
46. Deng, J., S.B. Jiang, T. Pawlicki, J. Li, and C.M. Ma, *Derivation of electron and photon energy spectra from electron beam central axis depth dose curves*. *Physics in Medicine and Biology*, 2001. **46**(5): p. 1429.

47. Faddegon, B.A. and I. Blevis, *Electron spectra derived from depth dose distributions*. Med. Phys., 2000. **27**: p. 514-526.
48. Siljamäki, S., L. Tillikainen, H. Helminen, and J. Pyyry, *TU-FF-A1-04: Determining Parameters for a Multiple-Source Model of a Linear Accelerator Using Optimization Techniques*. Med. Phys., 2005. **32**: p. 2113-2114.
49. Yang, J. and et al., *Modelling of electron contamination in clinical photon beams for Monte Carlo dose calculation*. Physics in Medicine and Biology, 2004. **49**(12): p. 2657.
50. Fippel, M., *Fast Monte Carlo dose calculation for photon beams based on the VMC electron algorithm*. Med. Phys., 1999. **26**: p. 1466-1475.
51. Heath, E., J. Seuntjens, and D. Sheikh-Bagheri, *Dosimetric evaluation of the clinical implementation of the first commercial IMRT Monte Carlo treatment planning system at 6 MV*. Med. Phys., 2004. **31**: p. 2771-2779.
52. Fan, J., J. Li, L. Chen, R. Price, K. Paskalev, Z. Chen, S. Stathakis, W. Luo, and C. Ma, *TH-E-224C-01: Generic Source Models for Commonly Used Clinical Accelerator Beams for Monte Carlo Treatment Planning*. Med. Phys., 2006. **33**: p. 2292-2292.
53. Fippel, M., F. Haryanto, O. Dohm, F. Nusslin, and S. Kriesen, *A virtual photon energy fluence model for Monte Carlo dose calculation*. Medical Physics, 2003. **30**(3): p. 301-311.
54. Fix, M.K., P.J. Keall, K. Dawson, and J.V. Siebers, *Monte Carlo source model for photon beam radiotherapy: photon source characteristics*. Med. Phys., 2004. **31**: p. 3106-3121.
55. Followill, D., J. Lowenstein, and G. Ibbott, *TU-D-303-01: High-Energy Photon Standard Dosimetry Data: A Quality Assurance Tool*. Med. Phys., 2004. **31**(6): p. 1782.
56. Ibbott, G. *TH-B-T-6B-01: The Radiological Physics Center's QA Activities*. in *AAPM Annual Meeting*. 2005. AAPM.

57. Rogers, D.W.O., B.A. Faddegon, G.X. Ding, C.M. Ma, J. We, and T.R. Mackie, *BEAM: A Monte Carlo code to simulate radiotherapy treatment units*. Medical Physics, 1995. **22**(5): p. 503-524.
58. Kawrakow, I., *VMC++, electron and photon Monte Carlo calculations optimized for radiation treatment planning*. Advanced Monte Carlo for Radiation Physics, Particle Transport Simulation and Applications: Proceedings of the Monte Carlo 2000 Meeting Lisbon, 2001: p. 229-236.
59. Sheikh-Bagheri, D. and D.W.O. Rogers, *Monte Carlo calculation of nine megavoltage photon beam spectra using the BEAM code*. Medical Physics, 2002. **29**(3): p. 391-402.
60. Liu, H.H., T.R. Mackie, and E.C. McCullough, *A dual source photon beam model used in convolution/superposition dose calculations for clinical megavoltage x-ray beams*. Med. Phys., 1997. **24**: p. 1960-1974.
61. Taylor, R.C., V.M. Tello, C.B. Schroy, M. Vossler, and W.F. Hanson, *A generic off-axis energy correction for linac photon beam dosimetry*. Medical Physics, 1998. **25**(5): p. 662-667.
62. Georg, D., G. Kragl, S.a. Wetterstedt, P. McCavana, B. McClean, and T. Knoos, *Photon beam quality variations of a flattening filter free linear accelerator*. Medical Physics, 2010. **37**(1): p. 49-53.
63. Horn, R.A., *Computer programs for output and depth dose from hyperbolic equations*. Medical Physics, 1981. **8**(1): p. 108-110.
64. *Pinnacle3 Physics Reference Guide*, 2005. p. 3-35.
65. Jaffray, D.A., J.J. Battista, A. Fenster, and P. Munro, *X-ray sources of medical linear accelerators: Focal and extra-focal radiation*. Medical Physics, 1993. **20**(5): p. 1417-1427.
66. Molineu, A., D.S. Followill, P.A. Balter, W.F. Hanson, M.T. Gillin, M.S. Huq, A. Eisbruch, and G.S. Ibbott, *Design and implementation of an anthropomorphic quality assurance*

- phantom for intensity-modulated radiation therapy for the Radiation Therapy Oncology Group*. J. Radiation Oncology Biol. Phys., 2005. **63**(2): p. 577-583.
67. Followill, D.S., D.R. Evans, C. Cherry, A. Molineu, G. Fisher, W.F. Hanson, and G.S. Ibbot, *Design, development, and implementation of the Radiological Physics Center's pelvis and thorax anthropomorphic quality assurance phantoms*. Medical Physics, 2007. **34**(6): p. 2070-2076.
68. Low, D.A., J.M. Moran, J.F. Dempsey, L. Dong, and M. Oldham, *Dosimetry tools and techniques for IMRT*. Medical Physics. **38**(3): p. 1313-1338.
69. Keall, P.J., J.V. Siebers, B. Libby, and R. Mohan, *Determining the incident electron fluence for Monte Carlo-based photon treatment planning using a standard measured data set*. Medical Physics, 2003. **30**(4): p. 574-582.
70. Huq, M.S., H. Song, P. Andreo, and C.J. Houser, *Reference dosimetry in clinical high-energy electron beams: Comparison of the AAPM TG-51 and AAPM TG-21 dosimetry protocols*. Medical Physics, 2001. **28**(10): p. 2077-2087.
71. Devic, S., J. Seuntjens, G. Hegyi, E.B. Podgorsak, C.G. Soares, A.S. Kirov, I. Ali, J.F. Williamson, and A. Elizondo, *Dosimetric properties of improved GafChromic films for seven different digitizers*. Medical Physics, 2004. **31**(9): p. 2392-2401.
72. Kry, S.F., P. Alvarez, A. Molineu, C. Amador, J. Galvin, and D. Followill. *Algorithms used in heterogeneous dose calculations show systematic error as measured with the Radiological Physics Center's anthropomorphic thorax phantom used for RTOG credentialing*. in *ASTRO Annual Meeting*. 2012. Boston MA.
73. Papanikolaou, N., J.J. Battista, A.L. Boyer, C. Kappas, E. Klein, T.R. Macki, M. Sharpe, and J.V. Dyk, *Tissue Inhomogeneity Corrections for Megavoltage Photon Beams*, in *Task Group Report No. 85*, A.A.o.P.i. Medicine, Editor 2004.

Chapter 9: Vita

Austin Michael Faught was born in Wooster, Ohio on March 13th, 1987, the son of Lori Ann Faught and Michael Wayne Faught. After graduating from Triway High School in 2005, he enrolled at Kenyon College. He was awarded a Bachelor of Arts in Physics in 2009. In August of 2009 he enrolled at The University of Texas Health Science Center Graduate School of Biomedical Sciences.

Permanent Address:

1964 Sherck Boulevard

Wooster, Ohio 44691